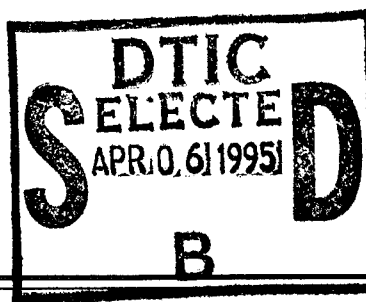


Naval Research Laboratory

Stennis Space Center, MS 39529-5004



NRL/MR/7322--95-7584

Proceedings of the ONR/NRL Workshop on Modeling the Dispersion of Nuclear Contaminants in the Arctic Seas October 18-19, 1994 — Monterey, California

RUTH H. PRELLER

*Ocean Dynamics and Prediction Branch
Oceanography Division*

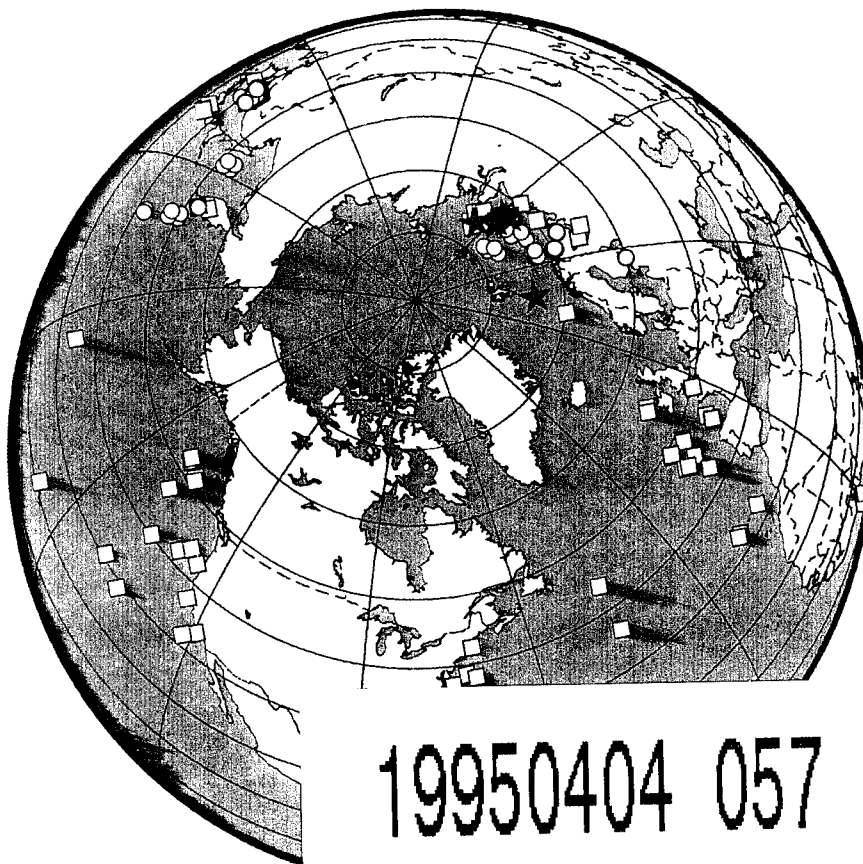
ROBERT EDSON

*Office of Naval Research
Arlington, VA 22217-5000*

Original contains color
plates: All DTIC reproductions
will be in black and
white.

OCEAN NUCLEAR WASTE SITES

- LIQUID
- ★ REACTOR
- SOLID



February 22, 1995

19950404 057

Approved for public release; distribution is unlimited.

DISCLAIMER NOTICE

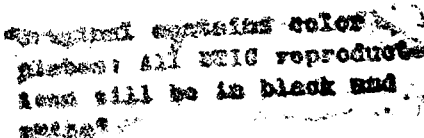


THIS DOCUMENT IS BEST QUALITY AVAILABLE. THE COPY FURNISHED TO DTIC CONTAINED A SIGNIFICANT NUMBER OF COLOR PAGES WHICH DO NOT REPRODUCE LEGIBLY ON BLACK AND WHITE MICROFICHE.

REPORT DOCUMENTATION PAGE

Form Approved
OBM No. 0704-0188

Public reporting burden for this collection of information is estimated to average 1 hour per response, including the time for reviewing instructions, searching existing data sources, gathering and maintaining the data needed, and completing and reviewing the collection of information. Send comments regarding this burden or any other aspect of this collection of information, including suggestions for reducing this burden, to Washington Headquarters Services, Directorate for Information Operations and Reports, 1215 Jefferson Davis Highway, Suite 1204, Arlington, VA 22202-4302, and to the Office of Management and Budget, Paperwork Reduction Project (0704-0188), Washington, DC 20503.

1. AGENCY USE ONLY (Leave blank)		2. REPORT DATE February 22, 1995		3. REPORT TYPE AND DATES COVERED Final	
4. TITLE AND SUBTITLE Proceedings of the ONR/NRL Workshop on Modeling the Dispersion of Nuclear Contaminants in the Arctic Seas October 18-19, 1994 — Monterey, California				5. FUNDING NUMBERS Job Order No. 573571504 Program Element No. 0603711H Project No. Task No. DNA Accession No. DN154-217	
6. AUTHOR(S) Ruth H. Preller and Robert Edson*					
7. PERFORMING ORGANIZATION NAME(S) AND ADDRESS(ES) Naval Research Laboratory Oceanography Division Stennis Space Center, MS 39529-5004				8. PERFORMING ORGANIZATION REPORT NUMBER NRL/MR/7322--95-7584	
9. SPONSORING/MONITORING AGENCY NAME(S) AND ADDRESS(ES) Defense Nuclear Agency 6801 Telegraph Road Alexandria, VA 22310-3398				10. SPONSORING/MONITORING AGENCY REPORT NUMBER	
11. SUPPLEMENTARY NOTES *Office of Naval Research 800 N. Quincy St. Arlington, VA 22217-5000					
12a. DISTRIBUTION/AVAILABILITY STATEMENT Approved for public release; distribution unlimited.				12b. DISTRIBUTION CODE	
13. ABSTRACT (Maximum 200 words) A workshop focusing on modeling the dispersion of radionuclides which have been dumped into the Arctic Ocean was held in Monterey, CA, in October 1994. This workshop was sponsored by the Office of Naval Research and hosted by the Naval Research Laboratory. Over 40 participants attended this meeting during which 23 oral presentations were given. The focus of this workshop was on the existing modeling effort within the Arctic Nuclear Waste Assessment program, complementary data sets and the future direction of these efforts. The goal of the workshop was to foster communication through presentations of ongoing work. The intent was that discussions, brought about by these presentations would help the most important processes, effects, and issues that should be addressed by present and future modeling efforts. 					
14. SUBJECT TERMS Kara Sea, nuclear waste, nuclear contamination				15. NUMBER OF PAGES 415	
				16. PRICE CODE	
17. SECURITY CLASSIFICATION OF REPORT Unclassified	18. SECURITY CLASSIFICATION OF THIS PAGE Unclassified	19. SECURITY CLASSIFICATION OF ABSTRACT Unclassified	20. LIMITATION OF ABSTRACT SAR		

Proceedings of the ONR/NRL
**Workshop on Modeling the Dispersion of Nuclear Contaminants
in the Arctic Seas**
October 18-19, 1994, Monterey California

Introduction	1
Workshop Agenda	3
Abstracts/Figures	
Data Presentations	7
Modeling Presentations	197
Workshop Summary and Conclusions	403
List of Attendees	409

Editors of Workshop Proceedings
Ruth H. Preller and Robert Edson

Workshop Support Staff
Charlene Parker, Thomas Kozo

Accession For	
NTIS GRA&I	<input checked="" type="checkbox"/>
DTIC TAB	<input type="checkbox"/>
Unannounced	<input type="checkbox"/>
Justification	
By	
Distribution	
Availability Codes	
Dist	Avail and/or Special
A-1	

Introduction

Ruth H. Preller

From October 18-19, 1994, the Office of Naval Research (ONR) sponsored a workshop on Modeling the Dispersion of Nuclear Contaminants in the Arctic. This meeting was hosted by the Naval Research Laboratory and held at the Naval Research Laboratory Facilities in Monterey, California. Over 40 participants attended the workshop, the majority of them, scientists working on the ONR Arctic Nuclear Waste Assessment Program (ANWAP).

The focus of this modeling workshop was to be on the existing modeling efforts, complementary data sets and the future direction of these efforts within the ANWAP program. The goal of the workshop was to foster communication between the modelers and the observationalists through presentations of ongoing work. The intent was that discussions, brought about by these presentations, would help determine the most important processes, effects and issues that should be addressed by present and future modeling efforts.

Twenty three presentations were given during this workshop. Ten of these presentations dealt with the gathering and analysis of data. Thirteen presentations dealt with various issues of modeling processes important to the study of Arctic Nuclear Waste Assessment.

The workshop was organized in such a way that the data presentations were given first, taking up the majority of the first day. Modeling presentations began in the afternoon of the first day and continued into the afternoon of the second day. The data presentations were organized such that an overview of the Naval Research Laboratory's development of a Geographical Information System (GIS) data base, containing a number of different sources of published data, was given first. Following that presentation was an overview of the 1993 and 1994 Geochemical and Environmental Research Group (GERG) field experiments in the Kara and Pechora Seas and their adjacent rivers. The four following presentations dealt with observations of sea ice and role sea ice might play in the transport of nuclear contaminants via sediment uptake. The seventh presentation was centered on river data for the Ob and Yenisei rivers. The next presentation was a discussion of the circulation of the Arctic Seas based on Russian data sources. The ninth presentation discussed seabed and fluid flow conditions from observations in the Barents Sea. The last data presentation was given on the second day and discussed the use of AVHRR data in studying river outflow and ice characteristics in the regions near river mouths.

The modeling papers were organized in such a way as to go from larger to smaller scale models. The first three presentations discussed large scale modeling efforts of the Arctic and its adjacent seas. The next four presentations looked at basin modeling efforts in regions such as the Kara and Laptev Seas. The eighth presentation discussed possible methods for modeling the release of radioactive contaminants into the environment from the Icebreaker Lenin. The two following papers discussed river and estuarine modeling efforts. The next paper switched focus from ocean modeling to atmospheric modeling and discussed

the development of a regional atmospheric model for the Kara Sea region. The final two papers discussed modeling the Sea of Okhotsk, another source site for nuclear contamination and the modeling of the motion of dense bottom currents which could affect the transport of contaminants trapped in bottom sediments.

The abstracts and figures presented here follow the order of presentation at the workshop. The text of these proceedings will contain the following

1. Introduction
2. Meeting Agenda
3. Abstracts and Figures
4. Summary and Conclusions
5. List of Attendees

WORKSHOP ON MODELING THE DISPERSION OF NUCLEAR CONTAMINANTS IN THE ARCTIC SEAS

Hosted by the Naval Research Laboratory

Sponsored by the Office of Naval Research

October 18-19, 1994

**Naval Research Laboratory
Monterey, CA**

Modeling Workshop Agenda

Tuesday, October 18, 1994

- 8:30 Opening remarks - Edson/Preller
- Data Presentations
- 9:00 Kathy Crane - Data Base Needs and Efforts
- 9:20 James Brooks - Overview of 1993 and 1994 Expeditions in the
 Kara Sea and Pechora Seas and Adjacent Rivers
- 9:40 Terry Tucker - Radionuclide Contaminants in Central Arctic Sea Ice
- 10:00 Coffee Break
- 10:20 Roger Colony - Patterns of Monthly Wind and Ice Motion in the
 Arctic Basin
- 10:40 Ignatius Rigor - Russian Historical Ice Charts and Dataset
 1967-1990
- 11:00 Erk Reimnitz - Transpolar Drift - The Garbage Scow from Siberia?
- 11:30 Lunch

- 1:30 Peter Becker - Data on the Ob River System, Yenisei River System and Kara Sea Region
- 1:50 Andrey Proshutinsky - Circulation of the Arctic Seas Based on Russian Sources of Information
- 2:10 Richard Sternberg - Time Series Observations of Seabed, Fluid, and Flow Conditions in the Barents and Norwegian Seas
- 2:30 Short wrap up discussion on data
- 2:50 Break

Modeling Presentations

- 3:10 Ruth Preller - Overview of the NRL Large Scale Modeling Effort Studying the Dispersion of Radioactive Contaminants in the Arctic
- 3:30 Abe Cheng - Model Results and Data Comparison for the Kara and Barents Seas
- 3:50 Rick Allard - The Effect of River Discharge in a Large Scale Ice/Ocean Model
- 4:10 Ignatius Rigor - Sea Ice Transport of Pollutants in the Laptev Sea
- 4:30 Meeting concluded for the day

Wednesday, October 19, 1994

- 8:30 Max Coon - An Oriented Sea Ice Dynamics Model with Contamination Incorporation, Transport, and Release
- 8:50 David Smith - A Numerical Study of Radionuclide Dispersal in the Kara Sea
- 9:10 David Brooks - Multiple-River Interactions in Buoyancy-Driven Coastal Currents

- 9:30 Mark Mount - Modeling the Release to the Environment in the Kara Sea from Radioactive Waste in the Dumped Reactor Compartment of the Icebreaker Lenin
- 9:50 Break
- 10:10 Terry Paluszkiwicz - Overview of Modeling from Land Based Sources Through the Ob and Yenisei Rivers and Estuaries to the Kara Sea
- 10:30 Lyle Hibler - Preliminary Assessment of Radioactive Contaminant Transports from Catastrophic Release Scenarios in the Ob and Yenisei River Systems
- 10:50 William Thompson - The NRL NORAPS Model
- Robert Fett - Use of Multi-channel NOAA AVHRR Data in Studying River Outflow Effects and Ice Thickness Patterns
- 11:10 Jiayan Yang - Modelling the Sea of Okhotsk
- Lin Jiang - Topographic Effects on Dense Bottom Currents
- 11:30 Lunch
- 1:30 Modeling discussions
Group discussion of the processes, effects and issues important to the study of the dispersion of radioactive contaminants in the Arctic seas. What are we doing, how can we collaborate and what else do we need to be doing to address the issue correctly.
- 4:30 Meeting adjourns

Data Base Needs and Efforts

Kathy Crane

DEVELOPMENT OF GIS DATA BASES TO DETERMINE THE STATE OF THE RADIONUCLIDE CONTAMINATION IN THE ARCTIC

Kathleen Crane¹ and Clare Brown²

¹Marine Physics

Naval Research Laboratory

Washington DC 20375

kathyc@hp8c.nrl.navy.mil, 202-767-0522 (phone), 202-767-0167 (fax)

²cbrown@boudin.nrlssc.navy.mil, 601-688-4422 (phone)

LONG TERM GOALS

Until recently, the Arctic has been thought of as remote and pristine, far from the environmental problems associated with industrial and agricultural development of lower latitudes. The Cold War cloaked many activities in the region under a curtain of secrecy and for most of the world, the Arctic remained largely out of sight and out of mind.

Information released in 1992 on deliberate dumping of nuclear materials in shallow Arctic Seas raised even more disquiet about pollution of the Arctic marine environment. However, adequate data sets for the distribution of anthropogenic radionuclides in the Arctic Ocean and its surroundings did not yet exist because of the paucity of data particularly in the western Arctic Ocean near North America, in the Central Arctic Ocean, and north of Siberia.

Given the presently unstable situation in Russia (with regard to the state of radioactive dumping in the seas, the sorry condition of its nuclear reactors and the uncertain future of its stockpile of weaponry), it became necessary to investigate all avenues by which airborne radioactive fallout and water transported waste may reach the shores of North America. Given the lack of adequate radionuclide data, it is necessary to observe how winds, currents and ice move and to what degree they may transport radionuclide pollution from the former Soviet Union across the Arctic Ocean to North America.

Existing time series data needed to be collected and compiled from Russian monitoring programs and integrated into western data sets including information on concentrations of radionuclides in the water, sediment, ice, snow, flora and fauna and how these concentrations have varied over space and time. It was also important to gather data from the neighboring seas to provide us with a means by which we can measure the degree of radionuclide pollution in the Arctic relative to the rest of the world's population centers.

The Naval Research Laboratory was tasked with the function of setting up a GIS to address the Arctic radionuclide

contamination issue and to create a data base of information collected from ONR funded expeditions in 1993 and 1994

OBJECTIVES

The goals of the 1994 NRL radionuclide GIS are:

- 1) to create a data base of existing radionuclide data in the water, sediment, ice and biota;
- 2) to create data bases of bathymetry, rivers, sedimentation, biota and physical and chemical oceanographic, riverine and estuarine processes and
- 3) to provide the platform for prediction and determination of the degree of risk these radionuclides pose to the Arctic environment and its inhabitants and to those who depend upon the Arctic marine life for sustenance (this includes many people in the mid latitudes).

APPROACH

Our approach has been multifaceted, incorporating a compilation of preexisting radionuclide data, the digitization of preexisting bathymetric, sediment and physical and chemical oceanographic data, the development of connections with Russian colleagues to further the compilation of preexisting data and the development of collection efforts for new radionuclide, sediment and bathymetric data. In addition, some of our efforts have been directed towards developing interfaces with the ARC/INFO system to enable individuals to query the data bases and to gather statistical information related to the distribution of and correlation's between the parameters entered. Efforts have also been placed in developing a more inexpensive and user friendly GIS operating system with pertinent subsets of the data bases upon which individuals may perform their own analyses of the information provided.

STATUS

As of October, 1994, data bases have been constructed for:

- 1) the distribution of nuclear events (e.g. bomb tests, reactor accidents, etc.) which have occurred around the Arctic, and the location of radionuclide dump sites in the Arctic, Atlantic and Pacific Oceans (figures 1,2). Parameters entered include: ID#, country, site, Start Year of Dumping, End Year of Dumping, Package?, Nature of Waste, # of Reactors with/without fuel, # of containers, Container Type, Container Matrix, Total Weight, (Tons), Total Volume (Liters), Total GBq, Total

Alpha GBq, Total Beta-gamma GBq, Total H-3 GBq, Total Ra-226 GBq, Comments, References

2) the location of stations and ship tracks of the 1993 and 1994 expeditions in the Arctic Seas (figures 3,4),

3) the distribution and concentration of radionuclides in the water column in the Arctic and its neighboring seas from the surface to the seafloor and from 1950 to the present. These include, ^{137}Cs , ^{90}Sr , ^{226}Ra , ^{238}Pu , $^{239/240}\text{Pu}$, ^{241}Am , ^{99}Tc and ^{129}I (figures 5-9).

4) the distribution and concentration of radionuclides in marine, lacustrine and riverine sediments in the Arctic and in its neighboring regions (data are still being added). These isotopes include, ^{137}Cs , ^{60}Co , ^{90}Sr , ^{228}Th , ^{232}Th , ^{234}Th , ^{238}U , ^{55}Fe , ^{226}Ra , ^{210}Pb , ^{212}Pb , ^{214}Pb , ^{40}K , ^{238}Pu , $^{239/240}\text{Pu}$, ^{241}Am , ^{144}Ce , ^{95}Nb , ^{106}Ru , ^{95}Zn , ^{99}Tc , ^{129}I , and ^7Be (figures 10-13).

Other parameters entered into the sediment-radionuclide data base include: ID#, Cruise, Station, Year, Day/Month, Bottom Depth, (m), depth in core (cm), sediment type, %sand, %silt, %clay, %carbonate, %H₂O, grain size, Porosity, Sedimentation rate, macrofauna /m², biomass (mg/m²), year of deposition, comments and references.

5) the distribution of nuclear power plants, weapons factories, and labs, sites of plutonium and uranium production and enrichment, nuclear test sites and military sites around and in the Arctic.

6) digitized Arctic bathymetry from 500 m to ocean depths

7) digitized Arctic Rivers, and

8) digitized distribution of important fish stocks, marine mammals, birds (used as food sources in the Arctic)

In addition, efforts are being taken to gather up-to-date bathymetry shallower than 500 m along the Russian Shelves with the assistance of Russian oceanographers. In addition, sediment type, physical properties, physical and chemical oceanography for the Kara Sea and the Arctic Ocean are being entered into the GIS.

Further development of ARC/INFO interfaces have progressed as well as the development of a MAPINFO GIS with subsets of the data (designed for use by scientists who may not have the resources to purchase or access the full ARC/INFO system).

PROPOSED DEVELOPMENT

In addition, we are planning to add to the GIS the following data bases, depending on levels of funding:

BIOTA

- 1) distribution and contamination of benthic biota;
- 2) distribution, concentrations, seasonal variation and contamination of fish in the Arctic and near-Arctic
- 3) distribution and contamination of other important food sources such as seals, walrus, beluga, narwhal,
- 4) distribution of indigenous and other Arctic people;
- 5) statistics on food sources of the peoples of the Arctic and dose assessments where available.

MARINE GEOLOGY

- 1) seafloor sediment type;
- 2) seafloor sedimentary thickness
- 3) recent sedimentation rates
- 4) detailed bathymetry of the Arctic Seas;
- 5) detailed acoustic backscatter information;
- 6) characterization of the transition from the riverine environment to the oceanic environment.

PHYSICAL OCEANOGRAPHY

- 1) compilations of temperature, salinity, density, and oxygen.
- 2) seasonal oceanographic and riverine information pertinent to the spring thaw and flushing of the Arctic rivers (including salt wedge and flocculation zones in estuaries); rare events (such as unusually large riverine fluxes)
- 3) "remote sensing" compilations of ice movement and transport on a daily, monthly and yearly basis,

IMPACT FOR APPLICATIONS AND RELATIONSHIP TO OTHER PROJECTS

The NRL GIS is an integral part of an international attempt to provide base line information to oceanographic modeling and monitoring efforts. Data from the GIS have been used by the Norwegian Radiation Protection Agency, Tokai University in Japan, the University of Edinburgh, the Norsk Polarinstitutt, KEMA, Netherlands, the IAEA, Vienna, the IAEA Marine Environmental Lab in Monaco, and KORDAI, from the South Korean Institute of Oceanography, and the German Hydrographic Service under the auspices of the IAEA and the AMAP program.

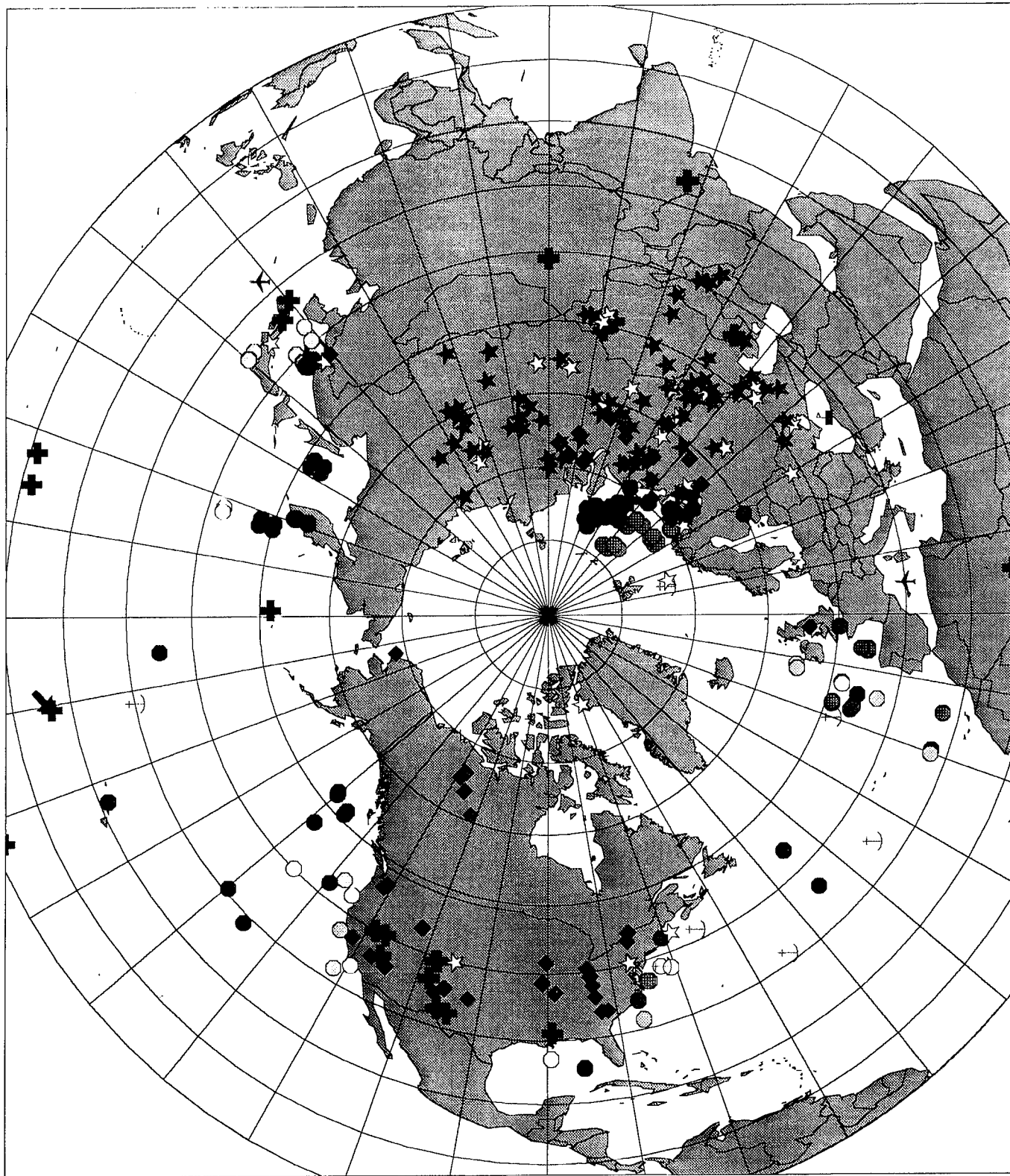


Figure 1

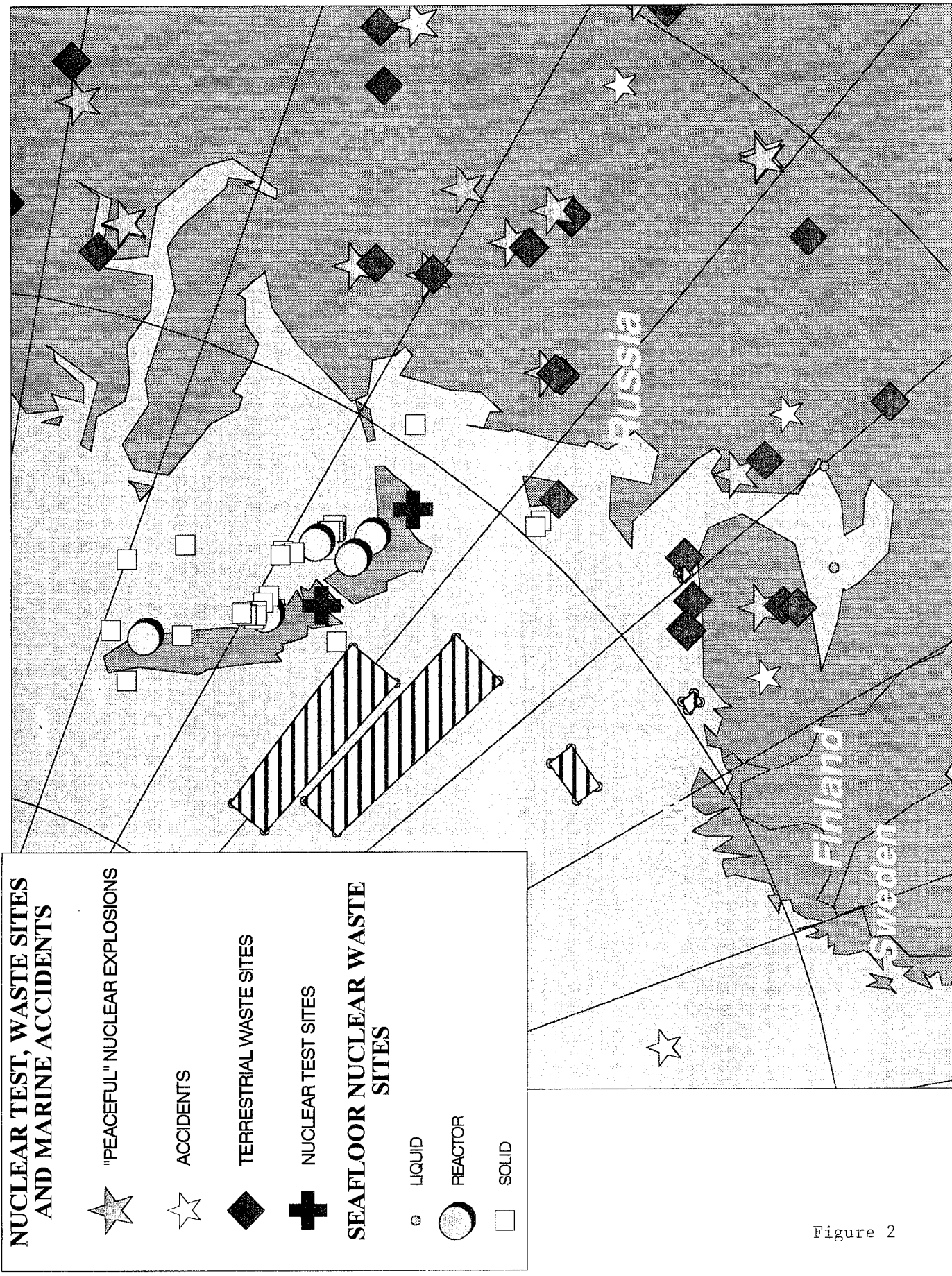


Figure 2

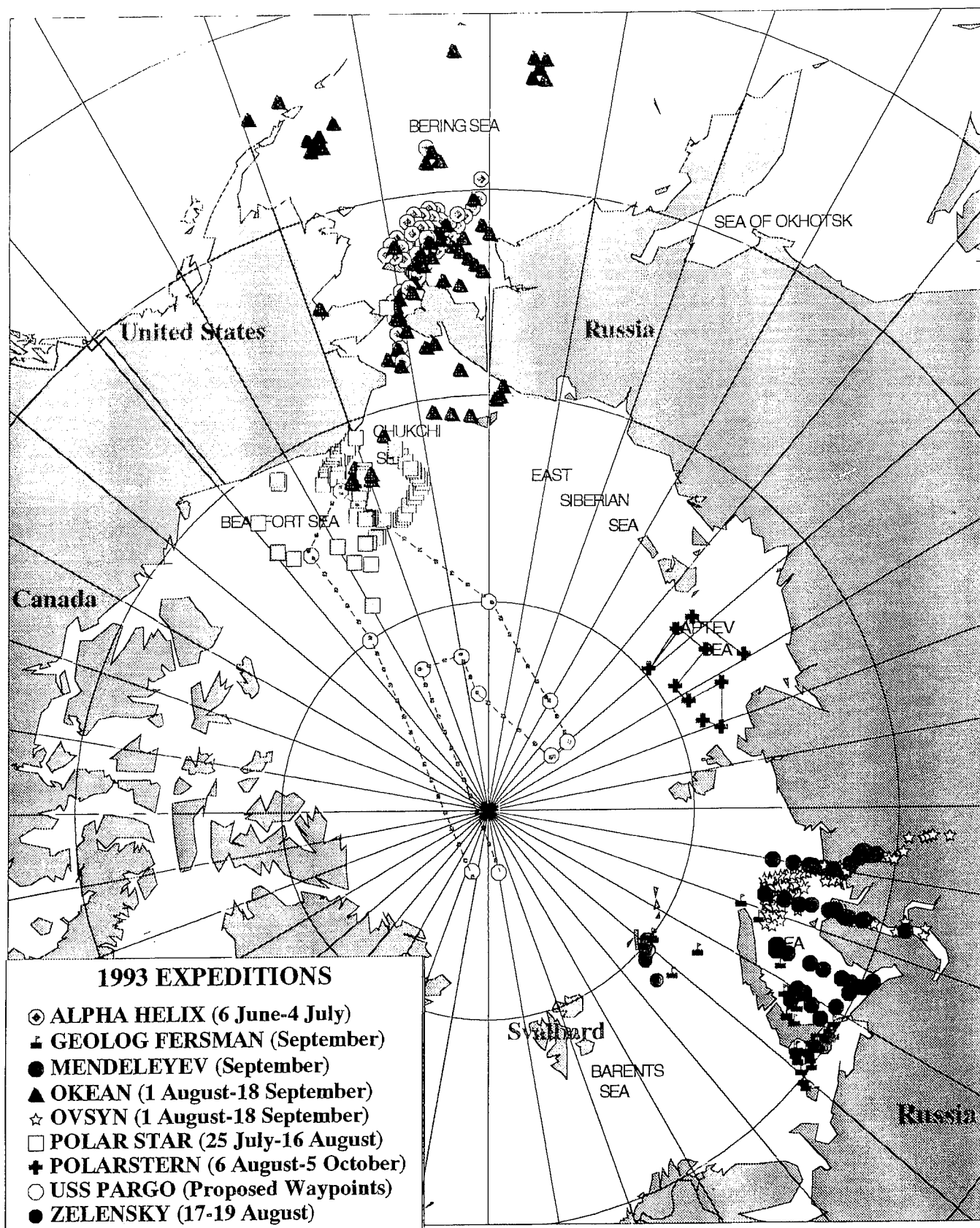
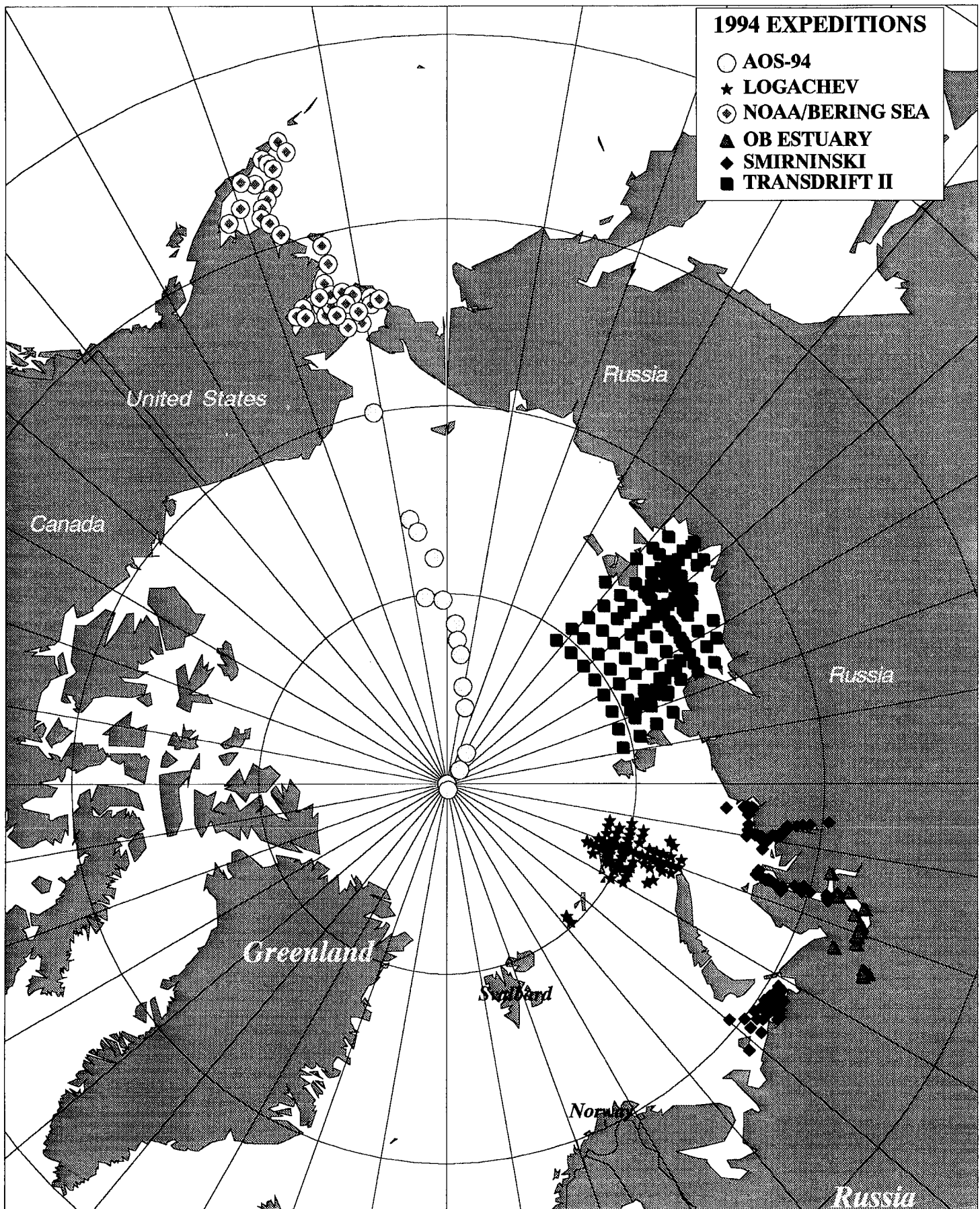


Figure 3



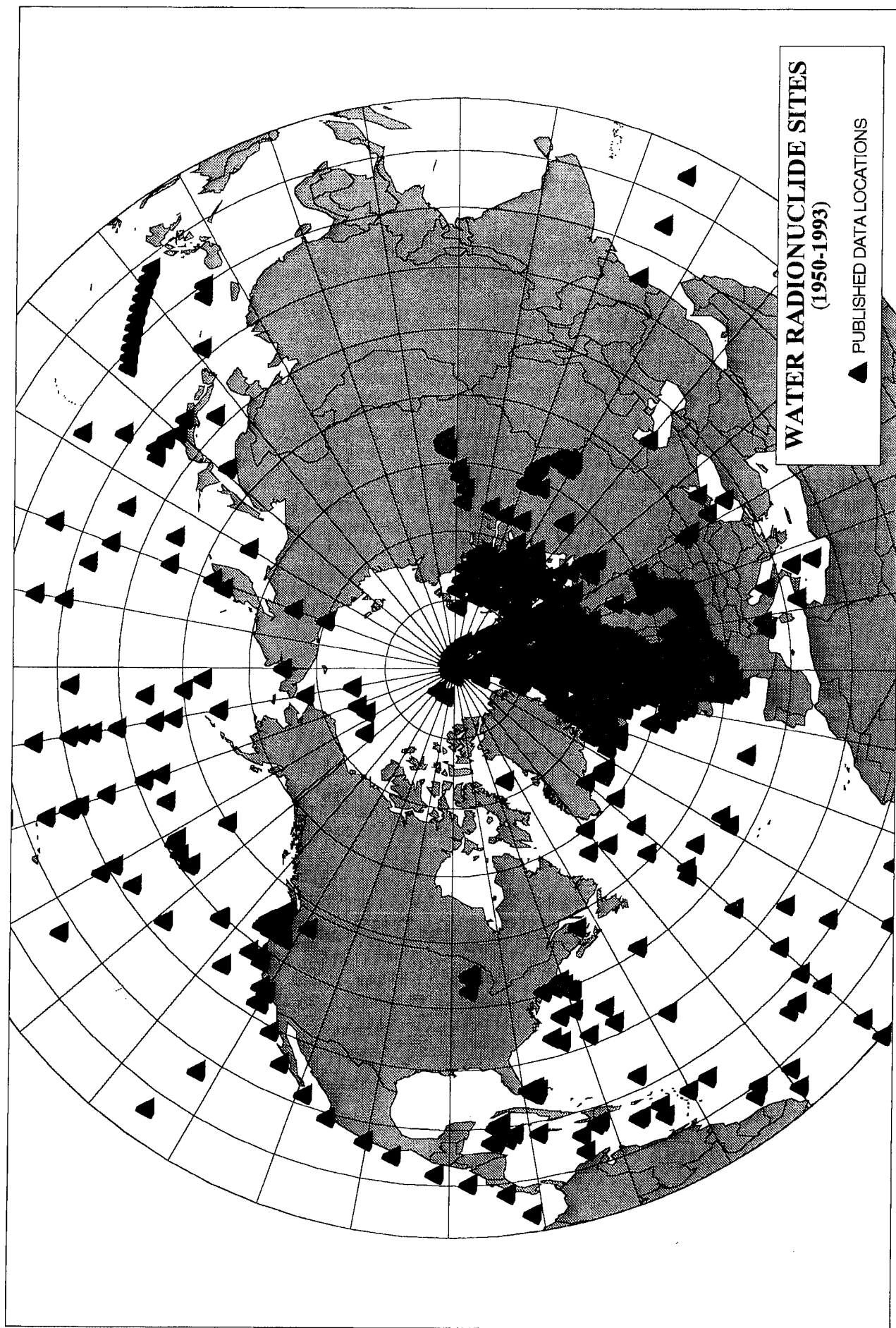


Figure 5

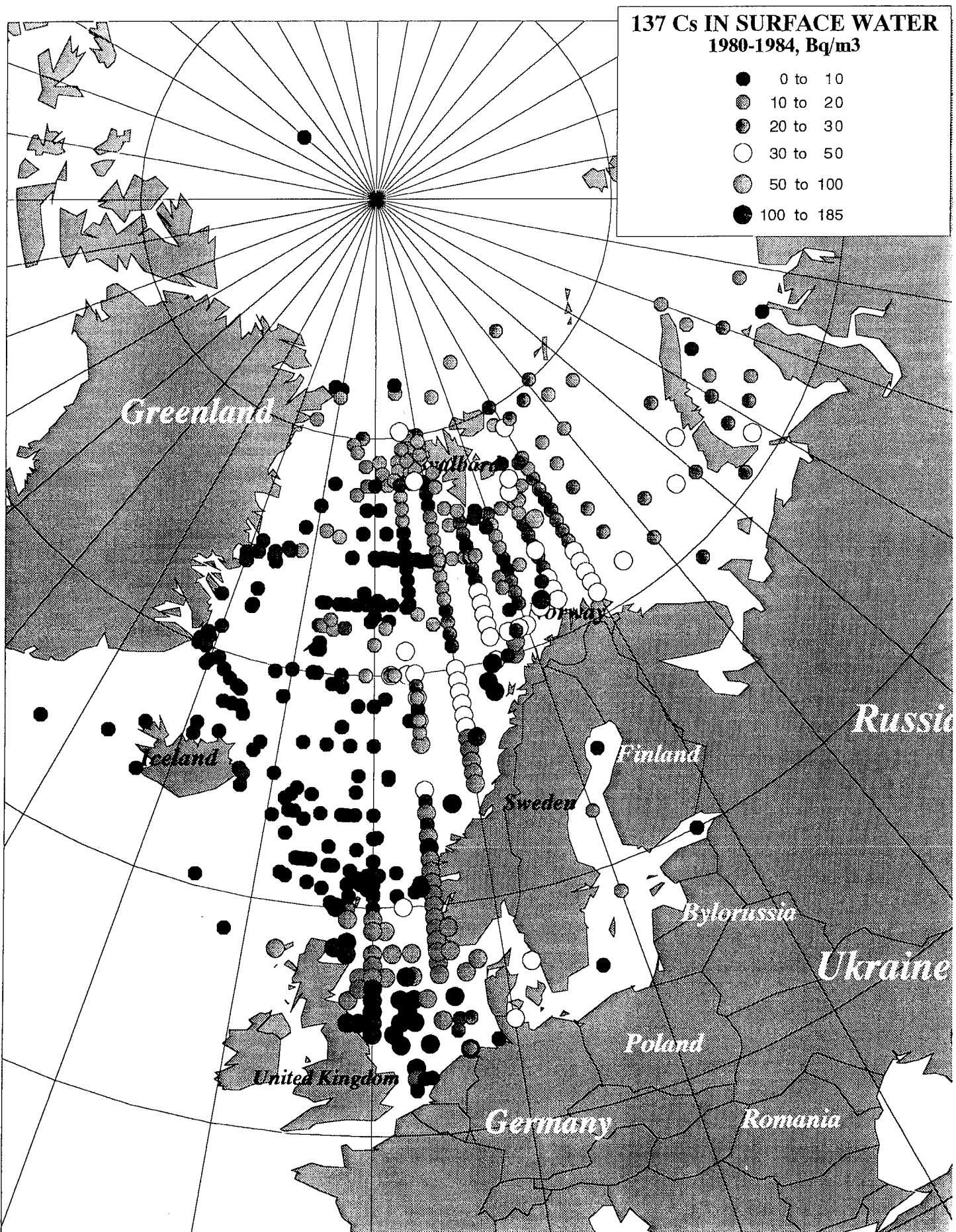


Figure 6

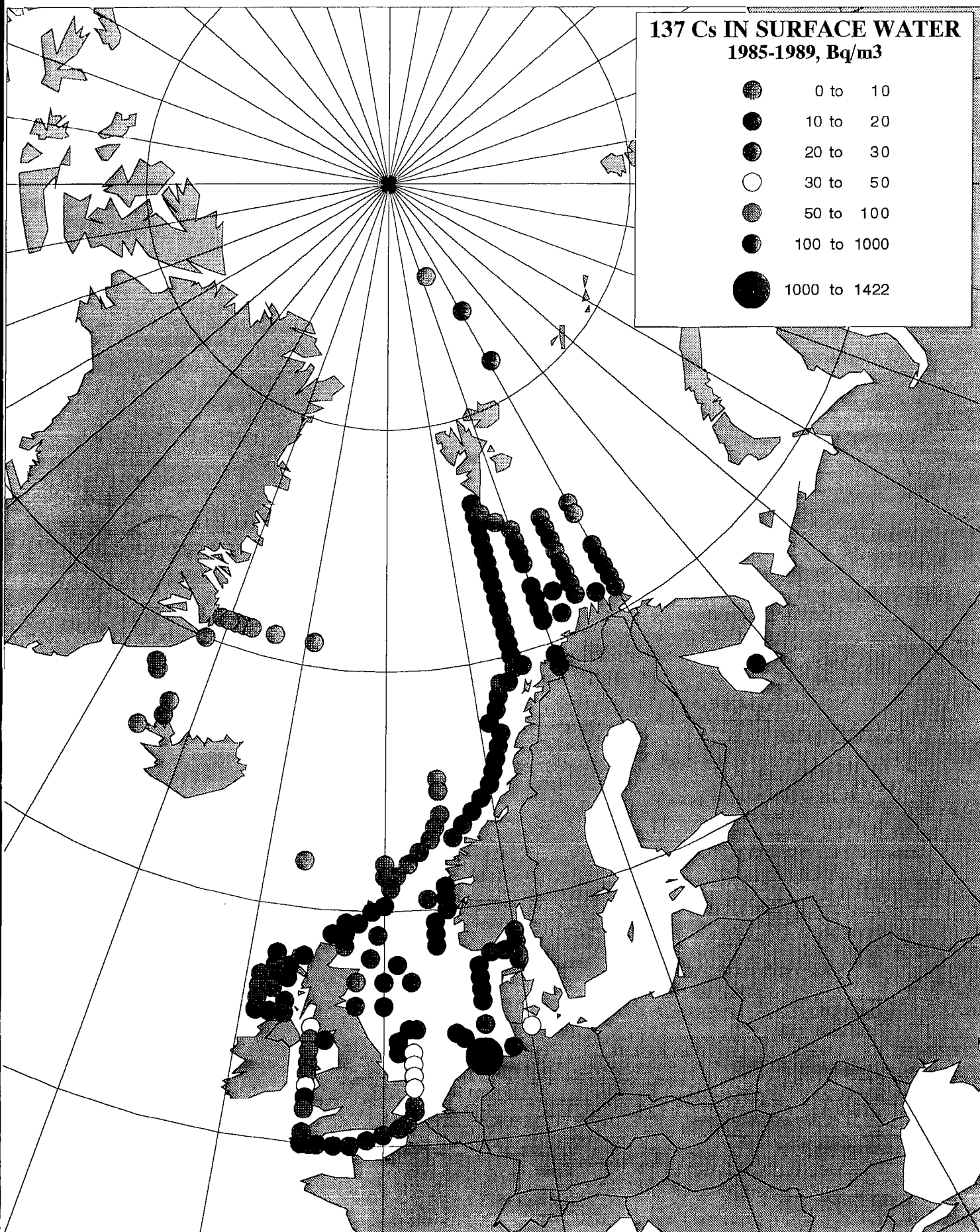


Figure 7

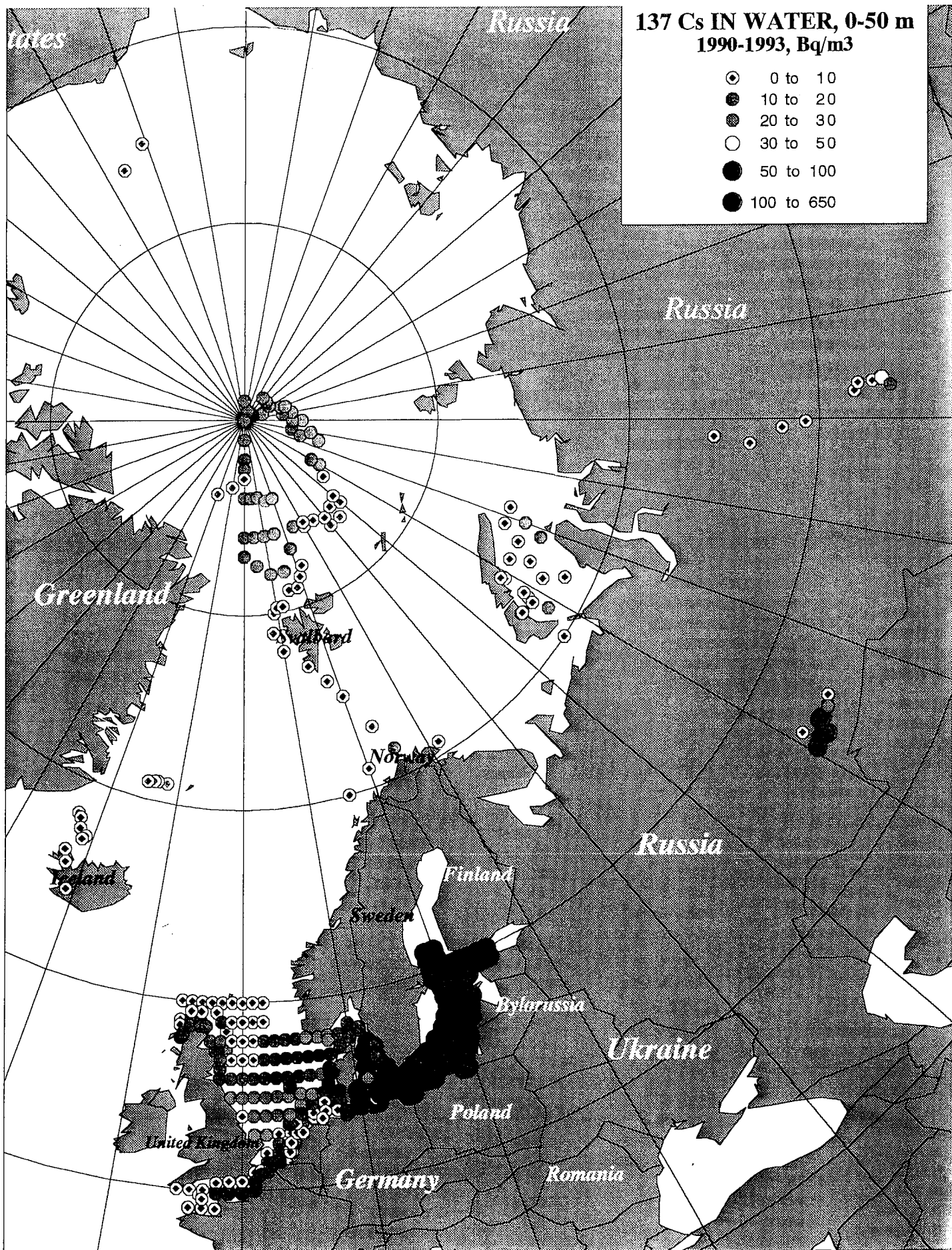


Figure 8

**90 Sr IN WATER 0-50 m
1990-1993 Bq/m³**

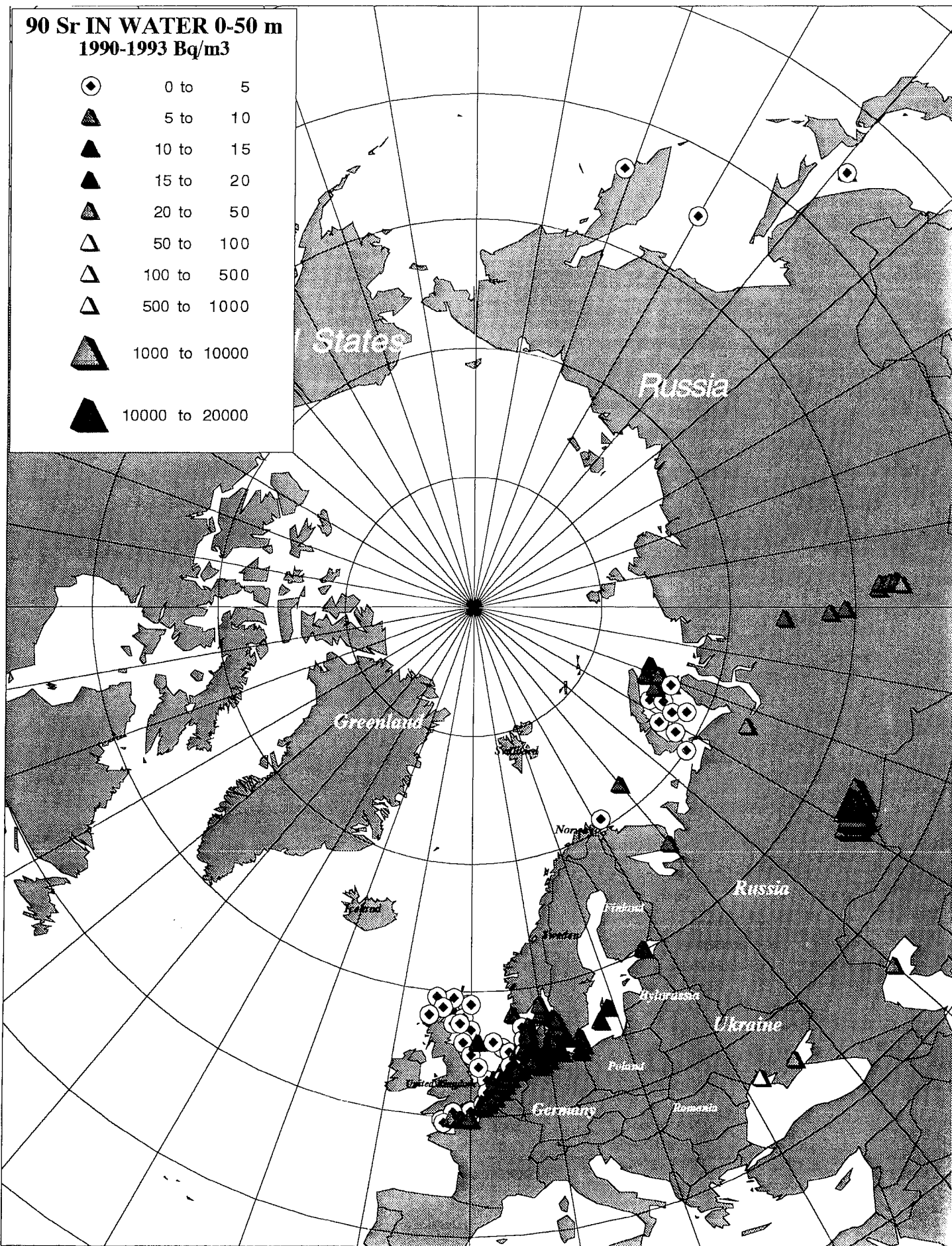
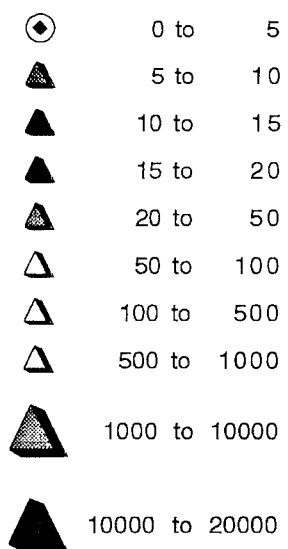


Figure 9

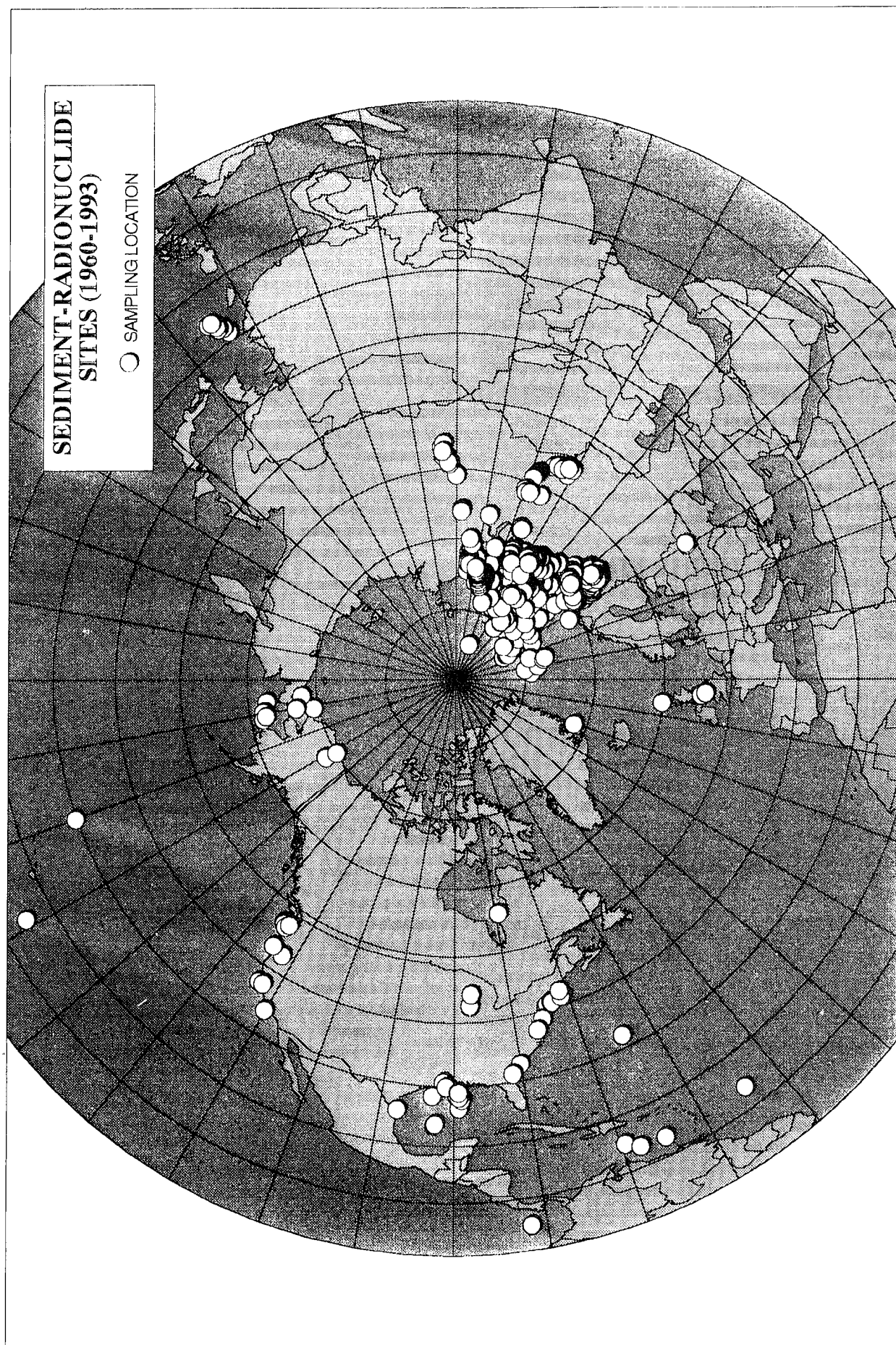


Figure 10

¹³⁷Cs IN SURFACE SEDIMENT **1990-1994 (Bq/Kg)dw**

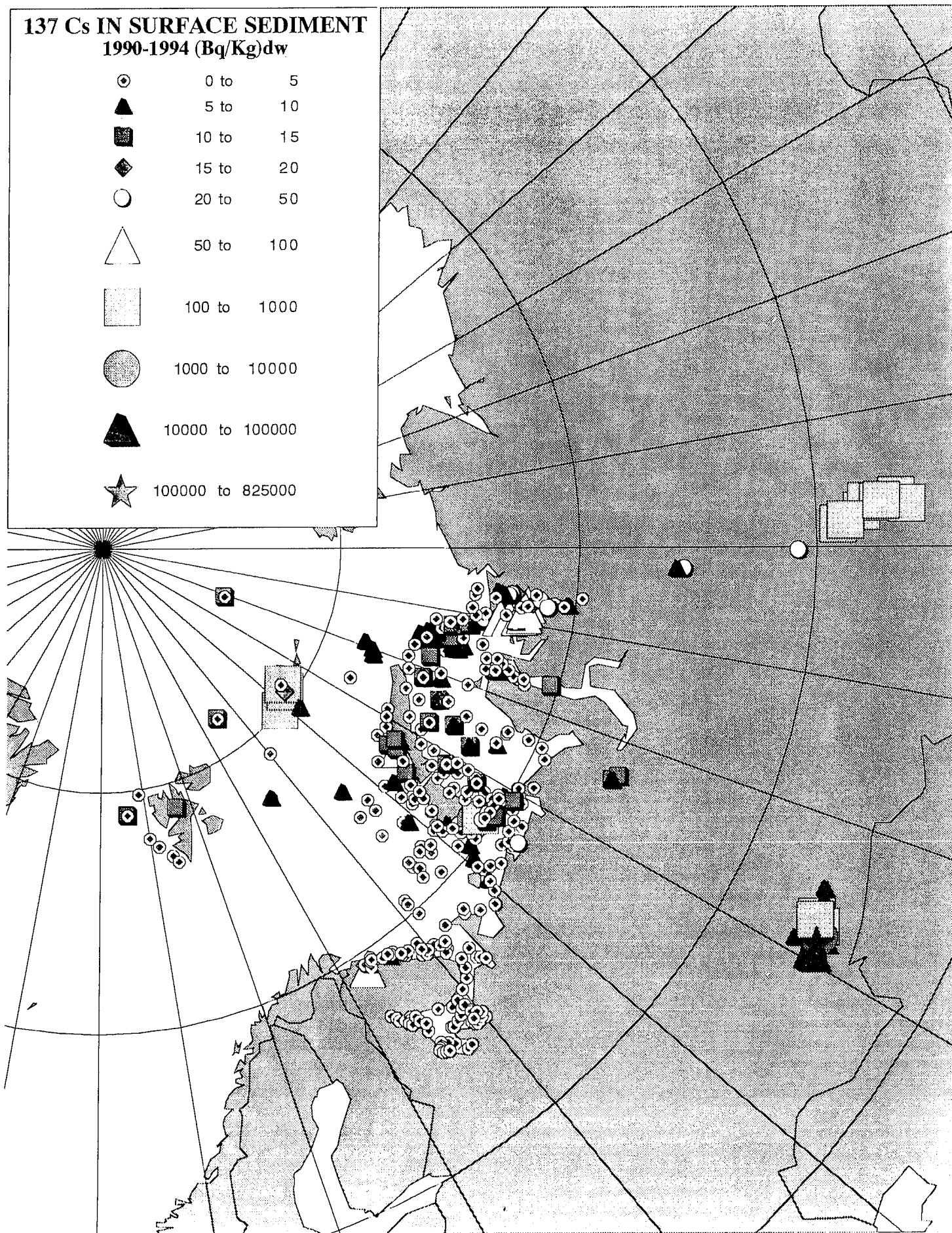
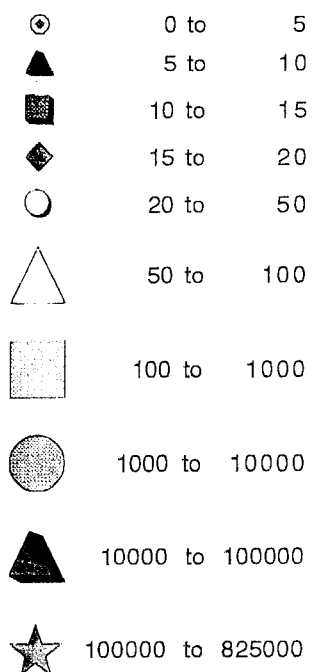


Figure 11

**239-240 Pu IN SURFACE SEDIMENT
1990-1994 (Bq/Kg) dw**

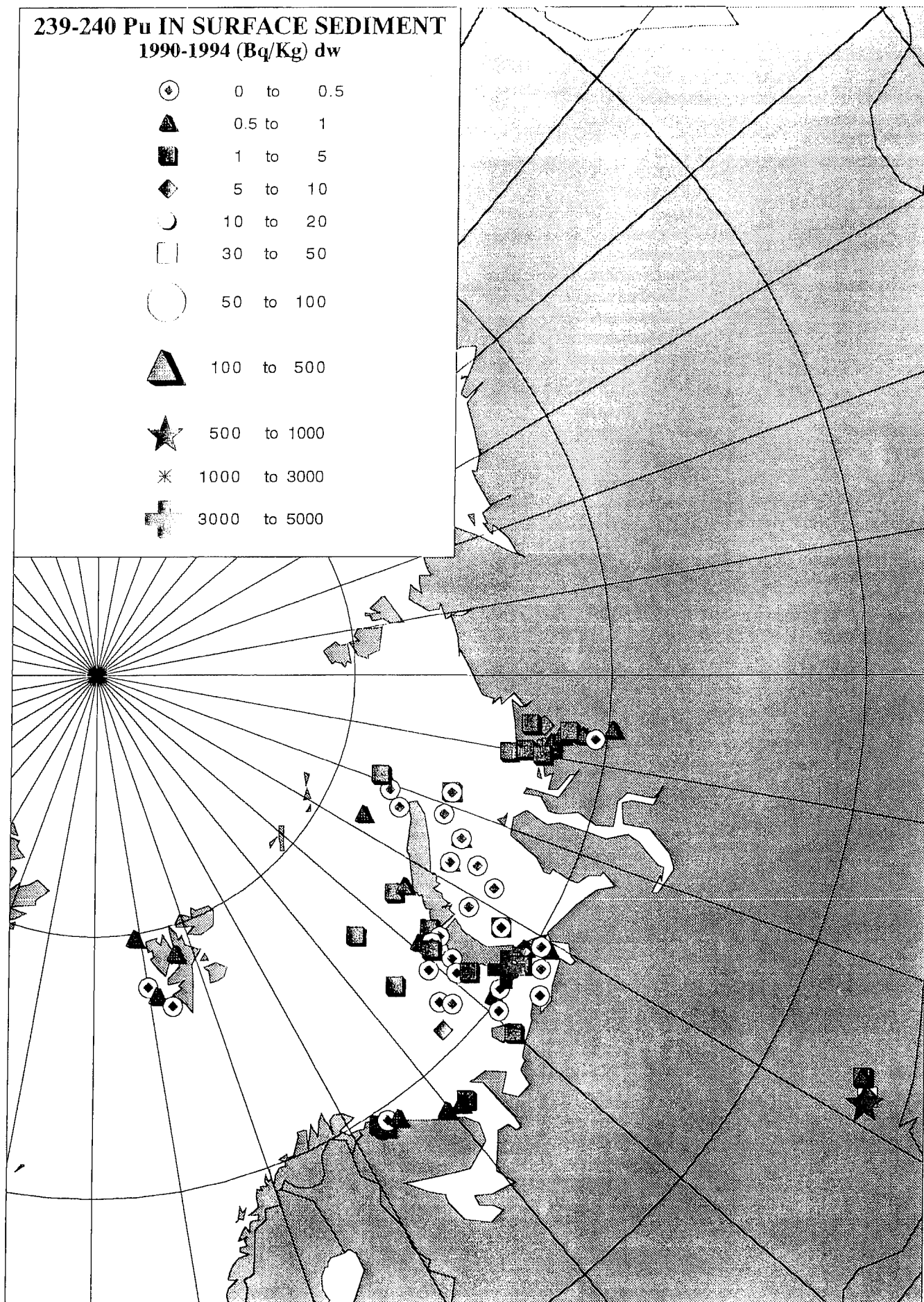
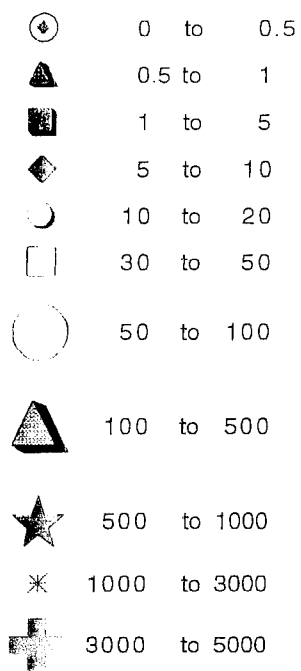


Figure 12

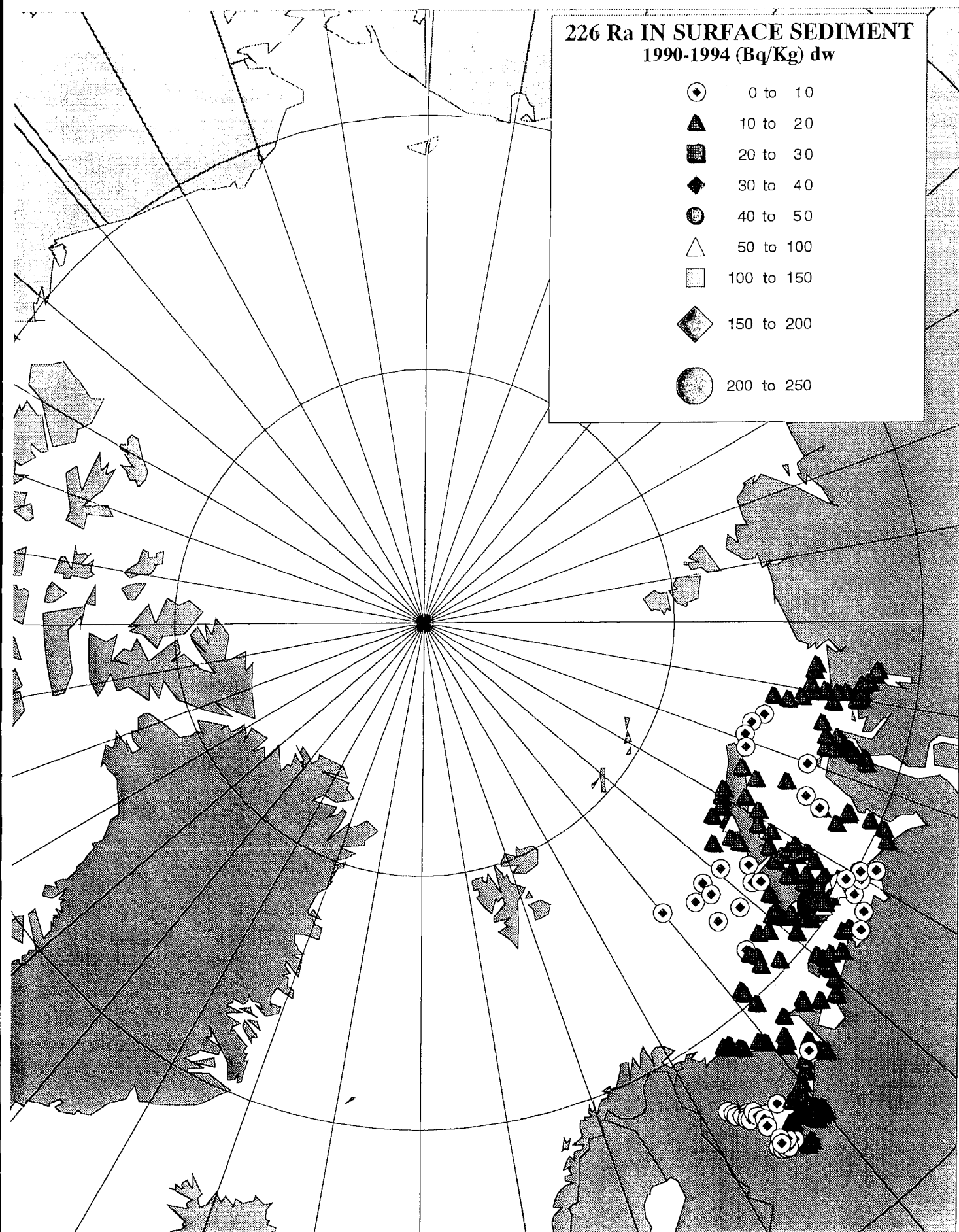


Figure 13

Overview of 1993 and 1994 Expeditions in the Kara Sea and Pechora Seas and Adjacent Rivers

James Brooks

Overview of 1993 and 1993 Expeditions in the Kara and Pechora Seas and Adjacent Rivers.

James M. Brooks, Michael A. Champ and M. Baskaran

Presented at Workshop on
"Modeling of Nuclear Contaminants in Arctic Seas"
18-19 October 1994
Monterey, California

Abstract

GERG conducted two extended sampling expeditions in 1993 and 1994 in the Russian Arctic. The first year expedition was conducted in August and September 1993 using the M/V OLFSON from the Hydrobase in Igarka on the Yenisey River. This cruise successfully sampled ~80 stations in the Ob and Yenisey Rivers and Kara Sea. Figure 1 shows the station locations sampled during the 1993 expedition.

The 1994 expedition was conducted using the M/V YAKOV SMIRNITSKIY out of Arkhangelsk, Russia on the White Sea. The vessel left Arkhangelsk on 10 July with a scientific party of 18 (10 Americans and 8 Russian participants). Five graduate students participated in the cruise collecting samples for M.S. and Ph.D. degrees. The Russian participants included groups from the Zoological Institute of St. Petersburg and the Arctic and Antarctic Research Institute. The M/V SMIRNITSKIY expedition successfully sampled stations in the Pechora and Kara Seas, and Ob, Yenisey and Pechora Rivers (Figures 2 and 3) during July and August 1994. A total of 88 stations were occupied during the 2-month expedition. Approximately 500 miles of geophysical data were collected using the Chirp subbottom profiler. Fifteen (15) cores were collected and logged with the multi-sensor core logger. Biological tissue samples were collected from 37 sites. Permits for these cruises were provided by Mr. Danilov-Danilian Minister of the Protection of the Environment and Natural Resources and closely coordinated with the Research Institute for Nature Conservation of the Arctic and North (RINCAN).

The M/V SMIRNITSKIY was equipped to provide full oceanographic sampling capabilities for:

- Chemical Contaminant Studies (full sampling capabilities for bottom and suspended sediment, biota and water);
- Physical Oceanographic Studies (hydrographic and CTD instrumentation);
- Biological Studies (trawls, box cores and traps); and
- Geological Studies (side scan sonar, subbottom profiler, piston cores and box cores).

Sampling efforts consisted of sampling water, surficial sediment and organisms for radionuclide analysis. All sediment and tissue samples were

placed in clean containers and returned to the US for analyses. Surficial sediments (upper 2-cms) were collected with a small box corer. Benthic sentinel-indicator organisms, including filter feeder bivalve molluscs were collected. Selected water samples were collected and processed through special extraction columns to remove Cs and Pu. Samples of particulates and colloidal material were collected for radionuclide analysis to determine transport phases and partitioning of isotopes. One of the major routes through which transportation of many of the reactor-derived radionuclides in the coastal waters take place are through the association with the colloidal material. Rates of deposition and transport will be determined. The samplings were closely coordinated with the sedimentological and geological component of this study that identified the depositional areas (i.e., troughs, fine grained sediment depositional areas, etc.) of the marginal seas.

GERG's 1993 expedition to the Ob and Yenisey Rivers and Kara Sea provided some of the first samples taken by USA scientists of the sediments, waters and biota from this Arctic region. One of the most interesting findings of the initial survey was the discovery of a depositional lobe of radionuclides in sediments in the Yenisey River below the salt wedge (Figure 4). Before our survey, the general expectation was that the Ob River would have higher levels of radionuclide contamination in its estuarine waters.

An initial evaluation of plutonium concentrations in samples from the 1993 expedition to quantitatively evaluate the contribution of Pu from the nuclear reactors dumped in the Kara Sea has been conducted and published in Applied Radiation and Isotopes. The distribution of Pu concentrations and inventories in surficial sediments (upper 3 cm) depends on many factors besides local inputs, including sedimentation rate, organic-matter content, variations in mineralogy, grain size parameters, and water content of the sediments. The $^{239,240}\text{Pu}$ concentration in the surficial sediments of the rivers and the Kara Sea varied between 9.4 and 627 mBq kg⁻¹, with a mean of 250 mBq kg⁻¹. In the five sediment cores collected from the Ob and Yenisey Rivers and Kara Sea, the maximum depths at which $^{239,240}\text{Pu}$ was detected varied between 6 and 12 cm. Assuming that the Pu was introduced to the sedimentary layer in the year 1952 (Koide et al., 1975), the penetration depths of $^{239,240}\text{Pu}$ can be utilized to obtain the average apparent sedimentation rates. These estimates of sedimentation rates vary between 1.5 and 3.0 mm yr⁻¹. The ^{238}Pu concentration varied between below detection limit and 26.5 mBq kg⁻¹, with a mean of 8.5±6.1 mBq kg⁻¹. The distribution of $^{239,240}\text{Pu}$ concentrations in the surficial sediments is shown in Figure 5. There is no systematic trend, either with distance from the coast line or with water depth, on the $^{239,240}\text{Pu}$ concentrations.

The Pu inventory obtained from the ocean water column as well as soil samples from the Arctic region are given in Table 1. Since a major portion of Pu in the world ocean still remains in the water column and the scavenging of particle-reactive radionuclides is poor in the open ocean Arctic waters where the particle concentrations are low, most of the Pu is

likely to remain in the water column. The Pu inventory for five sediment cores from the Ob and Yenisey Rivers and the Kara Sea varied between $2.69 \pm 0.45 \text{ Bq m}^{-2}$ and $24.42 \pm 2.21 \text{ Bq m}^{-2}$, with a mean of 8.86 Bq m^{-2} . In the three sediment cores from Kara Sea, the Pu inventories varied between 2.61 ± 0.63 and $10.9 \pm 1.3 \text{ Bq m}^{-2}$. Among the two sediment cores collected at adjacent sites in Kara Sea (water depth = 39 m) within a distance of less than 1 km, Pu inventories varied by a factor of 4.2 (2.61 and 10.9 Bq kg^{-1}). These values are comparable to the soil inventory values of $^{239,240}\text{Pu}$, 14.8 Bq m^{-2} , measured at Barrow (71.6° N), Alaska (Hardy et al., 1973). Also, these values are considerably lower than the water column inventory of $^{239,240}\text{Pu}$, 24.2 and 35 Bq m^{-2} , near the North Pole (89° N) reported by Livingston et al. (1984). If all the Pu from the dumped naval reactors (i.e., $2\text{-}5 \times 10^{13} \text{ Bq}$) would be released to the sediments uniformly over the entire Kara Sea, then that could result in an additional Pu inventory of $19.6\text{-}48.3 \text{ Bq m}^{-2}$. From the average value of the measured inventory of Pu ($8.5 \pm 6.1 \text{ Bq m}^{-2}$) in the five sediment core samples collected from the Ob and Yenisey Rivers and Kara Sea, and taking the area of Kara Sea to be $9.95 \times 10^5 \text{ km}^2$, the total inventory of Pu in the Kara Sea is estimated to be $(8.5 \pm 6.1) \times 10^{12} \text{ Bq}$.

The different sources of radionuclides; such as global fallout due to nuclear weapons testing, nuclear reprocessing plant effluents such as from Sellafield, leachates from dumped nuclear reactors in the seabed, etc.; have distinct $^{238}\text{Pu}/^{239,240}\text{Pu}$ activity ratios. The published data on the $^{238}\text{Pu}/^{239,240}\text{Pu}$ activity ratio, decay-corrected for the year 1993, for the Arctic region is given in Table 2. The $^{238}\text{Pu}/^{239,240}\text{Pu}$ activity ratio in the surficial sediments varied between 0.009 and 0.065 with a mean value of 0.034. If most of this Pu is derived from the global fallout of nuclear tests, then during the past 30 years, the ^{238}Pu has undergone radioactive decay, by about 27%. Thus, variations in the sedimentation rate could affect the activity ratio in the surficial sediments. The best-fit-line between ^{238}Pu and $^{239,240}\text{Pu}$ concentration in these samples yields an activity ratio of 0.034 ± 0.003 . Comparing this value with the published values on the European nuclear effluents discharged into the coastal waters, fallout values of the nuclear weapons tests, and the estimated Pu inventories in the dumped reactors in Kara Sea, we conclude that there is virtually no detectable input from either the European nuclear effluents or the dumped nuclear reactors in the Kara Sea.

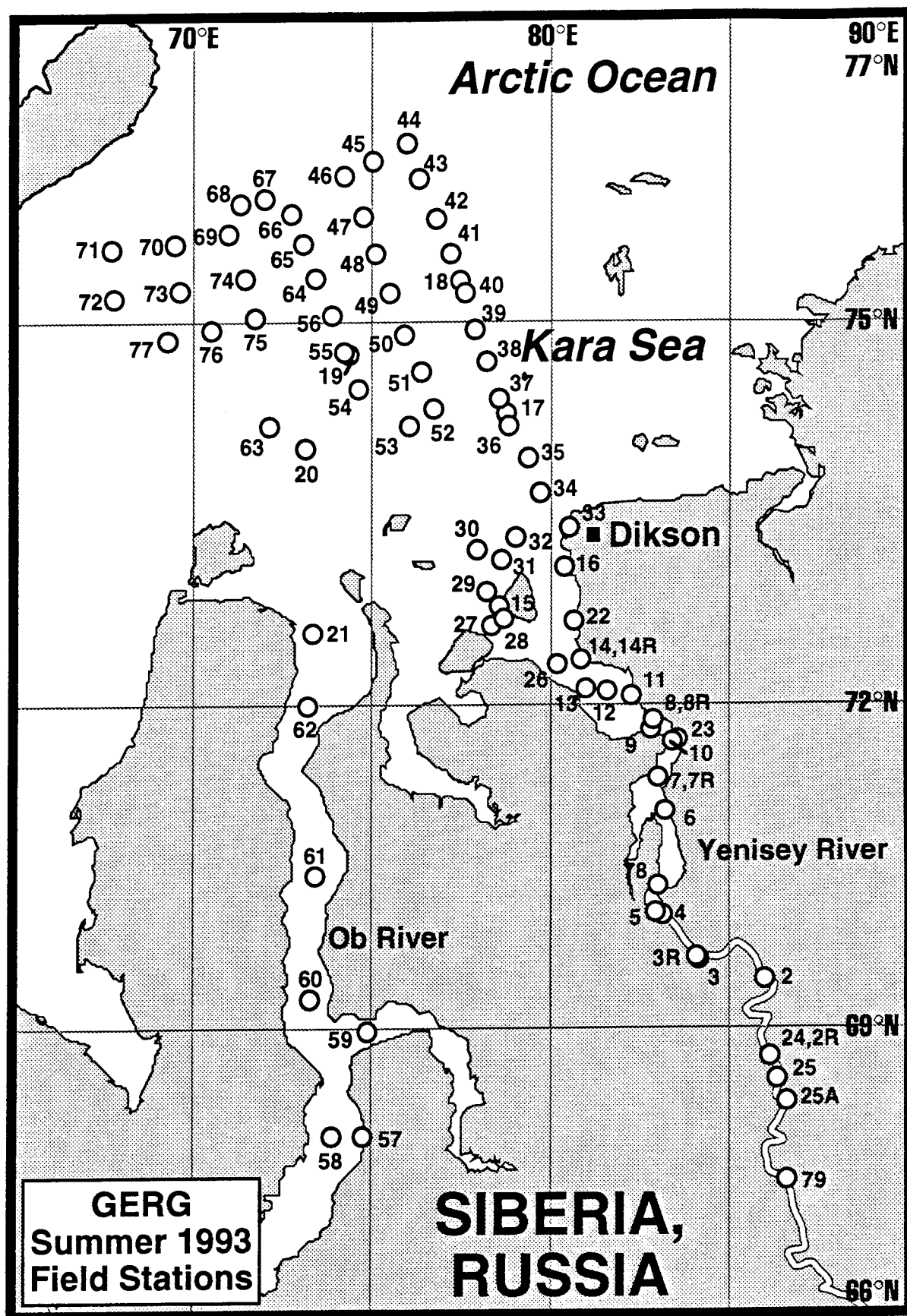


Figure 1. 1993 Kara Sea sampling stations.

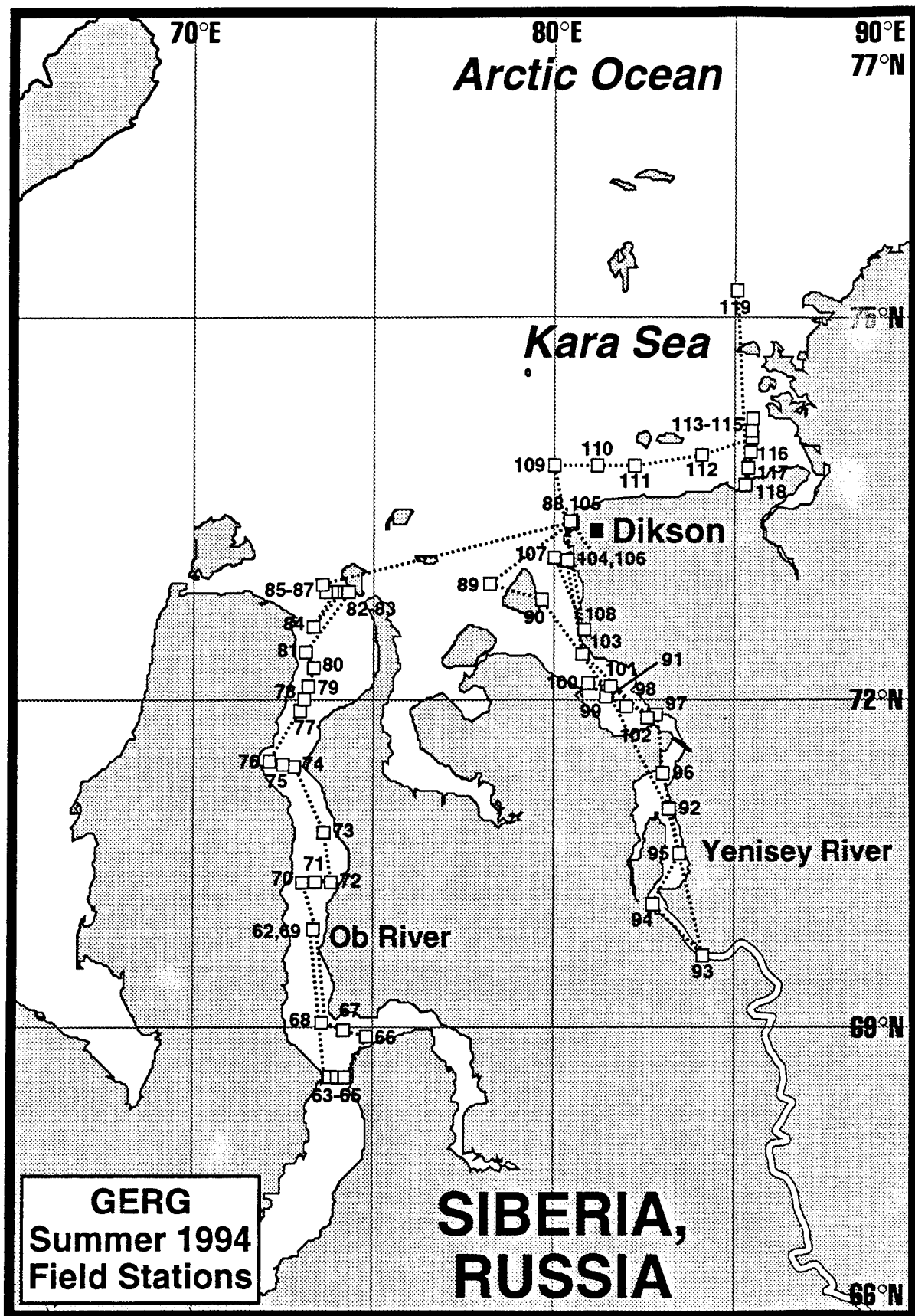


Figure 2. 1994 Kara Sea sampling stations.

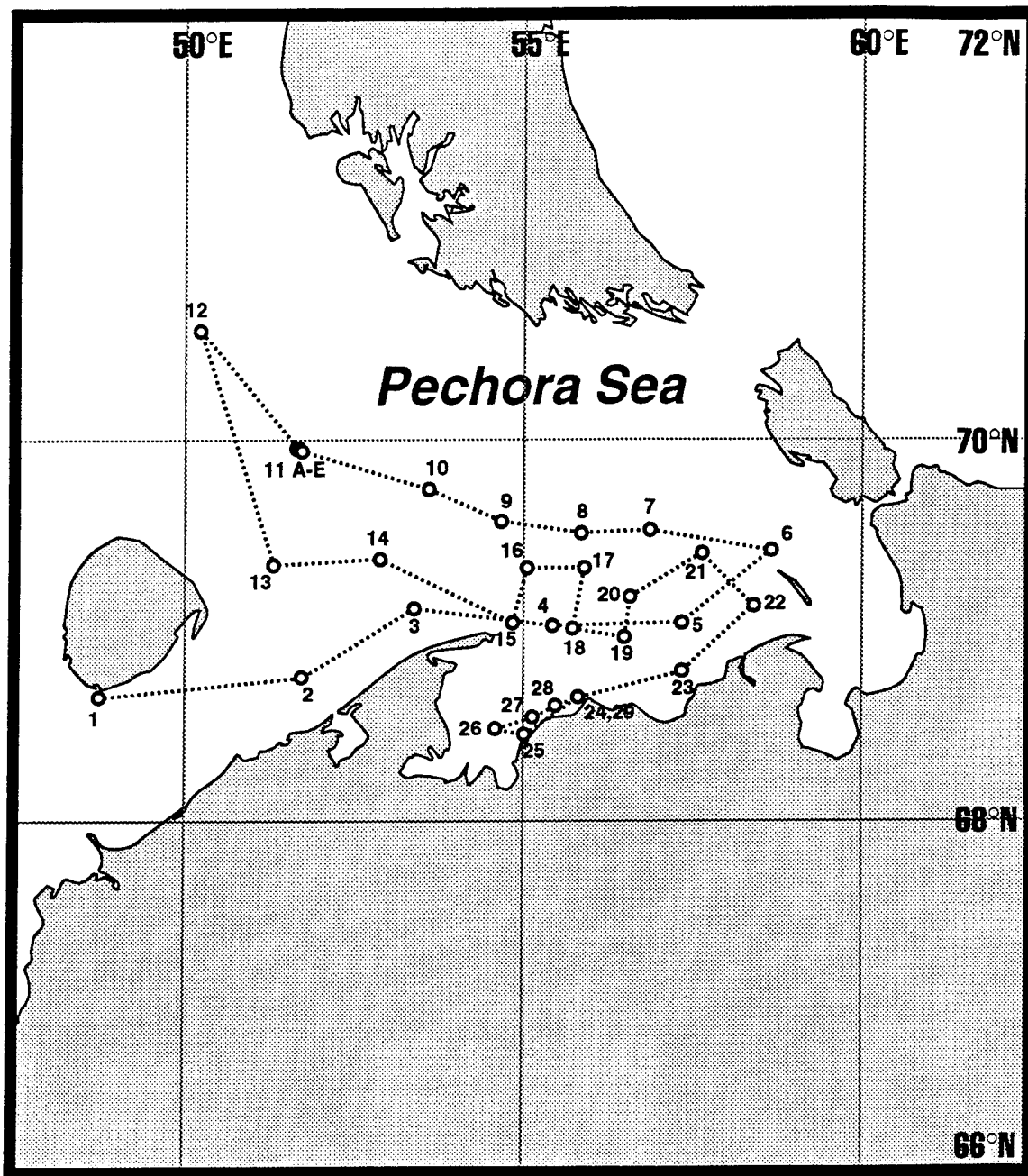


Figure 3. 1994 Pechora Sea sampling stations.

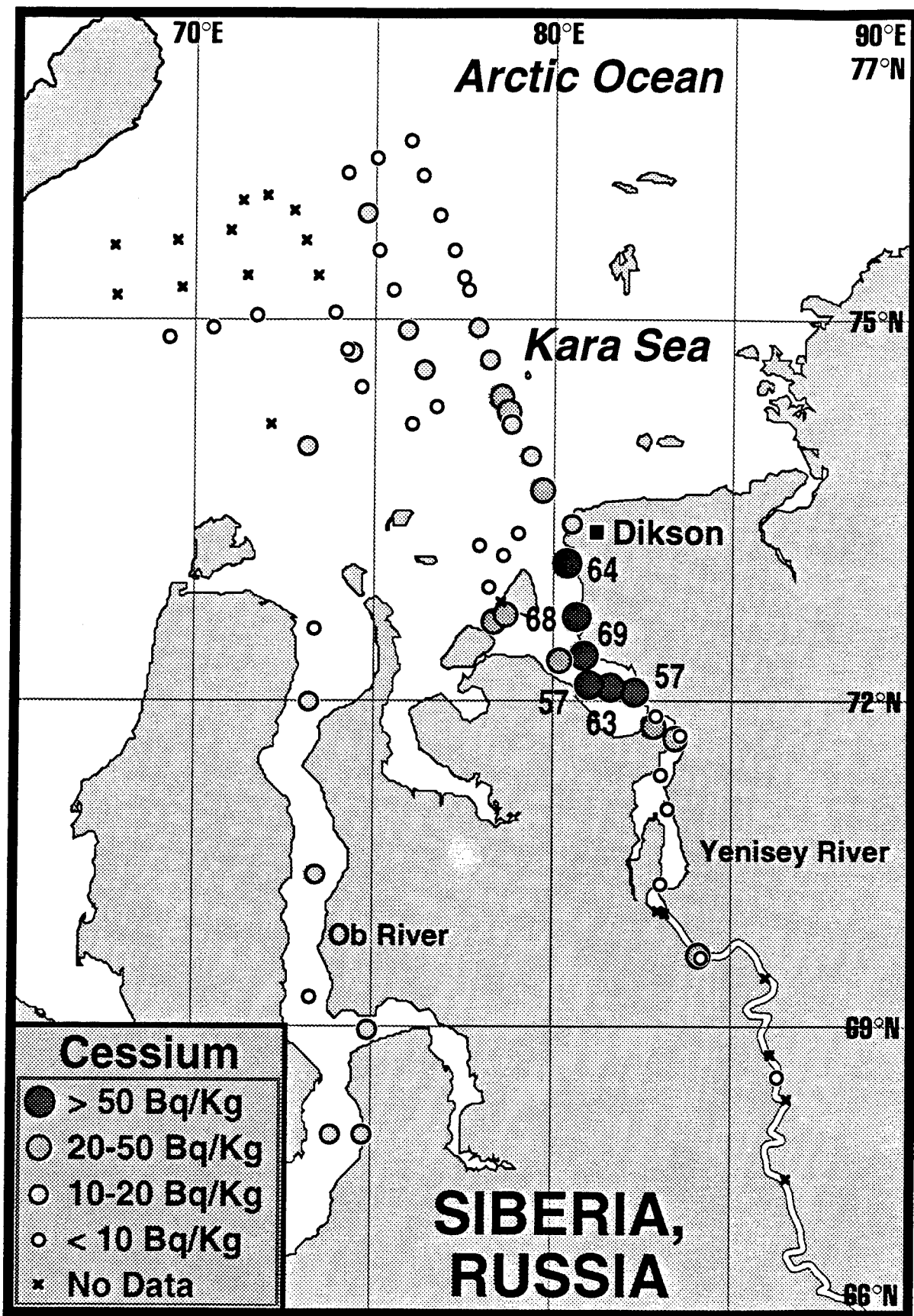


Figure 4. Cs^{137} distributions from 1993 Kara Sea sampling stations.

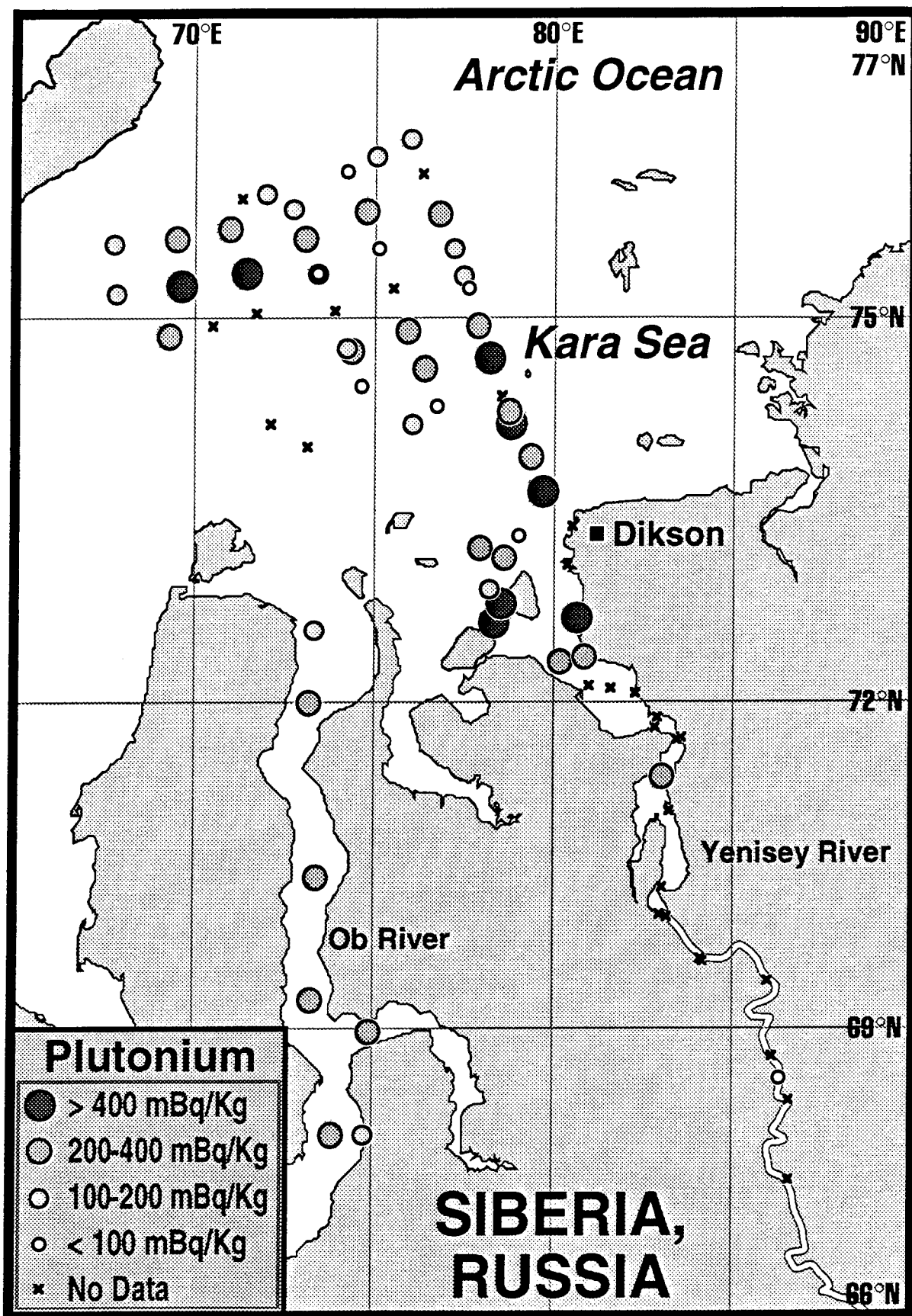


Figure 5. $^{239,240}\text{Pu}$ concentrations in surficial sediments at 1993 sampling stations.

Table 1. $^{239,240}\text{Pu}$ Inventories in the Water Samples and Sediments from the Arctic Regions.

Location and Nature of Sample	Water Depth (m)	Year of Collection	$^{239,240}\text{Pu}$ (Bq m^{-2})*	Source
76.6° N; Thule, Greenland Soil Sample	-	1971	12.2	<i>Hardy, 1973</i>
71.3° N; Barrow, Alaska Soil Sample	-	1971	14.8	<i>Hardy, 1973</i>
64.8° N, Fairbanks, Alaska Soil Sample	-	1971	31.5	<i>Hardy, 1973</i>
65°55.7 N; 27°27.0 W Water Samples	646	1972	20	<i>Livingston, 1985 Data reported in Aarkrog, 1989</i>
74°56.2 N; 1°7.2 W Water Samples	3740	1972	54	<i>Livingston, 1985 Data reported in Aarkrog, 1989</i>
89° N; 89° W Water Samples	2497	1979	35.0	<i>Livingston et al., 1984</i>
89° N; 111° W Water Samples	3000	1979	24.2	<i>Livingston et al., 1984</i>
89° N (Expected from Fallout)	-	-	5.13	<i>Livingston et al., 1984</i>
68° - 76° N; 67° - 84° E Sediment Cores from Ob and Yenisey Rivers and Kara Sea	7-290	1993	8.85 (2.61 - 24.4)	<i>this study</i>

* Numbers in parenthesis denote the range of values reported.

Table 2. $^{238}\text{Pu}/^{239,240}\text{Pu}$ Activity Ratios in Nuclear Effluents from Sellafield and Cap de la Hague, Dissolved, Particulate Phases, Surficial Sediments and Terrestrial Samples in the Arctic Region.

Nature of Sample	Location	Number of Samples	Year of Collection	$^{238}\text{Pu} / ^{239,240}\text{Pu}$ * Activity Ratios in 1993	Source
Effluents from Sellafield	Irish Sea	7	1978-1984	0.29±0.02	<i>British Nuclear Fuels 1985</i>
Effluents from Cap de la Hague	English Channel	7	1962-1982	0.46	<i>Calmet and Guegueniat, 1985</i>
Dumped Reactors in Kara Sea	Kara Sea	Estimate	-	0.26-0.49	<i>Mount et al. 1993</i>
Global Fallout (+SNAP)	Northern Hemisphere		1982	0.021 (0.030)	<i>Aarkrog, 1989</i>
Water samples- Dissolved phase	Barents, Greenland, Norwegian and North Seas	41	1980	0.060±0.010 (0.037±0.016 - 0.078±0.012)	<i>Holm et al. (1986)</i>
Water samples- Particulate phase	Barents, Greenland, Norwegian and North Seas	41	1980	0.052±0.018 (0.019±0.025 - 0.084±0.066)	<i>Holm et al. (1986)</i>
Terrestrial samples (Lichen, Moss, Soil)	Svalbard Isfjord, NE Greenland	12	1980	0.042±0.007 (0.036±0.005 - 0.055±0.005)	<i>Holm et al. (1986)</i>
Surficial sediments	79.2-82.3°N; 25.3-33.7°E	10	1980	0.062±0.006	<i>Holm et al. (1986)</i>
Surficial Sediments	Ob, Yenisey Rivers and Kara Sea	55	1993	0.036±0.003 (0.009-0.065)	this study

* Numbers in parenthesis denote the range of values reported.

Radionuclide Contaminants in Central Arctic Sea Ice

Terry Tucker

Radionuclide Contaminants in Central Arctic Sea Ice

Debra A. Meese and Walter B. Tucker III

U.S. Army Cold Regions Research and Engineering Laboratory
Hanover, NH

The U.S./Canada Arctic Ocean Section (AOS-94), which took place during July and August, 1994, was the first science expedition in 100 years to make a complete transect of the Arctic Ocean. Investigations of oceanography, biology, geology and geophysics, ice physics, meteorology and contaminants were conducted by researchers on board the USCGC Polar Sea and the CCGS Louis S. St. Laurent. The overall goals of the expedition were to establish a baseline data set of ocean structure and ice properties relating to global climate change research in a very sparsely sampled part of the Arctic, to investigate paleoclimate and plate tectonics in the central Arctic, and to determine the pervasiveness of radionuclide and persistent organic contaminants.

Our objective was to determine whether radionuclide contaminants are currently present in central Arctic sea ice. Should contaminants be observed, it would indicate that ice is an effective mechanism for transporting and releasing radionuclides far from source areas. A total of 5 ice samples and 12 sediment samples were collected, essentially from the ice edge in the Chukchi Sea to the North Pole, as shown in Figure 1. Radionuclide analysis of ice requires a minimum of 200 l of meltwater, which translates to about 25 m of ice core. The cores for a single site filled 4 large sample containers (plastic garbage pails) which were melted for further processing. Subsequent processing required treating the meltwater with various tracers and co-precipitating agents, and decanting the precipitates. The entire procedure required 5 - 7 days. Sediment samples were simply scraped from the ice surface, collected from cryoconite holes, and from the bottom of melt ponds.

Somewhat surprising was the fact that sediment was observed on the ice from the ice edge to the Pole. In some areas, sediment covered an estimated 10% of the ice surface. The amounts of sediment observed varied, yet on this part of the transect, there was nearly always some in evidence. The photographs in Figure 2 show examples of the sediment observed on the expedition. In stark contrast, virtually no sediment was observed from the Pole through the entire eastern Arctic. This was unusual because it has frequently

been observed in the eastern Arctic on previous expeditions. It indicates that sediment incorporation is episodic, likely occurring on the shallow circum-Arctic shelves during storms in the freezing season. The mechanisms of sediment incorporation in ice are not well understood. It is thought that the sediment suspended in the water column is entrained into frazil by various mechanisms. The frazil later consolidates into a solid ice cover with its sediment load. Anchor ice formation on the shallow seafloor, may also incorporate sediment into the consolidating ice cover when it rises from the bottom. It is clear from our observations that incorporated sediment is capable of being moved large distances from the areas of initial entrainment by the ice. This implies that contaminants may be transported and released throughout the Arctic if they are preferentially sorbed by the sediment, or incorporated directly into the ice.

The collected samples are now being analyzed for radionuclides by Dr. Lee Cooper and Dr. Jacqueline Grebmeier at Oak Ridge National Laboratory. We are collaborating with Roger Colony, University of Washington and Dr. Stephanie Pfirman, Barnard College to determine probable trajectories of the ice and ice-borne sediment samples. The sedimentological analysis is being conducted out by Dr. Erk Reimnitz, an expert in ice-borne sediment from the USGS, who was also a member of the AOS-94 expedition. In conjunction with the ice physical properties measurements, we should be able to delineate likely source regions.

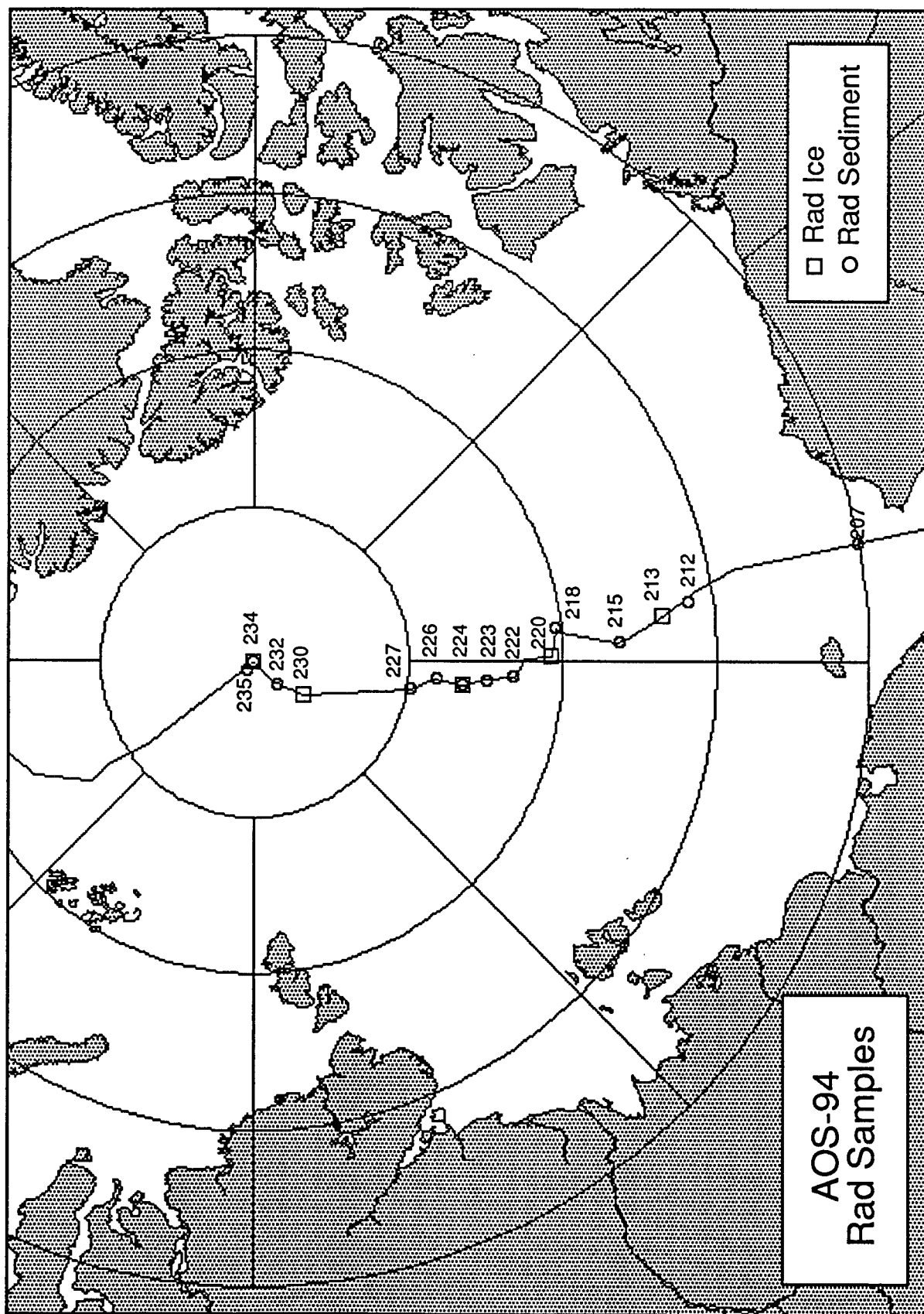


Figure 1. Locations of the ice and sediment samples collected for radionuclide testing on the 1994 U.S./Canada Arctic Ocean Section.



Figure 2. Surface sediment on sea ice observed during AOS-94.

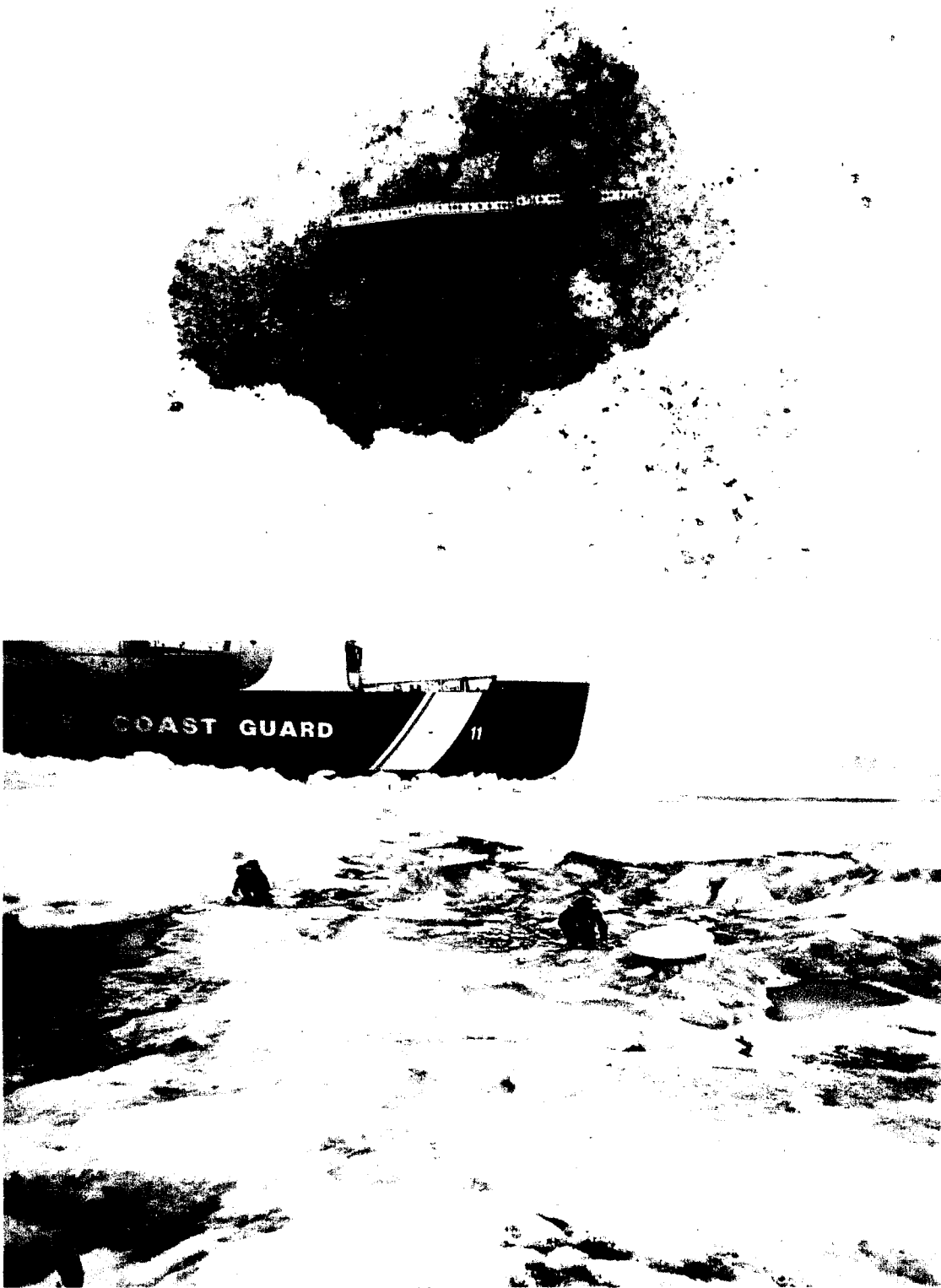


Figure 2. Continued - Surface sediment on sea ice during AOS-94.

Patterns of Monthly Wind and Ice Motion in the Arctic Basin

Roger Colony

Patterns of Monthly Wind and Ice Motion in the Arctic Basin

Roger Colony, Polar Science Center, University of Washington

Monthly fields of surface atmospheric pressure, geostrophic wind, and ice motion have been analyzed for the years 1979 through 1993. We apply a principle component analysis (PCA)(also known as empirical orthogonal function analysis) to the aggregate of the 180 monthly fields of ice motion. This type of analysis extracts the spatial pattern most resembling the aggregate of monthly fields. By continuing the analysis, a sequence of patterns, $P_i(x)$, may be determined such that each monthly field can be constructed as

$$U(x, t) = \sum_i \alpha_i P_i(x) f_i(t).$$

Our analysis shows that only three spatial patterns are required to capture 96% of the variance of monthly fields of ice motion in the central Arctic Basin. Applying the same analysis to the monthly fields of geostrophic wind, we find that another three patterns capture 97% of the variance of the monthly fields. Furthermore, the patterns of ice motion and wind bear a remarkable resemblance and are temporally correlated.

Borrowing from recent research in the atmospheric sciences, we apply the single valued decomposition (SVD) method to the pairs of monthly wind- and ice-motion patterns. The SVD analysis identifies pairs of patterns which explain the covariance between spatial patterns of wind and spatial patterns of ice motion. This analysis verifies that monthly wind anomaly patterns are primarily responsible for the monthly anomalies in large-scale ice motion. Initially used in forecasting and predictability studies, the PCA and SVD analyses are powerful tools in identifying the large-scale spatial patterns of several variables and in synthesizing particular realizations.

The findings are relevant to the design of a buoy array to monitor monthly wind and ice motion. We conclude that relatively few buoys are required to characterize the monthly patterns in the central Arctic Basin.

DATA SET, MEANS, AND VARIANCES

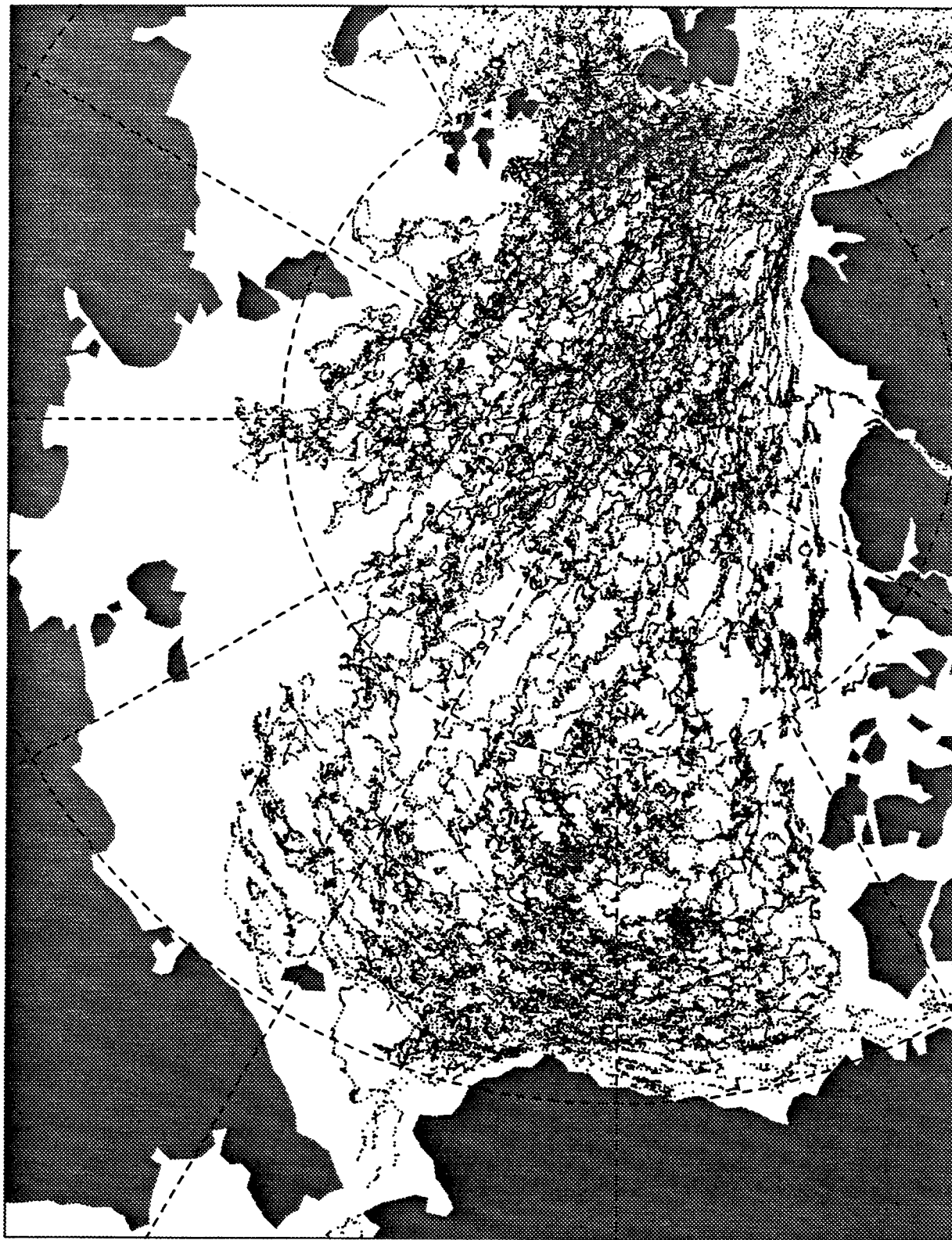


Figure 1. Illustration of buoy trajectories, 1979-1993 (the analysis will include manned station data for this period) (data set is collection of monthly wind and ice motion fields)

Optimal Monthly Ice Velocity - May 1980

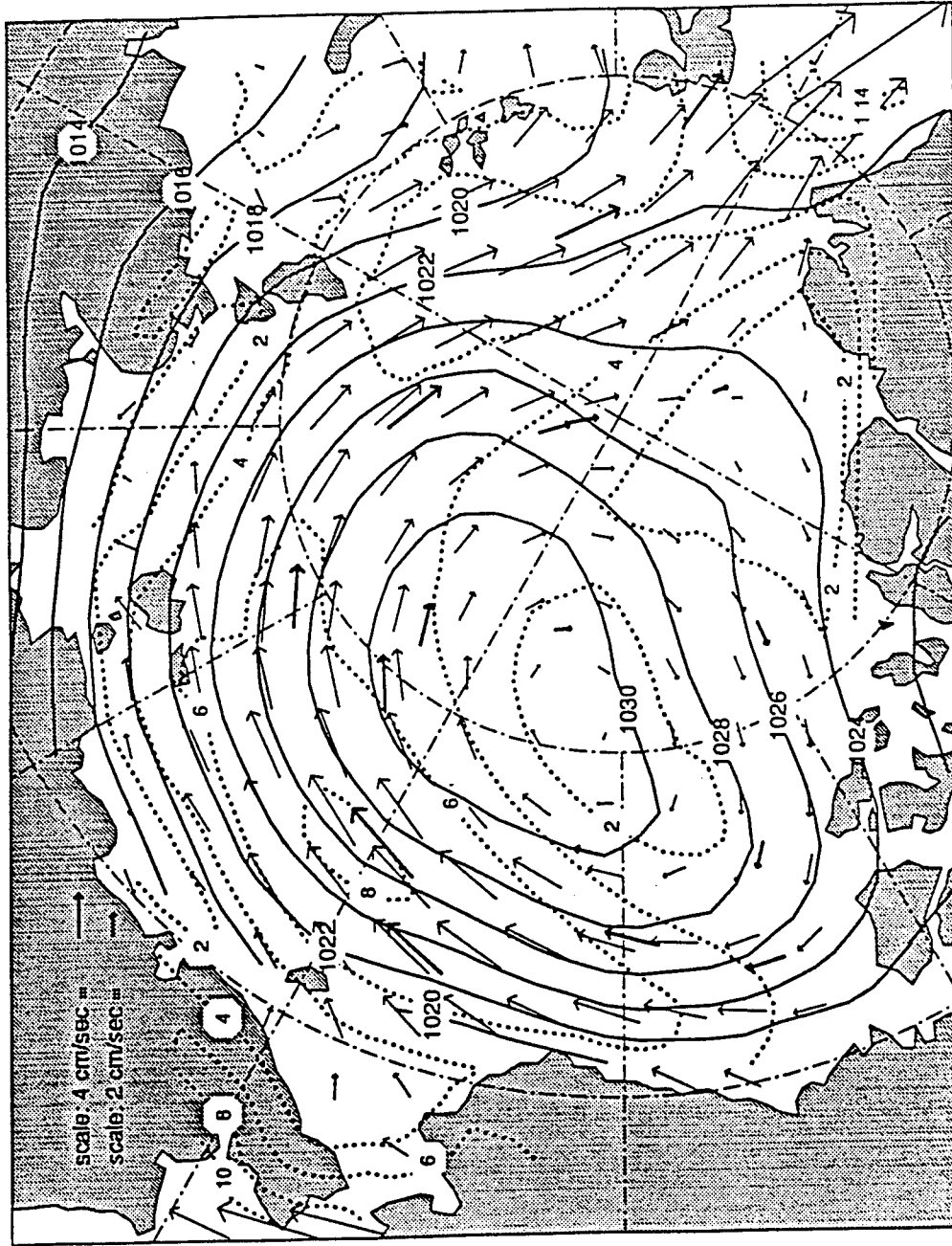


Figure 2. Example of analysis for May 1980
 (one analysis uses only ice motion data, alternative uses wind)
 (highlight buoy motions, analysis on 110 km grid)

Optimal Monthly Ice Velocity - May 1990

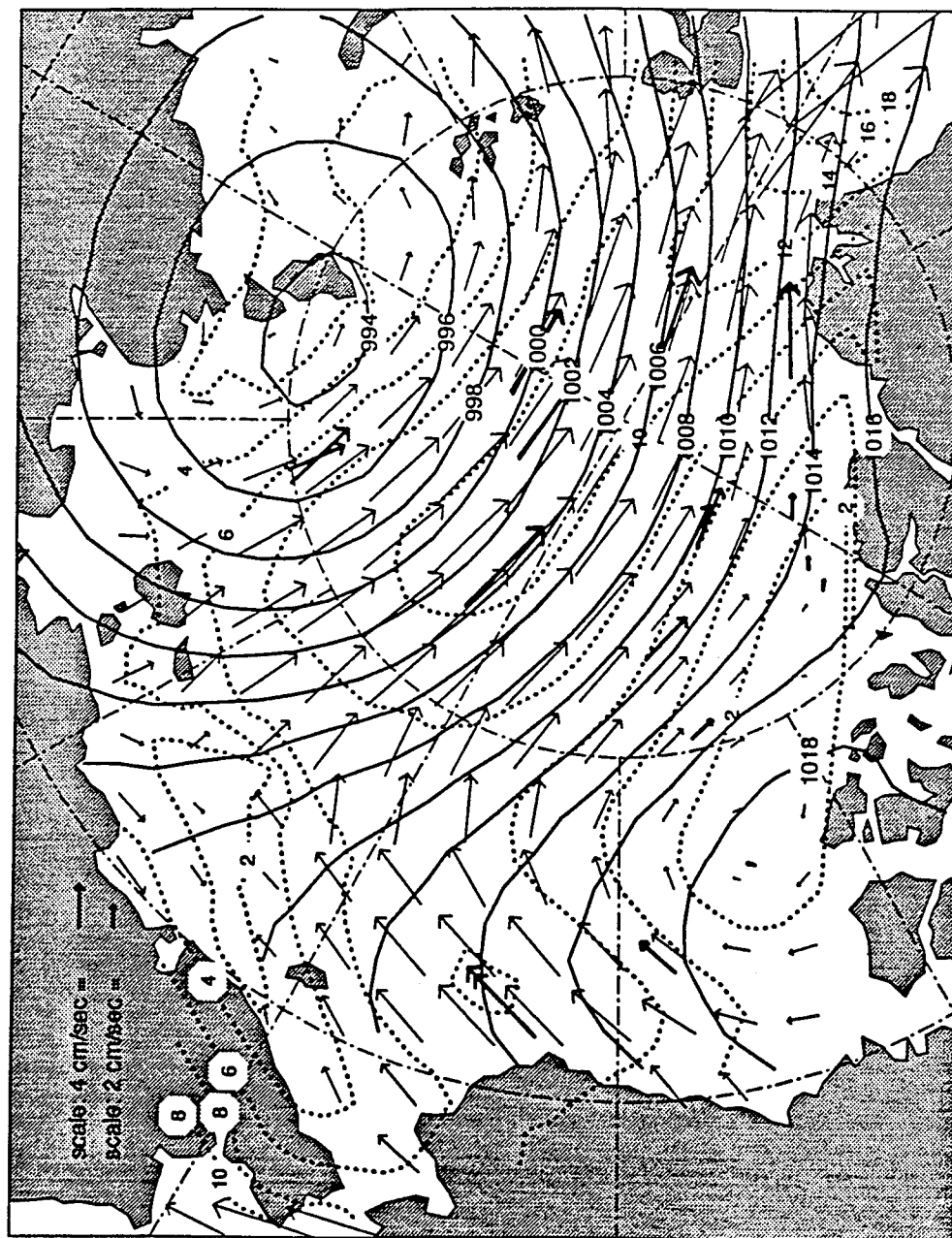


Figure 3. Example of analysis for May 1990
(note interannual variability)

Statistics of Monthly Wind and Ice Motion

denote $u(x, t)$ as monthly ice motion for each month.

$t=1,2,3,4,...,180$ (Jan. 79 - Dec. 93)

- Annual Mean

$$\bar{u}(x) = \sum_{t=1}^{180} u(x, t)$$

- Monthly Mean

$$\bar{u}(x, \tau) = \sum_{y=1}^{15} u(x, \tau, y)$$

- Variance (several)

$$\text{var} \{u(x)\}_a = \sum_{t=1}^{180} [u(x, t) - \bar{u}(x)]^2$$

$$\text{var} \{u(x, \tau)\}_m = \sum_{y=1}^{15} [u(x, \tau, y) - \bar{u}(x, \tau)]^2$$

$$\text{var} \{u(x)\}_s = \sum_{t=1}^{180} [u(x, t) - \bar{u}(x, \tau)]^2$$

$$\text{var} \{\bar{u}_s(x)\}_a = \sum_{i=1}^{12} [\bar{u}(x, \tau) - \bar{u}(x)]^2$$

Figure 4. Equations for means and variances, annual and seasonal cycle.

Annual Mean Pressure 1979-1993

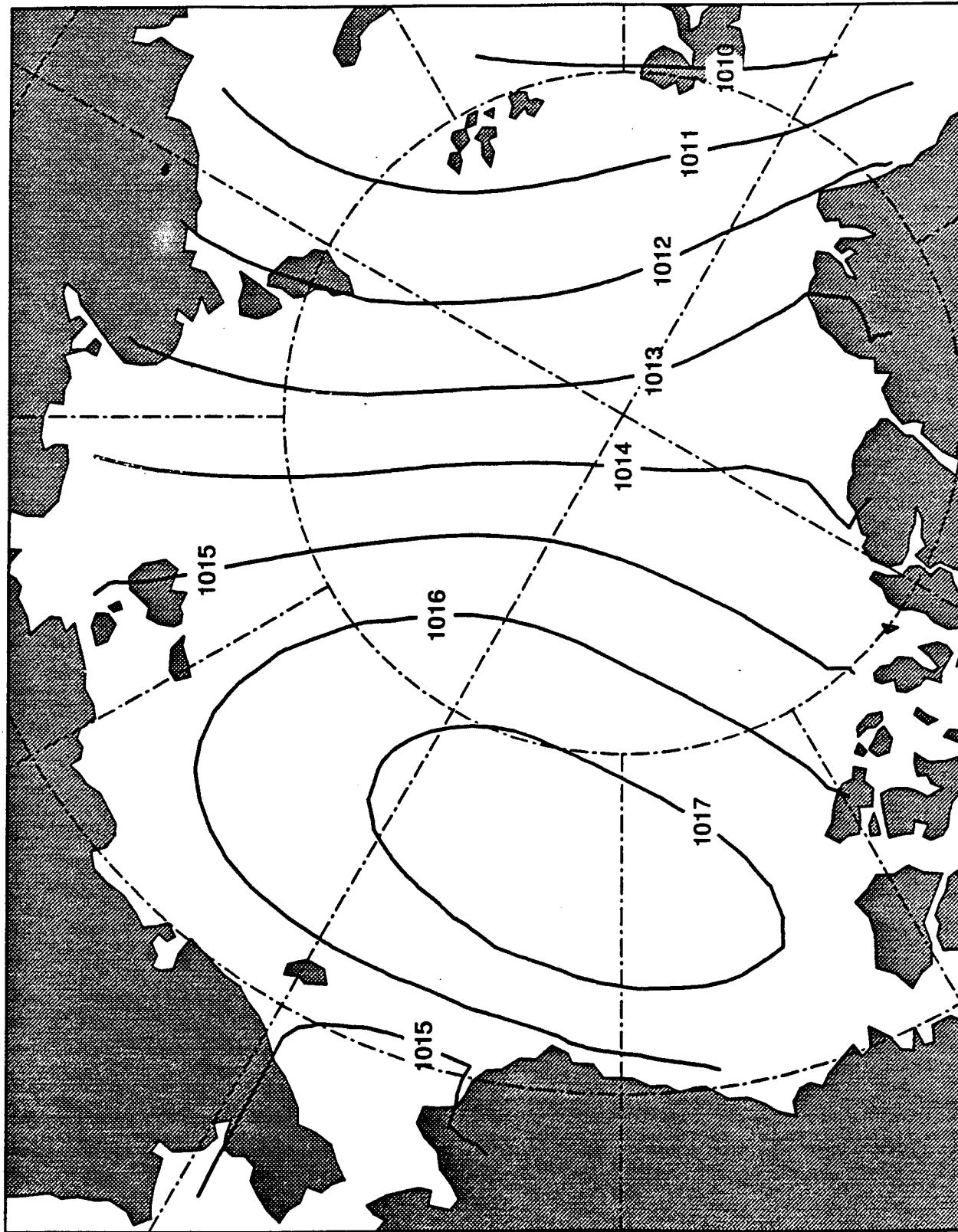


Figure 5a

Annual Mean Geostrophic Wind 1979-1993

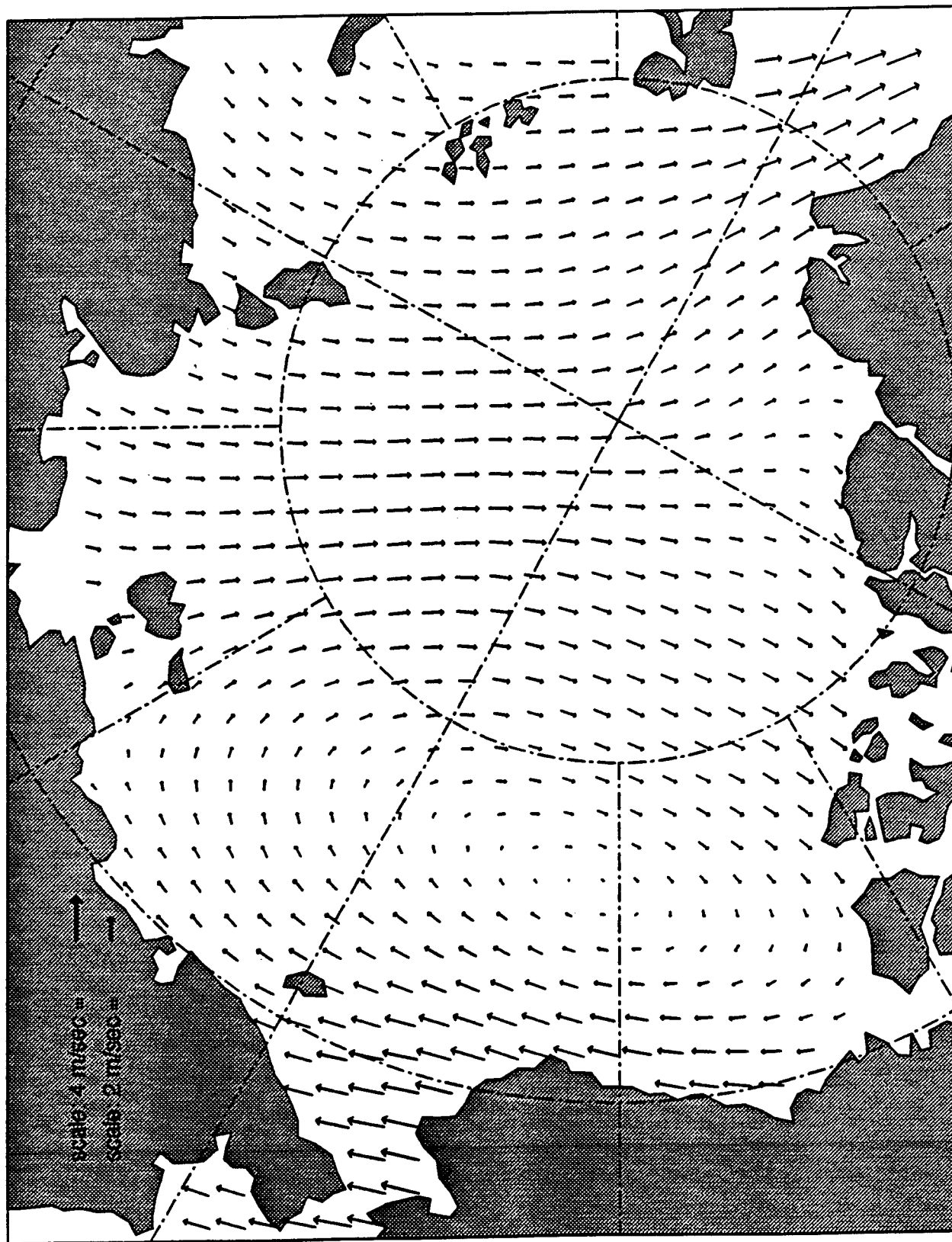


Figure 5b

Optimally Interpolated Current

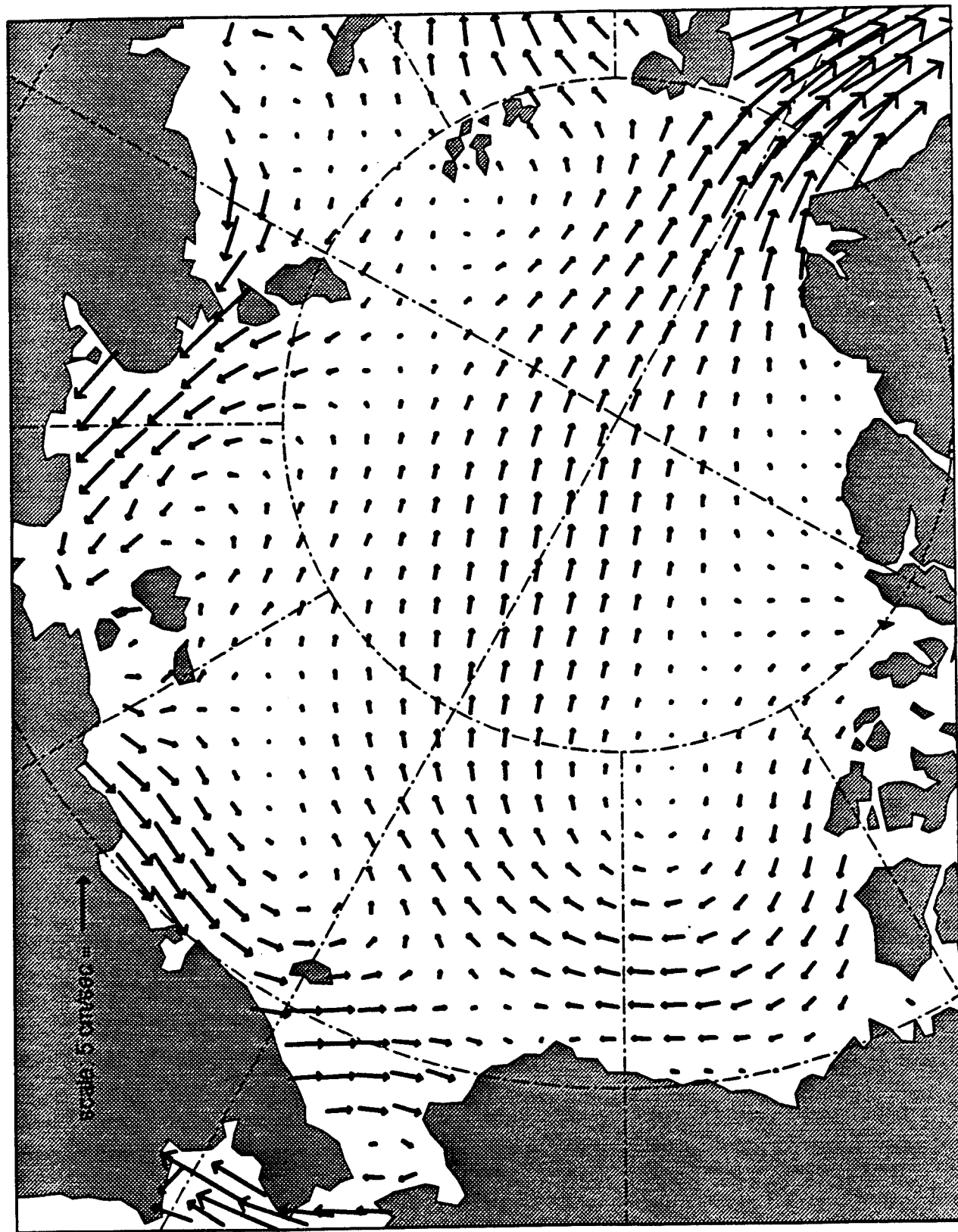


Figure 5c

Mean Sea Ice 1979-1993

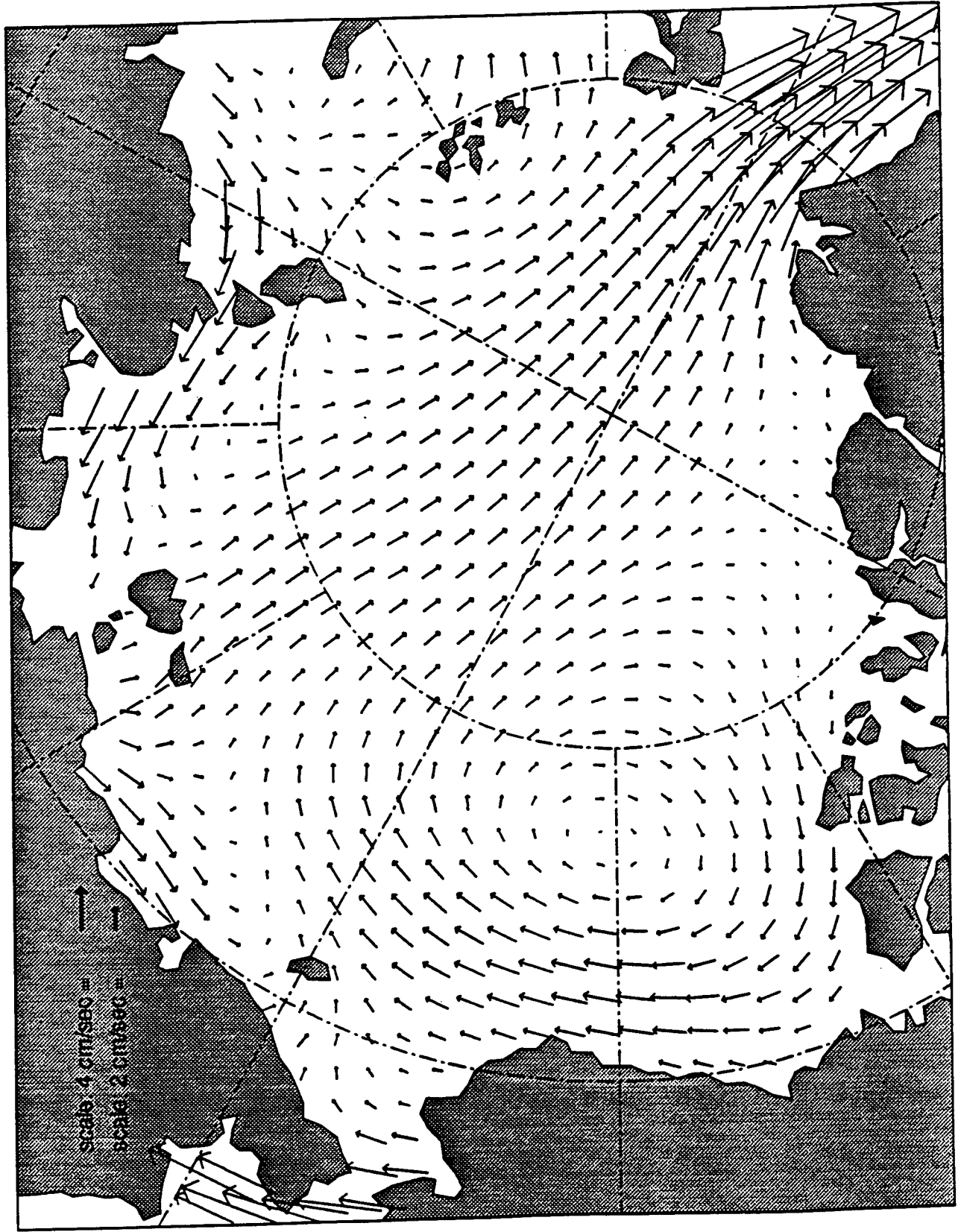


Figure 5d

Pressure Total Variance about Annual Mean in mb^2

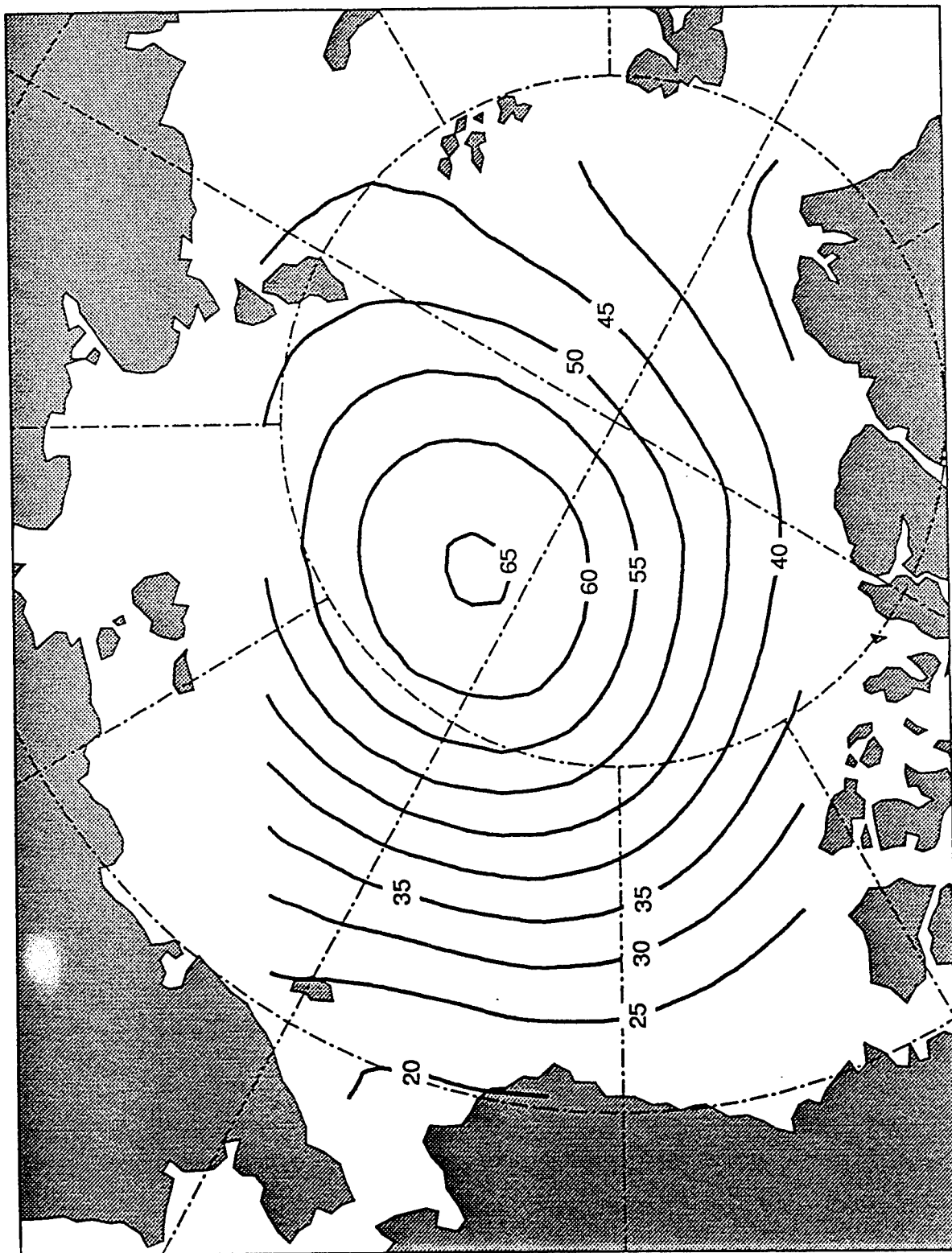


Figure 6. Variance of monthly pressure (departure from annual mean).

Pressure Variance of Climatological Annual Cycle in mb^2

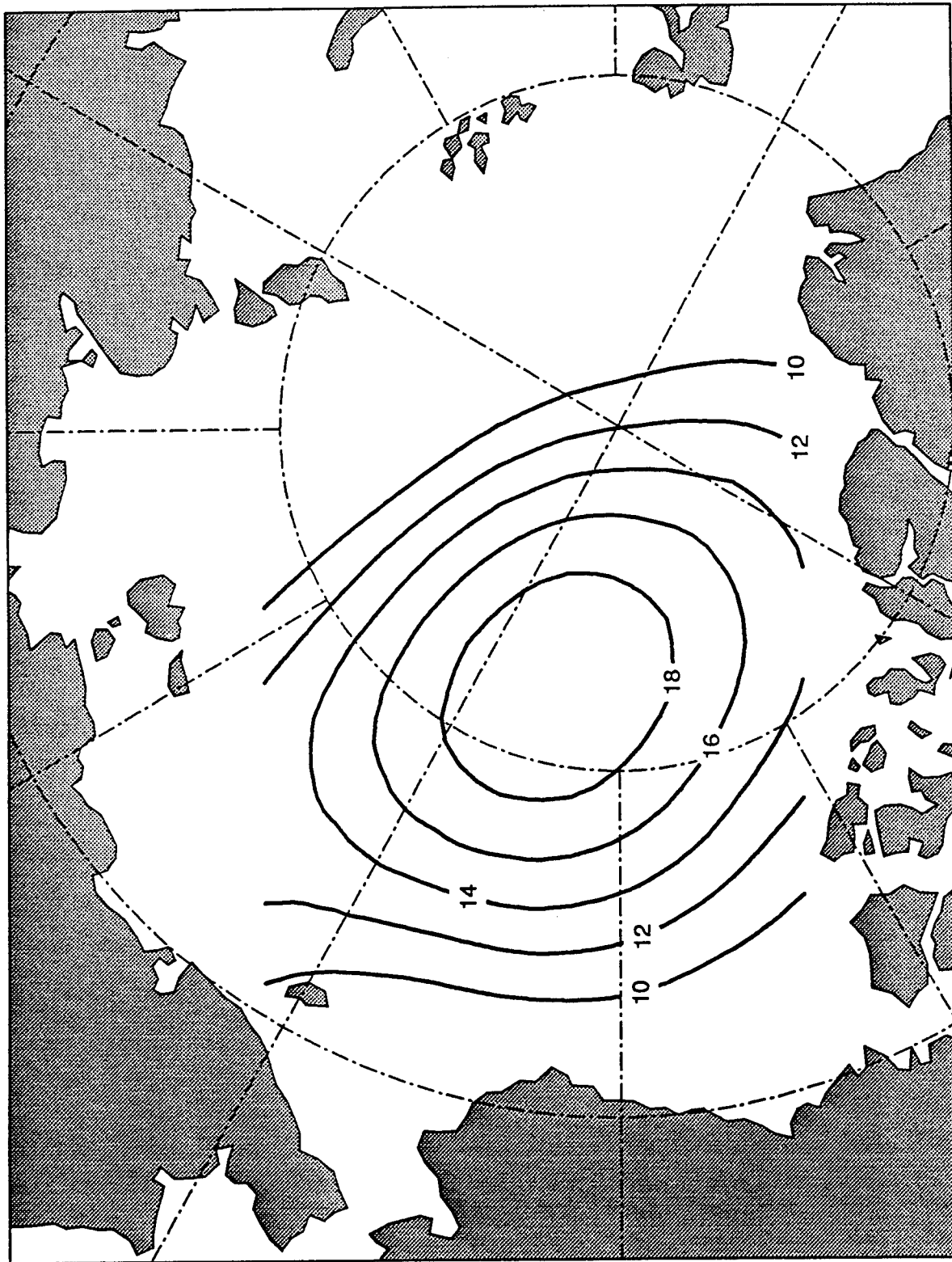


Figure 7. Variance of mean seasonal cycle of pressure (from annual mean).

Geostrophic Wind Total Variance about Annual Mean in m^2/s^2

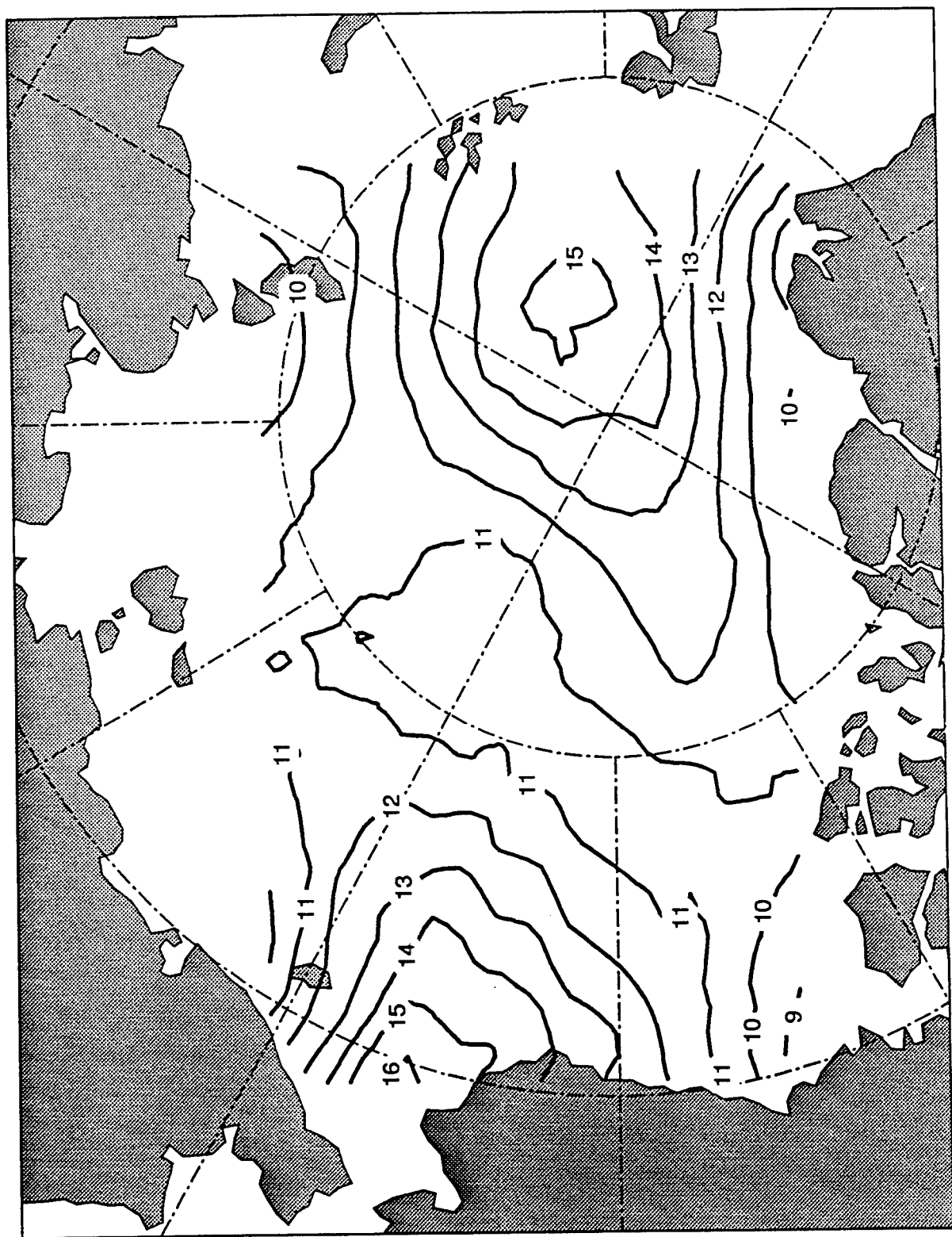


Figure 8. Variance of monthly geo. wind (departures from annual mean).

Geostrophic Wind Variance of Climatological Annual Cycle in m^2/s^2

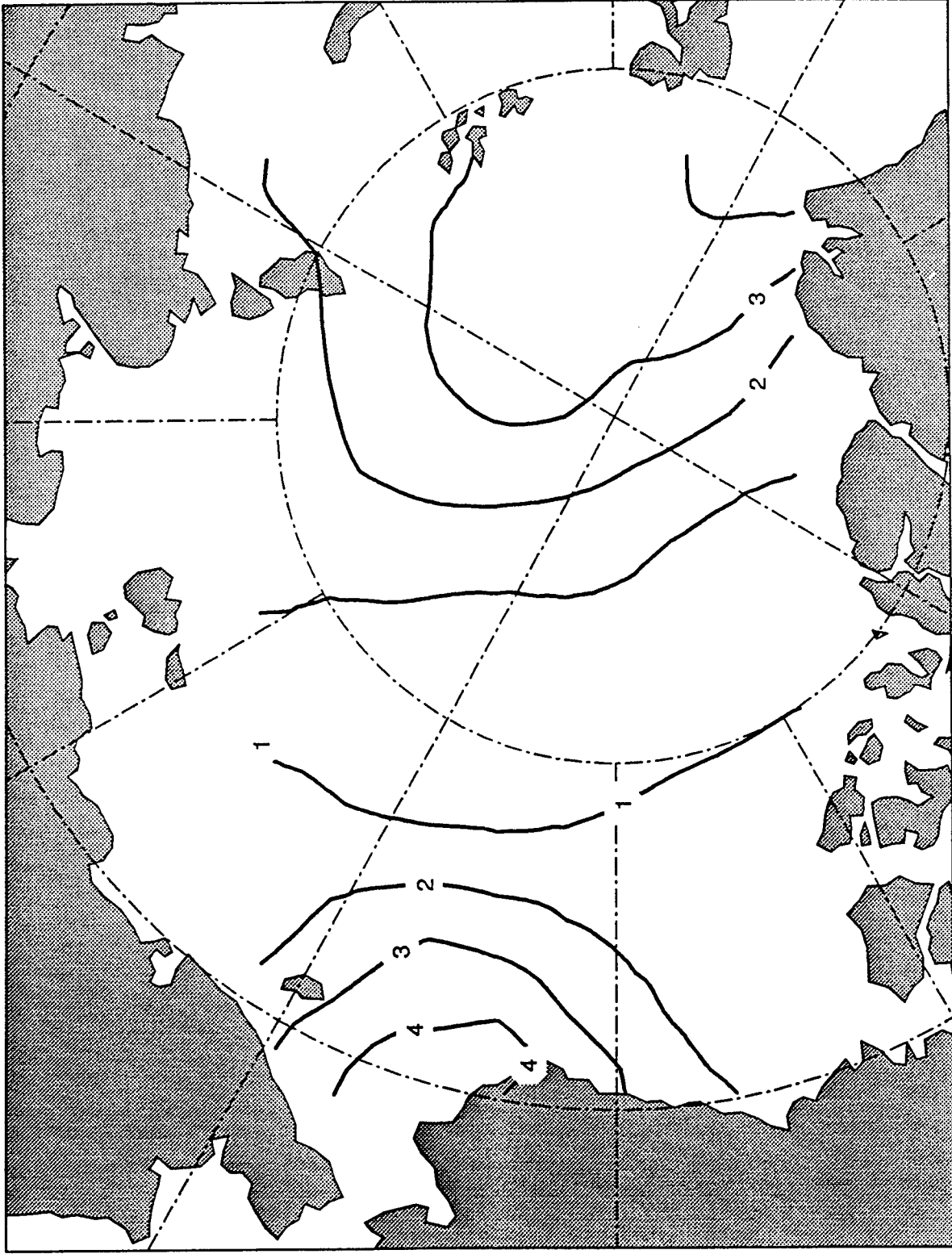


Figure 9. Variance of the mean seasonal cycle of geostrophic wind.

Ice Velocity Total Variance about Annual Mean in cm^2/s^2

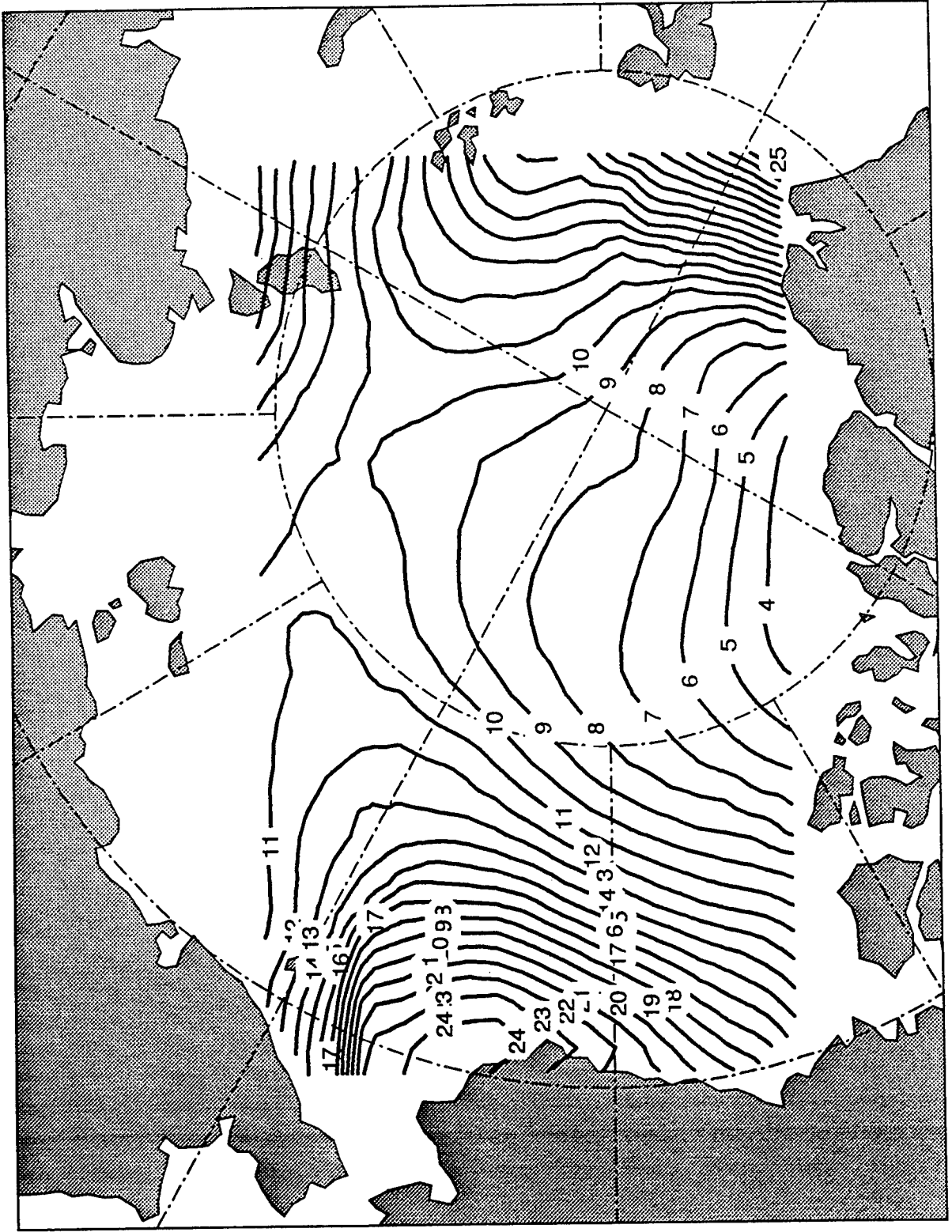


Figure 10. Variance of the monthly ice motion (from annual mean).

Ice Velocity Variance of Climatological Annual Cycle in cm^2/s^2

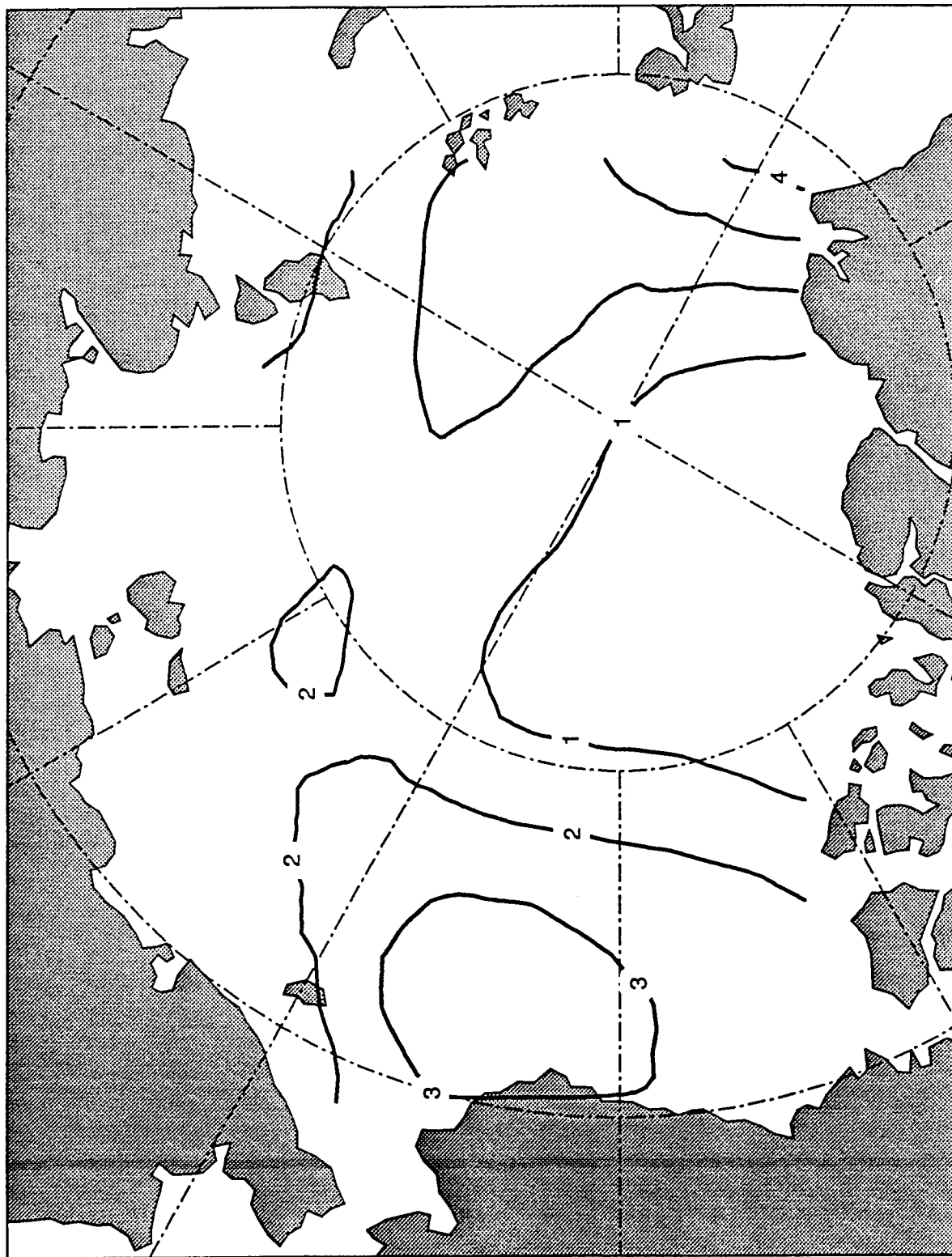


Figure 11. Variance of the mean seasonal cycle of ice motion.

GENERAL APPROACH

General Approach

Investigate a representation of the form:

$$U(x, t) = \bar{U}(x) + \sum_i \alpha_i P_i(x) Q_i(t)$$

$\bar{U}(x)$ = mean annual field

α_i = constant scalar associated with mode i

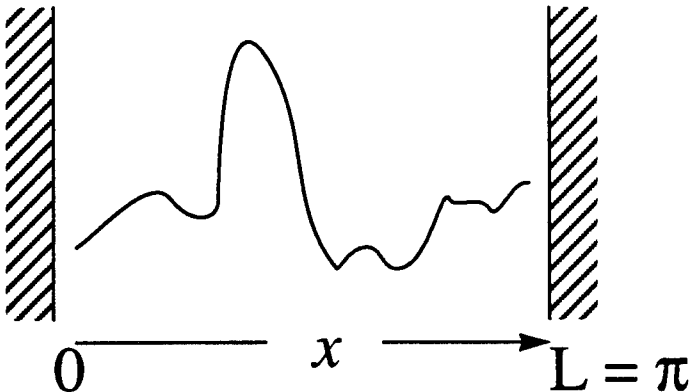
P_i = stationary pattern for mode i

$Q_i(t)$ = scalar time series for mode i

Figure 1. Represent U as sums of products (separation of time and space).

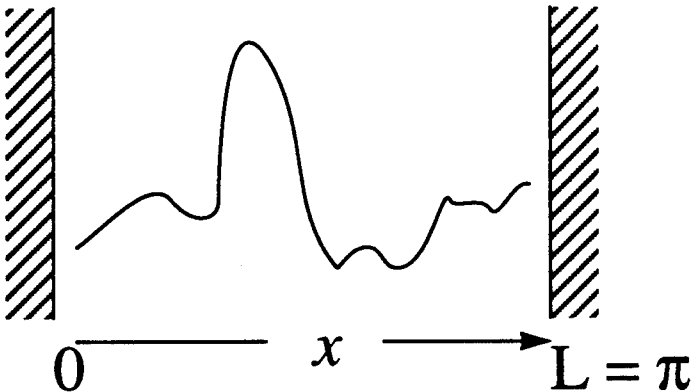
Familiar Patterns

Vibrating String

$$\frac{\partial^2 X}{\partial t^2} = \alpha^2 \frac{\partial^2 X}{\partial x^2}$$


$$X(x, t) = \sum_{k=1} a_k \sin(kx) \exp(-ik\alpha t)$$

Heat Conduction

$$\frac{\partial^2 T}{\partial t^2} = \alpha^2 \frac{\partial^2 T}{\partial x^2}$$


$$T(x, t) = \sum_{k=1} a_k \sin(kx) \exp(-k^2 \alpha^2 t)$$

Figure 2. Wave equation, diffusion equation.

Principle Component Analysis

- remove mean annual field from each monthly field
- for each month define a super vector $U(t)$ built from $U'(x,t)$
- determine a pattern P which looks “most like” the aggregate of perturbation fields $U'(t)$
- find the P to maximize

$$\sum_t \{ P \cdot U(t) (P \cdot U(t))^T \}$$

subject to the constraint

$$PP^T = I$$

Figure 3. Principle component analysis.

JIC: ----- Ice Edge, Fast Ice Edge

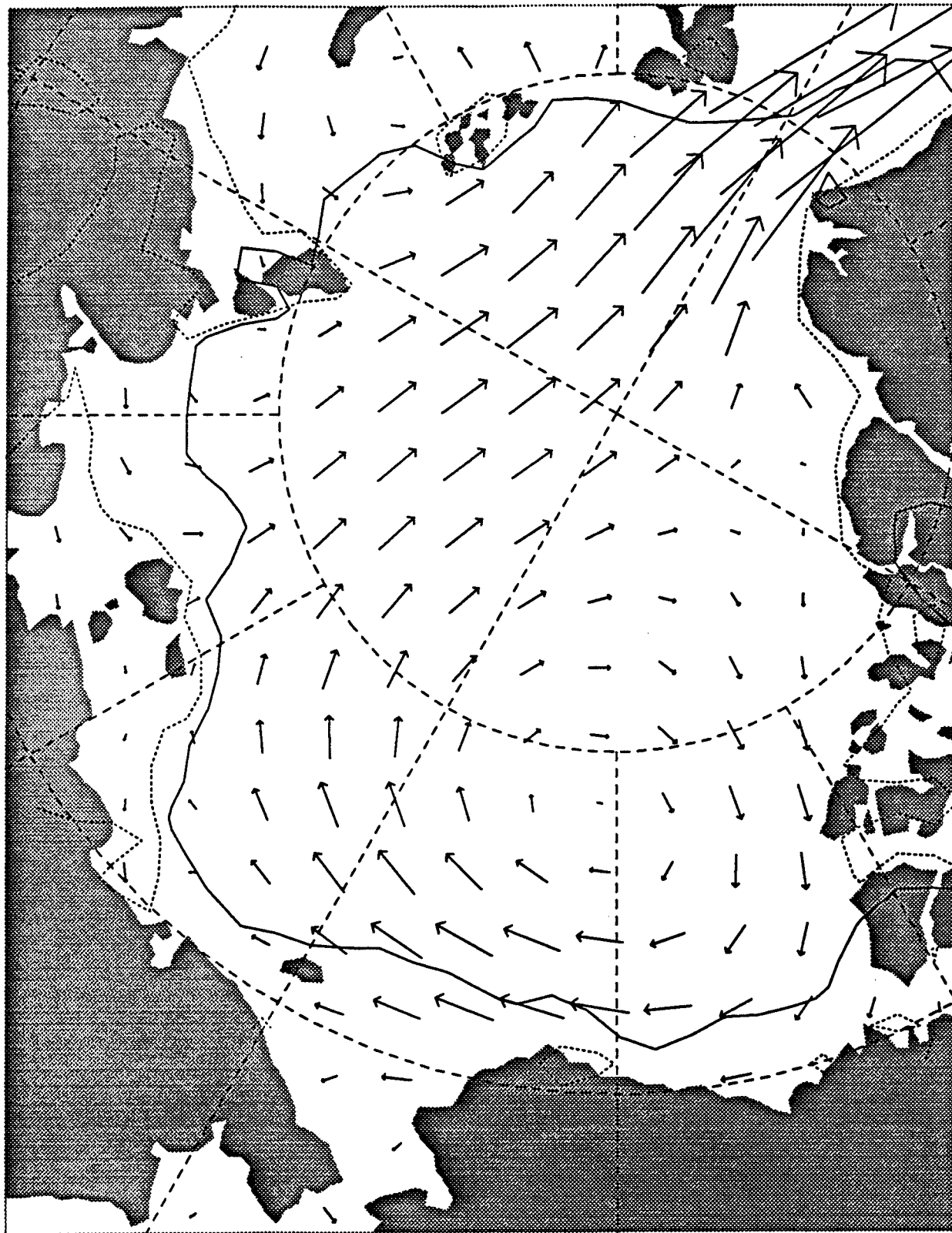


Figure 4. Mean annual ice motion ice edge and fast ice boundary (emphasize homogeneous, data rich area).

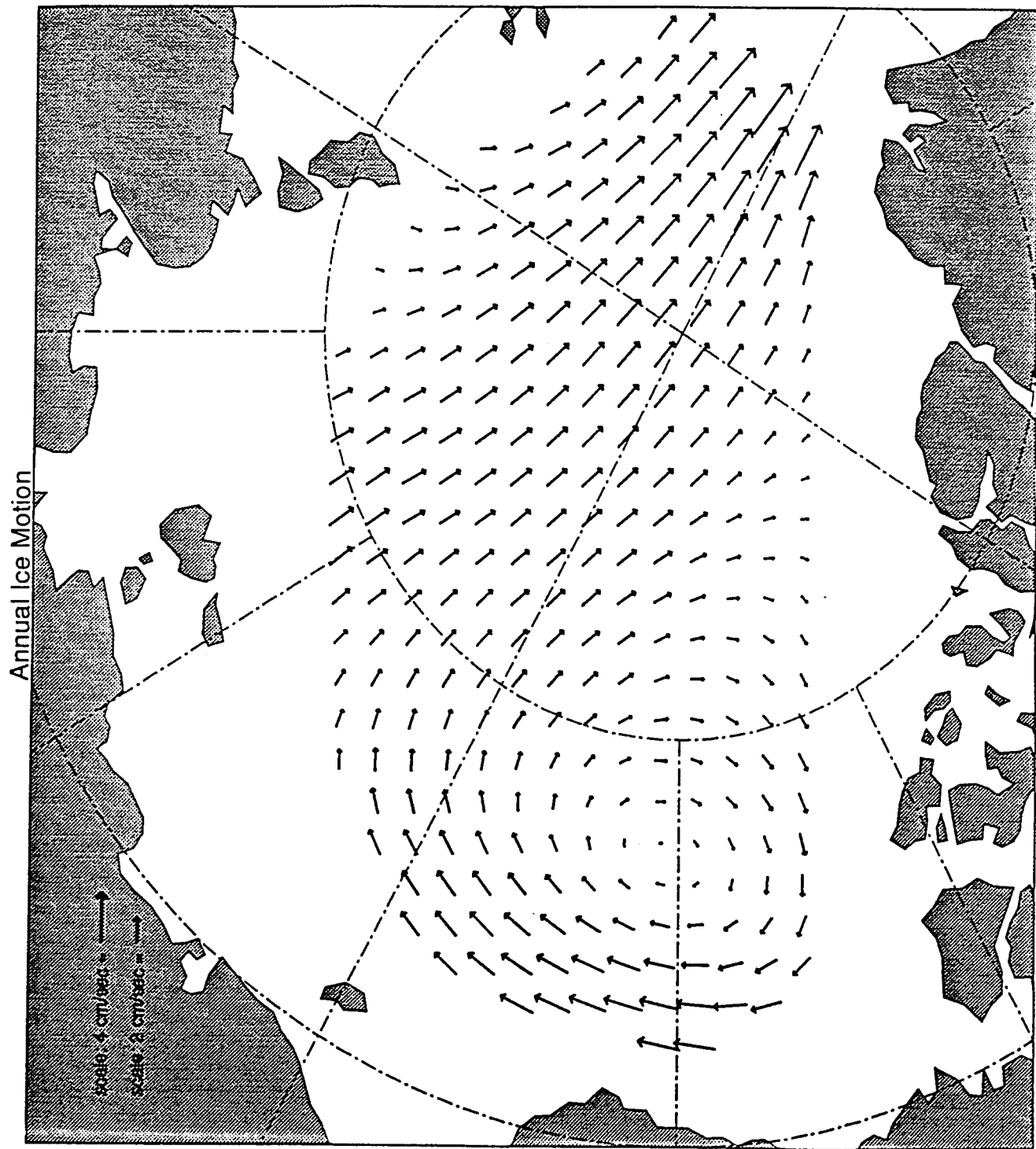


Figure 5. Annual ice motion (show study region, vector of 600 elements).

RESULT OF PRINCIPLE COMPONENT ANALYSIS

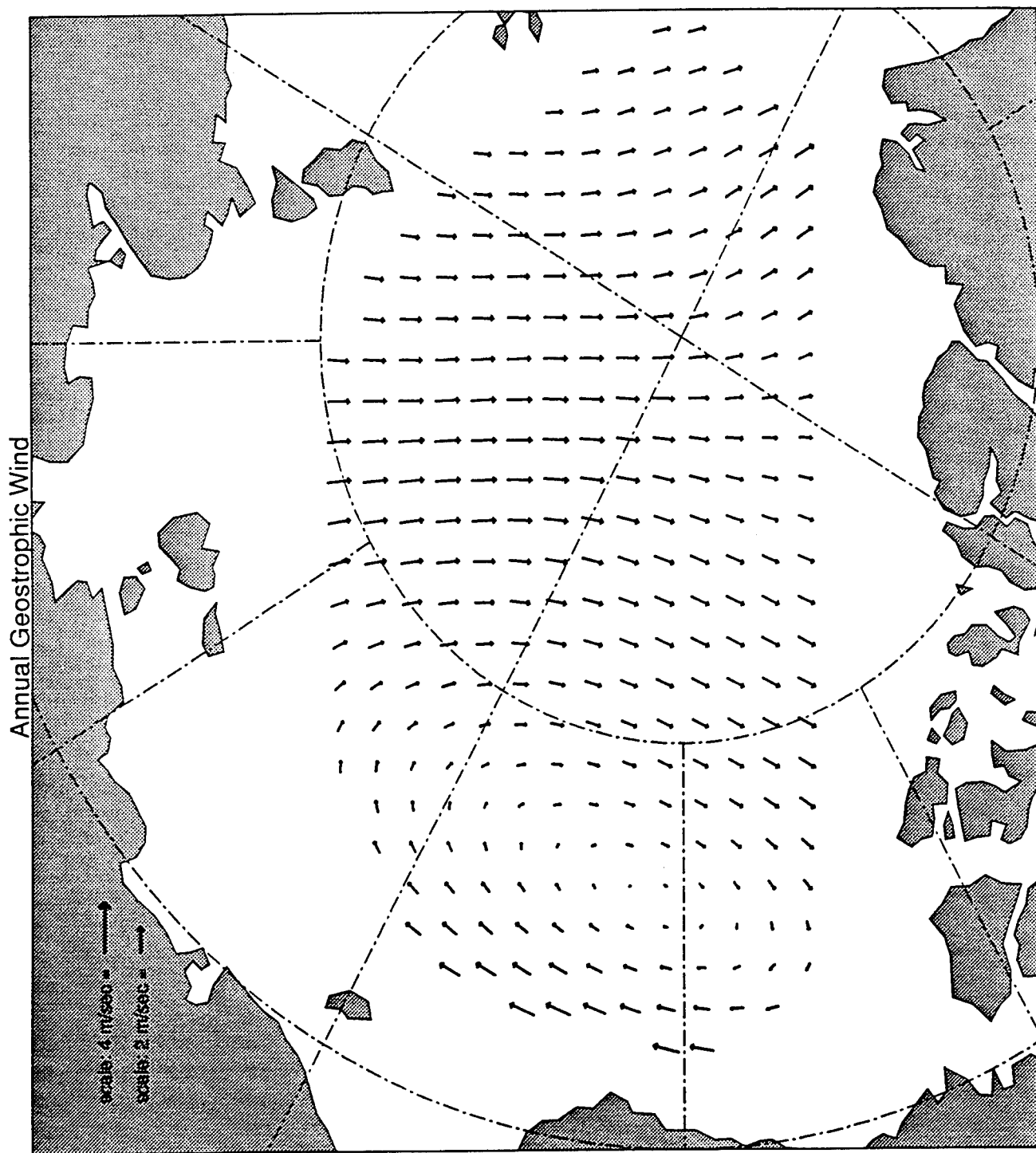


Figure 1. Begin with the wind, first subtract the mean annual wind vector.

Wind Velocity EOF, Mode 1

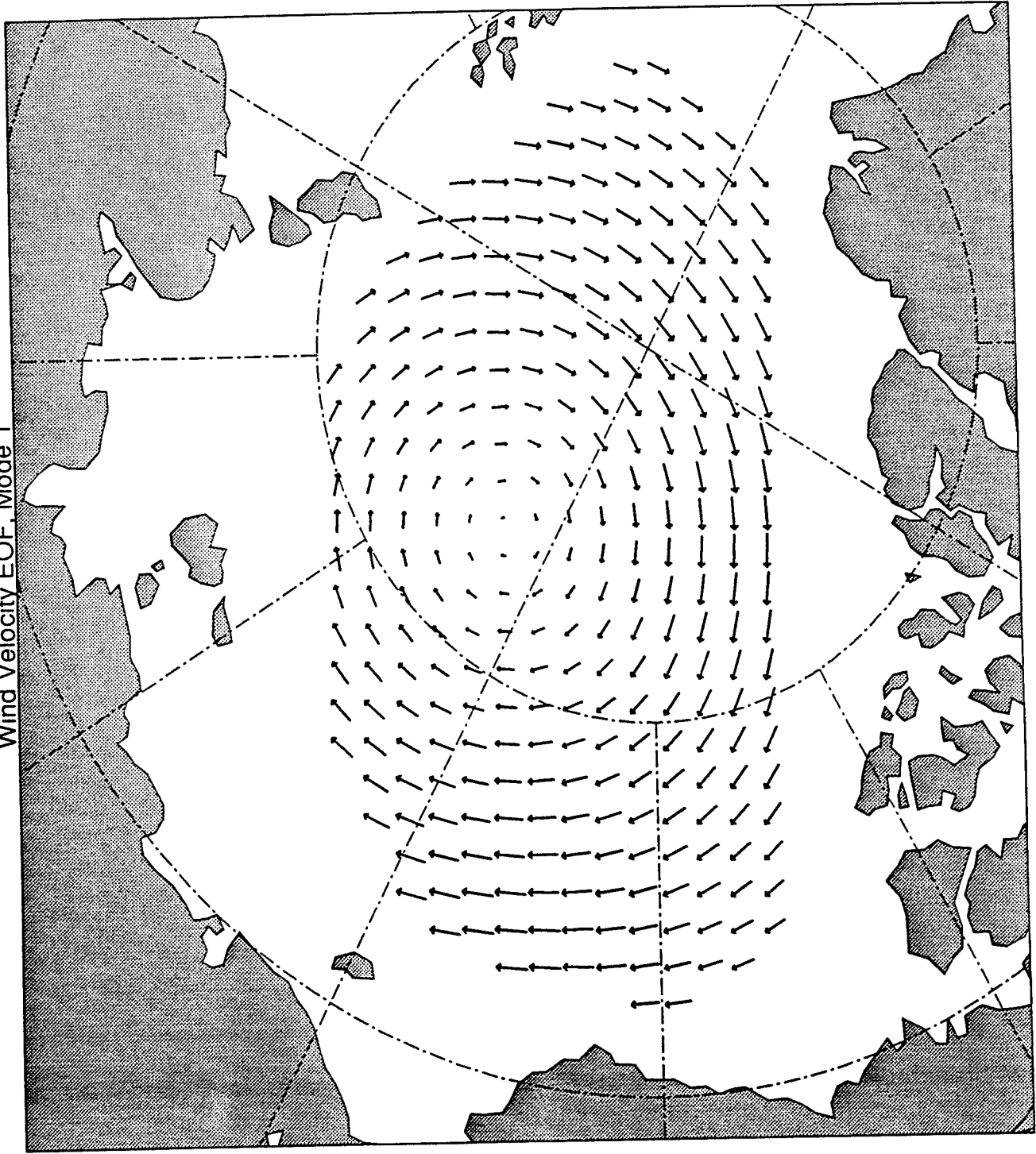


Figure 2a. Patterns of wind, mode 1.

Wind Velocity EOF, Mode 2

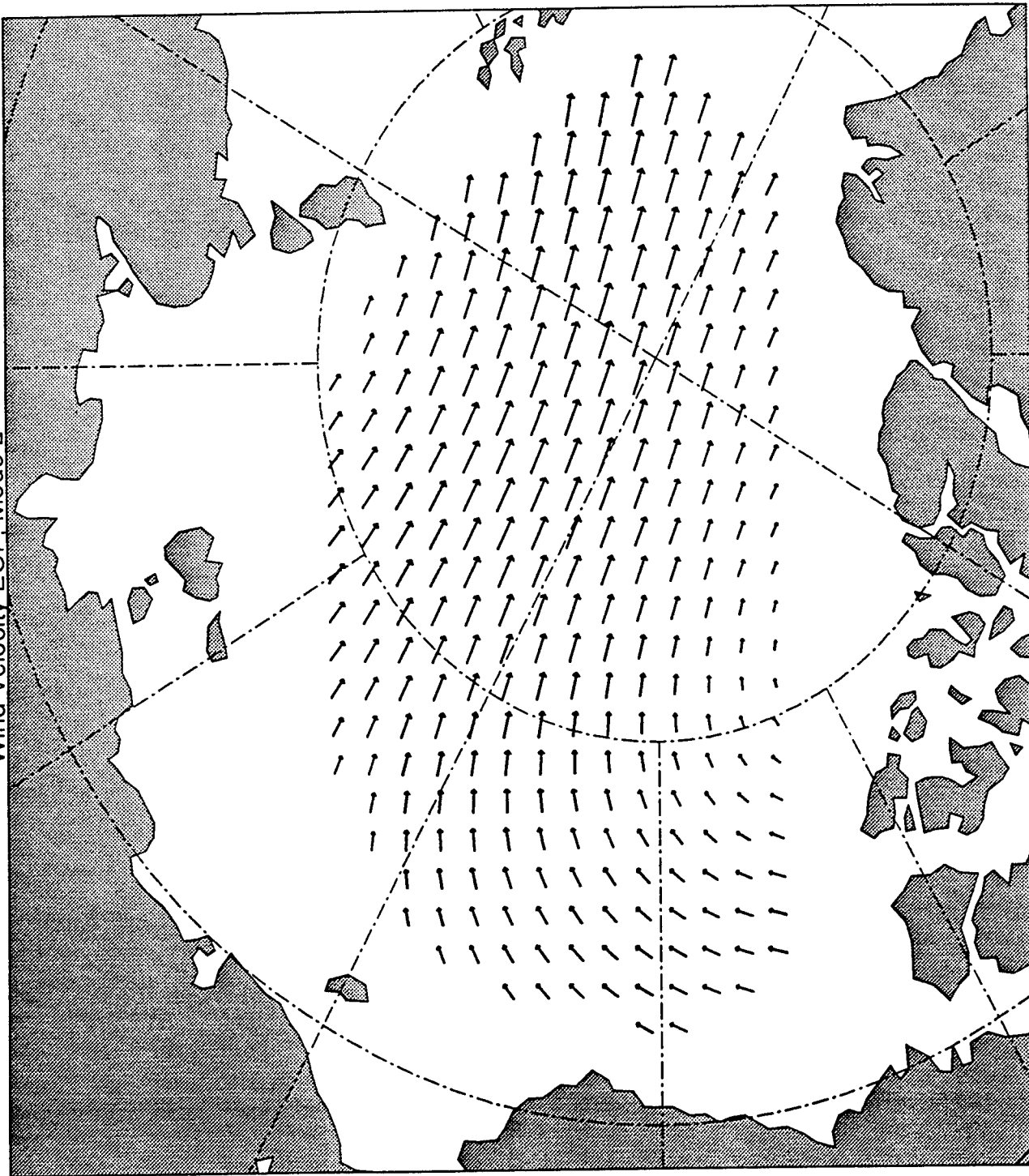


Figure 2b. Patterns of wind, mode 2.

Wind Velocity EOF, Mode 3

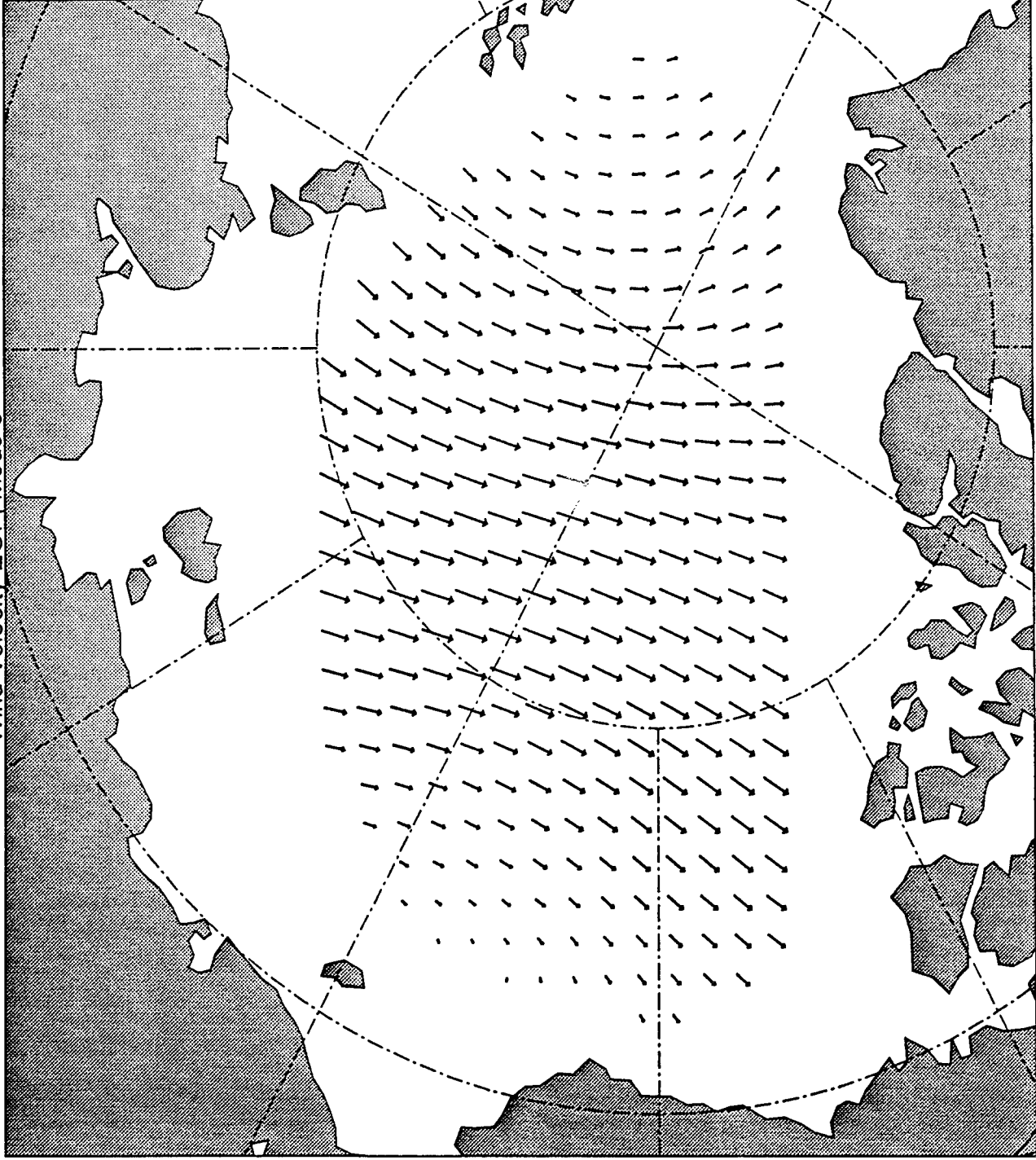


Figure 2c. Patterns of wind, mode 3.

EOF Geostrophic Wind, Departures from Annual

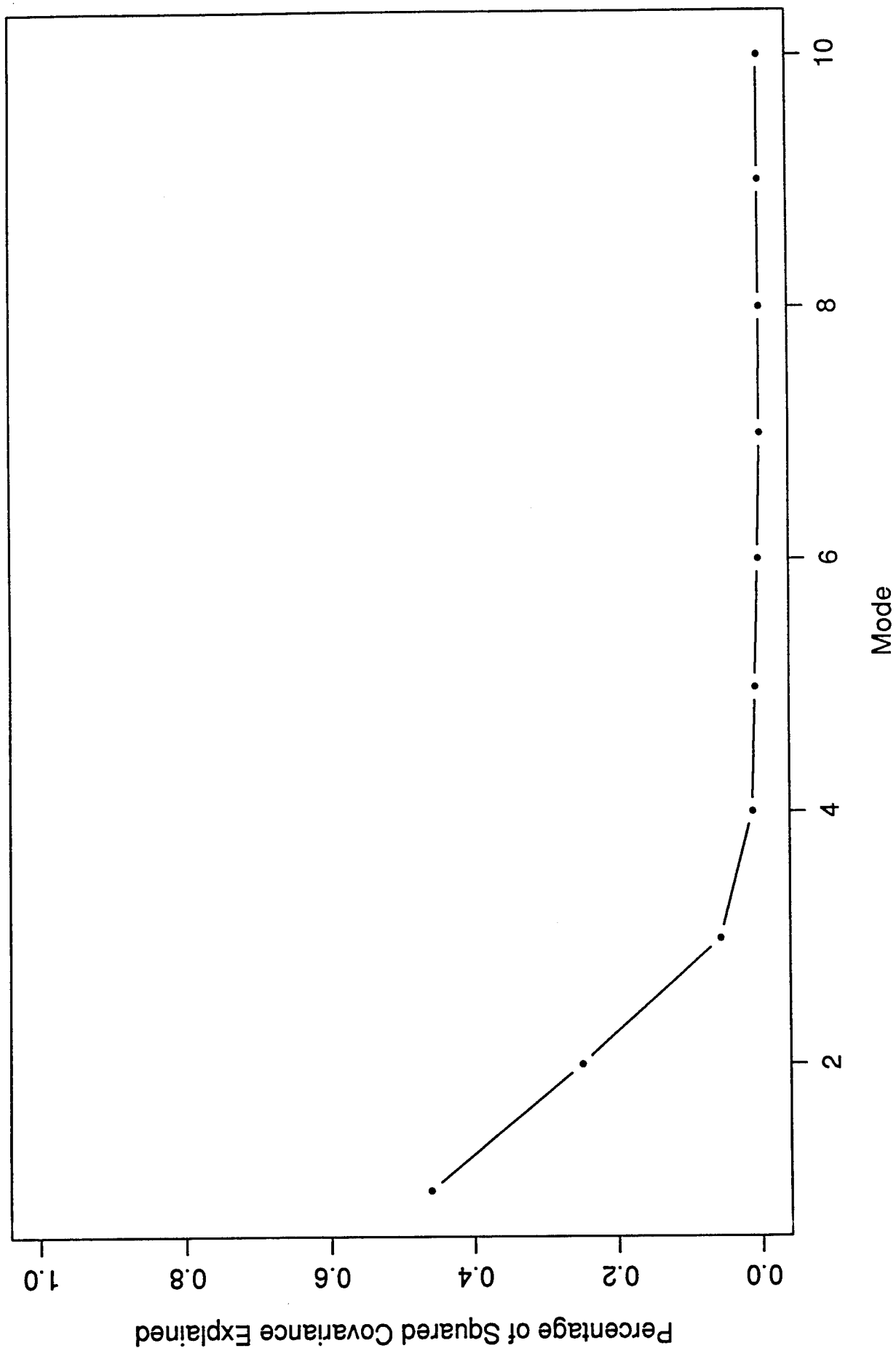


Figure 3. Scalar multiplier ALPHA, modes 1, 2, and 3.

EOF, Multiplier of Wind, mode = 1

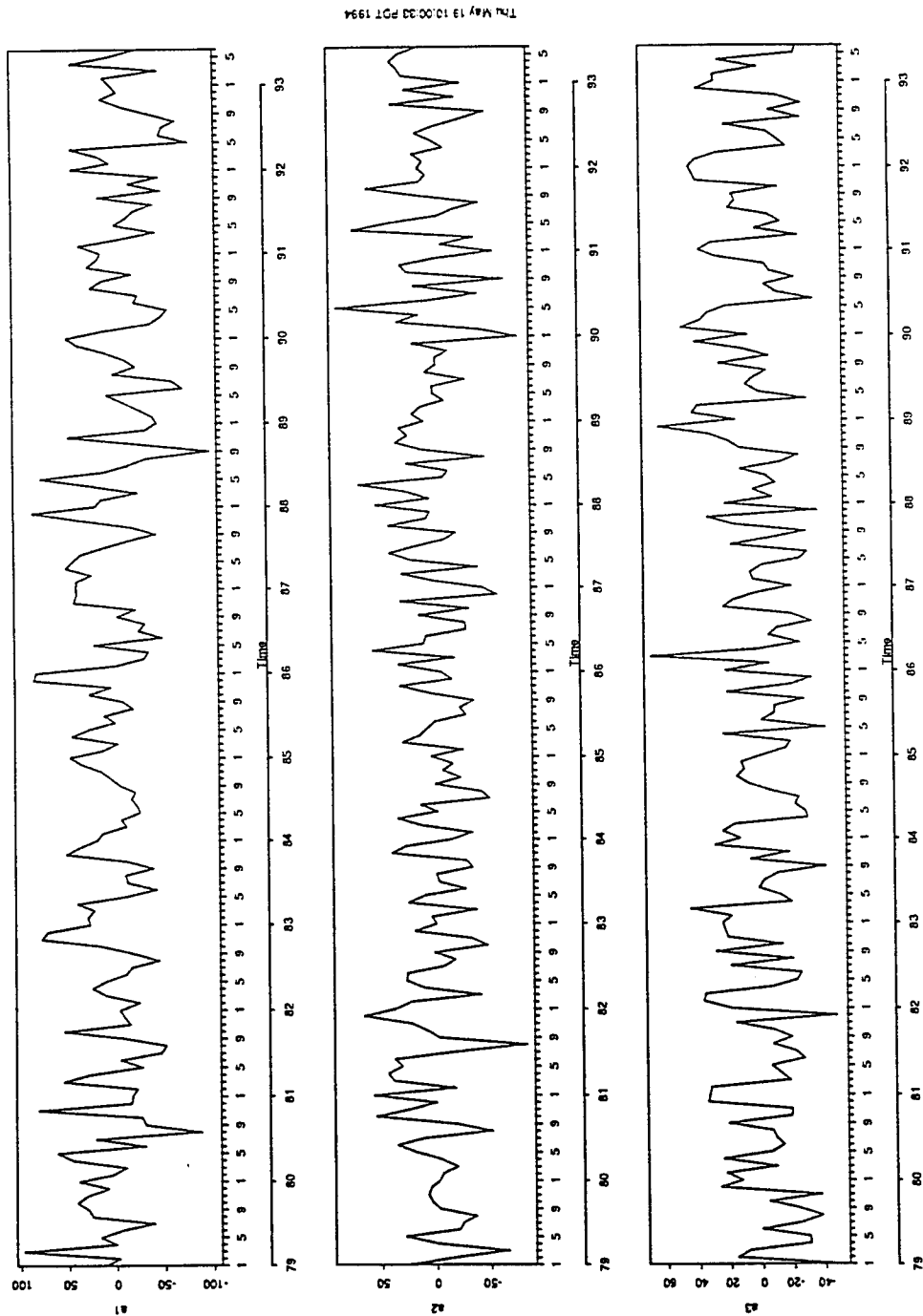


Figure 4a. Time series of pattern multiplier, mode 1.
(persistence, spectra, predictability)

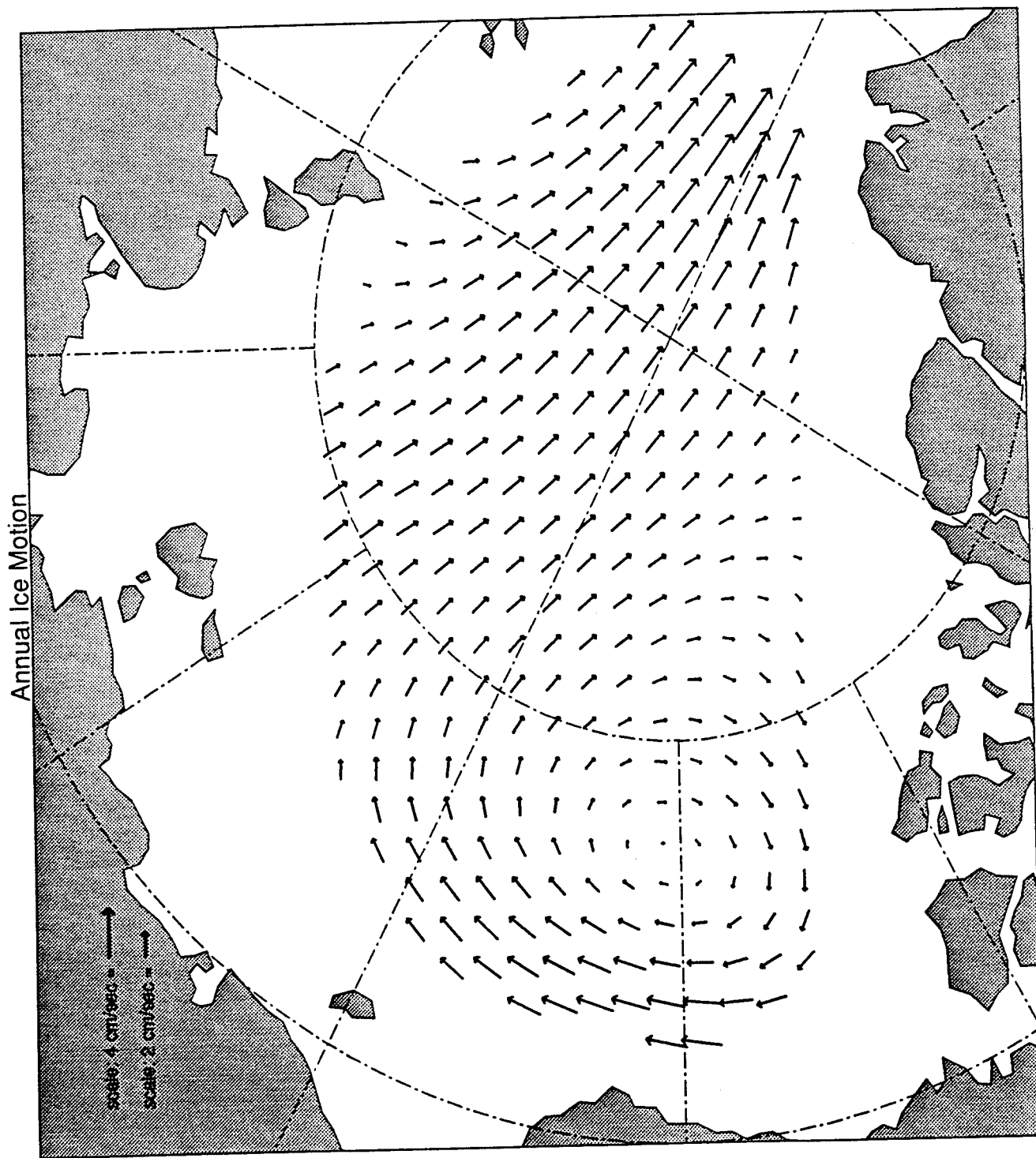


Figure 5a. Patterns of ice motion.

Ice Velocity EOF, Mode 1

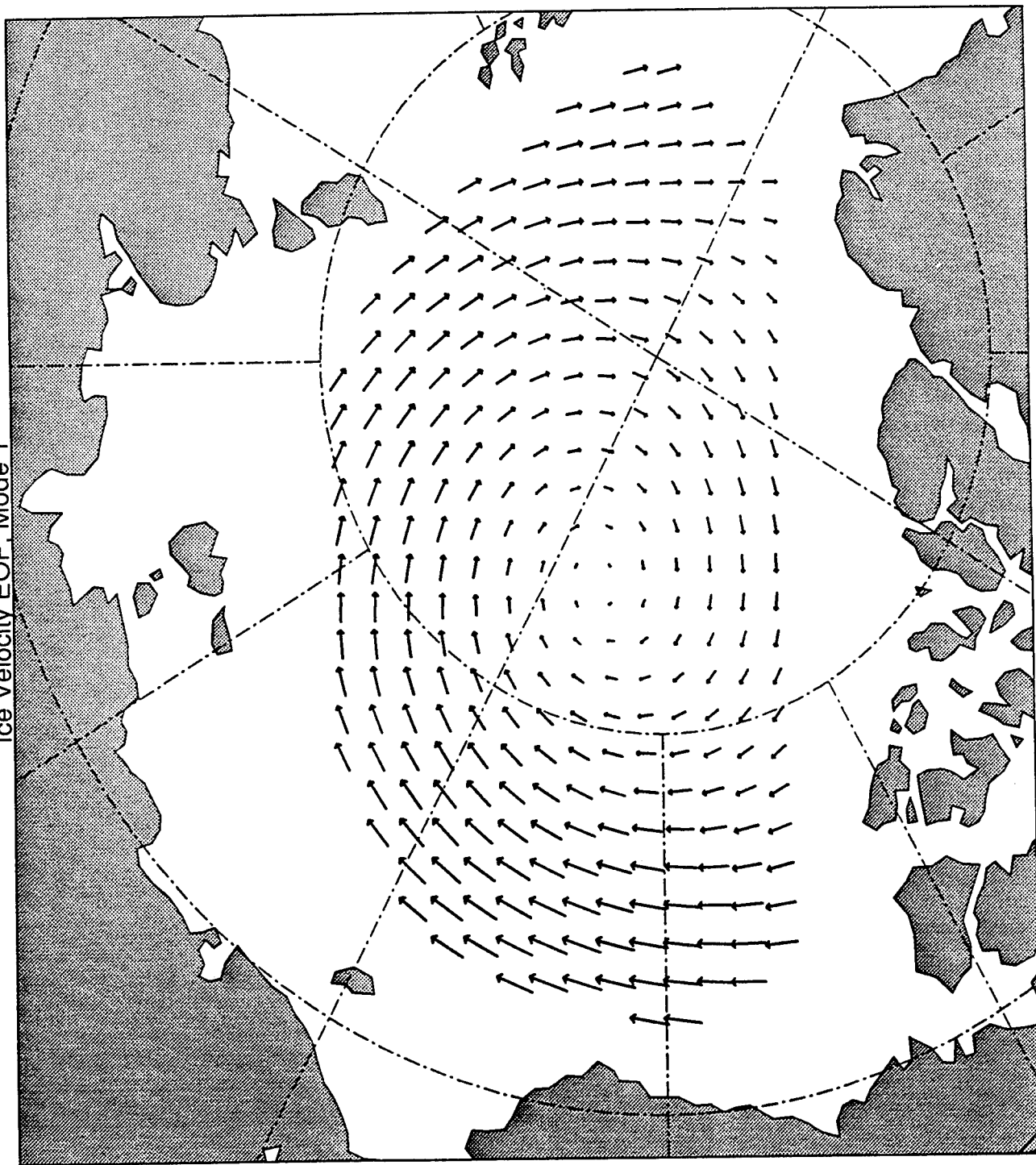


Figure 5b. Patterns of ice motion, mode 1.

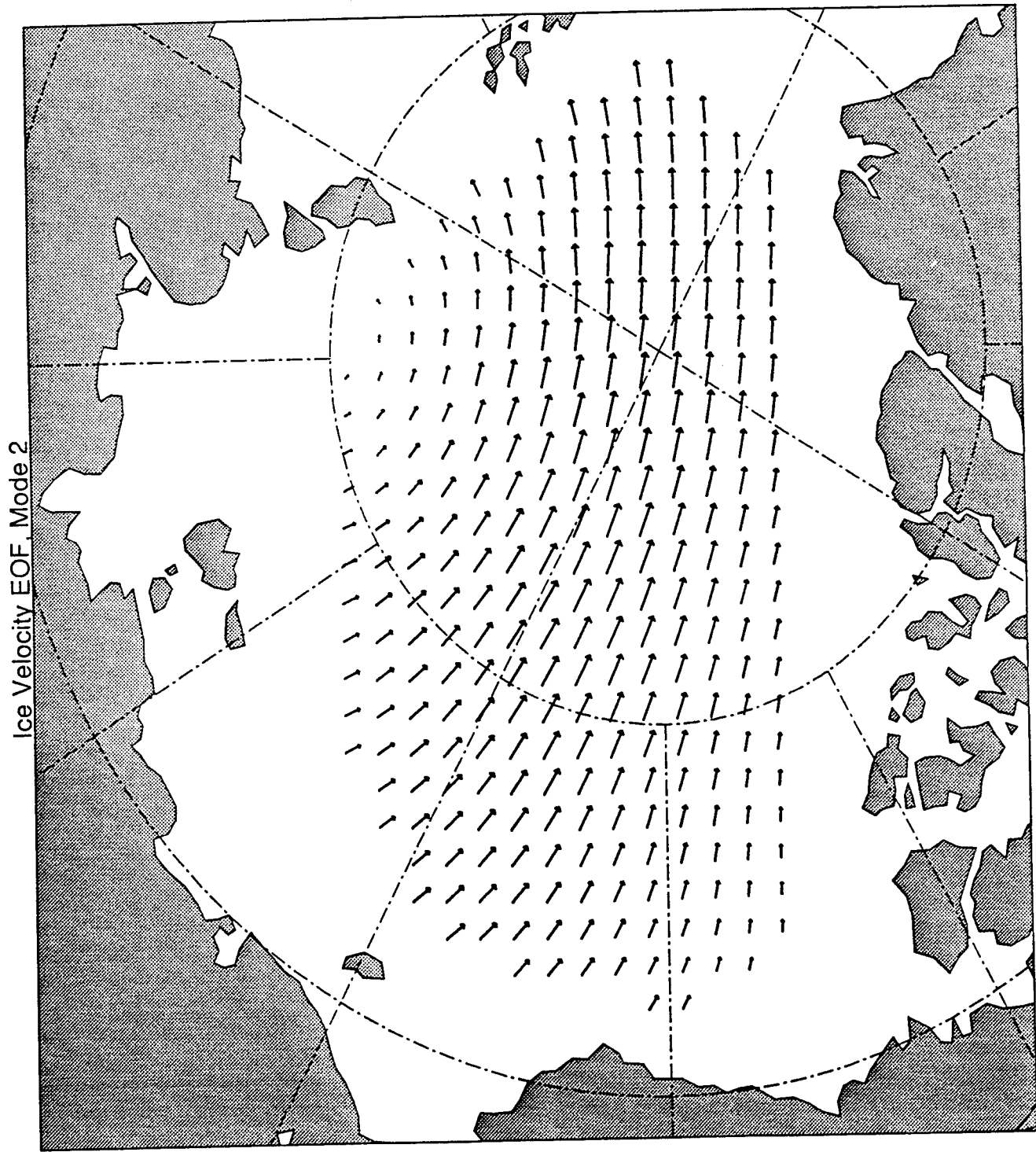


Figure 5c. Patterns of ice motion, mode 2.

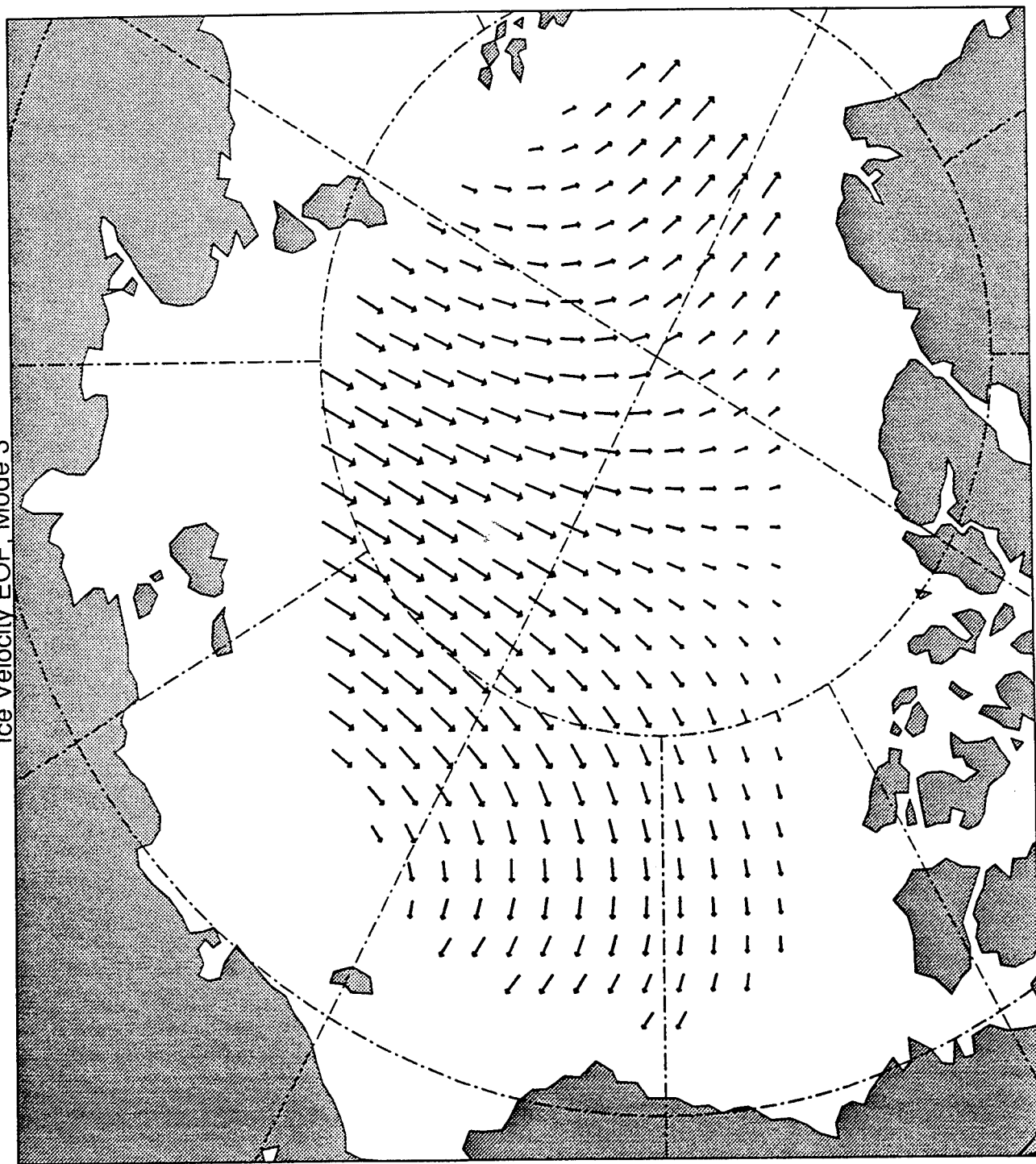


Figure 5d. Patterns of ice motion, mode 3.

EOF Ice Velocity, Departures from Annual

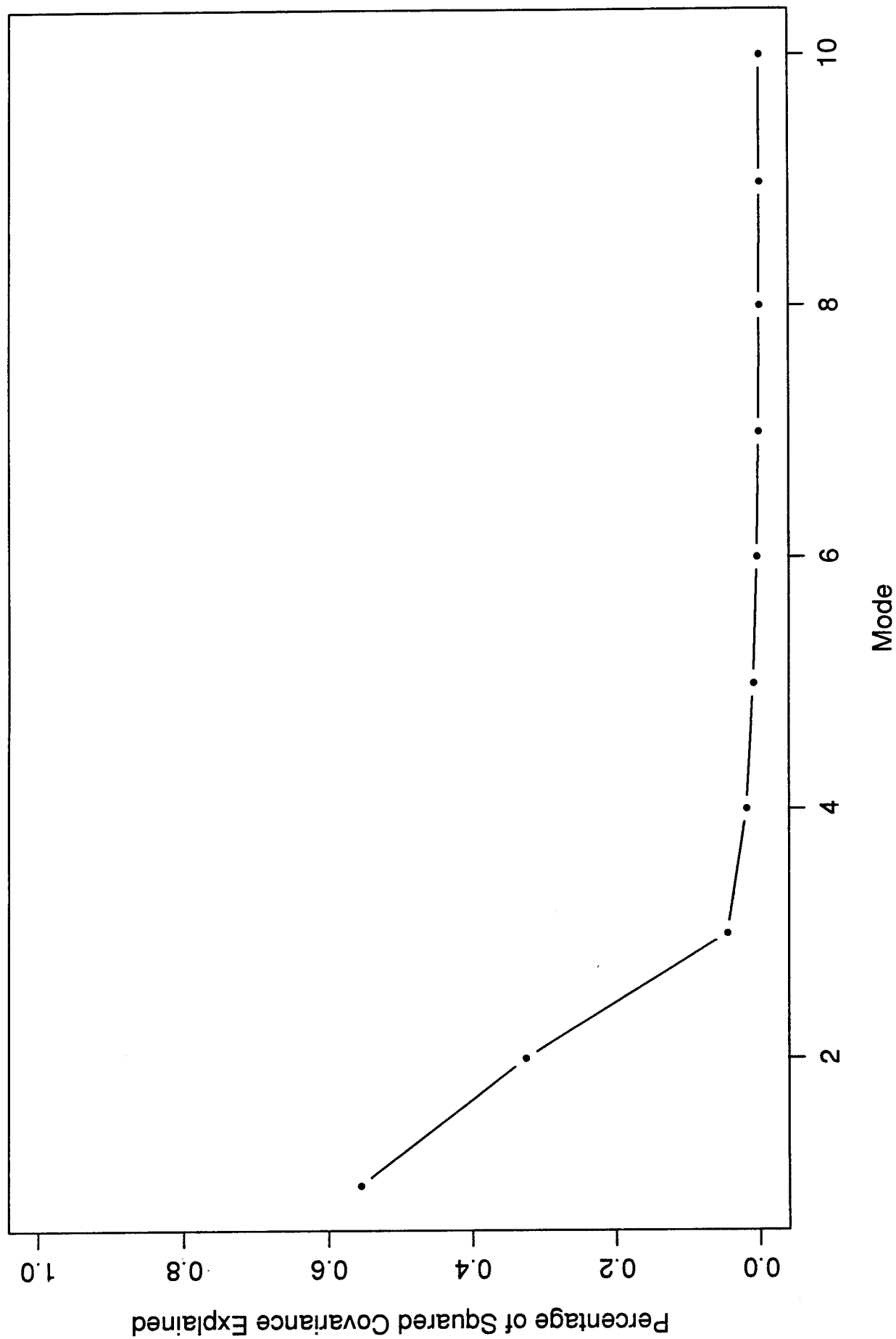


Figure 6. Scalar multiplier ALPHA, modes 1, 2, and 3.

EOF, Multiplier of Velocity, mode = 1

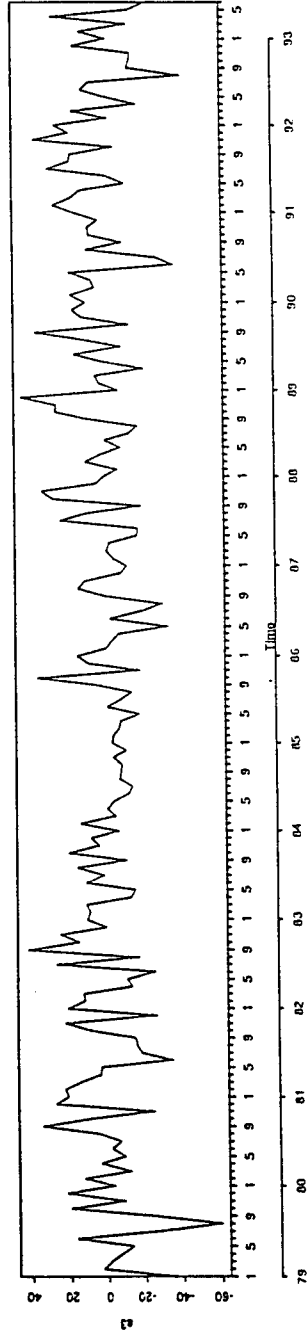
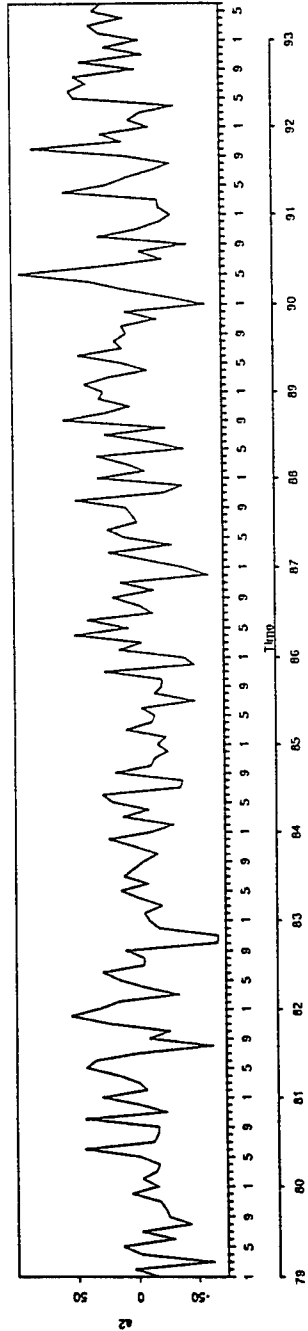
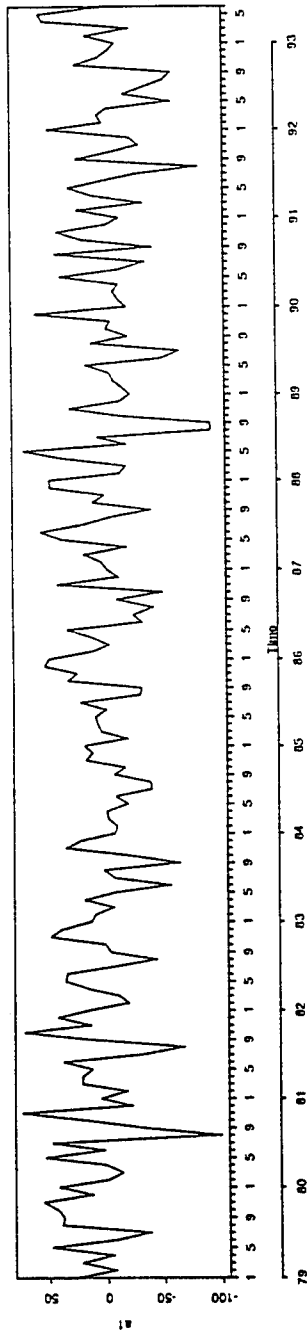


Figure 7. Time series of pattern multiplier, modes 1, 2, and 3.

CONCLUSION

Relatively few modes explain a large portion of variance (not surprising as correlation length scale is 1400 km).

1992 EOF, Multiplier of Wind, mode = 1, Departures From Monthly Means

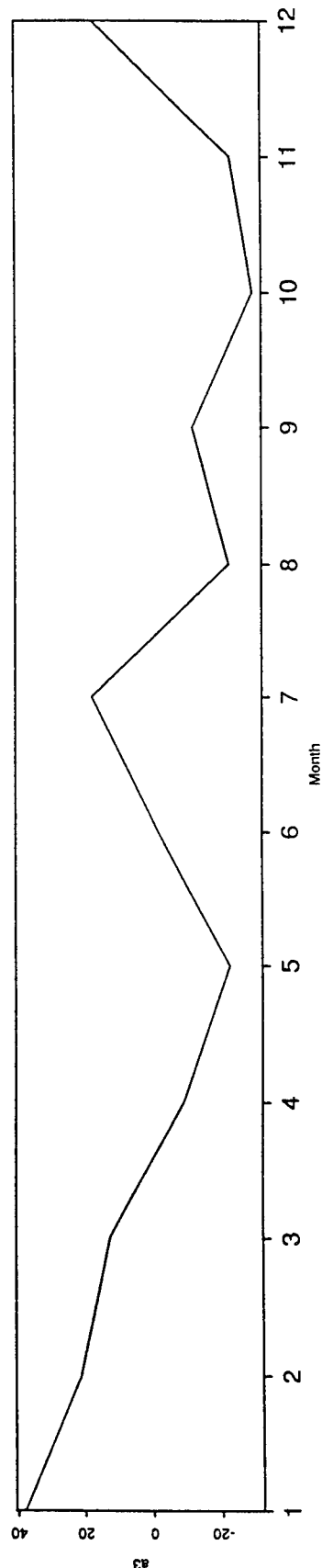
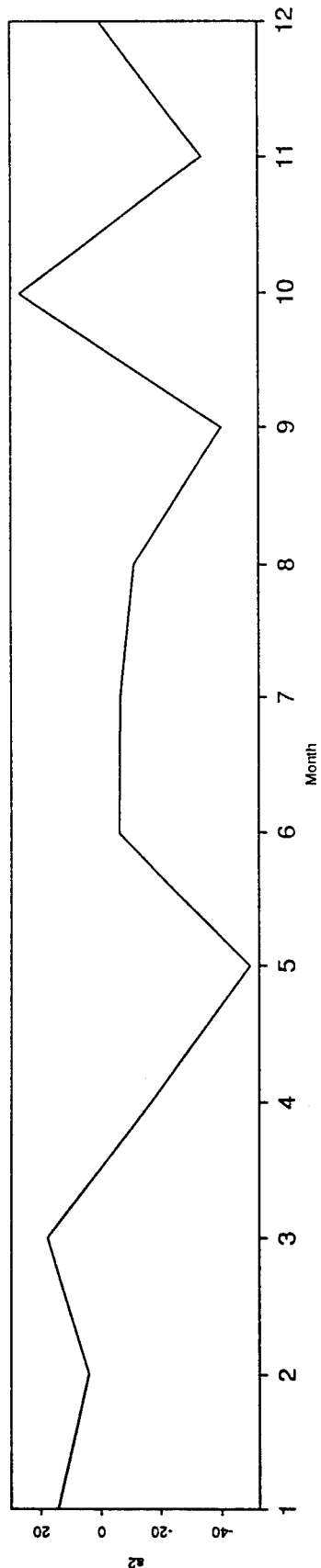
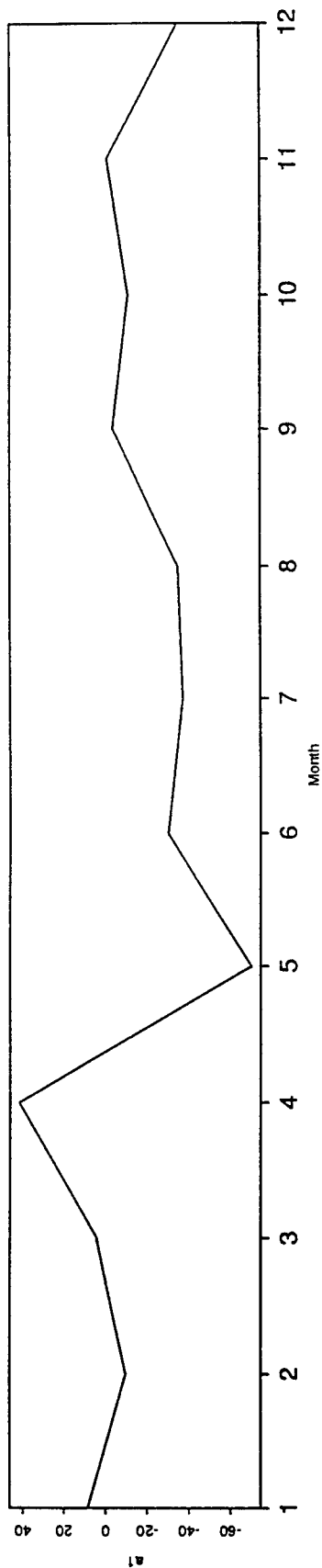


Figure 9a. Comparison of pattern multipliers, wind (these multipliers are for departures from mean seasonal cycle).

1992 EOF, Multiplier of Velocity, mode = 1, Departures From Monthly Means

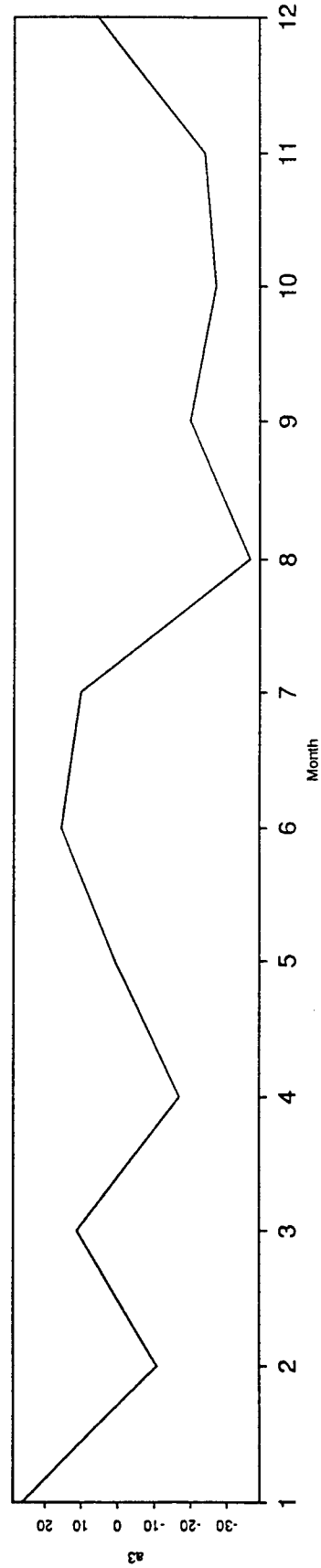
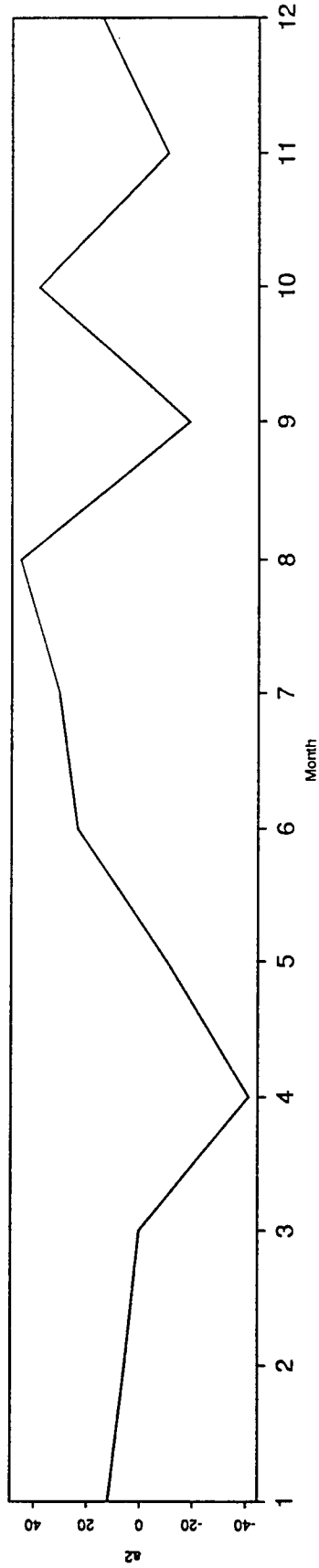
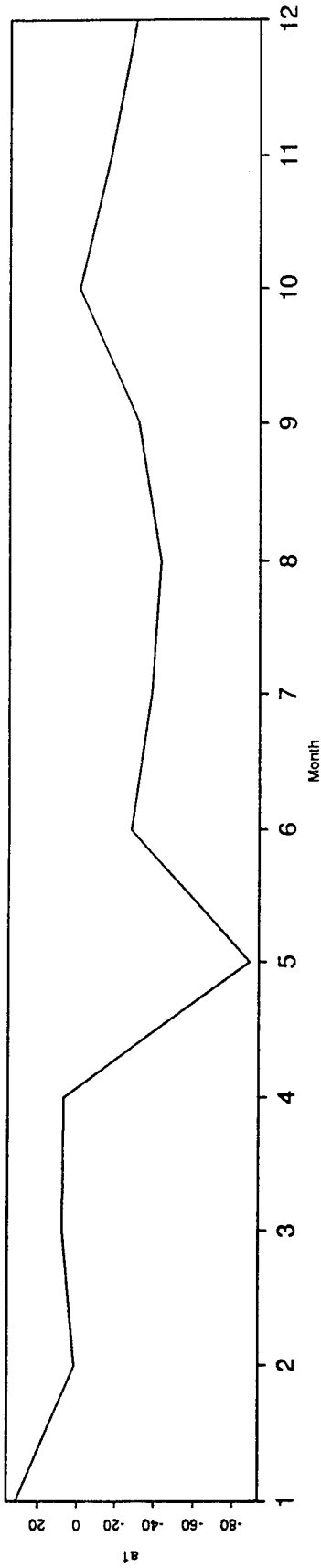


Figure 9b. Comparison of pattern multipliers, ice motion (these multipliers are for departures from mean seasonal cycle).

COVARIANCE OF PAIRS OF FIELDS

(Singular Value Decomposition)

Correlation Coefficients

Covariance of x and y (scalars)

$$\text{cov} \{x, y\} = E \{ (x - \bar{x}) (y - \bar{y}) \} \approx \sum_i (x_i - \bar{x}) (y_i - \bar{y})$$

$$\rho^2 = \frac{[\text{cov}(x, y)]^2}{[\text{var}(x) \text{var}(y)]}$$

$$1 - \rho^2 = \frac{\text{var} \{x - \alpha y - \beta\}}{\text{var}(x)} = \frac{\text{var} \{y - \gamma x - \delta\}}{\text{var}(y)}$$

Covariance of x and y (vectors)

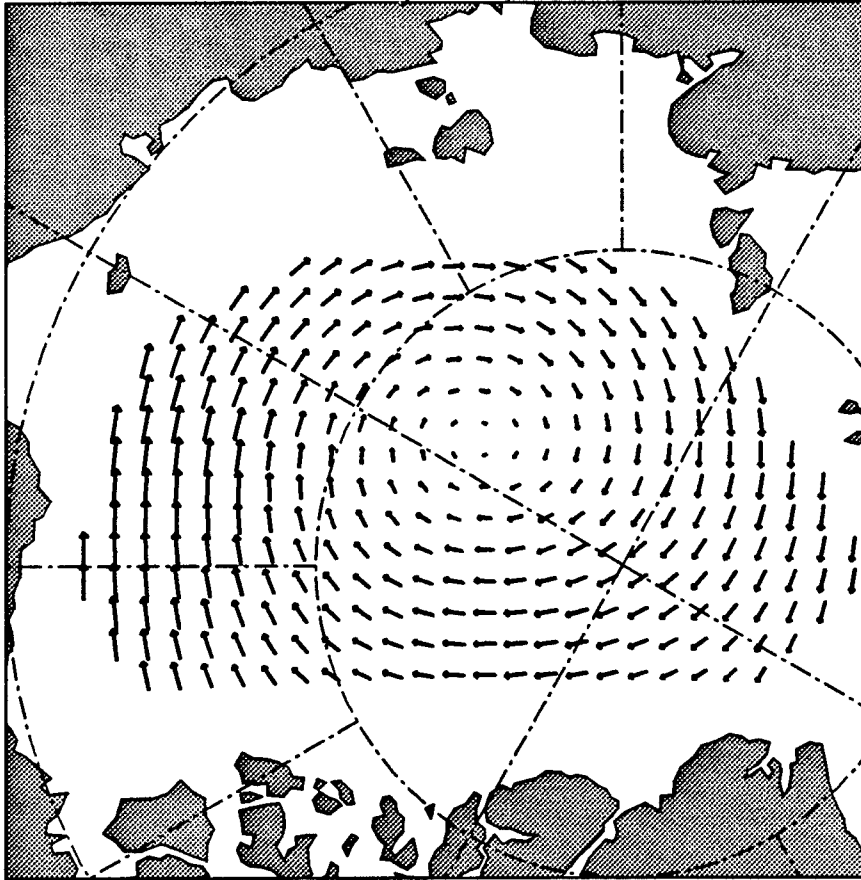
$$C_{xy} = E \{ (x - \bar{x}) (y - \bar{y})^T \} \quad = \text{matrix with elements } \{c_{m,n}\}$$

$$\|C_{xy}\|^2 = \sum_m \sum_n c_{m,n}^2 \quad \text{Frobenius norm}$$

$$\rho^2 = \frac{\|C_{xy}\|^2}{\|C_{xx}\| \|C_{yy}\|}$$

Figure 1. Define covariance for a pair of vectors.

Ice Velocity SVD, Mode 1



Wind Velocity SVD, Mode 1

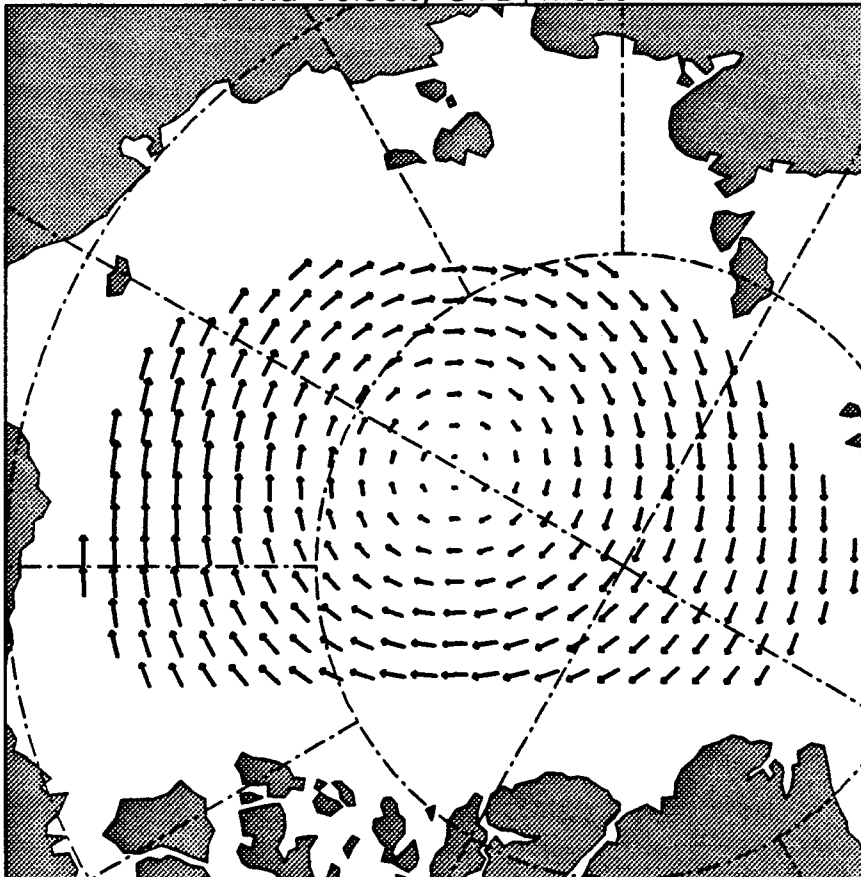
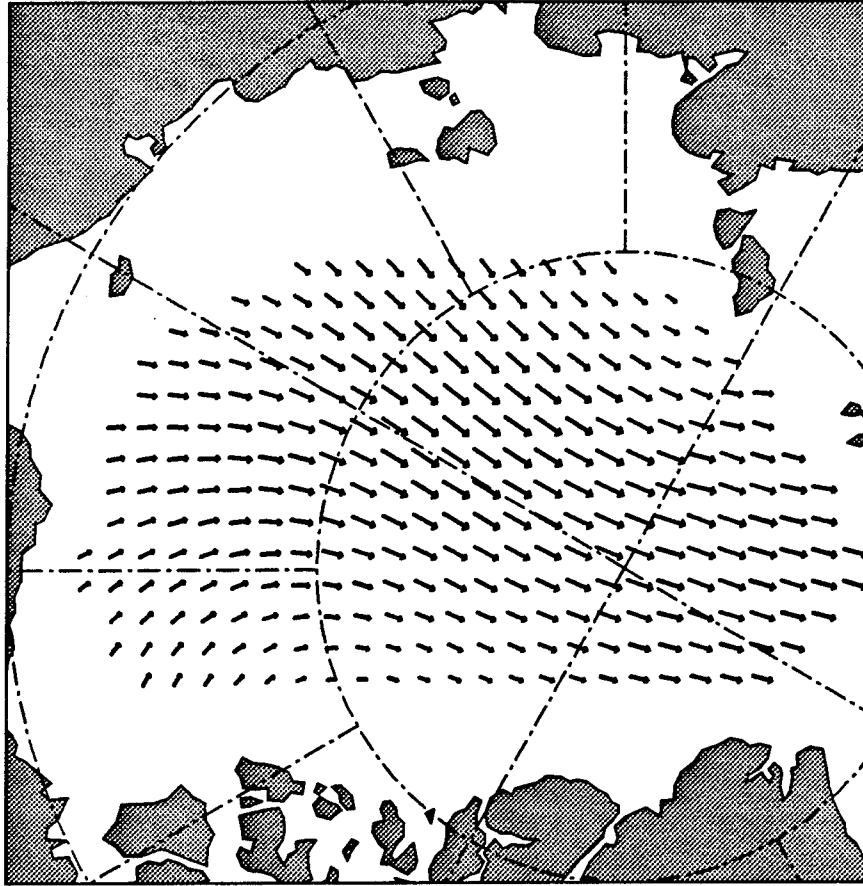


Figure 2a. Pattern pairs for wind and ice motion, mode 1.

Ice Velocity SVD, Mode 2



Wind Velocity SVD, Mode 2

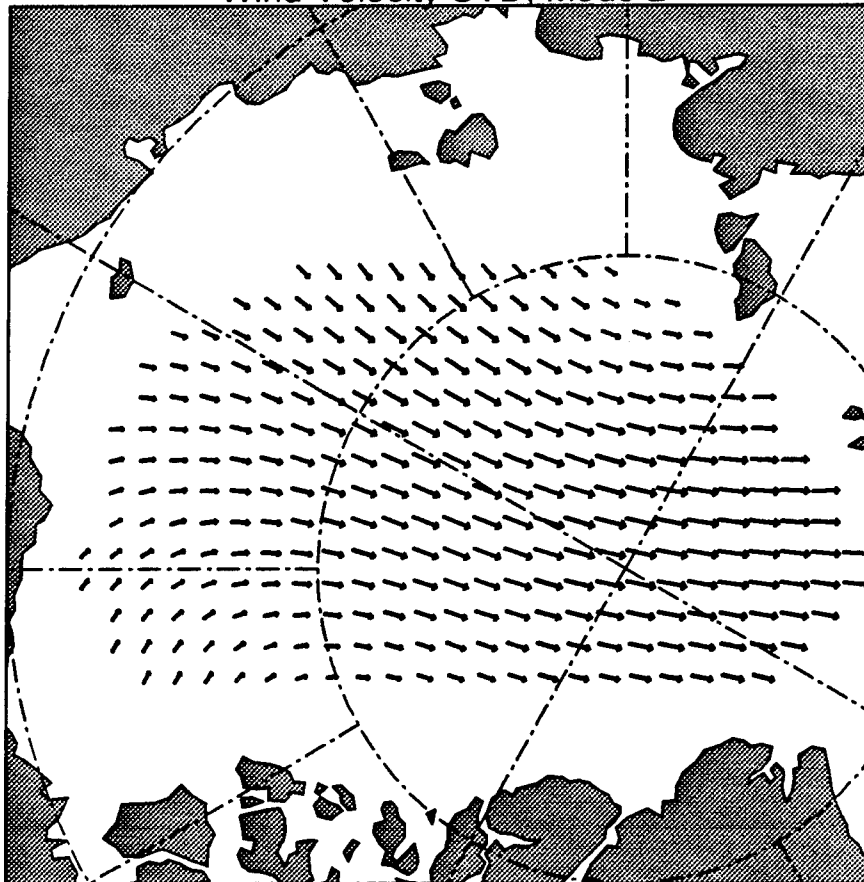
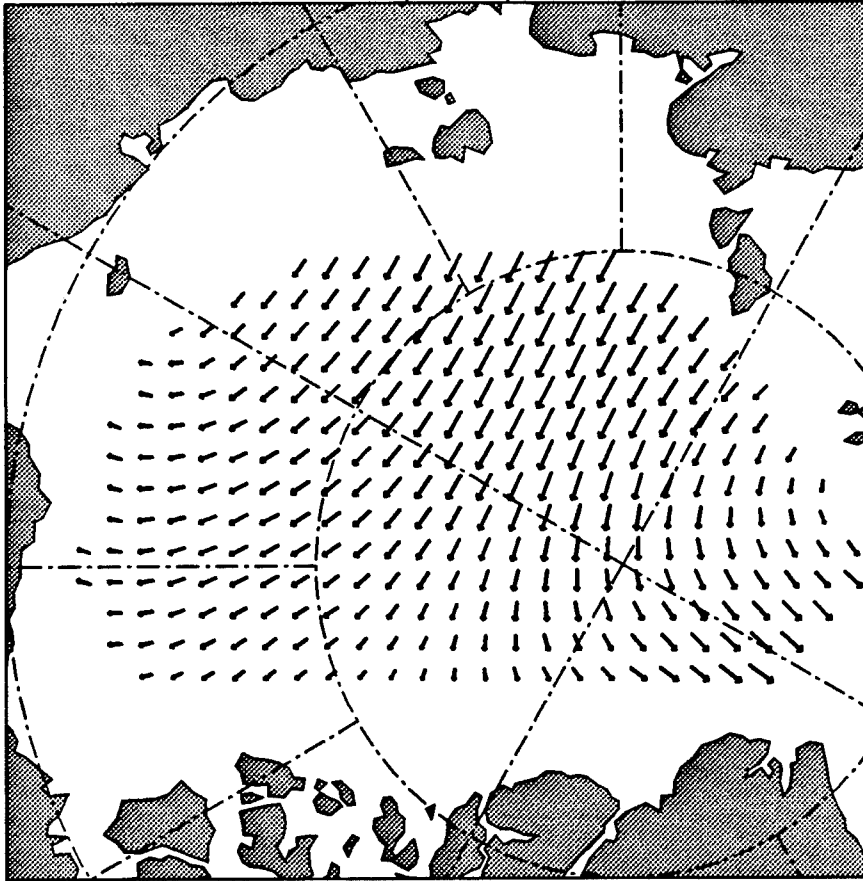


Figure 2b. Pattern pairs for wind and ice motion, mode 2.

Ice Velocity SVD, Mode 3



Wind Velocity SVD, Mode 3

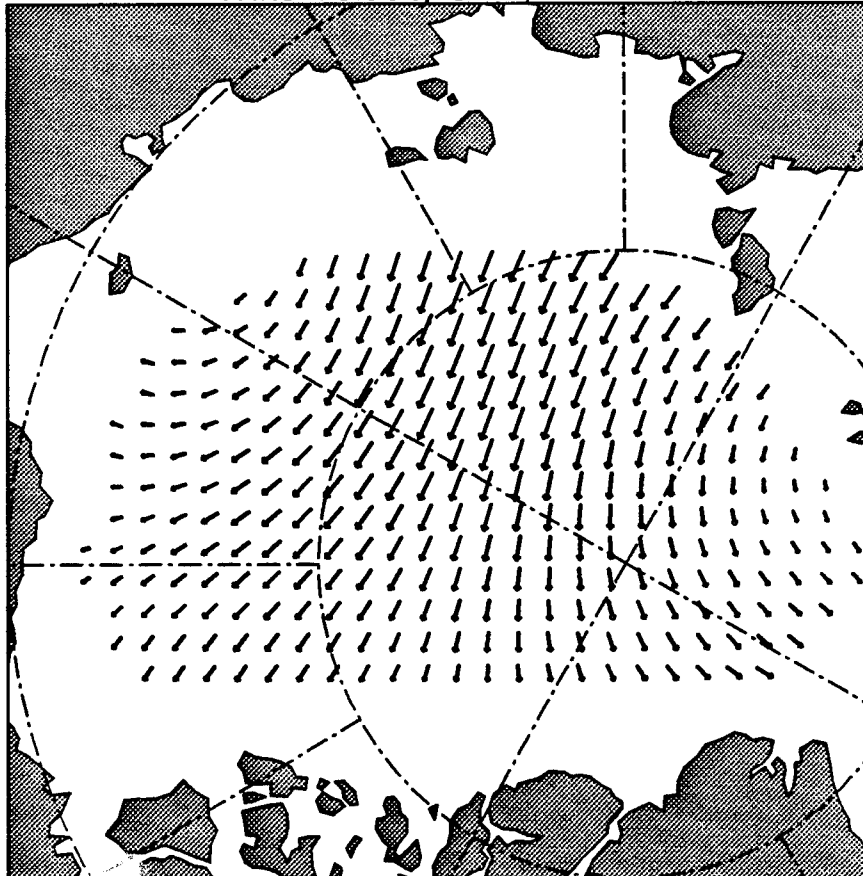
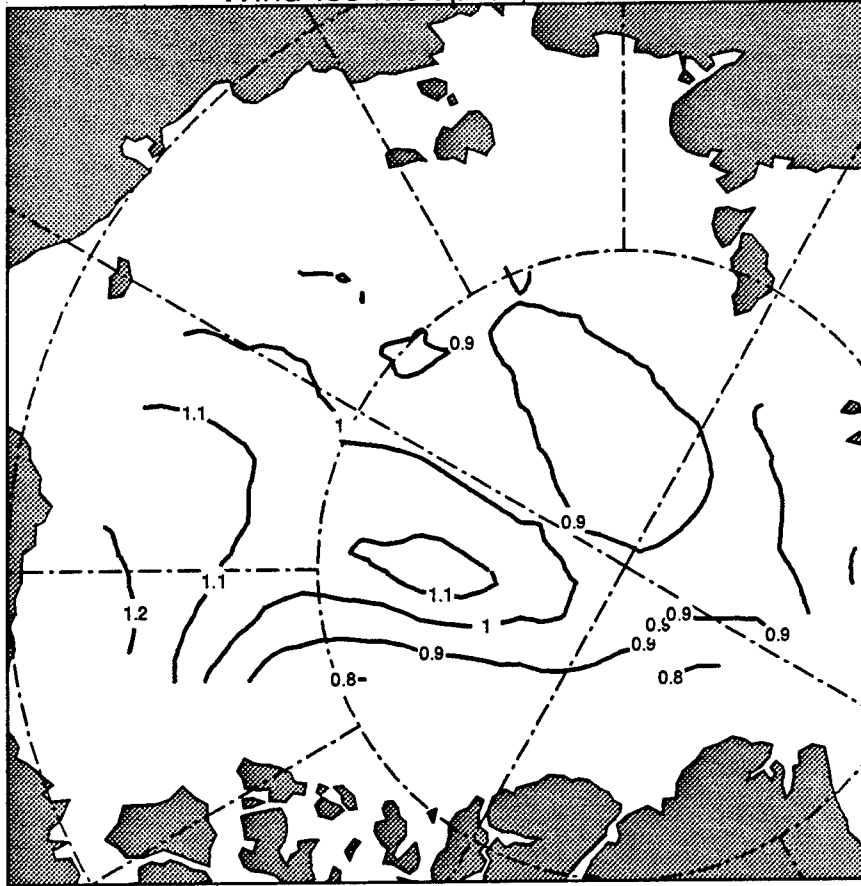


Figure 10. Pattern pairs for wind and ice motion, mode 3.

Wind-Ice Multiplier, Mode 1



Turning Angle, Mode 1

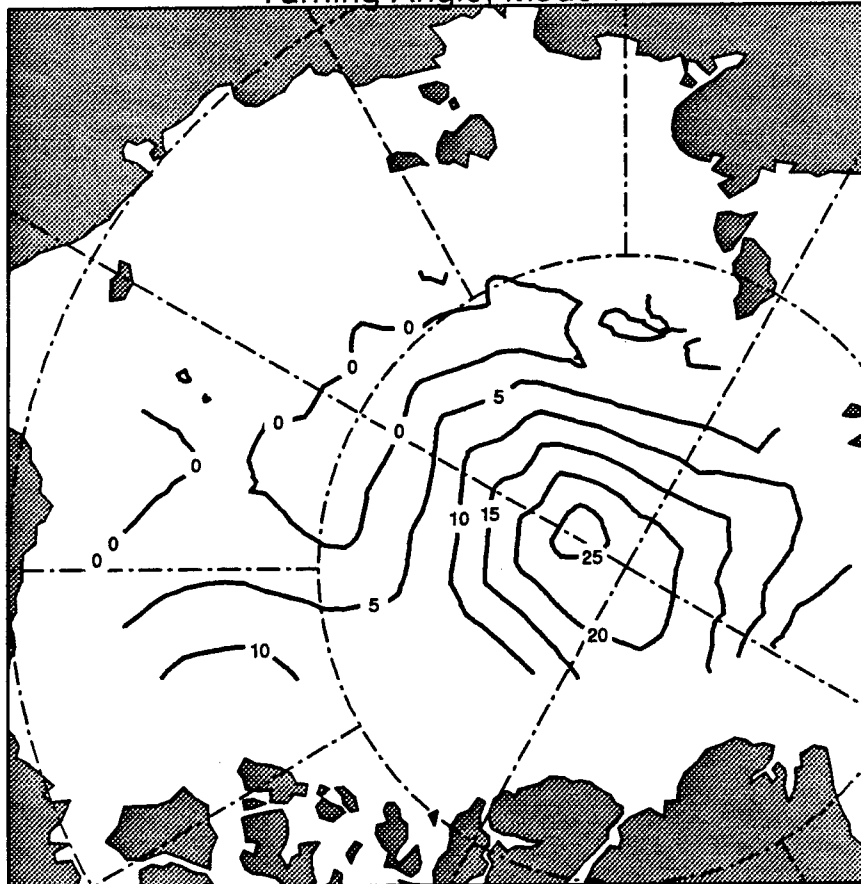
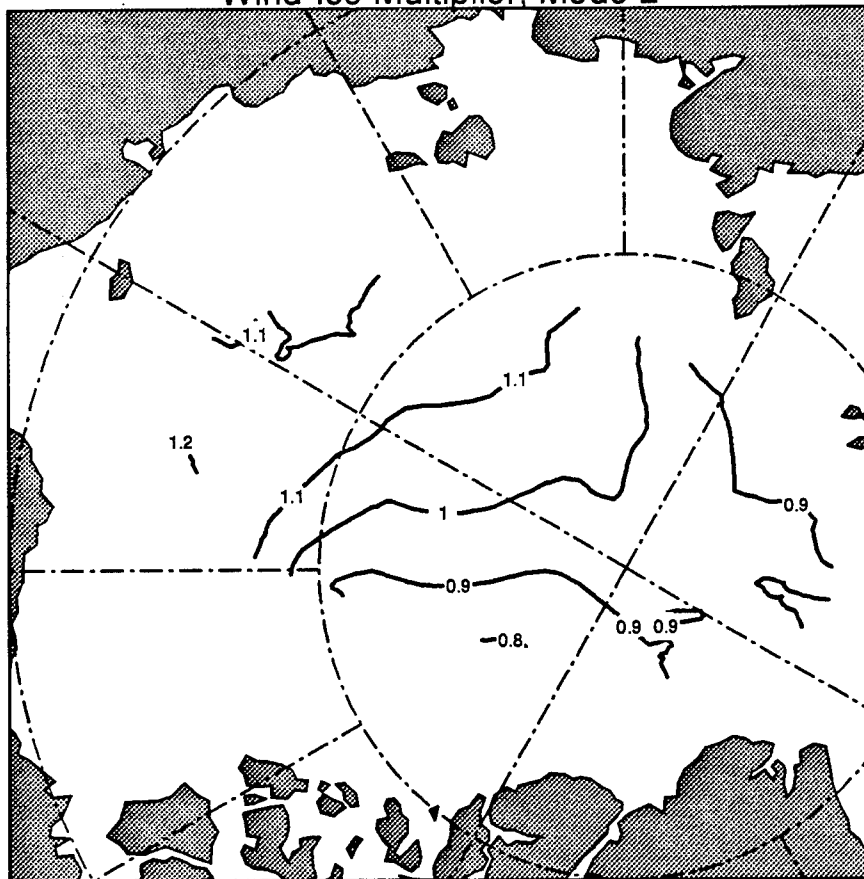


Figure 3a. Interpretation as $U = AG$ for Mode 1.

Wind-Ice Multiplier, Mode 2



Turning Angle, Mode 2

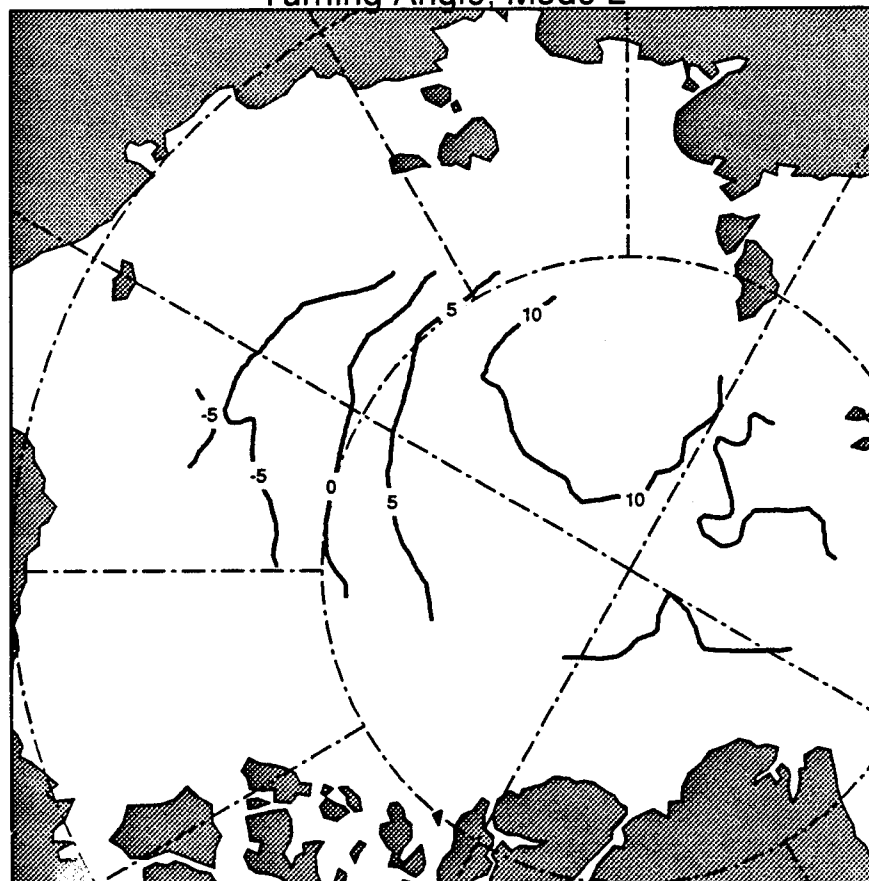
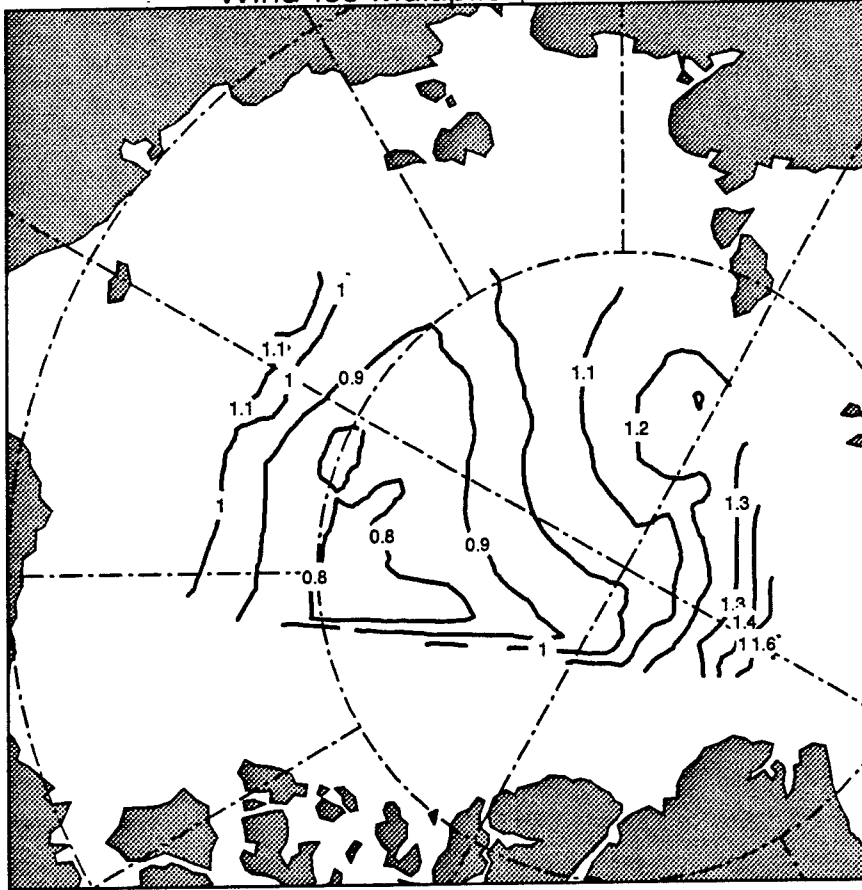


Figure 3b. Interpretation as $U = AG$ for Mode 2.

Wind-Ice Multiplier, Mode 3



Turning Angle, Mode 3

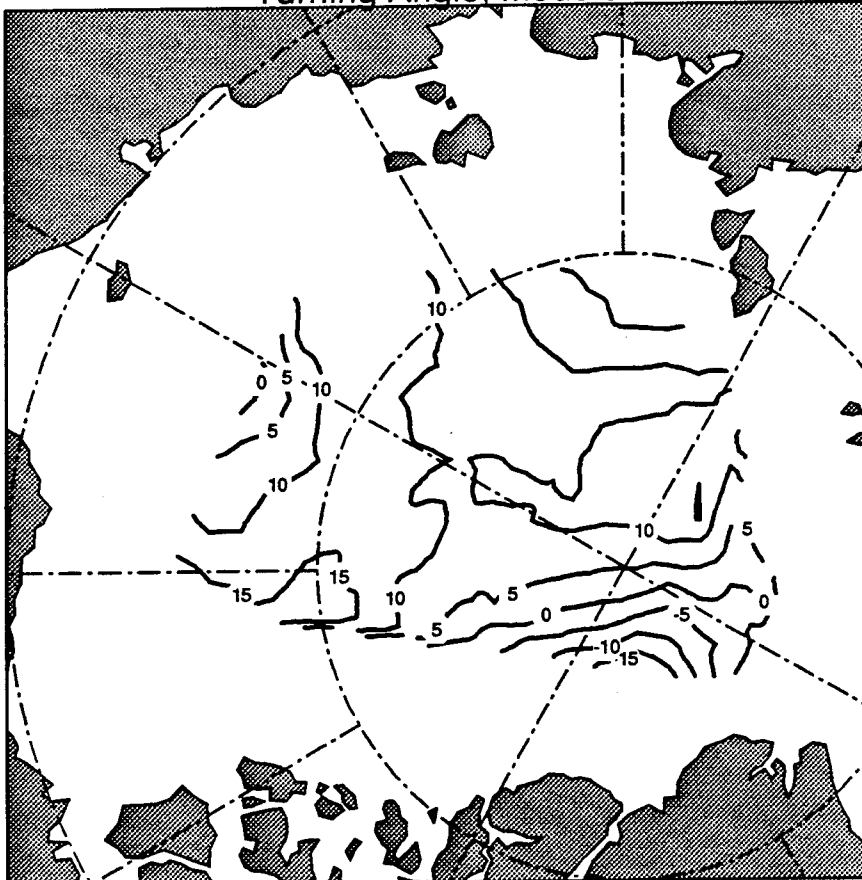


Figure 3c. Interpretation as $U = AG$ for Mode 3.

SVD Velocity - Geostrophic Wind, Departures from Annual

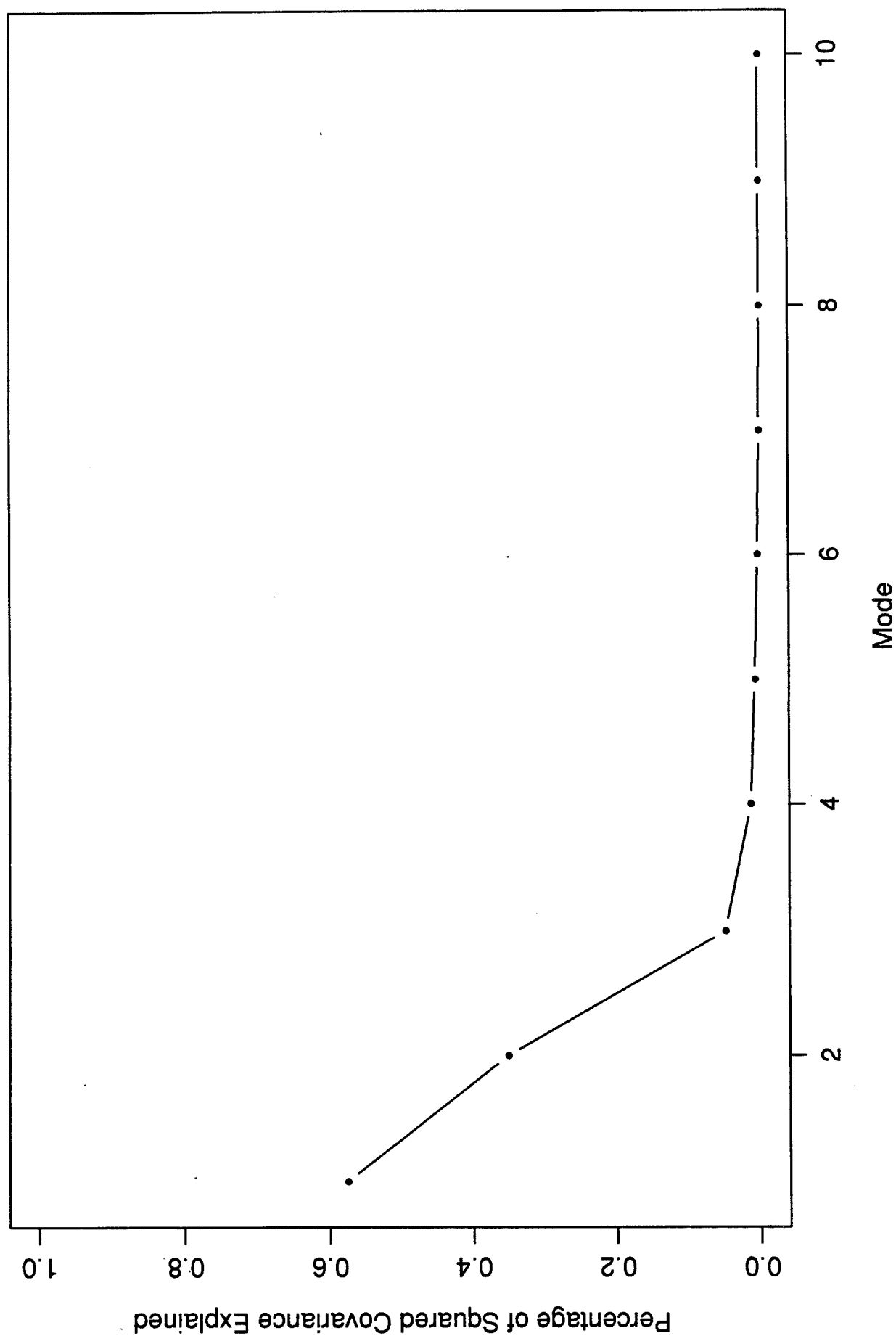


Figure 4. Scalar multiplier ALPHA, modes 1, 2, and 3.

SVD, Multiplier U-G, mode = 1

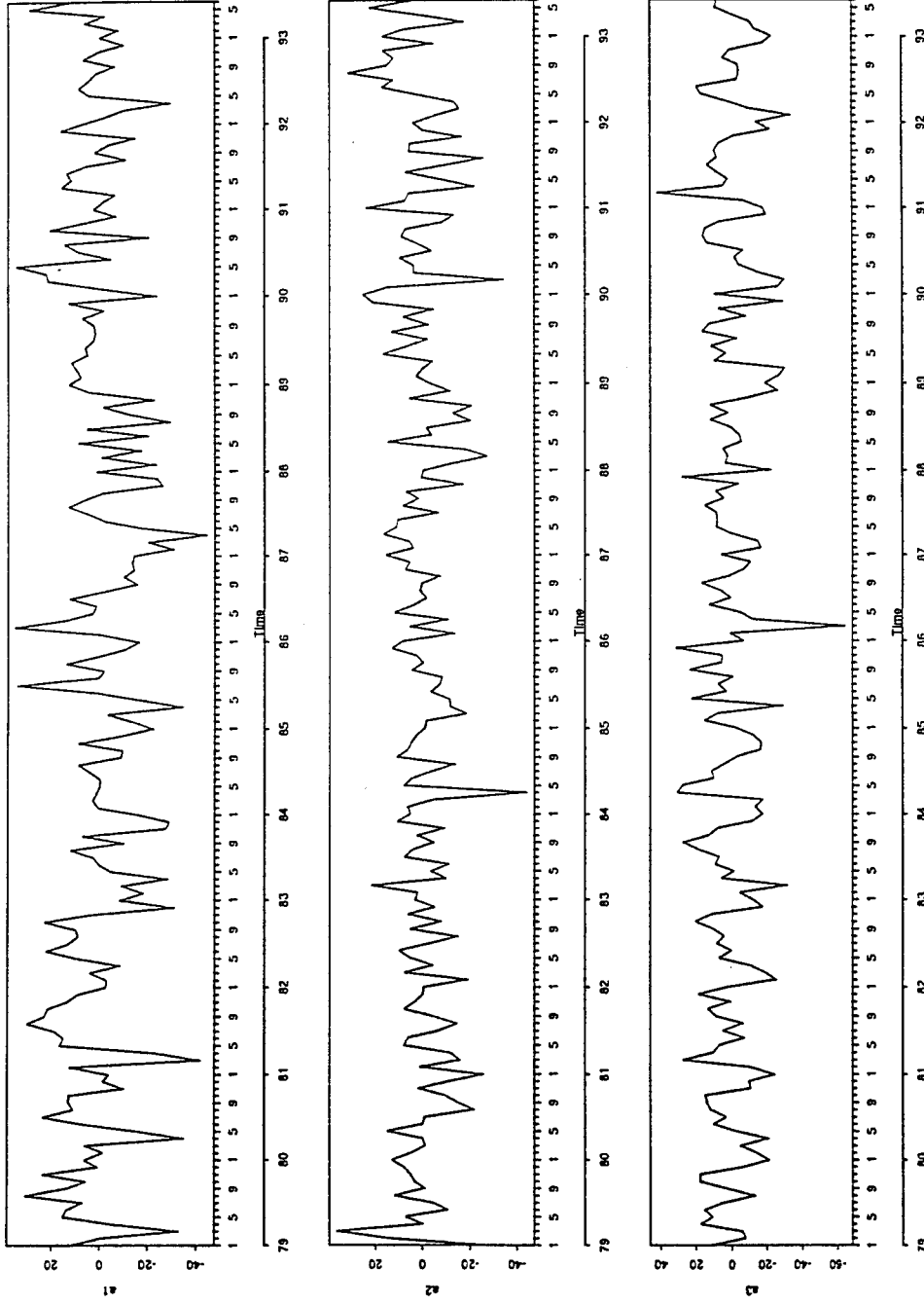


Figure 5. Time series of pattern multiplier, modes 1, 2, and 3.

1992 SVD, Multiplier U-G, mode = 1, Departures From Monthly Means

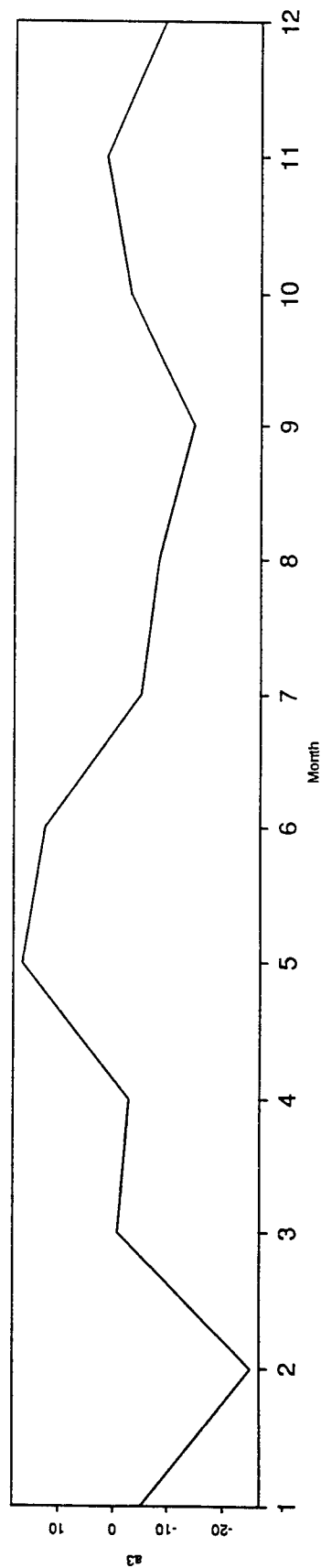
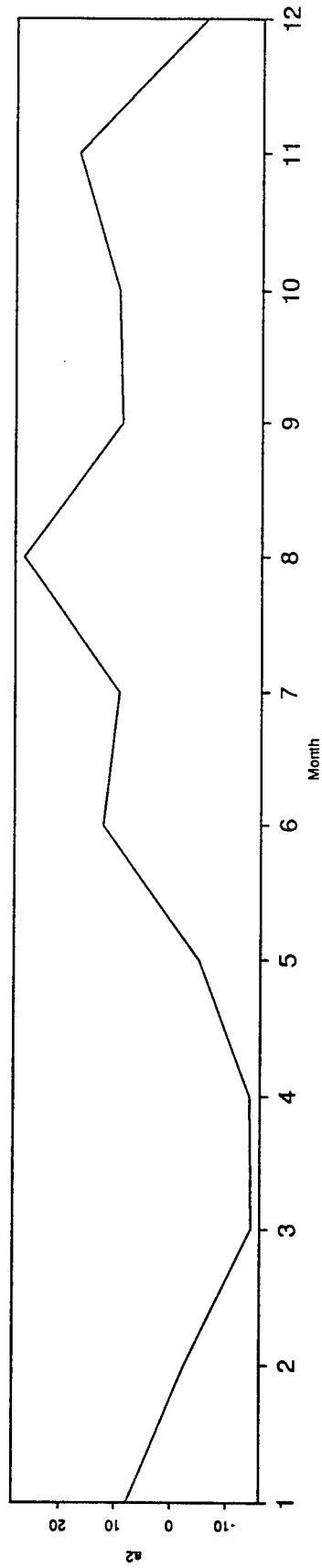
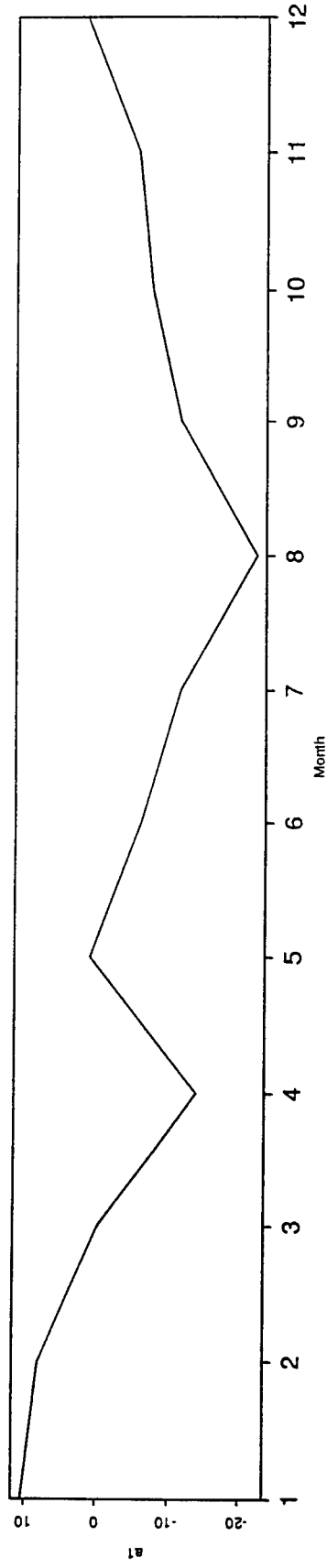


Figure 6.

Thu May 19 10:50:15 PDT 1994

CONCLUSIONS

WIND AND ICE MOTION ARE GLOBALLY COUPLED

Things to Do

- EOF and SVD analysis of monthly ice motion strain
- EOF and SVD analysis of microwave data
- Use monthly pressure fields 1953-1978 to synthesize ice motion fields (validate with obs from NP, DARMS, ARLIS)
- Use coastal wind-pressure data 1920's - 1990 to synthesize ice motion fields
- Investigate systematic differences between wind driven patterns and obs. patterns
- Investigate coastal regions - Fram Strait
- Spectral analysis of $A(t)$, $B(t)$ (predictability)

Russian Historical Ice Charts and Dataset 1967-1990

Ignatius Rigor

Russian Historical Ice Chart Dataset, 1967 - 1990

Analysis of ice conditions for the arctic regions have been prepared to support high latitude sealing and whaling activities since the 17th century. These early charts documented the position of the ice edge, conditions within the ice pack, and access to arctic ports. Ice charts for specific regions of the Arctic Basin began to be routinely prepared in the 1940's in support of commercial and military requirements. Presently, operational ice charts for the arctic are prepared at the Arctic and Antarctic Research Institute (AARI), the US National Ice Center (NIC), and the Norwegian Meteorological Institute.

Modern analyses of ice conditions are based on a combination of observations, ice feature persistence, mathematical models, and climatology. The most important ingredients are the observational data-- ship and shore station reports, aerial reconnaissance, and satellite imagery. Current satellite imagery makes global ice analysis possible. Much of the earlier (1966-1972) satellite data were low resolution visual and infrared imagery limited by the polar darkness and cloud cover. In 1972 the Advanced Very High Resolution Radiometer (AVHRR) provided one km resolution in the visual; this sensor is still used in the preparation of ice charts. In 1973 the US launched the Electronically Scanning Microwave Radiometer (ESMR) which provides for all weather remote sensing capability. The Russians have placed great emphasis on active, all weather, microwave systems, such as airborne and satellite based Sideways Looking Airborne Radar (SLAR).

The Arctic and Antarctic Research Institute began preparing routine ice charts in 1947, to support shipping along the Northern Sea Route. Since 1964 AARI has prepared 10 day ice charts throughout the Arctic Basin, emphasizing the Kara, Laptev, and East Siberian Seas.

A digital form of these ice charts is available as a sea-ice dataset in Sea-ice Data in Digital Form (SIGRID) format. The Commission for Marine Meteorology of the World Meteorological Organization (WMO) recognized the need for a uniform data base to facilitate the archival and distribution of sea-ice data. In 1989, the WMO adopted the SIGRID format, see WMO report No 558 (19ZZ). MANUAL ON MARINE METEOROLOGICAL SERVICES,--- The SIGRID format was adopted, in part, because it was able to focus on conventional sea-ice variables while accommodating flexibility. SIGRID data are encoded on a geographical grid. For the above marginal seas, the standard resolution is 1/4 degree of latitude and 1 degree of longitude north of 75N latitude and 1/4 degree of latitude and 1/2 degree of longitude south of 75N. In the Laptev Sea, for instance, this amounts to about 1200 grid points.

For each grid point the sea-ice variables are divided into ten categories. Each data category may contain specific and detailed information, or it may be flagged as containing no reported data. Most of the information in the AARI SIGRID charts is found in the concentration/stage/form category. This information includes total ice concentration and partial concentration, stage, and form of the three thickest ice types. The encoded form information includes floe size estimates, bands and patches of ice, and fast ice.

SIGRID Sea-Ice categories:

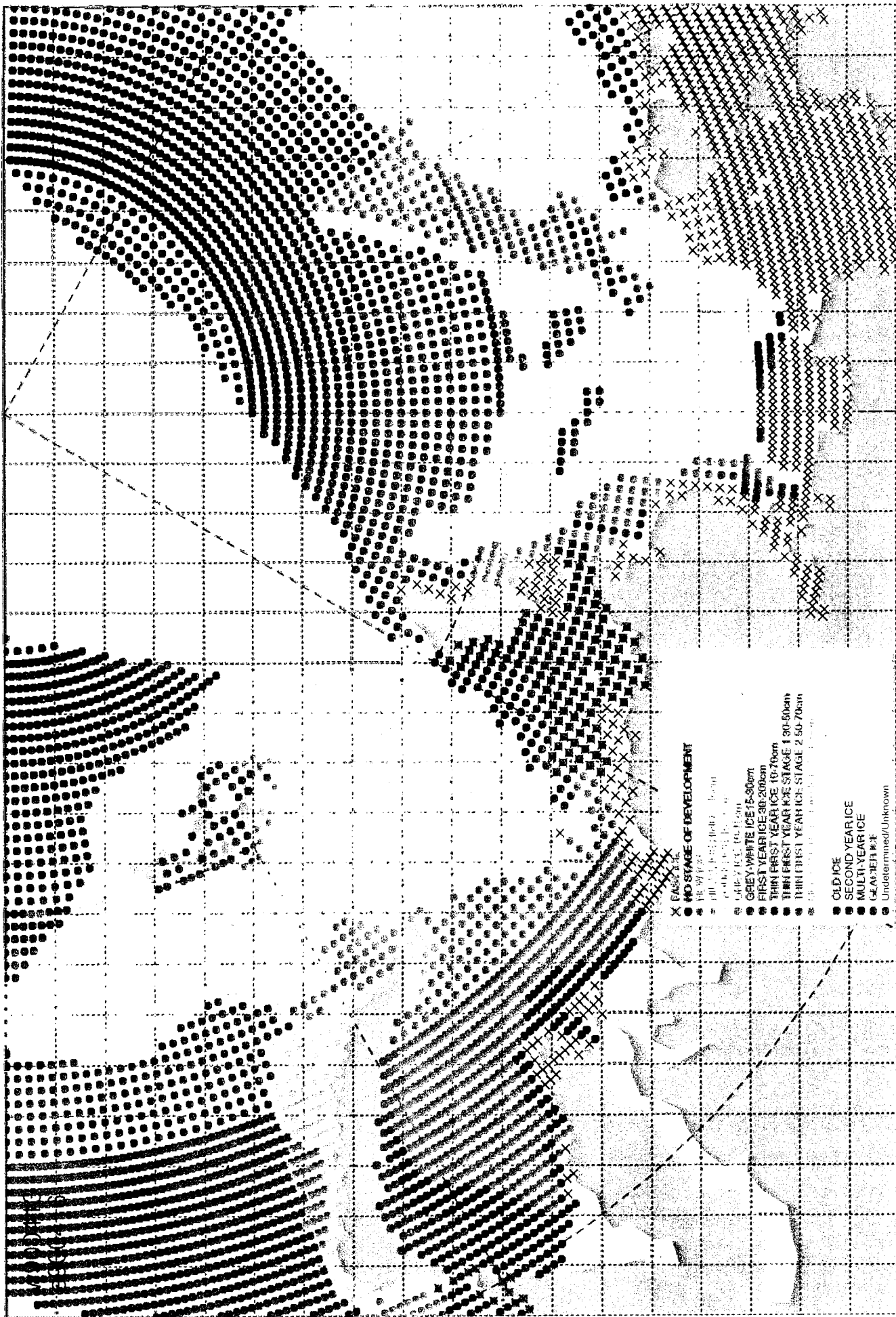
- concentration, stage of development, and form of ice
- dynamic processes
- water openings
- topography features
- thickness of ice
- surface features and melting forms
- icebergs or ice of land origin
- sea-surface temperature
- source of information on which chart is based
- land area

Concentration / Stage / Form category.

This information includes total ice concentration and partial concentration, stage, and form of the three thickest ice types.

Stage of development is coded as:

- open water
- new ice
- nilas, ice rind < 10 cm
- young ice 10-30 cm
- grey ice 10-15 cm
- grey-white ice 15-30 cm
- first year ice 30-200 cm
- thin first year ice 30 70 cm
- thin first year stage 130-50 cm
- thin first year stage 250-70 cm
- medium first year ice 70-120 cm
- thick first year ice > 120 cm
- old ice
- second year ice
- multiyear ice
- glacier ice
- undetermined/unknown



Transpolar Drift - The Garbage Scow from Siberia?

Erk Reimnitz

Transpolar Drift - The garbage scow from Siberia?

Erk Reimnitz, U.S. Geological Survey

A video by the dirty-ice group of the USGS demonstrates drift-ice related processes on the shallow shelf and in the coastal zone. That work has shown that the classic fast-ice entrainment mechanisms: aeolian deposition, river flooding, slumping from coastal cliffs, bottom adfreezing, and ice plowing, are insignificant compared to the mechanism of suspension freezing in supercooled water. That mechanism is most effective on shallow, circum-Arctic shelves landward of the 30-m isobath (Figure 1). Comparing sediments in sea ice of the Beaufort Gyre (Figure 1) to those of the bordering <30-m deep shelf surface to assess sorting by entrainment, we find them much finer (10% vs. 48% sand), having a much higher organic carbon content, and lower carbonate content than those of the source surface. Clay mineral composition and lithology of sand grains do not show differences that suggest suspension freezing is selective. No data are available about radio-nuclide entrainment, but we may assume an affinity for fine particulate and organic matter.

In the Beaufort Gyre off North America, sediment loads are highly variable, ranging upward to over 1,000 tonnes/km², depending on whether the necessary strong, freezing winds occurred during the generally short open-water period in late fall. The loads can be much higher than the sediment supply from local rivers feeding the area, and therefore lead to shelf erosion. To emphasize the importance of sediment transport by sea ice for the Arctic Ocean sediment budget we compare the above sediment load in sea ice to the low annual denudation rate of about 10 tonnes/km² on continents surrounding the basin. In years between such sediment pulses spaced 5 to 10 yrs apart, the ice of the Beaufort Gyre has been observed and measured to be very clean.

In the Laptev Sea of Siberia, which is dominated by a major, perennial polynya (Figure 2), conditions for suspension freezing to occur apparently are met yearly, resulting in a rather continuous sediment flux to Fram Strait and the North Atlantic. Very preliminary calculations of sediment flux in sea ice actually exported from the Laptev Sea are in the same order of magnitude as sediment supply by the Lena River feeding it.

Very little is known about pollutants in Arctic pack ice. Many mud samples collected from sea ice by the USGS in different expeditions to the Beaufort Gyre and the Siberian Branch of the Transpolar Drift over the last 5 years are undergoing sedimentological, mineralogical, and paleontological investigations. These samples are also being compared to surficial deposits in the deep basins. Portions of 26 of these valuable samples (Figure 3) were originally offered to the ONR program for radio nuclide analyses, but are presently being analyzed through funding from other sources.

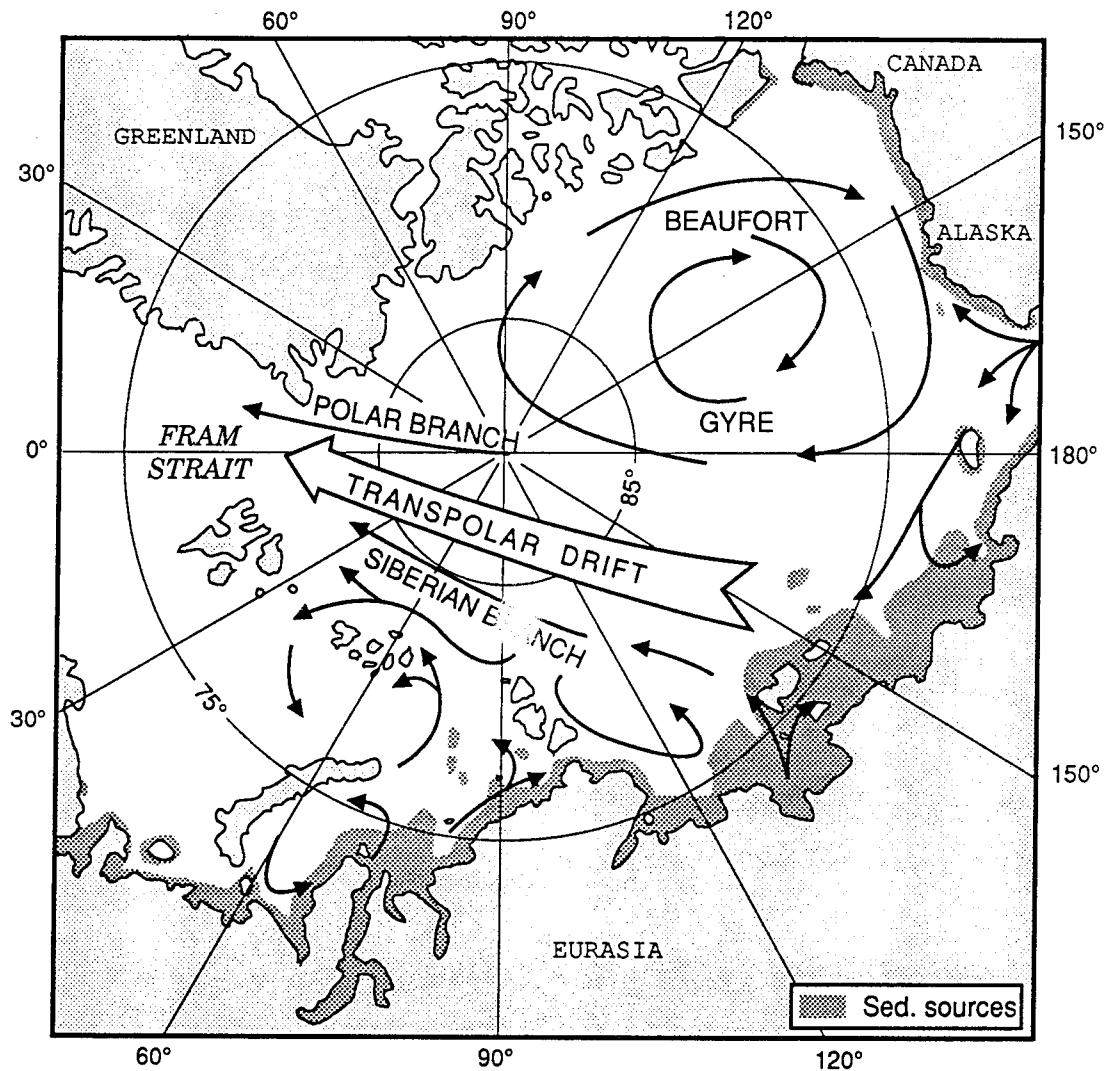


Figure 1.- Generalized Arctic Ocean ice circulation pattern, showing the sediment sources on shelf areas <30 m deep.

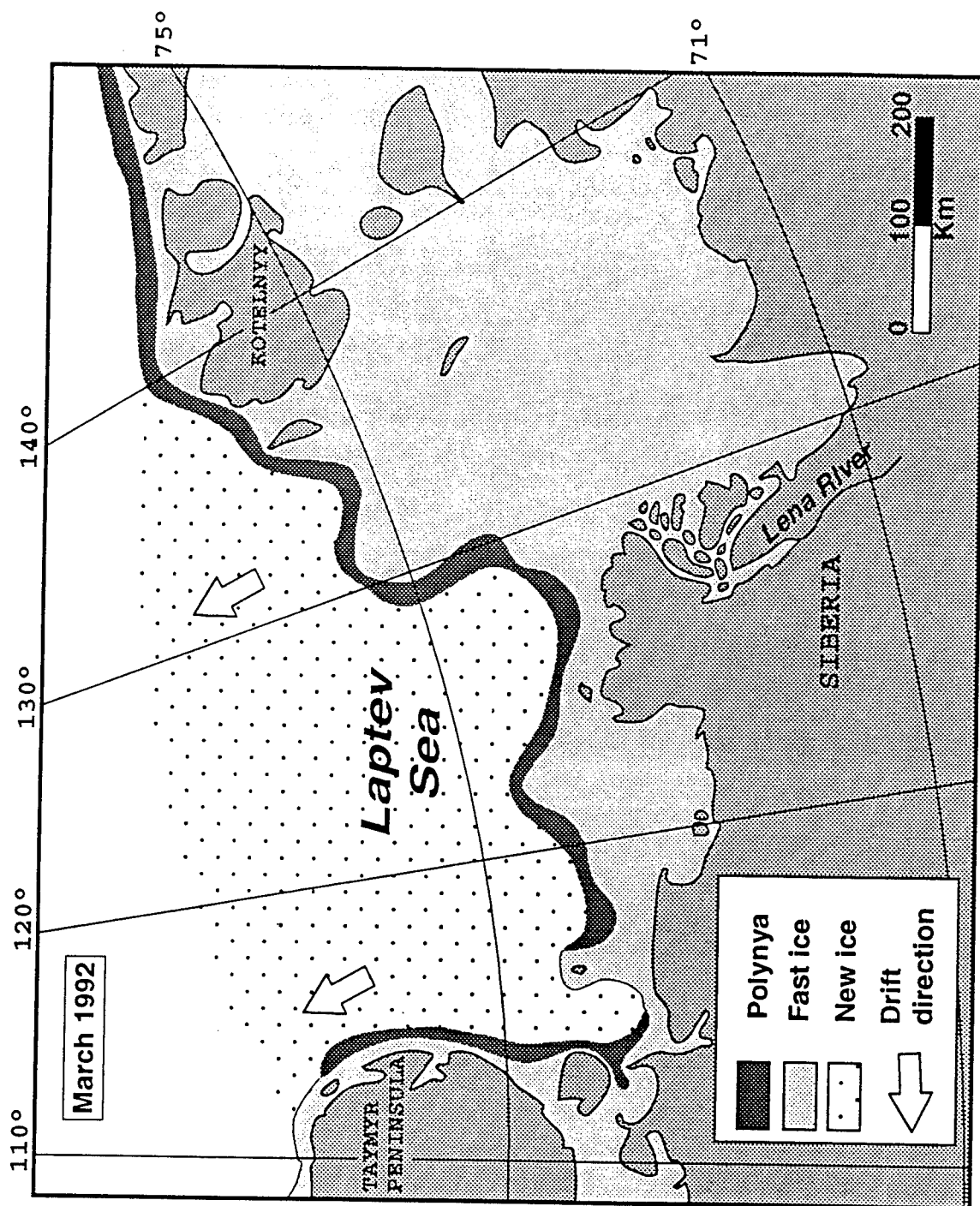


Figure 2. - The fast ice and perennial flaw lead with ice thinner than 15 cm as mapped for the period March 20 to 24, 1992 by the Arctic and Antarctic Research Institute in St. Petersburg.

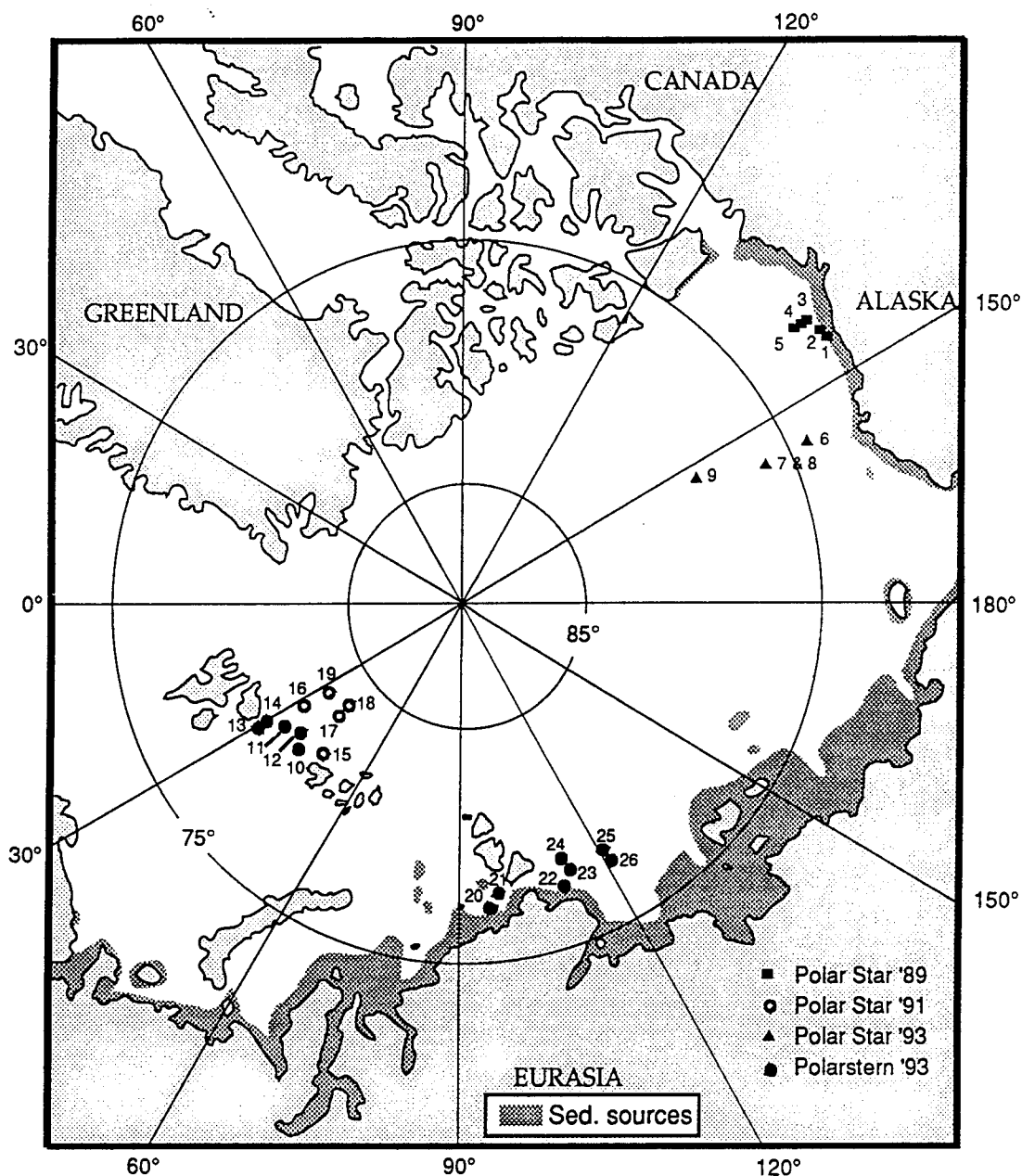


Figure 3. - Locations of 26 mud samples collected from pack ice by the U.S.G.S. from different ships during a 4-year time span, and presently being analyzed for radio nuclide contamination.

Data on the Ob River System, Yenisei River System and Kara Sea Region

Peter Becker

Data on the Ob River System, Yenisei River System and Kara Sea Region:

What we have, don't have... and need.

Peter Becker

CCPO, Old Dominion University, Norfolk, Virginia

Abstract

At the outset we were concerned that a dearth of actual field data on the Ob and Yenisei Rivers and Kara Sea would limit our ability to establish baseline values for the various parameters necessary to help model the transport of radionuclides by the large Arctic rivers to the Kara Sea and Arctic Ocean. Instead we find that there are both many different data sets and a rich literature to assist us and that much is in english or english translation.

These data sets include, but are not limited to:

- Drift Bouy
- Hydrographic
- Hydrological
- Meteorological
- Radionuclide Surveys
- Tidal Constants

The Drift Buoy data encompass both US and Russian sets (eg. Fig. 1a,b with two of the Russian sets indicated by I's in the Kara Sea.)

The Hydrographic data sets include US icebreaker cruises in 1965 and 1967. Other data sets include:

- Ostlünd et al. (Tritium)
- Anderson et al. (salinity/temperature/etc. ODEN data)
- Schlosser et al. (^{18}O /Salinity; ^3H :He ARKTICA-IV Data)
- Gloersen et al. (Seaice passive microwave 1978-1987)
- Wallace et al. (CFC's)

The Hydrological and Meteorological and Radionuclide data sets include Russian data through 1992 at stations in Figure 2,

Tidal constants are available for all the stations in Figure 3 as well as 200 other stations about the Arctic.

A Bibliography of over 600 citations has been compiled and placed along with all open data sets in a anonymous FTP archive at:

<ftp.ccpo.odu.edu/cd/pub/becker/IAEA>

The Bibliography contains all of the relevant translated Russian Literature citations from:

- Oceanology
- Problems of the North
- Soviet Hydrology
- Soviet Geography
- Soviet Geology and Geophysics
- Water Resources

as well as:

- Annual Review of Energy
- Health Physics
- J.G.R.
- J.P.O.
- Deep Sea Research
- Others...

The literature citations cover a range of topics as seen in Figure 4.

Intensive Russian studies of the Kara Sea resulted from the economic necessity of predicting the ice conditions on the Northern Sea Route (Figure 5) and resulted in numerous expeditions starting before 1928 and covering the entire Arctic Ocean. This included ice stations (Figure 6) and numerical circulation models (Figure 7). and coastal observations (Figure 8).

The literature also includes citations on the effect of anthropogenic influences on the river discharge of the Ob and Yenisei (Figure 9)

We have recently succeeded in obtaining higher resolution data sets for the Ob and Yenisei Rivers including the following:

- Hydrographic Data
- Hydrologic Data
- Kara Sea
- Ob River
- Radioisotopes
- Suspended Sediments
- Yenisei River

These data sets will assist in improving our understanding of the Ob and Yenisei river transports and their interaction with the Kara Sea and Arctic Ocean.

In conclusion:

- Data on hand is extensive at mean monthly time and basin size scales.
- Data on hand is now adequate to resolve short term flow (≤ 30 days) and storms.
- Data on hand is inadequate to resolve features of estuary stratification.
More data is needed but it is available.
- Radionuclide data available do not yet fully resolve nuclide transfer from river to estuary to ocean.
- Impact of reservoirs is significant and must be built into models.

1 Acknowledgements

The author wishes to thank the ONR Arctic Nuclear Waste Assessment Program for support in conducting this program.

2 References

Avakyan, A. B., Reservoirs of the USSR and tasks of their investigations, *Water Resources*, 6, 538-549, 1988.

Björk, G., A one dimensional time-dependent model for the vertical stratification of the upper Arctic Ocean, *J. Phys. Oceanogr.*, 19, 522-67, 1989.

Björk, G., The vertical distribution of nutrients and oxygen 18 in the upper Arctic Ocean, *J. Geophys. Res.*, 95, 11407-1422, 1990.

Gudkovich, A. M. and Ye.G. Nikiforov Some Important Features of the Formation of Water density Anomalies and Their Effect on Ice and Hydrological Conditions in the Arctic Basin and Marginal Seas

Oceanology, 5 , 2, 49-57, 1965.

Östlund, H.G., and G. Hut, Arctic Ocean water mass balance from isotope data, *J. Geophys. Res.*, 89, 6373-6381, 1984.

Östlund, H.G., and C. Grall, *Arctic Tritium: 1973 - 1991*, Tritium Laboratory Data Report No. 19, R.S.M.A.S. University of Miami, Miami, 1993.

Schlosser, P., D. Grabitz, R. Fairbanks and G. Bönisch, Arctic river-runoff: mean residence time on the shelves and in the halocline, submitted *Deep-Sea Res.* 1993.

Treshnikov, A. F. and G. I. Baranov; *Water circulation in the Arctic Basin*, Translation by: Israel Program for Scientific Translations, Jerusalem, 1973; Hydrometeorological Data Service, Leningrad, 1972, p145.

Arctic Ocean Buoy Program Data Report for 1 January 1986 – 31 December 1986

by Roger L. Colony and Ignatius Rigor

Technical Memorandum

APL-UW TM 6-89

April 1989



Applied Physics Laboratory University of Washington
1013 NE 40th Street Seattle, Washington 98105-6698

Figure 1 b

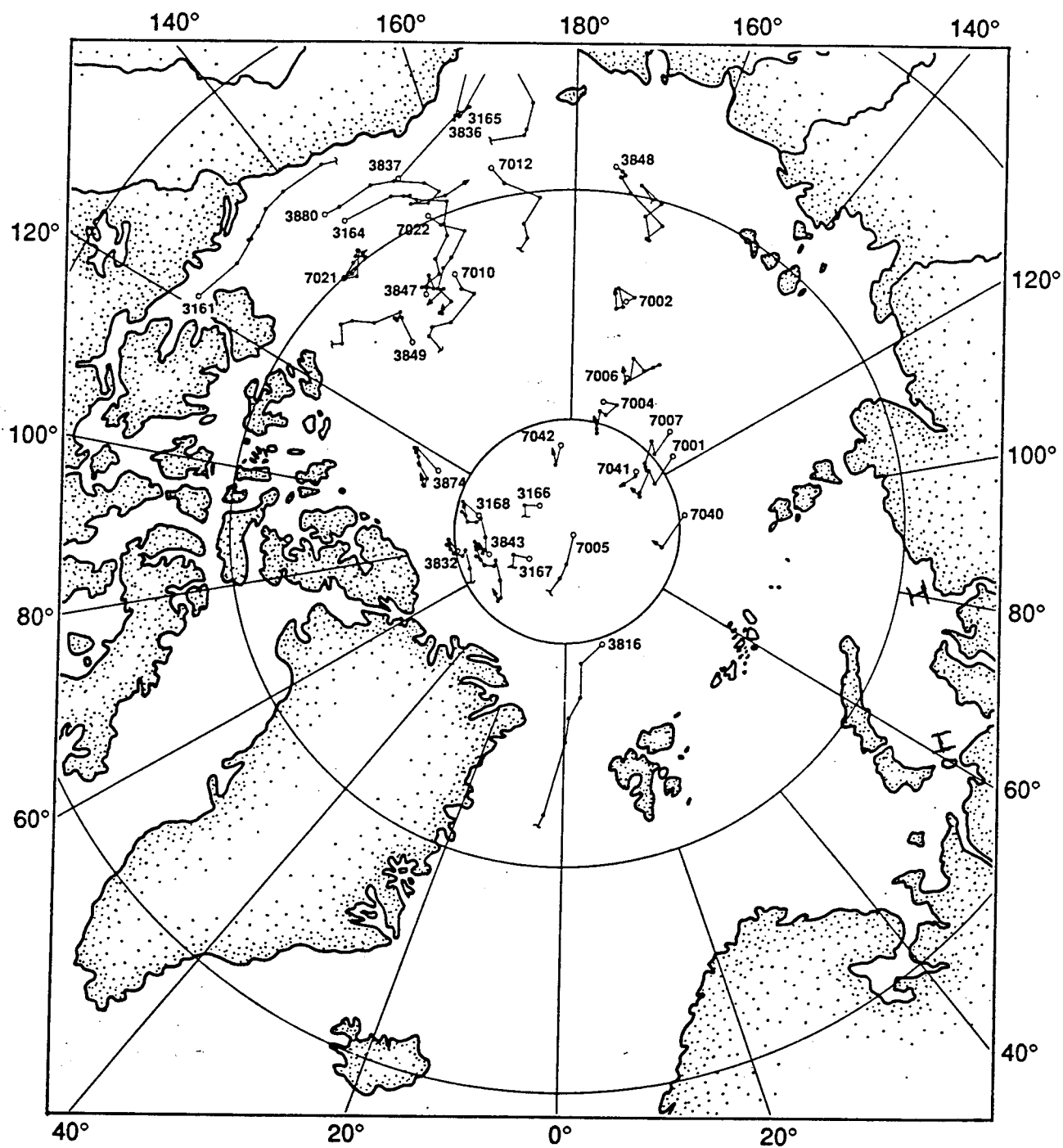


Figure 2

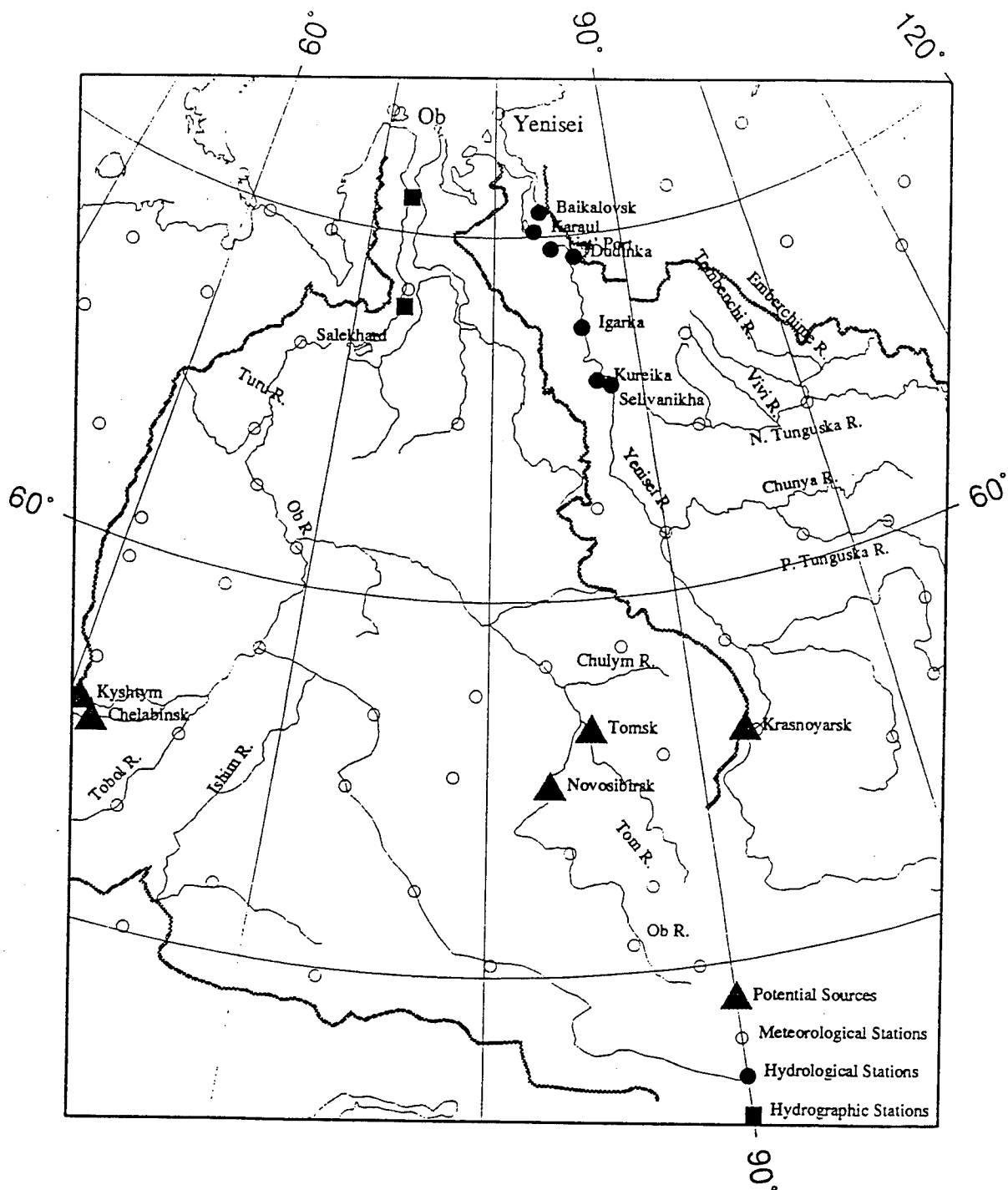


Figure 1. Map of the Ob and Yenisei Rivers and their watersheds. The hatched lines denote the watershed boundaries. Potential sources of radionuclide contaminants are marked with triangles. Many of the meteorological, hydrological, and hydrographic stations that are being used in the riverine modeling are shown.

Figure 3

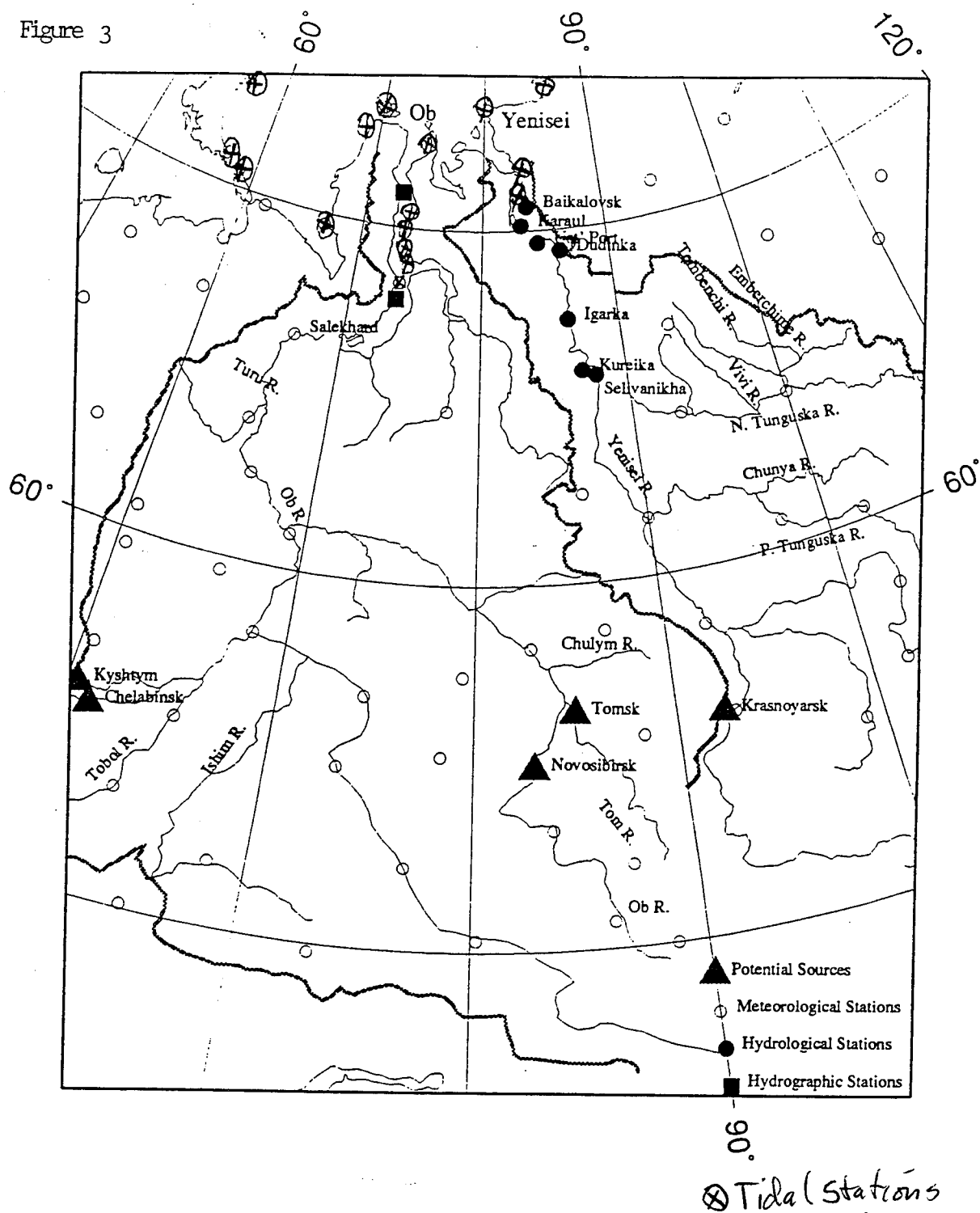


Figure 1. Map of the Ob and Yenisei Rivers and their watersheds. The hatched lines denote the watershed boundaries. Potential sources of radionuclide contaminants are marked with triangles. Many of the meteorological, hydrological, and hydrographic stations that are being used in the riverine modeling are shown.

Literature Sets:

- Estuaries
- Freshwater Ice
- Geology
- Ground Water
- Interannual Variation
 - Kara Sea
 - Lena River
 - Miscellaneous
 - Ob River
 - Permafrost
 - Radioisotopes
 - River Models
 - Sea Ice
- Suspended Sediments
 - Yenisei River

Figure 5

Map 3.1 The Northern searoute

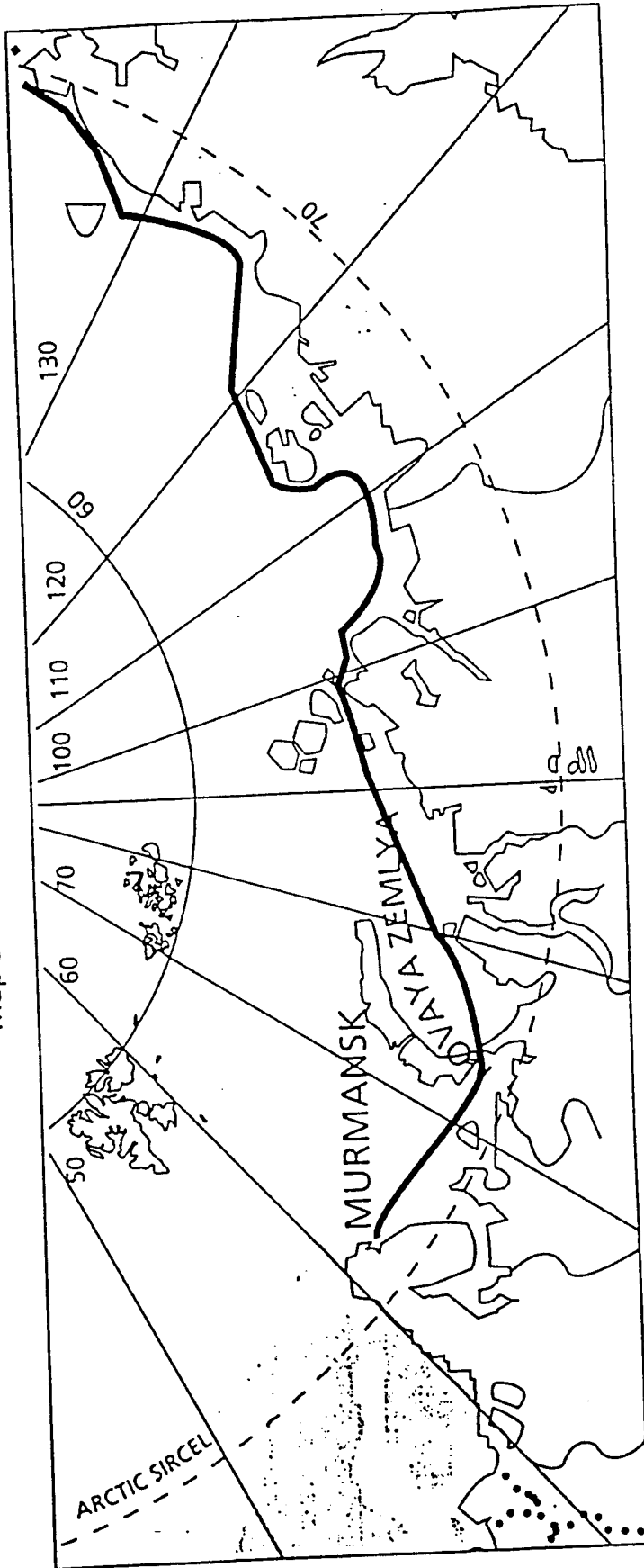


Figure 6

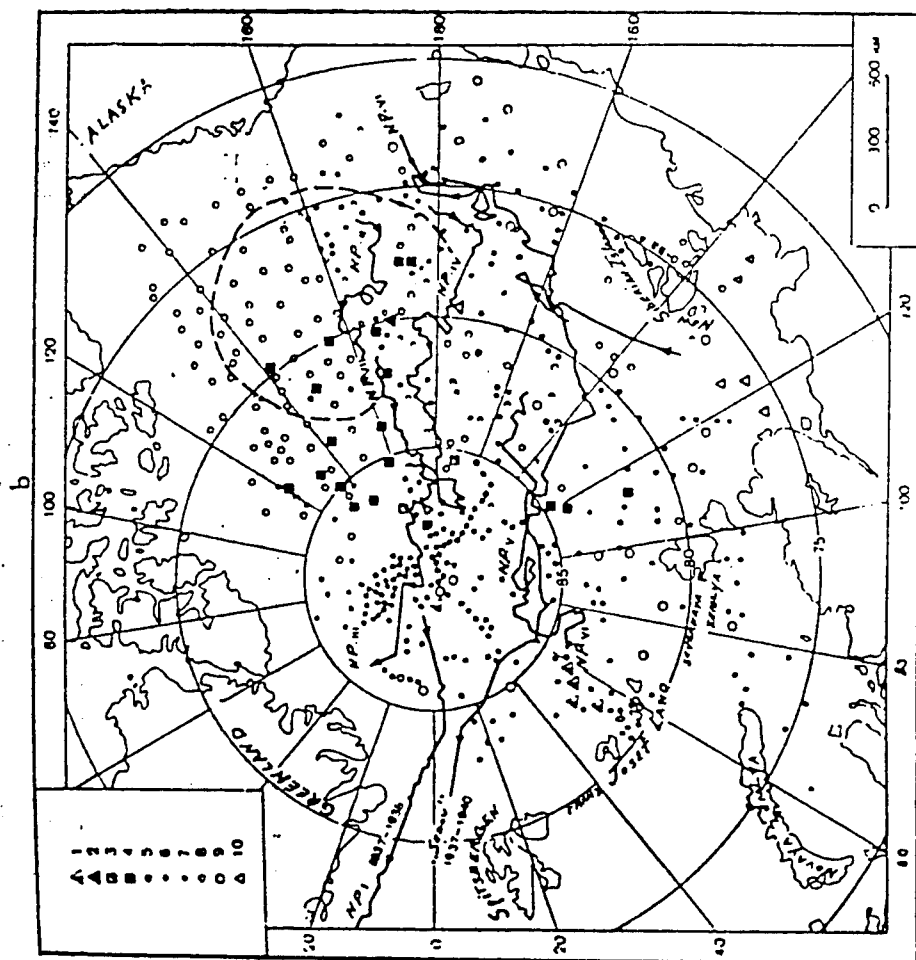


Fig. 1

Comparative density of points where regular meteorological, aerological and hydrological observations were made at the time of the Second International Polar Year (a) and in recent years (b):

1. - 1937 expedition; 2. - 1941 exp.; 3. - 1948 exp.; 4. - 1949 exp.; 5. - 1950 exp.; 6. - 1954 exp.; 7. - 1955 exp.; 8. - 1956 exp.; 9. - drifting radio beacons; 10. - stations operating from seaplanes in 1950

(after Dzerdevskii, 1959)

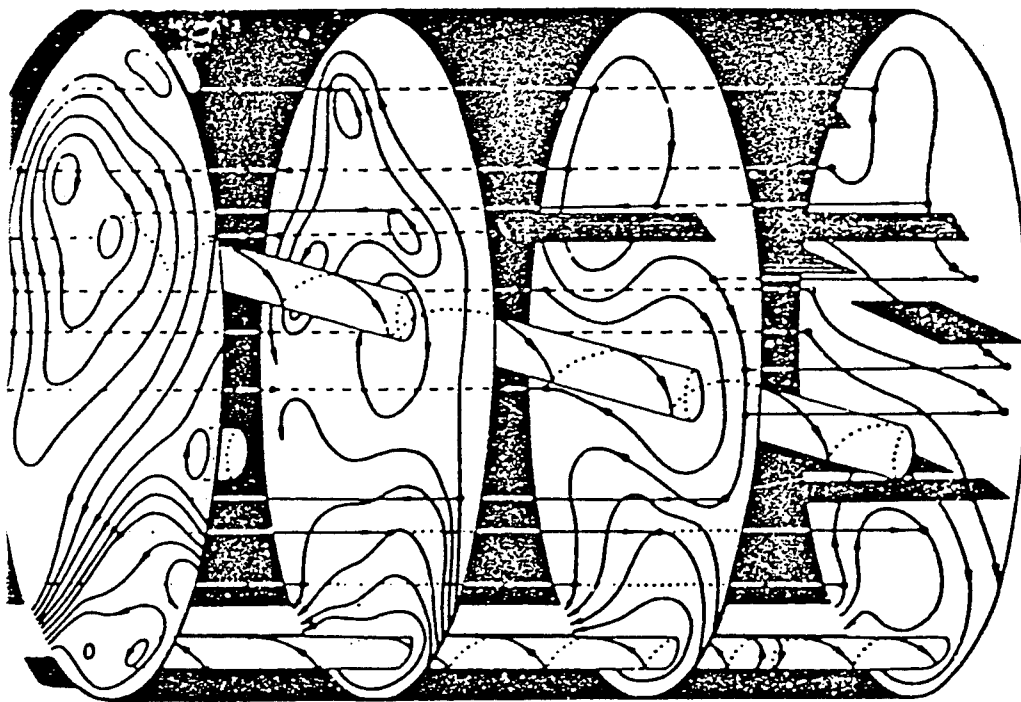
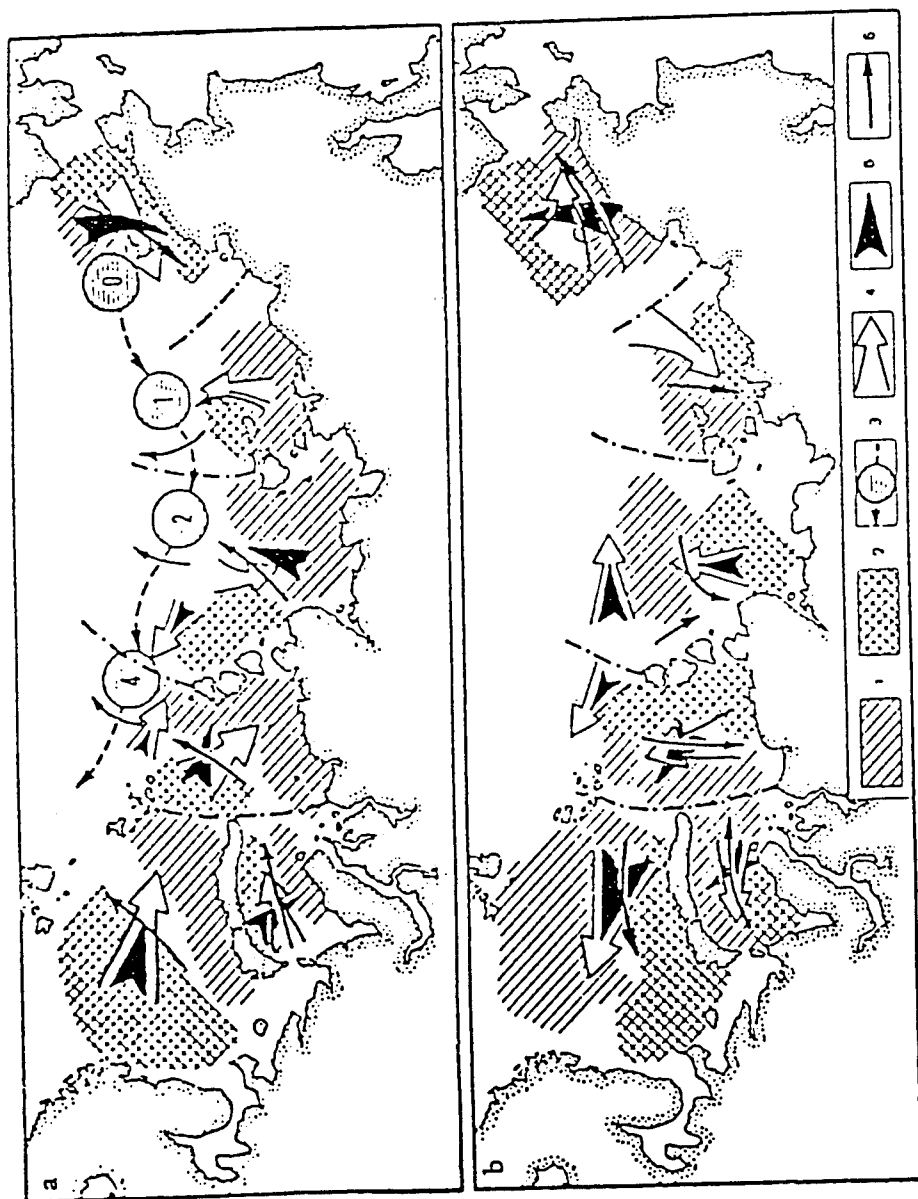


FIGURE 17. Three-dimensional structure of water circulation in the Arctic Basin.

(after Treshnikov and Baranov, 1972)

Figure 8



Basic outline of the formation of water density anomalies in Arctic seas: a) anomalies conducive to subsequent improvement of ice conditions, b) anomalies conducive to the formation of more severe ice conditions. The arrows denote the directions of spring-summer (4) and the following autumn (5) air transport, and also the components of currents and ice drift (2) produced by the distribution of the negative (1) and positive (2) water density anomalies. Diagram of the displacement of density anomalies from the Wrangel area (3) (the figures in circles give the mean duration of displacement in years).

(after Galkovich and Nikiforov, 1965)

Figure 9

Table 1. Suspended matter flux in the mouths of rivers regulated by reservoir systems [2]

System	Number of reservoirs	Average annual suspended matter discharge across the mouth, in million tons	
		prior to regulation	after regulation
Volga	7	25.9	7 - 8
Kama	2	10.0	1.3 - 1.9
Dnieper	6	2.0	0.4
Irtys	2	11.2	2.5 - 3
Yenisey	2	12.4	1.8 - 2.2
Angara	3	2.4	0.5

(after Avakyan, 1988)

Circulation of the Arctic Seas Based on Russian Sources of Information

Andrey Proshutinsky

CIRCULATION OF THE ARCTIC SEAS BASED ON RUSSIAN SOURCES OF INFORMATION

Short review of sources of information and methods of simulation of the Arctic Seas water circulation is presented. Summary currents in Arctic Seas are composed of permanent, wind-induced and tidal currents. In the Kara, East-Siberian and Chukchi Seas permanent currents are formed as a result of fresh water inflow from rivers and water exchange with adjacent areas. These currents in the Arctic Seas have a relatively stable pattern. The rate of the permanent currents is 0.1-0.3 knots in most of the Arctic Seas area. In some regions, mainly in straits and adjoining mouths of large rivers, the rate of the permanent currents increase to 0.4 - 1.2 knots.

Schemes of wind-driven currents in the surface layer of Arctic Seas for steady (i.e. lasting not less than 12 hours) northeast, southeast, southwest and northwest winds with a speed 10 m/s were published in 1992.

In the Laptev, East-Siberian and Chukchi seas, southeast wind drives a current flowing mainly northwest at a magnitude of 0.4-0.8 knots. In the Kara Sea similar wind drives a current flowing mainly northeast at the same magnitude. In Proliv Dmitriya Lapteva, Proliv Sannikova and Proliv Longa currents flow west and in Proliv Karskiye Vorota and in Bering Strait they are flow northeast. In the Bering Strait current velocity ranges from 1 to 1.2 knots. In Proliv Vil'kitskogo southeast wind drives currents flowing east and northeast at 1.3 knots.

Southwest wind drives currents flowing predominantly to the east and northeast. Current speed in the open sea ranges from 0.3 to 0.8 knots, in the Bering Strait is 1.7 knots, in Proliv Sannikova is 2.1 knots, and in Proliv Yugorskiy Shar is 2 knots. In Proliv Vil'kitskogo this wind drives a current east at 1.3 knots.

In the Laptev, East-Siberian and Chukchi seas, northwest wind drives currents flowing southeast at 0.4 to 0.6 knots. In the Kara Sea, similar wind drives currents flowing south and southwest at 0.2 to 0.5 knots. Current is south-going in Bering Strait reaching a speed of 1.1 knots.

Maximum speed of the wind currents is generally 1.5 - 2 knots, in some places reaches 2.5 to 3 knots, and may be as much as 5 to 6 knots in Proliv Matochkin Shar, Proliv Yugorskiy Shar and Proliv Matisena. Currents of such speed are usually observed during winds of 20 m/s and greater.

Tidal currents in the Arctic Seas are dominantly semidiurnal. In the narrow straits and bays they have a reverse character, i.e., they change direction every 6 hours on 180°. In the open regions of the Kara and western Laptev Seas, the spring tide velocities range from 0.4 to 0.8 knots. In the eastern Laptev and in the East-Siberian Seas, tide currents are about 0.2-0.4 knots and in the Chukchi Sea velocities range from 0.4 to 0.6 knots. In several regions of the Arctic Seas tidal currents reach extremum and have velocities of over 1.5 - 2 knots. For example, measurements show velocities of 1.5-1.8 knots in the Baidaratskaia Bay, to the north of Belii Island, in the Obskaia Guba, and in the region of Khatanga Bay. In the straits of Karskie Vorota, Yugorskii Shar, Malygina Strait and Nordvik Bay, they reach 2-2.8 knots.

Project:

**HIGH RESOLUTION MODELING AND REMOTE SENSING
OF THE EAST-SIBERIAN SEA AND ALASKAN SHELF**

P.I. - M. Johnson, Institute of Marine Science UAF

CO-P.I. - A. Proshutinsky, Institute of Marine Science UAF
(modeling)

CO-P.I. - J. Groves, Geophysical Institute UAF
(remote sensing)

**I. CIRCULATION OF THE ARCTIC SEAS BASED ON
RUSSIAN SOURCES OF INFORMATION**

1. Sources of information
2. Observed circulation
3. Numerical models
4. Simulated circulation
5. Two-dimensional transport of pollutants
in the East-Siberian and Chukchi Seas
6. Plans

1. Objective:

The objective is to understand the coastal circulation from the Kolyma River on the eastern Siberian shelf to Pt. Barrow Alaska. The domain includes the eastern Siberian shelf, the Chukchi Sea, Bering Strait, Bering Sea and part and a section of Alaska's shelf. This region was determined to be an important part of the Arctic's circulation as it relates to the potential pathway for radionuclides or other pollutants.

2. Motivation:

Motivation stems from the hypothesis that the eastern Siberian shelf provides the boundary conditions upstream of the Chukchi Sea and Alaska's coast. Speculation is that most of the eastern Siberian shelf volume transport is in the eastward flowing Siberian Coastal Current, a narrow boundary current that roughly parallels the coastline until reaching Bering Strait. Yet the lateral extent of the Siberian Coastal Current, its alongstream coherence, and its seasonal variability are all poorly known.

3. Approach:

The dominant physical mechanisms in this region will be examined by using several 2 and 3-d models with high resolution to determine main features of the Siberian Coastal Current (buoyancy forcing due to Kolyma River discharge, wind and ice cover effects).

Sources of information:

Books:

1. Soviet Arctic, 1970
2. Treshnikov, Baranov, 1973
"Water circulation in the Arctic Basin"
3. Krutskikh B.A., 1978
"Main rules of variability of the Arctic Seas
in natural hydrologic periods"
4. Nikiforov, Shpaikher, 1980
"Roles of formation of the large-scale
variations of hydrological regime of
the Arctic Ocean"
5. Proshutinsky A.Yu., 1993
"Sea level oscillations of the Arctic Ocean"

Journals:

Proceedings of the Arctic and Antarctic Research
Institute (AARI). (about 300 volumes)

Problems of the Arctic and Antarctic
(about 100 volumes)

Meteorogiia i Gidrologia (Meteorology
and Hydrology)

Oceanologiia (Oceanography)

Atlases:

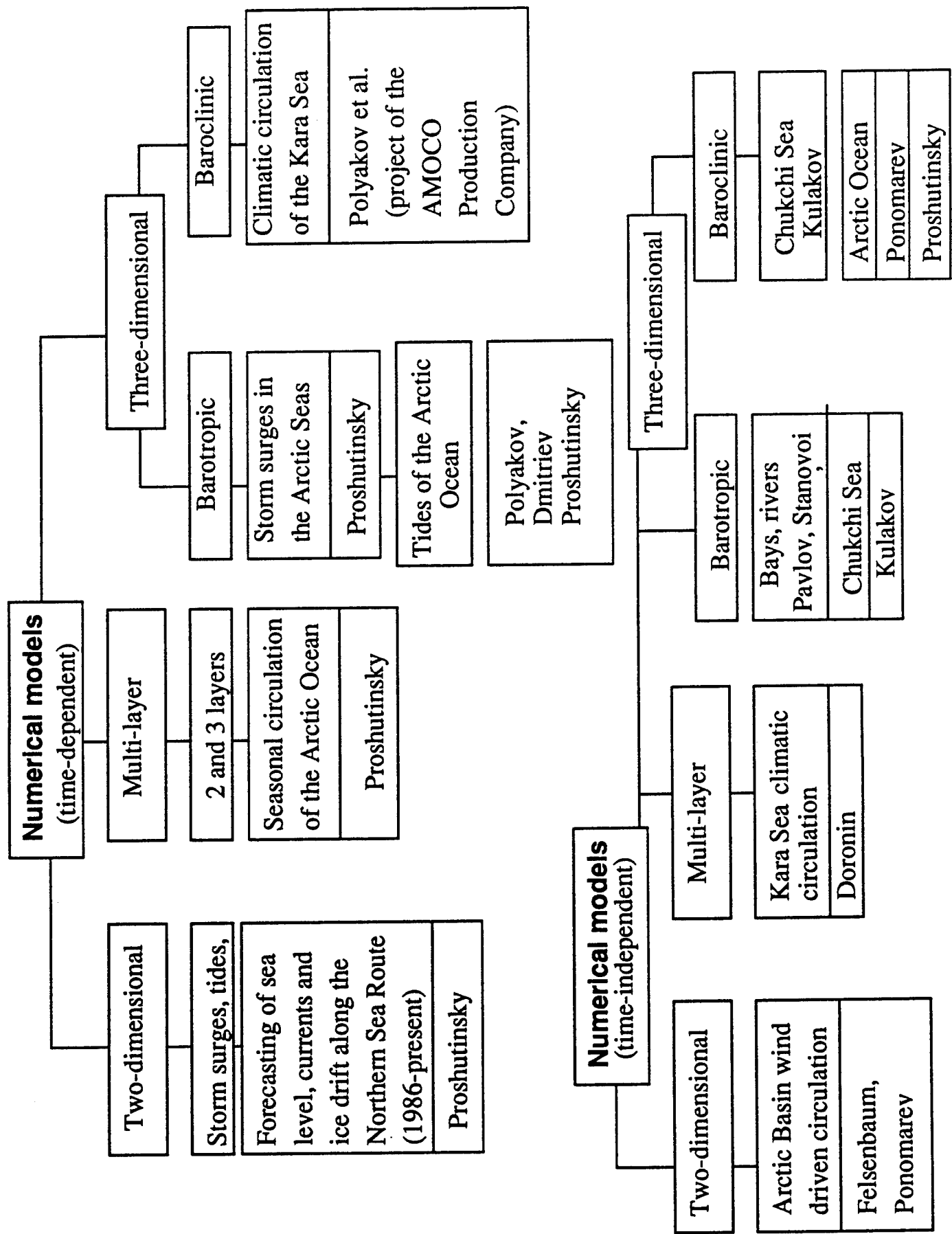
1. Atlas of the Arctic, 1985

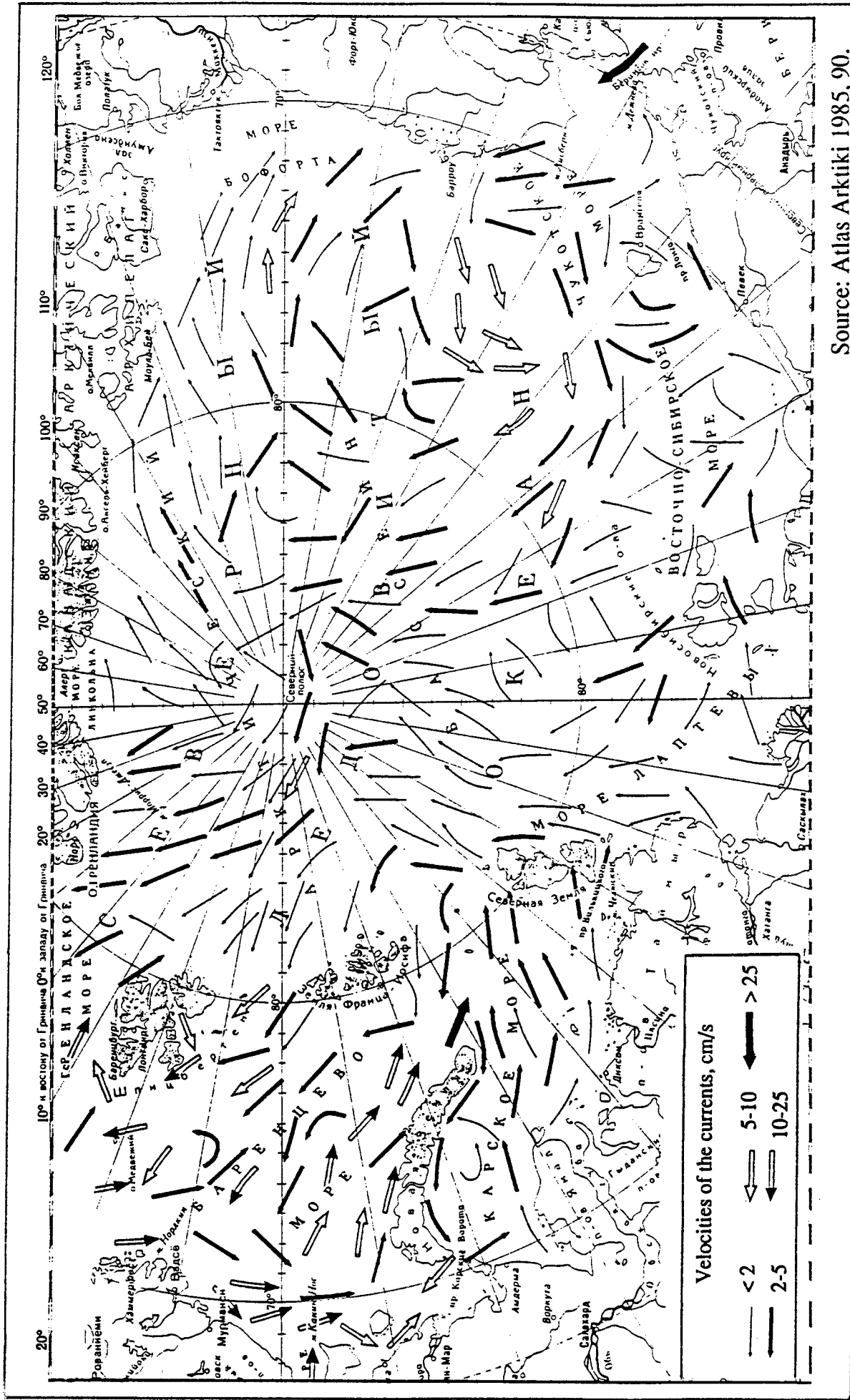
Reference books:

1. Guide to navigation through the
Northern Sea Route, 1992

AARI reports:

Available in the
AARI library only





Source: Atlas Arktiki 1985, 90.

FIGURE 3-7.-- Surface currents in the Arctic Seas (Atlas Arktiki, 1985).

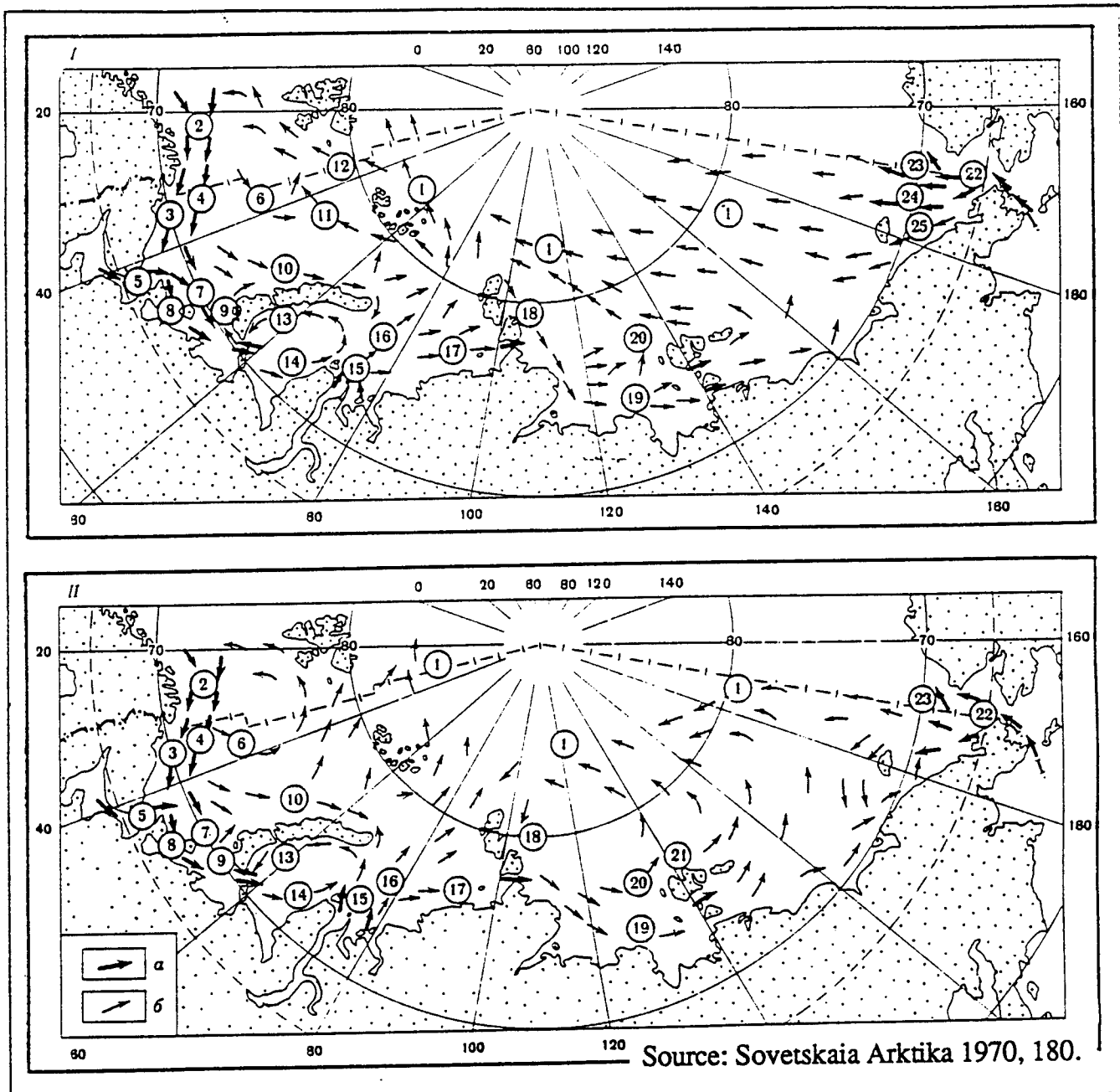


FIGURE 3-8.--Surface currents in the Arctic Seas (Sovetskaia Arktika, 1970)

I - first type of water circulation, II - second type of water circulation;

a - velocities are less than 0.1 knots (18.5 cm/s);

b - velocities are greater than 0.1 knots.

Currents: 1 - Transarctic; 2 - Nordkapskoe; 3 - Pribrezhnoe Murmanskoe; 4 - Murmanskoe; 5 - Belomorskoe; 6 - Yan-Mayenskoe; 7 - Kolguevskoe; 8 - Kaninskoe; 9 - Litke; 10 - Zapadno-Novozemel'skoe; 11 - Medvezhie; 12 - Vostochno-Shpitsbergenskoe; 13 - Vostochno-Novozemel'skoe; 14 - Yamal'skoe; 15 - Ob'-Yeniseyskoe; 16 - Sv. Anny; 17 - Zapadno-Taimyrskoe; 18 - Vostochno-Taimyrskoe; 19 - Lenskoe; 20 - Novosibirskoe; 21 - Sedova; 22 - Tikhookeanskoe; 23 - Gerd'arovskoe.

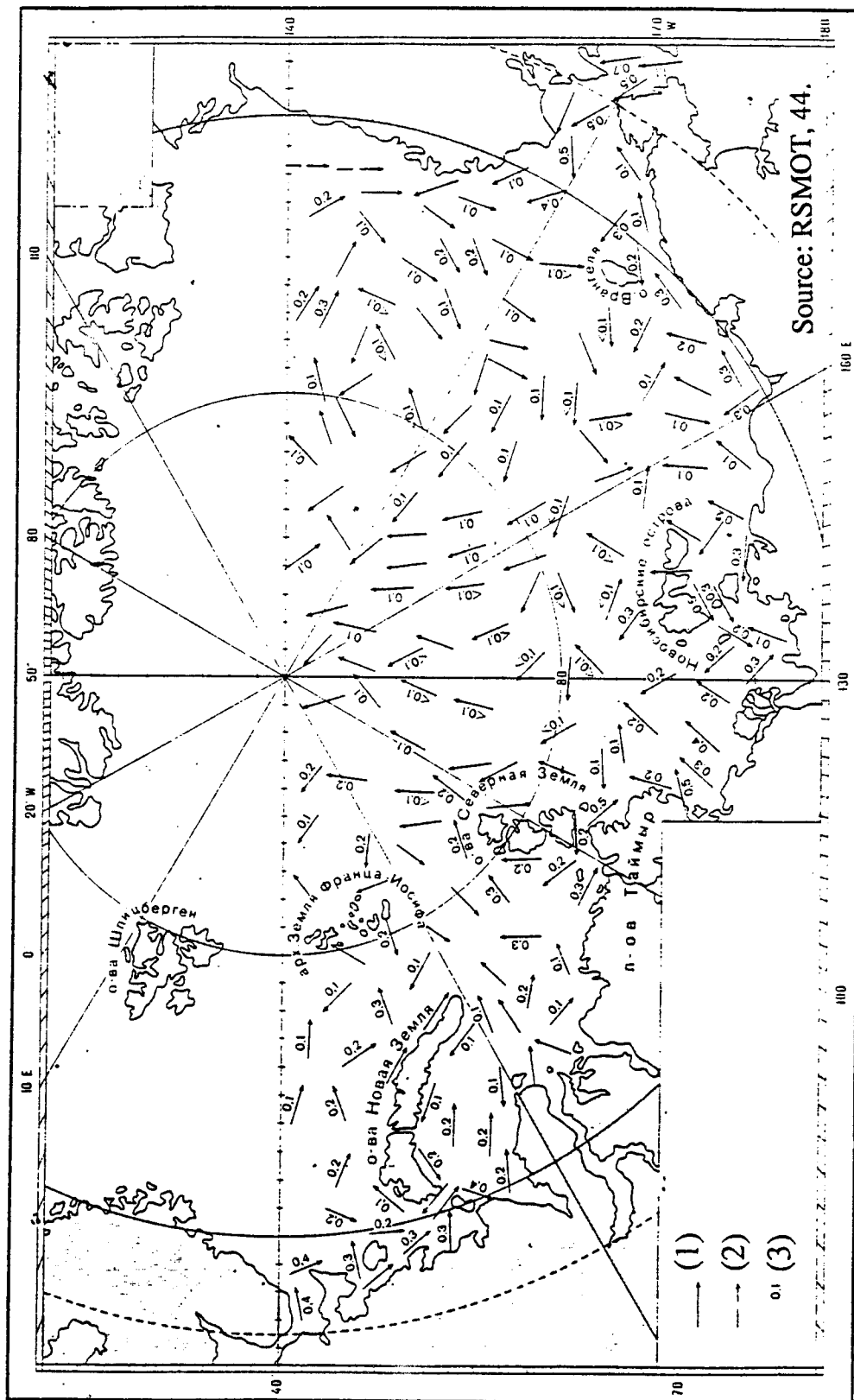
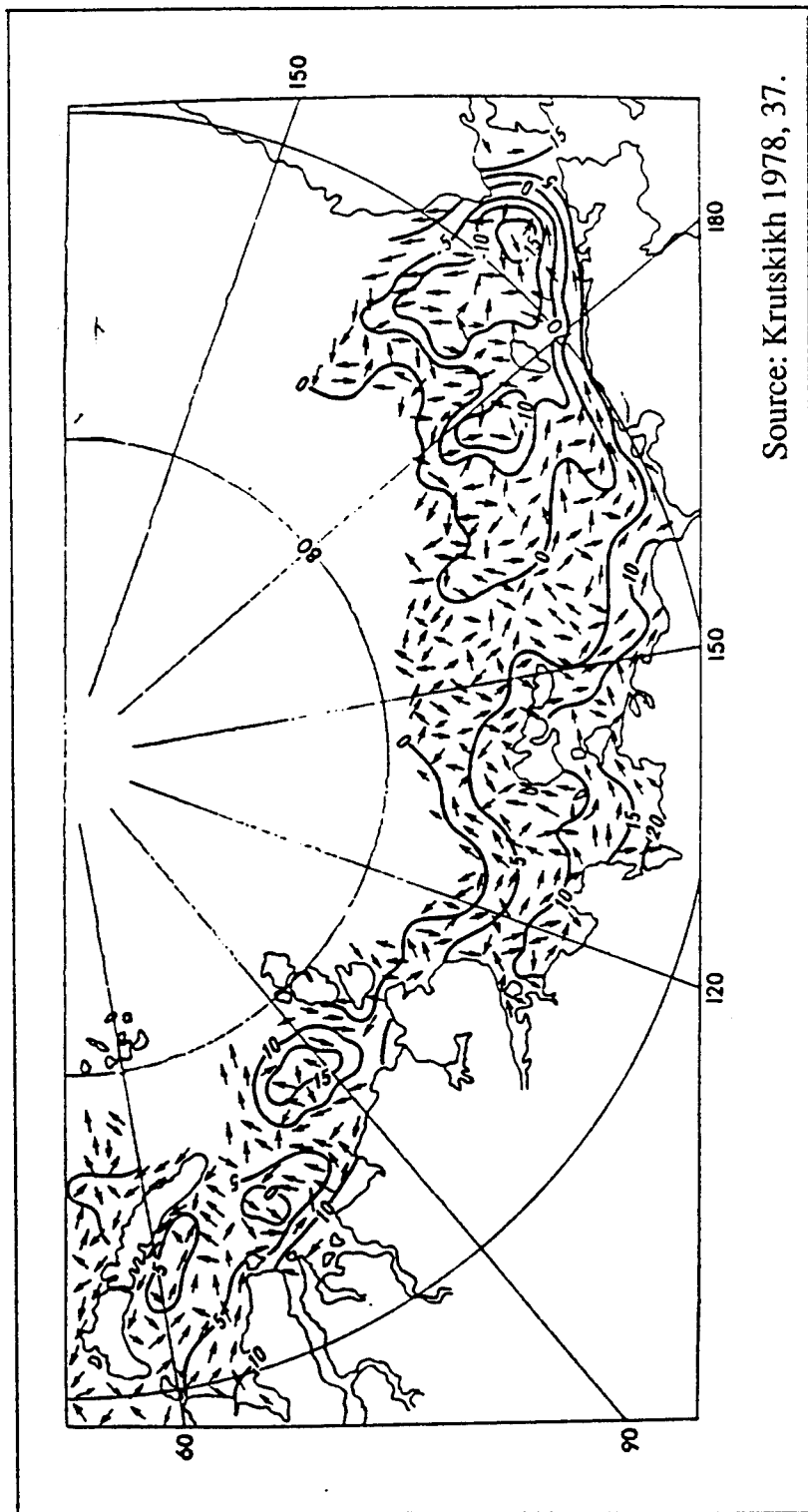


FIGURE 3-9.--Scheme of currents in 0-10 m layer.

1 - direction of a current; 2 - direction of a supposed current; 3 - velocity of a current, knots.



**FIGURE 3-10.--Integral circulation of the water and sea level distribution in the Arctic Seas under influence of cyclonic atmosphere circulation (Figure 3-12a).
Adopted from Krutskikh, 1978 (First type of ice and water dynamics).**

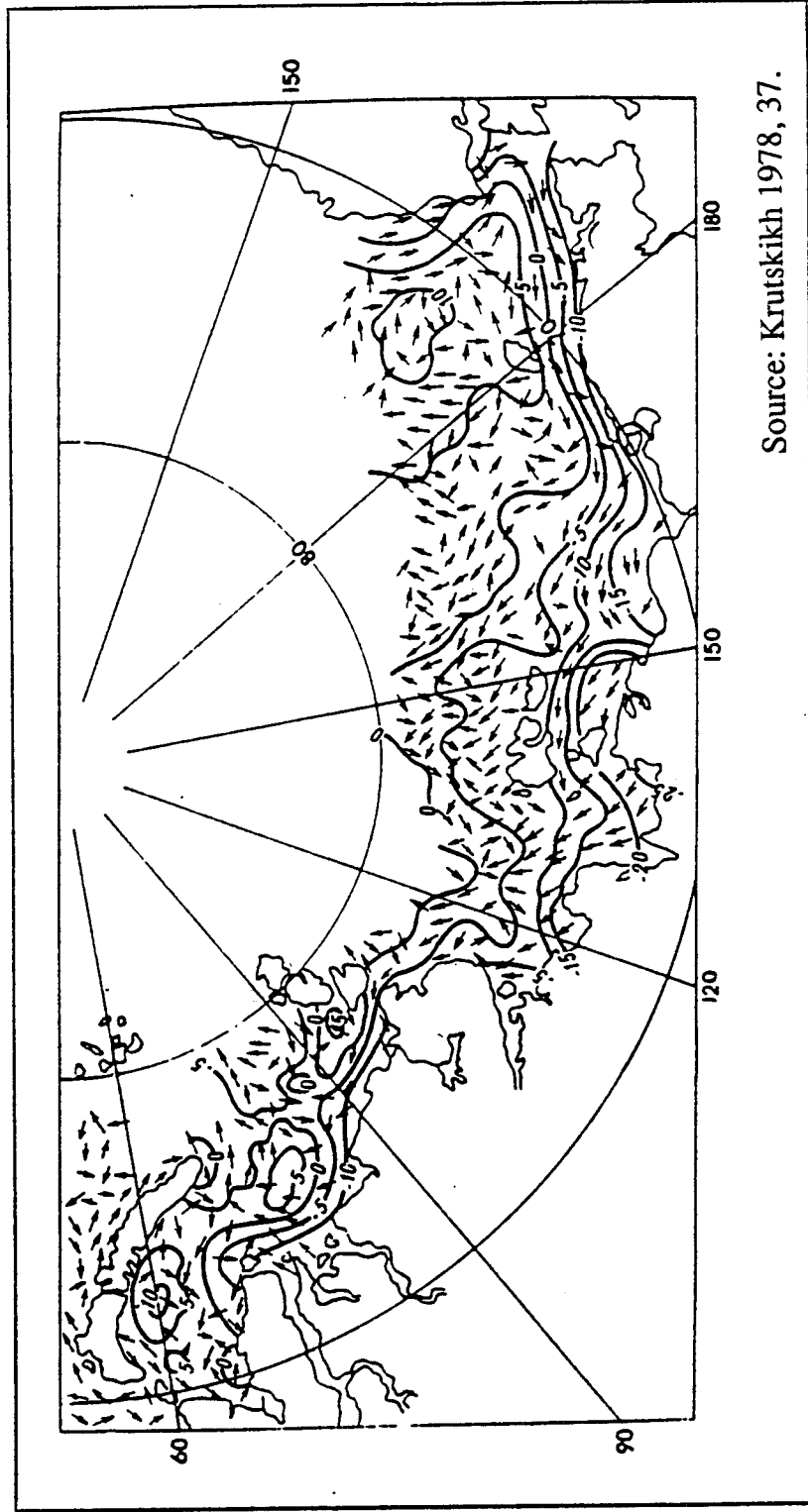
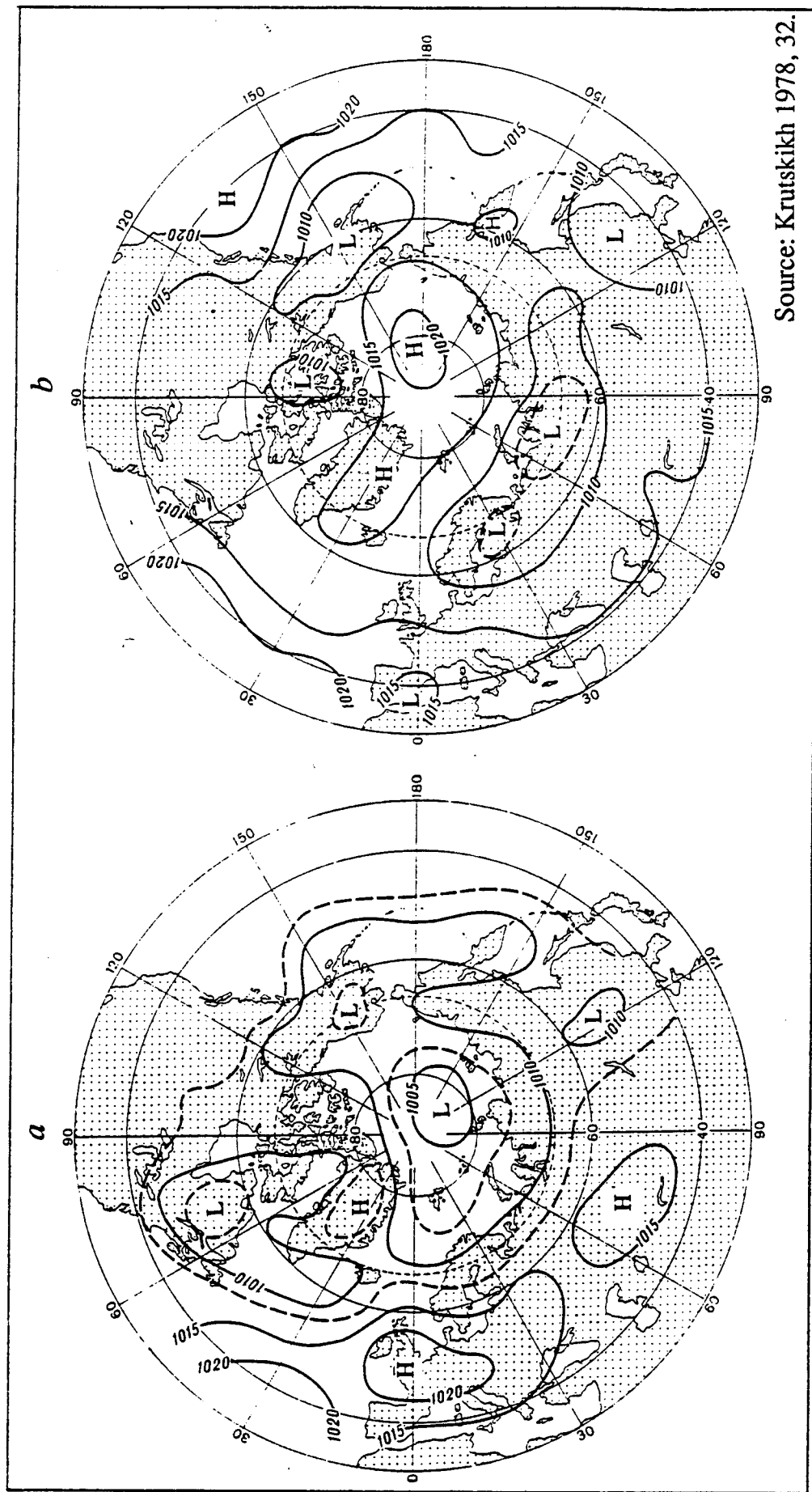


FIGURE 3-11. --Integral circulation of the water and sea level distribution in the Arctic Seas under influence of anticyclonic atmosphere circulation (Figure 3-12b). Adopted from Krutskikh, 1978 (Second type of ice and water dynamics).



Source: Krutskikh 1978, 32.

FIGURE 3-12.--Synoptic location of baric systems corresponded to first (a) and second (b) types of water and ice dynamics (Krutskikh,1978).

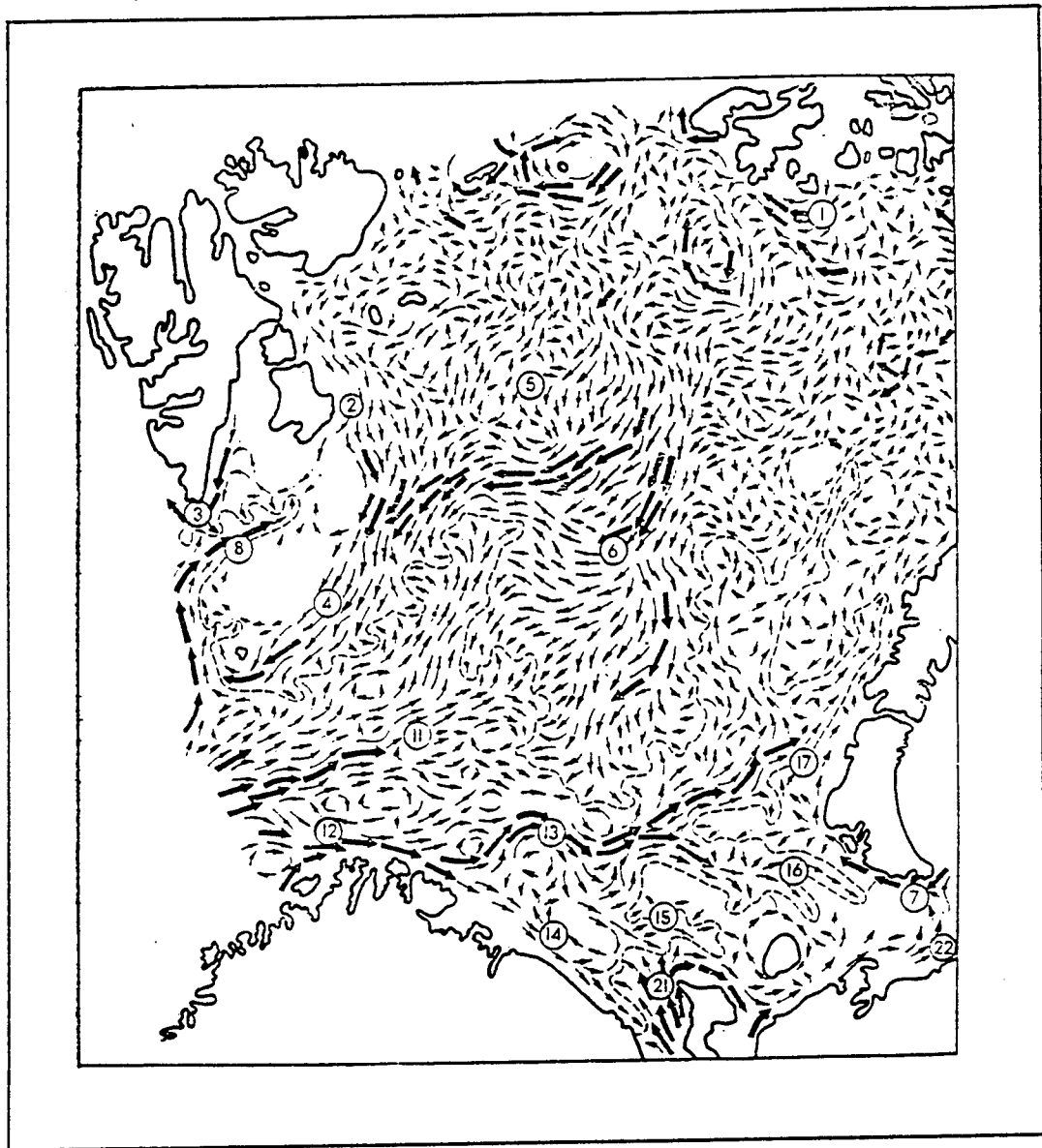


FIGURE 3-13. Surface permanent currents of the Barents Sea . Adopted from Tantsiura (1959) and Novitsky (1961).

Currents:

- 1 - Near coastal current of the Frants Josef Land ; 2 - Barents current (East Spitsbergen).
 3 - South Nord Cap current; 4 - Bear current (Bear-hope current); 5 - Persei current;
 6 - Central current; 7 - Litke current; 8 - South Spitsbergen current; 9 - Nord Cap current;
 10 - North branch of Nord Cap current; 11 - Central branch of Nord Cap current;
 12 - South branch of Nord Cap current; 13 - Murmansk current; 14 - Nurmansk coastal
 current; 15 - Kaninskoe current; 16 - Kolguevo-Pechorskoe current; 17 - Novozemelskoe
 current; 18 -Coastal branch of Novozemelskoe current; 19 - East branch of Novozemelskoe
 current; 20 - West branch of Novozemelskoe current; 21 - White Sea current;
 22 - Pechora current.*

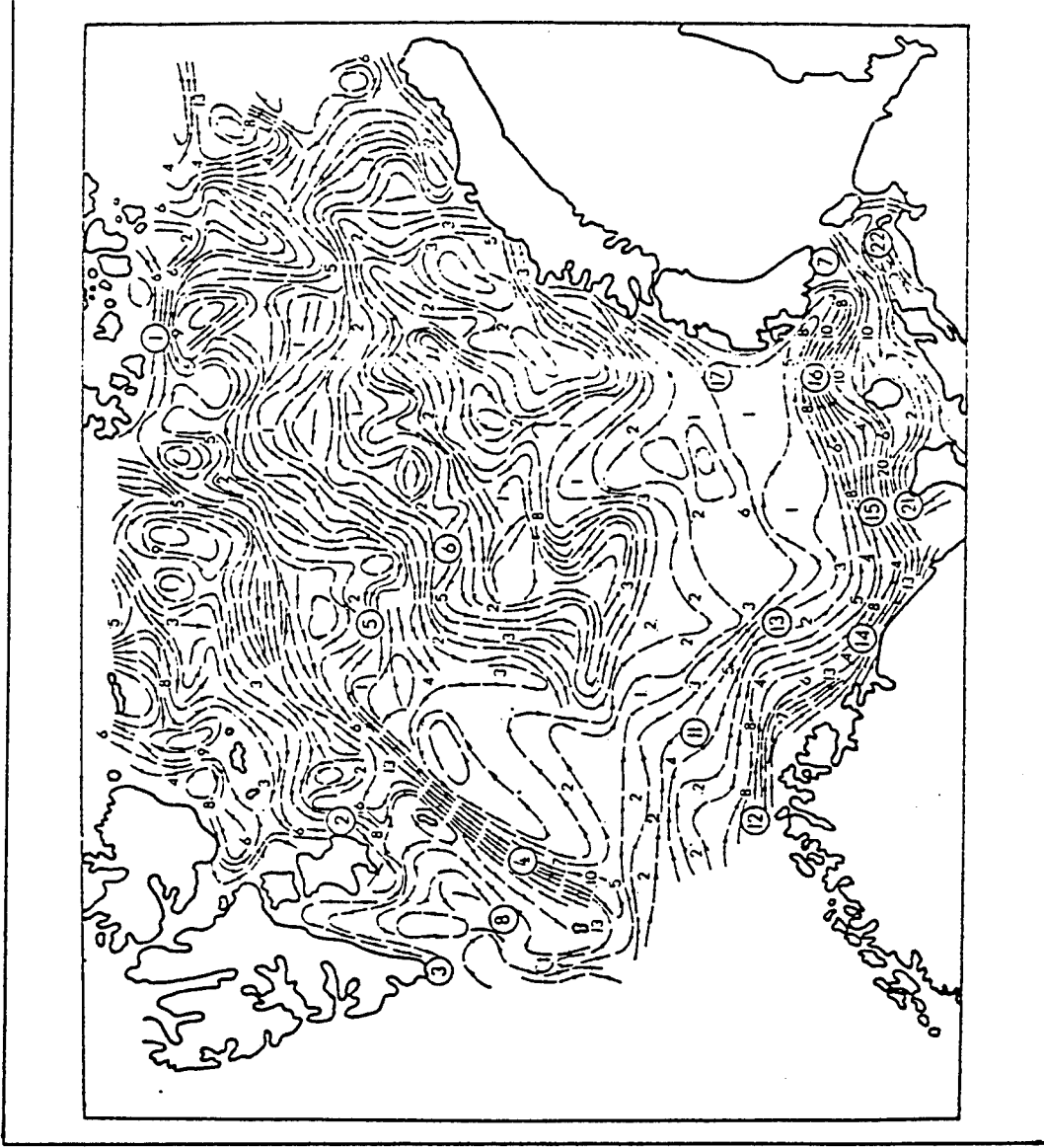


FIGURE 3-14. Surface permanent currents of the Barents Sea simulated using geostrophical balance method . Adopted from Potanin et al (1989).

Definition of the currents (numbers) is the same as in Figure 3-13.

Numbers near arrows are calculated velocities, cm/s



FIGURE 3-15. Surface permanent currents of the Barents Sea simulated using Burkov's model (Burkov, 1980).

Definition of the currents (numbers) is the same as in Figure 3-13.

Numbers near arrows are calculated velocities, cm/s

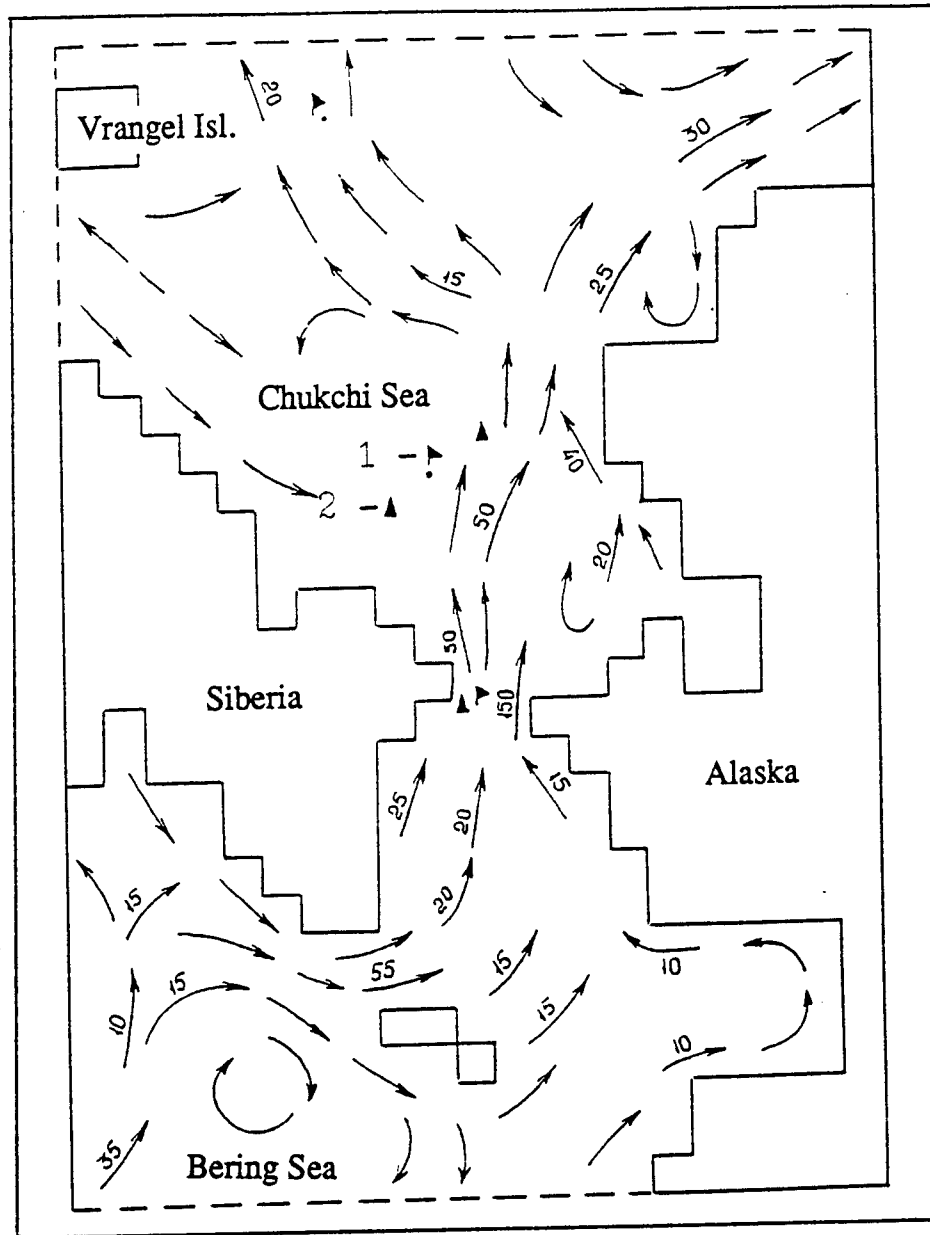


FIGURE 3-16.-- Surface currents of the Chukchi Sea
 Adopted from Proshutinsky, 1986. Numbers are velocities
 of currents, cm/s.

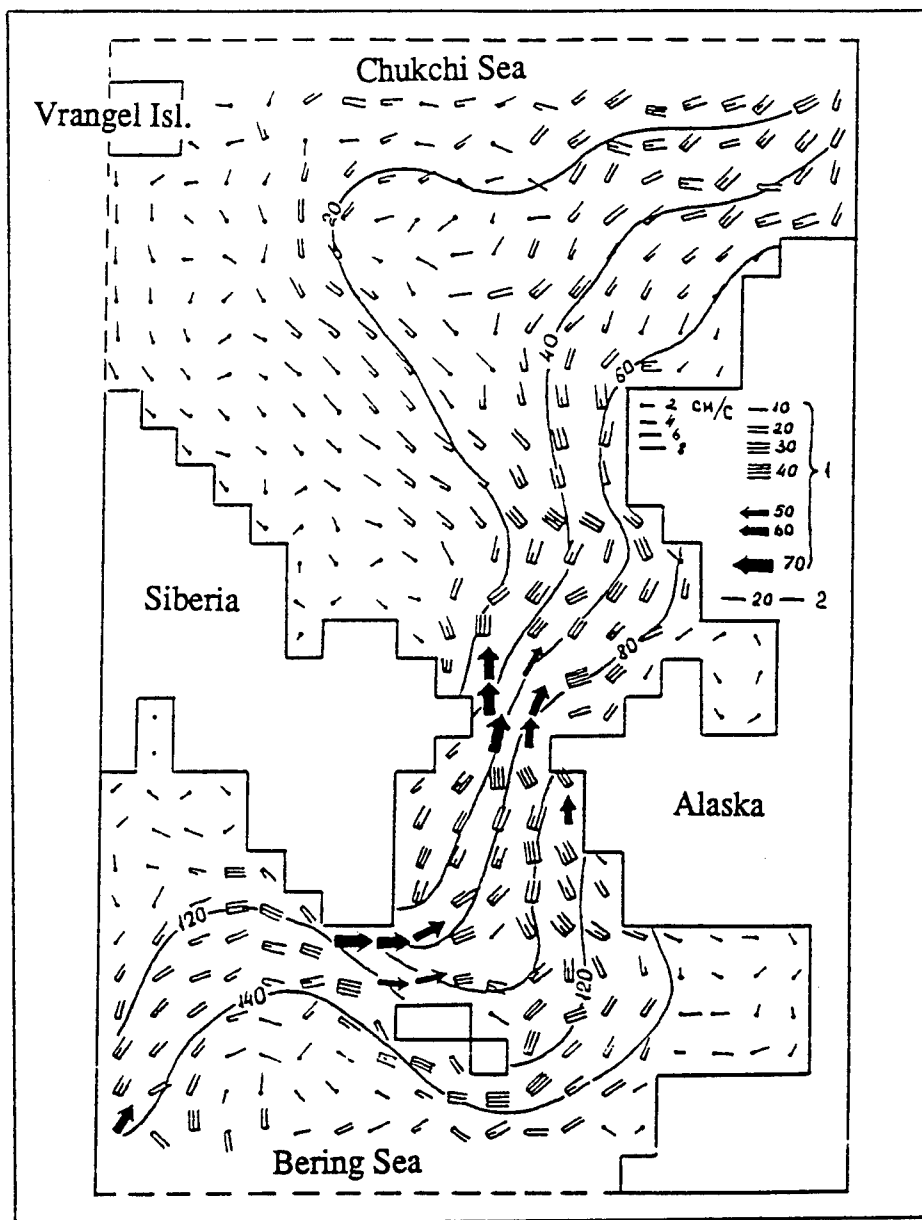


FIGURE 3-17.-- Integral currents of the Chukchi Sea.
Result of numerical simulation. Adopted from Proshutinsky,
1986.

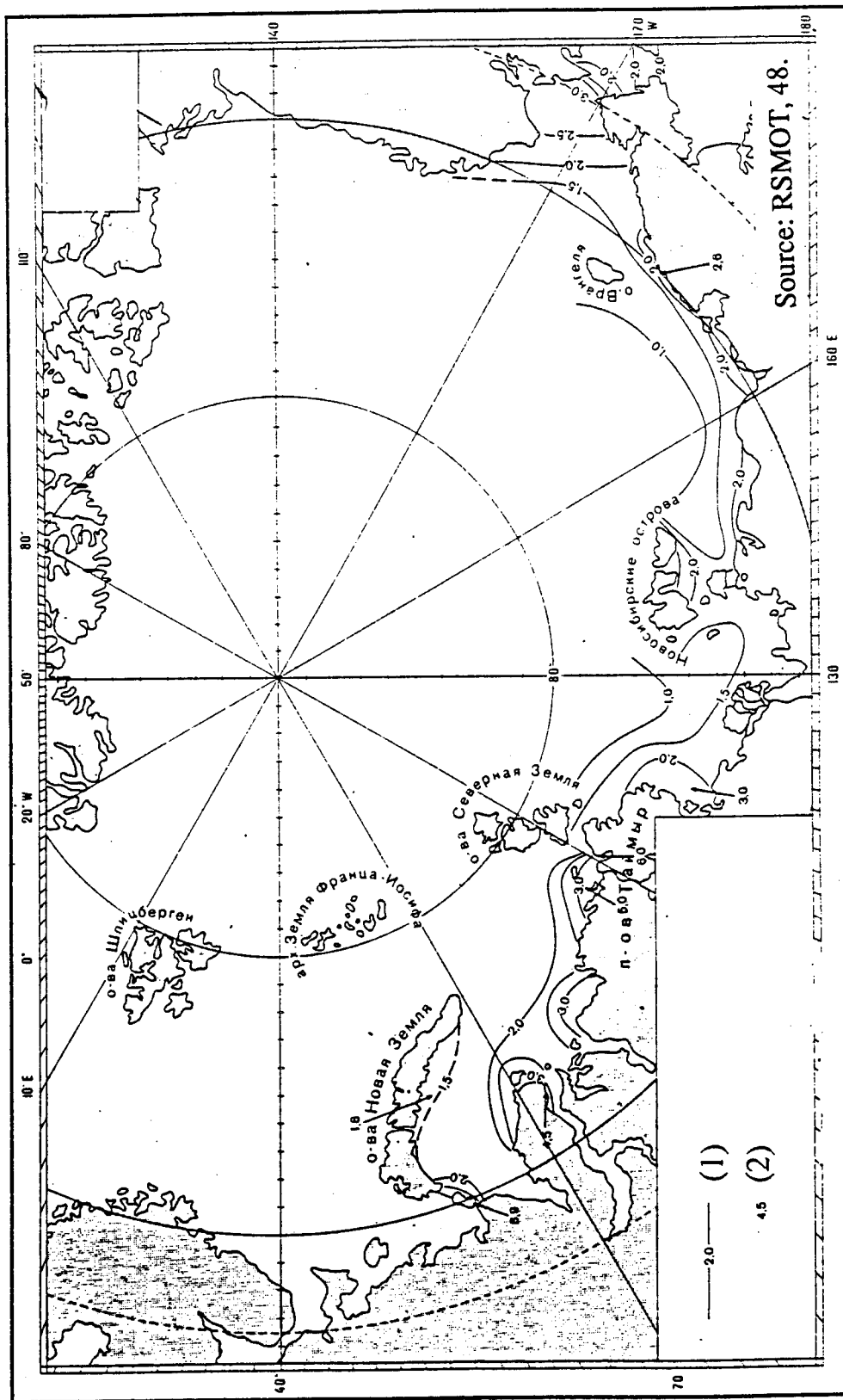


FIGURE 3-17a.--Scheme of maximum velocity of summary currents in 0-10 m layer.

Navigation period.

(1) - maximum, currents, knots;

(2) - local maximum of current.

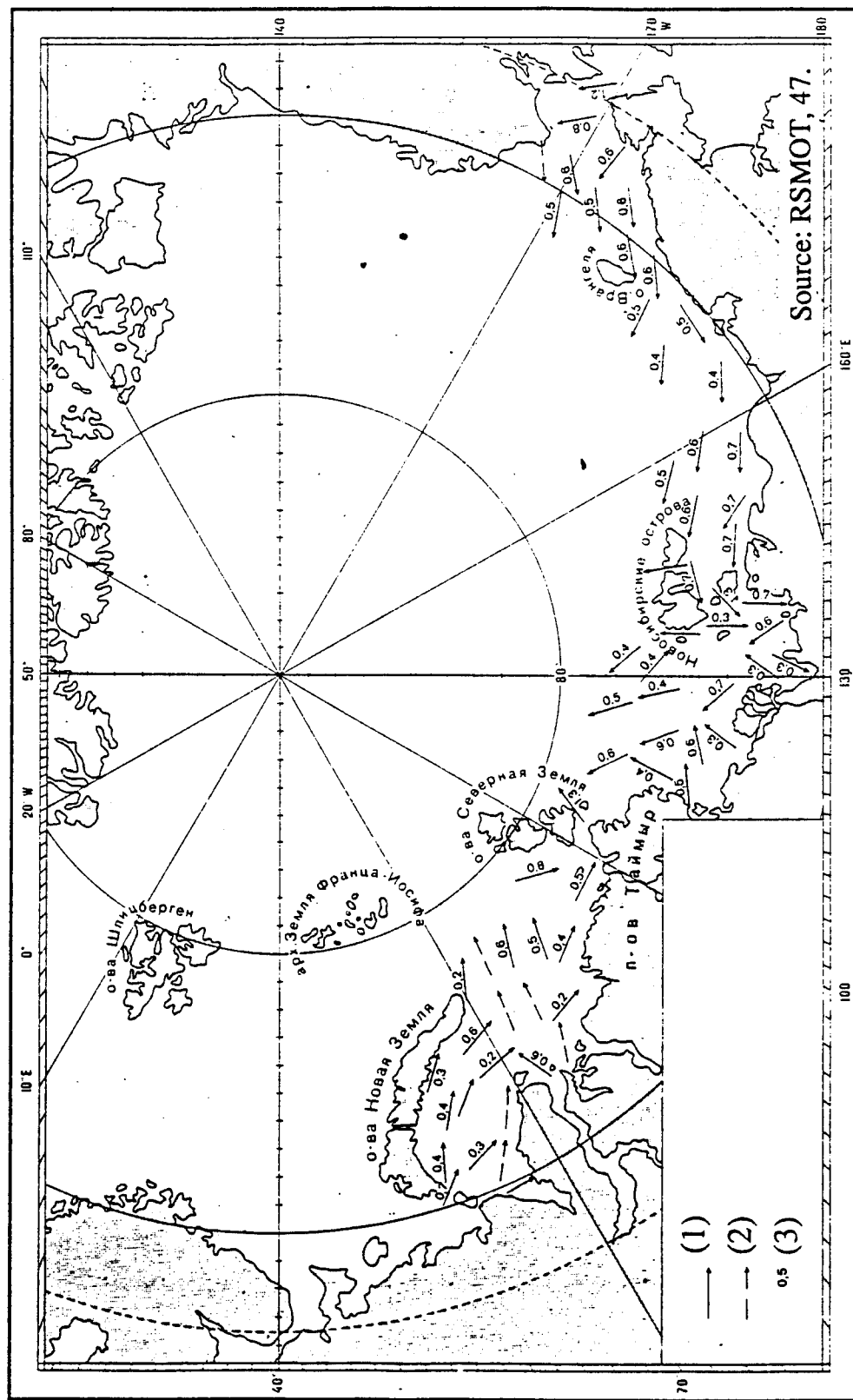


FIGURE 3-17b.--Scheme of currents in 0-10 m layer driven by SE 10 m/s wind.

1 - direction of a current; 2 - direction of a supposed current; 3 - velocity of a current, knots.

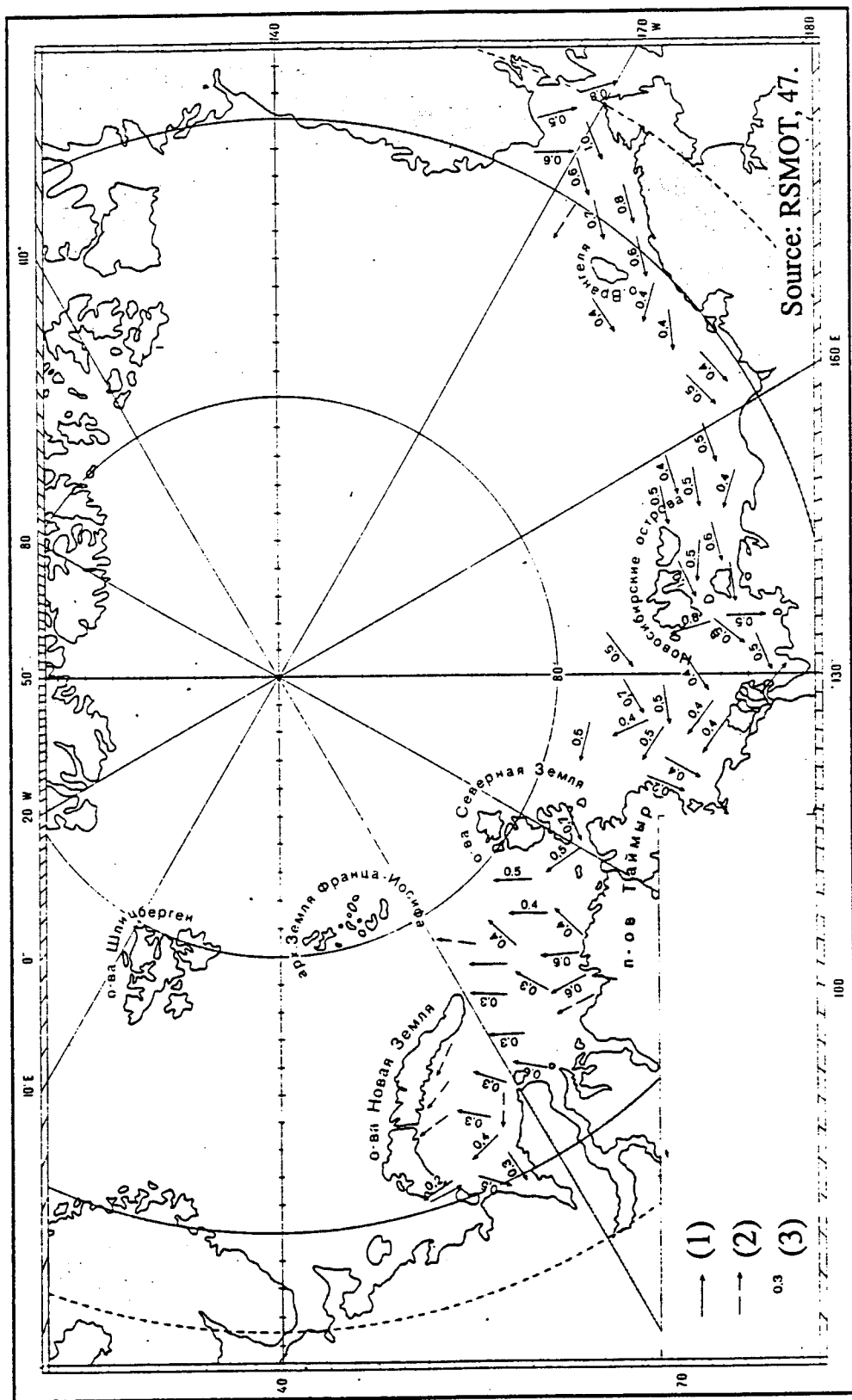


FIGURE 3-17c. --Scheme of currents in 0-10 m layer driven by NE 10 m/s wind.

1 - direction of a current; 2 - velocity of a supposed current; 3 - velocity of a current, knots.

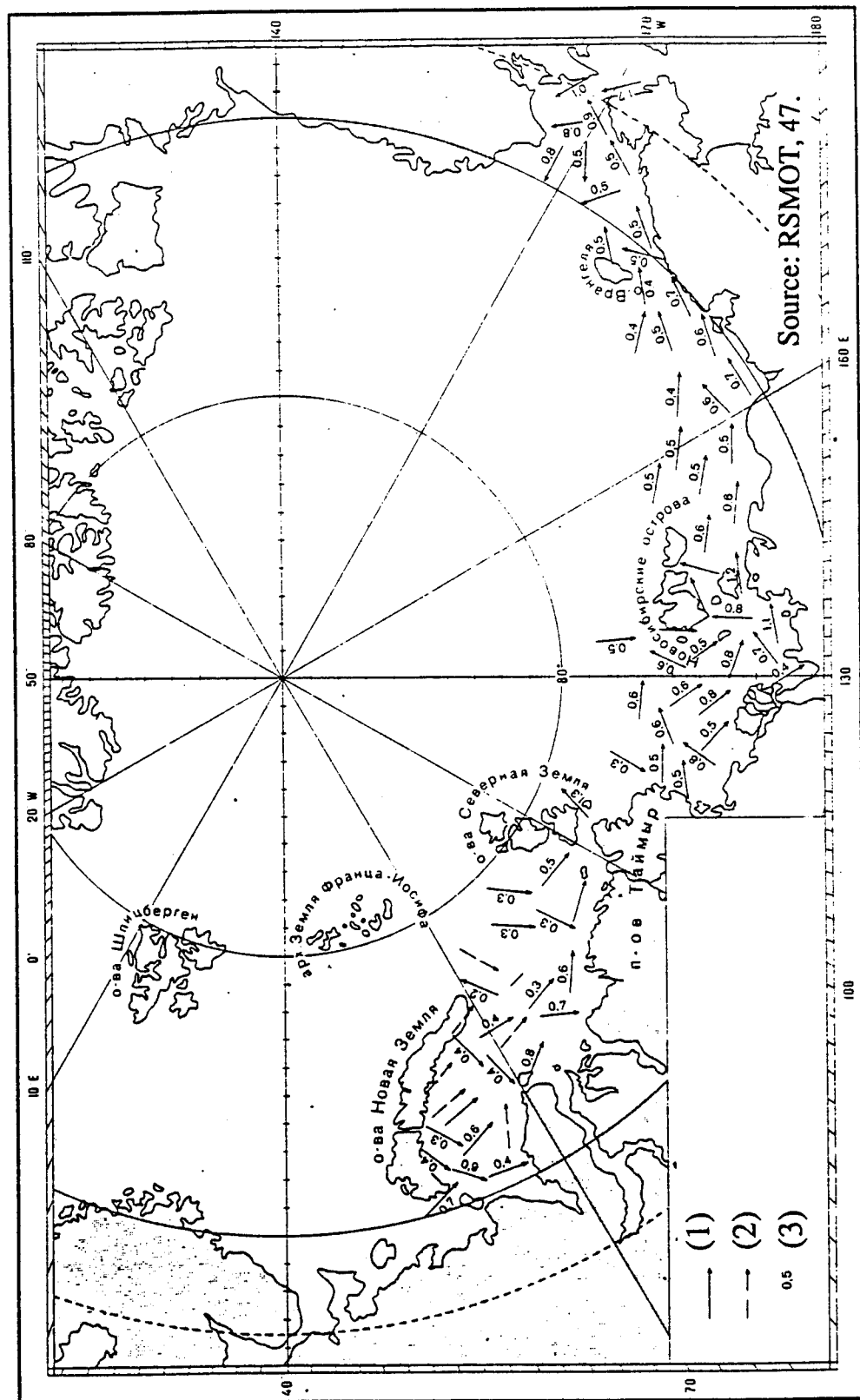


FIGURE 3-17d.---Scheme of currents in 0-10 m layer , driven by SW 10 m/s wind.
 1 - direction of a current; 2 - direction of a supposed current; 3 - velocity of a current, knots.

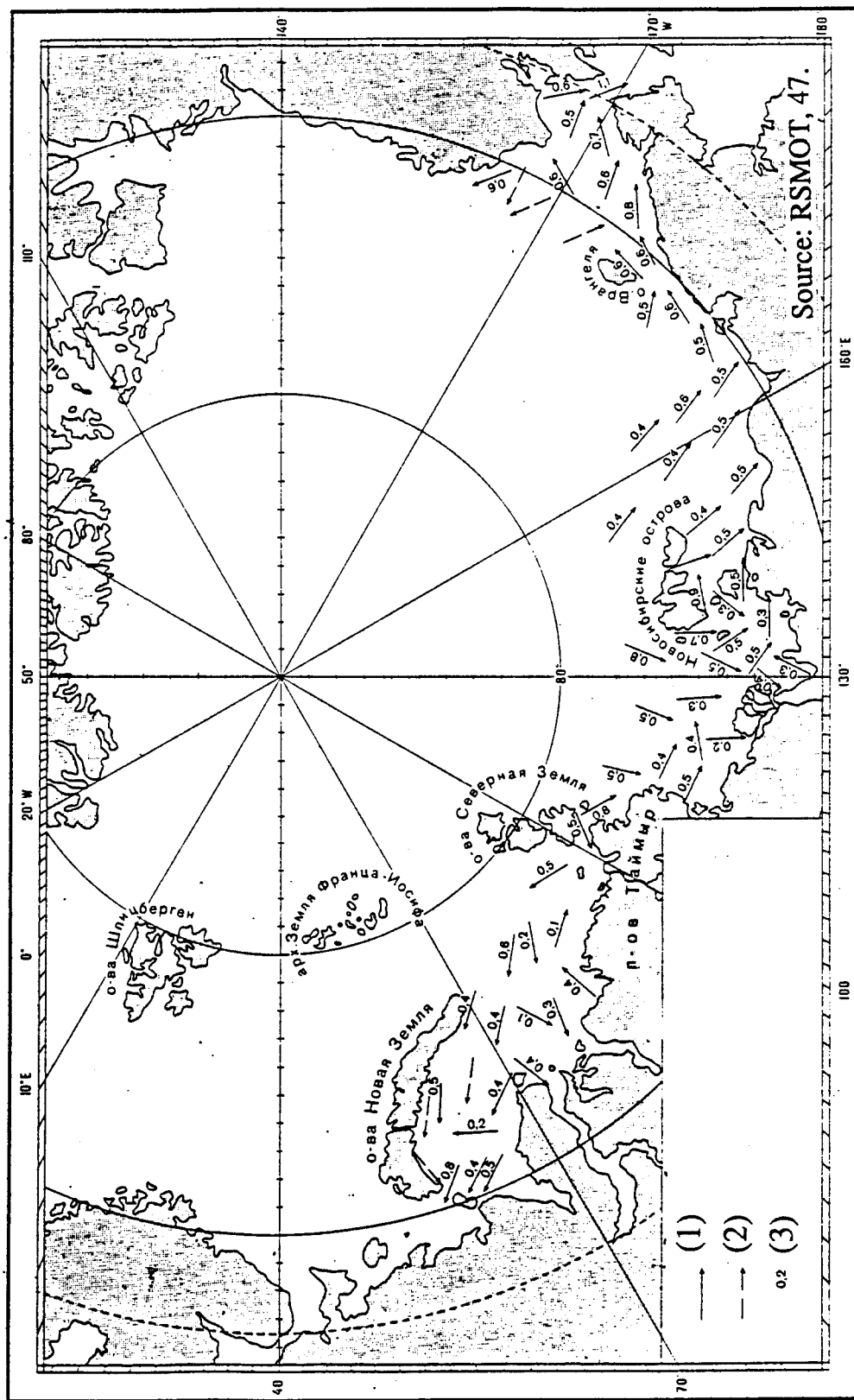


FIGURE 3-17e. --Scheme of currents in 0-10 m layer , driven by NW 10 m/s wind.

1 - direction of a current; 2 - direction of a supposed current; 3 - velocity of a current, knots.

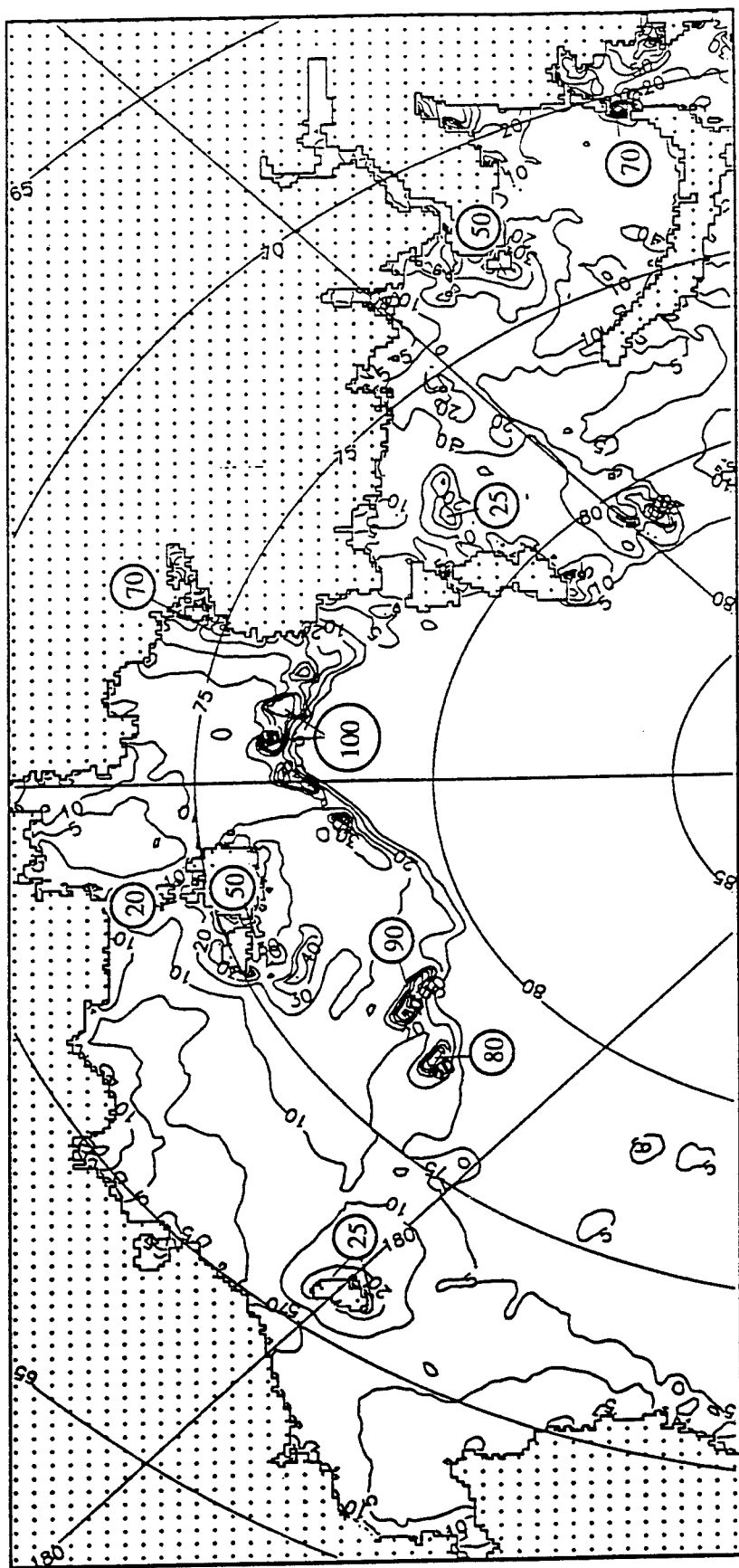


FIGURE 3-18. --Maximum tidal currents (cm/s) in the Arctic Seas.
Result of numerical simulation. Adopted from Kowalik and Proshutinsky,
1994.

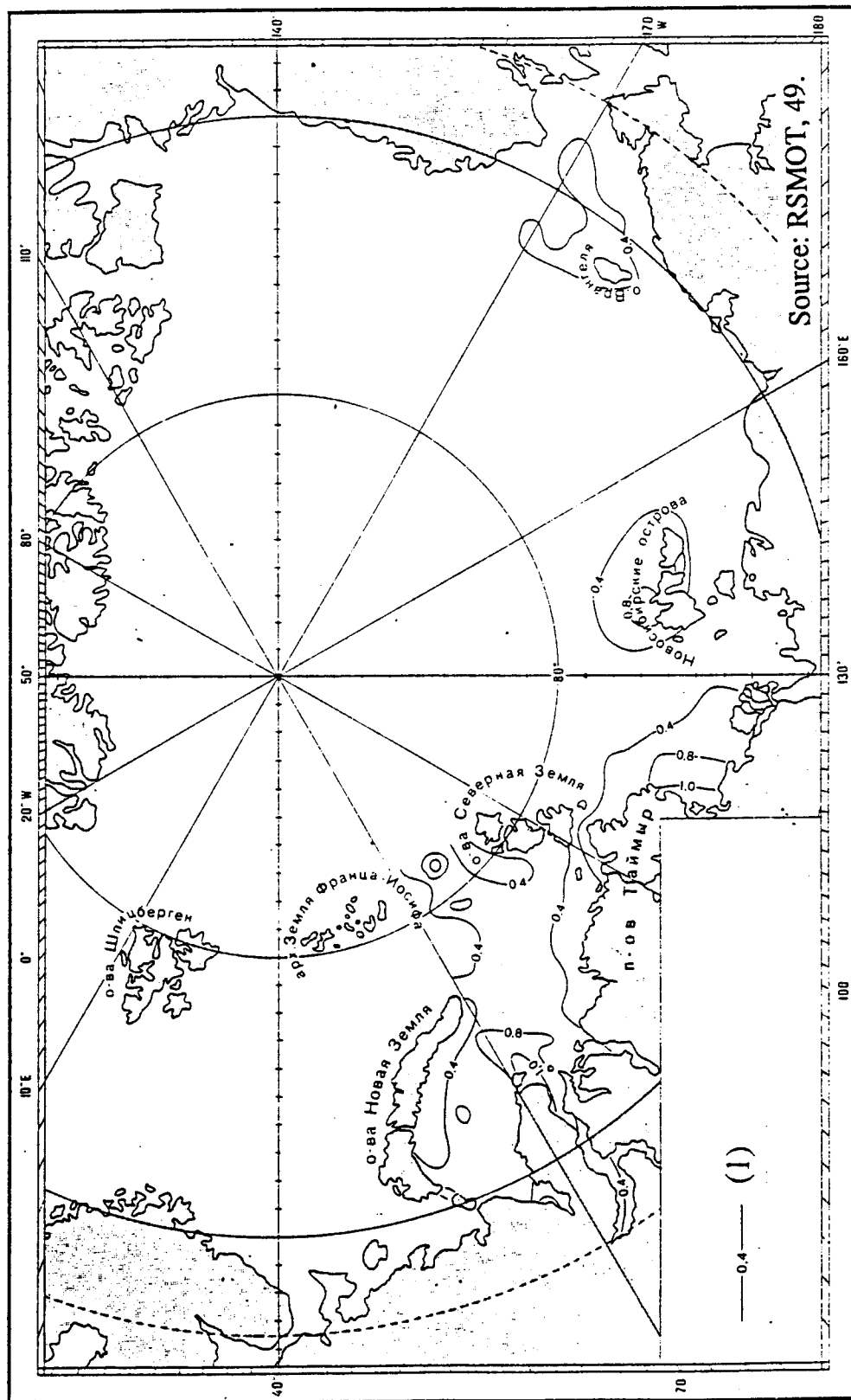
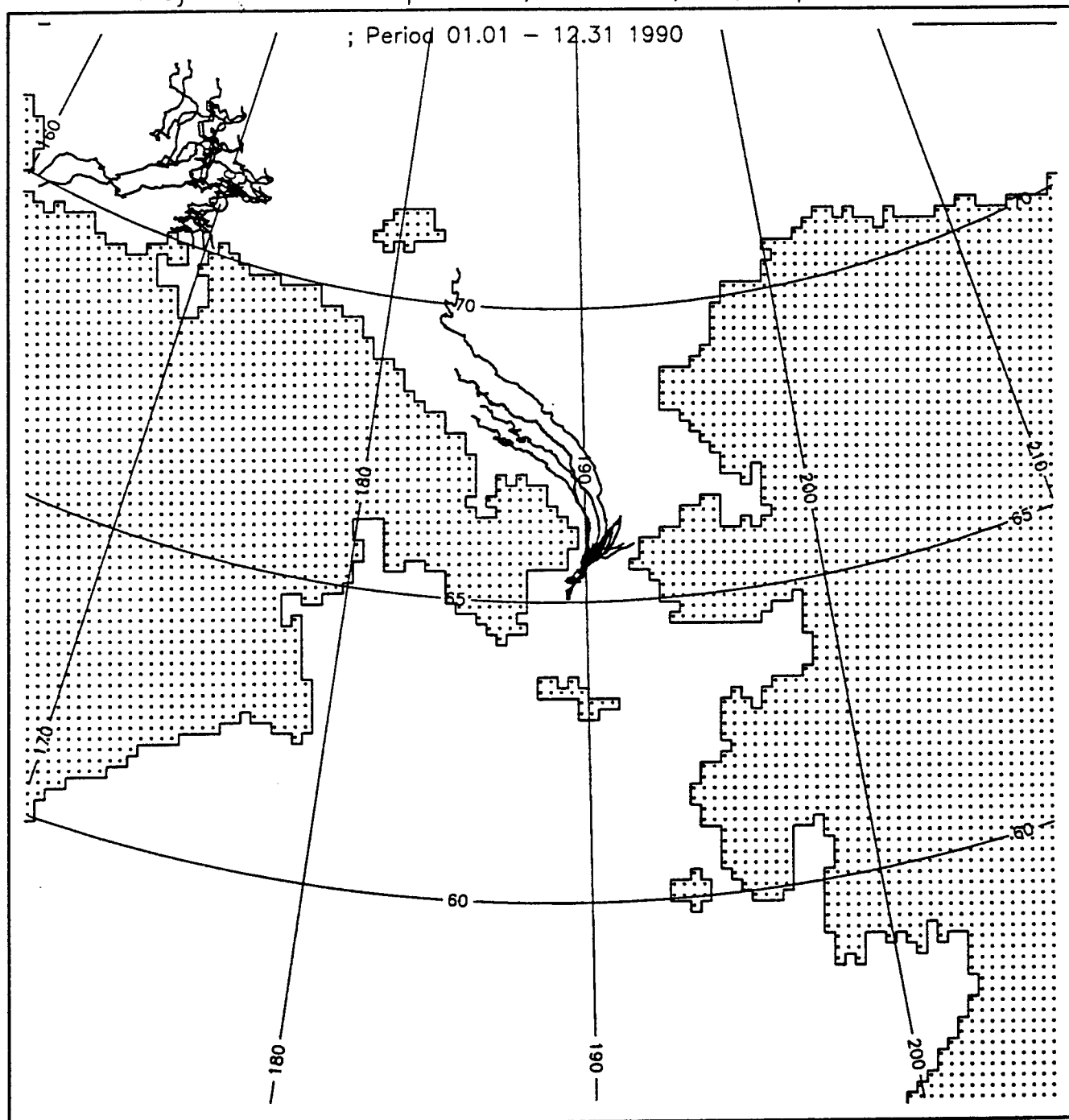
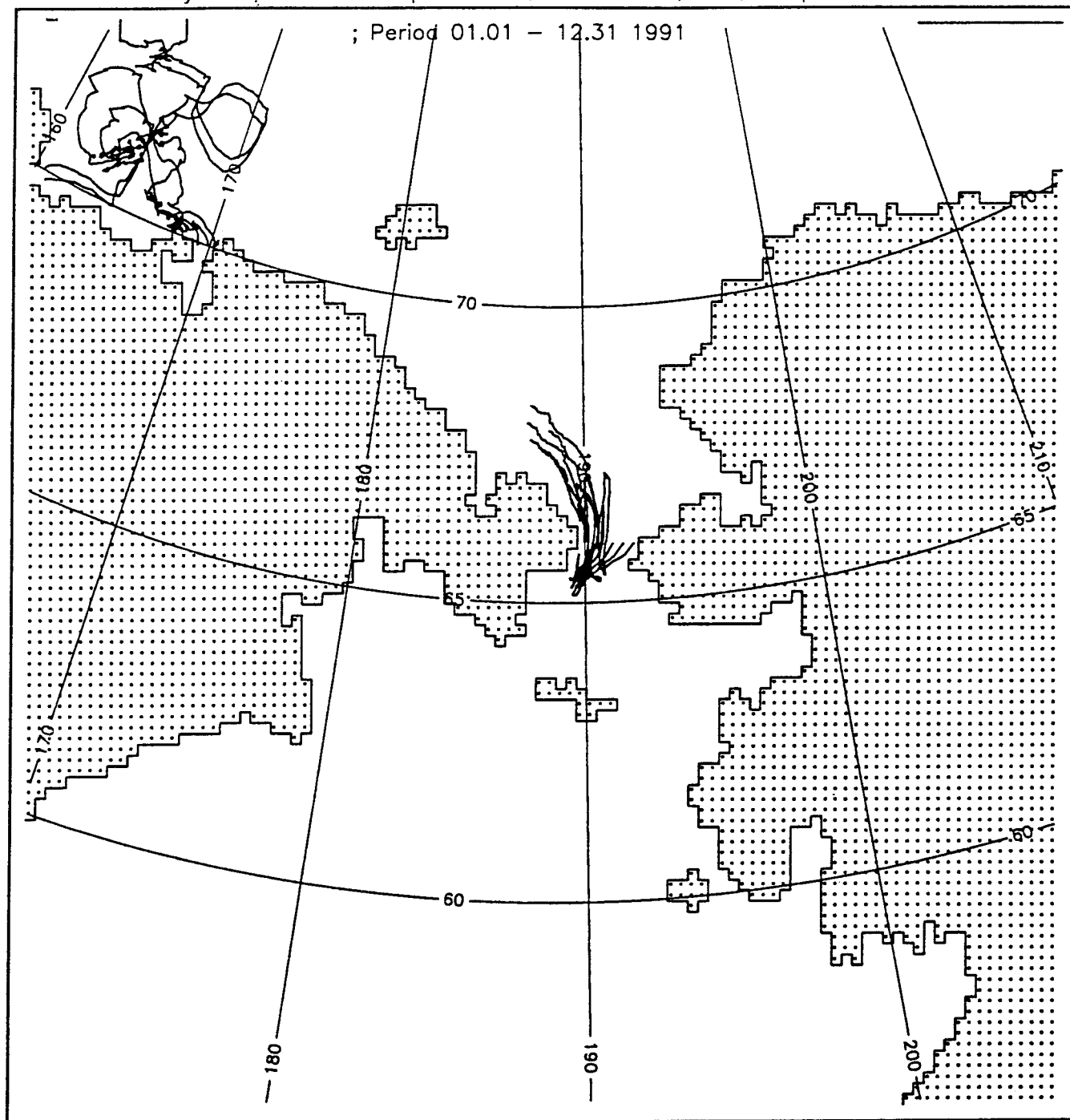


FIGURE 3-19.--Mean velocity of spring tidal currents, knots.

; Period 01.01 - 12.31 1990

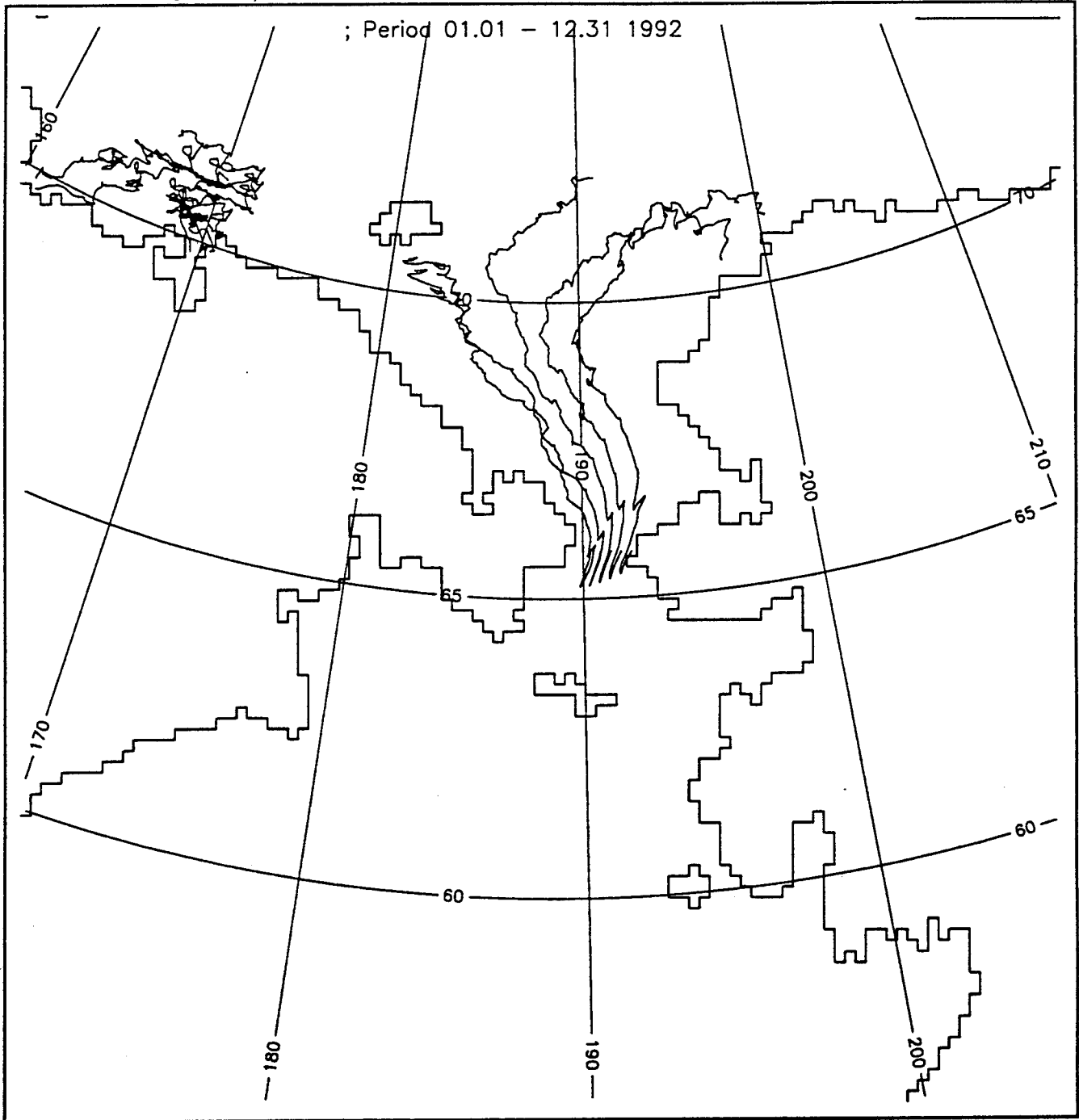


Trajectories of ice particles; real wind; ice; slope $1.1E-6$

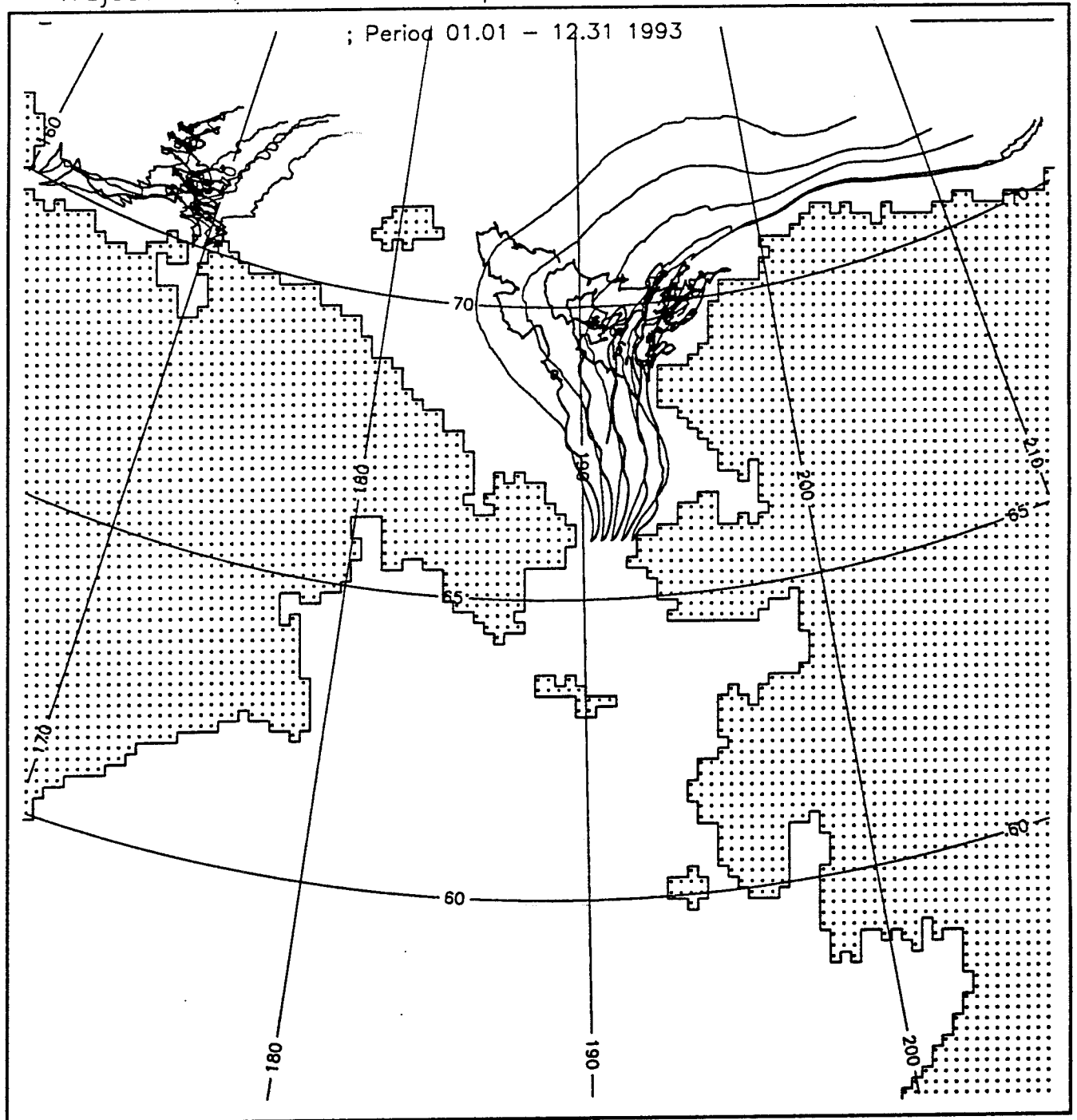


Trajectories of ice particles; real wind; ice; slope $1.1E-6$

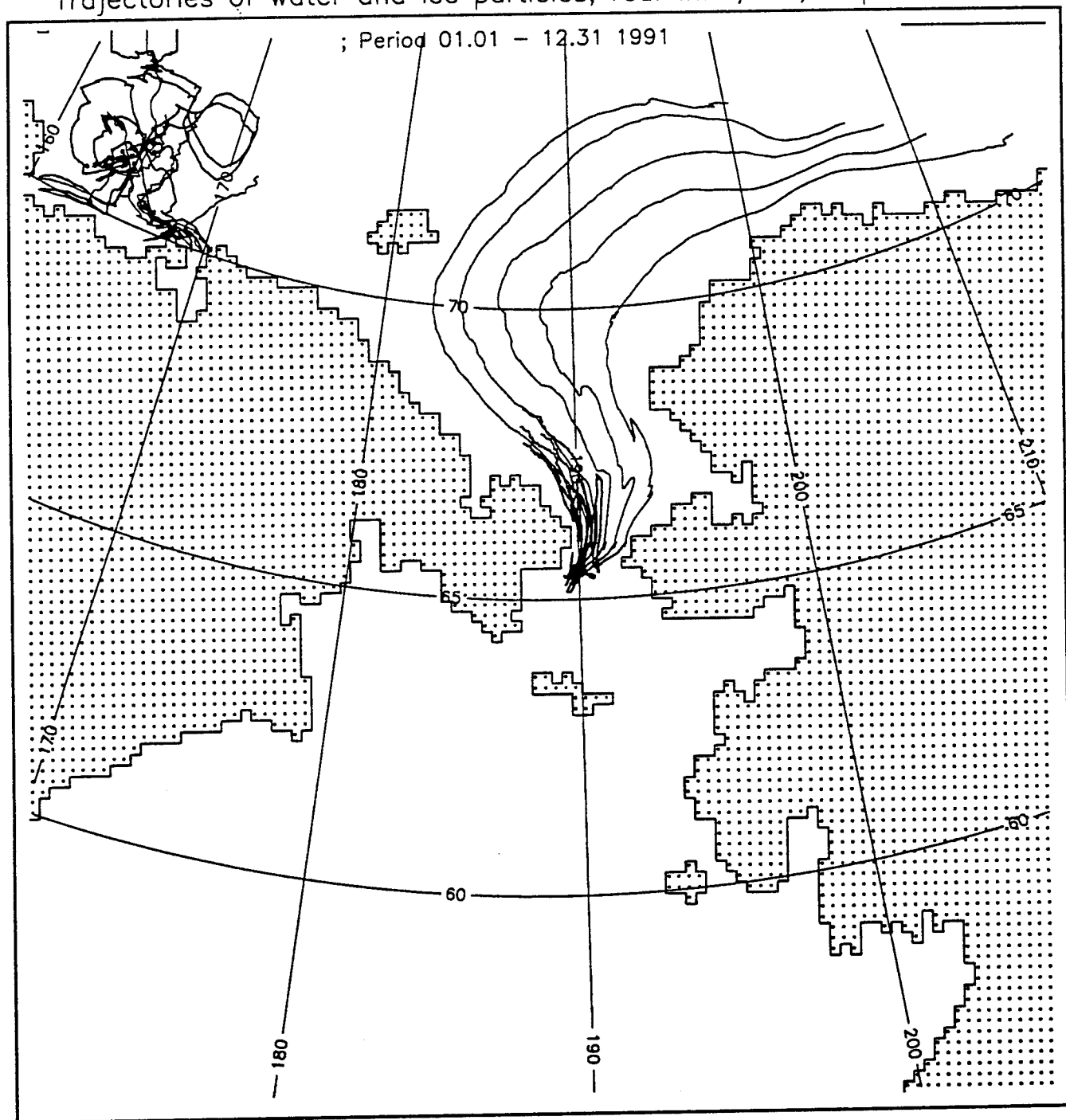
; Period 01.01 - 12.31 1992



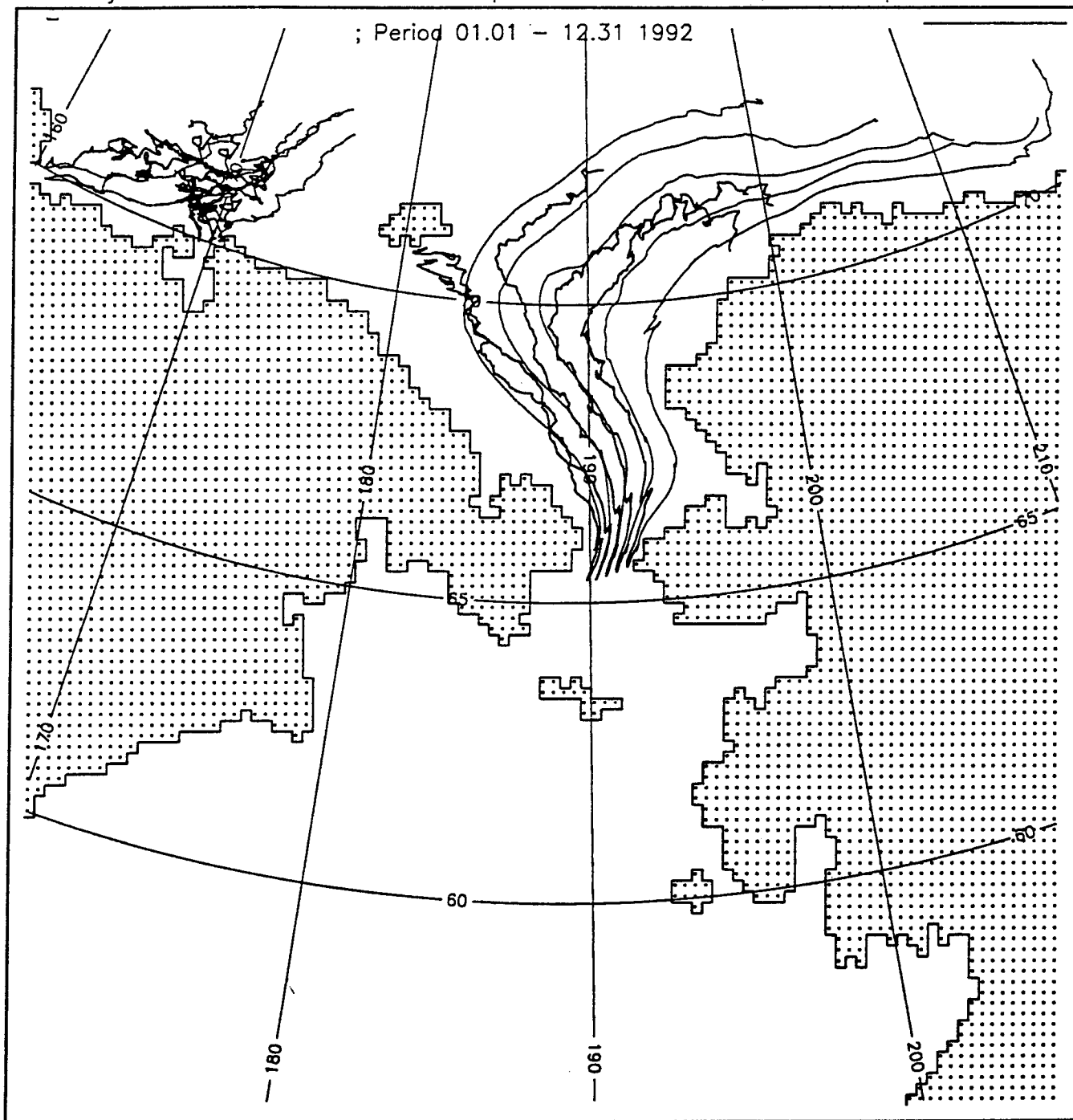
Trajectories of water and ice particles; real wind; ice; slope $1.1E-6$



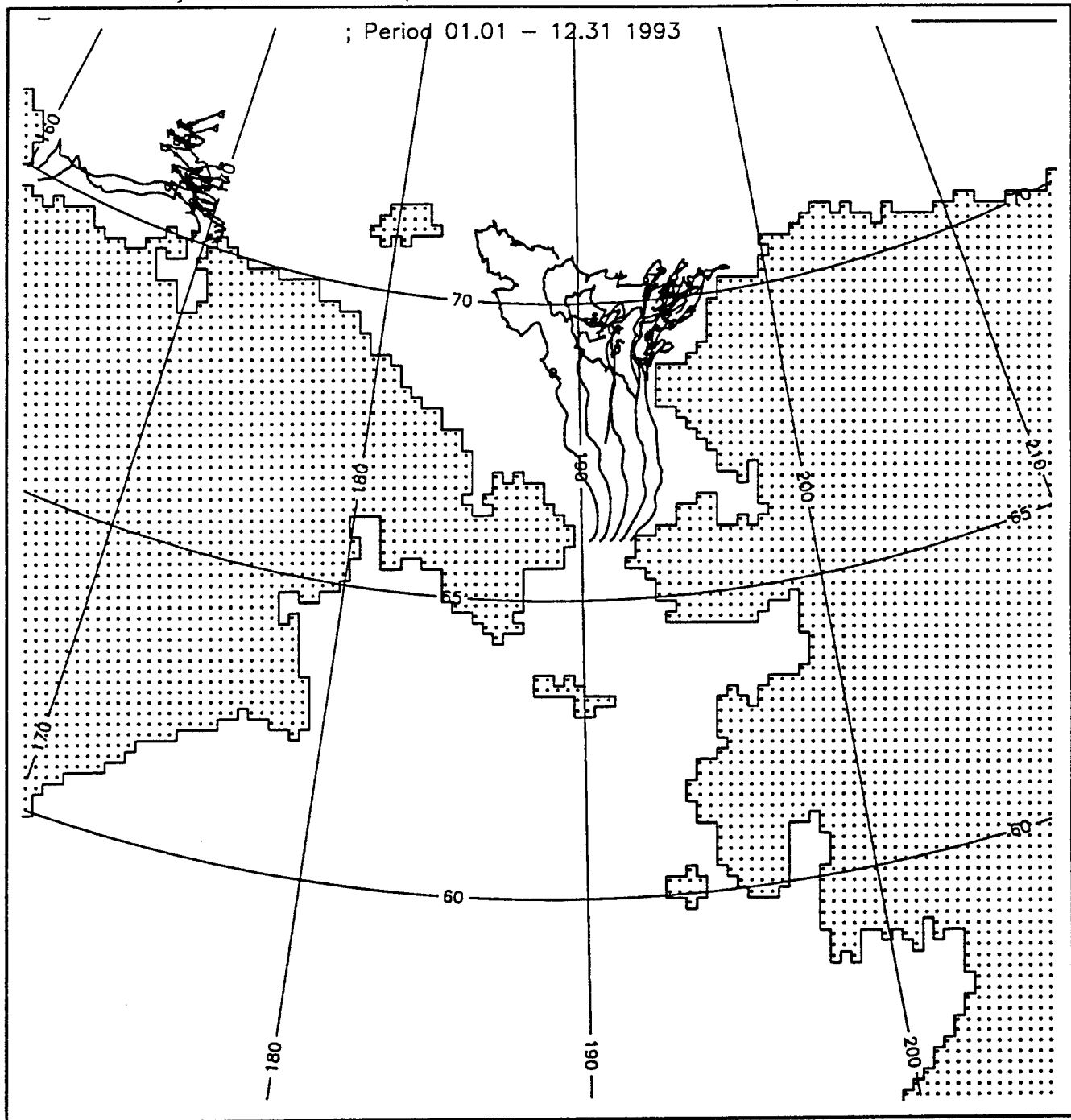
Trajectories of water and ice particles; real wind; ice; slope $1.1E-6$



Trajectories of water and ice particles; real wind; ice; slope $1.1\text{E}-6$



Trajectories of ice particles; real wind; ice; slope $1.1E-6$



Time Series Observations of Seabed, Fluid, and Flow Conditions in the Barents and Norwegian Seas

Richard Sternberg

Time Series Observations of Seabed, Fluid, and Flow Conditions in the Barents and Norwegian Seas

A.R.M. Nowell, R.W. Sternberg, K. Aagaard
School of Oceanography, WB-10
University of Washington
Seattle, WA 98195

D. Cacchione
U.S. Geological Survey
345 Middlefield Rd
Menlo Park, CA 94025

R. Wheatcroft
Woods Hole Oceanographic Institution
Woods Hole, MA 02543

This presentation summarizes long-term observations carried out from moored instruments and benthic tripods located in the vicinity of Svalbard and downslope of the Bear Island Trough. Measurements from moored instruments include (1) current speed, direction, conductivity, temperature, and depth at two levels in the water column at locations in Storfjorden and east of Hopen Island in the Barents Sea and (2) current speed, direction, conductivity, temperature, and light transmission at 20 m above the seabed at two locations in approximately 700 m depth west of Bear Island in the Norwegian Sea (Figure 1). Measurements from benthic tripods were made within 2.2 m of the seabed and include current speed, direction, pressure, conductivity, temperature, light transmission or scattering, and bottom photographs at stations located in Storfjorden, east of Hopen Island, and Olgastretet. Additionally, a benthic camera tripod was located in Olgastretet (Figure 1).

Generally, all sensors were sampled hourly and the length of time-series varied from 3-15 months. All instruments were not deployed simultaneously; the total experiment duration was from June 1991 through July 1994. At present, initial data reduction has been carried out and detailed analysis and interpretation is underway. This study is sponsored by the Marine Geology and Geophysics Program of the Office of Naval Research.

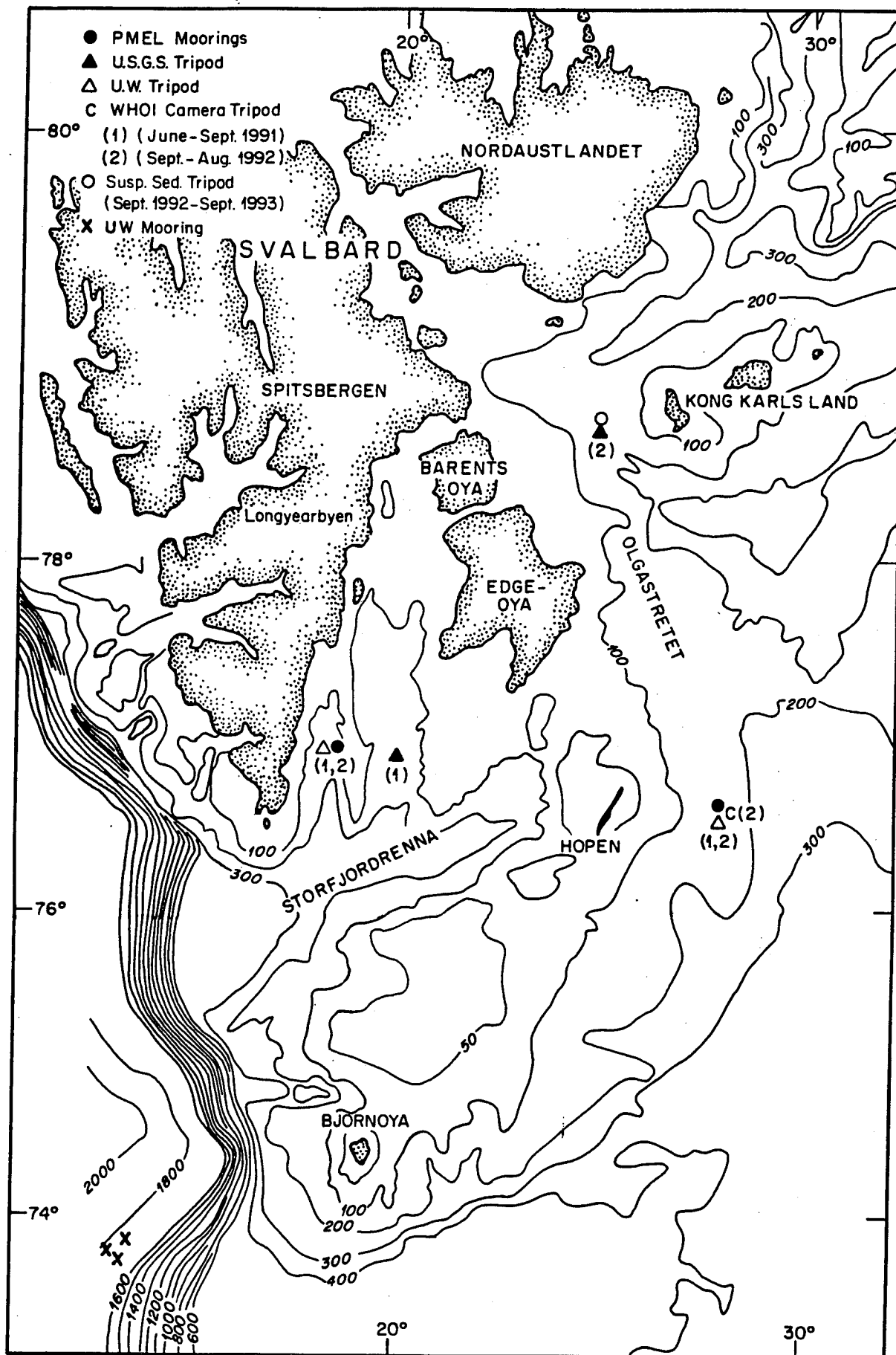


Figure 1. Station locations.

**SEDIMENT TRANSPORT MEASUREMENTS
IN A REGIONAL SEASONAL ICE COVER**

**BOUNDARY LAYER MEASUREMENTS:
DOWNSLOPE OR CONTOUR PARALLEL STORMS
IN THE NORWEGIAN SEA**

**Arthur R.M. Nowell and Richard Sternberg
Erika McPhee**

**School of Oceanography
University of Washington
Seattle, WA 98195**

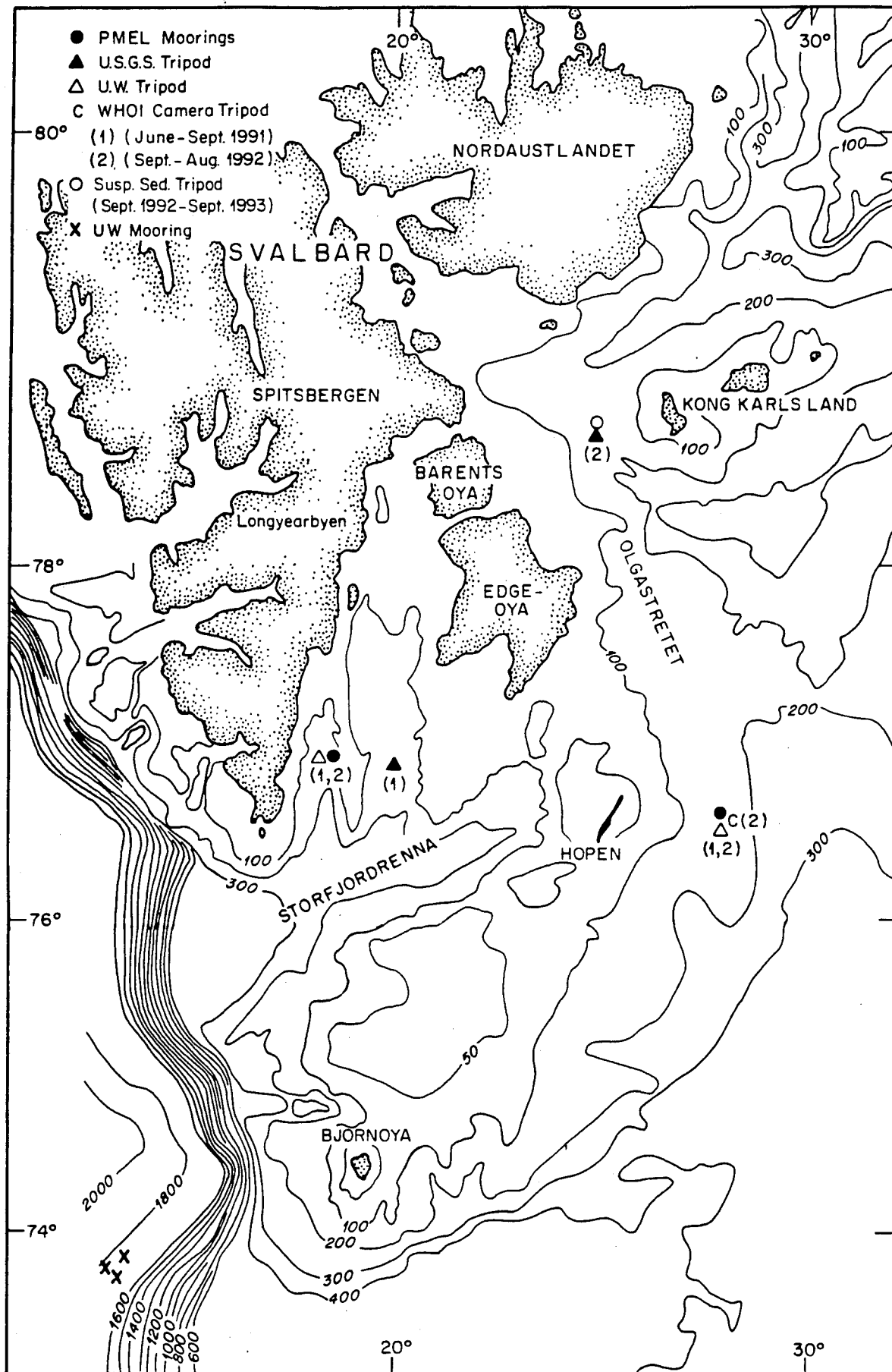
**Sponsor: Office of Naval Research
MG&G program managed by Dr Joe Kravitz**

SEDIMENT TRANSPORT MEASUREMENTS IN A REGION OF SEASONAL ICE COVER

Objectives:

Understand the transport of sediment under the seasonal ice cover in arctic environments

- time varying concentrations of suspended sediment
- modifications in small-scale bed roughness
- erosion and dispersal of water and sediment
- forcing mechanisms
- sediment transport modeling



OBSERVATION SUMMARY

BARENTS SEA

• STORFJORDEN

PMEL (APL) mooring

CTD	116 m	CTD	144 m
UV	115 m	UV	143 m

UW tripod

UV	1 mab
CTD	1 mab
Camera	2 mab
P	2 mab
Suspended sediment	0-3 mab

USGS GEOPROBE tripod (Summer '92)

UV	4 levels ≤ 1.2 mab
CTD	1 mab
Camera	
P	2 mab
Sediment concentration	2 levels ≤ 1.2 mab

• HOPEN ISLAND

PMEL (APL) mooring

CTD	156 m	CTD	183 m
UV	155 m	UV	182 m

UW tripod

UV	1 mab	2 mab
CTD	1 mab	
Camera	2 mab	
P	2 mab	
Suspended sediment	0-3 mab	

WHOI tripod

Bottom photographs

• OLGASTRETET

GEOPROBE tripod

UV	4 levels ≤ 1.2 mab
CTD	1 mab
Camera	
P	2 mab
Sediment concentration	2 levels ≤ 1.2 mab

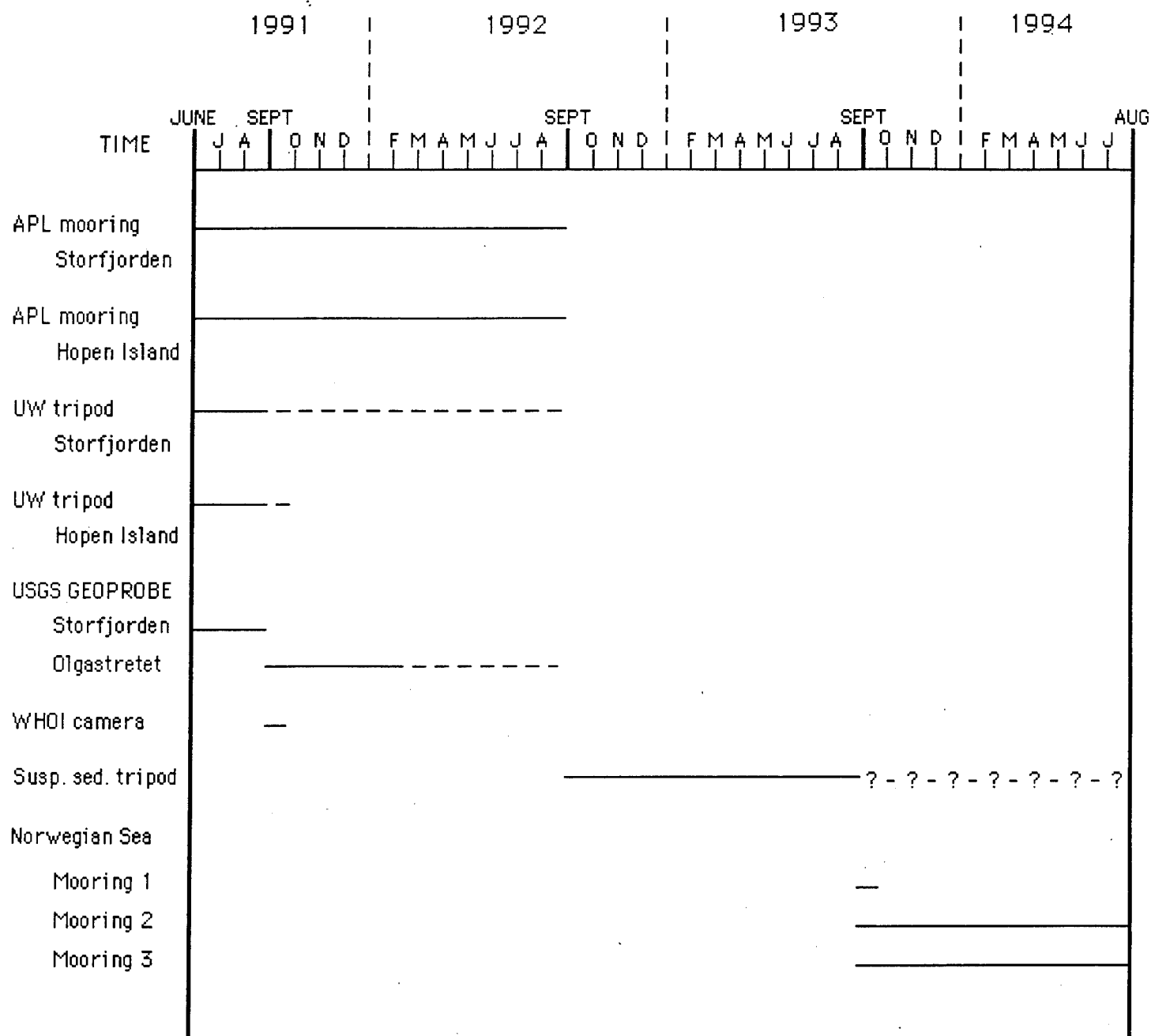
Suspended sediment tripod

Particle size	
U, V	
Particle settling velocity	

NORWEGIAN SEA

Mooring 1, 2, 3

U, V, temperature, conductivity	
Suspended sediment concentration	20 mab



Summary of time series observations at each location in the Barents and Norwegian seas.

Figure 1. Example of 15-month time series from 150 m depth in Storffjorden.
Instrument elevations approximately 2 m above the seabed.

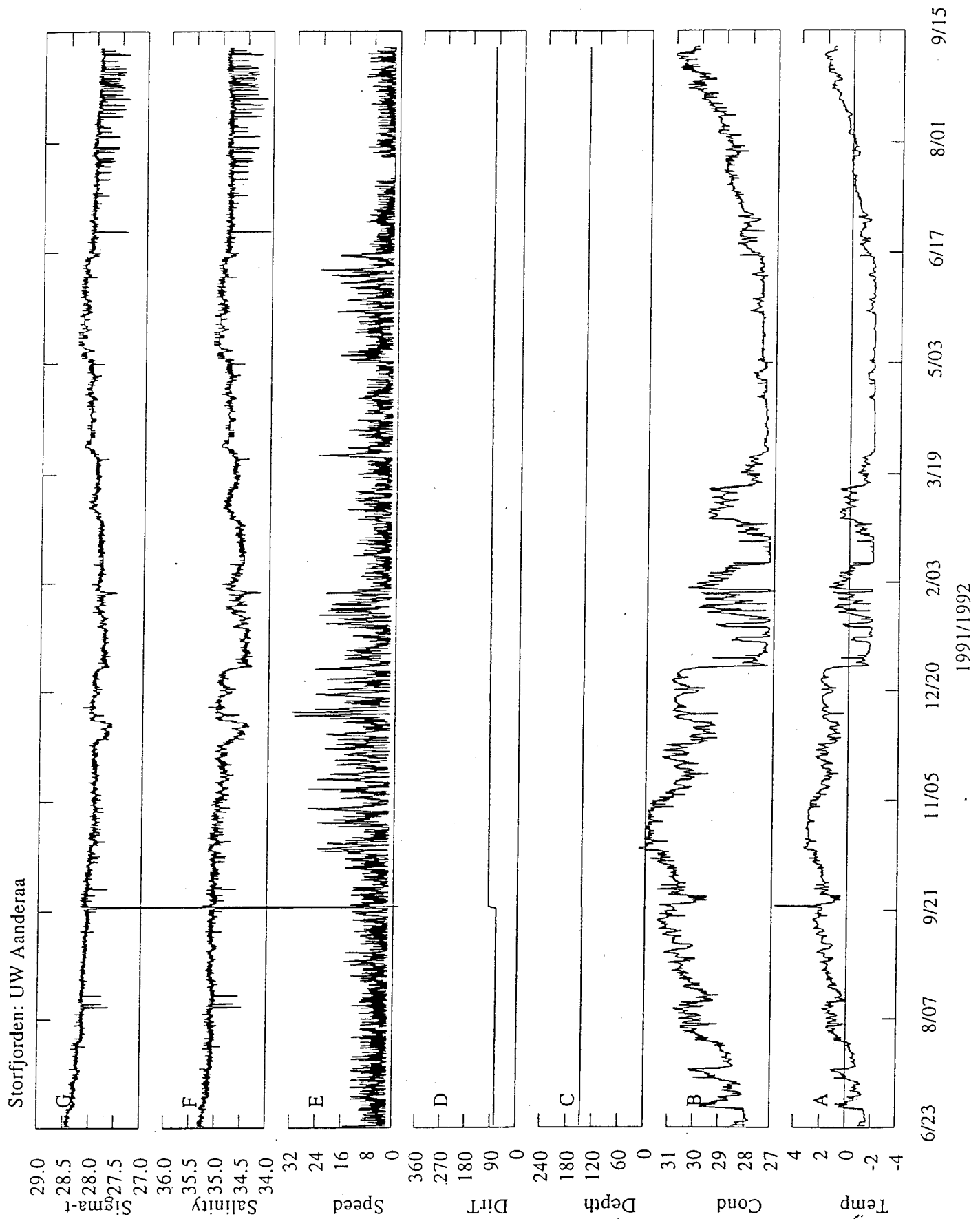


Figure 2. Example of 5-month time series from Olgastretet showing depth, speed, and u (eastward) and v (northward) components of velocity at 0.80 1.20 m above the seabed.

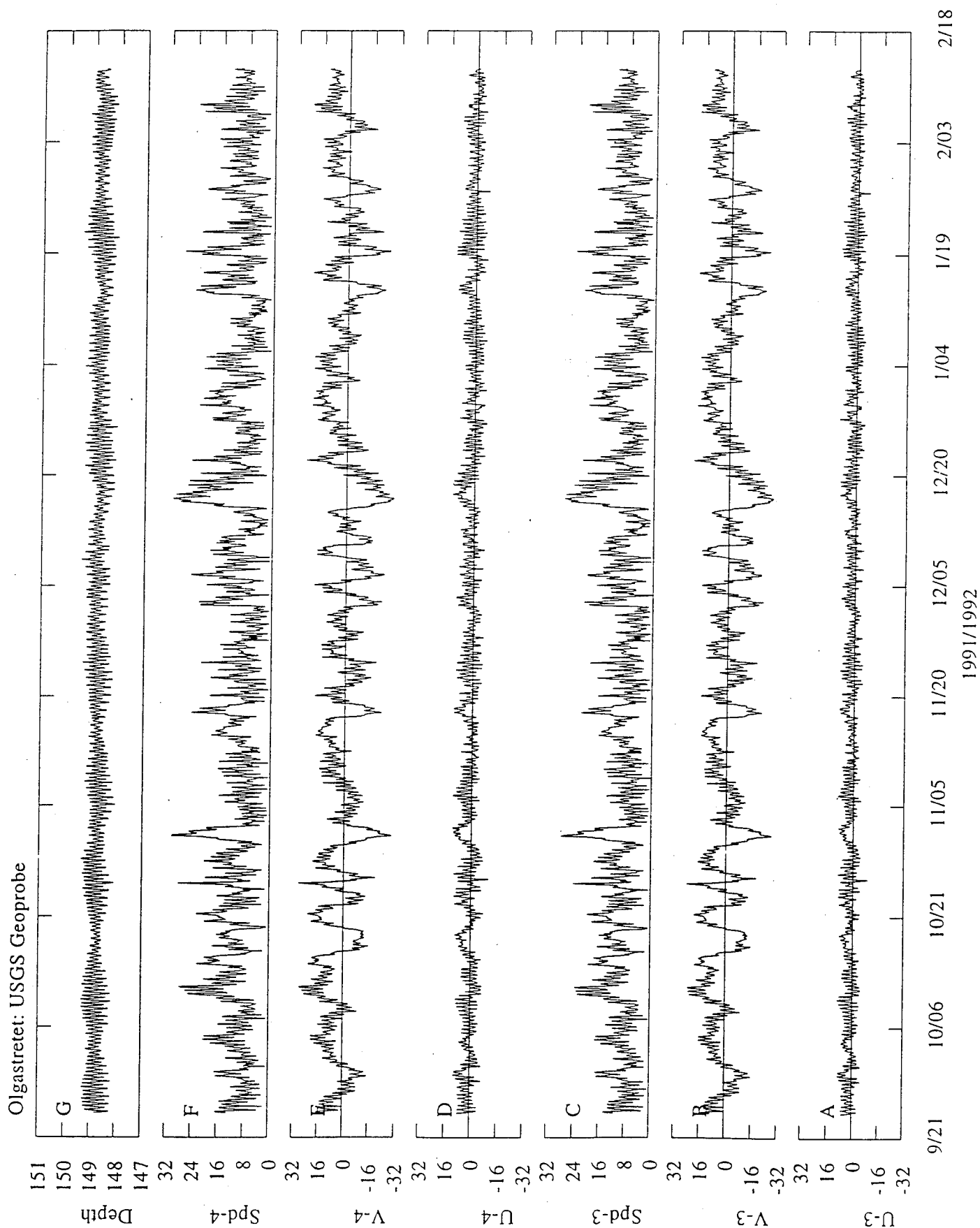


Figure 3. Example of 5-month time series from Olgastreret showing voltage output and light attenuation from transmissometers located at 20 cm (L) and 80 cm (U) from the seabed.

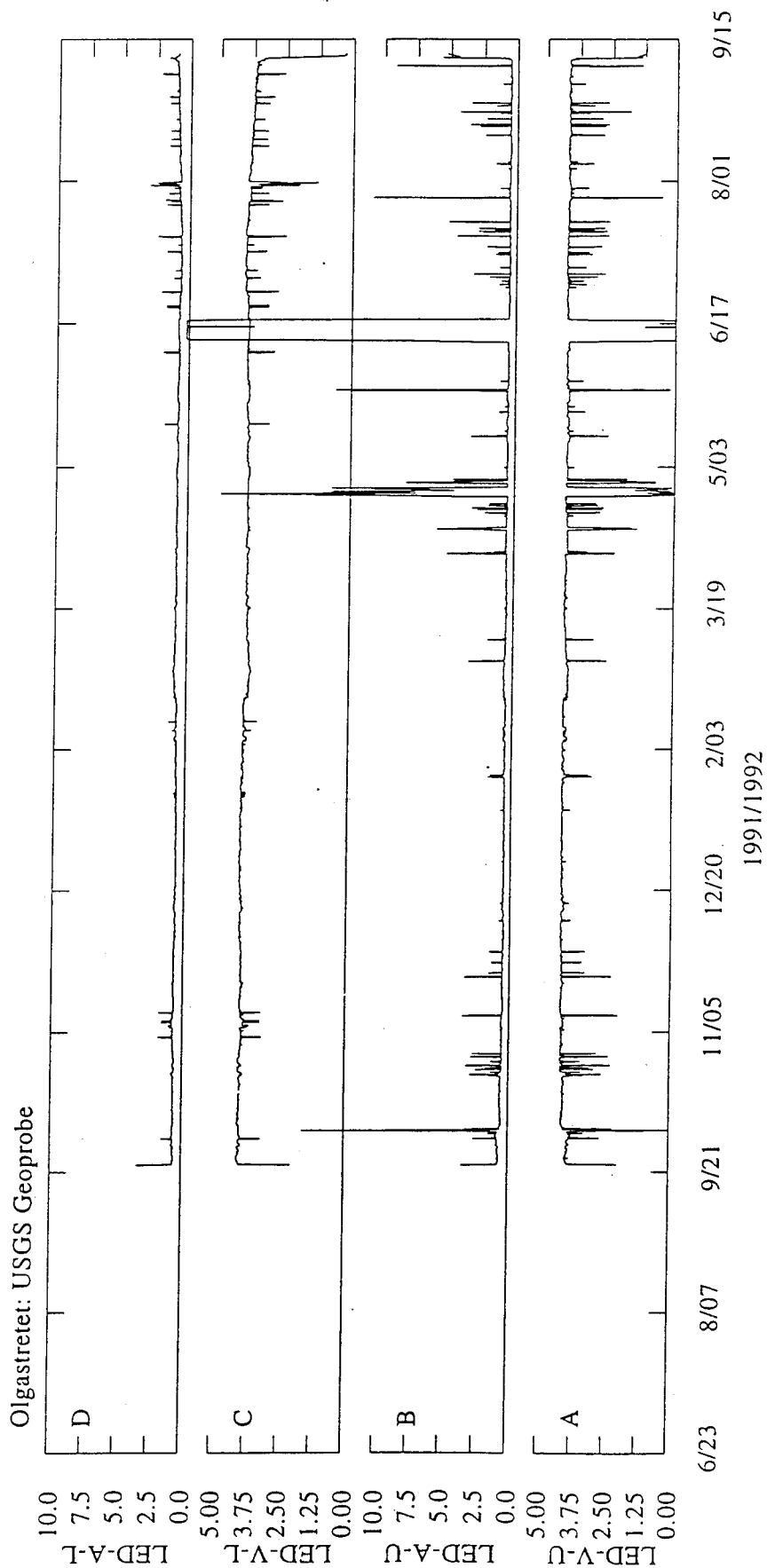


Figure 4A. Seabed photograph taken in Olgastretet.

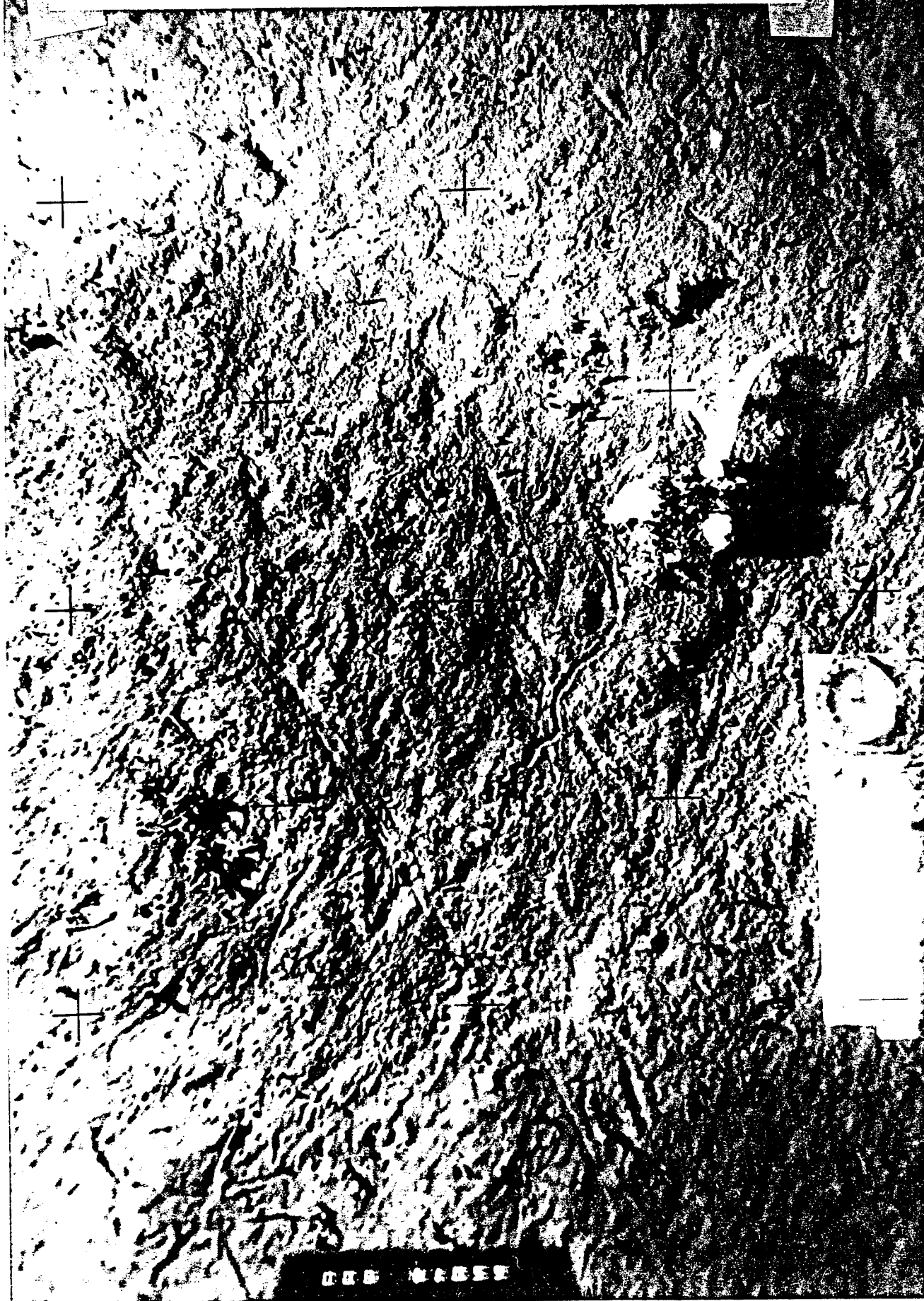


Figure 4B. Similar photograph taken one day later showing accumulation of sediment on compass and scale bar.



Bear Island 3, rotated velocity components

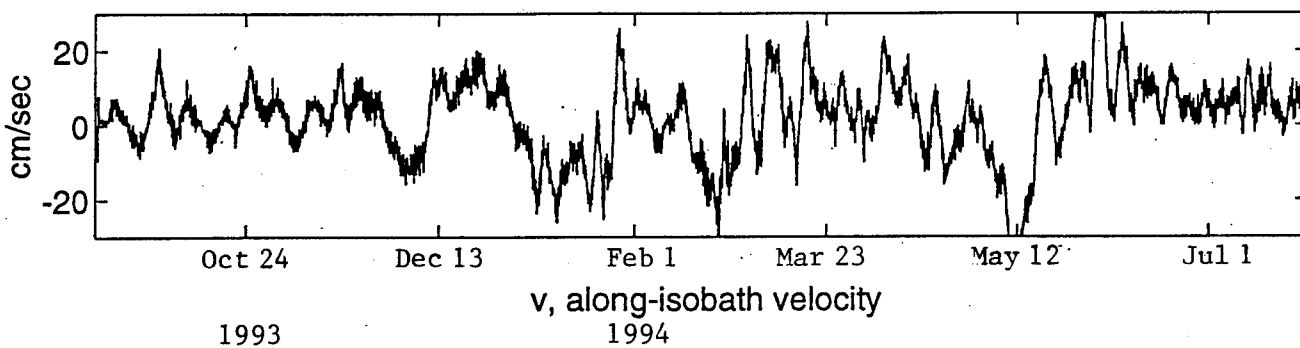
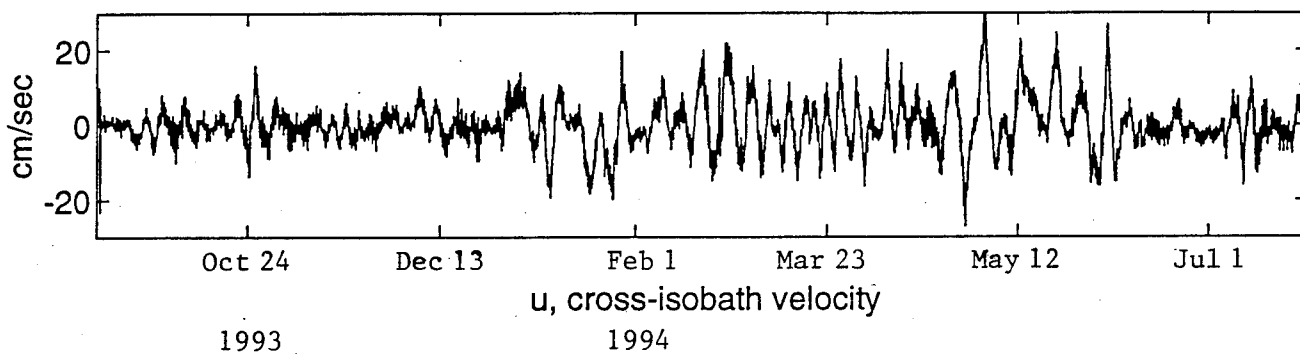
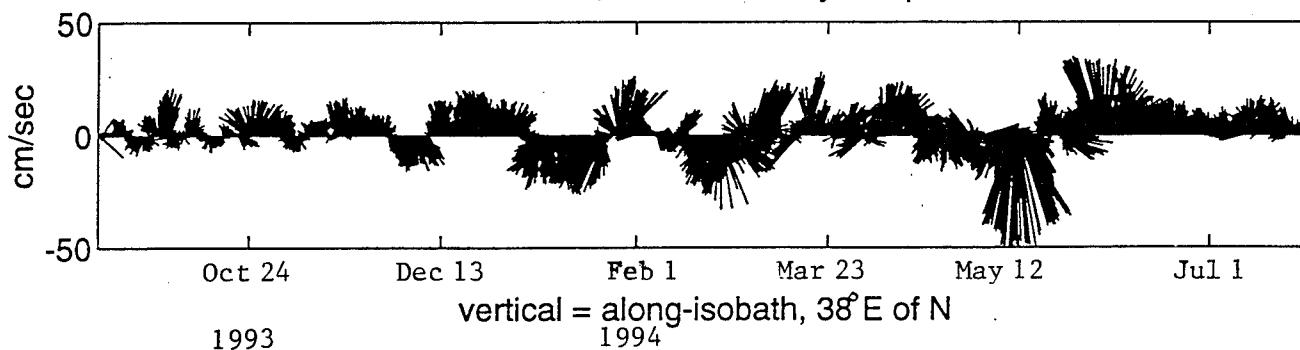


Figure 5. 11-month time series of velocity from Bear Island mooring. Measurements were made 20 m above the seabed and have been rotated to represent along (v) and across isobath (u) flow directions.

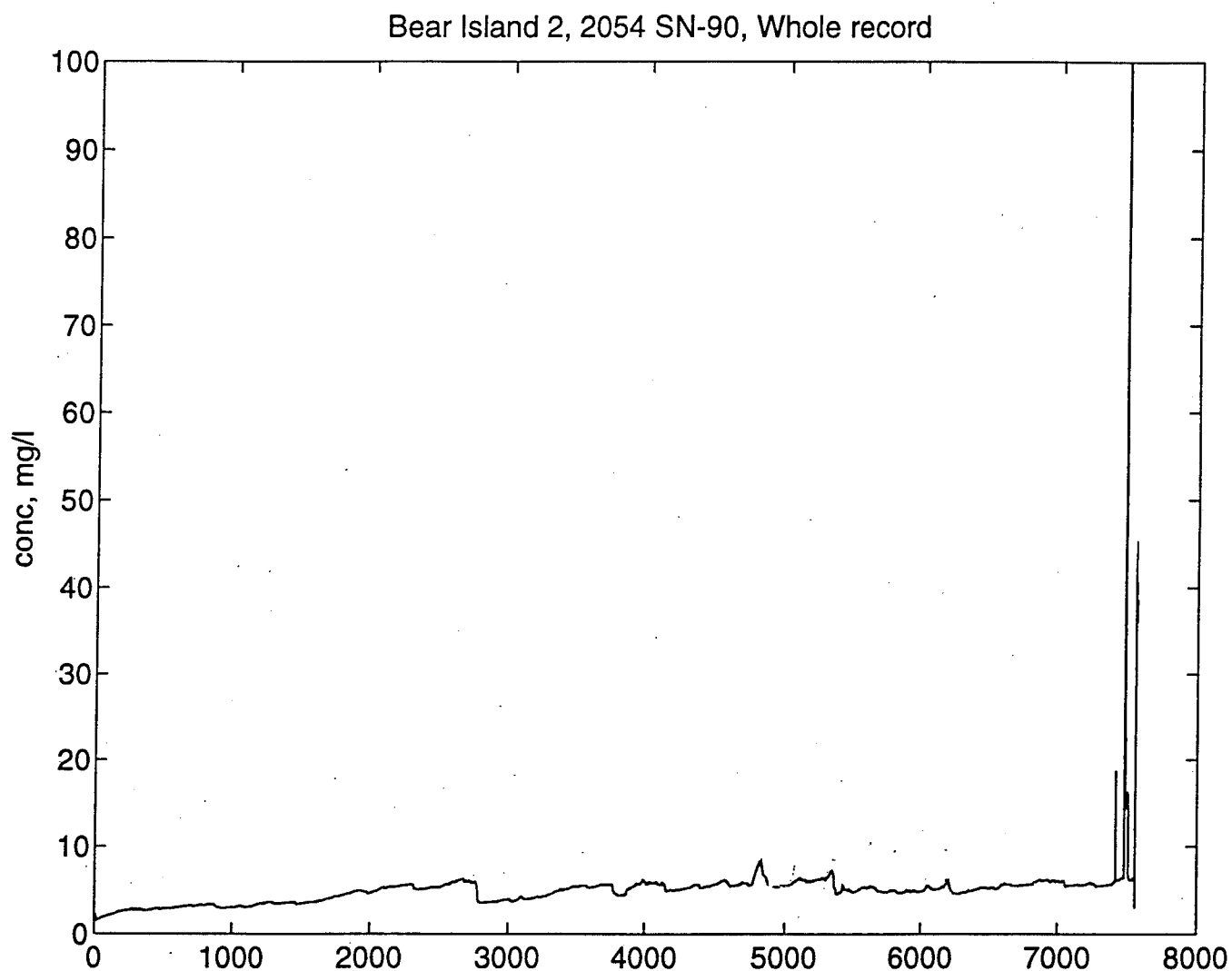


Figure 6. 11-month time series from the Bear Island mooring 2 showing suspended sediment concentration 20 m above the seabed. Record numbers represent hourly measurements beginning on Sept 15, 1993.

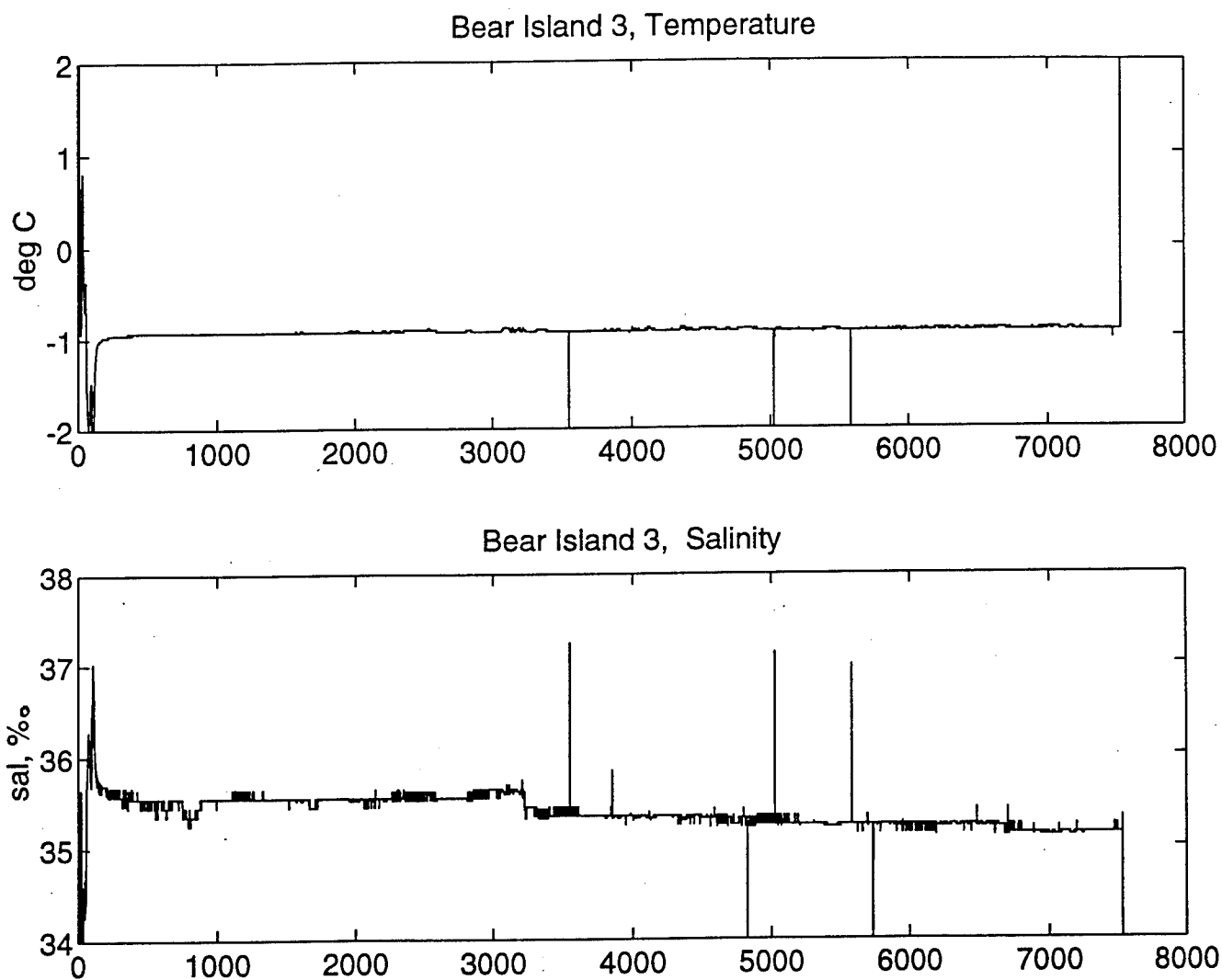


Figure 7. 11-month time series from the Bear Island mooring 2 showing temperature and salinity at 20 m above the seabed. Record numbers represent hourly measurements beginning on Sept 15, 1993.

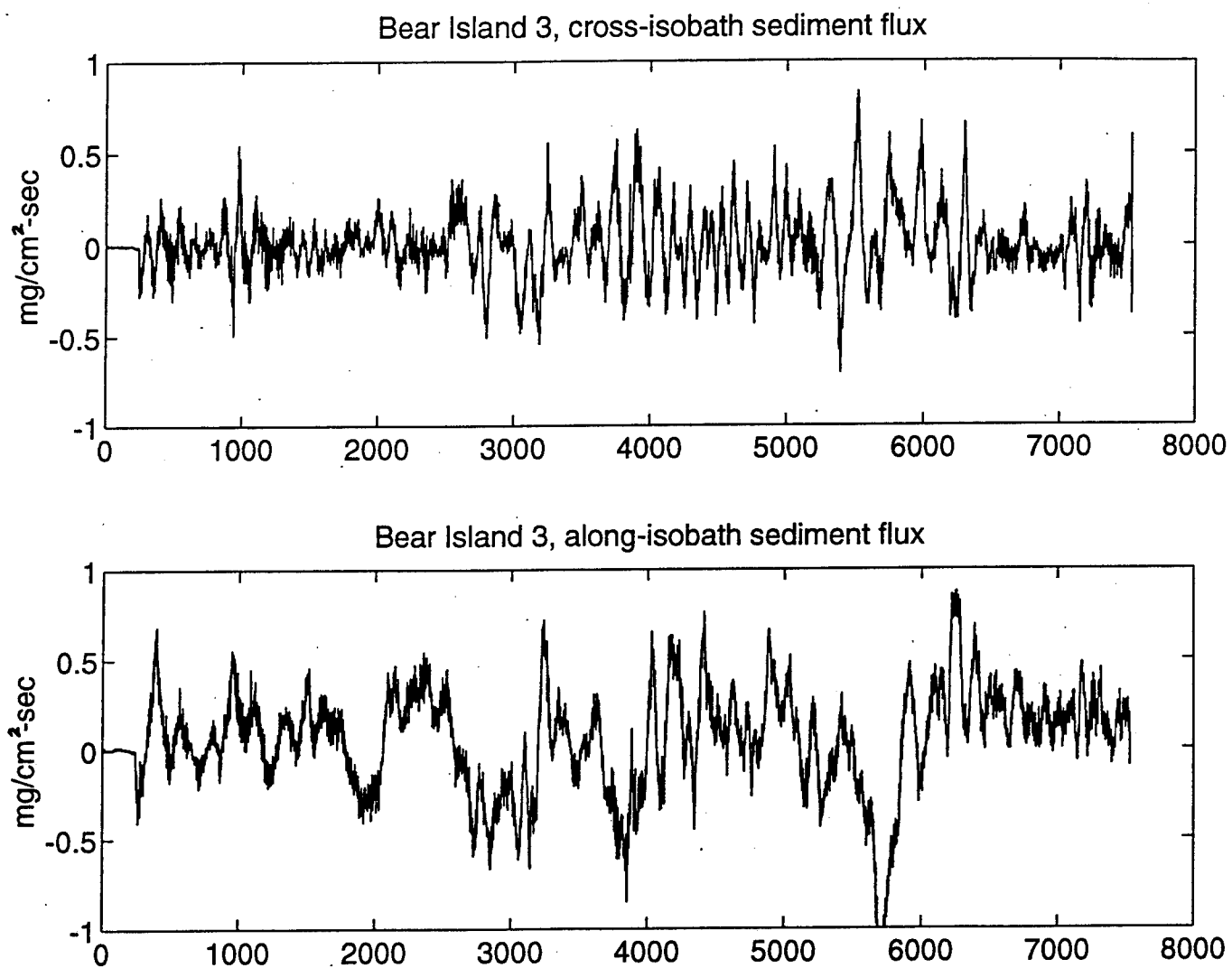


Figure 8. 11-month time series from Bear Island mooring 3 showing suspended sediment flux 15 20 m above the seabed oriented in along-isobath and cross-isobath directions. Record numbers represent hourly measurements beginning on Sept 15, 1993.

Overview of the NRL Large Scale Modeling Effort Studying the Dispersion of Radioactive Contaminants in the Arctic

Ruth Preller

An Overview of the NRL Large Scale Modeling Effort Studying the Dispersion of Radioactive Contaminants in the Arctic

Ruth H. Preller

Presented at the Workshop on
Modeling the Dispersion of Nuclear Contaminants
in the Arctic Seas

In 1993, the former Soviet Union released information pertaining to the dumping of nuclear waste into the Arctic Seas. A paper known as the Yablokov report or the "White Paper" was published containing data on both source locations and the amount and type of material dumped at these locations. This report indicated that the sources were low-level solid and liquid waste, high-level waste in the form of nuclear reactors, fuel rods with spent nuclear fuel and even discarded vessels containing nuclear waste. In addition, the Ob, the Yenisei and the Pechora rivers were sited as sources of nuclear contamination. The first figure included in this abstract is a table from this report showing the radionuclide budget for the Kara and Barents seas.

The object of this study is to determine what might happen to this radioactive material if and when it enters the water column. To look at possible answers to this question, we have made use of the Naval Research Laboratory's coupled ice ocean model. This model consists of the Hibler ice model coupled to the Cox ocean model and uses a 0.28 degree grid resolution (approximately 25 km). The model extends from the North Pole southward to approximately 30 degrees North latitude. For the initial phase of this study, we have decoupled the ice from the ocean model and will restrict our simulations to the ocean model.

Several ten year numerical model simulations have been run. In each case, the model was driven by an annually averaged wind field from 1986 atmospheric data from the U.S. Navy's global model and initialized from Levitus climatology. The following five test cases are presented using sources described in the Yablokov report: low-level solid and liquid waste, high level waste, rivers (Ob, Yenisei and Pechora), Sellafield (Irish Sea) and finally a combination of Sellafield and the rivers. Data from a recent 1992 joint Russian-Norwegian cruise indicated that levels of radiation in the Kara were ranging from 5-25 Bq/m³. Models results indicated that when the low level sources were used, the resulting levels of radiation were too weak. When the high level sources were used, the resulting levels of radiation were too strong. When river outflow was used as a source, the resulting levels of radiation were consistent with those measured in the Kara. The second figure included with this abstract shows the model results at the end of the tenth year for the case using rivers as a source. Note that 5 Bq/m³ is approximately 0.1 PCi/l which is represented by the pink color contour in this plot. When a simulation was run using Sellafield as a source, the ten year result agreed well with observation in the Norwegian, Greenland and Barents Seas, but appeared to give results that were too weak in the Kara Sea (see the abstract by Kathy Crane in this proceedings). The final test (see final figure) combining these two sources, the rivers and Sellafield, appeared to give the best results when compared to observations.

Future work will include a more detailed comparison to data as it become available (see the abstract by Cheng in this proceedings), continued modeling of the rivers as a source of radioactivity in conjunction with the river modeling project also presented at this workshop (see abstracts by Paluszkiewicz and Hibler), and modeling the possible transport of radioactive material via sediment trapped in sea ice.

**Table 5. Anthropogenic Radionuclide Budget
of the Barents and Kara Seas Ecosystem, 1961-1990**

Source of Long-Lived Radionuclides	Barents Sea		Kara Sea		Ecosystem as a Whole	
	Activity		Activity		Activity	
	kCi	TBq	kCi	TBq	kCi	TBq
1. Atmospheric fallout	100	3700	70	2600	170	6300
2. River runoff	6.0	200	33.0	1200	39	1400
3. Contributions from Gulf Stream system	200	7400	—	—	200	7400
4. Dumping of solid and liquid RW	13	480	16	600	30	1100
5. Sinking of SRW with SNF	—	—	2300*	85300*	2300*	85100
6. Underwater and surface nuclear explosions	...(No data)...					
Total (upper limit)	319	11780	2419	89700	2739	101300

*—Expert estimate of the upper limit of activity at the time of disposal.

Figure 1. Table 5 from the Yablokov report, page 29.

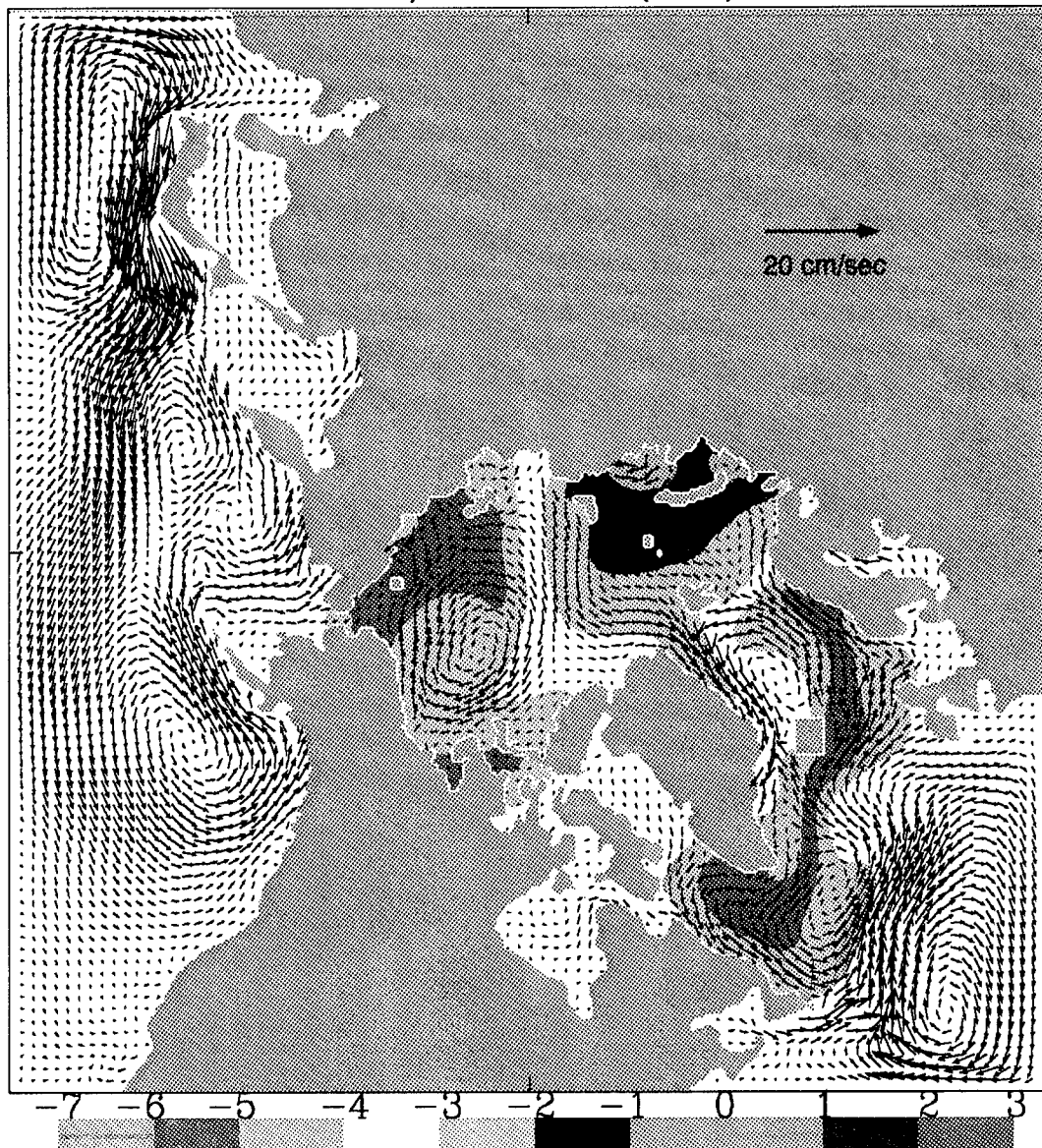


Fig. 2 The dispersion of the river outflow radionuclides at 15 meters deep at year 10. The colors which are in a logarithm scale represent the radionuclide level in PCi/l. The arrows are the ocean currents plotted at every fourth point..

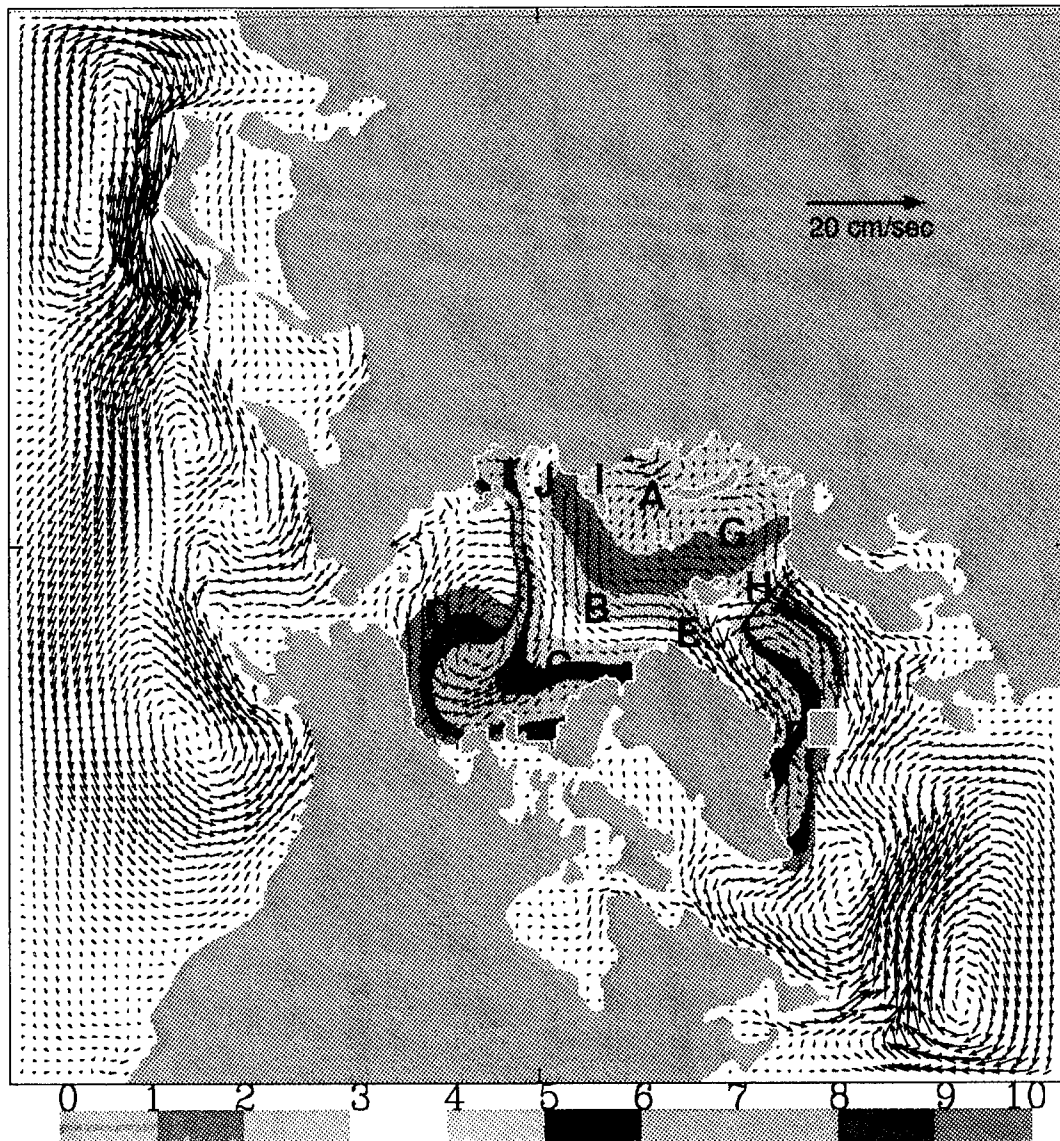


Fig. 3 A contour plot of the 10^5 PCi/l contours from Year 1 to 10 in the top mixed-layer based on the river outflow radionuclides. The color scale represents the end of each year. The arrows are the ocean currents.

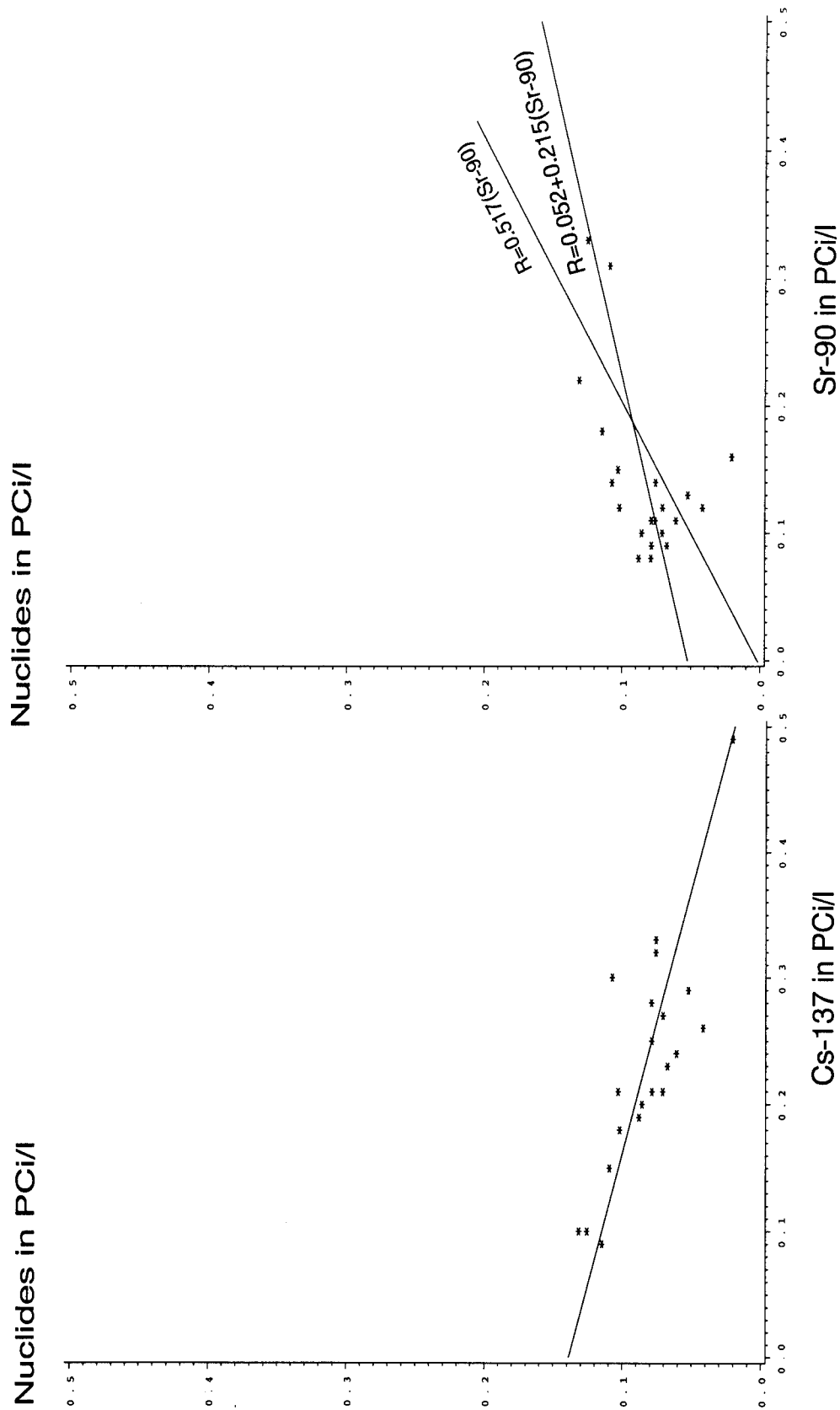


Fig. 4 Plots of the estimated radionuclides versus the measured Cs-137 and Sr-90.

The Effect of River Discharge in a Large Scale Ice/Ocean Model

Rick Allard

The Effect of River Discharge in a Large Scale Ice/Ocean Model

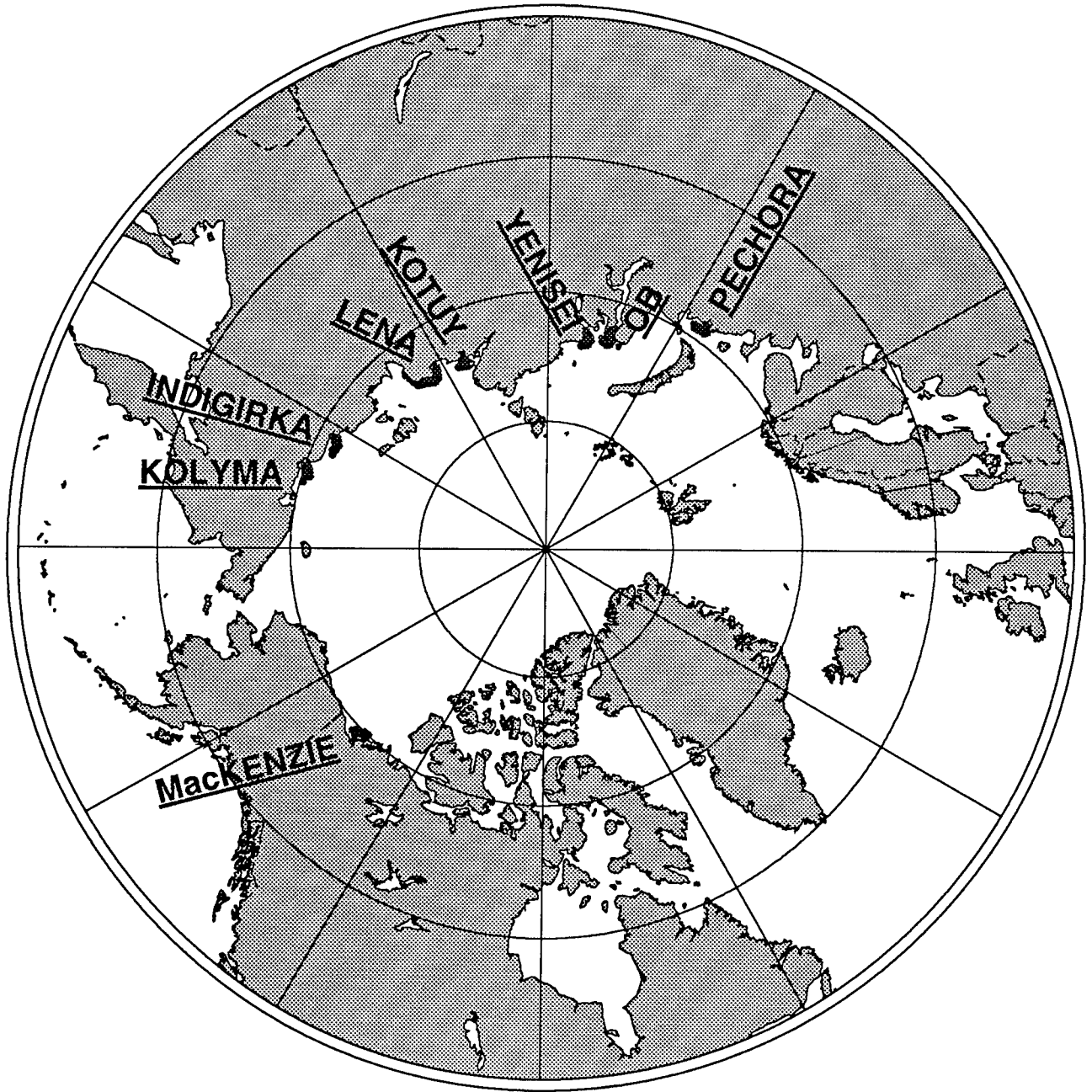
Richard Allard
Naval Research Laboratory
Stennis Space Center, MS 39529

Abstract

The effect of river inflow on the growth and melt of ice along the Siberian Shelf is examined with PIPS2.0, the spherical version of the Hibler model with a .28 deg resolution in the Arctic Basin coupled to the Cox ocean model. This coupled model encompasses a hemispheric domain from near 30.0 °N to the North Pole and includes most sea ice-covered areas such as the Gulf of St. Lawrence, the Yellow Sea, the Seas of Okhotsk and Japan as well as the Arctic and sub-Arctic areas. The model is forced by the Navy Ocean Global Atmospheric Prediction System (NOGAPS). A 50-year (1937-1986) data set of volume fluxes from 9 major rivers emptying into the Arctic Basin (8 Russian and the Mackenzie) is used. Each discharge is specified at several grid points. The largest river discharges (Lena, Yenisei) always show maxima in June. The rivers are specified as source regions of 0 ppt salinity and monthly varying runoff temperatures. Test cases examined include a "no-river" case, mean (1937-1986) rivers and an "extreme" river case in which the maximum monthly discharge during a 50-year period was used.

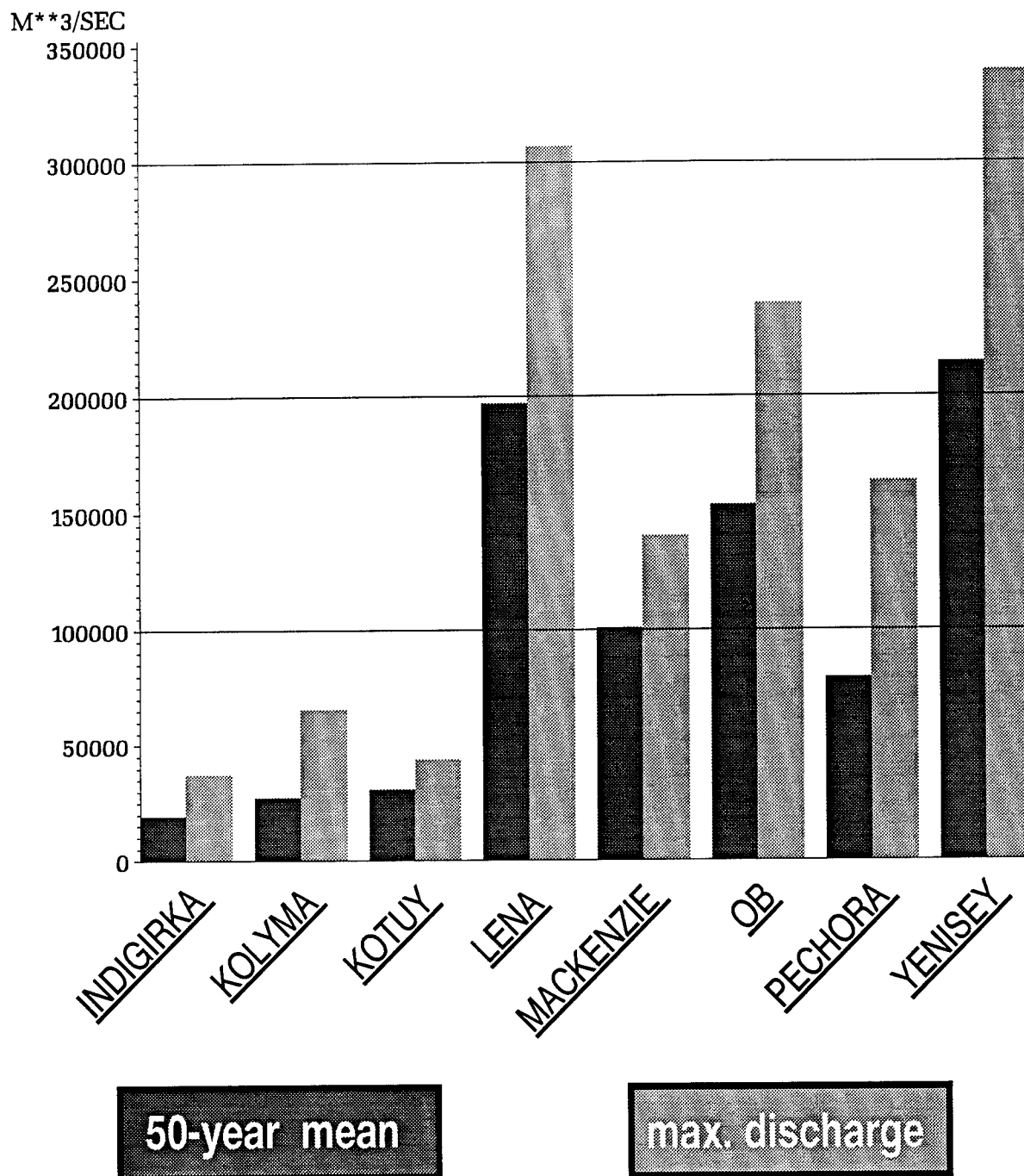
The inclusion of river discharge produces initially northward flowing surface currents with peak velocities of 6 cm/sec near the Lena River in June. As discharge decreases during the summer and autumn, these surface currents decrease in magnitude. The combination of warmer, fresher river water during summer promotes a thinner ice cover in the vicinity of the rivers. In the Laptev Sea, there is about 1 meter less ice by late August when compared to the test case without rivers. In autumn, the fresher water has a warmer freezing temperature, allowing thin ice to grow quicker when air temperatures are below freezing. The extreme river case shows a quicker ice melt in late spring and summer, and more ice growth in the Laptev Sea in autumn as a consequence of a warmer freezing temperature. The Arctic interior shows ice differences from 0 to 20 cm, when rivers are included.

RIVER LOCATIONS IN PIPS2.0 MODEL DOMAIN



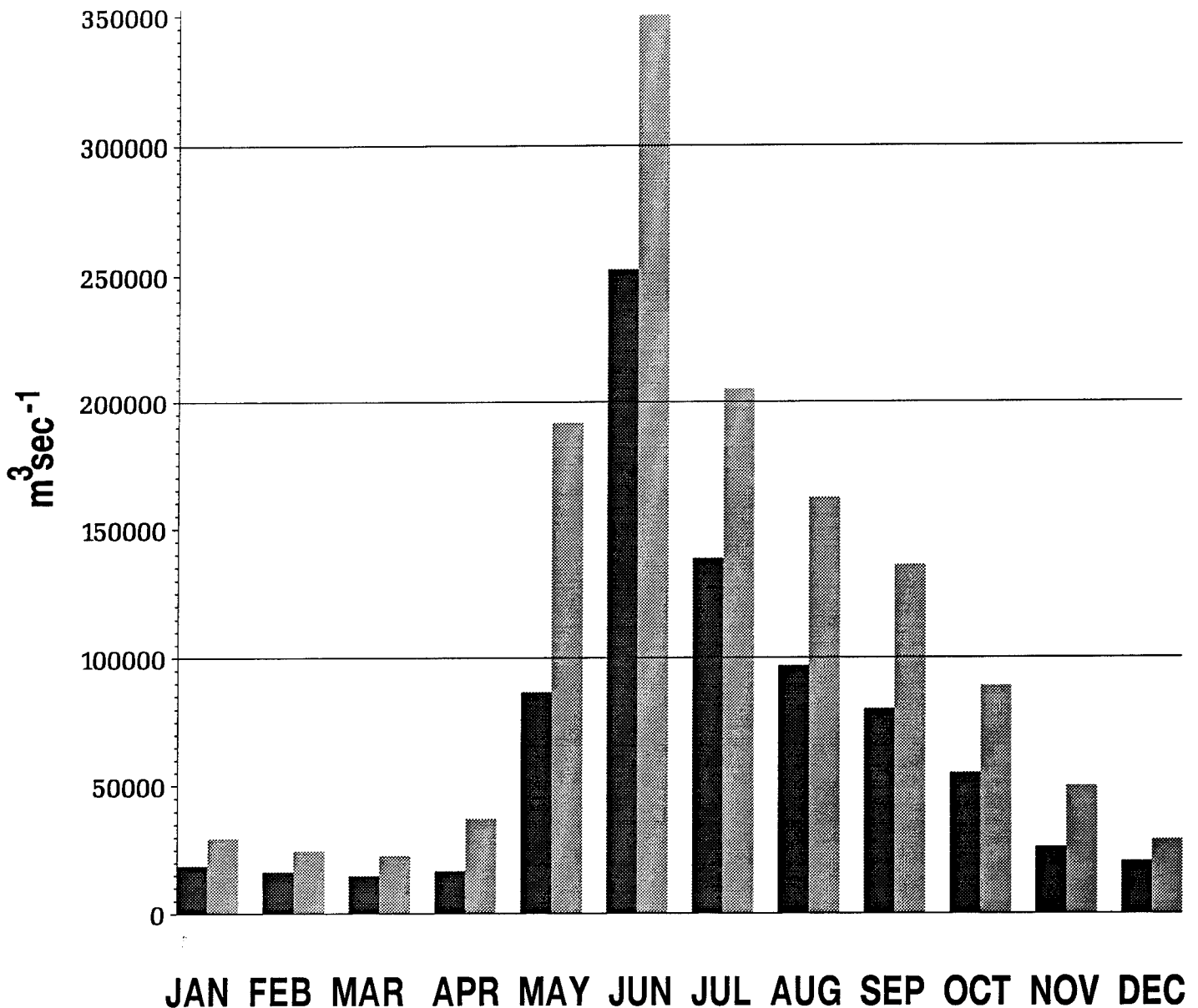
ANNUAL ARCTIC RIVER DISCHARGE

1937 - 1986



MONTHLY ARCTIC RIVER DISCHARGE

FOR 9 MAJOR RIVERS (1937-1986)

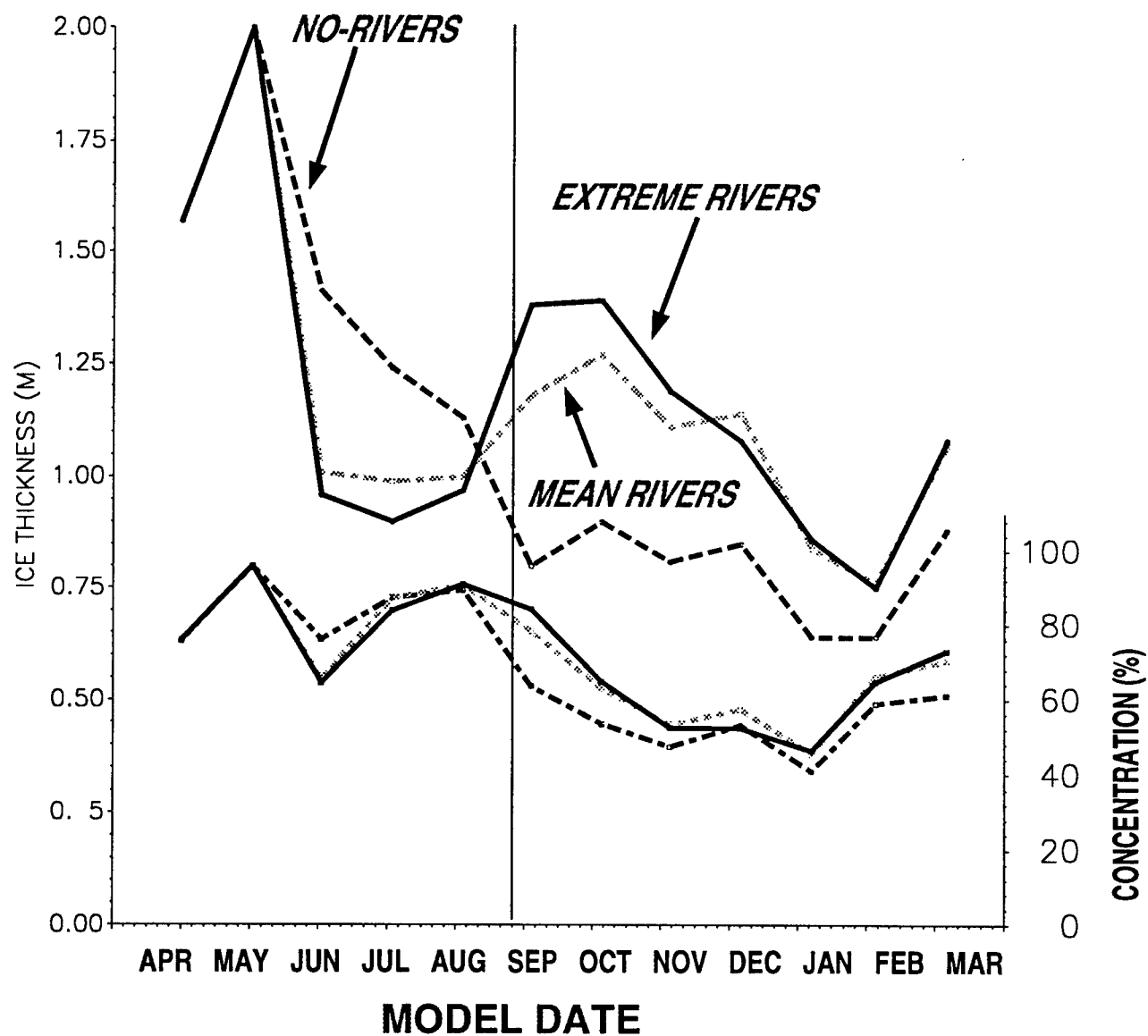


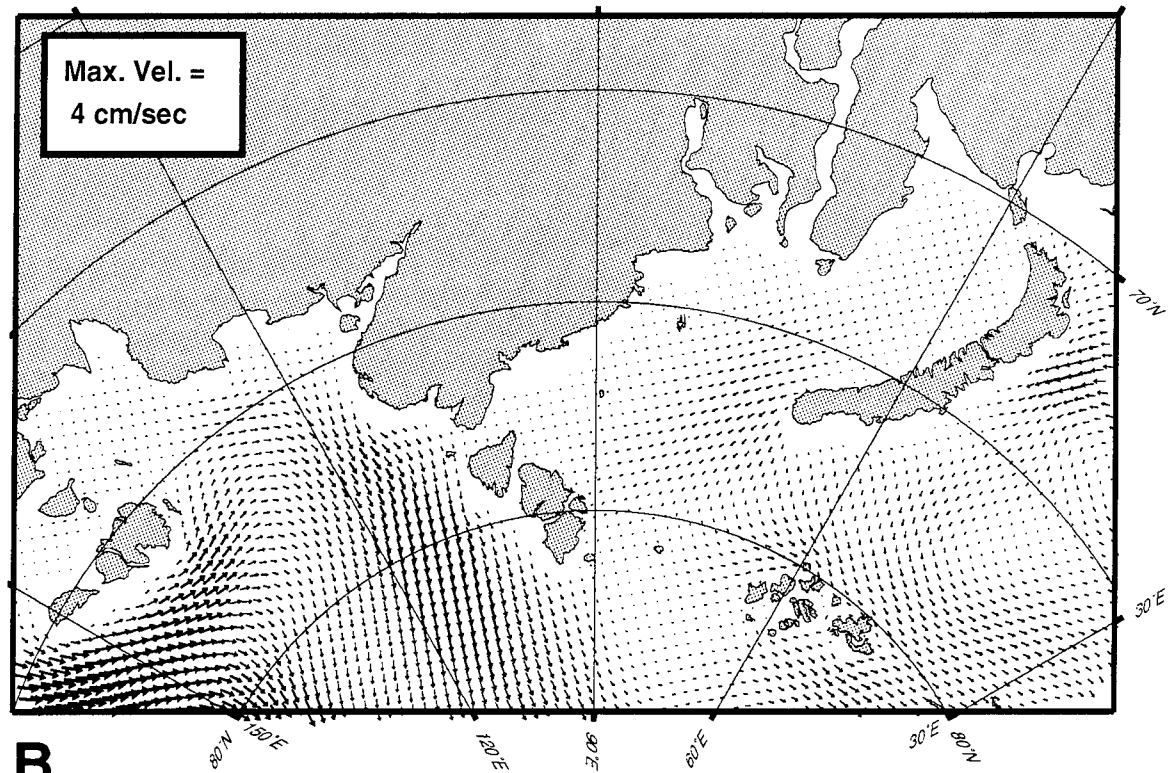
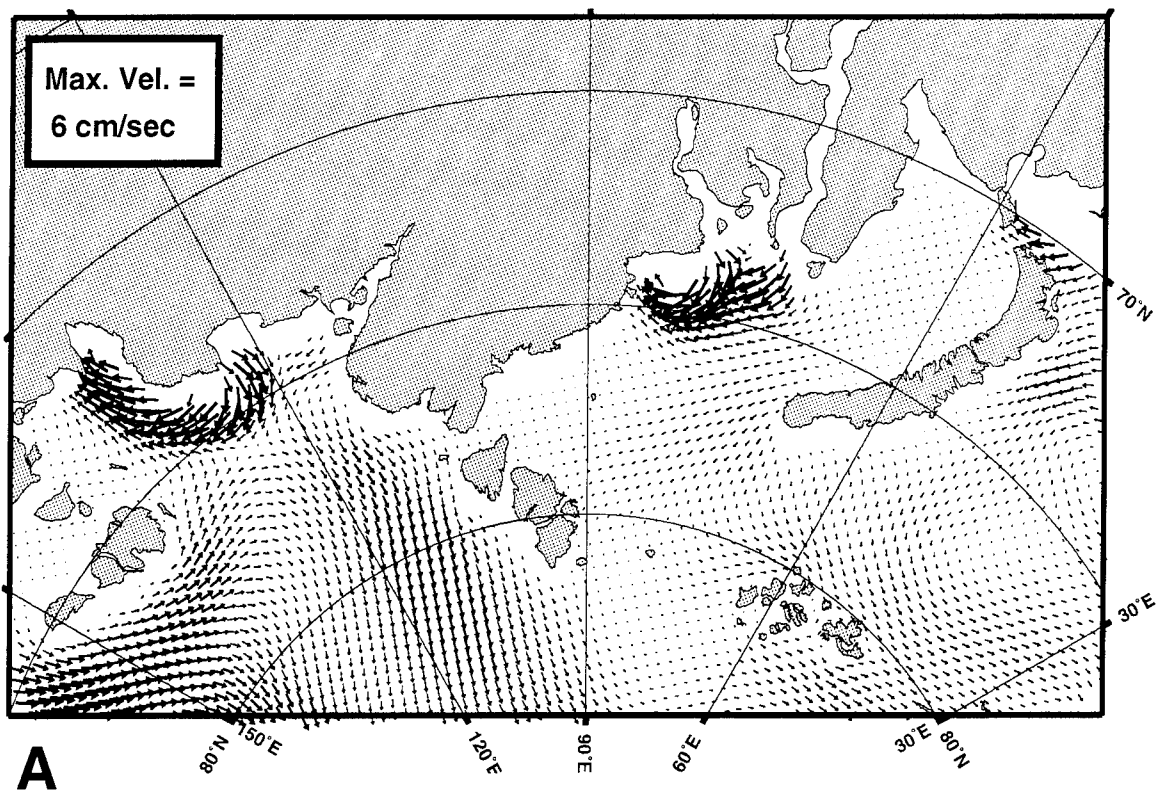
50 year mean

max. discharge

PIPS2.0 ICE THICKNESS/CONCENTRATION

LENA RIVER REGION





Surface ocean currents in the Laptev and Kara Seas a): with rivers,
b): without rivers.

Sea Ice Transport of Pollutants in the Laptev Sea

Ignatius Rigor

Sea Ice Transport of Pollutants in the Laptev Sea

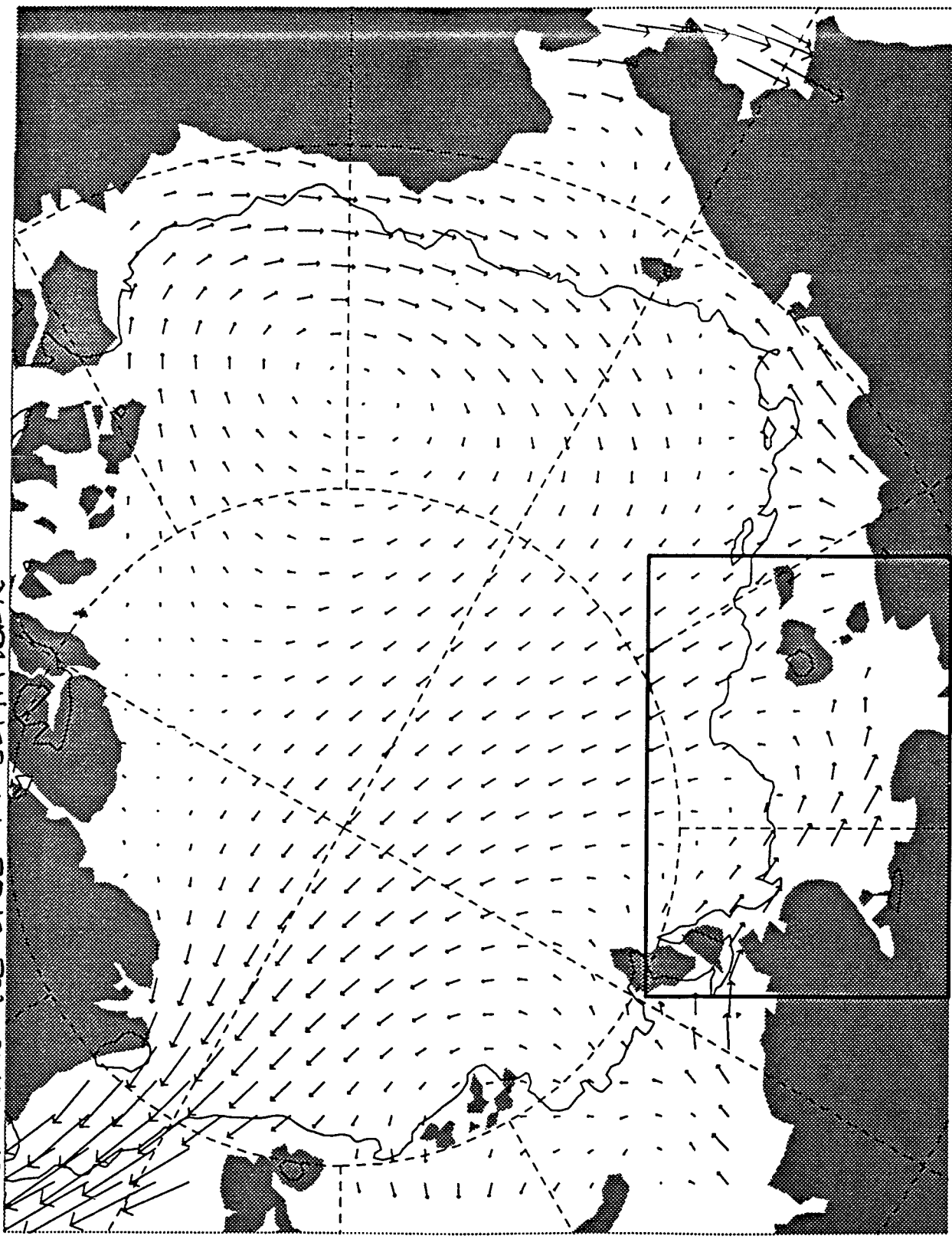
About 900,000 km² of the polar pack ice is transferred annually from the Arctic Basin to the North Atlantic. The largest portion of this exported ice cover is created by the large scale divergence within the ice pack. A smaller portion of the ice cover originates in the marginal seas, either by fall freezing of the seasonally ice free waters or by wintertime advection away from the coast.

The main objective of this study is to estimate the annual production of ice in the Laptev Sea and to determine its ultimate fate. The study is motivated by the possibility that ice formed in the Laptev Sea may be an agent for the long range transport of pollutants such as radionuclides.

The strongest evidence for long range, non-diffusive, pollution transport is the ubiquitousness of "dirty ice" throughout the eastern Arctic, e.g Pfirman et al (1990) and Nuernberg et al (1993). Although much of the ice is discolored by biogenic material, there is clear evidence of fine grained lithogenic material. While the biogenic material grows throughout the arctic, the lithogenic material can only be incorporated into ice formed in the coastal waters.

In this study we attempt to characterize the mean and interannual variability of ice production by investigating the winter production and subsequent melt of ice in the Laptev Sea from 1979 through 1992. The general approach is to associate pollution transport with the net exchange of ice area from the Laptev Sea to the perennial ice pack. The primary data sets supporting the study are ice charts, ice motion, and geostrophic wind. Unfortunately we have no direct measurement of pollutants.

MEAN FIELD OF ICE MOTION USING (PUG) + DAZHUS DATA +
MULTI-YEAR ICE EDGE IN SEPTEMBER



Shallow Water Ice Production Areas in October

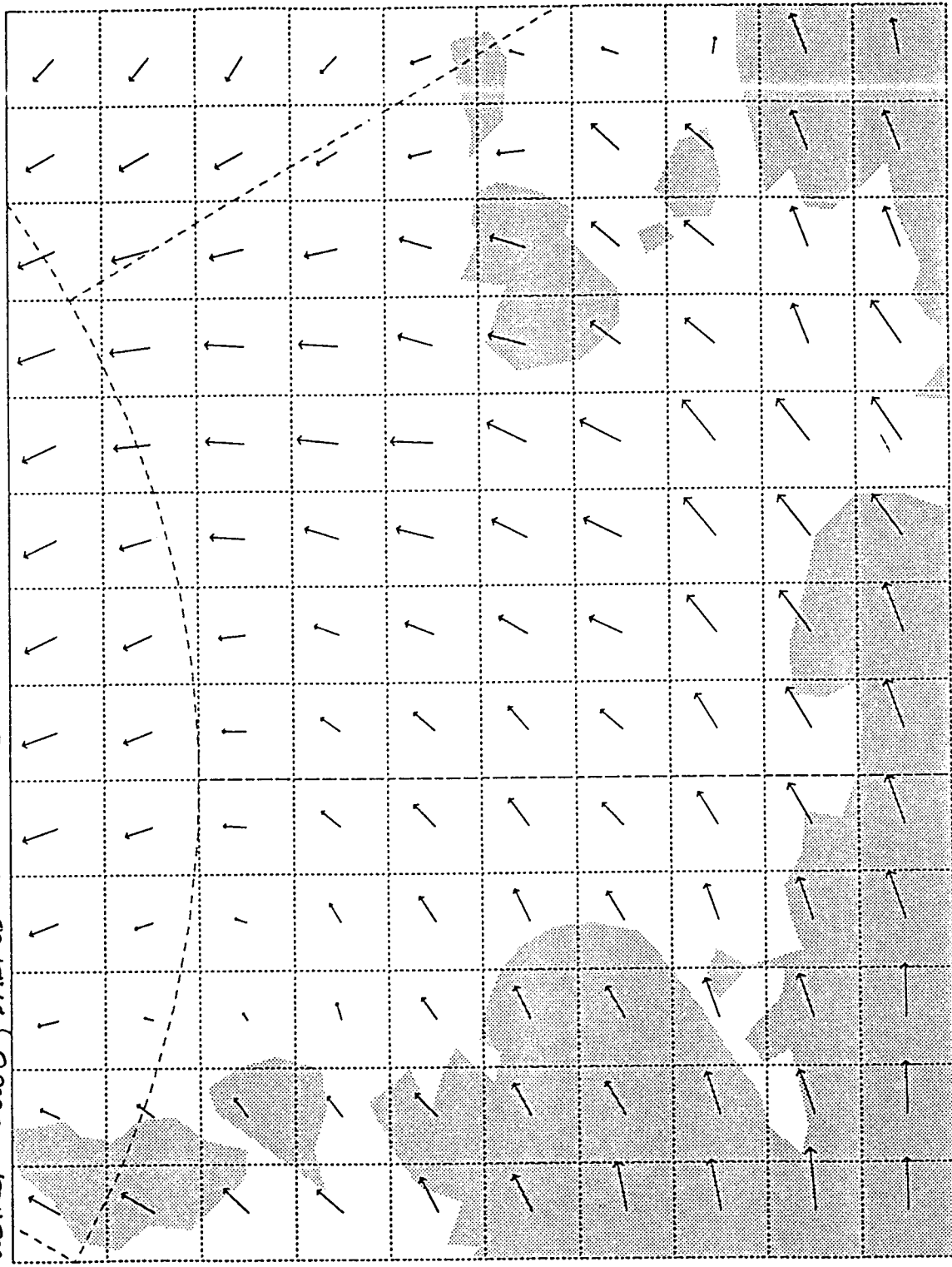


Interannual Variability of Ice Production Areas

October

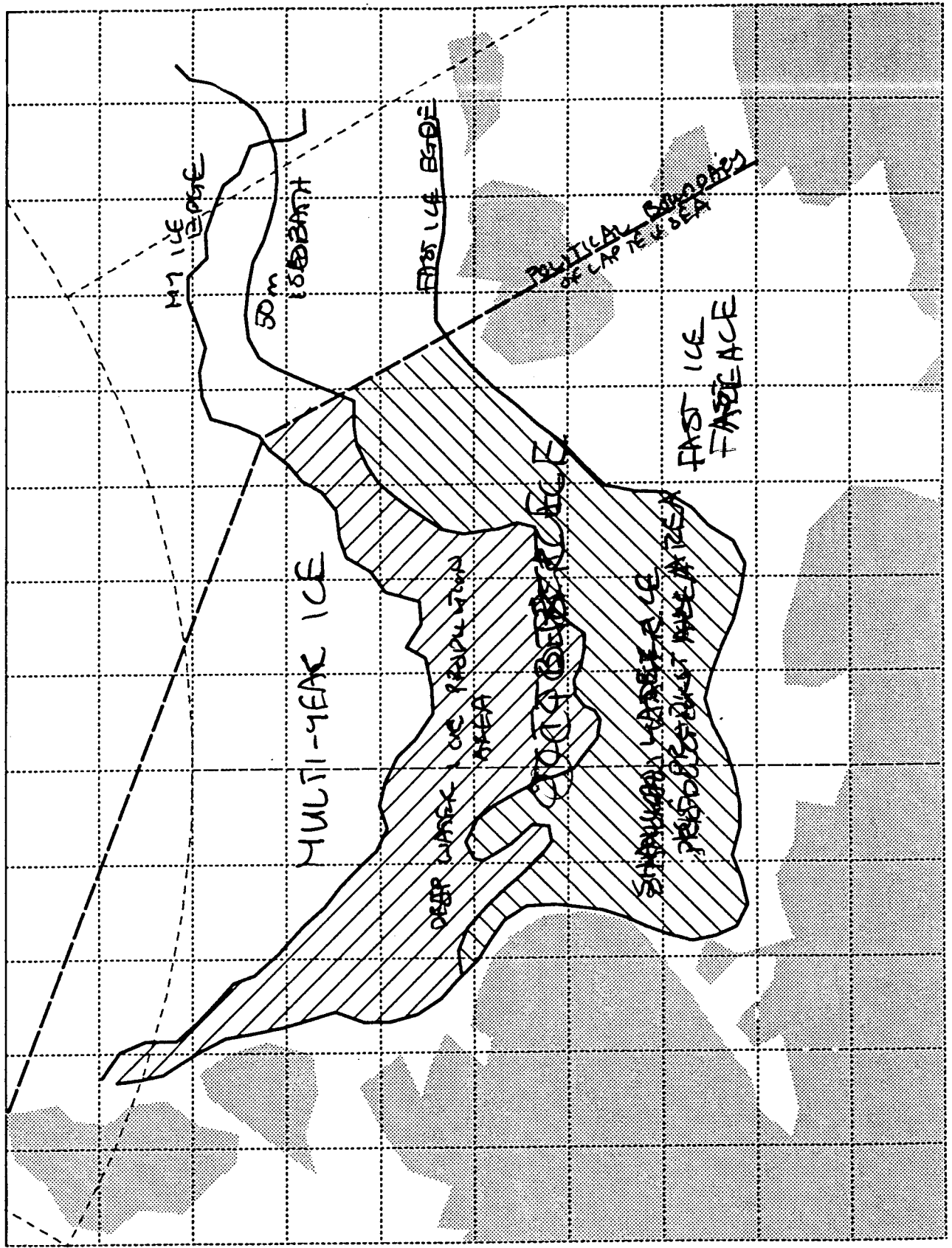
Year	Deep	Shallow	Very Shallow
1978	159000	147000	197000
1979	65000	132000	197000
1980	45000	132000	197000
1981	106000	147000	197000
1982	109000	147000	197000
1983	129000	147000	197000
1984	116000	147000	197000
1985	165000	141000	197000
1986	52000	147000	197000
1987	0	97000	197000
1988	0	129000	197000
1989	0	63000	197000
1990	166000	145000	197000
1991	96000	140000	197000
1992	0	111000	197000
Means:	80000	125000	197000

MEAN FIELD of ICE MOTION
USING BUOY, DARRMS & WINDS

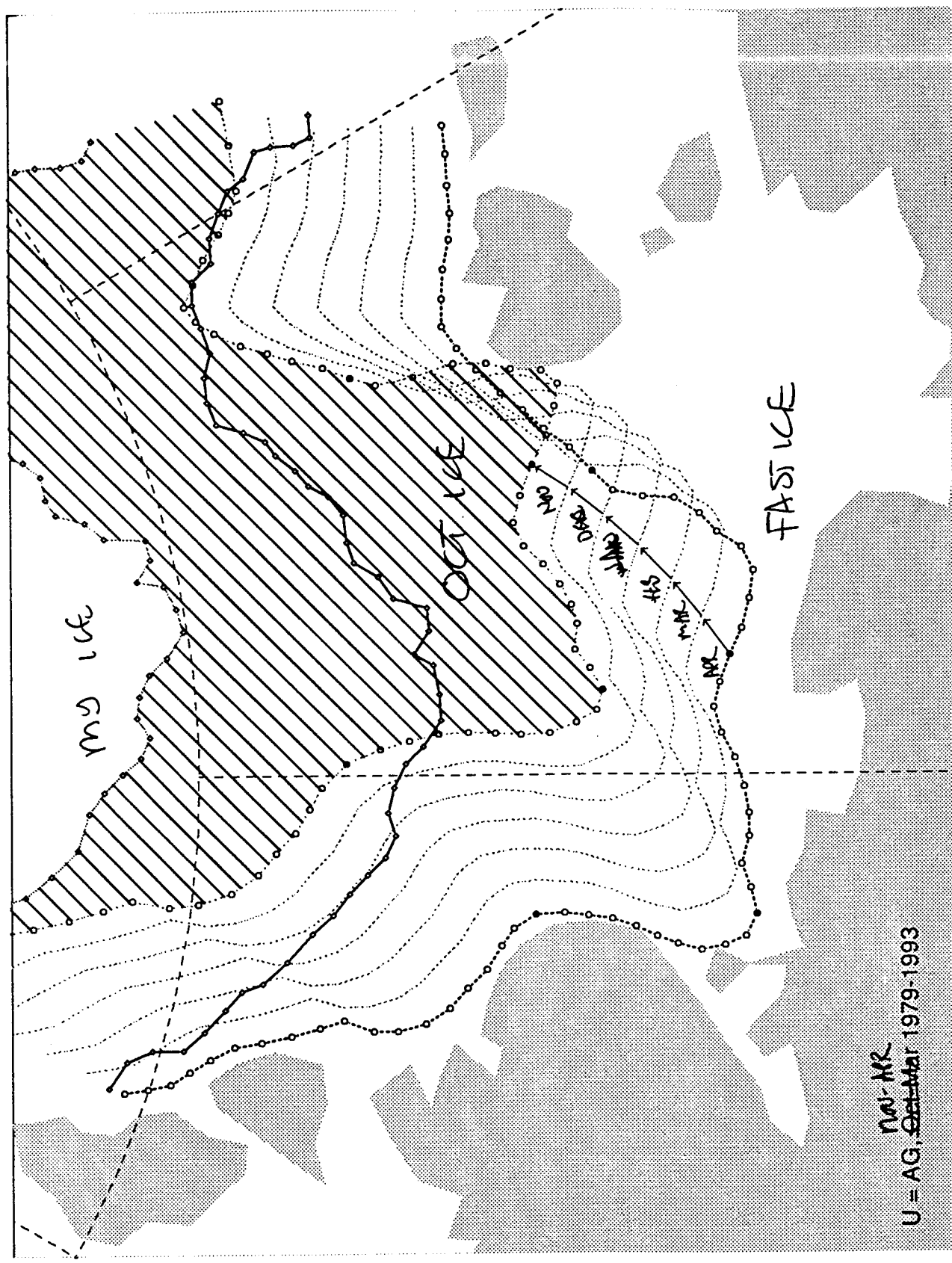


SCALE: \rightarrow 5 cm/s

OCTOBER ICE AREAS

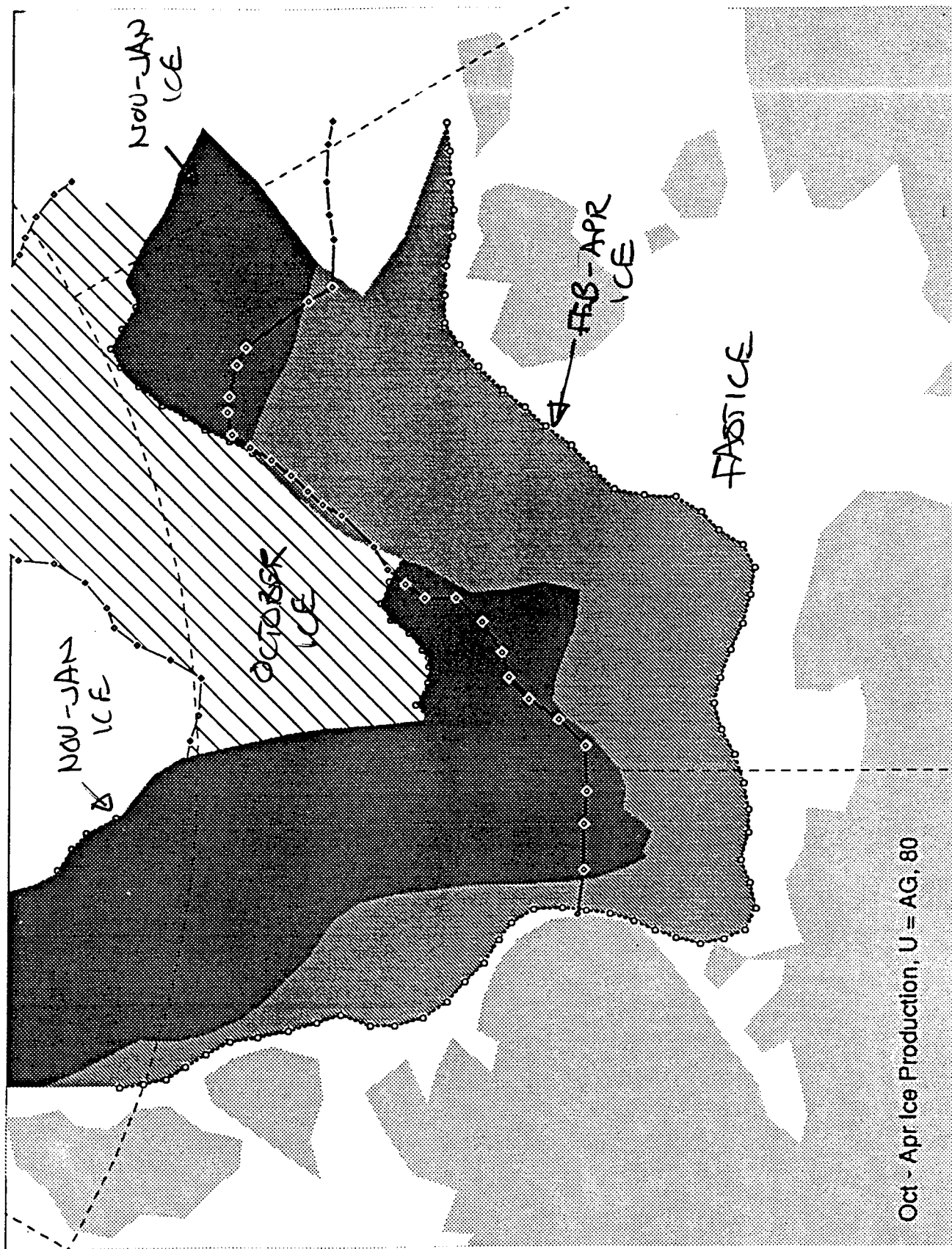


FLAW LEAD PRODUCTION OF ICE MODEL



U = AG, ~~Oct-Mar~~ 1979-1993

- 1980 FLAW LEAD ICE PRODUCTION AREAS



1990 FLAW LEAD ICE PRODUCTION AREAS



Oct - Apr Ice Production, U = AG, 90

Flaw Lead Production of Ice

(AREAS: km²)

Year	November - January	February - April
79-80	113,000	120,000
80	173,000	189,000
81	99,000	138,000
82	79,000	104,000
83	177,000	103,000
84	25,000	63,000
85	129,000	164,000
86	178,000	115,000
87	126,000	94,000
88	204,000	106,000
89	65,000	97,000
90	123,000	63,000
91	130,000	113,000
92	140,000	174,000
MEANS	125,000	117,000

Shallow Water Production of Ice

(AZFAS: km²)

Year	Oct	Winter Nov - Apr.	Total	Surviving
1979-80	132,000	233,000	365,000	245,000
1980-81	132,000	362,000	494,000	305,000
1981-82	147,000	237,000	384,000	246,000
1982-83	147,000	183,000	330,000	226,000
1983-84	147,000	280,000	427,000	324,000
1984-85	147,000	88,000	235,000	172,000
1985-86	141,000	293,000	434,000	270,000
1986-87	147,000	293,000	440,000	325,000
1987-88	99,000	220,000	319,000	225,000
1988-89	129,000	310,000	439,000	333,000
1989-90	63,000	162,000	225,000	128,000
1990-91	147,000	186,000	333,000	270,000
1991-92	140,000	243,000	383,000	270,000
1992-93	111,000	314,000	425,000	251,000
	131,000	243,000	373,000	256,000

An Oriented Sea Ice Dynamics Model with Contamination Incorporation, Transport and Release

Max Coon

AN ORIENTED SEA ICE DYNAMICS MODEL WITH CONTAMINATION INCORPORATION, TRANSPORT, AND RELEASE

by Max D. Coon
North West Research Associates, Inc.

and

Robert S. Pritchard
IceCasting, Inc.

Workshop on Modeling the Dispersion of Nuclear Contaminants in the Arctic Seas
Hosted by the Naval Research Laboratory
Sponsored by the Office of Naval Research
October 18-19, 1994
Naval Research Laboratory
Monterey, CA



North West Research Associates, Inc.

An Oriented Sea Ice Dynamics Model with Contamination Incorporation, Transport, and Release

by Max D. Coon
NorthWest Research Associates, Inc.

and

Robert S. Pritchard
IceCasting, Inc.

A model is being developed that will account for the essential physical processes of sea ice as a pathway for the transport of radionuclides; to characterize incorporation of radionuclides into a ice cover; advection of the contaminated ice, and dispersal of the material during transport and melting. This model will incorporate a new anisotropic constitutive law for sea ice which accounts for lead dynamics directly (See Coon et al, 1992).

Viewgraph 1 shows the mechanism to be considered in the model.

Viewgraph 2 lists mechanics of radioactive waste incorporated into sea ice.

Viewgraph 3 shows radionuclides released into the nearshore through river outflow. The fresh water from the river is in contact with the floating ice cover. Radionuclides in the river water are incorporated within the ice cover as additional freezing takes place.

Viewgraph 4 lists features of an oriented ice thickness distribution. In this ice model, which accounts for the dynamics of a lead, ice redistribution occurs in the leads which results in an oriented ice thickness distribution.

Viewgraph 5 shows a sea ice element with a lead at angle θ to the x axis and a local coordinate system fixed to the lead.

Viewgraph 6 shows a lead along the x axis in physical space and the failure surface for the lead in stress space. The failure surface for this model depends on direction, which is required to describe the ice dynamics on the physical scale of a few to tens of kilometers.

Viewgraph 7 shows a refrozen lead containing three ice categories (including open water and nilas). The three failure surfaces shown represent three lead ice thickness categories.

Viewgraph 8 lists the assumptions about the ice thickness distribution.

Viewgraph 9 illustrates how the assumptions of Viewgraph 7 lead to equations for the growth and redistribution of ice in the thickness categories for both lead opening and closing.

Viewgraph 10 lists radioactive waste release mechanisms from ice to water.

Viewgraph 11 shows that the goal of NWRA and ICI is to provide Ruth Preller of NRL with our model. Our methodology will include interaction with other P.I.s from ANWAP.

Coon, M.D., G.S. Knoke, and D.C. Echert (1992), "Anisotropic Pack Ice Constitutive Law" in proceedings of *IAHR 11th International Ice Symposium*, Banff, Alberta, June 15-19.

Mechanisms to consider in the model

- **Incorporation of rad. waste into sea ice**
- **Transport using the oriented ice dynamics model**
- **Release of waste from sea ice into water**

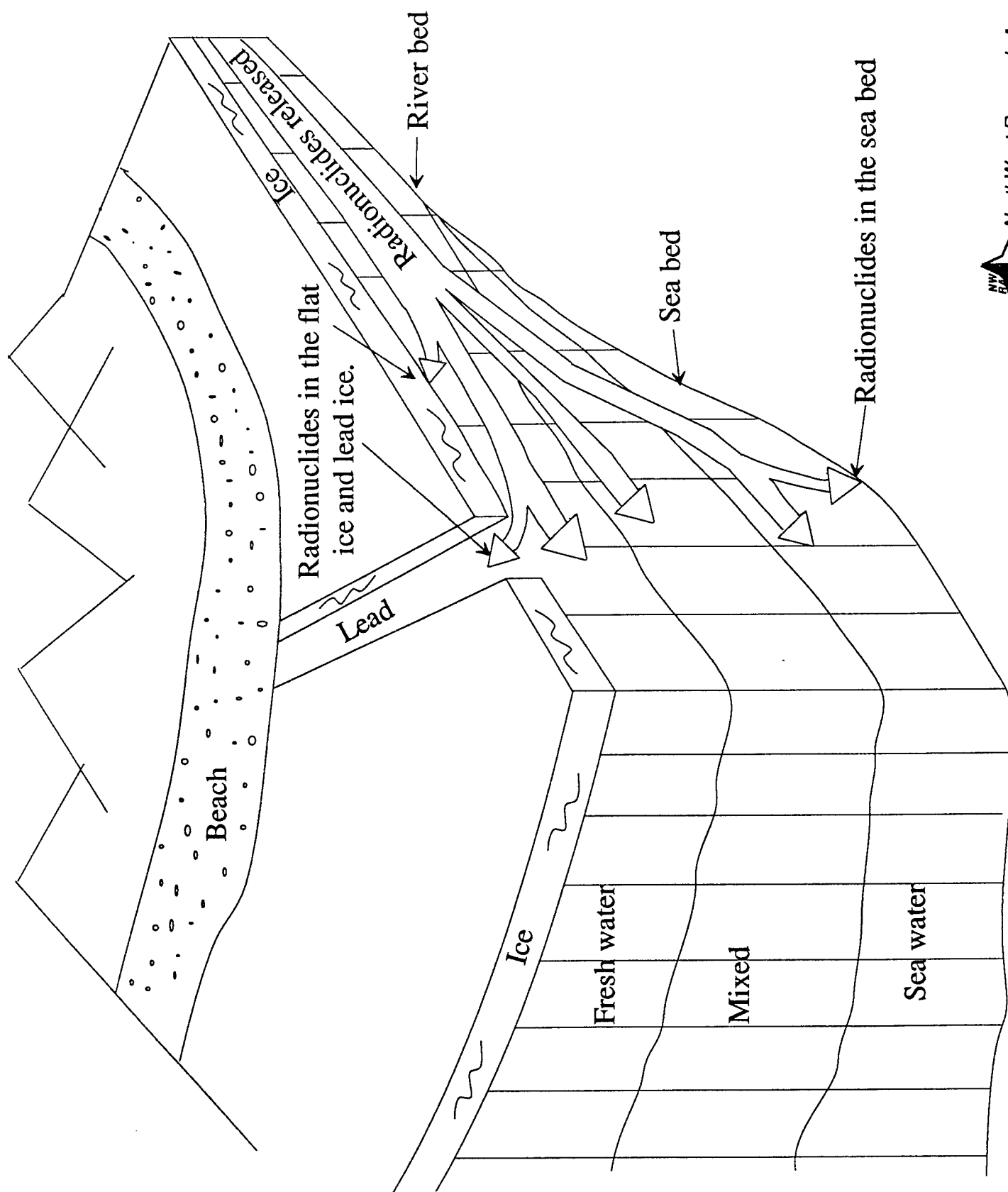


NorthWest Research Associates, Inc.

Incorporation of rad. waste into sea ice

- Contaminated river water flows under nearshore sea ice and is frozen
 - Buoyancy holds it against to the bottom of the sea ice
 - Some brine and particles are excluded during freezing
- Rad. waste tends to sorb onto particles, changing state
- Particles adhere to frazil ice during formation and become incorporated within the sea ice
- Anchor ice raises sediment from bottom
- Deposition on sea ice surface during spring overflowing



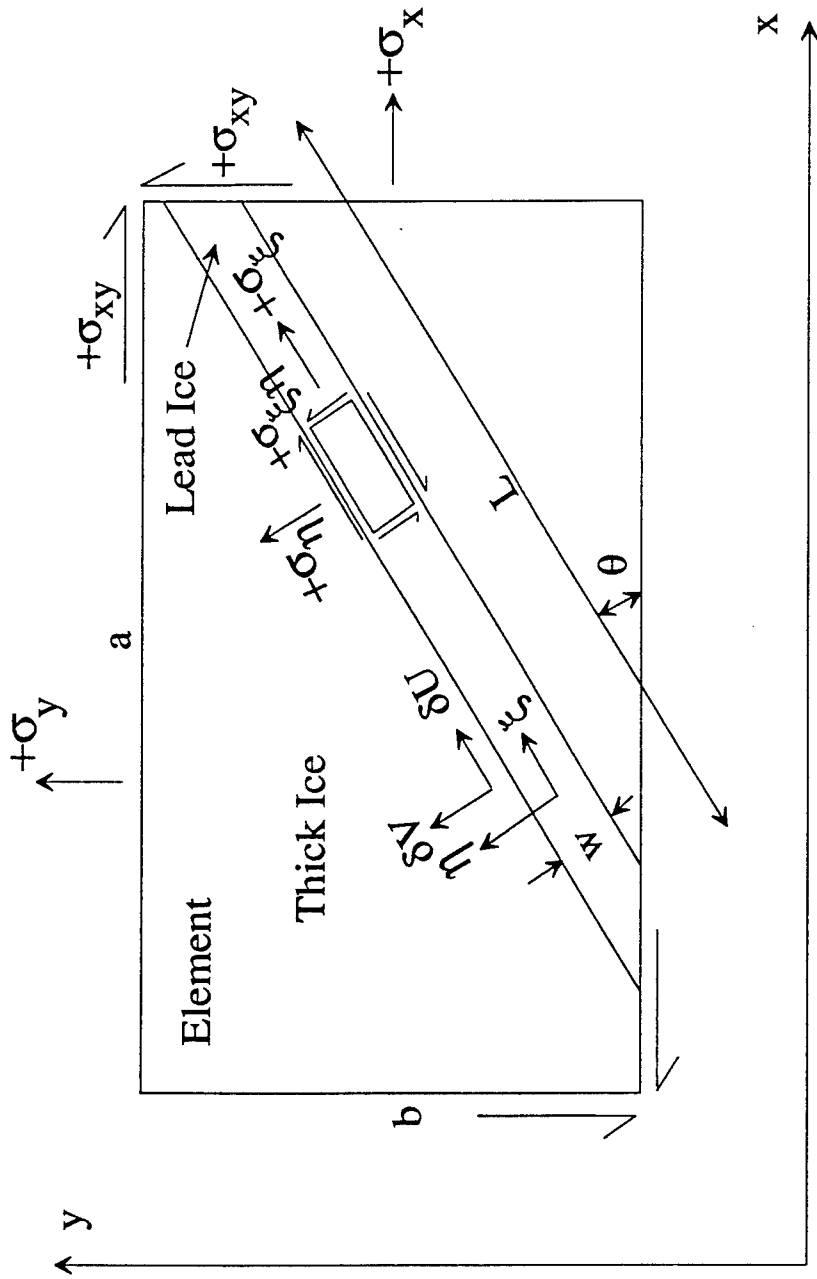


ACCOUNTING FOR ORIENTED ICE THICKNESS CATEGORIES

A model which considers oriented ice thickness categories (resulting from the orientation of the leads and refrozen lead ice) must include the following features:

- Ice thickness distribution in each lead and amount of thick ice
 - ⇒ Ice failure surface in ice stress space
- Ice stress state
 - ⇒ When combined with ice failure surface, defines ice motions such as
 - No activity
 - Normal/shear motion of one lead
 - Normal/shear motion of two leads
 - New lead creation
 - ⇒ Shear and normal strain rate in active leads or new leads
- Ice redistribution in active leads
- Thermal growth in all ice categories





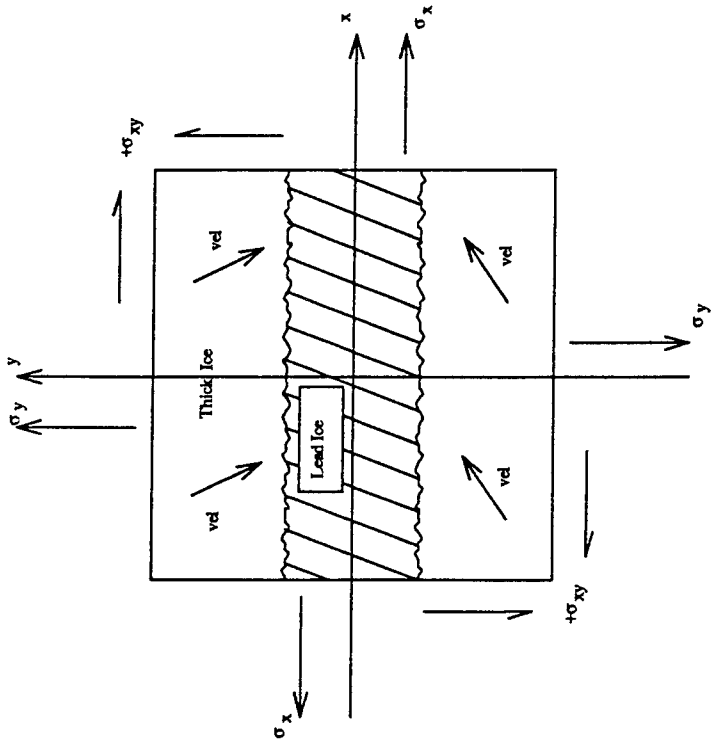
$\sigma_x, \sigma_y, \sigma_{xy}$ - Stress in element coordinates
 $\sigma_\xi, \sigma_\eta, \sigma_{\xi\eta}$ - Stress in lead coordinates
 $\delta U, \delta V$ - Relative velocity across lead
 ξ, η - Lead coordinate system

x, y - Element coordinate system
 L, w - Length and width of lead within element
 θ - Angle of lead relative to x axis:
 $-90 < \theta < 90$

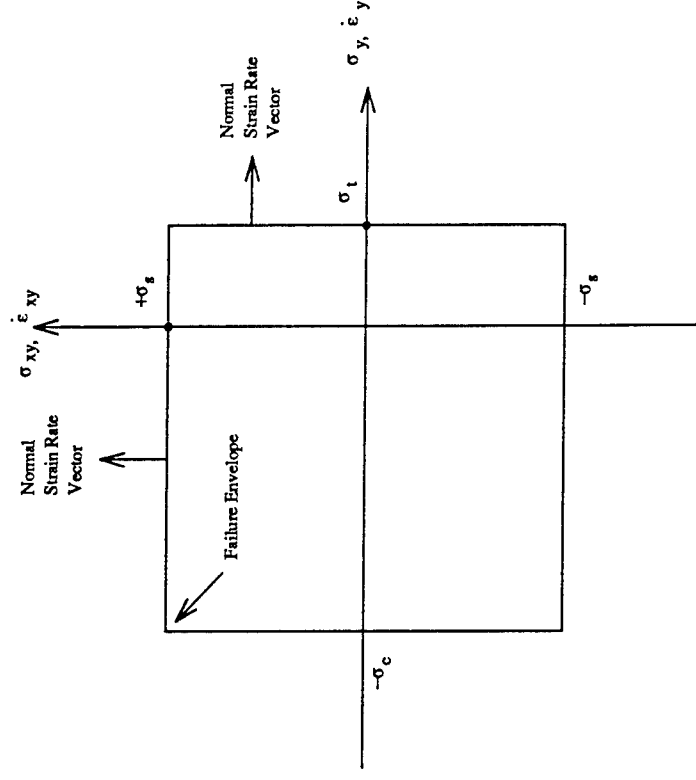
Single lead nomenclature.



North West Research Associates, Inc.



Physical space

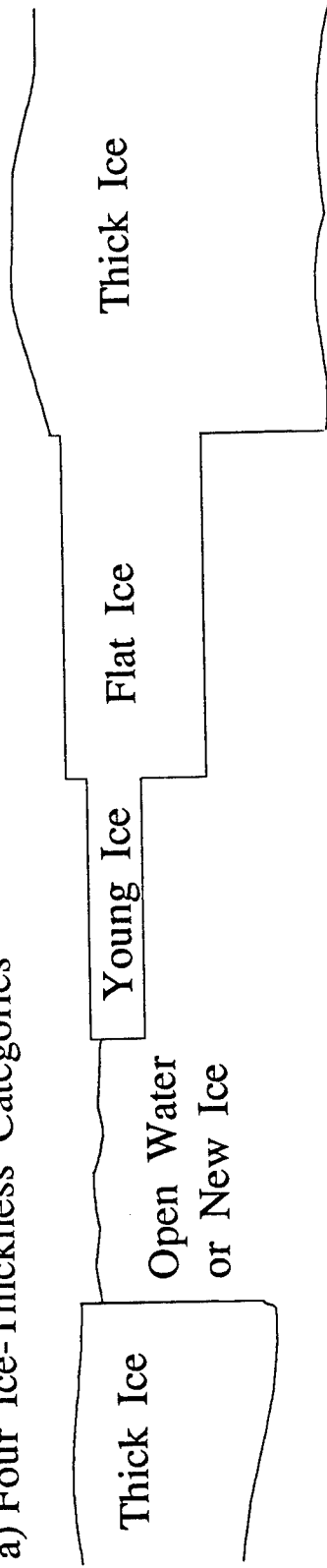


Failure surface for a lead

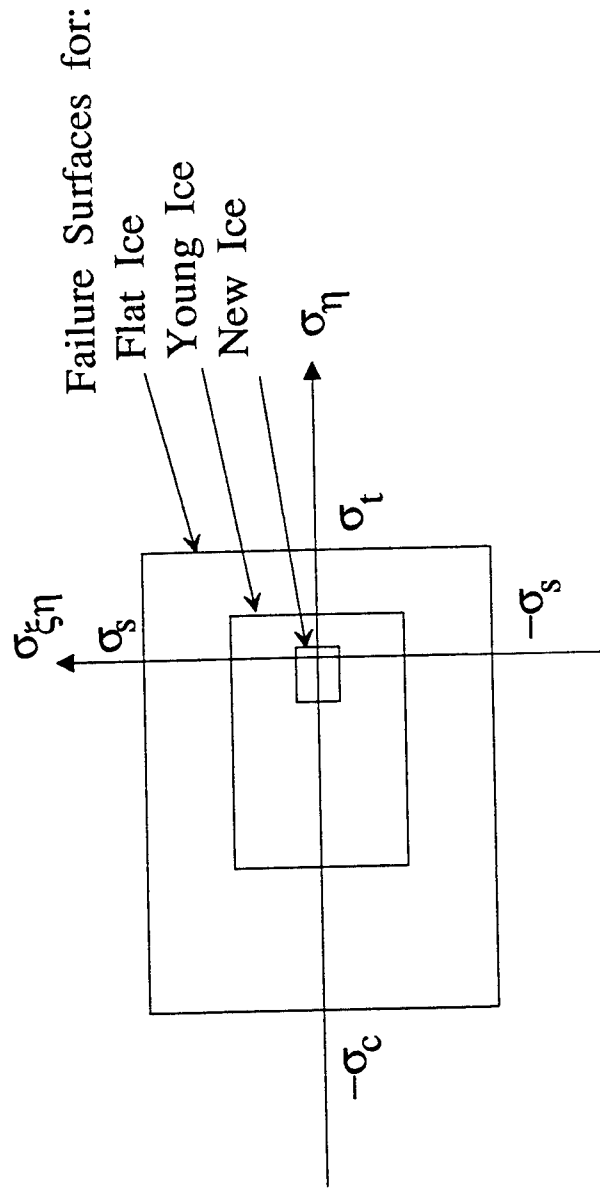
The stress and deformation data for an ice failure event will provide a stress data point on the failure surface and the strain rate vector for the lead (x-axis is along the lead)



a) Four Ice-Thickness Categories



b) Failure Surfaces for Refrozen Lead Ice



Ice thickness categories and their failure surfaces.



NorthWest Research Associates, Inc.

ASSUMPTION ABOUT ICE THICKNESS DISTRIBUTION

- The mathematical equations and calculation procedures are being developed for the ice thickness distribution with four ice thickness categories, based on Reimber, Pritchard, and Coon (1980).
- It is assumed that lead systems will have three thickness categories and the thick non-lead ice will have one thickness category.
- Thickness categories: open water and nilas, young ice, flat ice, and thick ice
 - The open water and nilas category includes ice up to a thickness where heat transfer is significantly reduced (about 10 cm)
 - Young ice continues from 10 cm to a thickness providing significant strength (say 30 cm)
 - Flat ice is strong lead ice (30 cm - 2 m)
 - The thick ice category thus includes ridges, rubble areas, old first year ice, and multiyear floes
- Rules for redistributing the lead ice thickness as a result of deformation are being formulated.
- The SAR data, when combined with ice stress data, can be used to form the plastic strain rate as a function of the stress state (the "plastic flow rule") for lead ice and thick ice.



When the j -th lead is opening, i.e., for $\delta V_j > 0$, the following equations describe the rate of change of area fraction of the four ice categories.

$$\begin{aligned}\frac{d\emptyset_j}{dt} &= \frac{L_j \delta V_j}{ab} - \Phi_{0j} & \frac{dT_j}{dt} &= \Phi_{0j} \\ \frac{dF_j}{dt} &= 0 & \frac{dR_j}{dt} &= 0\end{aligned}$$

where F_j is the area fraction of flat ice in the j -th lead and R_j is the area fraction of rubble ice in the j -th lead. When the j -th lead is closing, i.e., for $\delta V_j < 0$, the following equations describe the rate of change of area fraction of the four ice categories.

$$\begin{aligned}\frac{d\emptyset_j}{dt} &= \frac{L_j dV_j}{ab} \frac{\bar{h}_{1j}}{h_{1j} - \bar{h}_0} u_0(\emptyset_j) - \Phi_{0j} \\ \frac{dT_j}{dt} &= -\frac{L_j dV_j}{ab} \frac{\bar{h}_0}{h_{1j} - \bar{h}_0} u_0(\emptyset_j) + \frac{L_j dV_j}{ab} \frac{\bar{h}_{2j}}{h_{2j} - \bar{h}_{1j}} u_0(T_j) [1 - u_0(\emptyset_j)] + \Phi_{0j} \\ \frac{dF_j}{dt} &= -\frac{L_j dV_j}{ab} \frac{\bar{h}_{1j}}{h_{2j} - \bar{h}_{1j}} u_0(T_j) [1 - u_0(\emptyset_j)] \\ &\quad + \frac{L_j dV_j}{ab} \frac{\bar{h}_{3j}}{h_{3j} - \bar{h}_{2j}} u_0(F_j) [1 - u_0(T_j)] [1 - u_0(\emptyset_j)] \\ \frac{dR_j}{dt} &= -\frac{L_j dV_j}{ab} \frac{\bar{h}_{2j}}{h_{3j} - \bar{h}_{2j}} u_0(F_j) [1 - u_0(T_j)] [1 - u_0(\emptyset_j)]\end{aligned}$$



Release of rad. waste from sea ice to water

- Release of brine during ice deformation
- Brine drainage at formation, and at ultimate melt area
 - Is drainage important during transport?
- Release of all contaminants during melting (may be in MY ice)
 - Injected into surface water



GOAL: Provide Ruth Preller, NRL, an oriented ice dynamics model with transport of rad. waste in the sea ice pathway.

APPROACH: NWRA and ICI will develop the model using all data available (including past ONR- and NASA-sponsored work and ANWAP results) and

Through interaction with ANWAP P.I.s:

James Brooks, Texas A&M

Roger Colony, U. of Washington

Martin Jeffries, U. of Alaska, Fairbanks

Jamie Morison, U. of Washington

Terry Paluszkiwicz, Battelle Pacific N.W. Laboratories

Stephanie Pfirman, Barnard College

Ruth Preller, NRL, Stennis

David Smith, IV, U. of California, Santa Cruz

Terry Tucker and Debra Meese, U.S.A. CRREL



NorthWest Research Associates, Inc.

A Numerical Study of Radionuclide Dispersal in the Kara Sea

David C. Smith

1 A numerical study of radionuclide dispersal in the Kara Sea

David C Smith IV

Institute of Marine Sciences

University of California Santa Cruz

Santa Cruz CA 95064

Fax: 408-459-4882

phone: 408-4595136

email: dcsiv@cascade.ucsc.edu

A number of physical processes may be important in the transport of radionuclides from Russian rivers into the Arctic Ocean. These include transport by ocean currents, sea ice and geological pathways. The amount of radionuclide transported by each of these paths is dependent on time of year, as river flow rates, nearshore ice fields and atmospheric mixing of the ocean change seasonally. The long term goals of this research are to understand how river borne contaminants are partitioned between sea-ice, sea water at various depths and sediment on the shelves? The emphasis of this study is on the Kara Sea and in the inflow from the adjacent Ob and Yenesei river systems.

A regional ocean circulation model, presently in use in numerous ocean circulation studies, is being adapted for application to the Kara Sea. The model will be used in a study of the various processes that may contribute to the redistribution of radionuclides in the Kara Sea. The important modifications of the coastal ocean model for Kara Sea application involve incorporating ice and radionuclide loss terms.

Presently we are forcing the model with a coastal buoyancy source over simple shelf topography. The magnitude of the buoyancy forcing will be adjusted to correspond to Ob and Yenesei flow rates for different seasons. In subsequent simulations the added effects of winds will then be considered. Initial simulations will not involve existing ocean flow fields. It is possible to incorporate these in subsequent simulations by relaxing offshore density fields back to a prescribed ocean climatology. After the sensitivity of river plume distributions to the above factors is understood, we will repeat simulations with bathymetry fields appropriate to the Arctic shelf adjacent to the Ob and Yenesei rivers.

It will not be feasible to examine the transport of radionuclides in all the possible paths discussed above. We will however consider some aspects of these. It will be possible to include the dynamical (but not thermodynamical) effects of ice. In nearshore regions for example, the inclusion of free drift ice cover can be readily implemented to examine ice edge ocean transport phenomena. The effects of pack ice may be incorporated by the presense of lateral boundaries which simply restrict river flow. Incorporation of convective forcing, associated with ice formation is illustrated below.

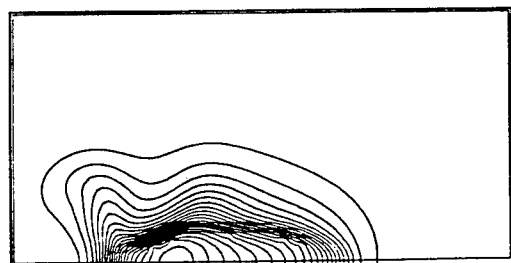
As a first step, we have been working to identify space and times scales associated with river forced flow in the Kara Sea. These determine model resolution and duration of simulations. At present, it appears that model resolution of order several kilometers and seasonal time scales are important. At these resolutions we have been able to reproduce the results of other investigators using the same model to study near shore buoyancy forced flows.

Because this effort is new this year, no major results are yet available. Several preliminary

simulations are shown in figure 1 and contrast the different responses of the coastal ocean to dense versus fresh coastal ocean buoyancy forcing. Bottom topography is represented by a simple linear sloping bottom which slopes away from the coast, ranging in depth from 20 to 100 m. Experiment 1 is forced with dense water source at the surface adjacent to the coast and is representative of the flow forced in a nearshore polynya, where ice formation and brine rejection are occurring. Experiment 2 is forced with a fresh water source at the surface representative of river inflow into the coastal ocean in the absence of ice. Both processes may occur in the Kara Sea depending on season. The physical processes occurring in the two experiments are quite different. In experiment 1, convective instability leads to baroclinically unstable wave growth and breakup of the flow into eddies. The sloping bottom enhances the unstable wave growth. The river plume in experiment 2 is surface trapped and evolves stably as a coastal Kelvin wave.

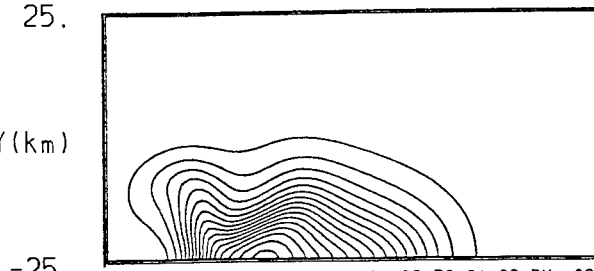
The Kara Sea model effort interfaces with the research of a number of other investigators. Researchers at the University of Washington are in the process of obtaining Russian data sets for the Kara Sea, which will provide valuable input for model initialization and verification. Data sets taken by Jim Brooks at TAMU will also provide information about the distribution of river plumes near the mouth of the Ob and Yenesei rivers. Flow rates and geological transport processes in the Ob and Yenesei river -estuary system are being studied by the group at the Pacific Northwest Laboratory. Input to the Kara Sea modeling will be taken from their findings. The results of regional Kara Sea modeling should also benefit the larger scale Arctic basin modeling being done at NRL, in the form of improved assessment of radionuclide residence time in the Kara Sea and improved boundary conditions for the larger domain model. Finally it will be possible to assess the importance of tides in redistribution of river borne contaminants. This will be done in collaboration with David Brooks at TAMU who will perform compatible experiments using a tidally driven model.

S(Z = .0, DAY = 12.0)



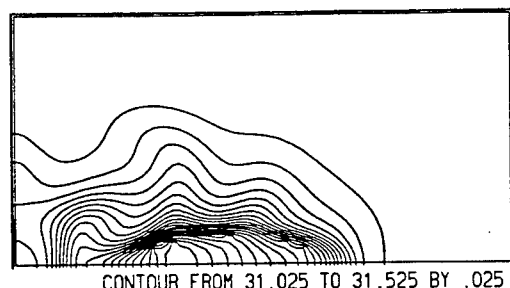
-50. X(km) 50.

S(Z = -20.0, DAY = 12.0)



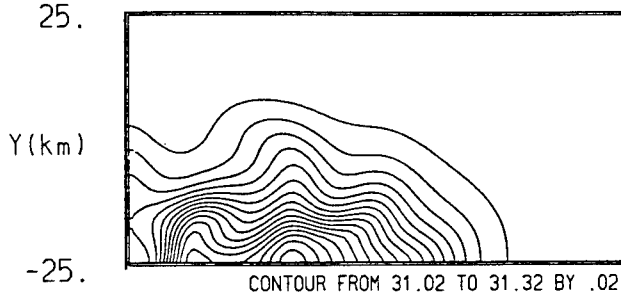
-50. X(km) 50.

S(Z = .0, DAY = 18.0)



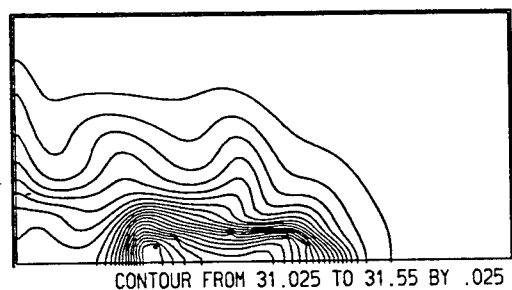
-50. X(km) 50.

S(Z = -20.0, DAY = 18.0)



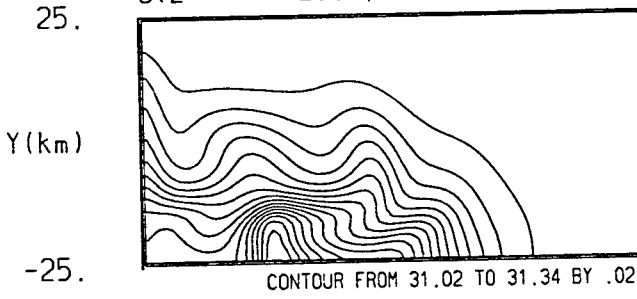
-50. X(km) 50.

S(Z = .0, DAY = 24.0)



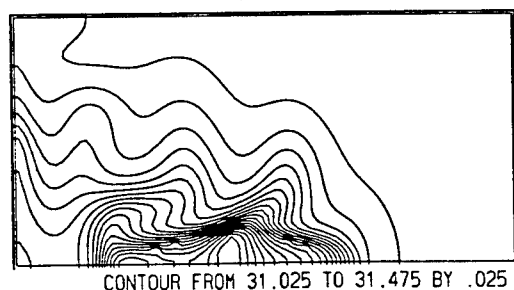
-50. X(km) 50.

S(Z = -20.0, DAY = 24.0)



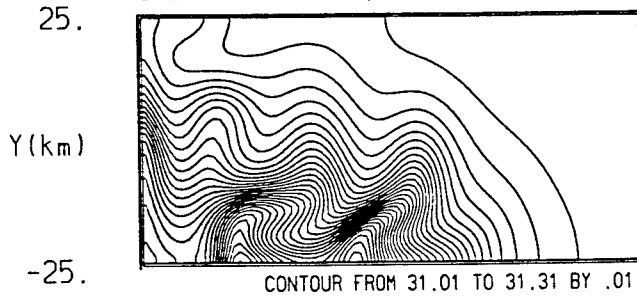
-50. X(km) 50.

S(Z = .0, DAY = 30.0)



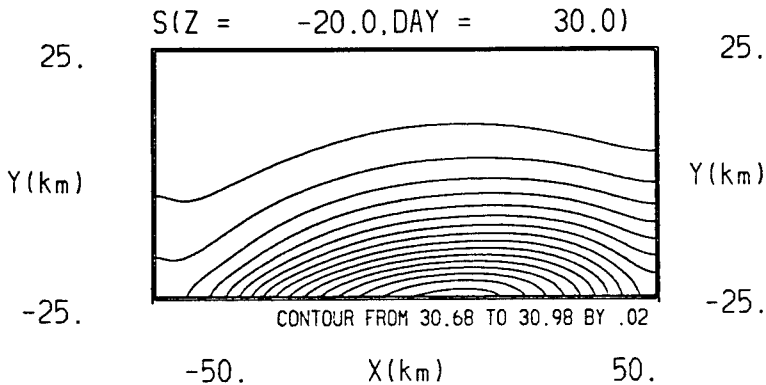
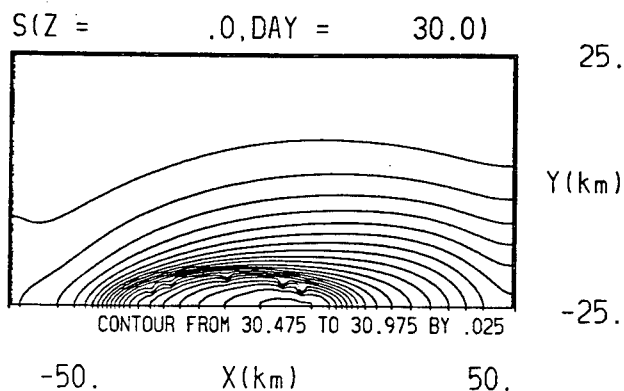
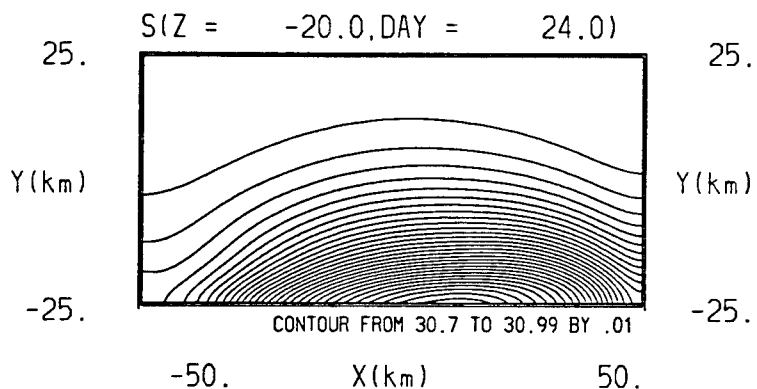
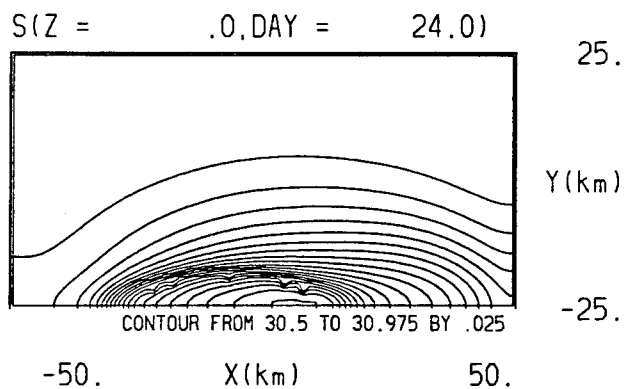
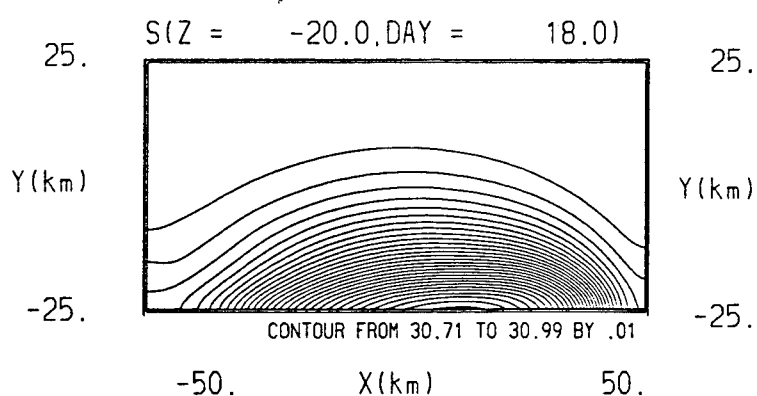
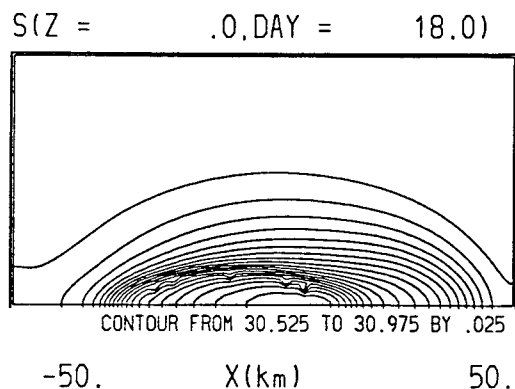
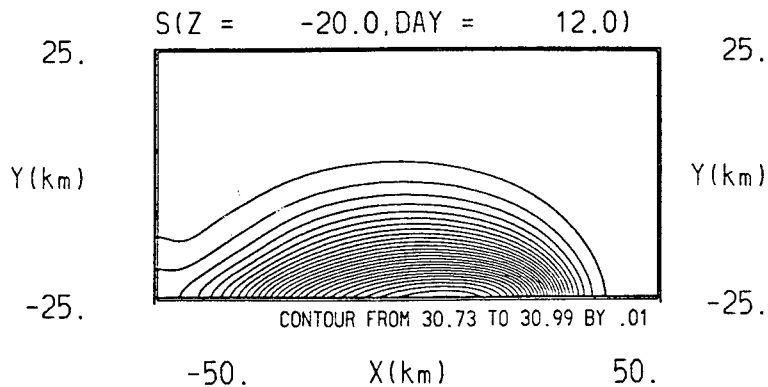
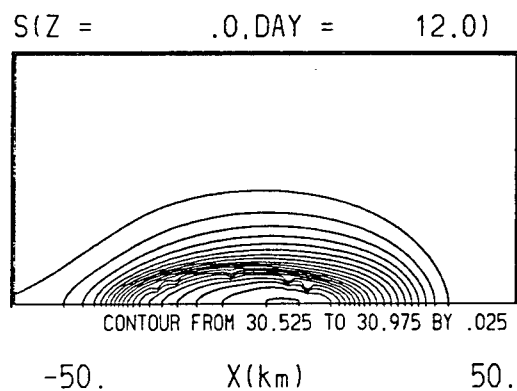
-50. X(km) 50.

S(Z = -20.0, DAY = 30.0)



-50. X(km) 50.

Experiment 1. Dense water source at the surface. Left column is salinity distribution at the surface. right column is salinity distribution at z=-20 m.



Experiment 2. Fresh water source at the surface. Left column is salinity distribution at the surface. right column is salinity distribution at $z=-20$ m.

Multiple-River Interactions in Buoyancy-Driven Coastal Currents

David A. Brooks

Multiple-River Interactions in Buoyancy-Driven Coastal Currents

David A. Brooks
Department of Oceanography
Texas A&M University
College Station, TX 77843

Coastal and shelf circulation patterns are often strongly influenced by fresh water outflows from rivers. The fresh-water buoyancy injection provides a potential energy source that, due to the earth's rotation, eventually sets up a nearshore current that is trapped against the coast in the Kelvin-wave sense (right bounded in the Northern Hemisphere). Numerical models and observations indicate that near the river mouth the freshened water first forms a bolus or bulge of low salinity water that spreads in both directions along the coast. The buoyancy driven coastal current eventually escapes the bulge and spreads along the coast.

In a coastal region influenced by multiple rivers, complex interactions can occur. When the river mouths are nearby, the bulges from the adjacent rivers can merge and act essentially as a single source for a coastal current. On the other hand, when the mouths are separated sufficiently that, for prescribed flow rates, the bulges remain distinct, the 'upstream' coastal current can be redirected offshore as it encounters the strong thermohaline fronts associated with the 'downstream' river bulges. Such a case occurs, for example, in the Gulf of Maine, where the combined plume from the Kennebec and Androscoggin Rivers interrupts the Maine coastal current that is set up in part by outflow from the Penobscot River farther to the east (see Figure). Model results show that the Kennebec-Androscoggin plume partially deflects the coastal current offshore into the central Gulf of Maine, where the nutrient flux influences the annual cycle of productivity.

Multiple rivers are common on continental shelves, so a similar effect can be expected in many regions. For example, the Ob and Yenisee Rivers in the Kara Sea of the Arctic Ocean have very large run-off in spring months and no doubt interact in complex ways. Pollutant pathways in the Kara Sea and toward the Alaska shelf in the associated coastal current therefore depend to some extent on the way in which the individual river plumes interact. Model studies are planned to begin examining the ways in which these interactions occur and how they depend on river flow rates and timing of maximum volume fluxes.

Surface velocity and salinity, t=20 days, June, 1982

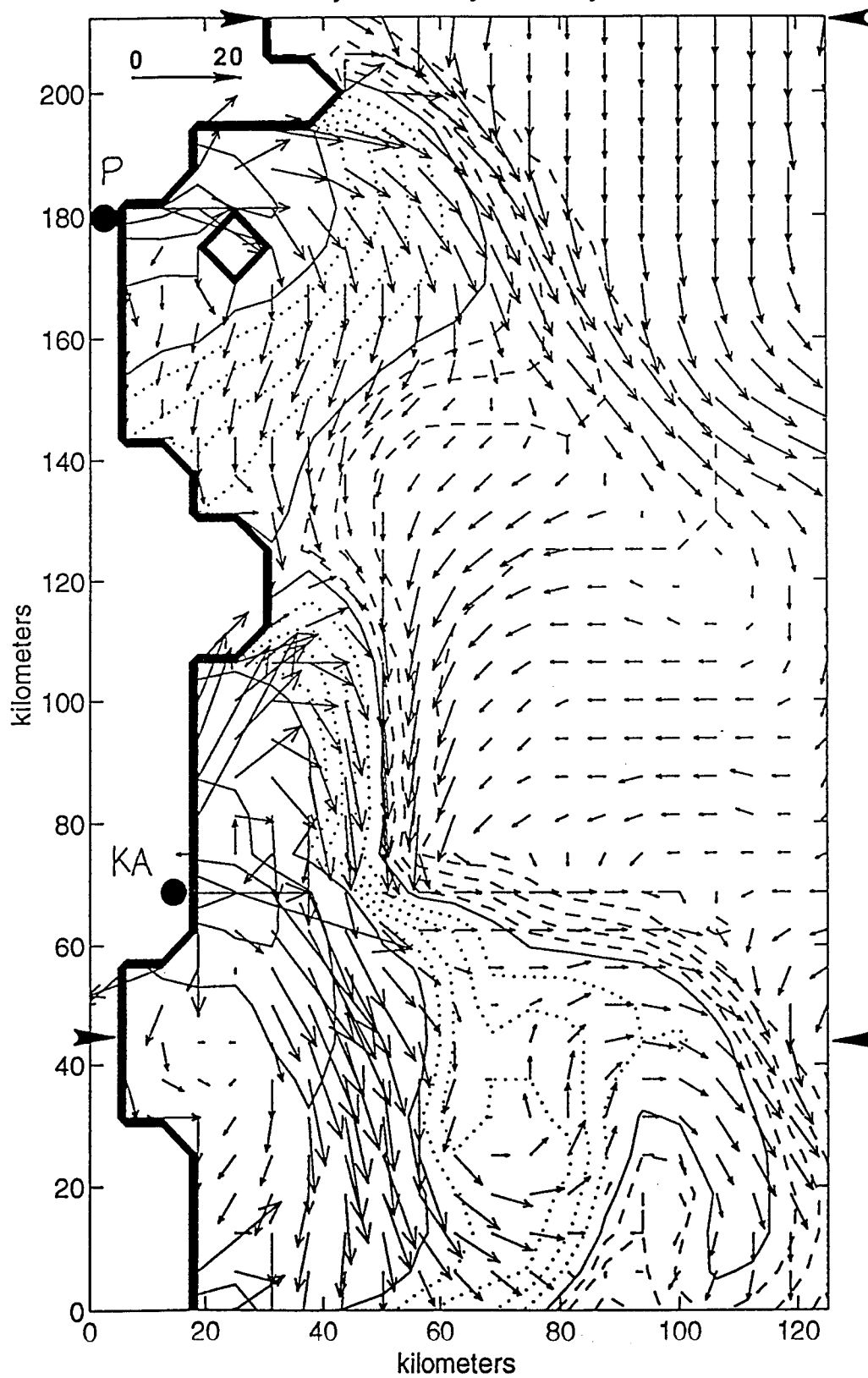


FIGURE CAPTION

Model tidal-residual surface current and salinity, showing the interaction of river plumes 20 days after the start of a run initialized with hydrographic data from June, 1982. The region shown is a coastal subregion of the full modeled domain, which included the Gulf of Maine, Bay of Fundy and Georges Bank on the continental shelf. The mouths of the Penobscot (P) and Kennebec-Androscoggin (KA) Rivers are shown by the filled circles. The contour interval is 5 ppt for salinity <30 ppt and 0.5 ppt for salinity >30 ppt. Dotted contours show detail between 25 and 30 ppt with 1 ppt interval. Vector speed scale (cm s^{-1}) is indicated. The horizontal arrowheads identify vertical sections not shown here (see Brooks, 1994, for additional details).

Reference:

Brooks, D.A., 1994: A Model Study of the Buoyancy-Driven Circulation in the Gulf of Maine. *J. Phys. Oceanogr.*, 24(11), 2387-2412.

**Modelling the Release to the Environment in
the Kara Sea from Radioactive Waste
in the Dumped Reactor Compartment
of the Icebreaker Lenin**

Mark Mount

MODELLING THE RELEASE TO THE ENVIRONMENT IN THE KARA SEA FROM RADIOACTIVE WASTE IN THE DUMPED REACTOR COMPARTMENT OF THE ICEBREAKER LENIN

S.J. Timms¹, N.M. Lynn¹, M.E. Mount², Y. Sivintsev³

¹Department of Nuclear Science and Technology, Royal Naval College
Greenwich, London, England

²Lawrence Livermore National Laboratory, University of California
Livermore, California, United States of America

³Russian Research Centre, Kurchatov Institute, Moscow, The Russian
Federation

ABSTRACT

In progressing its work for the International Arctic Seas Assessment Project (IASAP), under the auspices of the International Atomic Energy Agency (IAEA), the Source Term Working Group developed a simple spreadsheet model to predict a radiation release profile into the Kara Sea from reactor fuel and activated components dumped within the reactor compartment of the icebreaker *Lenin*.

The model accounts for the degradation of containment materials through corrosion and other mechanisms, and predicts annual release rates to four thousand five hundred years into the future. Five scenarios are modelled, depending on the integrity of the levels of containment, a major factor being the very slow rate of corrosion of the UO₂ fuel. At the turn of the century, total release rates are shown to vary between <0.01 to 50 Ci/yr (0.37 GBq to 1.85 TBq/yr) depending on the model. By 2050, the best of the scenarios are predicting release rates on the order of 0.6 Ci/yr (22 GBq/yr) and at 2500, the rate is down to 0.2 Ci/yr (7.4 GBq/yr), dropping by a decade until the year 4000; after this, the radioactive components will all have been released from their containment or decayed away.

The model is being applied to other forms of solid radioactive waste dumped in the Kara and Barents Seas, in a programme of work for the IASAP, aimed at assessing the collective release profile from all significant dump sites in this region.

INTRODUCTION

Background

1. In the Spring of 1993, an English translation of the Russian report, *Facts and Problems Related to Radioactive Waste Disposal in Seas Adjacent to the Territory of the Russian Federation*,¹ was released. The findings presented in this report were the result of a scientific study commissioned in October 1992 by the Office of the President of the Russian Federation. The White Book, as the report was later called, reported that: (1) between 1965 and 1988, 16 naval reactors from seven former Soviet Union submarines and the icebreaker *Lenin*, each of which suffered some form of reactor accident, were dumped at five sites in the Kara Sea;

(2) between 1959 and 1991, low level liquid radioactive waste was discharged at sites in the Baltic, White, Barents, and Kara Seas; and (3) between 1964 and 1991, low and intermediate level solid radioactive waste was dumped at sites in the Barents and Kara Seas.

2. Of the discarded naval reactors, six of the 16 contained their spent nuclear fuel (SNF). In addition, approximately 60% of the SNF from one of the three *Lenin* naval reactors was disposed of in a reinforced concrete and stainless steel shell container. The vast majority of the low and intermediate level solid radioactive waste was disposed of in containers of unknown composition. The Kara Sea disposal sites for the 16 naval reactors and low and intermediate level solid radioactive waste varied in depth from 12 to 380 m.

3. The White Book also reported estimates of total radioactivity at the time of disposal, these were (1) 2,300 kCi (85 PBq) of fission products in the SNF; (2) 100 kCi (3.7 PBq) of ^{60}Co in the reactor components; (3) 24 kCi (0.89 PBq) of unspecified origin in the low level liquid radioactive waste, over 50% of which was discharged in the Barents Sea; and (4) 16 kCi (0.59 PBq) of unspecified origin in the low and intermediate level solid radioactive waste, over 95% of which was discarded in the Kara Sea.¹ With rare exception, no radionuclides were identified and no estimate provided for the current levels of radioactivity.

International Arctic Seas Assessment Project

4. International concern over the possible health and environmental effects from disposal of these aforementioned radioactive wastes in the shallow waters of the Arctic Seas prompted the International Atomic Energy Agency (IAEA), as part of their responsibilities to the London Convention of 1972, to initiate the International Arctic Seas Assessment Project (IASAP).² The IASAP formally began on February 1, 1993 in Oslo, Norway at the meeting on the Assessment of Actual and Potential Consequences of Dumping Radioactive Waste into Arctic Seas.

5. The stated objectives of the IASAP are to: (1) assess the risks to human health and to the environment associated with the radioactive waste dumped in the Kara and Barents Seas, and (2) examine possible remedial actions related to the dumped wastes and to advise on whether they are necessary and justified.² To meet these objectives, four working groups were established: (1) Source Term, (2) Existing Environmental Concentrations, (3) Transfer Mechanisms and Models, and (4) Impact Assessment and Remedial Measures.

Source Term Working Group

6. The first Consultants Meeting of the Source Term Working Group, hereafter identified as the Group, was held at the IAEA, in Vienna, Austria on January 10-14, 1994. The purposes of this meeting were to: (1) review progress and needs on the source term evaluation for the assessment of risks to human health and the environment associated with nuclear reactors dumped in the Kara Sea, and (2) prepare a preliminary source term description to be used by the Transfer Mechanisms and Models Working Group.

7. During the meeting, the Group reviewed and discussed source term reports prepared by consulting members, one from the United States and one from Russia. The estimate prepared by the consulting member from the United States was for the inventory of selected actinides and fission products in the SNF and activation products in the reactor components and primary

system corrosion products of the 16 naval reactors.³ Estimates for the *Lenin* radionuclide inventory were based upon core history information obtained from translations of Russian articles available in the open literature, while the estimates of the nuclear submarine radionuclide inventories were based upon core history information developed from open literature Western estimates of their operating characteristics. The estimate prepared by the consulting member from Russia was for the inventory of selected actinides and fission products in the SNF and activation products in the reactor components of the *Lenin*.⁴ In addition to the inventory estimate, this report provided detailed information on the operating history of the *Lenin*; condition of the reactor compartment, reactor pressure vessels (RPV), and the SNF prior to disposal, and the disposal operations. From the standpoint of the Group, the later of these two source term estimates was definitive for the *Lenin*.

8. The Group was also provided with preliminary information from the September - October 1993 joint Norwegian/Russian expedition to the Tsivolka Inlet, Stepovoy Inlet, and Novaya Zemlya Depression disposal sites in the Kara Sea.⁵ Included among this information were preliminary results from underwater camera investigations of specific objects and *in situ* gamma spectroscopy of bottom sediments.

9. As the information from the joint Norwegian/Russian expedition was preliminary at best, and because Russian estimates for the radionuclide inventories in the nuclear submarine naval reactors would not be available for evaluation before the Fall of 1994, the Group focused its efforts on the *Lenin*. The following section summarizes the information pertinent to development of the *Lenin* source term.

LENIN SOURCE TERM⁴

Background

10. Launched in Leningrad in 1959, the icebreaker *Lenin* was the first nuclear merchant ship in the world. During her 31 years in commission, the *Lenin* had two separate steam generating plants (SGPs). The first SGP contained three pressurized water reactors (PWRs) of 90 MW maximum thermal power each and operated from 1959 to February 1965, when during routine repair of the SGP, an operator error allowed the core of the N2 PWR to be left without water for some period of time. As a consequence, a part of the reactor core was damaged due to residual heat. It is the characteristics of this first SGP that form the basis for the *Lenin* source term.

Characteristics of the First SGP

11. The entire SGP, including the steam generators and pumps, was located in the centre of the ship in an isolated reactor compartment. The three PWRs were aligned vertically in a plane perpendicular to the keel and were surrounded by a large iron-water tank shield. The biological shield located above the three PWRs was made of limonite concrete and a heat resistant composition of graphite and boron.

12. Each cylindrical RPV was made from low alloy steel, with approximate dimensions: 2-m diameter, 5-m height, and 40-mm thick walls with a 5-mm internal stainless steel (SS) layer of cladding. The height and diameter of each PWR core was approximately 1.6 m and 1 m,

respectively, with each core containing 219 cylindrical technical fuel channels (TFCs) with 36 pin-type fuel elements. The fuel elements contained fuel pellets made from sintered UO_2 enriched to 5.0% ^{235}U and clad with a Zr-Nb alloy or SS.

13. To reduce heat and radiation effects on each RPV and subsequently extend their operating lives, thermal shields consisting of five concentric SS cylinders of 20- to 30-mm thickness each (185 mm total) were positioned around each reactor core. Two of these five concentric cylinders were welded to the upper and lower rings, which connected with the upper and lower plates used for fixation of the TFCs.

Reactor Operating Histories

14. The first fuel load lasted from 1959 to 1962 and consisted of 80 kg of ^{235}U in each reactor core. The integrated power productions with this first fuel load were equal to 17.8 GWd for the N1 PWR and 18.0 GWd for the N2 and N3 PWRs. Refuelling occurred in 1963. The second fuel load lasted from 1963 to 1965 and consisted of 129 kg ^{235}U clad in SS in the N1 PWR and 75 kg ^{235}U clad in Zr-Nb in the N2 and N3 PWRs. The N2 PWR operated from July 19, 1963 to November 17, 1963 and from June 22, 1964 to November 13, 1964 for a total period of 267 days. The mean power of the N2 PWR during the second fuel load was 53 MW. At the time of the reactor accident, the integrated power production for the N2 PWR was approximately 14.2 GWd thermal and the burnup was equal to 18.9 MWd/metric tonne initial heavy metal. Integrated power productions for the second fuel load were equal to 22.5 GWd for the N1 PWR and 17.5 GWd for the N3 PWR.

Reactor Compartment Disposal

15. Initially, all undamaged and damaged SNF was removed from the three RPVs. However, as a consequence of the accident, only 94 of the 219 TFCs from the N2 RPV could be removed for normal disposal. The remaining 125 TFCs were removed with three of the concentric SS cylinders of the thermal shield and placed into a cylindrical reinforced concrete and SS shell container of inner and outer diameter of approximately 1 m and 2 m, respectively. This reinforced concrete and SS shell container, hereafter identified as the box, was filled with a hardening compound based on furfural resin and then stored on land for approximately two years.

16. Before disposal, the primary circuit loops and equipment were washed, dried, and hermetically sealed; the most radioactive inner parts of each RPV were covered with the furfural based hardening compound; the ceiling of the reactor compartment was equipped with special pressure relief valves; the box with the SNF was transferred from its land storage location to the top of the SGP steel shielding; and the hole in the reactor compartment ceiling where the box was inserted was covered with a 10-mm thick carbon steel plate and sealed by weld.

17. In August 1967, the *Lenin* reactor compartment with her three RPVs and SNF was dumped in the shallow water of Tsivolka Inlet, as shown in Figure 1,⁵ at an estimated depth of 50 m directly from the *Lenin* through the bottom of her hull. A diagrammatic representation of the entire dumped assembly appears in Figure 2.⁴

Radionuclide Inventories

Fission Products and Actinides

18. Calculations of core cell burnup in the N2 PWR were performed by the spectral code GETERA.⁶ The fission product and actinide activities were estimated using the RECOL⁷ library data base, which was generated on the bases of the latest versions of the evaluated nuclear data files, ENDF/B-V, with corrections based on the results of critical experiments.⁸ The criticality problem was solved for a realistic 3-D geometry model of a TFC by Monte-Carlo with RECOL and checked with MCNP⁹ for fresh fuel load. One-group cross sections were prepared for burnup calculation of critical loads of both fresh and spent fuel and input to ORIGEN-2¹⁰ for detailed radionuclide content calculations.

Activation Products

19. All internal reactor constructions were made from SS; the RPVs were made from low alloy steel. Almost all activation products associated with the *Lenin* PWRs originated in the internal constructions made from SS.

20. Analysis of neutron activation shows that only four radionuclides are of consequence at 10 or more years after reactor shutdown. These are ⁶³Ni, ⁶⁰Co, ⁵⁹Ni, and ¹⁴C. Activities of ⁶³Ni and ⁶⁰Co were estimated from the following equation:

$$A = 3.1 \times 10^{16} (P_{\text{mean}}) [\rho_m + \rho_a + \Delta K (\Sigma_s / \Sigma_{s+w})] T \lambda \Psi,$$

where 3.1×10^{16} is the number of fissions/second-MW; P_{mean} is the mean thermal power of the reactor, MW; ρ_m is the fraction of the neutron flux captured in the main reactivity compensating lattices per unit fission; ρ_a is the fraction of the neutron flux captured in the additional reactivity compensating lattices per unit fission; ΔK is the fraction of the neutron flux captured in the shielding assemblage and lower plate per unit fission; Σ_s is the macroscopic capture cross section for thermal and intermediate neutrons in the steel of the shielding assemblage, in cm^{-1} ; Σ_{s+w} is the macroscopic capture cross section for thermal and intermediate neutrons in the steel and water of the shielding assemblage, in cm^{-1} ; T is the irradiation time, in days; λ is the radioactive decay constant for ⁶³Ni or ⁶⁰Co, in days^{-1} ; and Ψ is the ratio of the activation cross section of Ni or Co to the total activation cross section of the steel under irradiation.

Activities for ⁵⁹Ni and ¹⁴C were estimated from a British calculation of activation products in the reactor components of a generic nuclear powered submarine one year after shutdown.¹¹

Table 1 presents a summary of the estimated radioactivity in the box that is sealed within the reactor compartment of the icebreaker *Lenin* for 1993.^{3,4,11}

Table 2 presents a summary of the estimated radioactivity for activation products in the three reactor pressure vessels that are sealed within the reactor compartment of the icebreaker *Lenin* for 1993.^{4,11}

LENIN RELEASE MODEL

21. A spreadsheet model was developed to provide a workable estimate of the rate of release of activity into the environment. With so many unknowns, especially with respect to the behaviour of oxide fuel in sea water, corrosion rates, and the effectiveness of the various containment barriers, a number of simplifying assumptions were necessary as described below. In all cases, such assumptions are pessimistic so as to over rather than under-estimate the rate of release of activity. The model has the ability to vary most of the operating parameters, for instance, corrosion rates, material thicknesses and barrier effectiveness or containment lifetimes.

22. All the fission products and actinides are in the box placed on top of the SGP. This box also contains three thermal shields from the N2 RPV, representing an estimated 27% of the total inventory of activation products. The remaining 73% of activation products are in the RPVs. It is further assumed that the activation products in the RPVs are distributed in the ratio 80% thermal shields, 10% RPV cladding, 10% RPV walls.

23. To cope with the different forms of radioactive material and their containment arrangements, the model is based upon the four cases depicted in Figure 3, with each case representing escalating layers of containment. Case I assumes no containment whatsoever, with the radioactive material directly in contact with the sea. Cases II to IV progressively add containment barriers that have an inhibiting effect on the expected release profile from the radioactive sources in Case I. Finally, a Case V is assumed that adds a degree of realism by considering the collapse of support for the box and consequent displacement of its lid.

24. The process of release of radionuclides from the activated RPV walls and SS thermal shields is deemed to be by corrosion. For fission products and actinides in the oxide fuel, once sea water penetrates through to the fuel, the release process is assumed to be immediate from fuel grain boundaries followed by a very slow dissolution of fuel grains. Reasonably accurate rates of radioactive release into the sea are clearly crucial for realistic modelling, and have been predicted from a detailed survey of current literature. The result of this work by the Department of Nuclear Science and Technology, Royal Naval College, Greenwich, has been reported separately¹² and is the source document for the majority of rates of material decomposition used in this paper.

The constituent elements of the model are discussed in more detail under case headings:

Case I - No Containment Barriers

25. The three low alloy steel RPVs, complete with SS internal clad and concentric SS thermal shields (five each for the N1 and N3 RPVs, two for the N2 RPV); the fuel pins; and remaining three SS thermal shields from the N2 RPV are directly in contact with the sea.

Activation Release from the RPV Walls and Thermal Shields

26. Based on published data,¹ vessel geometry is assumed to be as shown in Figure: 4.

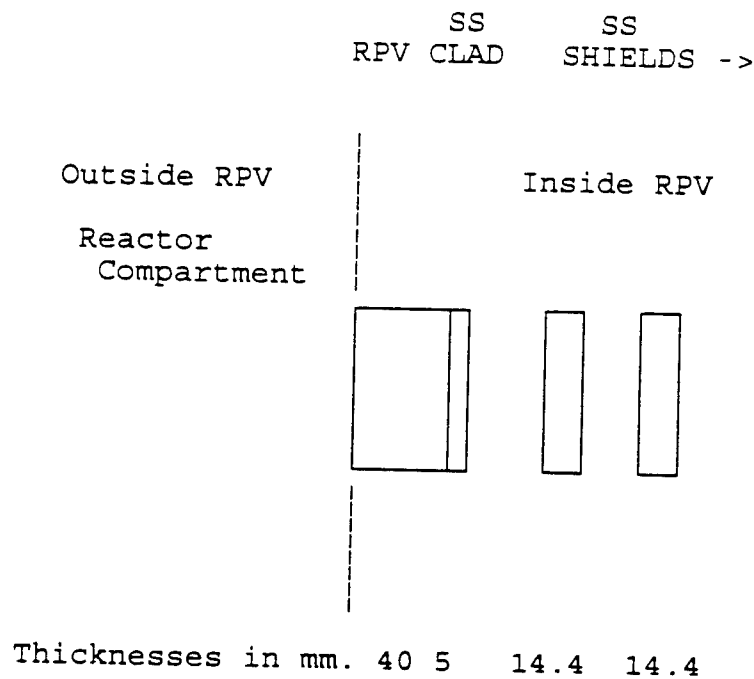


Figure 4: RPV geometry showing RPV wall, cladding and the internal stainless steel thermal shields

The low alloy steel RPV walls corrode immediately from the outside at an assumed rate of 0.075 mm/yr,¹² releasing activation products into the surrounding water. Similarly, the inner layers of SS cladding and SS thermal shields corrode into the sea, but at a rate of 0.02 mm/yr¹¹ from both sides simultaneously.

Activation Release from the N2 PWR Fuel Rods and Thermal Shields

27. As for the SS thermal shields in the RPVs, the three from the N2 RPV are assumed to corrode away on both sides at a rate of 0.02 mm/yr.¹¹ The damaged fuel from the N2 PWR is assumed to comprise UO₂ pellets, 5% enriched, 4.5-mm diameter, 10-g/cm³ density, carried in Zr-Nb alloy cladding. In the absence of details of the extent of damage to the 125 fuel pins, a conservative assumption is made that the cladding material has been fully breached, and does not constitute a barrier to fission product release from the fuel.

28. As soon as the fuel is in contact with sea water, an immediate release of 20% of the fission product inventory is assumed from fuel grain boundaries. The remaining fission products and the actinides are released through dissolution of fuel grains at a pessimistic rate of 30x10⁻⁷ g/cm²/day.¹² For fuel pins with a 4.5-mm diameter and 10-g/cm³ density, this equates to a constant dissolution rate of 1.1 mm/1000 yr. For ease of modelling, the model assumes a linear surface for the circular fuel pin and an evenly spread rate of dissolution. Allowing for

the geometry of the pins, activity release from dissolution will commence at its maximum rate, reducing until the pins finally disappear.

Model results

29. Figure 6: This shows the initial high release [36 kCi/yr (1.3 PBq/yr)] due to the 20% fission product inventory released immediately to the sea. This drops to 56 Ci/yr (2.1 TBq/yr) by the year 2000, and drops further after 2300 when the steels have largely corroded away. From then on, the only release is due to the corrosion of the remaining SNF. By the year 3000, the release rate is 0.11 Ci/yr (4.1 GBq/yr) and at 4000, it is 0.02 Ci/yr (0.74 GBq/yr). After the year 4000, the SNF has disappeared.

Case II - Reactor Compartment Containment Barrier

30. The reactor compartment walls are assumed to form a boundary around the radioactive waste material, and to thus modify the release into the surrounding sea by the containment effectiveness factor K_c , with the release at time t , in years, for fission and activation products given by:

$$A_i(t) = A_i[\text{Case I}(t)] \times K_c$$

31. As shown in Figure 2, pressure release valves allowed sea water into the reactor compartment on sinking. Corrosion is therefore assumed to occur on either side of the hull, but at a reduced rate internally because of low oxygen levels. The weakest area of containment is in the vicinity of the weld securing the mild steel cover plate. At a mean corrosion rate of 0.166 mm/yr,¹² on both sides, the estimated life of an assumed 10-mm thick weld is 30 years. To this point, the effectiveness of the containment boundary is considered to be 100% ($K_c=0$); thereafter, it is assumed to be 90% effective ($K_c=0.1$). General corrosion of the 10-mm thick mild steel hull in this area continues at a rate of 0.075 mm/yr¹² on both sides of the plating, until complete failure eliminates the effectiveness of this boundary ($K_c=1$) 67 years from first immersion in sea water in 1967. These values of K_c are injected into the model as step changes.

Model Results

32. Figure 7: Adding the reactor containment barrier to Case I reduces the initial release to the sea. It is assumed that the 20% soluble fraction escapes in 1996 [950 Ci/yr (35 TBq/yr)] when the reactor compartment closure weld fails and $K_c = 0.1$. Once the weld fails, release rates drop to below 10 Ci/yr (370 GBq/yr) and then rise to 15 Ci/yr (560 GBq/yr) as the full containment barrier corrodes away, then follow the same pattern as Case I.

Case III - Furfural Containment Barrier

33. Information is lacking on the precise composition of the hardening mixture furfural,¹ in which the radioactive material is encased. It is known that it is based on a chemical obtained from the acid hydrolysis of the polysaccharides of oat husks, corn cobs or straw, and that it can

be polymerized with compounds such as acetone or urea to form a hard resin. An effective lifetime of 500 years is quoted¹ for this material. However, in the absence of reliable data on the performance of furfural in such environmental conditions, a conservative lifespan of 100 years *in the radiation environment* is assumed in the model. It has the effect of inhibiting the activity released from all components encased in furfural by the factor K_f . The multiplying factor K_f is zero until the *Lenin* reactor compartment is dumped, and then ramps to unity over the ensuing 100 years. The breakdown of the material is assumed to be due to radiation damage, cracking, and decomposition in sea water.

Model Results

34. Figure 8: Adding the protection of furfural to the box and interior of the RPVs cuts down the release rates in the early years. The activation products corroding from the outside of the RPV walls, as they are unprotected by the resin, are still released, but the remainder is encapsulated in the resin. The form of the release rate follows Case II after the resin loses its complete effectiveness in 100 years, but the initial soluble pulse has been reduced by a third to 290 Ci/yr (11TBq/yr). Choosing a lifetime of 100 years for the resin means that its effectiveness is comparable to the reactor compartment itself (Case II). The spreadsheet model can be run with a range of furfural lifetimes and then its barrier properties can be shown to extend beyond the Case II protection.

Case IV - Box Containment Barrier

35. The fuel pins and three SS thermal shields from the N2 PWR are sealed within the box with welded closure lid, and the RPV heads are in place. For the latter, as bottom and top RPV enclosures are only bolted into position, sea water is assumed to have penetrated at the time of disposal and thus interfaced with the furfural to commence its degradation.

Corrosion of the SS Shell Around the Box

36. The box geometry is shown in Figure 5. Assuming a 10-mm thick closure weld and a mean pitting corrosion penetration rate of 0.5 mm/yr,¹² initial penetration will occur after 20 years, admitting sea water into the box to interface with the furfural and start its degradation. With a general bulk corrosion rate of 0.02 mm/yr,¹¹ complete penetration of the SS shell around the concrete can be expected 500 years later.

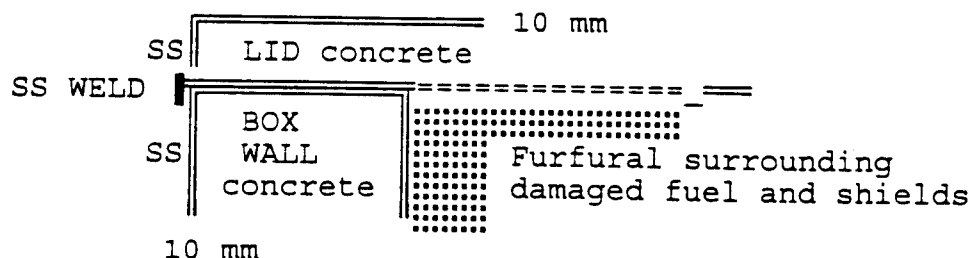


Figure: 5 Box Geometry showing stainless steel covering the concrete lid and wall, the stainless steel closure weld and the space for the fuel and thermal shields encapsulated in furfural.

Deterioration of the Concrete in Sea Water

37. There is little data on the performance of concrete in sea water. Available literature¹² indicates that a concrete structure such as this should have a long life if it does not suffer cracking from radioactive heating or mechanical damage. However, changes in the concrete structure over time are likely, and will alter its effectiveness as a barrier to the diffusion of radioactive species and to the inward diffusion of salt water and dissolved oxygen. The model assumes such diffusion commences after general sea water penetration of the clad, and increases at a linear rate for a further 200 years until the concrete is assumed completely porous. The box containment factor, K_b , therefore has a value of zero until failure of the box closure weld and then ramps to unity over the subsequent 200 years. This is less than the time for the complete degradation of the SS of the box itself.

Model Results

38. Figure 9: Although the outside RPV walls always contribute to the release rate after the reactor compartment walls have been breached (Case II and Case III), the box is shown to reduce the overall rate to below 1 Ci/yr (37 GBq/yr). The early activity release comes from the RPVs as the furfural degrades (Case III). When the box weld fails, additional activity will be released. The concrete, with its lifetime of 200 years, and the outer SS shell will inhibit the release. Overall rates do not exceed 0.7 Ci/yr (26 GBq/yr) by the year 2100. The concrete ceases to provide protection long before the outer SS shell corrodes completely, just before the year 2500.

Case V - Box Support Collapse

39. Assuming that the *Lenin* reactor compartment has remained upright on the sea bed, with the box securely located, this final case considers the consequences of the box losing its lid through displacement following failure of its supporting deck and hull structure. If the mild steel is assumed to corrode away at a rate of 0.075 mm/yr,¹² a 15-mm support framework, corroding on both sides, would collapse in 100 years from first immersion in sea water, nearly the same time of the complete failure of the surrounding hull structure and its containment (Case I). At this point the massive box is assumed to topple and lose the lid, eliminating its effectiveness as a containment barrier ($K_b=1$). All that remains to inhibit the release of fission products, actinides, and activation products will be the furfural, and with the lifetime chosen for this model of 100 years, this provides no barrier.

40. It was also assumed in this scenario, that the 20% soluble fraction of fission products will be released when the box support collapses.

Model results

41. Figure 10: Before the box collapse, release rates are identical to Case IV. When the hull frames corrode away in 100 years, the box lid breaks off and the SNF is exposed to the sea water, by now without the protection of furfural (and the box). Figure 10 shows the initial pulse

of the 20% soluble fraction of the fission product inventory, released when the box breaks open in 2066, at a rate of 1900 Ci/yr (70 TBq/yr) to the sea. Afterwards, the rate drops down to 1.9 Ci/yr (70 GBq/yr) at 2100, 0.5 Ci/yr (19 GBq/yr) by 2200, and then mirrors Case I, with no containment.

CONCLUSIONS AND FURTHER WORK

42. All the scenarios are brought together in Figure 11, which shows that Case IV provides the best level of protection, as might be expected. With all the pessimistic assumptions (paragraph 21) on the furfural and concrete lifetimes, release rates never exceed 0.7 Ci/yr (26 GBq/yr), and stay within the 0.1 to 0.2 Ci/yr (3.7 to 7.4 GBq/yr) band for the next 500 years.

43. The box collapse scenario, Case V, represents the greatest risk, allowing the soluble fraction of fission products to be washed out in the year the structure fails and the lid breaks off. This case is most sensitive to the lifetime assumed for furfural protection.

44. Recommendations:

a. As the box collapse scenario is deemed to be the "worst" of the scenarios that could be envisaged realistically, it is suggested that in the next exploratory cruise to the Kara Sea, the *Lenin* reactor compartment be located in Tsivolka Inlet and the state of the structure be photographed. In particular, the angle of repose and the state of the closure weld on the top deck should be checked, and any indication of general structural failure noted.

b. More data must be found on the lifetime of furfural in the Arctic Ocean environment and a research project should be initiated using the original formulation of the resin.

c. Similarly, the effective lifetime or barrier efficiency presented by the concrete in the box needs to be evaluated.

44. Further work:

a. The concepts of this spreadsheet model developed for the *Lenin* could equally well be applied to the other nuclear material that still remains on the sea floor. It is the intention of the Group to extend the study, using information on nuclide inventories, activation, composition, structures, and the containment boundaries of all the disposed material, when the data becomes available. This way, a realistic estimate can be made for the radionuclide release rates into the Barents and Kara Seas.

REFERENCES

1. A.V. Yablokov, et. al., *Facts and Problems Related to Radioactive Waste Disposal in Seas Adjacent to the Territory of the Russian Federation*, Office of the President of the Russian Federation, Moscow (1993), pp. 20-41.
2. K.L. Sjoebloom and G. Linsley, "IAEA Programmes Relevant to the Radioactive Waste Dumped in the Arctic Seas: Part 1. International Arctic Seas Assessment Project (IASAP)," in *Environmental Radioactivity in the Arctic and Antarctic*, P. Strand and E. Holm, Eds., Scientific Committee of the International Conference on Environmental Radioactivity in the Arctic and Antarctic, Osteras, Norway (December 1993), pp. 89-92.
3. M.E. Mount, M.K. Sheaffer, and D.T. Abbott, "Estimated Inventory of Radionuclides in Former Soviet Union Naval Reactors Dumped in the Kara Sea," in *Environmental Radioactivity in the Arctic and Antarctic*, P. Strand and E. Holm, Eds., Scientific Committee of the International Conference on Environmental Radioactivity in the Arctic and Antarctic, Osteras, Norway (December 1993), pp. 81-87.
4. Y. Sivintsev, *Study of Nuclides Composition and Characteristics of Fuel in Dumped Submarine Reactors and Atomic Icebreaker "Lenin": Part I - Atomic Icebreaker*, Russian Research Centre, "Kurchatov Institute," Moscow, Russia (December 1993).
5. L. Foyn and A. Nikitin, *The Joint Norwegian/Russian Expedition to the Dump Sites for Radioactive Waste in the Open Kara Sea, the Tsivolki Fjord, and the Stepovogo Fjord, September - October 1993: Report from the Expedition on Board R/V Viktor Buinitskiy, with Some Preliminary Results*, (in preparation).
6. N.N. Belousov, et. al., "The Use of the GETERA Code in Reactivity Effects Analysis," in *Proceedings of the VII All-Union Seminar on the Problems of Reactor Physics*, Moscow, (1991)
7. V.V. Kevrolev, "RECOL Continuous-Energy Monte-Carlo Code for Neutron Transport," Preprint RRC KI, IAE-5621/5, (1987).
8. M.L. Williams, "Analysis of Thermal Reactor Benchmarks with Design Codes Based on ENDF/B-V Data," *Nucl. Techn.*, **71** (November 1985), pp. 386-401.
9. J.F. Briesmeister, "MCNP - A General Monte-Carlo Code for Neutron Transport," Los Alamos National Laboratory, Los Alamos, NM, LA-7396-M-Rev.2, (1987).
10. A.G. Groff, "ORIGEN-2: A Versatile Computer Code for Calculating the Nuclide Composition and Characteristics of Nuclear Materials," *Nucl. Techn.*, **62** (September 1983), pp. 335-352.
11. House of Commons Defence Committee, "Decommissioning of Nuclear Submarines," 7th Report, Session 1988 - 1989, Her Majesty's Stationary Office, London (1990).

12. J.H. Carter, "Corrosion of LENIN Reactor Compartment Materials", Department of Nuclear Science and Technology, Royal Naval College, Greenwich, London, Technical Memorandum RNC/NS/TM431 (May 1994).

Acknowledgements

1. Ms. K.L. Sjoebloom, Division of Nuclear Fuel Cycle & Waste Management, IAEA Vienna, for her work in organizing the Source Term Working Group, and for permission to publish the study as part of the IAEA's International Arctic Seas Assessment Project.
2. Dr. J.H. Carter, Department of Nuclear Science & Technology, Royal Naval College Greenwich, for researching and sifting corrosion data in support of the modelling work for this paper.

Table 1. Estimated radioactivity in the reinforced concrete and stainless steel shell container within the reactor compartment of the icebreaker *Lenin* for 1993.^{3,4,11}

Radionuclide	Activity		
	Curies (Ci)	Becquerels (Bq)	Percent (%)
<i>Fission products</i>			
¹³⁷ Cs	1.331x10 ⁴	4.925x10 ¹⁴	26.14
^{137m} Ba	1.259x10 ⁴	4.658x10 ¹⁴	24.73
⁹⁰ Sr	1.208x10 ⁴	4.470x10 ¹⁴	23.73
⁹⁰ Y	1.208x10 ⁴	4.470x10 ¹⁴	23.73
⁸⁵ Kr	4.768x10 ²	1.764x10 ¹³	0.937
¹⁵¹ Sm	2.969x10 ²	1.099x10 ¹³	0.583
¹⁴⁷ Pm	4.827x10 ¹	1.786x10 ¹²	0.095
³ H	2.371x10 ¹	8.773x10 ¹¹	0.047
⁹⁹ Tc	3.629x10 ⁰	1.343x10 ¹¹	0.007
¹²⁵ Sb	2.034x10 ⁰	7.526x10 ¹⁰	0.004
¹²⁹ I	1.000x10 ⁻²	3.700x10 ⁸	0.00002
Subtotal	5.091x10 ⁴	1.884x10 ¹⁵	100.00
<i>Activation products</i>			
⁶³ Ni	1.350x10 ³	4.995x10 ¹³	77.23
⁶⁰ Co	3.510x10 ²	1.299x10 ¹³	20.08
⁵⁹ Ni	3.780x10 ¹	1.399x10 ¹²	2.16
¹⁴ C	9.180x10 ⁰	3.397x10 ¹¹	0.53
Subtotal	1.748x10 ³	6.468x10 ¹³	100.00
<i>Actinides</i>			
²⁴¹ Pu	1.908x10 ³	7.060x10 ¹³	82.13
²⁴¹ Am	1.891x10 ²	7.000x10 ¹²	8.14
²³⁹ Pu	1.363x10 ²	5.040x10 ¹²	5.87
²⁴⁰ Pu	6.105x10 ¹	2.260x10 ¹²	2.63
²³⁸ Pu	2.856x10 ¹	1.060x10 ¹²	1.23
Subtotal	2.325x10 ³	8.601x10 ¹³	100.00

Table 2. Estimated radioactivity in the three reactor pressure vessels within the reactor compartment of the icebreaker *Lenin* for 1993.^{4,11}

Radionuclide	Activity		
	Curies (Ci)	Becquerels (Bq)	Percent (%)
<i>Activation products</i>			
⁶³ Ni	3.650x10 ³	1.351x10 ¹⁴	77.23
⁶⁰ Co	9.490x10 ²	3.511x10 ¹³	20.08
⁵⁹ Ni	1.022x10 ²	3.781x10 ¹²	2.16
¹⁴ C	2.482x10 ¹	9.183x10 ¹¹	0.53
Subtotal	4.726x10 ³	1.749x10 ¹⁴	100.00

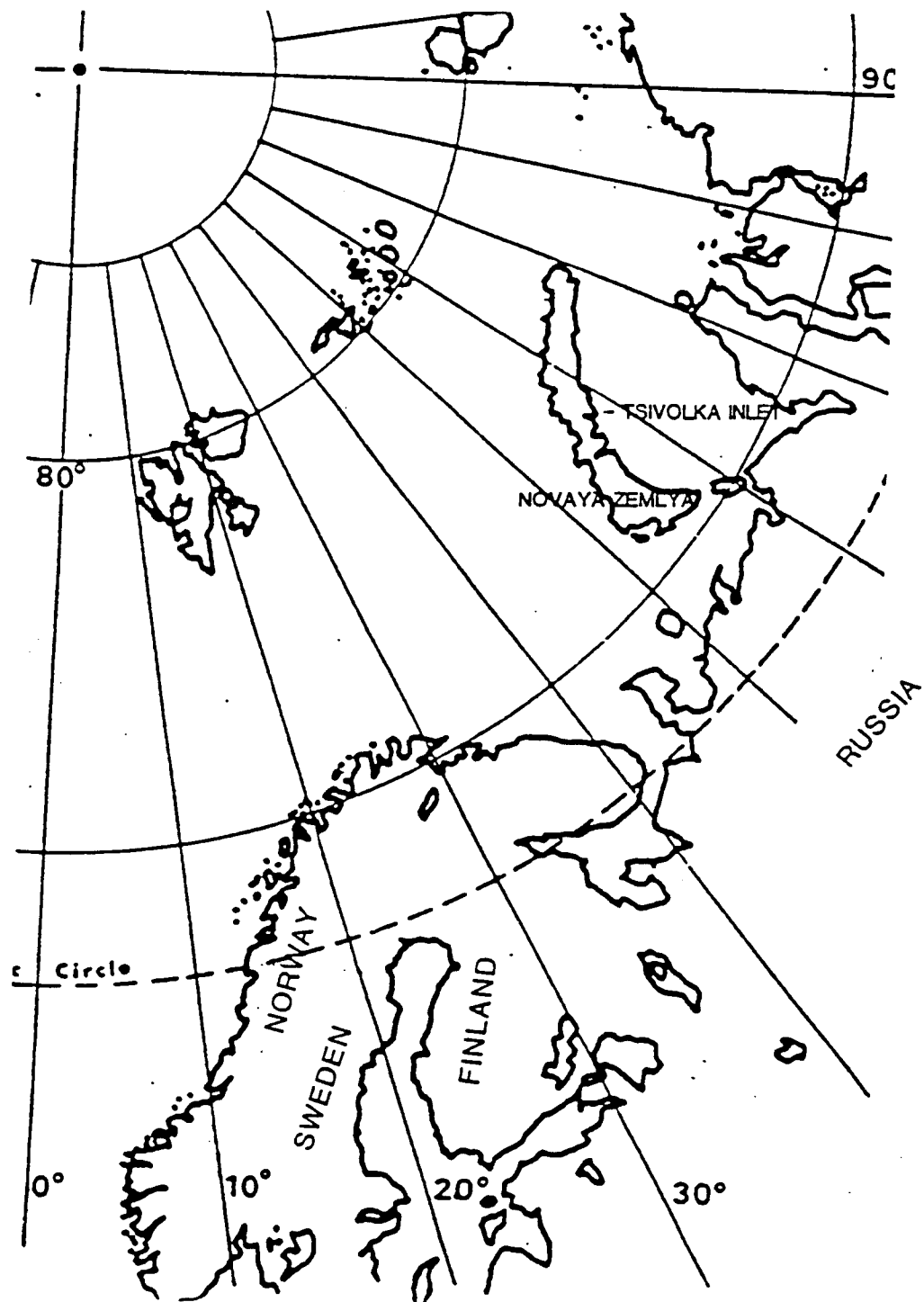


Figure 1: The LENIN dump site in Tsivolki Inlet, Novaya Zemlya

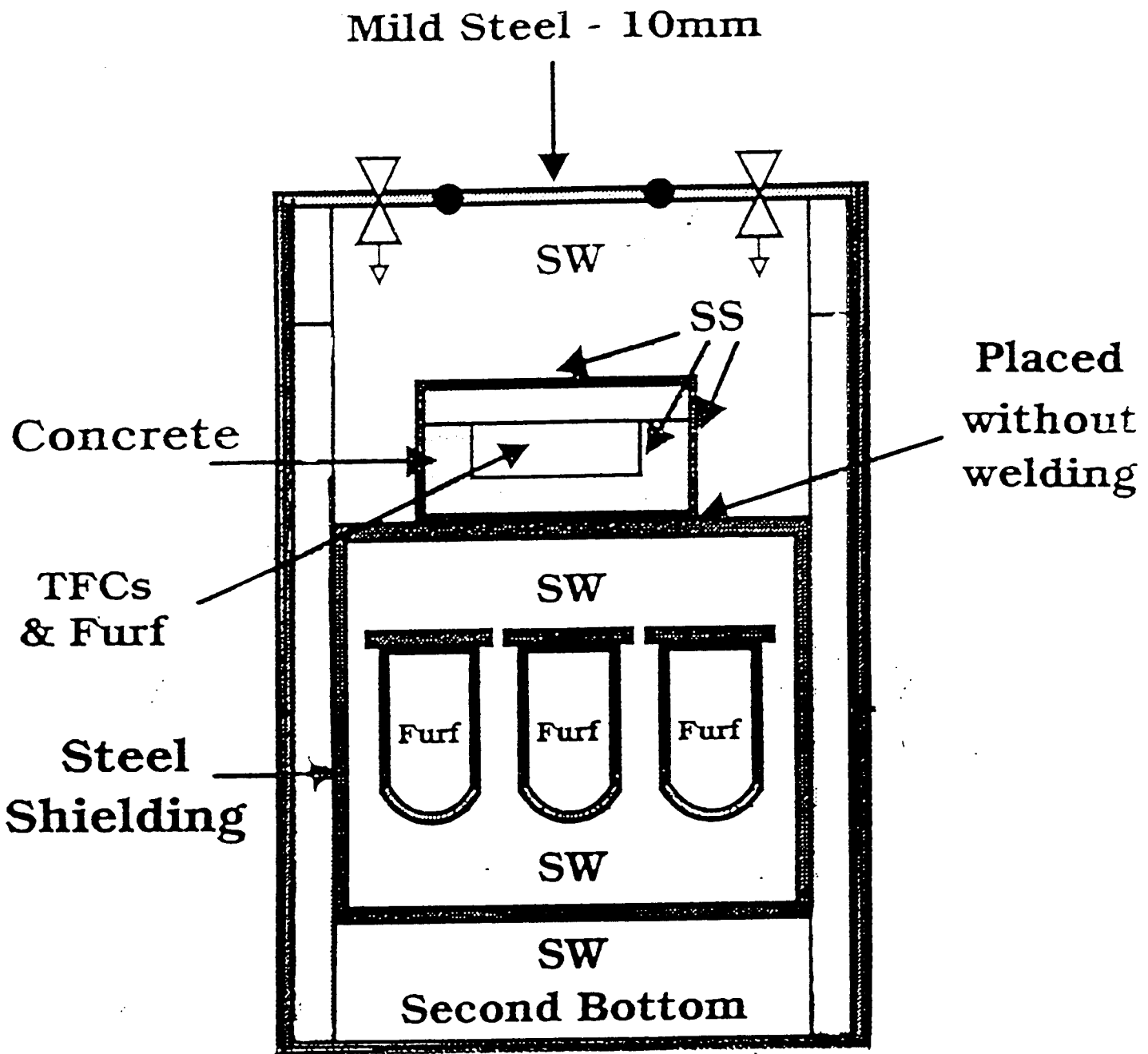
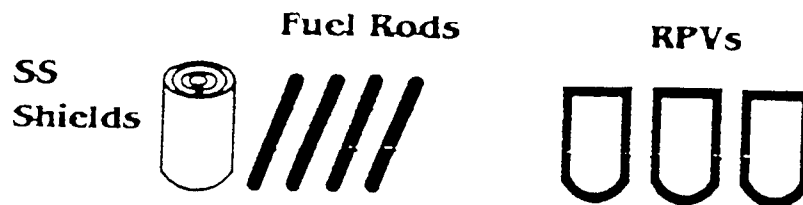


Figure 2: Diagrammatic representation of the LENIN reactor compartment. (Based on Reference 4)
 SW = seawater, SS = stainless steel, Furf = furfural, TFCs= Technological Fuel Channels (containing the damaged fuel)

CASE 1



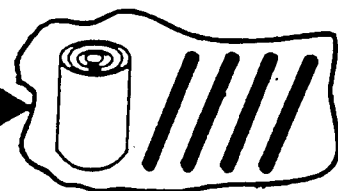
CASE 2

Containment
Boundary
(kc)



CASE 3

Furfural
(kf)



CASE 4

Concrete
Box
(k_B)

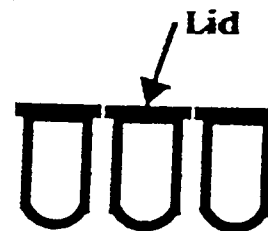
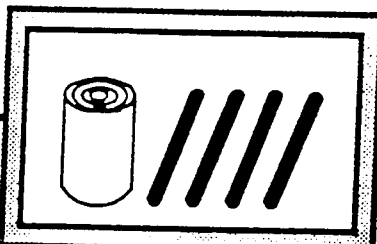


Figure 3: The four scenarios in the LENIN Release Model (See para 23 for description)

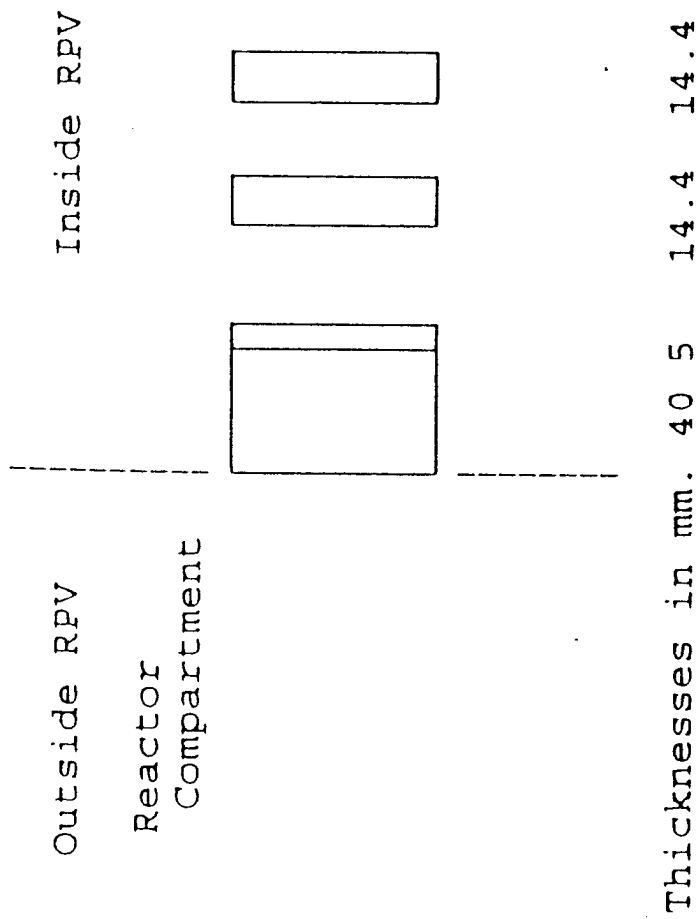


Figure 4: RPV geometry showing RPV wall, cladding and the internal stainless steel thermal shields

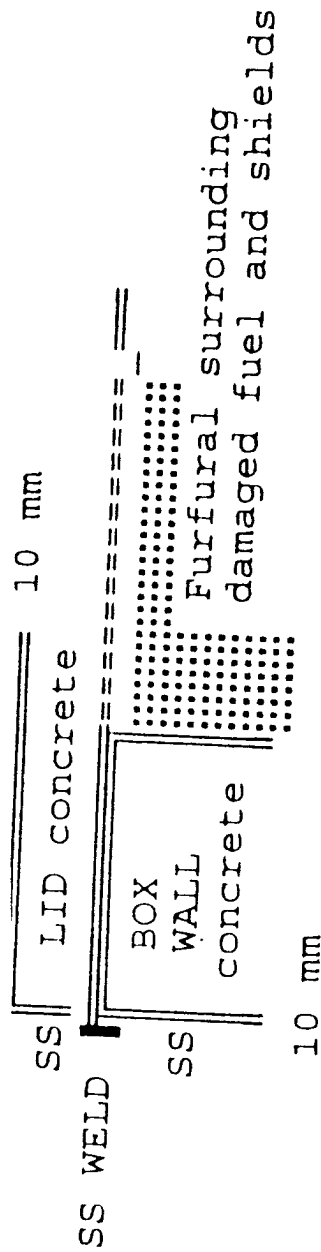
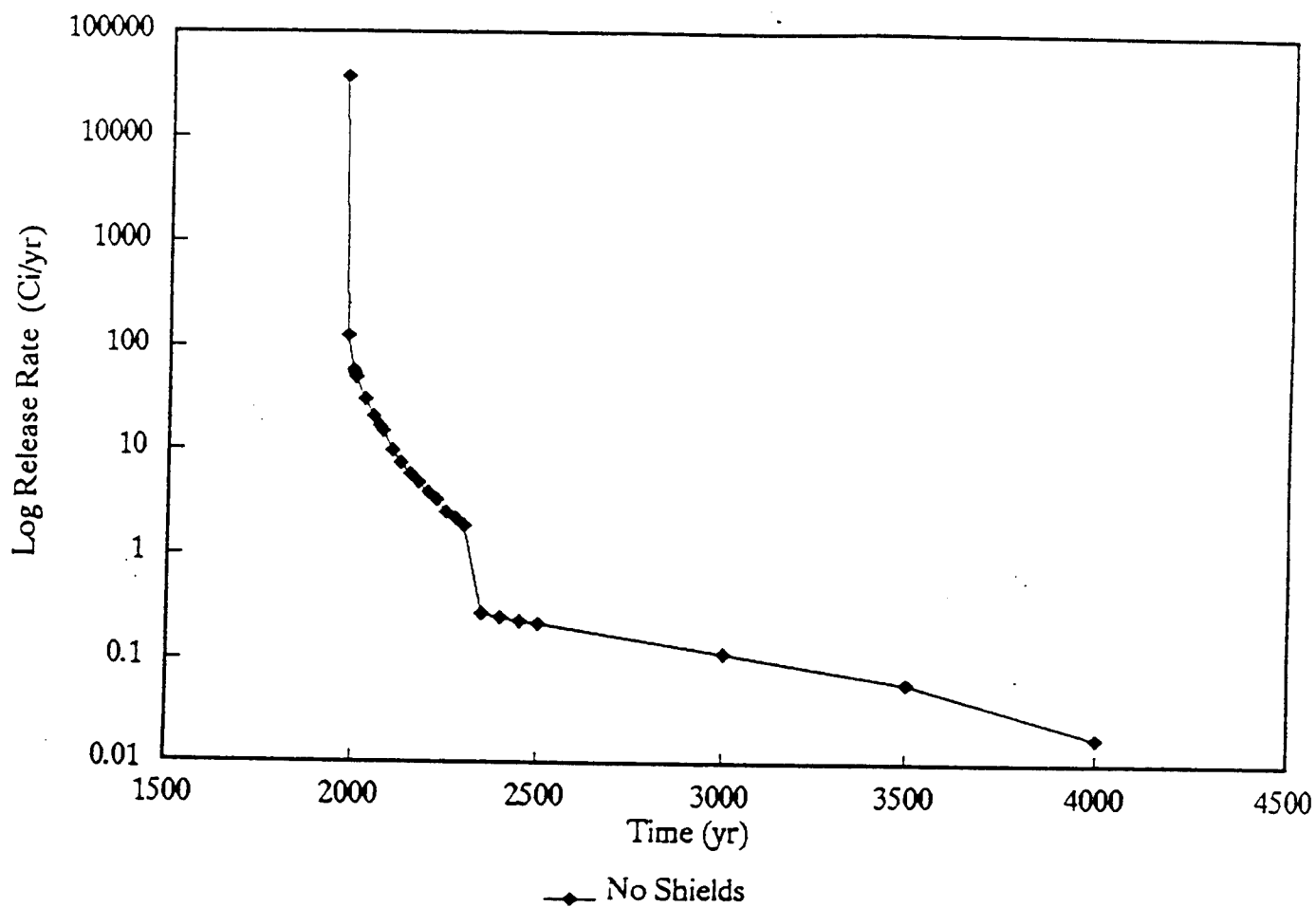


Figure: 5 Box Geometry showing stainless steel covering the concrete lid and wall, the stainless steel closure weld and the space for the fuel and thermal shields encapsulated in furfural.



Lenin.018

Figure 6: Case I No containment barriers

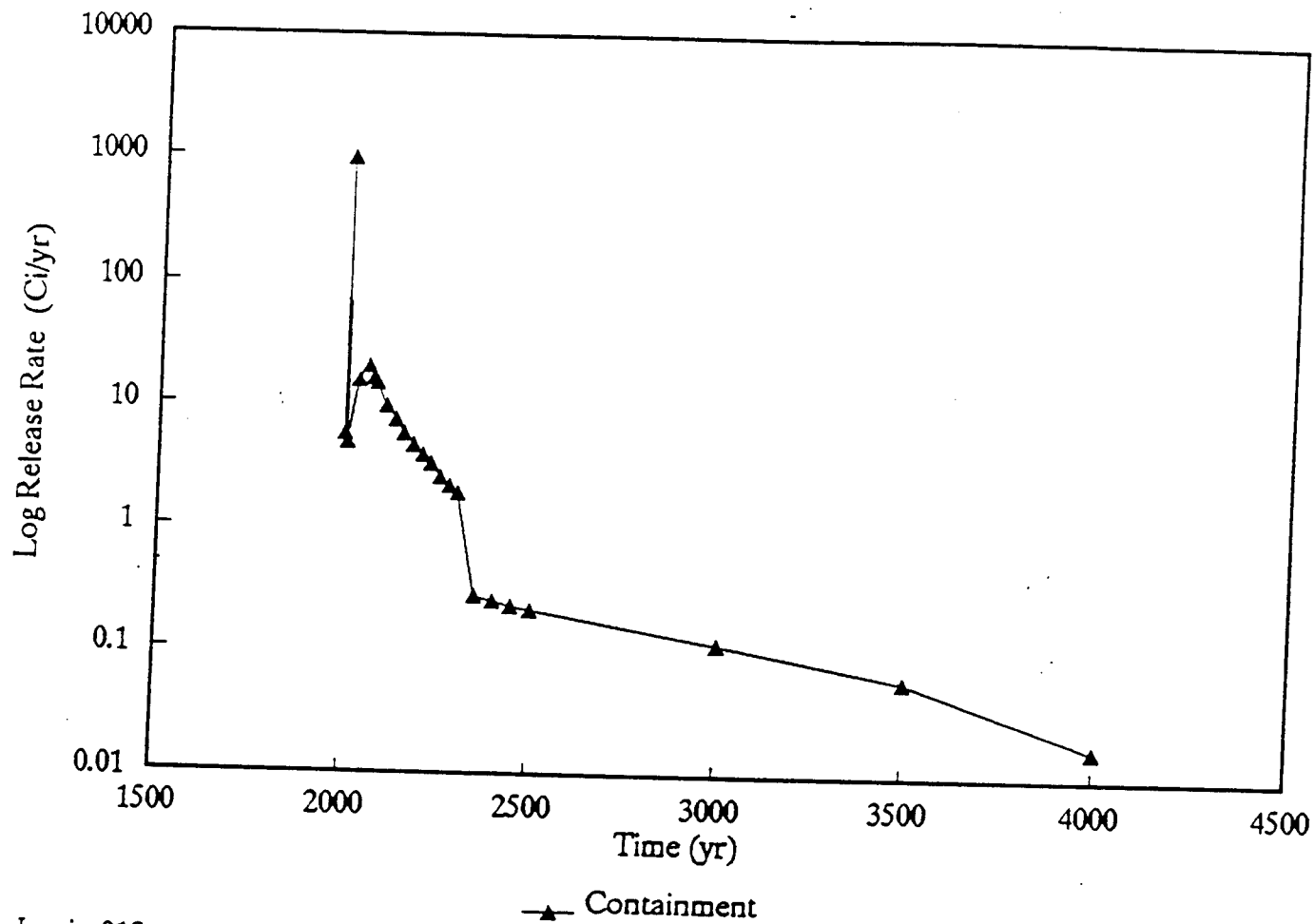
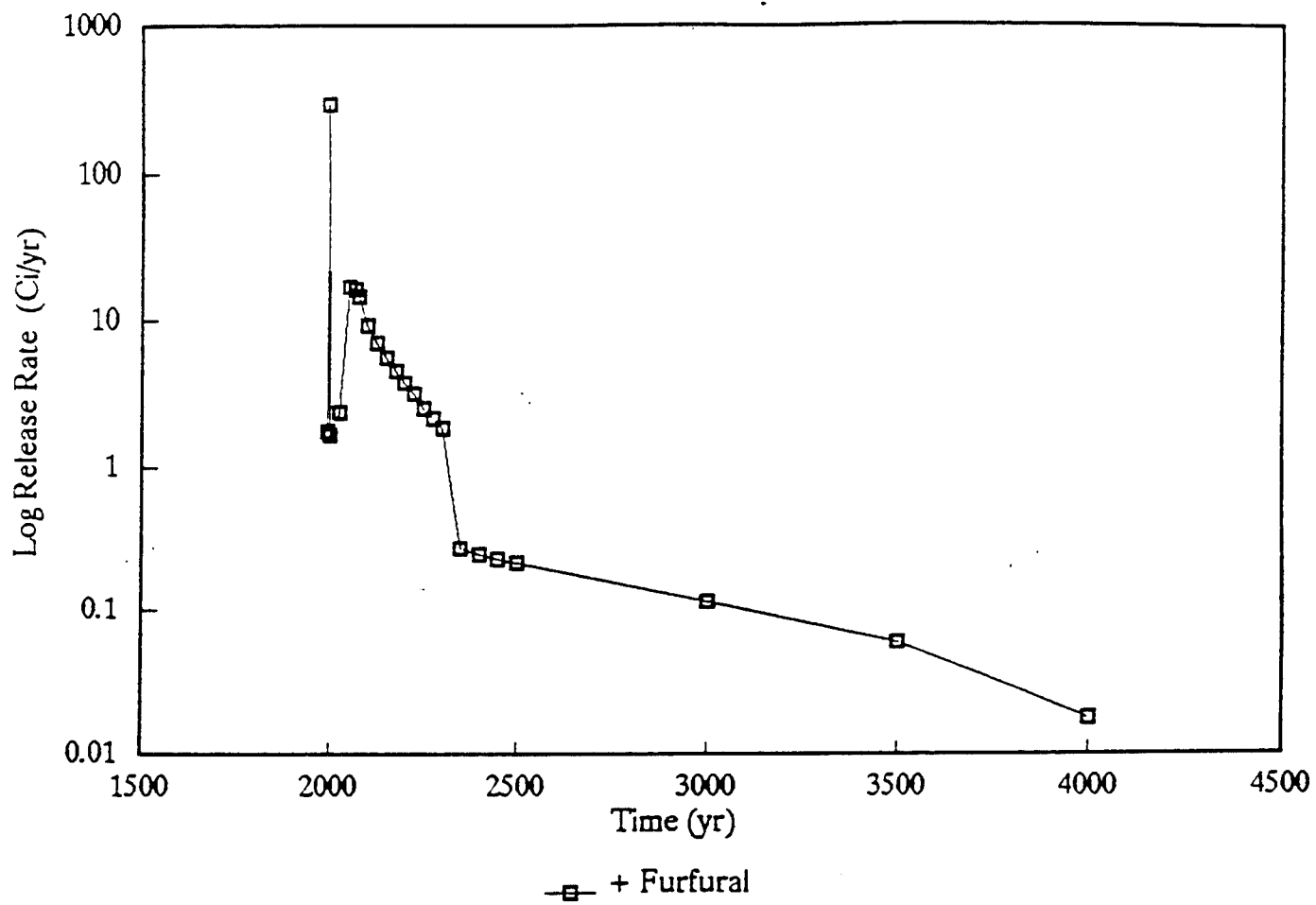
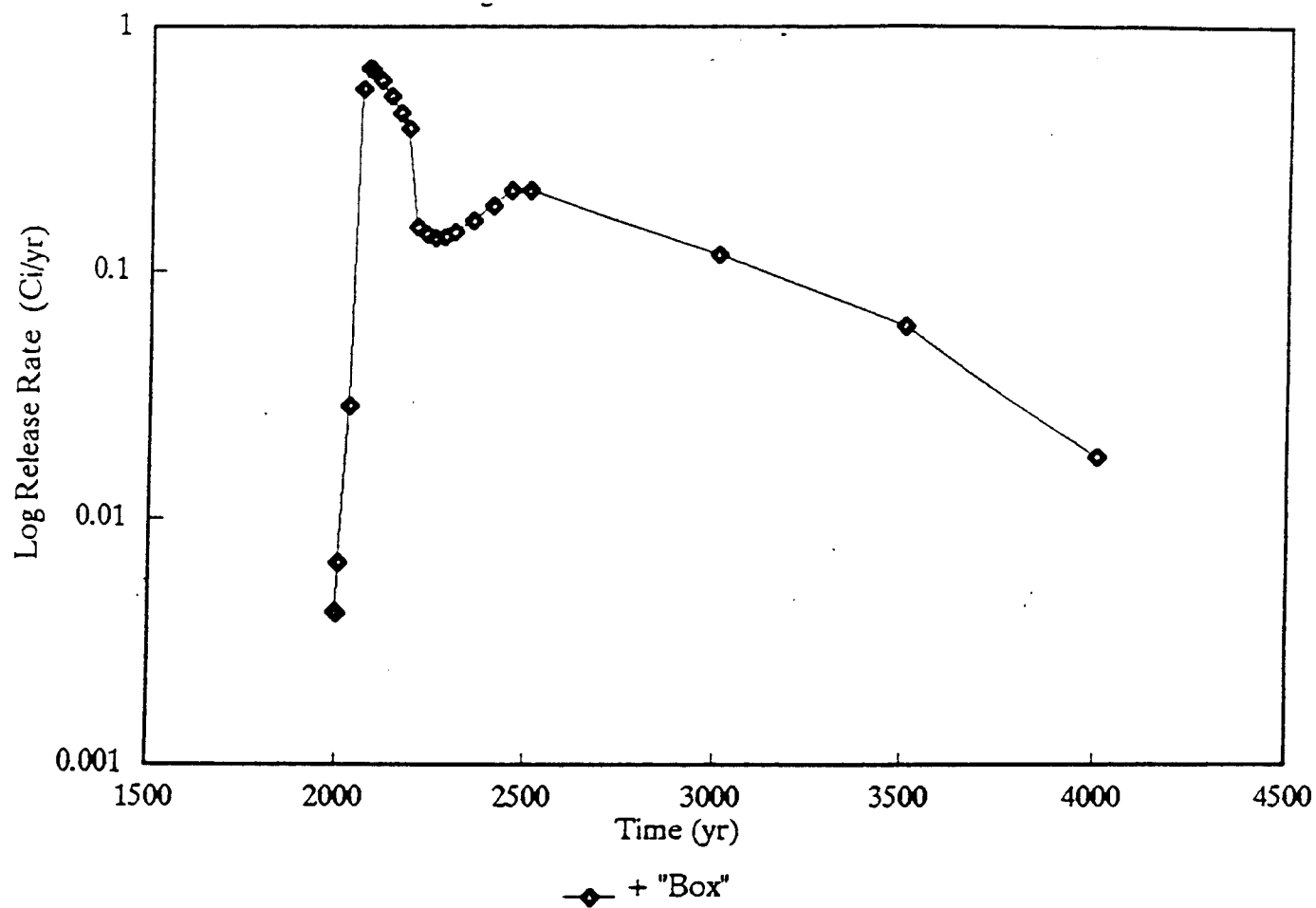


Figure 7: Case II Reactor Compartment Containment Barrier



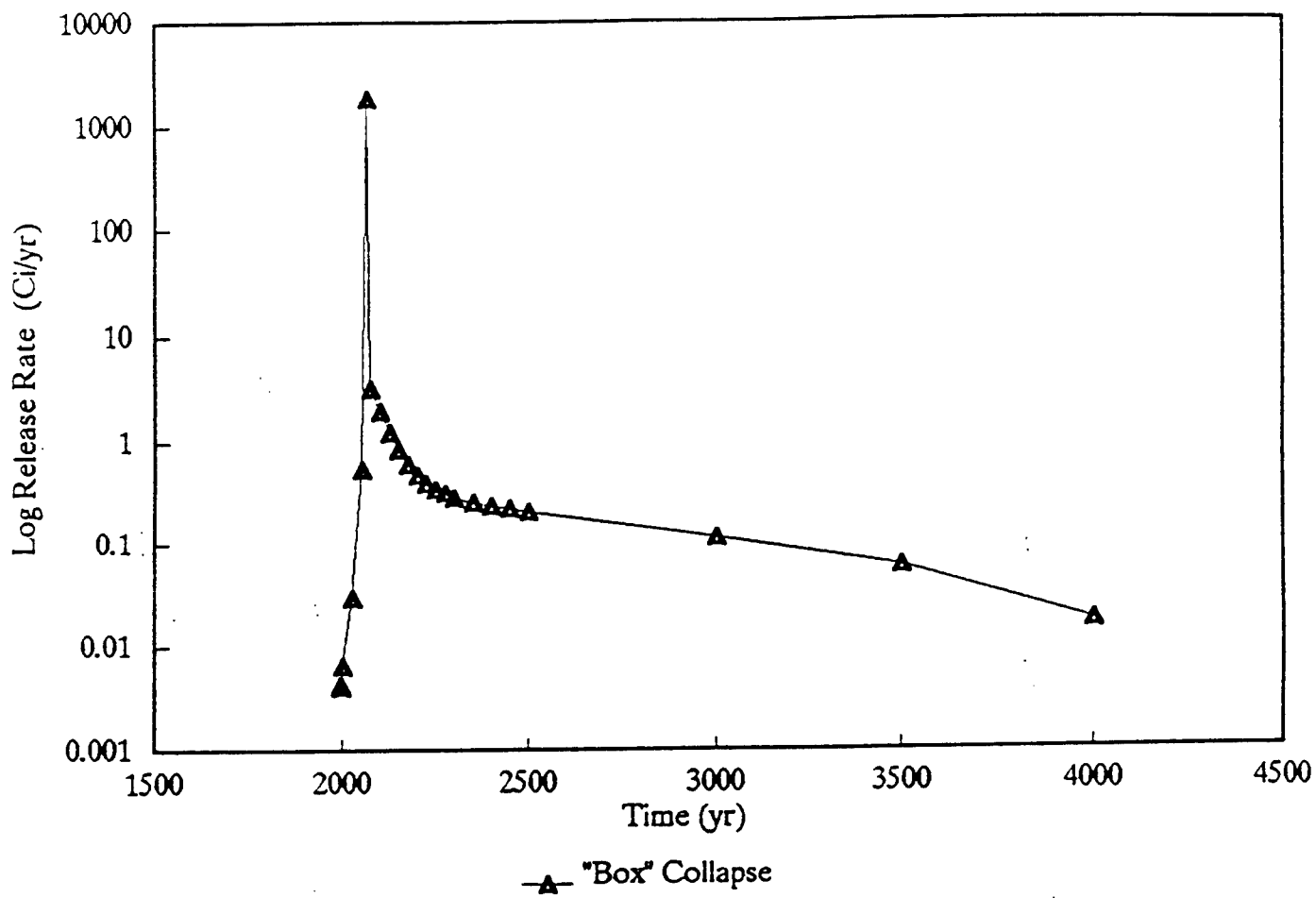
Lenin.018

Figure 8: Case III Furfural Containment Barrier



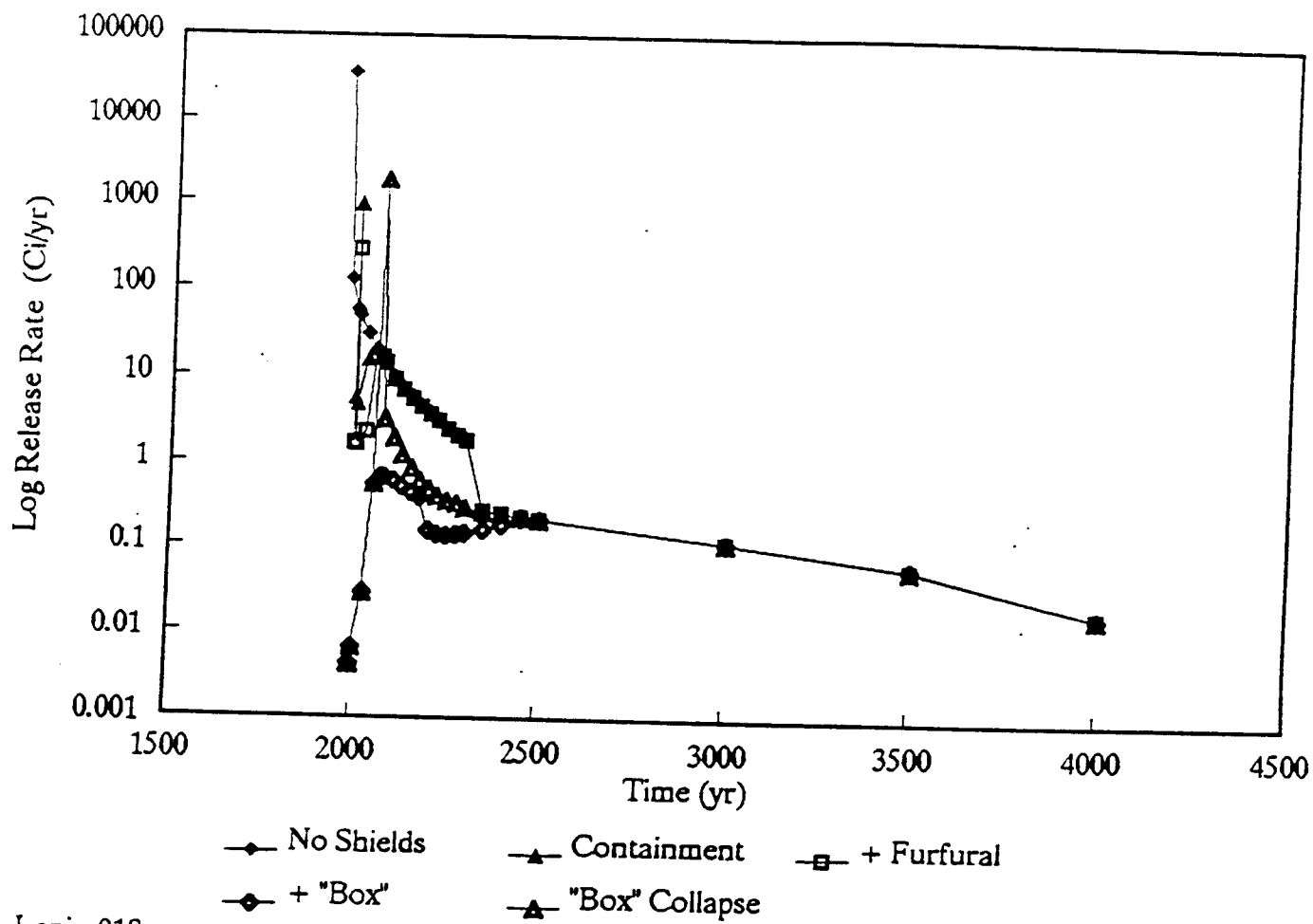
Lenin.018

Figure 9: Case IV Box Containment Barrier



Lenin.018

Figure 10: Case V Box Support Collapse



Lenin.018

Figure 11: Cases I to V All Scenarios Compared

Overview of Modeling from Land Based Sources Through the Ob and Yenisei Rivers and Estuaries to the Kara Sea

Terry Paluszkiewicz

Overview of Modeling from Land Based Sources Through the Ob and Yenisei Rivers and Estuaries to the Kara Sea

Terri Paluszkievicz
Pacific Northwest Laboratories
Marine Sciences Laboratory
1529 W. Sequim Bay Road
Sequim, Washington 98382

The objective of this research is to couple models with existing and forthcoming data to estimate radionuclide fluxes to the Kara Sea from the Ob and Yenisei River systems. Our approach is to use a hierarchy of simple models to quantify the transport and fate of radionuclide contaminants via various pathways through the system. The system consists of the sources of past and (possible) future contaminant releases from Russian nuclear defense sites on land, the environment (terrestrial, ground and surface water), between the location of the sources and the Ob and Yenisei Rivers, the Ob and Yenisei Rivers and their tributaries, the Ob and Yenisei Estuaries, and the confluence region where the estuaries flow into the Kara Sea. There are five integrated tasks that together provide data and numerical modeling to quantify the fluxes through the entire system and each component (riverine, estuarine, or inner shelf) within the system.

The contaminants that we are following through the system are ^{90}Sr , ^{137}Cs , and ^{239}Pu . The basic algorithms governing the adsorption and desorption of a dissolved contaminant with sediments and solids are used in the budget models. We are evaluating the following scenarios for both river systems: a steady release of contaminants and a catastrophic release, corresponding to a flood and dam failure and to the fast (in geological time) movement of groundwater from injection wells. Both scenarios will be evaluated over all seasons. The steady release simulations will yield a baseline for comparison with samples being taken in the estuary and on the shelf by other program participants.

An initial quantification has been made of the inventory at nuclear facilities that include research institutes, fuel fabrication facilities, uranium mining and materials, production reactors, and spent nuclear fuel reprocessing sites. The latter sites, Mayak, Tomsk-7, and Krasnoyarsk-26 are believed to be responsible for the majority of the radioactive contamination that is found in the major river systems that feeds into the Arctic Ocean through the Kara Sea. An analysis of basic residence times under simplified conditions has been used to establish that the models were configured properly for each river system. Multiple-parameter range studies were run to determine the sensitivity to ranges in the empirical coefficients used in the sediment transport, sediment-contaminant transport algorithms. Initial results indicate the need for further data on the composition of bed-load sediments and the need to use a calibration data set to establish the mass transfer coefficient.

Assessment of the Contamination of the Kara Sea from Radionuclide Transport through the Ob and Yenisei River Systems

and amended scope of work

Refinement and Data Calibration of the Radionuclide Transport Model for the Ob and Yenisei River Systems

Participants:

Terri Paluszkiewicz

Peter Becker

Don Bradley

Don Denbo

Mike Foley

Lyle Hibler

Chris Sherwood

Yasuo Onishi

Gene Whelan

Collaborators

Ted Callender

Ed Landa

Robert Meade

TYPHOON

Soviet Hydrological Institute

The study will address the following specific questions:

- Under conditions of normal river flow, with existing dam structures, and a steady continuous release of contaminants, what are the concentration levels of ^{90}Sr , ^{137}Cs and ^{239}Pu in the Ob and Yenisei Rivers, their estuaries, and the inner Kara Sea?
- Under catastrophic conditions, such as a dam-break, tank-failure, or flood, (i.e. a large pulse-like release of contaminants), what are the concentration levels of ^{90}Sr , ^{137}Cs and ^{239}Pu in the Ob and Yenisei Rivers, their estuaries, and the inner Kara Sea?

Project Objectives

- Couple simple models with existing and forthcoming data to estimate radionuclide fluxes to the Kara Sea from the Ob and Yenisei River systems.
- Answer the following questions using existing data, observations that are presently being collected, and simple but robust budget models.
 - What are the basic pathways and partitioning of the contaminants (dissolved, or sorbed) in the rivers, estuary, and inner shelf?
 - What are the dominant processes that control these pathways?
 - Which processes require additional study and what additional data is most critical?

Task Integration

River
Geo-
chemistry
USGS

Source Terms Bradley and Foley

Data
Becker
SHI/USGS
Typhoon

MEPAS
Whelan

River Modeling
[REDACTED] and Hibler
Richmond

Estuarine Modeling

Paluszkievicz & Sherwood

ICE, THERMODYN, MIXING
Denbo

Tracer Continuity with Ocean Modeling - Becker

Planned Approach

- Quantitative analysis of existing contaminant sources.
- Collaboration with Lawrence Berkeley Lab. (studies of Mayak).
- Collaboration with FSU Typhoon scientists on their ongoing riverine and estuarine studies.
- Collaboration with USGS Mobilization and Transport Study.
- Assessment of transport risk from terrestrial sources to the river using the MEPAS methodology.
- Refinement of contaminant transport parameterization if data are sufficient.

SPOT Image of the Mayak Site

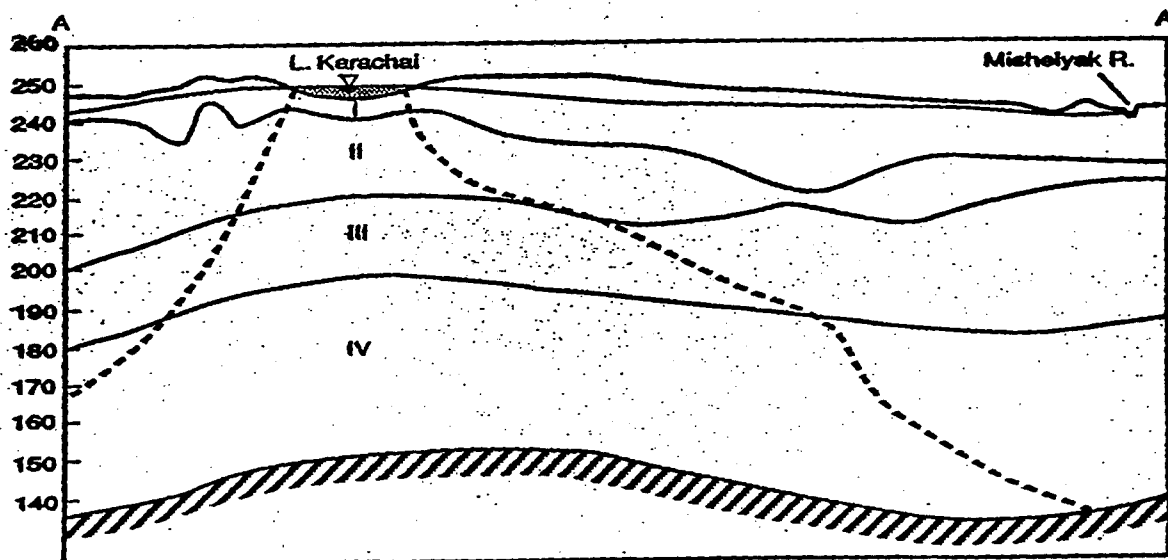
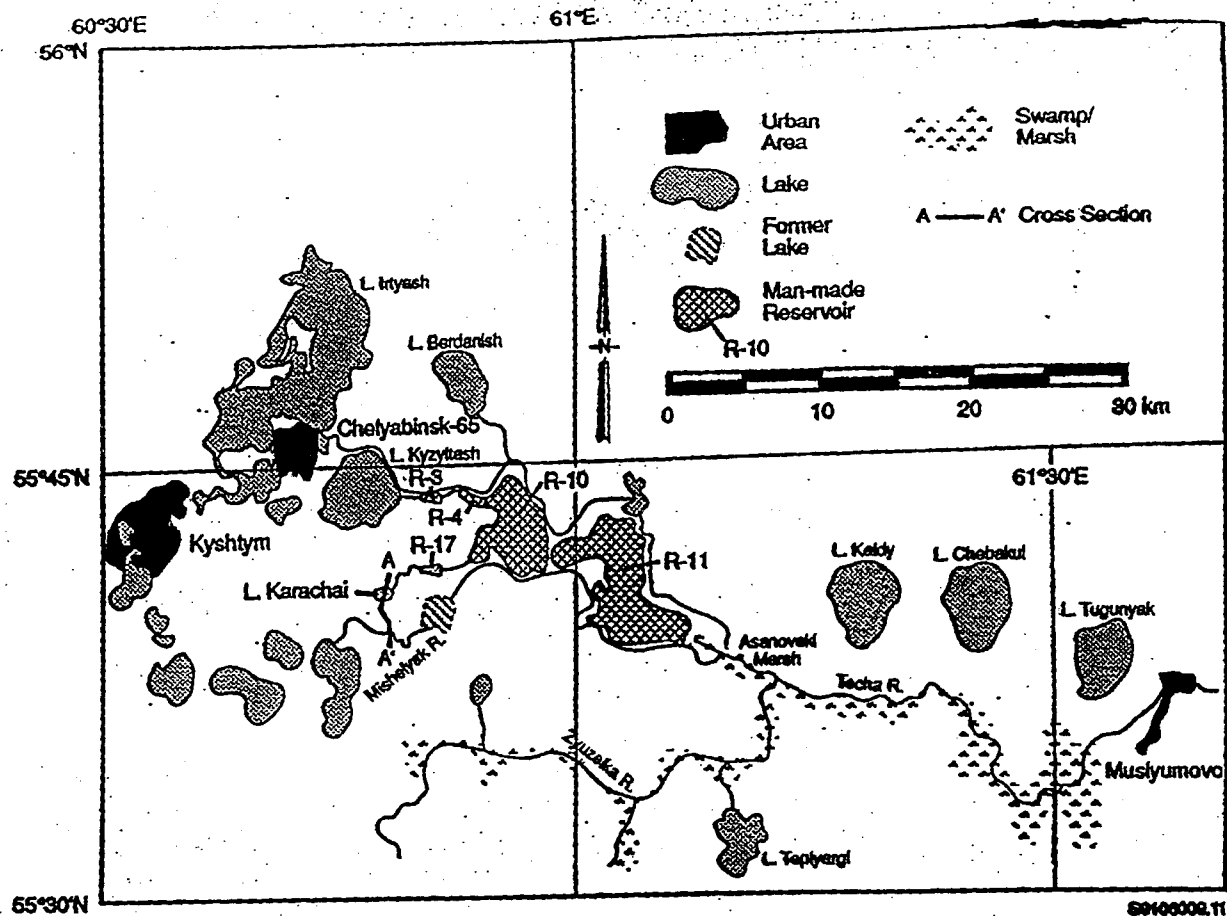


Production
Facilities

Lake Karachai

Reservoirs

Techa River



Explanation

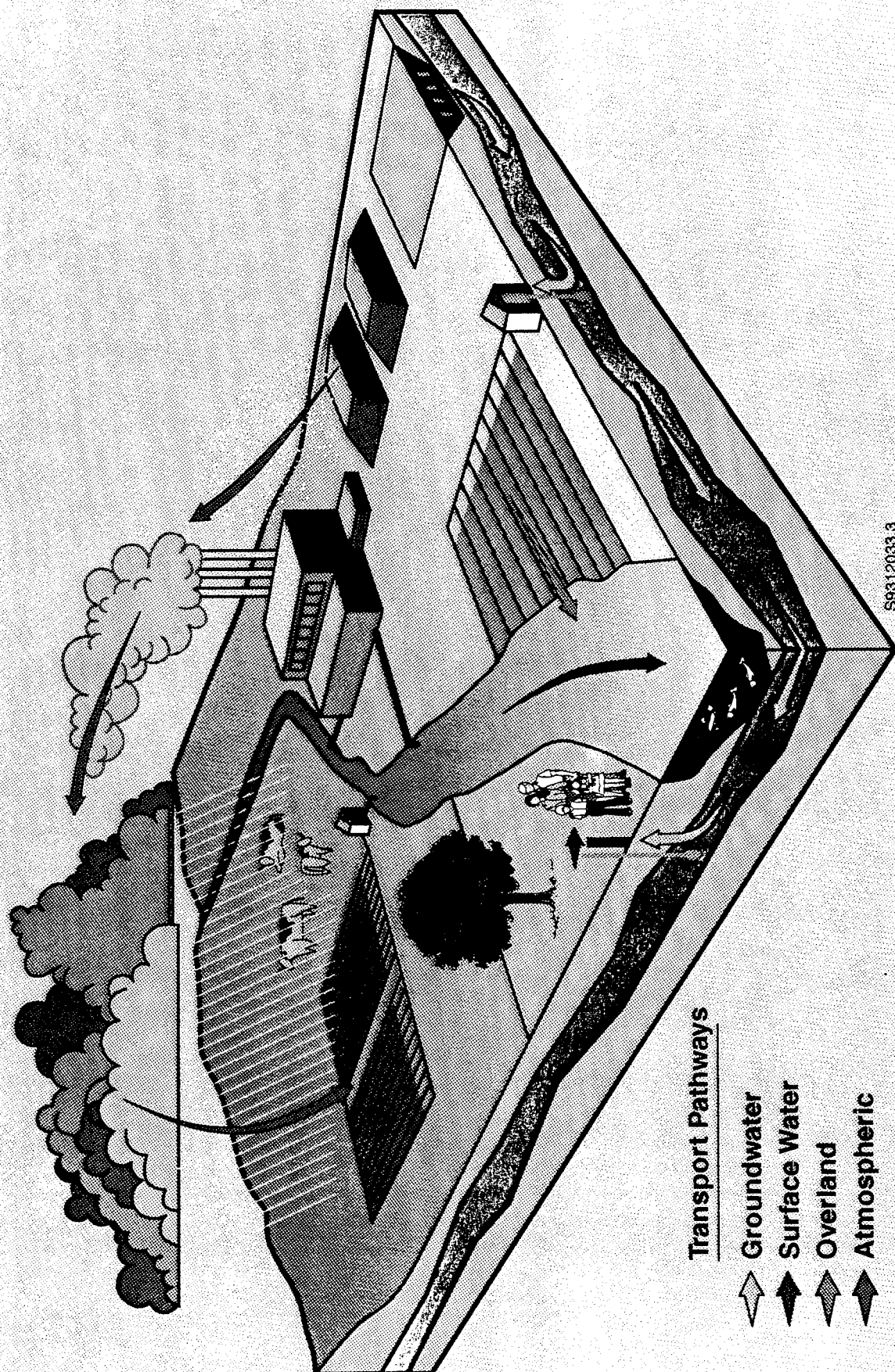
Zones of different hydraulic conductivity
 I = 1 m/d
 II = 4 m/d
 III = 0.5 m/d
 IV = 0.1 m/d

▽ Ground-water level

Lower boundary of permeable zone

--- Boundary of contaminant plume from Lake Karachai

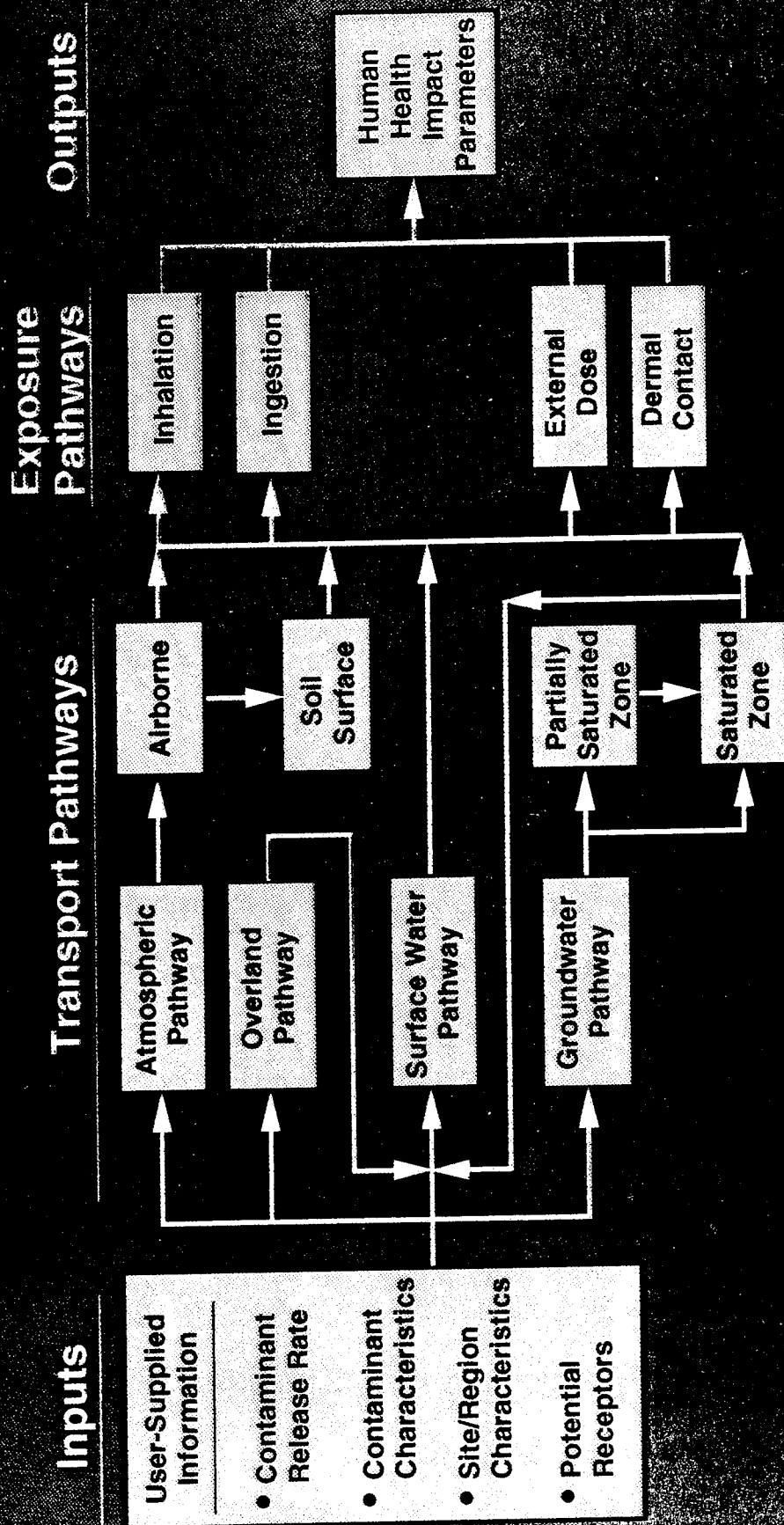
S9402054.2



Transport Pathways

- Groundwater
- Surface Water
- Overland
- Atmospheric

S9312033.3



Riverine Modeling

Some key processes in the conceptual model:

- Time-dependent transport of water, dissolved contaminants, sediments, contaminants sorbed onto sediments
- Deposition and Resuspension of contaminants and sediments, contaminants sorbed onto sediments
- Ice formation and breakup, ice damming of flow, ice-incorporation of sediment and contaminant

Incremental improvements in model complexity:

- Phase 1:
 - Evaluate sediment and contaminant transport parameterizations under simplified (steady) flow conditions;
 - "Tune" model using existing data and understanding;
 - Evaluate data and parameterization weaknesses;
 - Determine residence time and basic behavior of system.
- Phase 2:
 - Evaluate the system response for time-dependent flow conditions;
 - Examine the system response for key transport scenarios (flooding, ice damming, freshet, freeze-up);
 - Incorporate additional data, calibrate and validate when possible.
- Phase 3:
 - Evaluate system response to risk-related scenarios (container-rupture, dam-break, flood) using full set of data and algorithm improvements.

3-D Primitive Equation Model: Mellor and Blumberg, SPEM, Davies, Semtner and Chervin

Attributes: -Reveals more complex circulation and interactions
 -Could provide circulation estimates to box models of sediments and contaminants
 -Easily accepted by the unsuspecting viewer

Detractions: -Our level of observation-based knowledge would not support a consistency check with model results.
 -High level of complexity in adding ice
 -Requires considerable data
 -Parameterizations are inappropriate

Hierarchy of Estuarine Models

Box Model: Officer (1980a,b) Officer and Kester (1991)

- Attributes:
- Data requirement matches availability
 - Includes sediment transport
 - Inclusion of ice possible (Hamblin, 1989)
 - Will reveal basic patterns of distribution

- Detractions:
- Assumes steady state
 - Assumes tidal mixing < horiz. net circ.
ie. gravitational processes are dominant
 - Will not reveal new information about the
estuarine processes

2-D Numerical Models: Bowden and Hamilton (1975), Oey et al. (1985), Festa and Hansen (1976),
RMA2-RMA4(ACOE)

- Attributes:
- Reveals more complex interactions in
estuarine circulation
 - Will reveal more information about
circulation processes
 - Computational efficiency
 - More responsive to complex physical
forcing

- Detractions:
- Requires more data (N_z , R_i , U , V)
 - More complexity in including sediment
dynamics (except RMA4)
 - More complexity in including ice

*Box model solution of Festa and Hansen (1978) has been compared with box model of Officer(1980)

Estuarine Modeling

Identify the characteristics of the estuary:

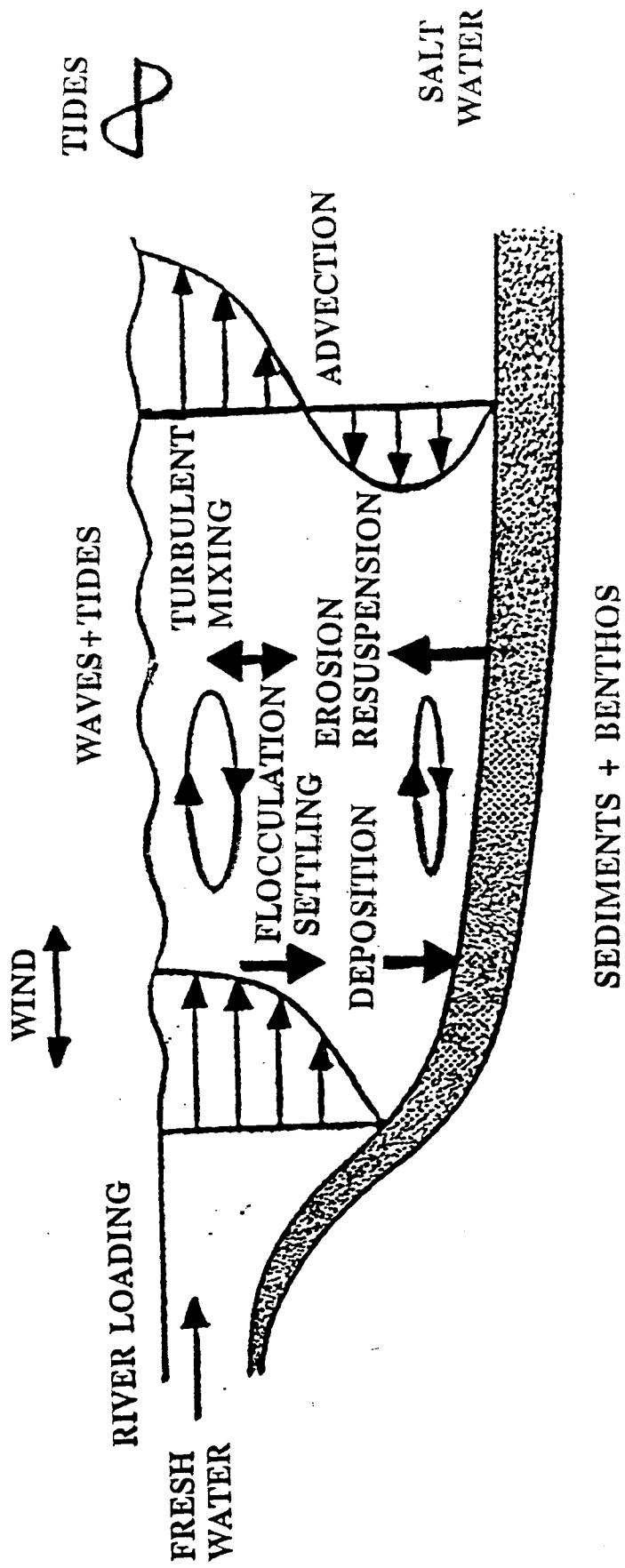
- Salt-wedge (river-flow dominant)
- Two-layer, entraining (river-flow dominant modified by tidal currents)
- Two-layer with vertical mixing (river flow and tidal mixing)
- Vertically homogeneous
 - with lateral variation
 - laterally homogeneous

Identify key processes in conceptual model:

- Time-dependent transport of fresh and salt water, dissolved contaminants, sediments, contaminants sorbed onto sediments
- Advection, dispersion, and diffusion due to tidal forcing, wind-forcing, river inflow
- Ice formation and breakup, ice damming of flow, ice-incorporation of sediment and contaminant

Scenarios to evaluate:

- Wind mixing and denevilation
- Brine rejection effects on stratification during ice season
- Degree of homogeneity during freshet



SEDIMENT TRANSPORT PROCESSES

Description of the Yenisei Estuary

Primary dynamic influences: river runoff, wind, tides, ice

360 km long, 35-100 km wide

Inflow: 20,000 m³ s⁻¹ average
8,000 m³ s⁻¹ low
80,000 m³ s⁻¹ high

Primarily semidiurnal tides

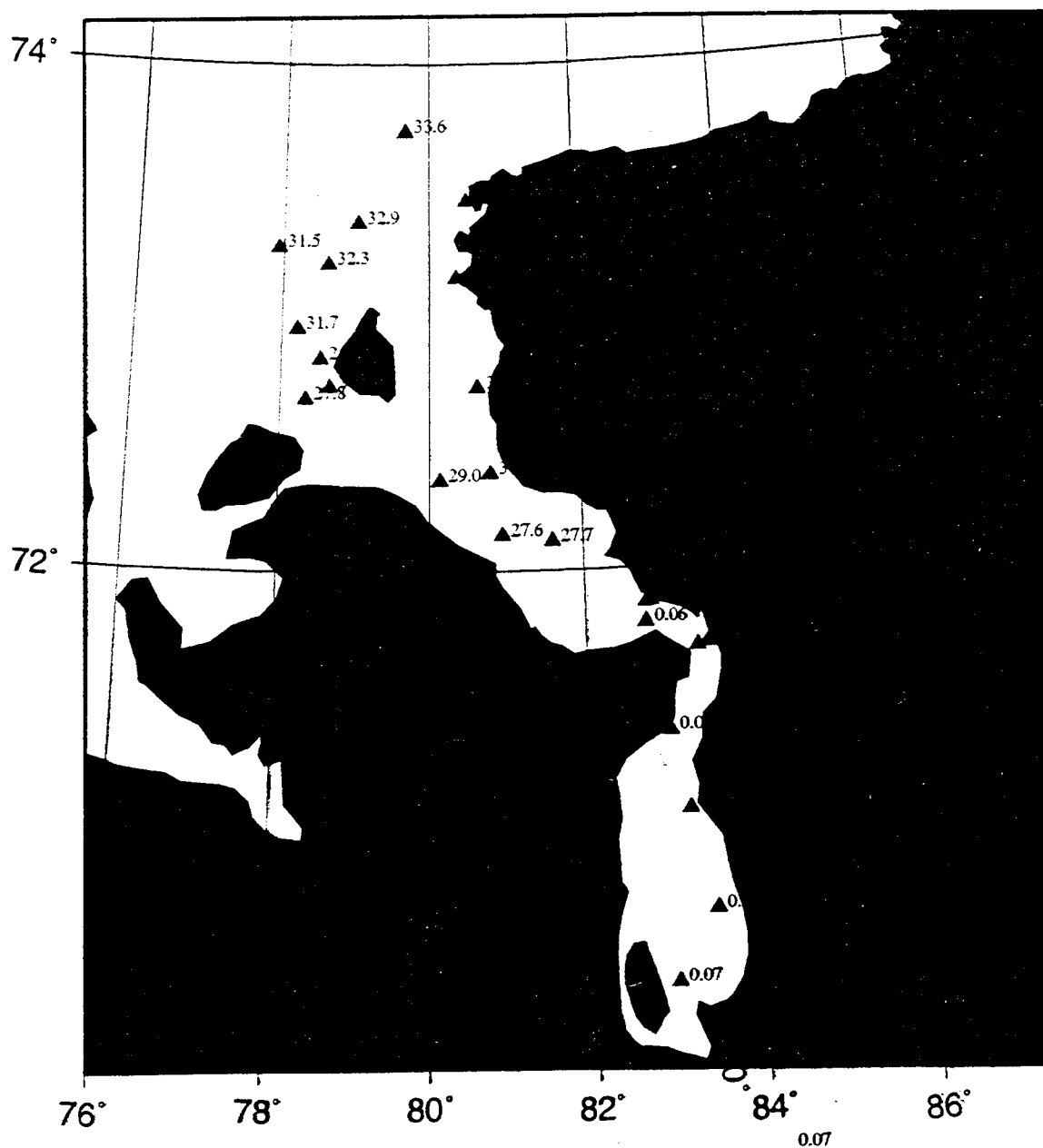
Flow: is dominated by river discharge with local currents up to 50 cm s⁻¹ northward;

Wind-driven "pile-ups" influence the head of the estuary with sea-level elevations of up to 6.0 m during minimum discharge and strong fall winds 15-20 m s⁻¹; related currents up to 8 cm s⁻¹; long-wave propagation noted.

Mixing Regime: the Yenisei estuary is stratified near the mouth. The extent of the salt wedge is not well documented

Longitudinal/Latitudinal Variations: No indications of latitudinal variations; indications are that in the shallower portions of the estuary the waters are more well-mixed and homogenous.

Bottom Salinity, August 1993



Data Courtesy of J. Brooks, GERG

Bottom Salinity, August 1993



Data Courtesy of J. Brooks, GERG

Description of the Ob Estuary

Primary dynamic influences: river runoff, wind, tides, ice

800 km long, 60-100 km wide

Inflow: 530.5 km³ yr⁻¹ (16,800 m³ s⁻¹) average
404.0 km³ yr⁻¹ (12,800 m³ s⁻¹) low
662.0 km³ yr⁻¹ (21,000 m³ s⁻¹) high

Volume of Ob is 450 km³; waters renewed completely during the year

Primarily semidiurnal tides; max amplitude 1.85 m at mouth decreasing to 0.30 m at head

Flow: is dominated by river discharge with local currents up to 50 cm s⁻¹ northward during freshet and < 2 cm s⁻¹ during minimum discharge;

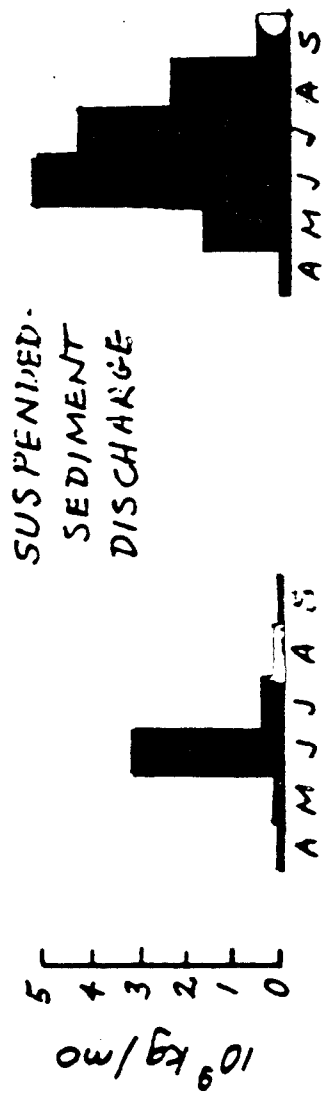
Wind-driven "pile-ups" influence the head of the estuary with sea-level elevations of up to 4.0 m during minimum discharge and strong fall winds

Mixing Regime: the Ob estuary is well mixed (homogenous from the head to 71 N) and somewhat stratified near the mouth. The extent of the salt wedge is not well documented

Longitudinal/Latitudinal Variations: Indications are that the freshwater flow is right-bounded along the estuary and tends right upon reaching the confluence region.

Yenisey R.
at Igarka

Ob R.
at Salekhard



Mean values for 1960-80.
Preliminary data provided by Nelly Bobrovitskaya,
SHI, 16 June 1994

Hierarchy of Estuarine Models

Box Model: Officer (1980a,b) Officer and Kester (1991)

- Attributes:
- Data requirement matches availability
 - Includes sediment transport
 - Inclusion of ice possible (Hamblin, 1989)
 - Will reveal basic patterns of distribution

- Detractions:
- Assumes steady state
 - Assumes tidal mixing $<$ horiz. net circ.
ie. gravitational processes are dominant
 - Will not reveal new information about the estuarine processes

2-D Numerical Models: Bowden and Hamilton (1975), Oey et al. (1985), Festa and Hansen (1976),
RMA2-RMA4(ACOE)

- Attributes:
- Reveals more complex interactions in estuarine circulation
 - Will reveal more information about circulation processes
 - Computational efficiency
 - More responsive to complex physical forcing

- Detractions:
- Requires more data (N_z , R_i , U , V)
 - More complexity in including sediment dynamics (except RMA4)
 - More complexity in including ice

*Box model solution of Festa and Hansen (1978) has been compared with box model of Officer(1980)

Preliminary Assessment of Radioactive Contaminant Transports from Catastrophic Release Scenarios in the Ob and Yenisei River Systems

Lyle Hibler

Preliminary Assessment of Radioactive Contaminant Transport from Catastrophic Release Scenarios in the Ob and Yenisei River Systems

L. F. Hibler
Battelle/MSL
1529 W. Sequim Bay Road
Sequim, Washington 98382
(206) 881-3642
e-mail: lf_hibler@ccmail.pnl.gov

M. C. Richmond
Battelle
Richland, WA 99352
(206) 376-8319

There are significant inventories of radioactive waste stored in the Ob and Yenisei watersheds of the Siberian Arctic. The purpose of this study was to provide a defensible means of estimating the contamination that would reach the Kara Sea under a catastrophic release scenario from three sites (Krasnoyarsk, Tomsk, and Mayak). A dynamic, one-dimensional sediment/contaminant transport model was used to study the transport of Cs-137 under a variety of flow conditions. Analysis of the sediment/contaminant transport algorithms showed that the interaction of key parameters (critical shear stress, erodibility, and partitioning and rate constants) had a pronounced effect on the calculated contaminant transport. A suite of sensitivity studies was performed to determine acceptable ranges for these parameters, and these ranges were compared with those from similar analyses of other river systems. This transport analysis provided contaminant boundary conditions for the complementary studies of the estuarine and shelf contaminant transport.

This research was supported by the Office of Naval Research under Contract 25110.

Ob and Yenisei River Modeling Study

Study Goals:

Estimate the Fate and Behavior of Radioactive Contamination Released from Krasnoyarsk(Yenisei), Mayak and Tomsk (Ob)

Provide Estimated Boundary Conditions for an Estuarine Model

Approach:

Use One-Dimensional Dynamic Models as Tools for Objective Characterization of Sediment and Contaminant Transport within the Ob and Yenisei Rivers

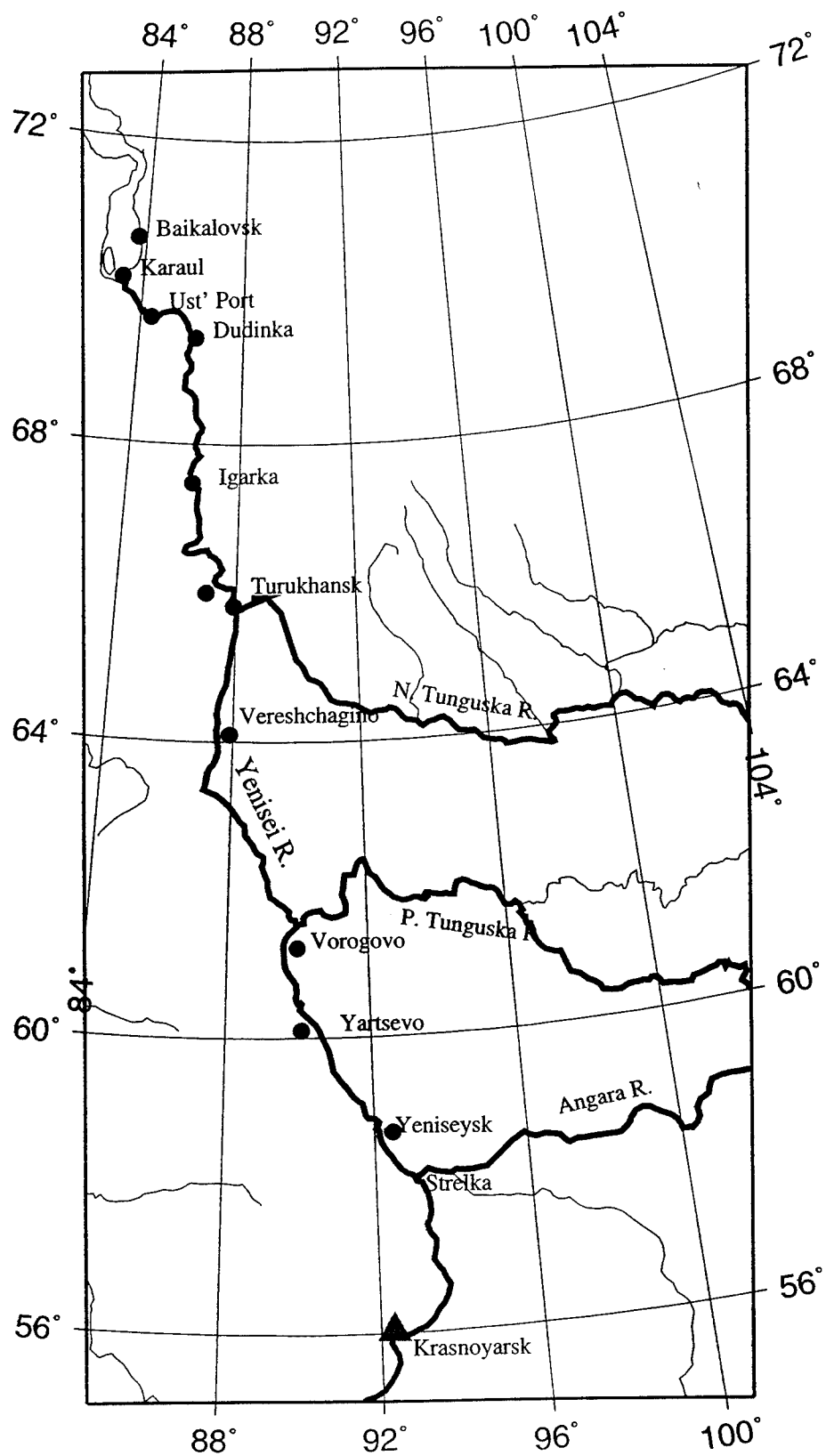
Status:

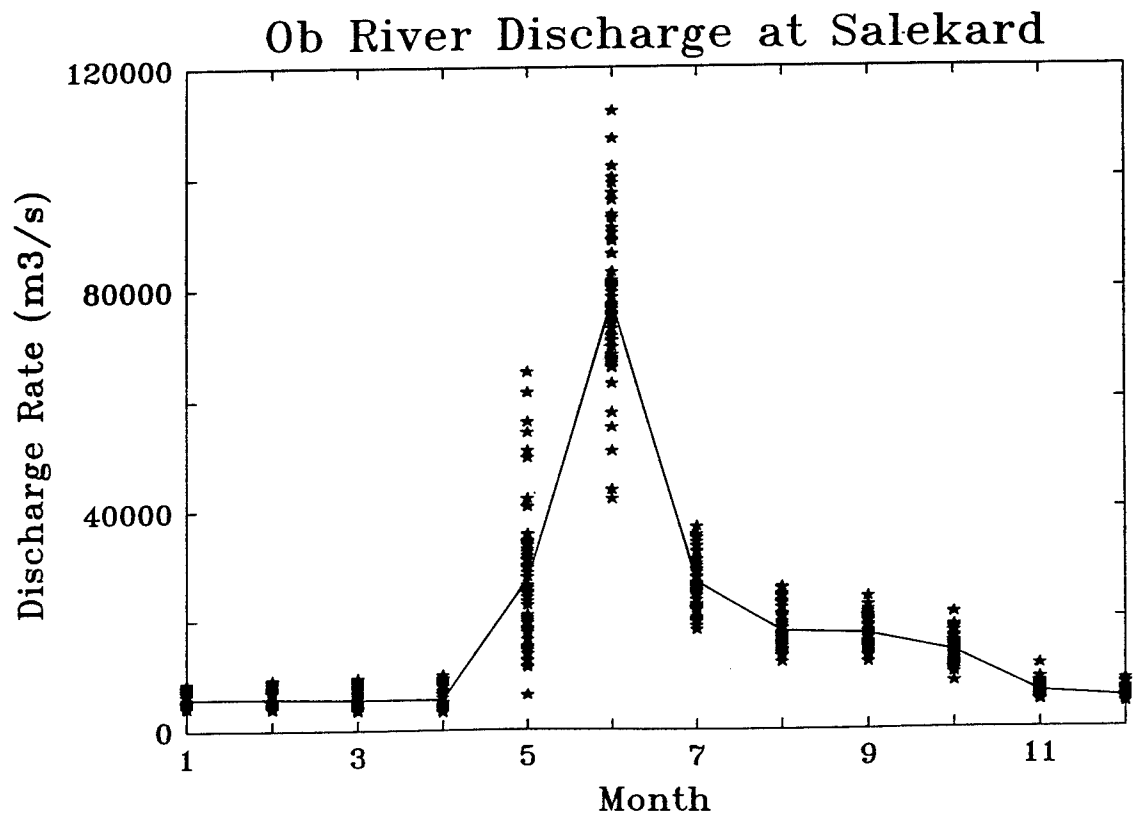
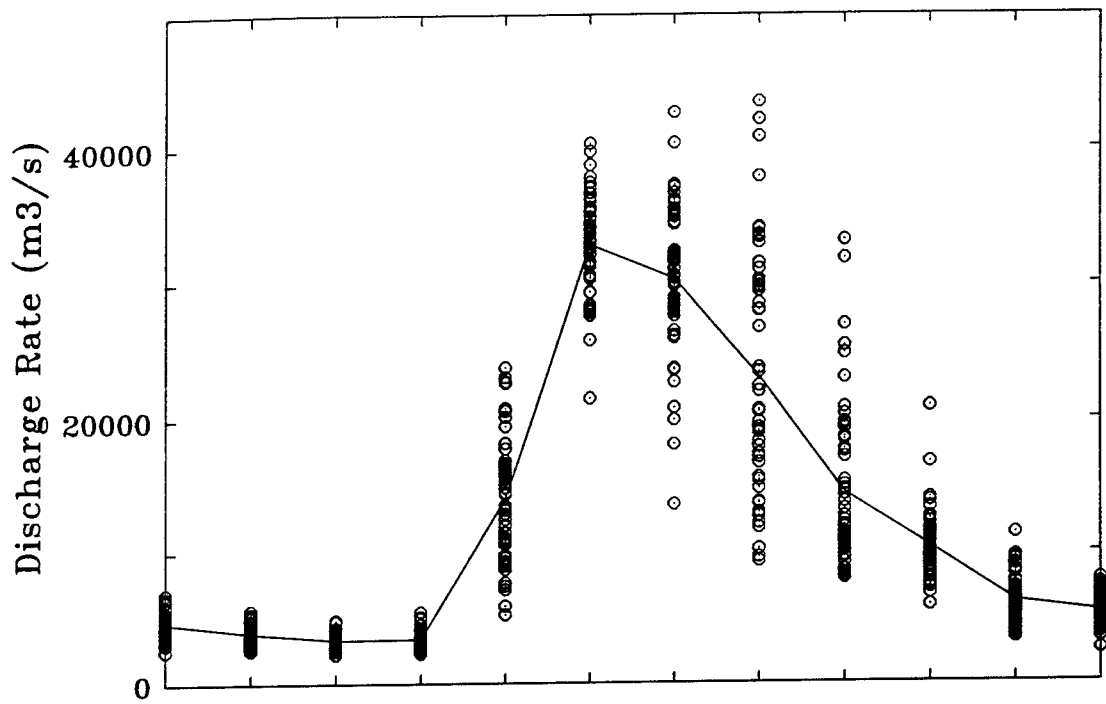
Performing Sensitivity Studies on the Yenisei River Application

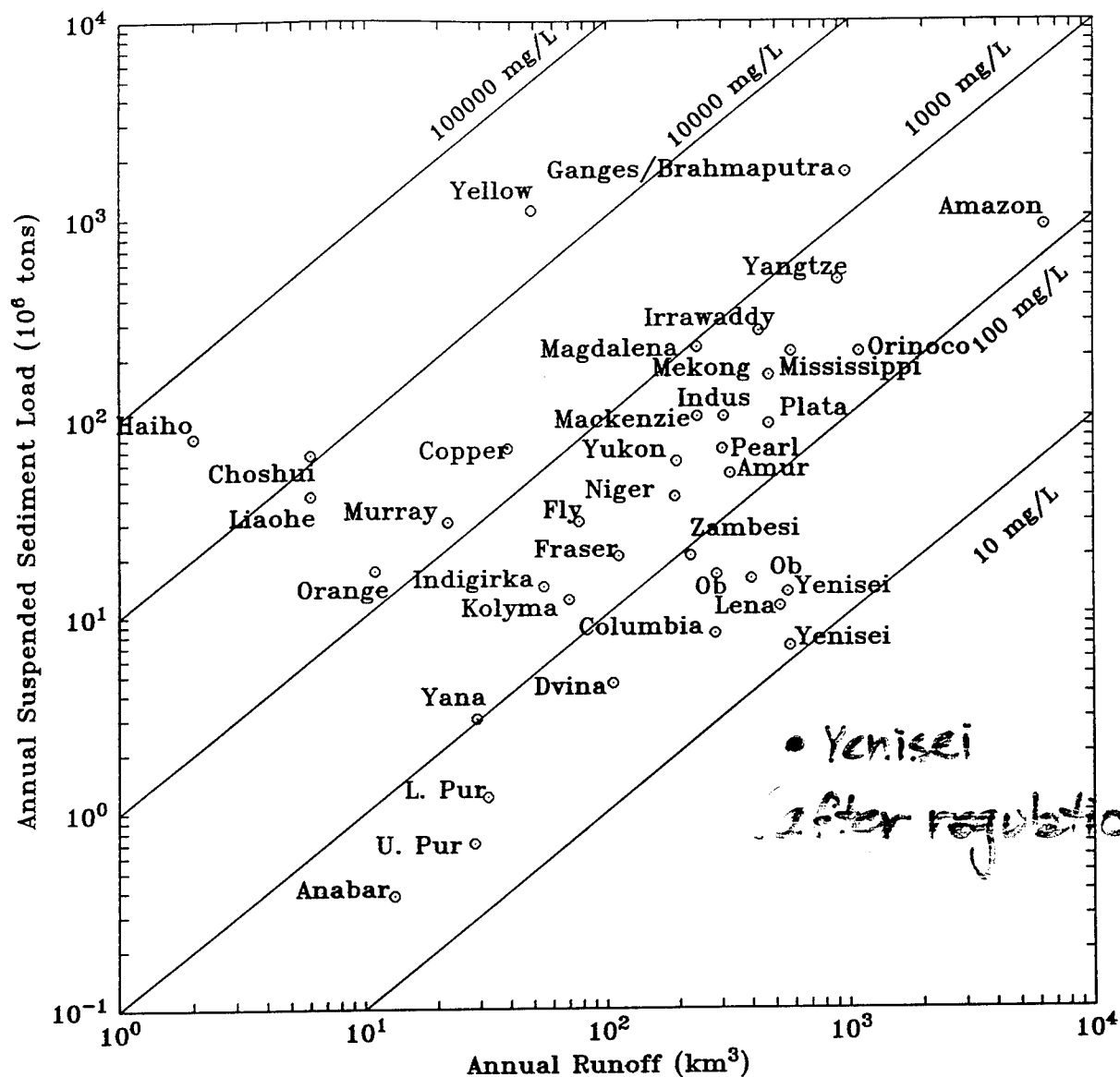
Configuring similar study for the Techa-Iset-Tobol-Irtysh-Tom-Ob Application

Future Work:

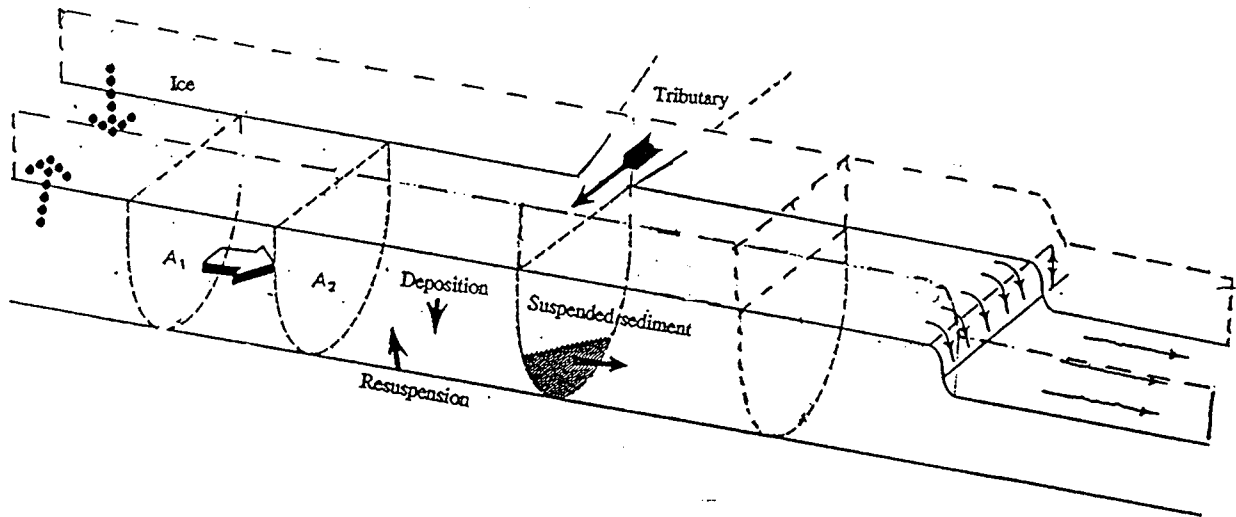
Use of CHARIMA Model for linked Hydrodynamic and Transport Modeling





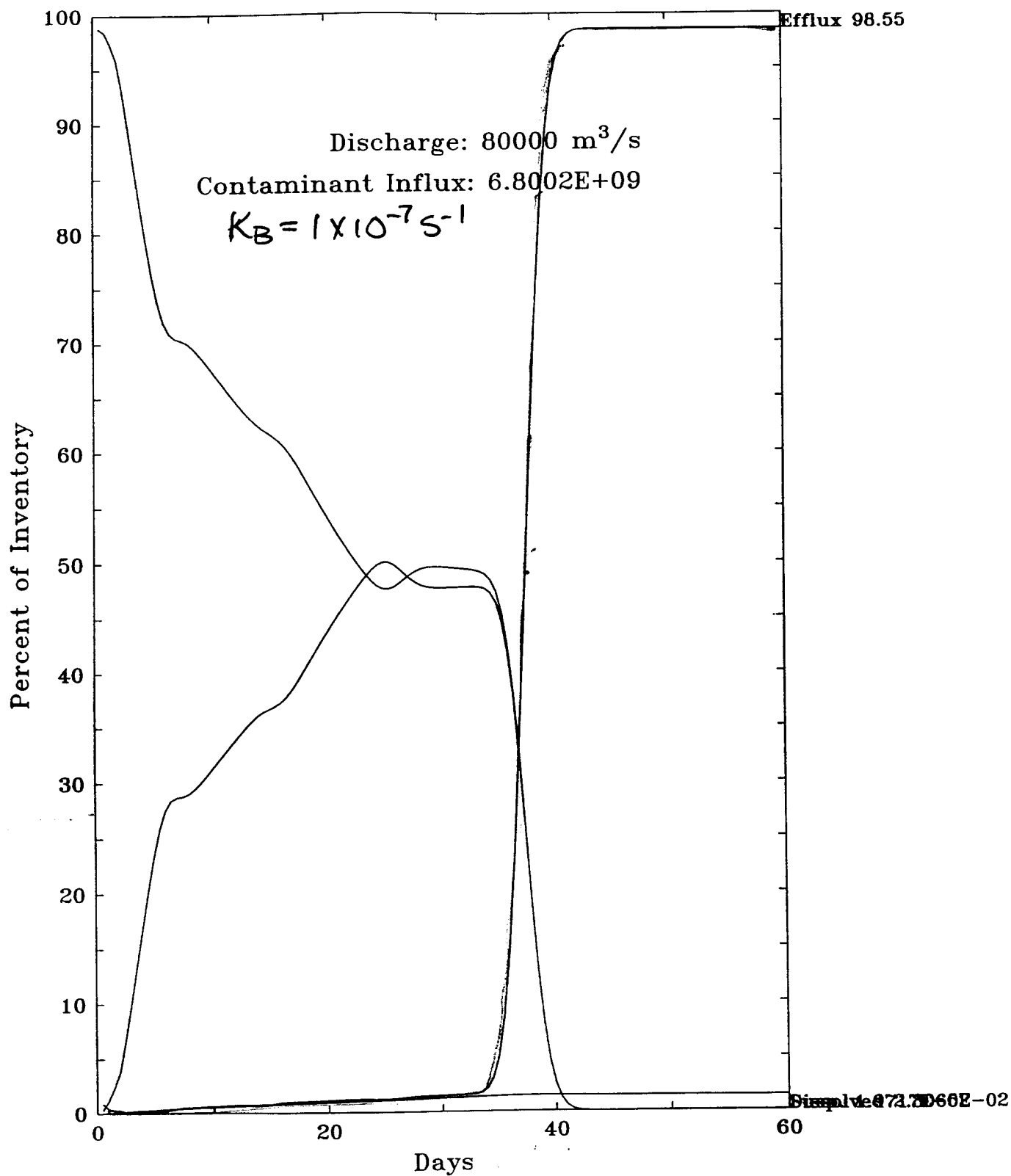


(Milliman & Meade, 1983)

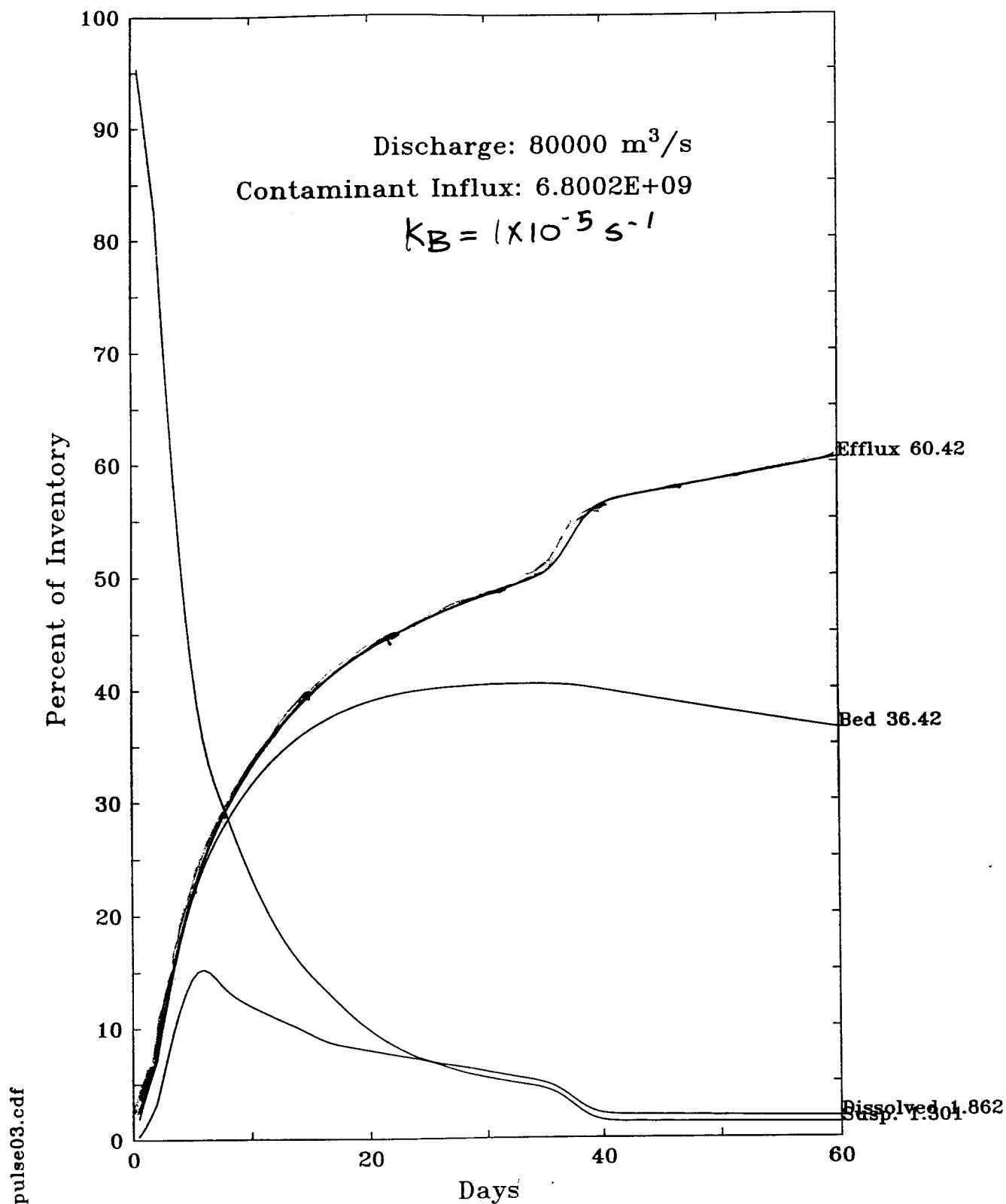


Conceptual Model for Riverine System

pulse02.cdf



Contaminant Inventory Distribution



Contaminant Inventory Distribution

Modeled Contaminant and Sediment Process:

Sediment Transport:

[Time rate of change in Suspended Sediment Concentration] +
[Advection] = [Dispersion] + [Sources] + [Erosion] + [Deposition]

$$A \frac{\partial S}{\partial t} + UA \frac{\partial S}{\partial x} = \frac{\partial}{\partial x} \left(\epsilon A \frac{\partial S}{\partial x} \right) - Q_l S + B (S_r - S_d)$$

Dissolved Contaminant Transport:

[Time Rate of change in Dissolved Contaminant Concentration] =
[Advection] = [Dispersion] - [Decay] + [Sources] -
[Sorbed Phase Exchange From Suspended Sediment] -
[Sorbed Phase Exchange From Bed Sediment]

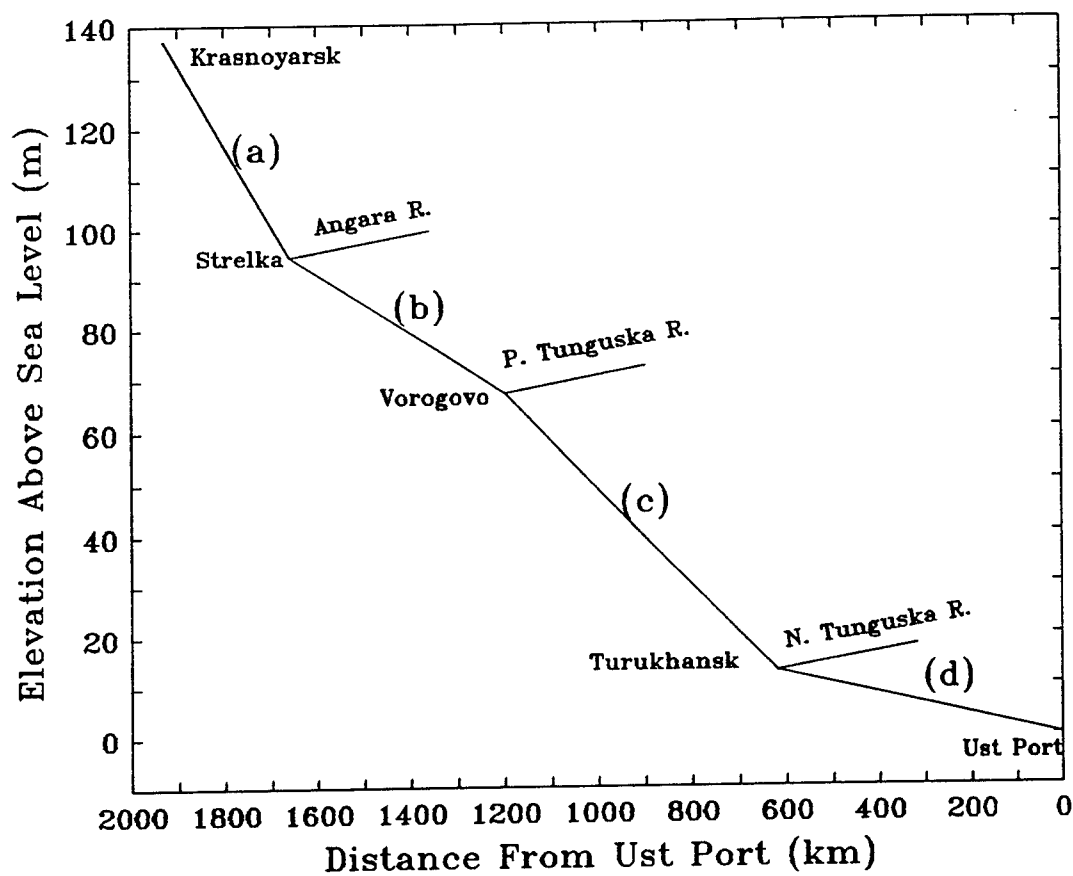
$$A \frac{\partial C}{\partial t} + UA \frac{\partial C}{\partial x} = \frac{\partial}{\partial x} \left(\epsilon A \frac{\partial C}{\partial x} \right) - \lambda AC \\ - Q_l C - AK (K_d SC - G) - BY (1 - \eta) \frac{dK_b}{dt} (K_d C - G_b)$$

Sediment-Sorbed Contaminant Transport:

[Time Rate of Change in Sediment Sorbed Contaminant Concentration] =
[Advection] =
[Dispersion] - [Decay] + [Sources] + [Erosion] - [Deposition] +
[Dissolved Phase Exchange]

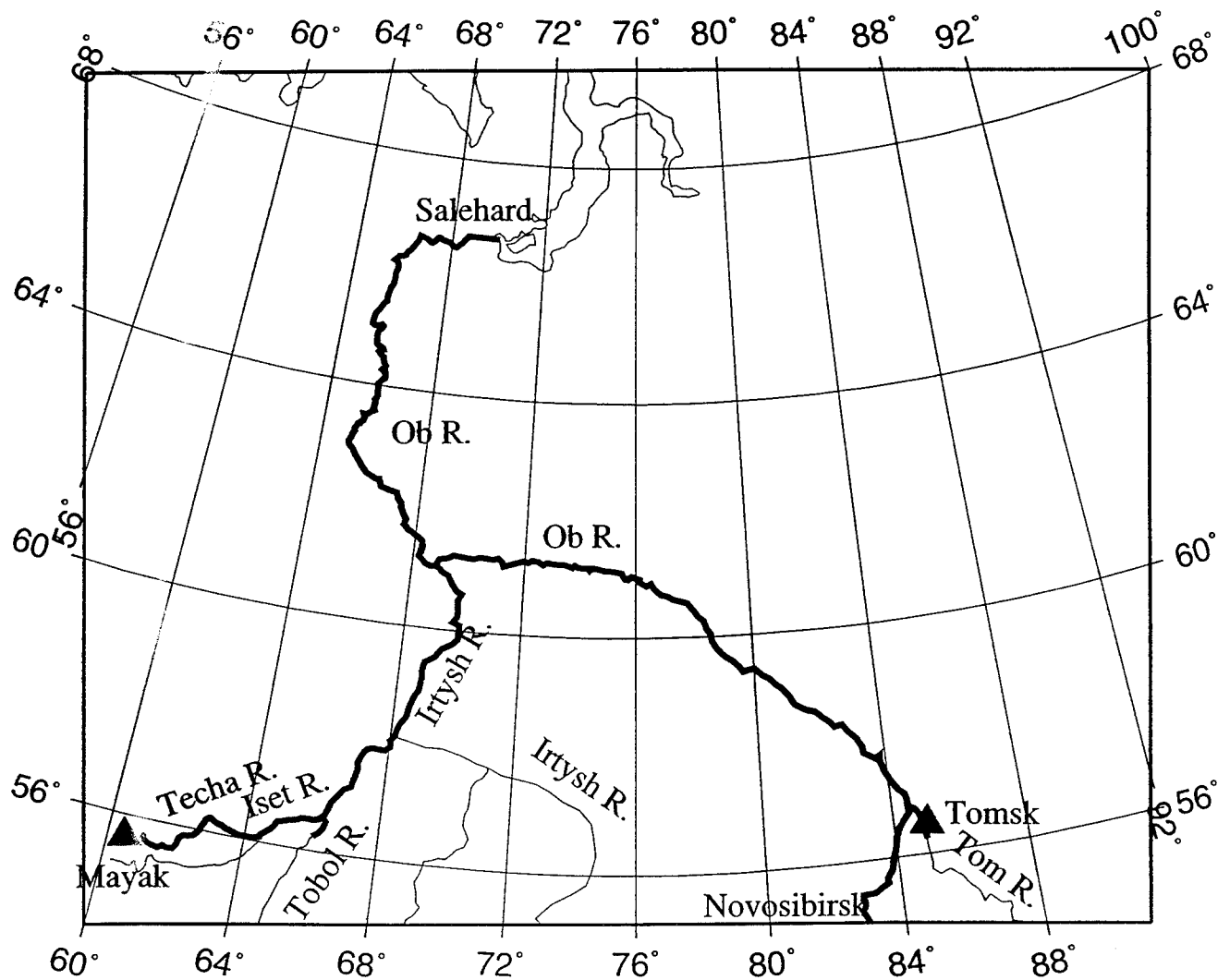
$$A \frac{\partial G}{\partial t} + UA \frac{\partial G}{\partial x} = \frac{\partial}{\partial x} \left(\epsilon A \frac{\partial G}{\partial x} \right) - \lambda AG \\ - Q_l G + B \left(G_b S_r - \frac{S_d G}{C} \right) + AK (K_d SC - G)$$

Summer (High Flow) Hydrology:



Reach	(a)	(b)	(c)	(d)
Length (km)	270	460	580	620
Slope	0.00016	0.00006	0.00009	0.00002
Area (m ²)	64977	93733	106822	130851
Depth (m)	19.3	22.7	24.0	26.3
Vol (km ³)	18	43	62	81
Q (m ³ /s)	39353	57050	65131	80000
U (m/s)	0.61	0.61	0.61	0.61
T (days)	5	9	10	12
τ_b (dynes/cm ²)	303	133	212	53

366



SPOT Image of the Mayak Site



Production
Facilities

Lake Karacha ⑨

Reservoirs

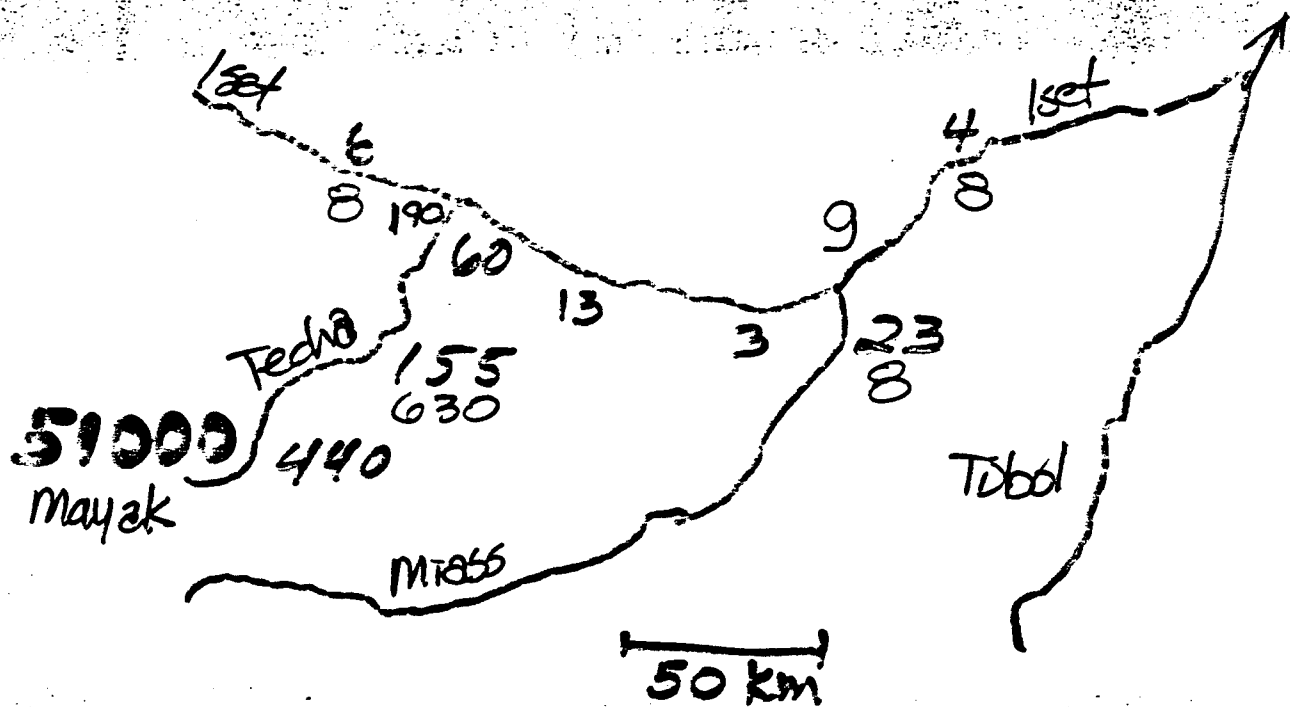
Techa River

② 4440000 ± 100000

⑤ 4440000 ± 100000
4 = 400000 m³

⑩ 4440000 ± 100000

⑪ 4440000 ± 100000



[Cs-137] water Bq/m³ 1990-92
 [Cs-137] bed sediment Bq/kg (dry wt) observations

Trapeznikov

Hydraulic and Radionuclide Transport Model

CHARIMA Model from Univ. of Iowa

Water Continuity Equation

$$\frac{\partial A}{\partial t} + \frac{\partial Q}{\partial x} = 0$$

Momentum Conservation Equation

$$\frac{\partial Q}{\partial t} + \frac{\partial}{\partial x} \left(\frac{Q^2}{A} \right) + gA \frac{\partial y}{\partial x} + gAS_f = 0$$

PNL-CHARIMA

Radionuclide Mass Conservation Equation

$$A \frac{\partial C}{\partial t} + Q \frac{\partial C}{\partial x} = \frac{\partial}{\partial x} \left(AK \frac{\partial C}{\partial x} \right) - \lambda AC + \text{Sediment Interaction}$$

SUMMARY:

- * TODAM. revealed the importance of river system processes & conditions (erosion/depositional zones, contaminant partitioning)
- * Yenisei River is relatively simple providing a good configuration for model testing
- * Ob River is more complex (channel braiding, more tributaries)
- * Future Work
 - time-variant hydrology (CHARIMA)
 - incorporation of more system data
 - more realistic release scenarios (MEPAS)
 - more extensive data comparisons (USGS)

The NRL NORAPS Model

William Thompson

ABSTRACT

A version of the Navy Operational Regional Atmospheric Prediction System (NORAPS) will be used to provide atmospheric forcing to PIPS over the Kara Sea. NORAPS is a hydrostatic primitive equation model with split explicit time differencing and time dependent lateral boundary conditions from NOGAPS. In the analysis and initialization phase, an optimum interpolation scheme is used to blend current observational data with a previous 12 h forecast and an incremental update is used. The physical parameterizations used in this version of the model include a second-order closure turbulence scheme, fully interactive clouds and radiation, and a surface energy budget for snow and ice covered surfaces. The physical parameterizations use implicit time differencing.

For the Kara Sea runs, 20 km horizontal resolution will be used with a domain extending 2100 km E-W by 1600 km N-S. The domain thus extends from the Eastern Barents Sea to the western Laptev Sea and from approximately 75N to 83N.

William T. Thompson
Naval Research Laboratory
Marine Meteorology Division
7 Grace Hopper Ave.
Monterey, CA 94943-5502
(408) 656-4733
(408) 565-4769 (fax)
thompson@nrlmry.navy.mil

COASTAL MESOSCALE DATA ASSIMILATION SYSTEM

ANALYSIS/INITIALIZATION

- Optimum Interpolation Analysis
- Incremental Update
- Nonlinear Vertical Mode Initialization

FORECAST MODEL FEATURES

- High Vertical and Horizontal Resolution
 - 20 km horizontal resolution
 - 30 levels in the vertical; 14 in the lowest 1 km
- Hydrostatic
- Primitive Equation
- Time Dependent Lateral Boundary Conditions from the Global Model (NO-GAPS)
- Split Explicit Time Differencing

MODEL PHYSICS

- Second-Order Closure Turbulence Parameterization

Mellor-Yamada (1974) level 3

- Fully Interactive Cloud-Radiation

Two-Stream Radiative Transfer

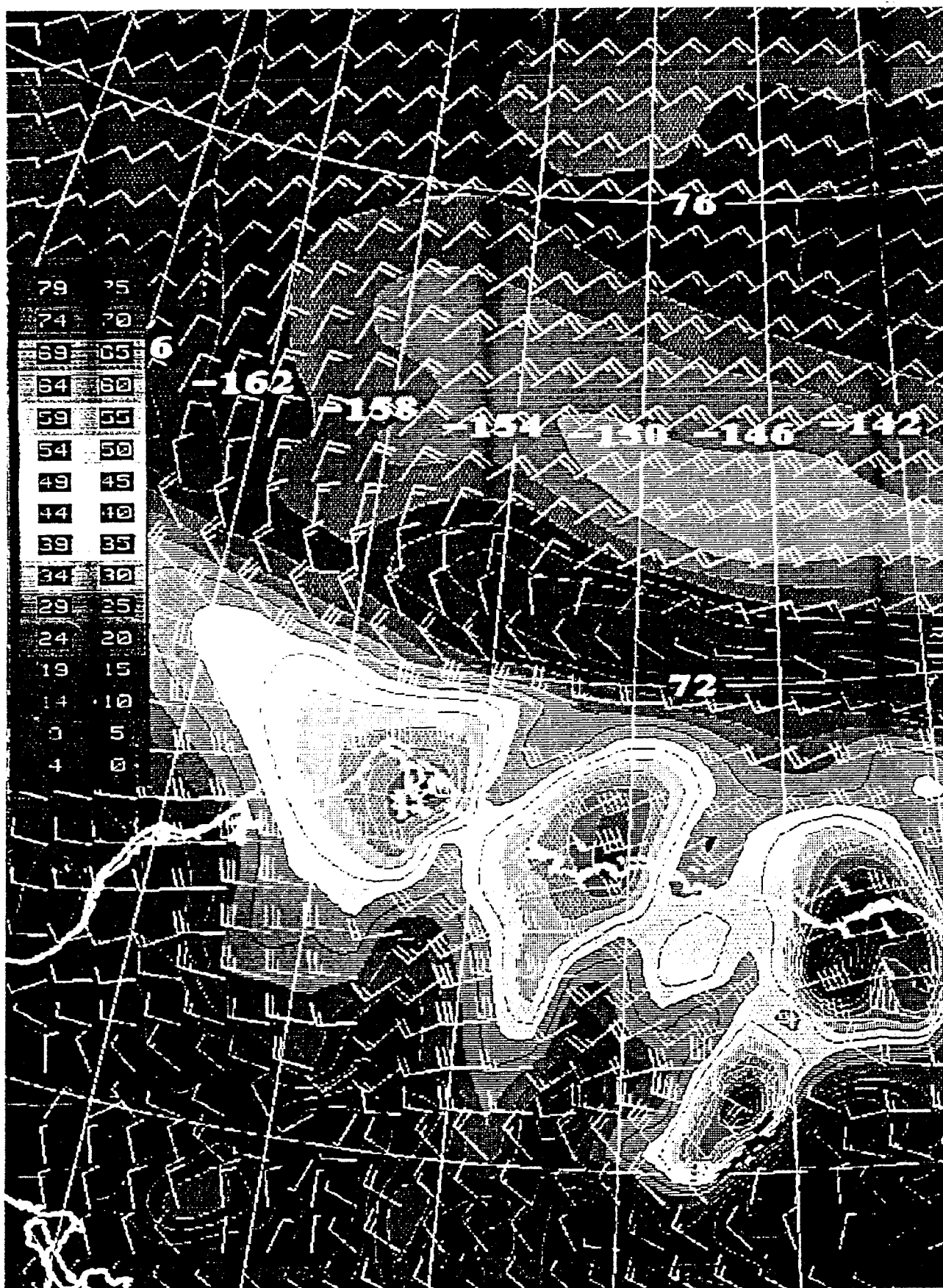
Cloud Parameterization follows Sommeria and Deardorff (1979)

- Surface Layer Parameterization

Loius (1979) over land and sea ice

Liu (1979) over open water

- Implicit Time Differencing for Physics

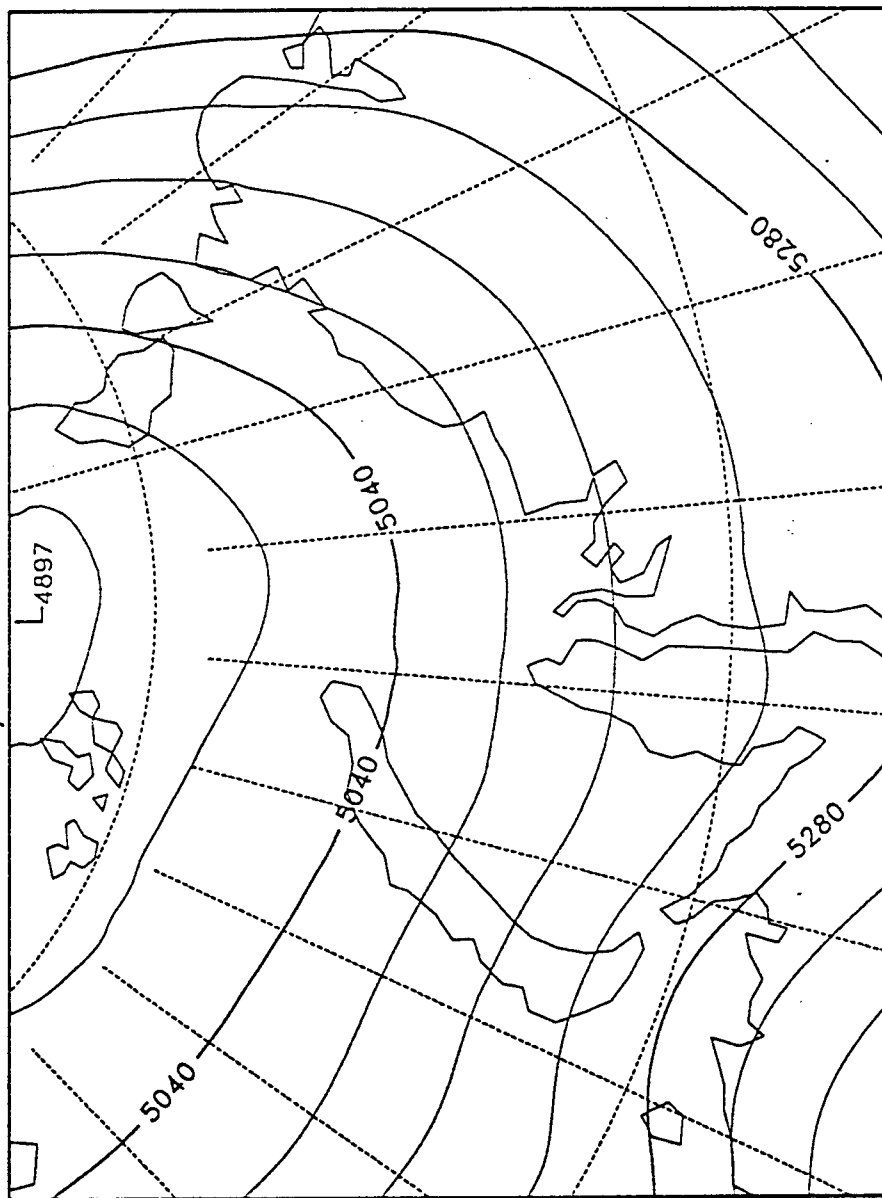


12h Est Wind Stress valid 12Z 6 April 1979.

NORAPS grid 1, 109 x 82 x 36 20.00 km

500.0 mb geop ht

analysis at 1994100700



$10^3 \times 20 = 2100$

$10^3 \times 20 = 1620$

Use of Multi-Channel NOAA AVHRR Data in Studying River Outflow Effects and Ice Thickness Patterns

Robert Fett

ABSTRACT

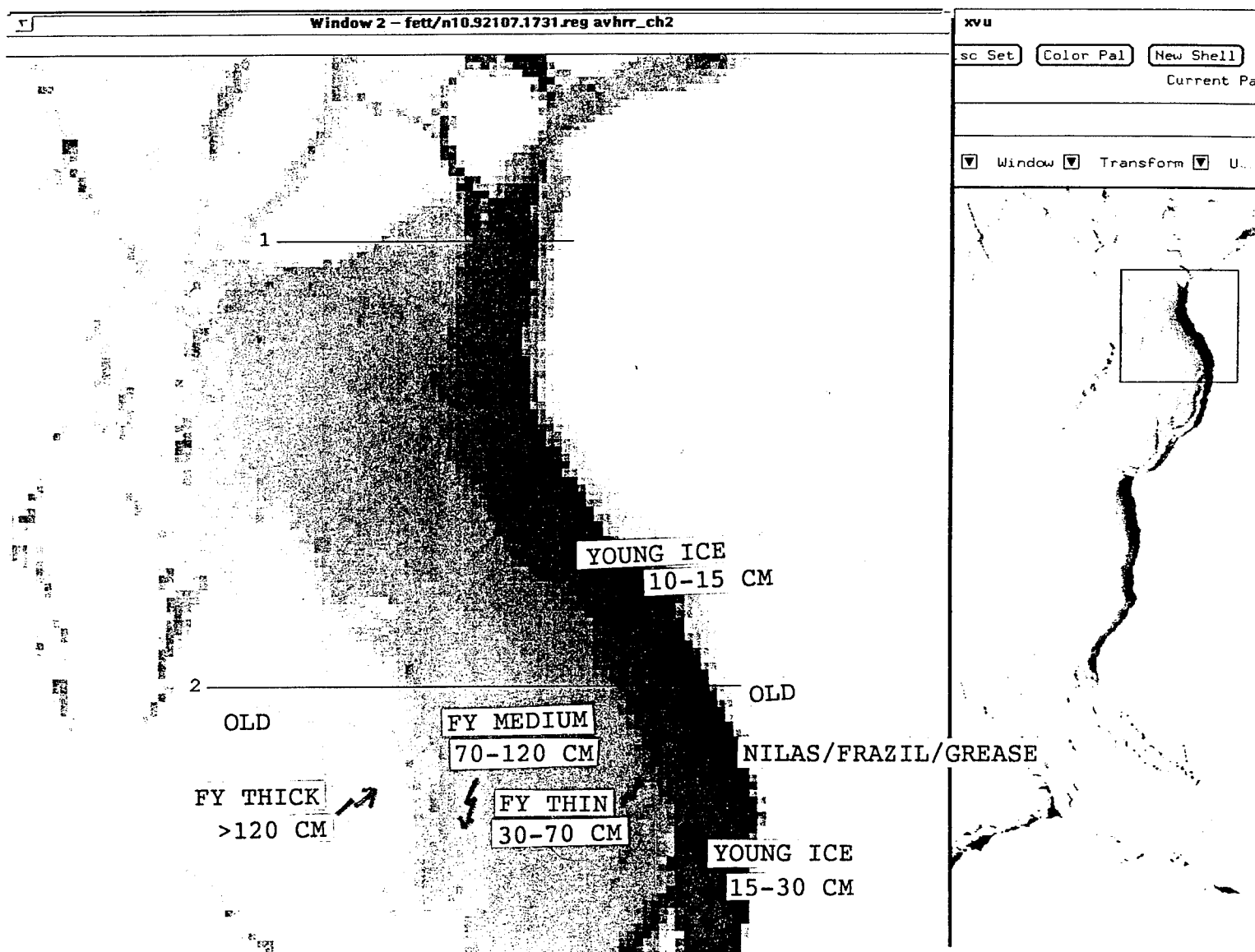
Use of Multi-channel NOAA AVHRR Data in Studying River Outflow Effects and Ice Thickness Patterns

Robert W. Fett
SAIC/Consultant

Characteristic albedo and temperature changes have been used to evaluate ice thickness in NOAA AVHRR data in the Banks Island - Beaufort Sea region. Similar attempts have been made in the past using research aircraft. A "spin-off" from this research using NOAA data in the Mackenzie Bay region revealed an anomalous warm plume extending several hundred kilometers westward along the North Slope of Alaska. This plume is believed to be an outflow effect of the Mackenzie River. Reduced albedo in the plume may be a result of river sediment which has become embedded in the ice and carried westward by the Beaufort anticyclonic gyre. The example suggests that river outflow effects and the effect of anomalous warm spots in the Laptev Sea may also be monitored using these data.

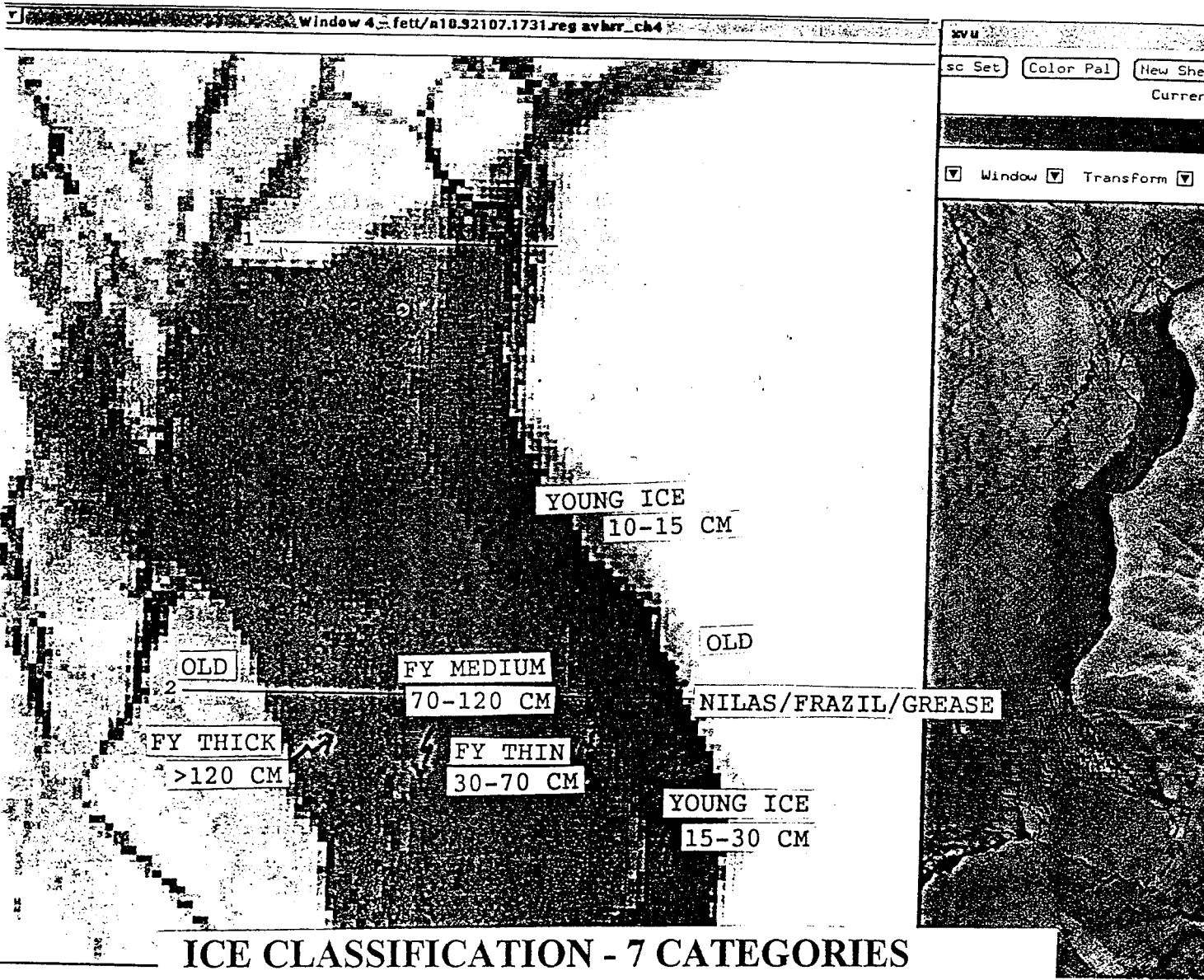
Table 1. Sea ice classification scheme (World Meteorological Organization, 1970).

Ice Type	Thickness	Gray Tone	Features
open water	0 cm	black	
new			
frazil	0 cm	black	unconsolidated
slush	0- 50 cm	very dark gray to gray	unconsolidated
shuga	0- 50 cm	dark gray to gray	unconsolidated
grease	0-100 cm	dark gray to gray	unconsolidated
nilas			
dark nilas	0- 5 cm	very dark gray	rafts
light nilas	5- 10 cm	dark gray to gray	rafts
young			
gray	10- 15 cm	gray to light gray	rafts
gray-white	15- 30 cm	light gray to almost white	rafts or ridges
first-year			
thin	30- 70 cm	white	ridges
medium	70-120 cm	white	ridges
thick	120-200 cm	white	ridges
old			
second-year	200-400 cm	white	ridges
multiyear	200-400 cm	white	ridges, hummocks



ICE CLASSIFICATION - 7 CATEGORIES

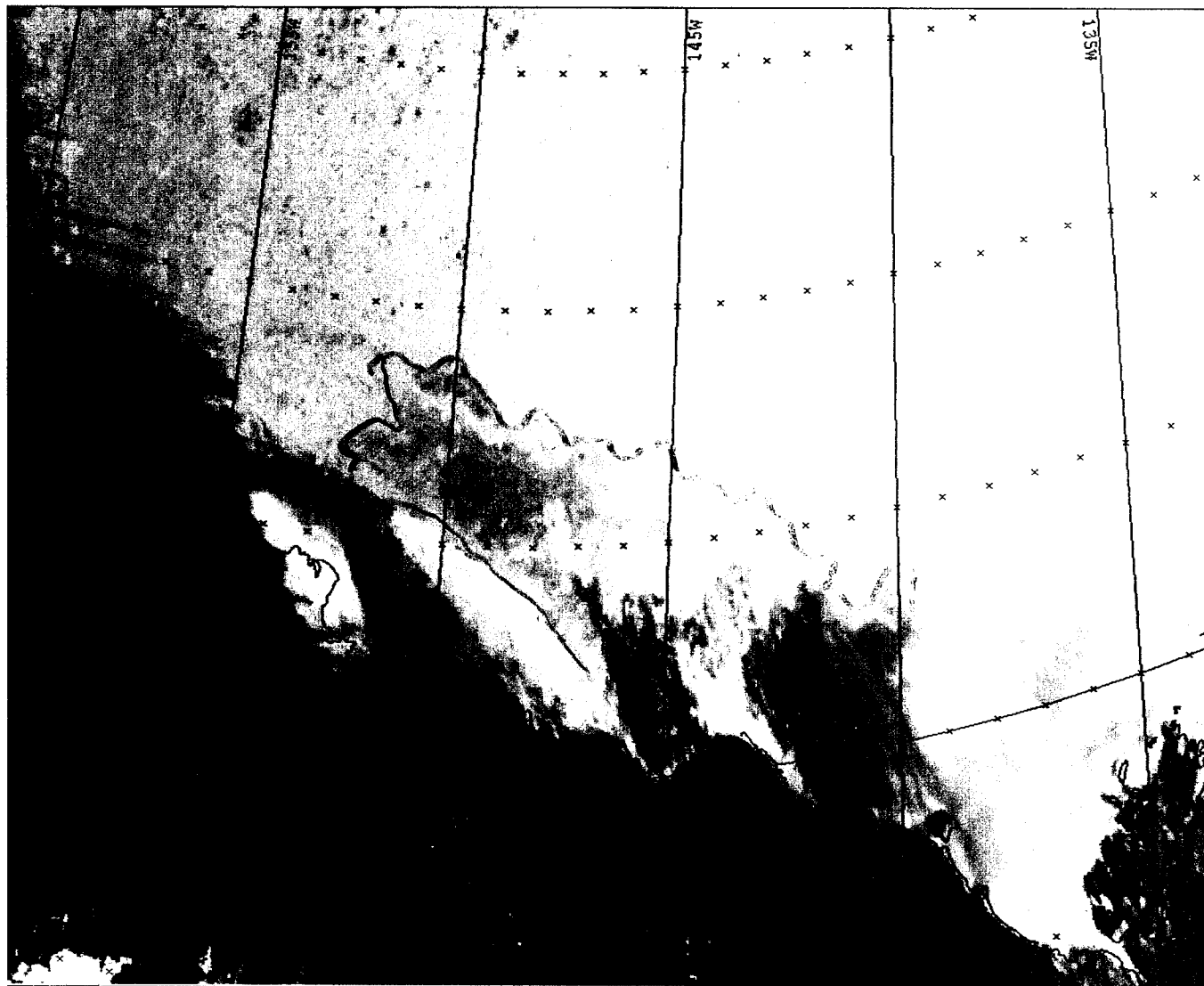
- ① OLD ICE > ONE MELT SEASON
- ② FIRST YEAR THICK ICE >120 CM
- ③ FIRST YEAR MEDIUM ICE 70-120 CM
- ④ FIRST YEAR THIN ICE 30-70 CM
- ⑤ YOUNG ICE GRAY-WHITE 15-30 CM
- ⑥ YOUNG ICE AND LIGHT NILAS 5-15 CM
- ⑦ DARK NILAS/FRAZIL AND GREASE ICE <5 CM



- ① OLD ICE > ONE MELT SEASON
- ② FIRST YEAR THICK ICE >120 CM
- ③ FIRST YEAR MEDIUM ICE 70-120 CM
- ④ FIRST YEAR THIN ICE 30-70 CM
- ⑤ YOUNG ICE GRAY-WHITE 15-30 CM
- ⑥ YOUNG ICE AND LIGHT NILAS 5-15 CM
- ⑦ DARK NILAS/FRAZIL AND GREASE ICE <5 CM

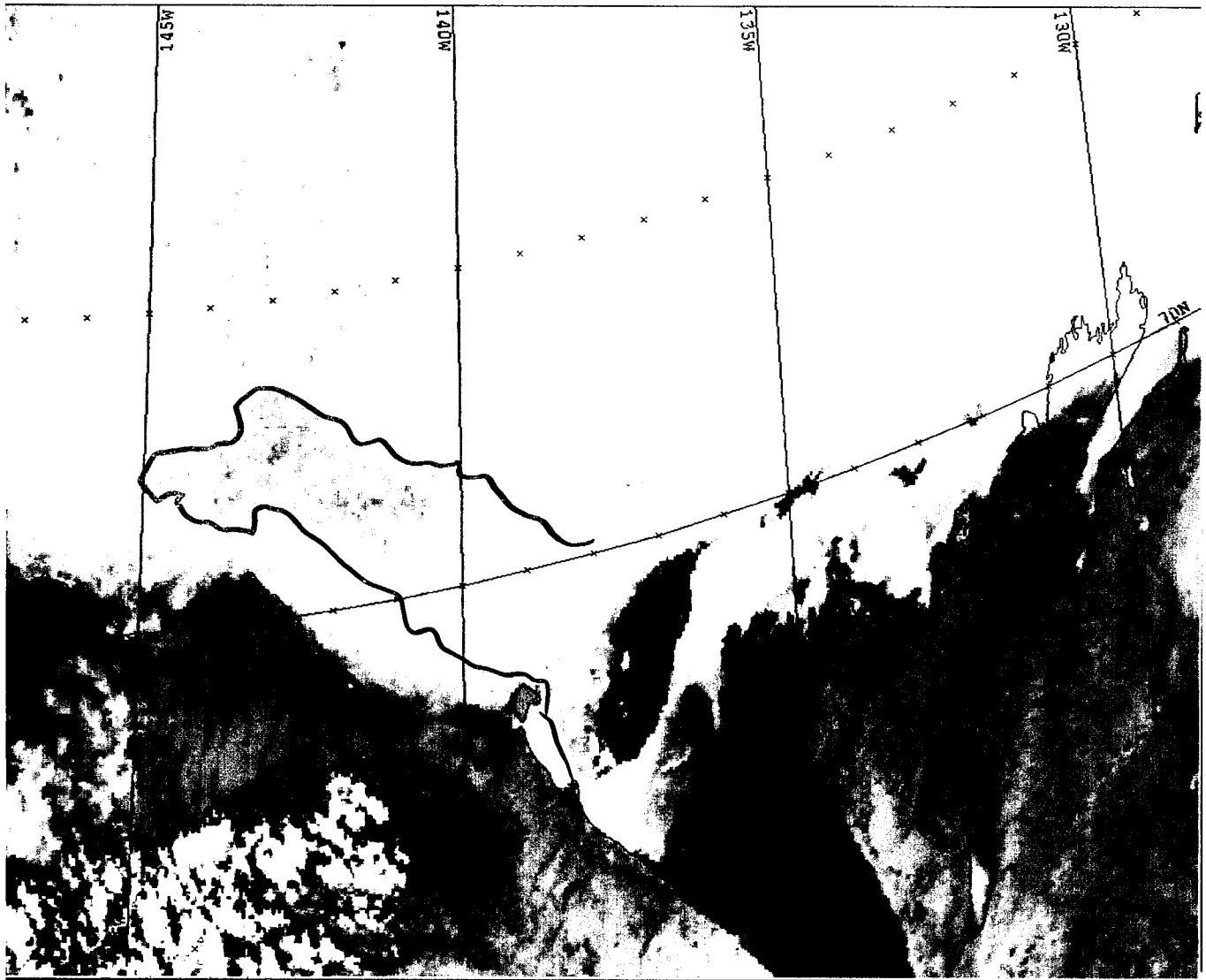
N10.92107.1731 PIXEL CHANNEL 1 DIFFERENCE CHANNEL 2 DIFFERENCE CHANNEL 4 DIFFERENCE

	1	21.88		18.8		-23.73	
	2	21.78	-0.1	18.8	0	-23.73	0
OLD ICE	3	21.78	0	18.69	-0.11	-23.73	0
>ONE MELT	4	21.99	0.21	18.9	0.21	-23.73	0
SEASON	5	21.78	-0.21	18.69	0	-23.58	0.17
	6	21.88	0.1	18.69	0	-23.73	-0.17
	7	21.88	0	18.8	0.11	-23.58	0.17
	8	21.99	0.11	18.8	0	-23.73	-0.17
	9	21.88	-0.11	18.8	0	-24.22	-0.49
TRANSITION	10	21.25	-0.63	18.27	-0.53	-23.07	1.15
	11	21.51	0.26	17.74	-0.53	-19.7	3.37
	12	20.72	-0.79	18.06	0.32	-19.7	0
FIRST YEAR	13	20.51	-0.21	17.74	-0.32	-19.23	0.47
THICK ICE	14	20.3	-0.21	17.63	-0.11	-19.23	0
> 120 CM	15	20.19	-0.11	17.26	-0.37	-18.77	0.46
	16	20.29	0.1	17.63	0.37	-18.92	-0.15
	17	20.19	-0.1	17.42	-0.21	-18.77	0.15
	18	20.19	0	17.42	0	-18.61	0.16
	19	20.08	-0.11	17.53	0.11	-18.61	0
	20	20.08	0	17.42	-0.11	-18.77	-0.16
	21	19.98	-0.1	17.31	-0.11	-18.77	0
	22	19.87	-0.11	17.21	-0.1	-18.61	0.16
	23	19.77	-0.1	17.21	0	-18.46	0.15
TRANSITION	24	18.91	-0.86	16.57	-0.64	-17.84	0.62
	25	18.81	-0.1	16.47	-0.1	-17.69	0.15
	26	17.75	-1.06	15.3	-1.17	-16.77	0.92
FIRST YEAR	27	18.28	0.53	15.72	0.42	-17.23	-0.46
MEDIUM ICE	28	18.28	0	15.61	-0.11	-17.08	0.15
70-120 CM	29	18.07	-0.21	15.51	-0.1	-16.93	0.15
	30	17.97	-0.1	15.4	-0.11	-16.93	0
	31	17.97	0	15.3	-0.1	-16.93	0
	32	17.86	-0.11	15.3	0	-16.93	0
	33	17.75	-0.11	15.3	0	-16.93	0
TRANSITION	34	17.54	-0.21	14.98	-0.32	-16.62	0.31
	35	17.65	0.11	15.09	0.11	-16.77	-0.15
	36	17.65	0	15.09	0	-16.77	0
FIRST YEAR	37	17.75	0.1	15.09	0	-16.77	0
THIN ICE	38	17.64	-0.11	14.78	-0.33	-15.42	1.35
30-70 CM	39	17.43	-0.21	14.66	-0.1	-16.62	-1.2
	40	17.54	0.11	14.34	-0.32	-16.77	-0.15
	41	17.11	-0.43	14.24	-0.1	-16.62	0.15
	42	17.01	-0.1	14.34	0.1	-16.62	0
	43	16.91	-0.1	14.23	-0.11	-16.67	-0.05
TRANSITION	44	16.91	0	14.02	-0.21	-16.62	0.05
	45	16.8	-0.11	13.92	-0.1	-16.47	0.15
YOUNG ICE	46	16.8	0	13.92	0	-16.47	0
GRAY-WHITE	47	16.27	-0.53	13.81	-0.11	-16.32	0.15
15-30 CM	48	16.27	0	13.6	-0.21	-16.32	0
	49	15.95	-0.32	12.75	-0.85	-16.32	0
TRANSITION	50	15.32	-0.63	11.27	-1.48	-15.42	0.9
YOUNG ICE AND	51	14.05	-1.27	11.27	0	-14.54	0.88
LIGHT NILAS	52	13.73	-0.32	11.27	0	-14.54	0
5-10 CM	53	13.62	-0.11	11.27	0	-14.68	-0.14
	54	13.41	-0.21	11.06	-0.21	-14.68	0
	55	13.31	-0.1	10.95	-0.11	-14.68	0
	56	13.31	-0.1	10.95	-0.11	-14.68	0
	57	12.46	-0.85	10.42	-0.53	-14.68	0
	58	12.25	-0.21	10.31	-0.11	-14.54	0.14
	59	12.04	-0.21	10.21	-0.1	-14.39	0.15
TRANSITION	60	11.72	-0.32	9.89	-0.32	-14.09	0.3
DK NILAS/FRAZIL	61	10.34	-1.38	8.72	-1.17	-12.21	1.88
GREASE ICE	62	9.81	-0.53	8.19	-0.53	-10.65	1.56
TRANSITION	63	15.32	5.51	12.43	4.24	-16.93	-6.28
	64	17.12	1.8	14.03	1.6	-19.08	-2.15
OLD ICE	65	19.45	2.33	16.78	2.75	-21.29	-2.21

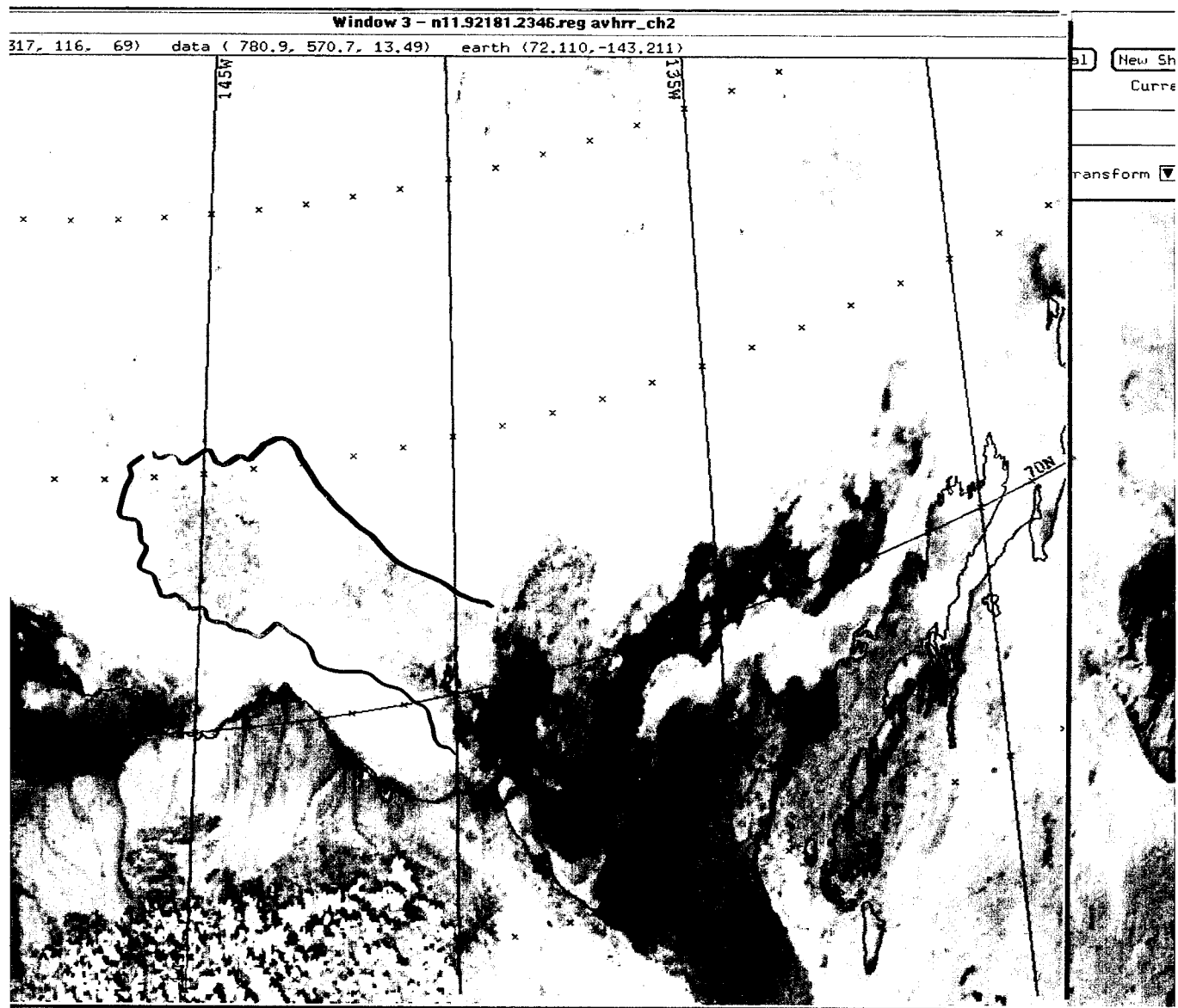


7 JULY 92

Window 5 - n11.92173.2341.reg avhrr_ch2



21 JUN 92

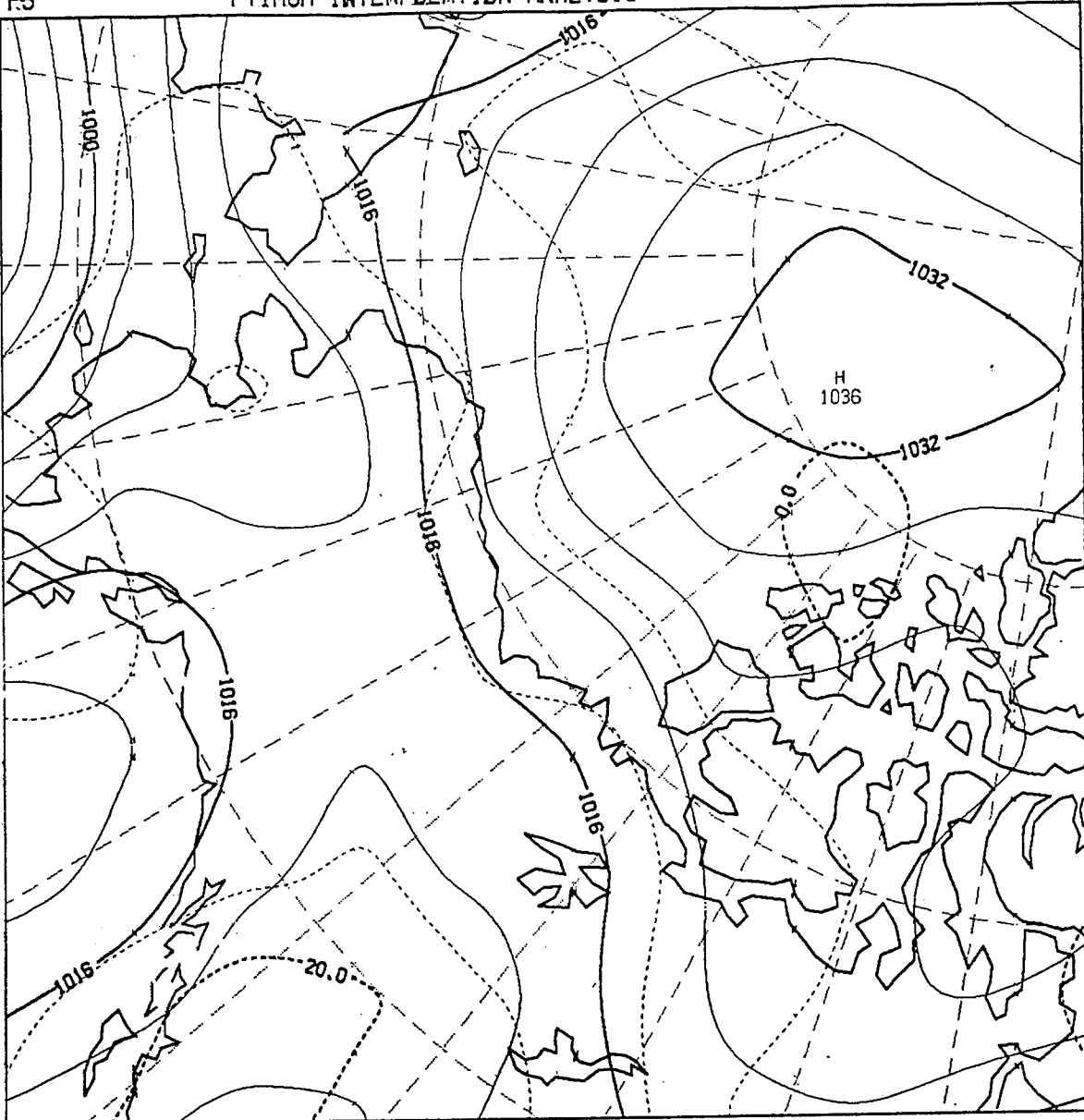


29 JUN 92

T 1000
P5

URE AT 1000 MBS-N0CAPS.T79-L18
PTIMUM INTERPOLATION ANALYSIS

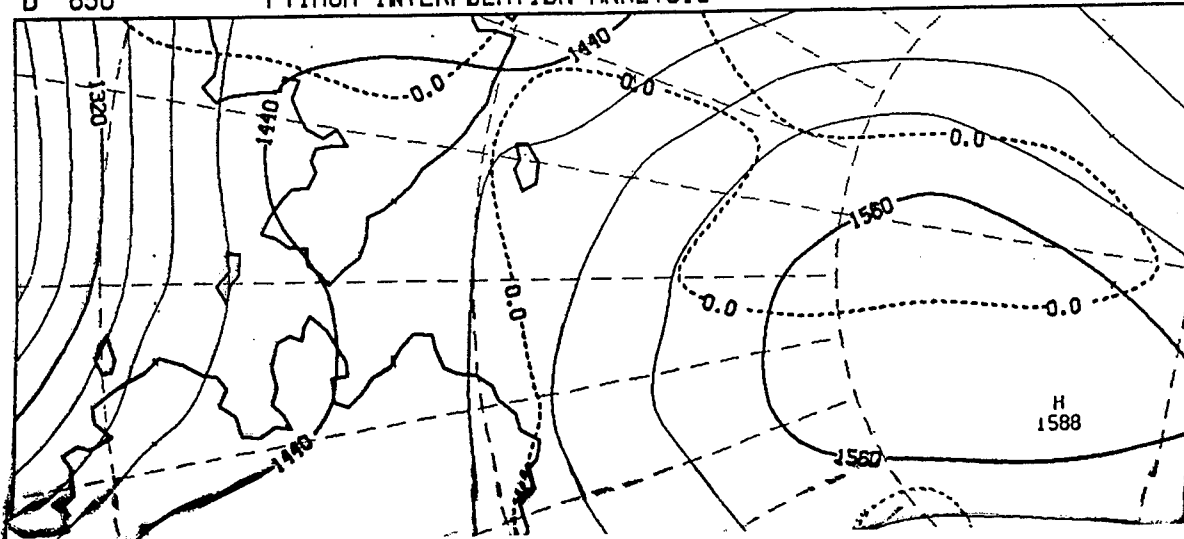
26 JUN 92



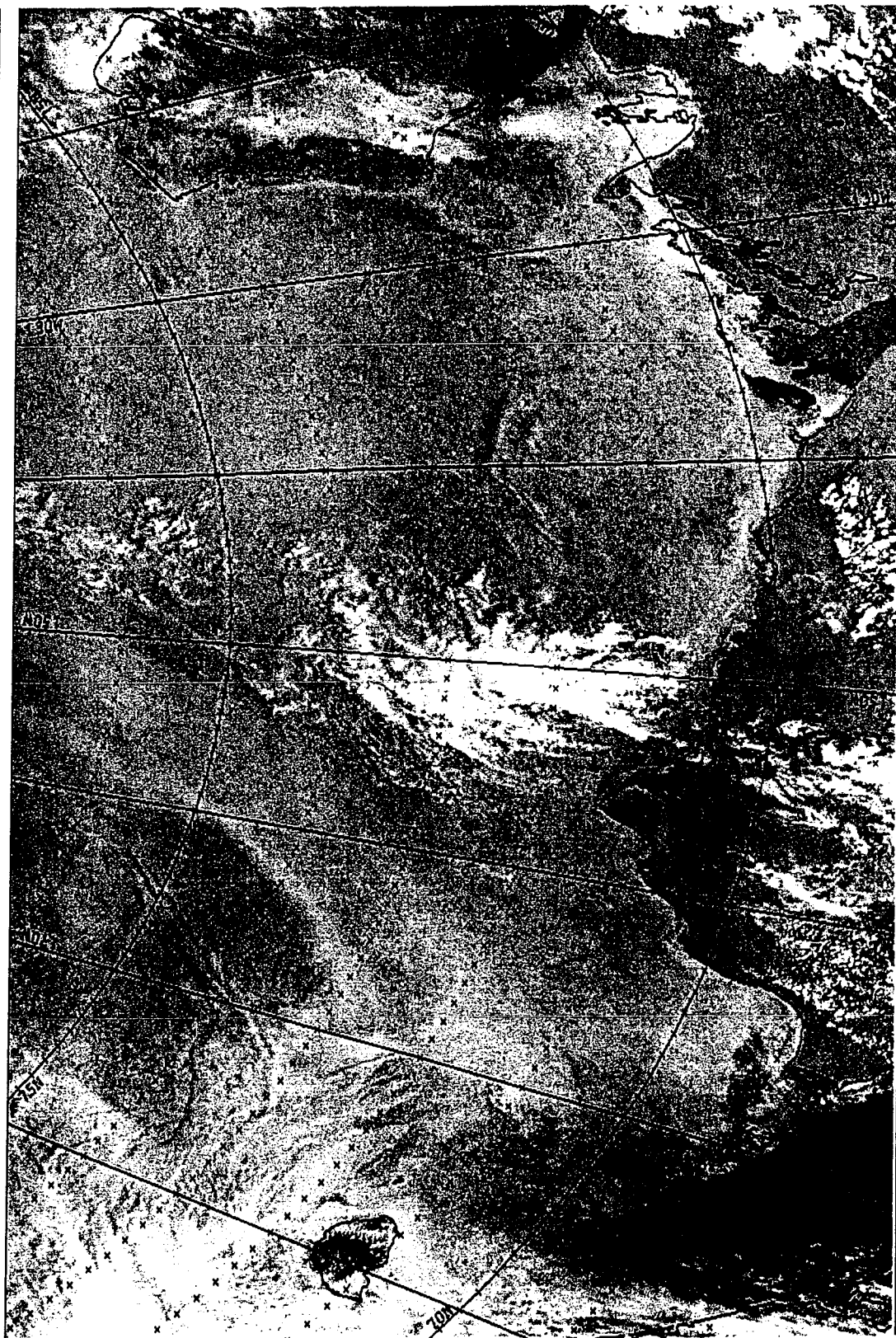
92062600
92032600

T 850
D 850

URE AT 850 MBS-N0CAPS.T79-L18
PTIMUM INTERPOLATION ANALYSIS

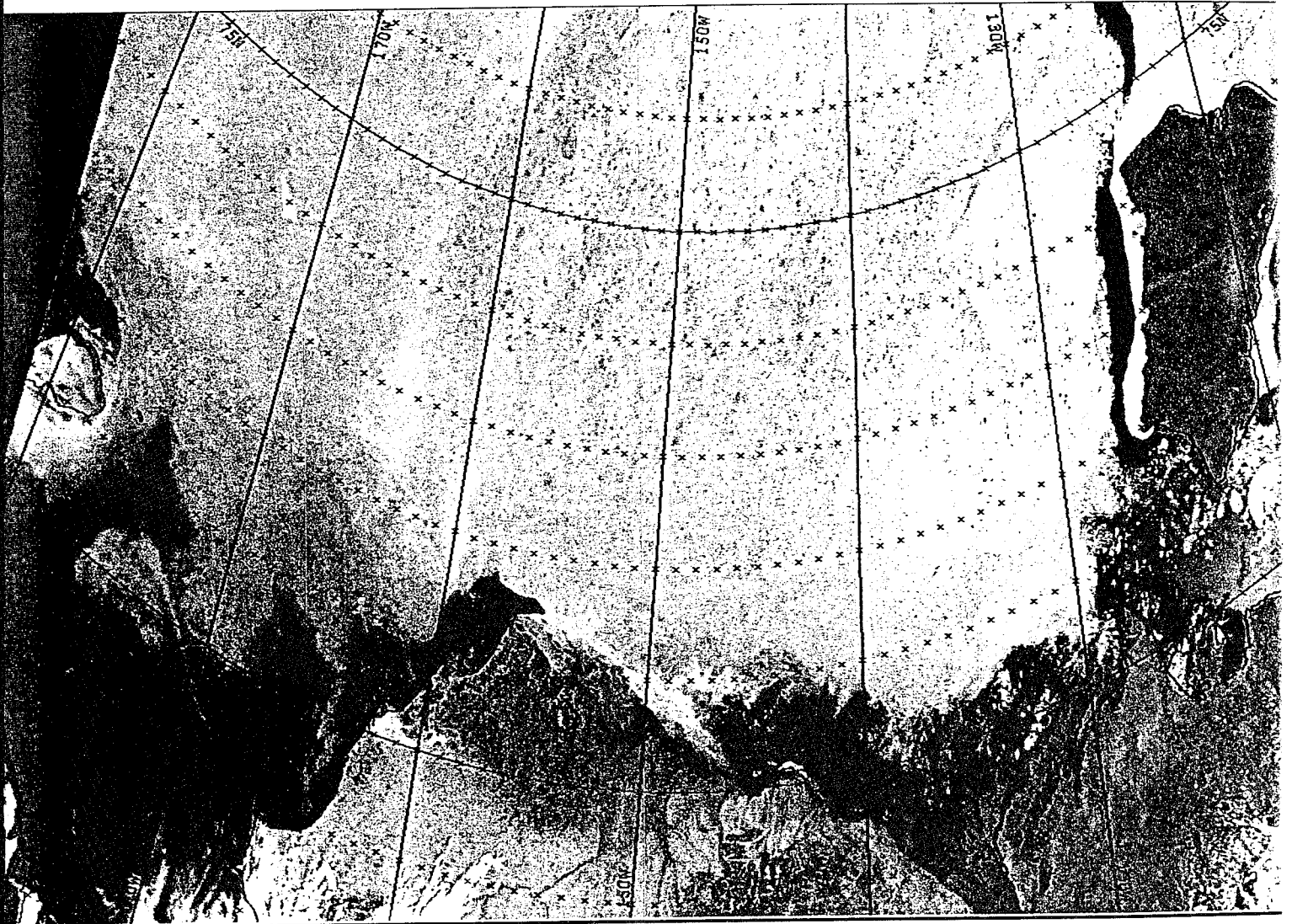


Window 1 - 011921732341768 avhr_ch2



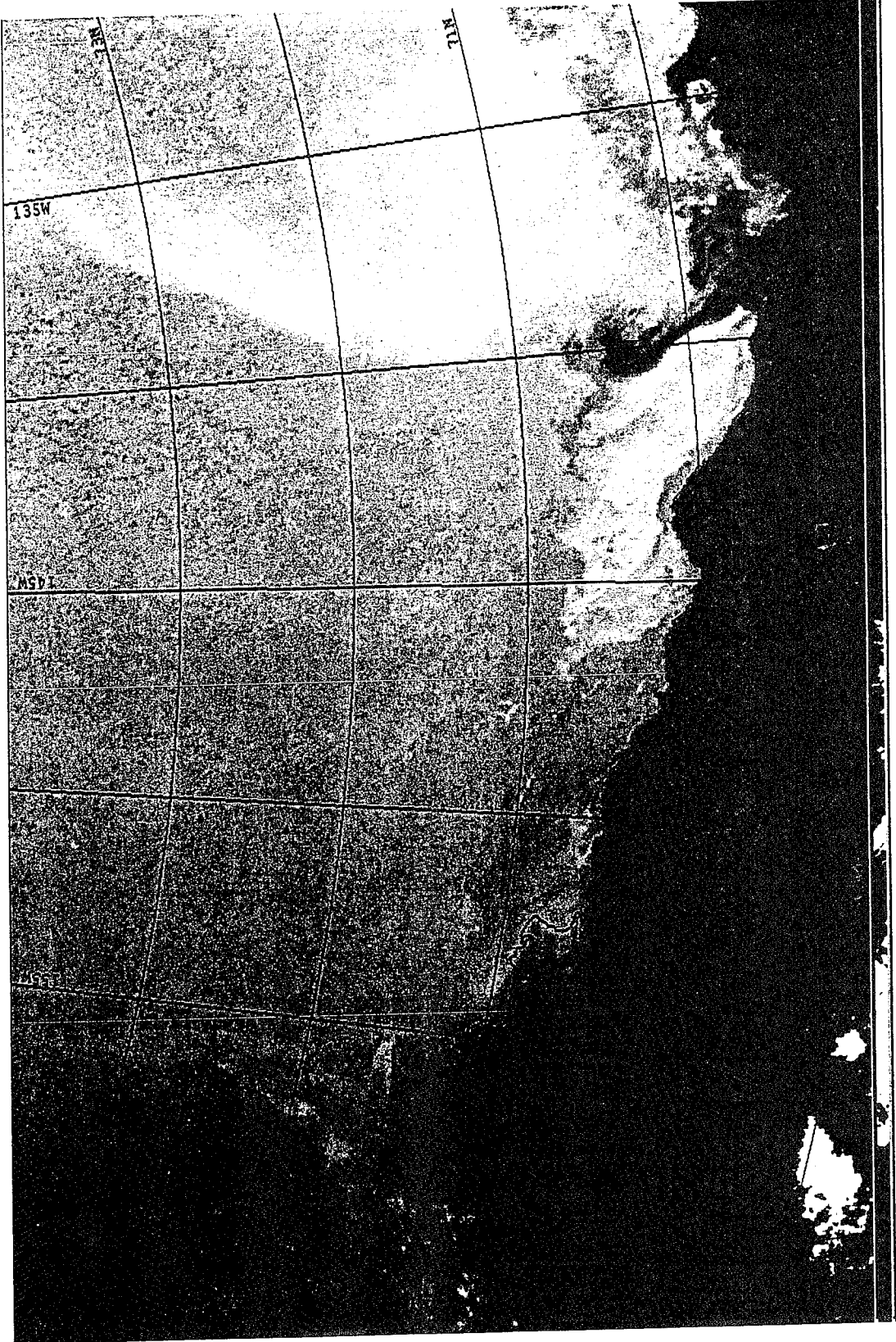
21 JUN 92

Window 1 - n10.92190.1752.reg avhrr_ch2



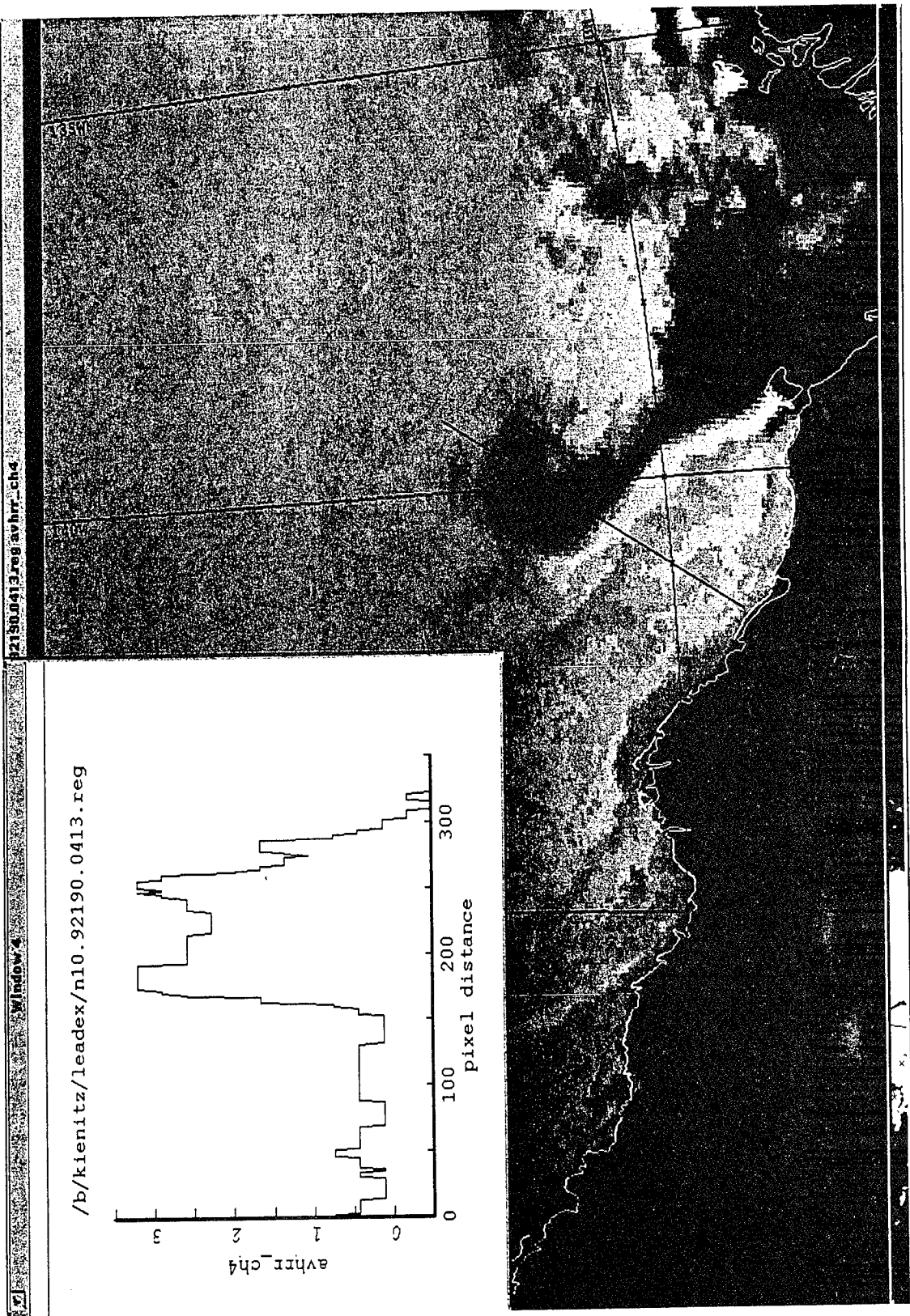
8 JUL 92

Window 4: leader/n10.92189.1955.mg avhrr_ch4



A Julian

7 JUL 92



Modelling the Sea of Okhotsk

Jiayan Yang

Modelling the Sea of Okhotsk

Jiayan Yang and Susumu Honjo
Woods Hole Oceanographic Institution
Woods Hole, MA 02543

The Sea of Okhotsk, located in the northwestern corner of the north Pacific Ocean between 45°N and 65°N, is covered by low-salinity water in the surface. This large marginal sea possesses a quite unique oceanographic setting that is not found elsewhere on a similar scale. First, it is mostly covered by sea ice during winter despite its relatively southern location. Second, it exhibits a very strong seasonal cycle. The sea surface temperature (SST) varies from over 15°C at the summer to near freezing point at winter. Unlike the Arctic Ocean, Okhotsk sea ice completely melts in the summer despite its extensive coverage in winter. Third, its deep basin is covered by a dicothermal layer between 30 and 150 meters in depth. The dicothermal layer water usually remains near freezing through the entire year. The Sea of Okhotsk also shows a very strong interannual variability as revealed from satellite passive-microwave observation of sea ice and from a few available in situ measurements.

A simple coupled sea ice and ocean model is used to examine some key physical processes that maintain this unique oceanographic state and to explore some plausible mechanisms that contribute to the observed interannual variability. The ocean model is a modified version of the 1.5-dimensional model of Killworth and Smith (1984). This model only resolves laterally-integrated vertical profiles of temperature, salinity and upwelling. It is forced by a prescribed inflow of the Pacific Ocean water, precipitation-evaporation, runoff, freshwater flux associated with sea-ice melting and freezing, sinking of shelf water, and inflow from the Sea of Japan. An outflow to the Pacific Ocean is also specified. A thermodynamic sea-ice model (Welander, 1973) is used to calculate the seasonal variation of sea-ice thickness. The forcings are specified by fitting them to some scarce observational data mainly from published Japanese and Russian literatures. Despite its simplicity, this model successfully captures the main features of the Sea of Okhotsk. For example, the model produces a dicothermal layer between 50 and 150 meters, a transitional layer beneath the dicothermal layer, and a highly seasonal surface mixed layer. In our model, the dicothermal layer is generated by the winter convection, and the transitional layer is due to a mixing between shelf water and Pacific Ocean intermediate water. These model results agree with the hypothesis of Kitani (1973). More interestingly, the model also exhibits a strong interannual variability characterized by alternating between two deep convections to the base of the dicothermal layer and two shallow convections to the base of the mixed layer. After two successive deep convections, the dicothermal layer is cold and salty. Sea ice is also thicker during these two deep convections. In the following two years, the increased melting water to the mixed layer together with a denser dicothermal layer restrict a winter convection only within the surface layer. Deep convection resumes after two years of shallower convection.

Reference:

- Killworth, P. D., and J. M. Smith, 1984: A one-and-a-half dimensional model for the Arctic halocline. *Deep Sea Research*, **31**, 271-293.
- Kitani, K., 1973: An oceanographic study of the Okhotsk Sea-particularly in regard to cold waters. *Bull. Far Seas Fish. Res. Lab.*, **9**, 45-57.
- Welander, P., Thermal oscillations in a fluid heated from below and cooled to freezing from above, *Dyn. Atmos. Oceans*, **1**, 215-223, 1977.

Modelling the Sea of Okhotsk

Jiayan Yang and Susumu Honjo

**Woods Hole Oceanographic Institution
Woods Hole, MA 02543
(508) 457-2000 ext. 3297, jyang@whoi.edu**

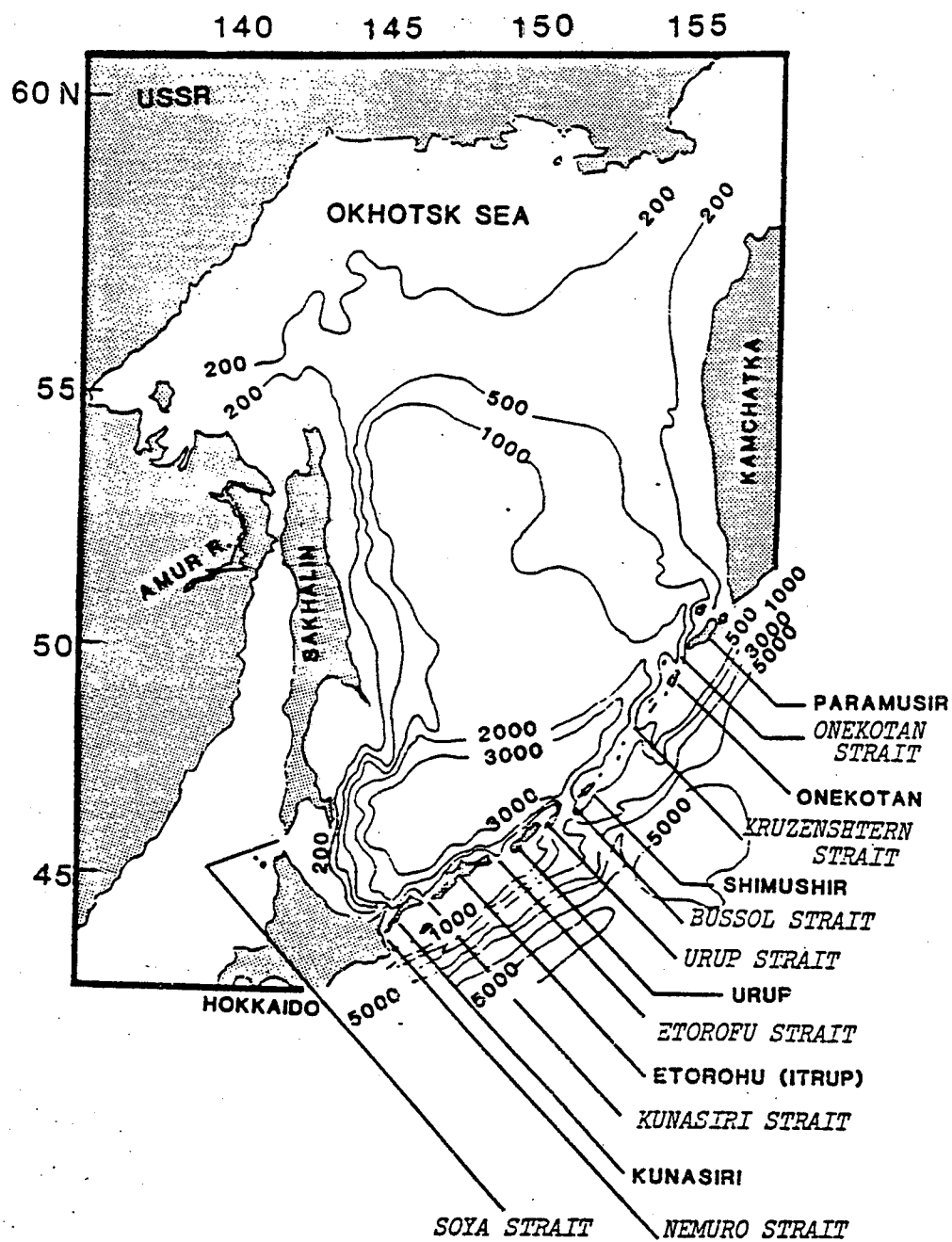


Figure 1-8. Key geographical features in the Okhotsk Sea.

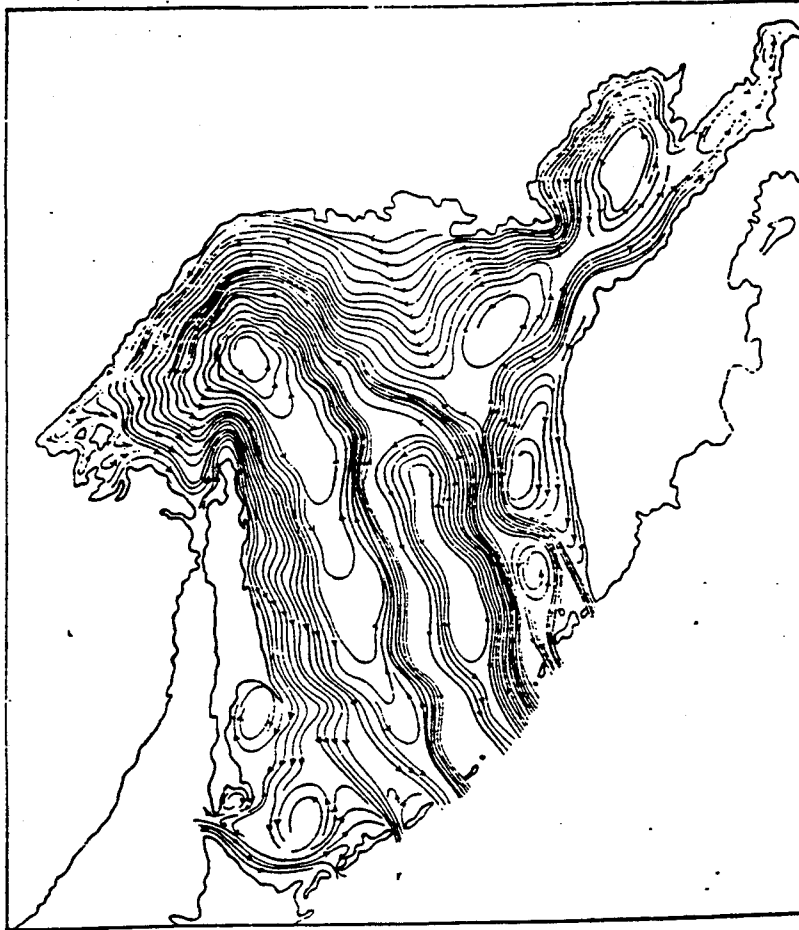
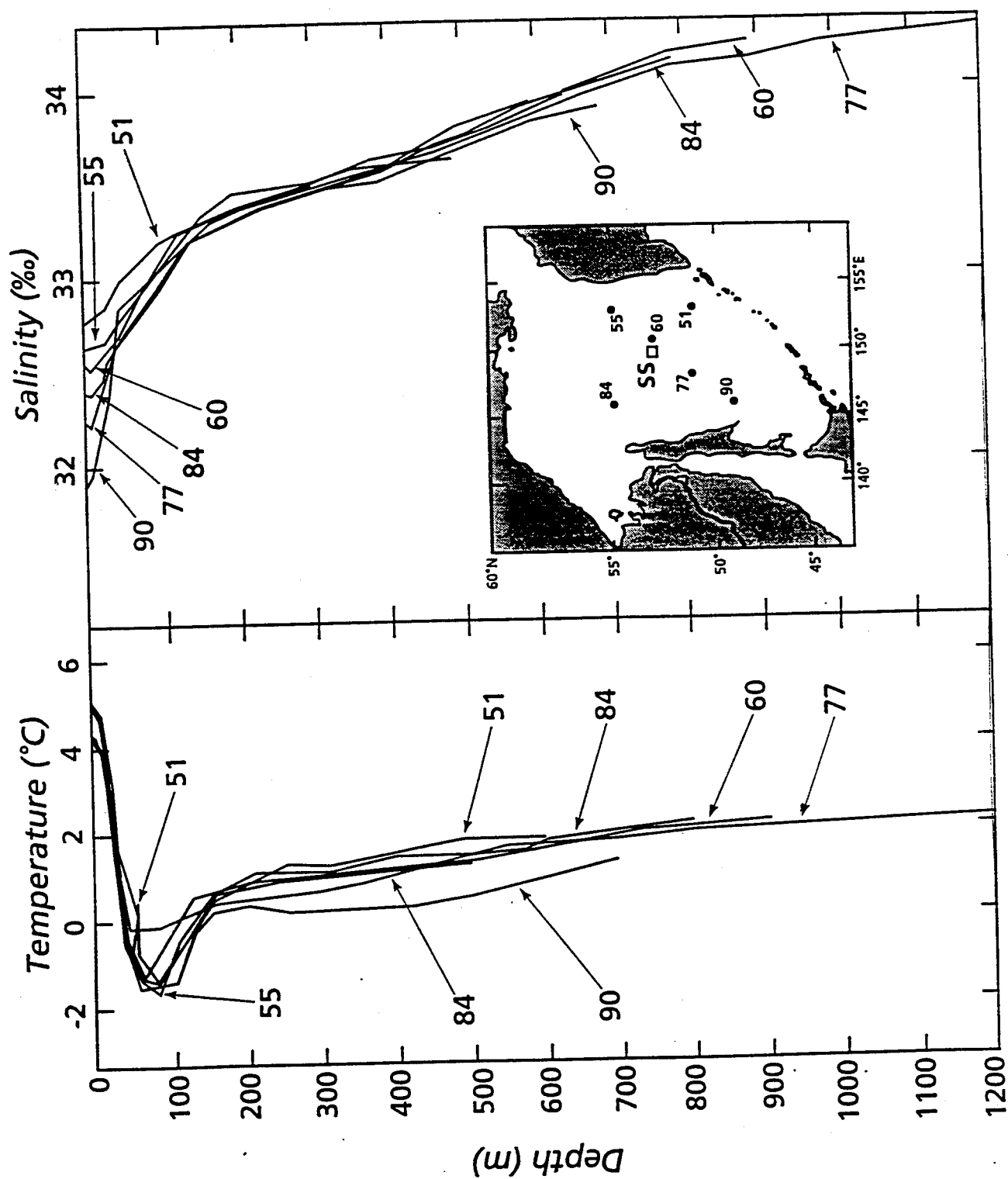
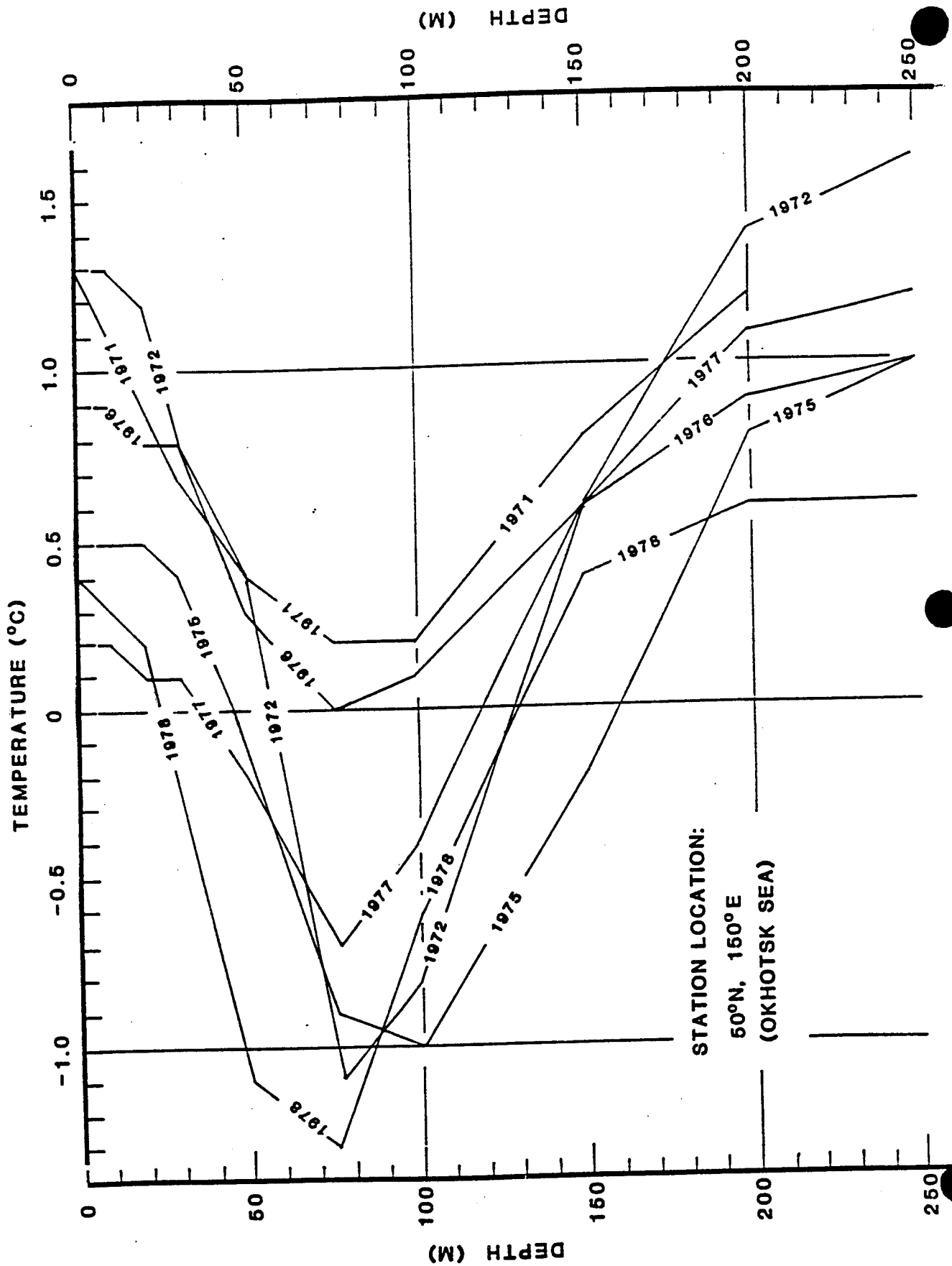
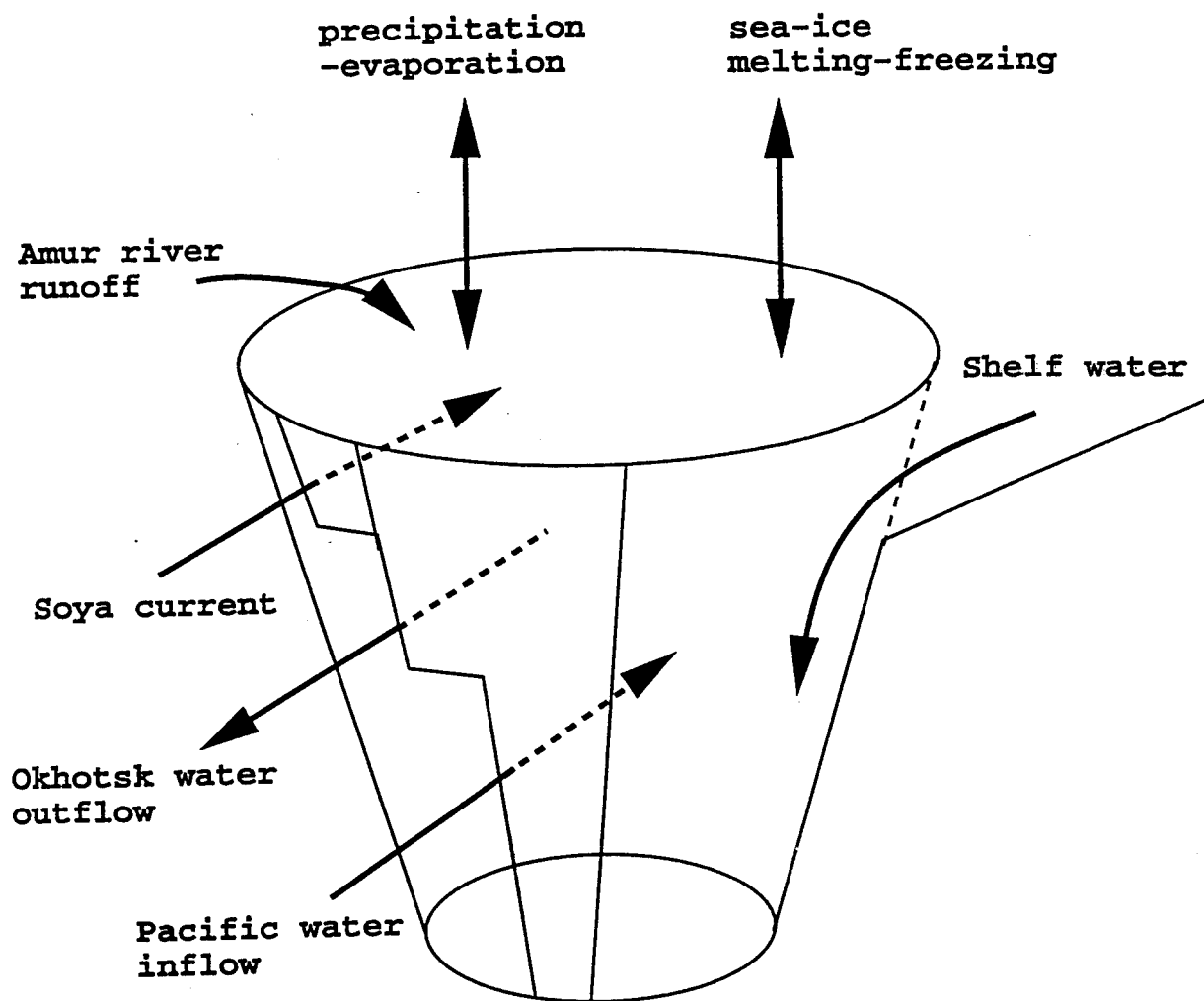


Fig. 38. A scheme of general circulation of water masses in the surface of the Sea of Okhotsk.







The Sea of Okhotsk and the Pacific are connected by 14 channels along Kurile Islands. Inflow mainly occurs at Bussol Strait and Kruzenshtern Strait; outflow at Etorofu Strait, Bussol Strait, and shallow western Kurile channels.

Ocean model (a modified Killworth and Smith model):

$$(A(z)W(z))_z = Q(z) \quad (1)$$

$$AT_t + (AWT)_z = \kappa(AT_z)_z + Qt + mix \quad (2)$$

$$AS_t + (AWS)_z = \kappa(AS_z)_z + Qs + mix \quad (3)$$

where:

$$Q(z, t) = Q_{pac} - Q_{out} + Q_{soya} + Q_{shf} + Q_{surface}$$

$$Qt(z, t) = Q_{pac}T_{pac} - Q_{out}T + Q_{soya}T_{soya} + Q_{shf}T_{shf} + Qt_{surface}$$

$$Qs(z, t) = Q_{pac}S_{pac} - Q_{out}S + Q_{soya}S_{soya} + Q_{shf}S_{shf}$$

$$Q_{surface} = A(0)(P(t) - E(t) - \delta_t) + Q_{runoff}(t)$$

$$Qt_{surface} = A(0)(P(t)T_p - E(t)T_e - \delta_t T_f) + Q_{runoff}(t)T_{runoff}$$

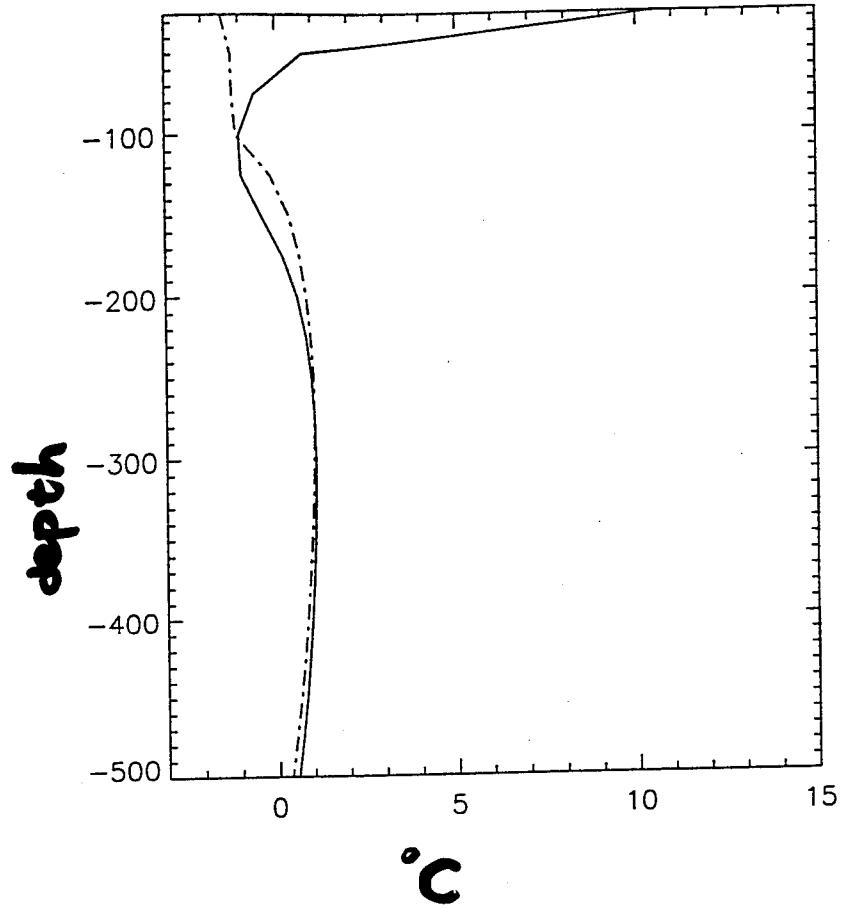
Sea-ice model:

$$\rho_i L_f \frac{d\delta}{dt} = \frac{\kappa_a K_i (T_f - T_a)}{K_i + \delta \kappa_a} - \kappa_w (T - T_f) \quad (4)$$

Data source:

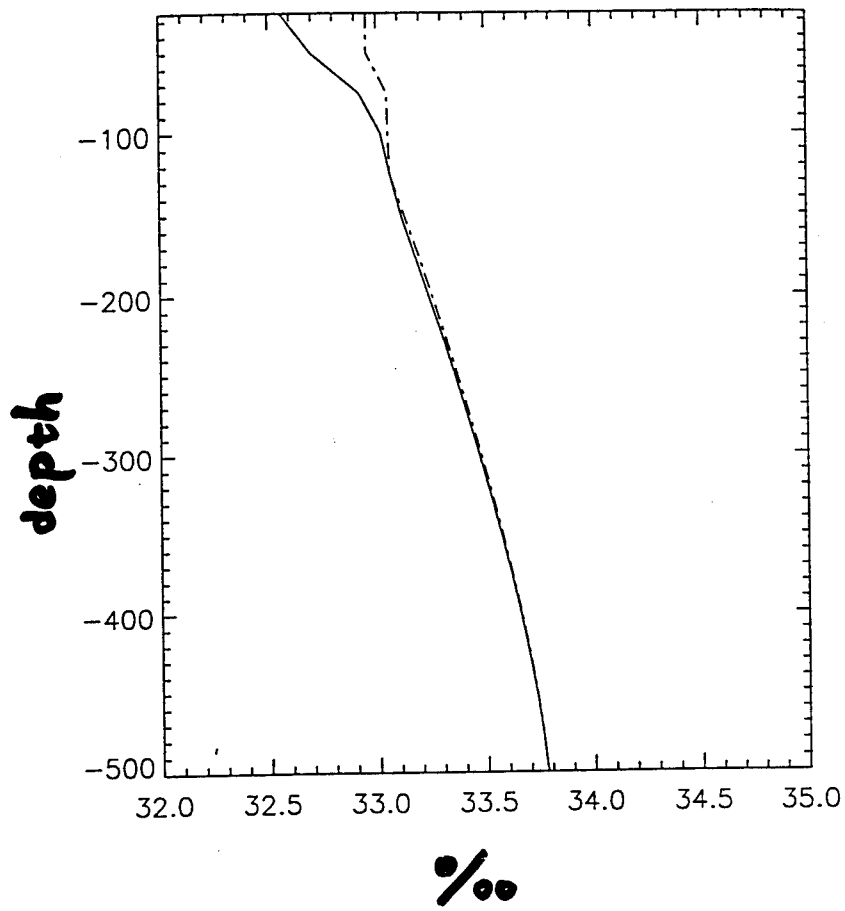
- Alfultis, M. A., and S. Martin, 1987: Satellite Passive microwave studies of Sea of Okhotsk ice cover and its relation to oceanic processes, 1978-1982. *J. Geophys. Res.*, **92**, 13,013-13,028.
- Cavalieri, D. J. and C. L. Parkinson, 1987: On the relationship between atmospheric circulation and the fluctuations in the sea ice extent of the Bering and Okhotsk Seas. *J. Geophys. Res.*, **92**, 7141-7162.
- Honjo, S. M. Honda, S. Manganini, and H. Ishii, 1994: Biogeochemical cycles in the Sea of Okhotsk, a temporarily ice-bound large marginal sea. *Deep-Sea Res.*
- Kajiura, K., 1947: On the hydrography of the Okhotsk Sea in summer. *J. Oceanogr. Soc. Jpn*, **5**(1), 19-26.
- Kitani, K., 1973: An oceanographic study of the Okhotsk Sea-particularly in regard to cold waters. *Bull. Far Seas Fish. Res. Lab.*, **9**, 45-57.
- Kitani, K. and K. Shimazaki, 1971: On the hydrography of the northern part of the Okhotsk Sea in summer. *Bull. Faculty of Fish., Hokkaido University*, XXII (3), 231-242.
- Kurashina, S., K. Nishida, and S. Nakabayashi, 1967: On the open water in the southern part of the frozen Okhotsk Sea and the currents through the Kuril Islands, *J. Oceanogr. Soc. Jpn.*, **23**, 57-62.
- Leonov, A. K., 1960: The Sea of Okhotsk, NTIS AD 639 585, Nat. Tech. Inf. Serv., Springfield, Va., 95pp.
- Parkinson, C. L. and A. L. Gratz, 1983: On the seasonal sea ice cover of the Sea of Okhotsk, *J. Geophys. Res.*, **88**, 2793-2802.
- Sonu, C. J., 1982: Descriptive Oceanography of the Okhotsk Sea and the Northern Sea of Japan.
- Wakatsuchi, M. and S. Martin, 1989: Satellite observations of ice/ocean eddies in the Okhotsk Sea and their relation to ocean structure. *J. Geophys. Res.*
- Yasuoka, T., 1967: Hydrography in the Okhotsk Sea (1), *Oceanogr. Mag.*, **19**(7), 61-72.
- Yasuoka, T., 1968: Hydrography in the Okhotsk Sea (2), *Oceanogr. Mag.*, **20**(7), 55-63.

$T(z)$



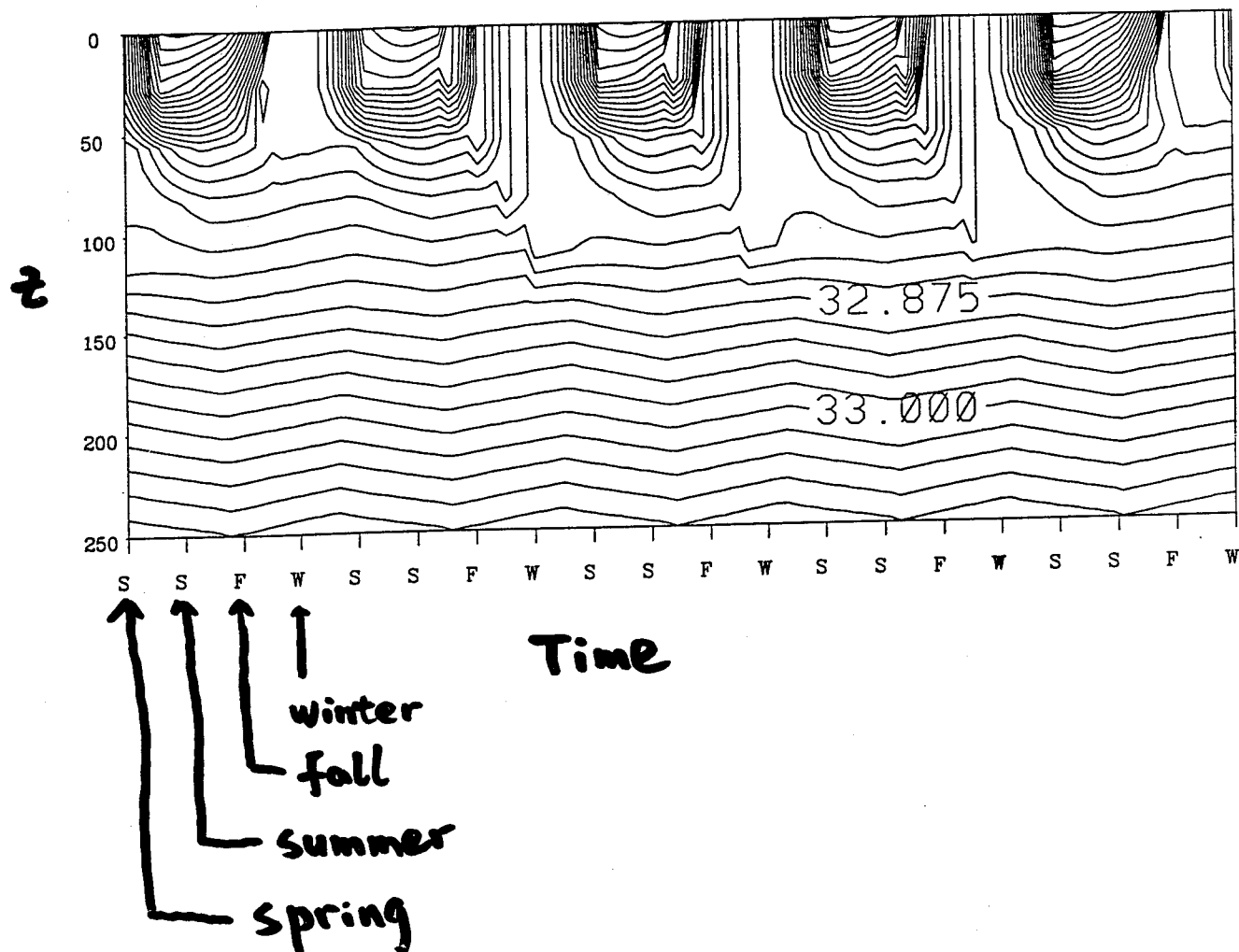
— summer
- - - winter

S(z)

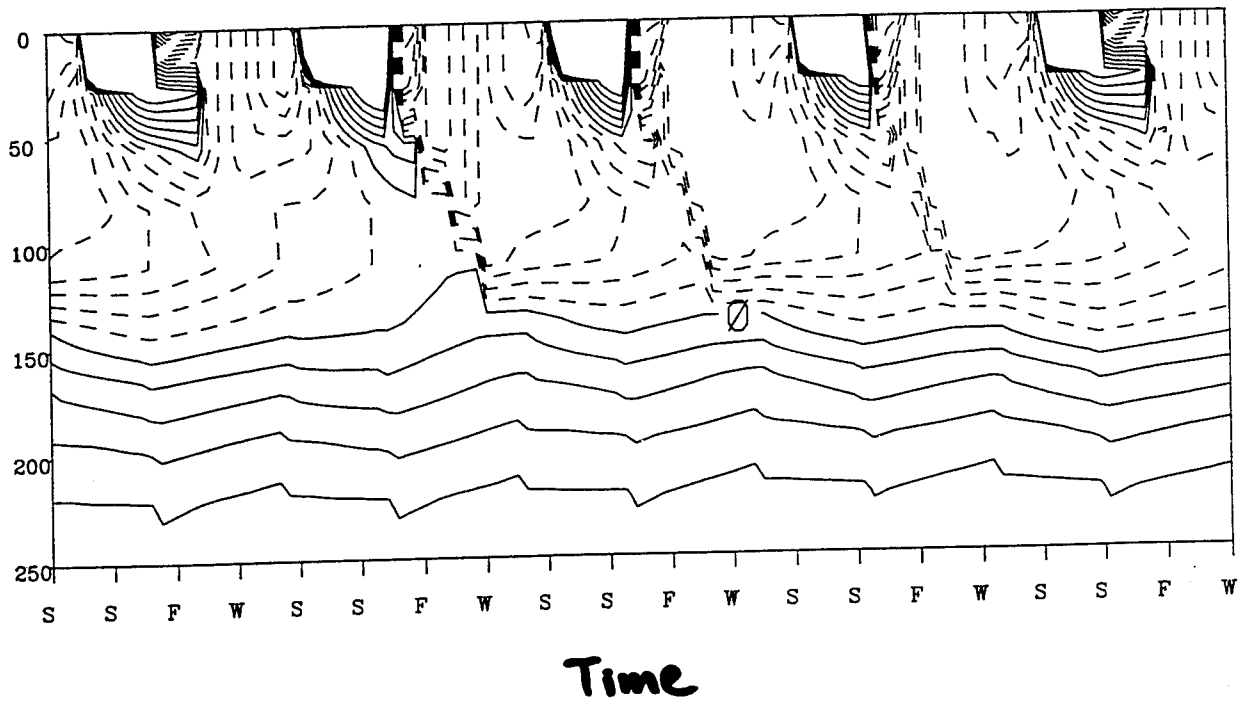


— summer
- - - winter

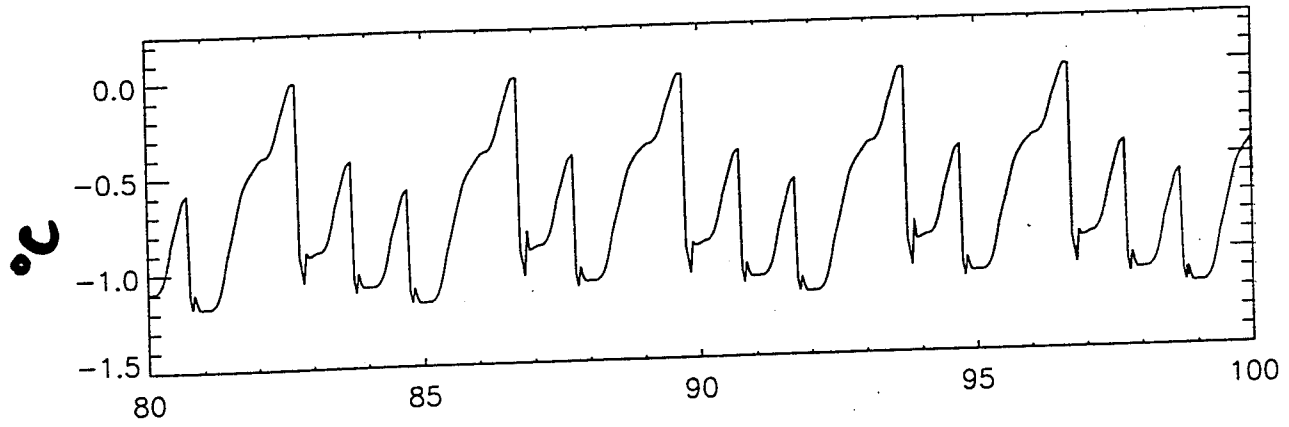
$$S(z, t)$$



$T(z, t)$

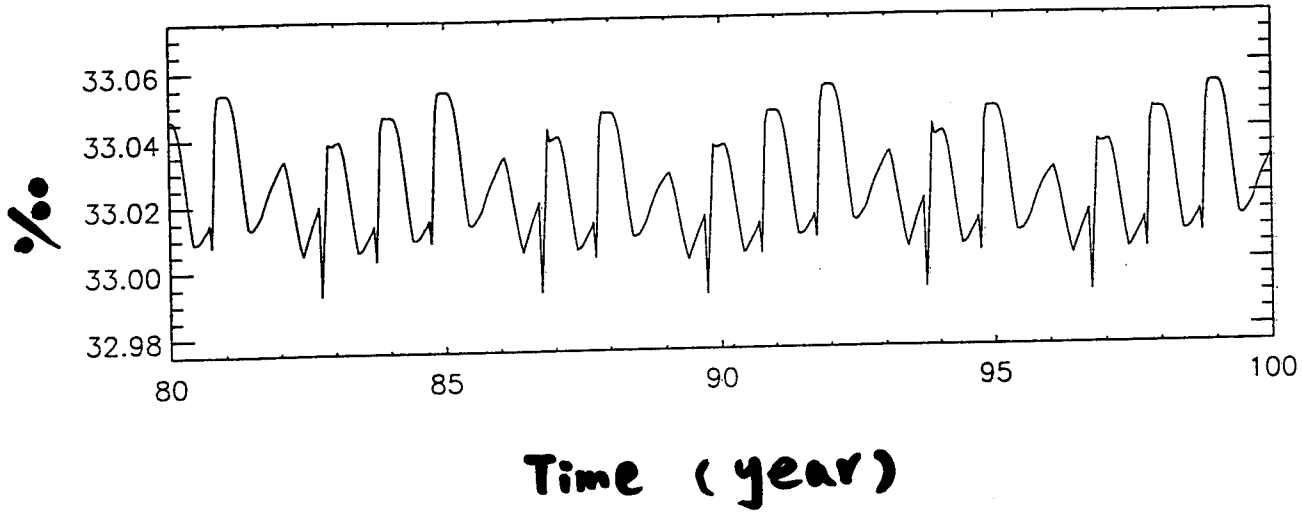


$T(z=100m)$



Time (year)

$S(z = -100m)$



Future work:

- Modelling wind-stress-driven and buoyancy-driven circulations in the Sea of Okhotsk;
- coupling a three-dimensional OGCM to a dynamic and thermodynamic sea-ice model;
- to understand the physical processes that maintain the unique oceanographic state in this large marginal sea;
- to examine various possible mechanisms that contribute to a strong interannual variability.

Topographic Effects on Dense Bottom Currents

Lin Jiang

Topographic Effects on Dense Bottom Currents

Lin Jiang and Roland W. Garwood, Jr.

Department of Oceanography, Naval Postgraduate School
Monterey, California 93943

ABSTRACT

Three-dimensional features of dense bottom plumes and deep water formation over continental slopes with or without along-slope topographic variations are investigated by simulating the evolution of a density front at a southern ocean continental shelf break, using a three-dimensional, primitive equation numerical model with a second-order turbulence closure scheme embedded. The focus of our investigation is the role of topography in determining mixing and deep water formation during the transient adjustment process of a density front over a continental slope. We compare and discuss the numerical simulations for two cases: a uniform shelf and slope case and a case with a canyon that leads from the coast to the deep ocean crossing the shelf and the slope.

The numerical simulations show that baroclinic instability together with the rotation deform the front into surface and bottom plumes along the shelf break. Correspondingly, a street of counter-rotating eddies form both at the surface and the bottom near the shelf break. The buoyant surface plumes are deflected to the left while intruding shoreward in this southern hemispheric case, with an intrusion scale controlled by rotation and buoyancy. The dense bottom plumes, which are dominated by the bottom friction and buoyancy, however, can penetrate downslope to much larger extent than do the surface plumes. Ultimately diffusion will limit the downward penetration of the shelf water. Eddy transport of shelf water is found to be very important in deep water formation on the continental slope.

The presence of a canyon in the shelf and slope enhances the penetration depth of the dense bottom currents in the canyon and thus increases deep water production, due to partial cancellation of the rotation effect in the lower part of the water in the canyon. A deep canyon has more significant effects in enhancing the deep water formation by draining more shelf water into deep ocean through the canyon, while a narrower canyon has reduced drainage.

Topographic Effects on Dense Bottom Currents

Lin Jiang and Roland W. Garwood, Jr.

Department of Oceanography, Naval Postgraduate School
Monterey, California 93943

ABSTRACT

Three-dimensional features of dense bottom plumes and deep water formation over continental slopes with or without along-slope topographic variations are investigated by simulating the evolution of a density front at a southern ocean continental shelf break, using a three-dimensional, primitive equation numerical model with a second-order turbulence closure scheme embedded. The focus of our investigation is the role of topography in determining mixing and deep water formation during the transient adjustment process of a density front over a continental slope. We compare and discuss the numerical simulations for two cases: a uniform shelf and slope case and a case with a canyon that leads from the coast to the deep ocean crossing the shelf and the slope.

The numerical simulations show that baroclinic instability together with the rotation deform the front into surface and bottom plumes along the shelf break. Correspondingly, a street of counter-rotating eddies form both at the surface and the bottom near the shelf break. The buoyant surface plumes are deflected to the left while intruding shoreward in this southern hemispheric case, with an intrusion scale controlled by rotation and buoyancy. The dense bottom plumes, which are dominated by the bottom friction and buoyancy, however, can penetrate downslope to much larger extent than do the surface plumes. Eddy transport of shelf water is found to be very important in deep water formation on the continental slope.

The presence of a canyon in the shelf and slope enhances the penetration depth of the dense bottom currents in the canyon and thus increases deep water production, due to partial cancellation of the rotation effect in the lower part of the water in the canyon. A deep canyon has more significant effects in enhancing the deep water formation by draining more shelf water into deep ocean through the canyon, while a narrower canyon has reduced drainage.

1. Introduction

The continental shelves in southern oceans comprise a vast area and play an important role in water mass formation and biological productivity. Antarctic Bottom Water forms in the southwestern Weddell Sea as a result of frontal mixing at the continental shelf break between the Warm Deep Water and the Western Shelf Water, as well as the result of deep open ocean convection [Foster and Carmack 1976; Killworth 1983; Foldvik et al. 1985].

Here we focus our attention on the deep water formation by dense shelf water flowing down a continental slope and mixing with the deep ocean interior water. Cold and dense shelf water is an important source of deep water even in the absence of deep open ocean convection [Foster and Carmack 1976; Foldvik et al. 1985]. Deep water formation on a continental slope has unique dynamic characteristics that differentiate it from open ocean deep water formation. The presence of a continental slope introduces a downslope gravitational component that enables cross-isobath transport of dense shelf water. Frictional bottom boundary layers also contribute to cross-isobath transport of mass, heat, salt. The shelf break constrains the flow around it and allows possibility of

trapped currents. Submarine canyons in the continental shelf and slope may facilitate the offshore transport of dense shelf water into deep ocean.

Early analytical studies on dense bottom plumes on continental slopes were steady stream-tube model simulations [Smith 1975; Killworth 1977] which exclude many processes that we find to be important. Smith [1975] described a rotating plume model that explains well the behavior of the Norwegian and Mediterranean outflows. Killworth [1977] considered both two-dimensional and three-dimensional plume models to investigate mixing processes on the Weddell Sea continental slope and found that the stream tube models gave results incompatible with observations, until the thermobaricity effect was incorporated in the model. The stream tube model has several limitations in dealing with outflow along very wide shelves with complex topography (e.g. the Antarctic continental shelves). Firstly it assumes that the ambient water is quiescent and does not allow baroclinic instability and cross-stream variations, and thus it neglects some important dynamic features of three-dimensional plumes. Secondly it can not deal with plumes flowing on a slope with abrupt bottom variations, such as a canyon or a sea mount.

Recently more complicated numerical models have been used to investigate dense water formation and transport on continental shelves and slopes. Jungclauss and Backhaus [1994] employed a hydrostatic, reduced gravity, two-dimensional primitive equation model to simulate the nonlinear and non-steady features of the Denmark Strait Overflow. Hsu [1993] used a two-dimensional primitive equation model to study negative buoyancy forcing adjacent to a coast and found that the dense water did not move offshore beyond the forcing region unless an along-shelf current was included. The model did not allow along-shelf variation in the flow field and thus could generate neither plumes nor eddies. Gawarkiewicz and Chapman [1994] modeled dense water formation and transport generated by an idealized coastal polynya over a gently sloping shallow continental shelf. The flow response to a constant negative surface buoyancy flux imposed over a half-elliptical region adjacent to the coast was discussed. The numerical results suggest that instability and eddy fluxes are the important mechanisms in the transport of dense coastal water off continental shelves and into marginal seas. To investigate offshore transport of dense bottom water and deep water formation on southern ocean continental slopes, we pursue a similar approach but focus on the transient response to topographic influences on bottom plume formation and penetration.

In this study we simulate the evolution of a density front at a southern ocean continental shelf break with a three-dimensional primitive equation model in which a second-order turbulence closure scheme is embedded. We consider a wide continental shelf and a continental slope for two cases: a uniform shelf and slope case and a case with a canyon in the shelf and the slope. The traditional "dam break" technique is adopted to simulate the adjustment processes of a density front at the shelf break in the absence of external forcing. In the dam-break experiment a vertical barrier that separates different salinities and temperatures of water at the shelf break is removed at time $t=0$ to allow the separated waters to exchange. This technique gives a good sense of the time development of the response of the front over the continental slope from an initial rest state.

2. Model Description

To investigate the topographic effects on the dynamical processes on the shelf and slope, two idealized topographies are introduced in the model domain. The first one is a uniform shelf and slope case which has no along-shelf topographic variations, as shown in Figure 1. The second case has a 100-km-wide and 200-m-deep canyon oriented in the East-West direction, halfway between the southern and the northern boundaries, as

shown in Figure 2. In this model study, the water mass system is greatly simplified, and we consider only the case for the adjustment of a density front, located at the shelf break, separating a well-mixed shelf water and a well mixed deep ocean interior. We do this in order to gain physical insight into the dynamics of the plumes and the topographic influences on the plume formation and penetration and as a prerequisite for understanding the more complicated case with stratification in both the shelf and the slope water. The temperature and salinity ranges used here are those from the water masses involved in forming deep water in the Antarctic, i.e., temperature from -2° to $+1^{\circ}$ C and salinity from 34.40 to 35.00 ‰ [Foster and Carmack 1976]. Figure 3 shows the idealized cross-shelf topography of the model domain without along-shelf topographic variations and the hypothetical initial temperature and salinity conditions from which the evolution of the density front starts.

The model used here is a three-dimensional primitive equation model which is hydrostatic, fully nonlinear, and applies the Boussinesq approximation. Vertical turbulent mixing processes are parameterized with the second-order turbulent closure scheme of Mellor and Yamada [1982]. Smagorinsky's [1963] lateral eddy mixing coefficient is used along sigma-coordinate surfaces with a purpose of purely removing spurious computational modes. The model uses a sigma-coordinate system for which the model equations and the method of solution are given in Blumberg and Mellor [1983].

High resolution in the horizontal and the vertical are used to ensure that instability processes due to both the horizontal and vertical velocity shears and density gradients are properly included. Altogether, 41 sigma levels are used in the vertical, with a logarithmic sigma distribution at the surface and the bottom in order to resolve the buoyant near-surface plumes and the bottom boundary currents. The horizontal grid sizes are $\Delta x = \Delta y = 10$ km throughout the model domain, which is able to resolve scales of $O(R_o) = 11$ km for the case considered. The value of f_0 is set a latitude of 72° S, so that $f_0 = -1.38 \times 10^{-4} \text{ s}^{-1}$.

At the free surface, there is no surface wind stress, and no heat and salinity fluxes. At the bottom, zero heat and salinity fluxes are specified. At land boundaries we use the condition of no diffusive fluxes of any property across the interface. The eastern open boundary is set such that interior energetic bores are allowed to pass through with little reflection to the interior. The model is integrated with an external time step of 10 s and a internal time step of 500 s, which is set by the CFL condition of the fast-moving external mode.

3. A uniform slope case

The uniform-slope case is taken as the benchmark experiment, whose results will be compared with the those for the cases with along-shelf topographic variations. The salinity fields at sigma level 1 (the surface), where the surface outflow is maximum, at days 14, 18, and 22, are shown in Figure 4. After the sudden removal of the 'dam', fresher and warmer deep ocean water intrudes onto the shelf near the surface, while more saline and colder water penetrates downslope from below. The initially straight front meanders and deforms into a number of light plumes at the surface, with a length scale of about 50 km in the along-shelf direction. The surface salinity fields display strong along-shelf asymmetry in the plumes. The plumes are almost uniformly aligned along the shelf break. They are deflected to their left-hand-side as they flow onto the shelf, apparently dominated by the planetary rotation. The surface plumes continue to spread shoreward, but the spreading speed slows and the intrusion is limited as the front becomes diffused. Eventually a quasi-steady state is reached where the surface plumes are trapped near the shelf break with the extent of shoreward intrusion of about 50-60 km in the interior of the model domain.

The salinity fields at level 40 (the bottom level) at days 14, 18, 22 are illustrated by Figure 5, respectively. Again the salinity field and the temperature field have almost identical patterns (so later on only one field will be shown). The dense cold, and saline bottom plumes form on the slope and penetrate away from the shelf break down the slope. During the initial stage of the bottom plume formation, a street of dense plumes appears in the form of individual plumes with a width of about 50 km, uniformly aligned along the shelf break while flowing downslope. They are deflected to the left slightly under the influence of rotation. Bottom friction increases with the increase of the current speed and it balances the Coriolis force in dragging the plumes further down the slope. The bottom plumes continue to penetrate downslope, but the spreading speed slows gradually with time due to mixing and entrainment with the surrounding water. Later, at $t=18$ days, the bottom plumes grow larger and wider as a result of mixing and they start to interact with each other. Gradually the bottom plumes lose their individual characteristics and merge into a bottom front with a wavy foreface which is almost parallel to the shelf break. The horizontal penetration extent of the bottom plumes is about 140 km from the shelf break, corresponding to a vertical penetration depth of about 1700 m from the surface.

To understand the dynamics of the spreading plumes, we examine the evolution of the lateral velocity fields at the surface. Figure 6 shows the velocity fields at days 14, 18, 22 at sigma level 1. Baroclinic instability causes a street of eddies in the form of pairs with opposite rotating directions, almost uniformly aligned along the shelf break. The eddies on the shelf side rotate anti-cyclonically, apparently controlled by the rotation. The eddies on the slope side are larger in the cross-shelf direction than those on the shelf, and they rotate cyclonically. They become elongated in the cross-slope direction as bottom plumes penetrate deeper downslope and at the same time drag the surface water offshore. The lateral velocity scale is about the same at both the surface and the bottom, which is about 10-20 cm/s.

Figure 7 shows the velocity fields at sigma level 40 at days 14, 18, and 22. Again baroclinic instability results in a train of eddies near the bottom along the shelf break. The eddies on the slope rotate anti-cyclonically, while the coupling surface eddies on the slope rotate cyclonically. The bottom eddies on the shelf rotate cyclonically, and the coupling surface eddies on the shelf rotate anti-cyclonically. They are trapped near the shelf break, apparently under more significant influence of planetary rotation and less significant influence of bottom friction. The velocity field near the bottom again indicates that the dense bottom plumes are dominated by the friction and buoyancy. This friction allows them to penetrate further downslope before being held back and flowing along isobars. The bottom plumes also turn to the left-hand-side of their flow direction due to the Coriolis effect as bottom friction enables a downslope flow. The magnitude of the lateral velocity in the interior of the model domain is on order of 10-20 cm/s.

4. A canyon in Shelf and Slope

To examine the influence of a cross-shelf canyon on the plume dynamics and deep water formation, we include a case with a 100-km wide and 200-m deep canyon that leads from the coast to deep water, crossing the shelf and the slope. Examination of the salinity fields at the bottom, Figure 8, reveals that a large plume forms in the canyon at $t=14$ days, and this plume grows quickly and spills over the north wall of the canyon as it progresses downslope. The large plume continues to penetrate deeper along the north wall of the canyon, with a considerably diffused front due to intense mixing and entrainment with the surrounding water. The plumes about two plume-sizes from the canyon are affected much less significantly. The cold saline shelf water progressed downslope much deeper (to about 2050 m) along the north wall of the canyon than for

the uniform slope case (to about 1600 m) at day 22. The canyon has an effect similar to that of the north wall of the model in draining shelf water into the deep ocean. A canyon, however, does not exactly act as a wall because it also affects the flows on the adjacent continental shelf and slope within a two plume-size region.

To study the effects of the depth of a canyon, an experiment is conducted for a 100-km wide and 300-m deep canyon. Figure 9 shows the salinity fields in the presence of a 200-m deep canyon and 300-m deep canyon at days 22 at level 40, respectively. It is found that colder shelf water penetrates much deeper downslope (to about 2800 m) than for the shallower canyon case (to about 2050 m), thus deep water generation is more effective.

Figure 10 illustrates the velocity fields in the presence of the 200-m deep canyon and the 300-m deep canyon at day 22 at level 40, respectively. The velocity in the canyon is strengthened along the north wall of the canyon because more available potential energy was converted to kinetic energy in the deep canyon case than in the shallow canyon case. Again the velocity field near the coastal end of the canyon shows that dense shelf water plunges over the south wall of the canyon.

To investigate the influence of the width of a canyon, we study a case with a 40-km wide and 300-m deep canyon. Figure 11 shows the salinity fields at day 22 at level 40 in presence of the 40-km wide canyon, together with the 100-km wide and 300-m deep canyon case. The penetration depth (to about 2200 m) in the 40-km wide and 300-m deep canyon is reduced considerably compared with the 100-km wide and 300-m deep canyon case. This results from the interaction between the flow and the two walls of the canyon, which are closer to each other than in the previous cases. The north wall of the canyon enhances penetration along it, while plume penetration downslope is hindered along the south wall. When the walls are far apart, they act as a step; their effects counter-act when the canyon width is close to order of the local deformation radius.

5 Conclusions

The numerical simulations show that baroclinic instability together with the rotation deform the front into surface and bottom plumes along the shelf break. Correspondingly, a street of counter-rotating eddies form both at the surface and the bottom near the shelf break. The buoyant surface plumes are deflected to the left while intruding shoreward in this southern hemispheric case, with an intrusion scale controlled by rotation and buoyancy. The dense bottom plumes, which are dominated by the bottom friction and buoyancy, however, can penetrate downslope to much larger extent than do the surface plumes. Ultimately diffusion will limit the downward penetration of the shelf water. Eddy transport of shelf water is found to be very important in deep water formation on the continental slope. The presence of a canyon in the shelf and slope enhances the penetration depth of the dense bottom currents in the canyon and thus increases deep water production, due to partial cancellation of the rotation effect in the lower part of the water in the canyon. A deep canyon has a more significant effect in enhancing the deep water formation by draining more shelf water into deep ocean through the canyon, while a narrower canyon has reduced drainage.

REFERENCES

- Blumburg, A.F., and G.L. Mellor, A description of a three-dimensional coastal ocean circulation model, in *Three-Dimensional Coastal Ocean Models*, ed. N. Heaps, pp. 208, American Geophysical Union, Washington D.C., 1983.
Foldvik, A., Current and tidal measurements in the Weddell Sea (Abstract), Int. Union Geod. and Geophys. 17th Assembly, Canberra, 421 pp., 1979.

- Foldvik, A., T. Kvinge, and T. Torresen, Bottom Current near the continental shelf break in the Weddell Sea, *Oceanology of the Antarctic Continental Shelf*, Antarctic Research Series, 43, 21-34, 1985.
- Foster, T.D. and E.C. Carmack, Frontal zone mixing and Antarctic bottom water formation in the southern Weddell Sea, *Deep-Sea Research*, 23, 301-317, 1976.
- Gawarkiewicz, G. and D.C. Chapman, A numerical study of dense water formation and transport on a shallow, sloping continental shelf, *J. Geophys. Res.*, in press, 1994.
- Hsu, H.M., 1993: The response of the shallow polar shelf water to negative buoyancy forcing: a numerical study, Submitted to *J. Phys. Oceanogr.*, 1993.
- Jungclauss, J.H., and J.O. Backhaus, Application of a transient reduced gravity plume model to the Denmark Strait Overflow, *J. Geophys. Res.*, 99(C6), 12375-12396, 1994.
- Killworth, P.D., Mixing on the Weddell Sea continental slope, *Deep-Sea Res.*, 24, 427-488, 1977.
- Killworth, P.D., Deep Convection in the world ocean, *Rev. Geophysics*, 21, 1-264, 1983.
- Mellor, G.L., and T. Yamada, Development of a turbulence closure model for geophysical fluid problems, *Rev. Geophys. Space Phys.*, 20, 851-875, 1982.
- P.C., Smith A streamtube model for bottom boundary currents in the ocean, *Deep-Sea Res.*, 22, 853-973, 1976.
- Smagorinsky, J., General circulation experiments with the primitive equations, *Mon. Wea. Rev.*, 91, 99-165, 1963.
- Sugimoto, T. and J.A Whitehead, Laboratory models of bay-type continental shelves in the winter, *J. Phys. Oceanogr.*, 13, 1819-1828, 1983.
- Whitehead, J.A, A laboratory model of cooling over the continental shelf, *J. Phys. Oceanogr.*, 23, 2412-2427, 1993.

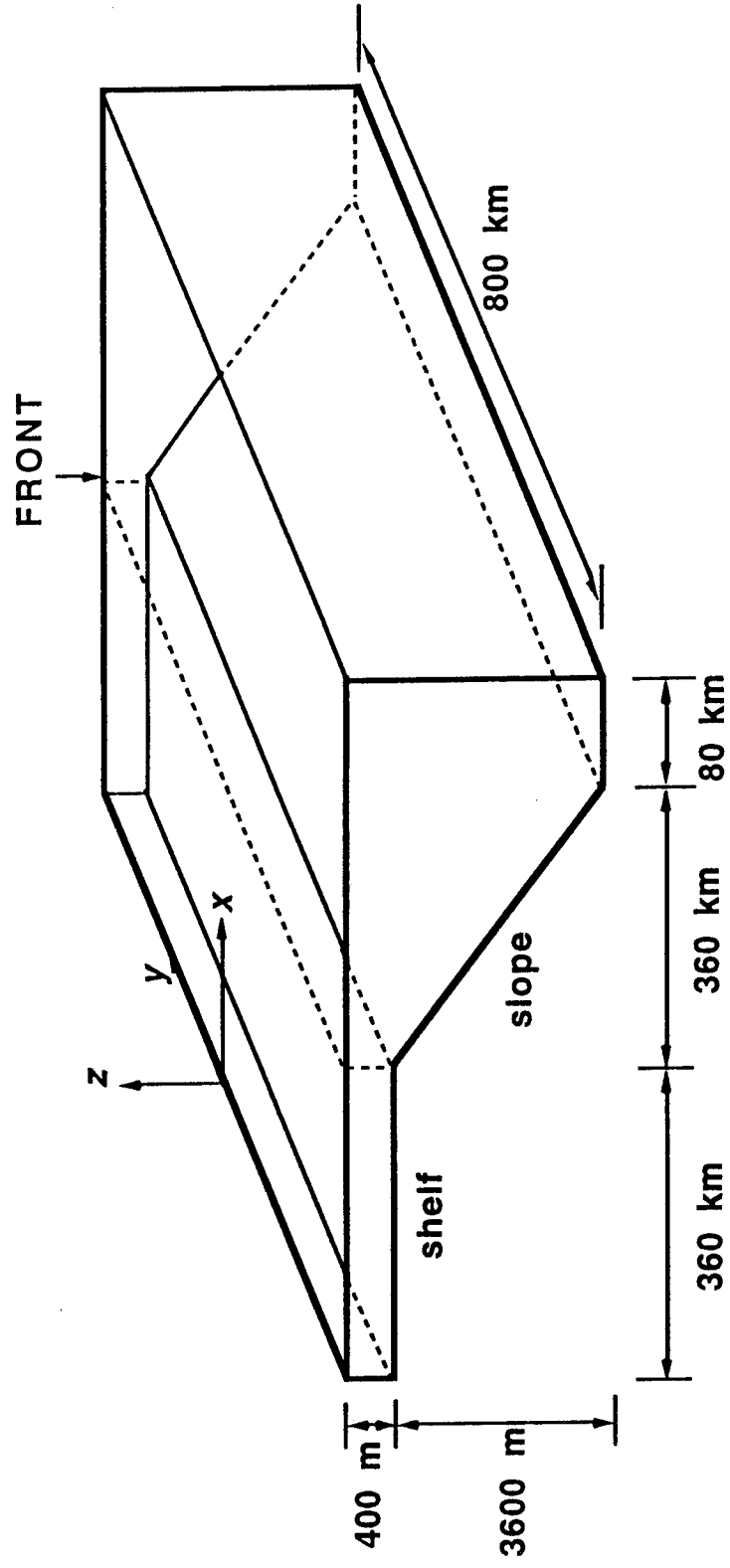


Fig 1 Perspective View of the Model Domain
- A Uniform slope and Shelf

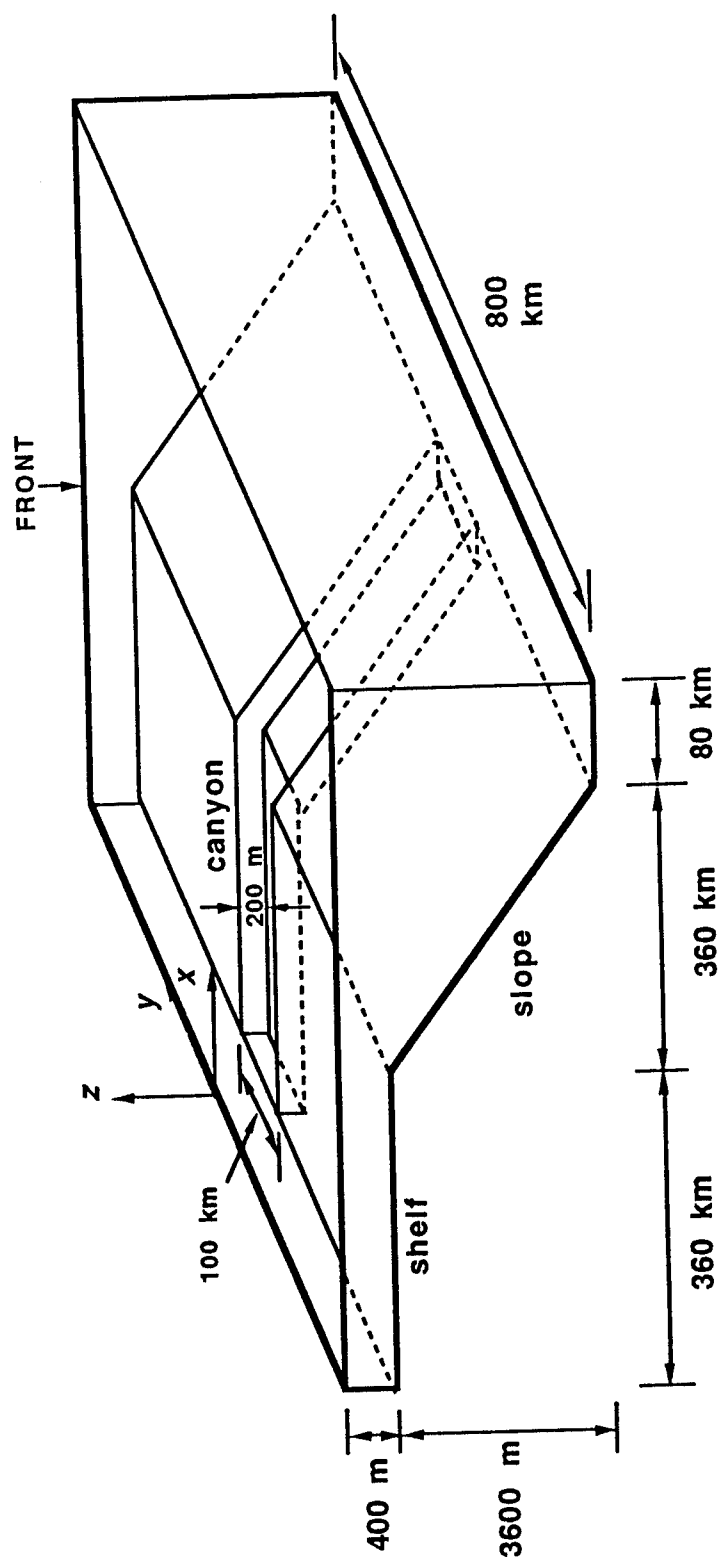


Fig. 2 Perspective View of the Model Domain
- A Canyon in the shelf and slope

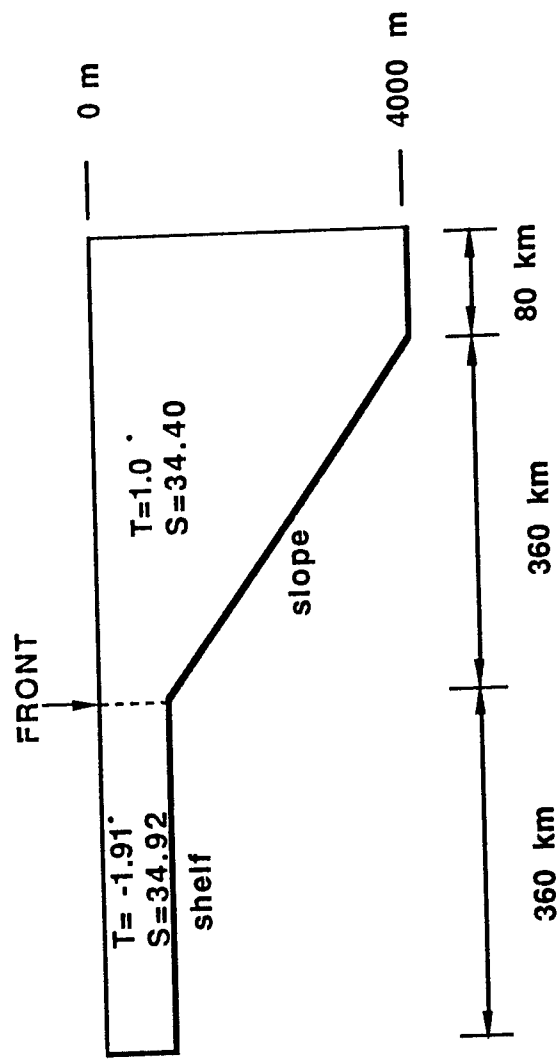
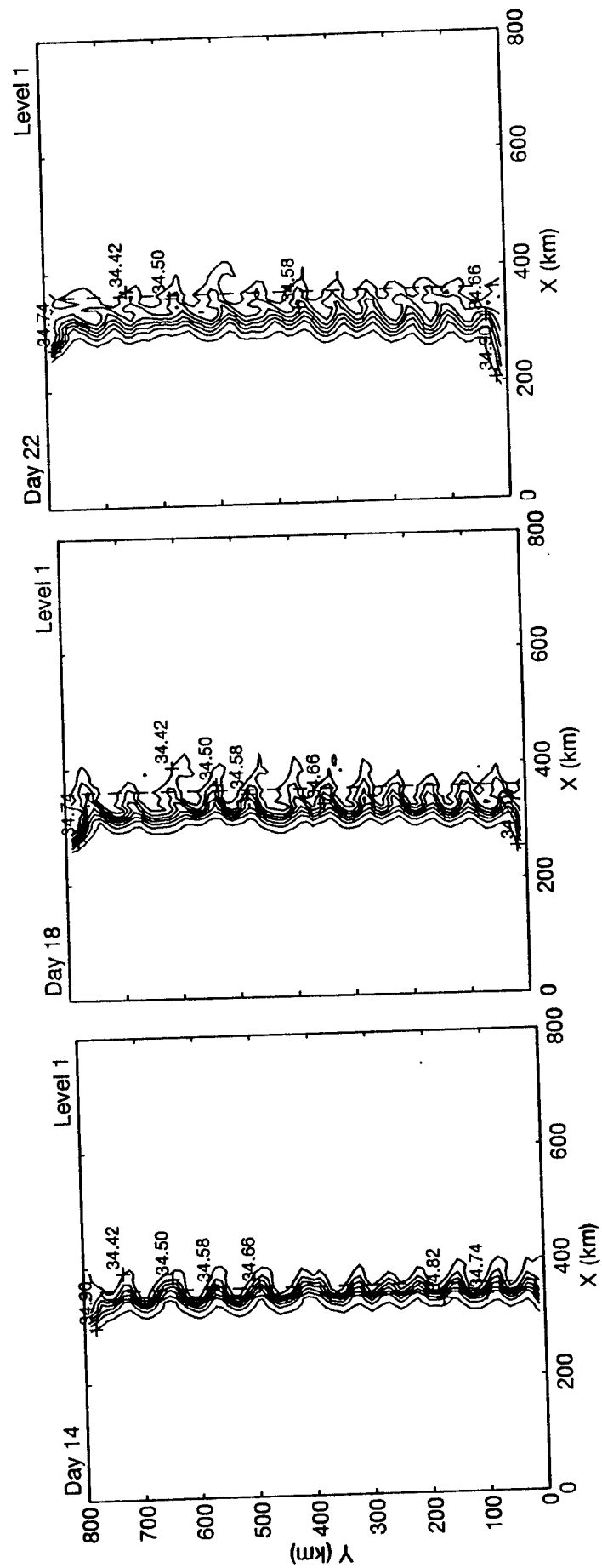


Fig.3 Cross-shelf Section of the Model Domain and Initial Conditions



The salinity fields at sigma level 1 at days 14, 18, 22.

Fig. 4

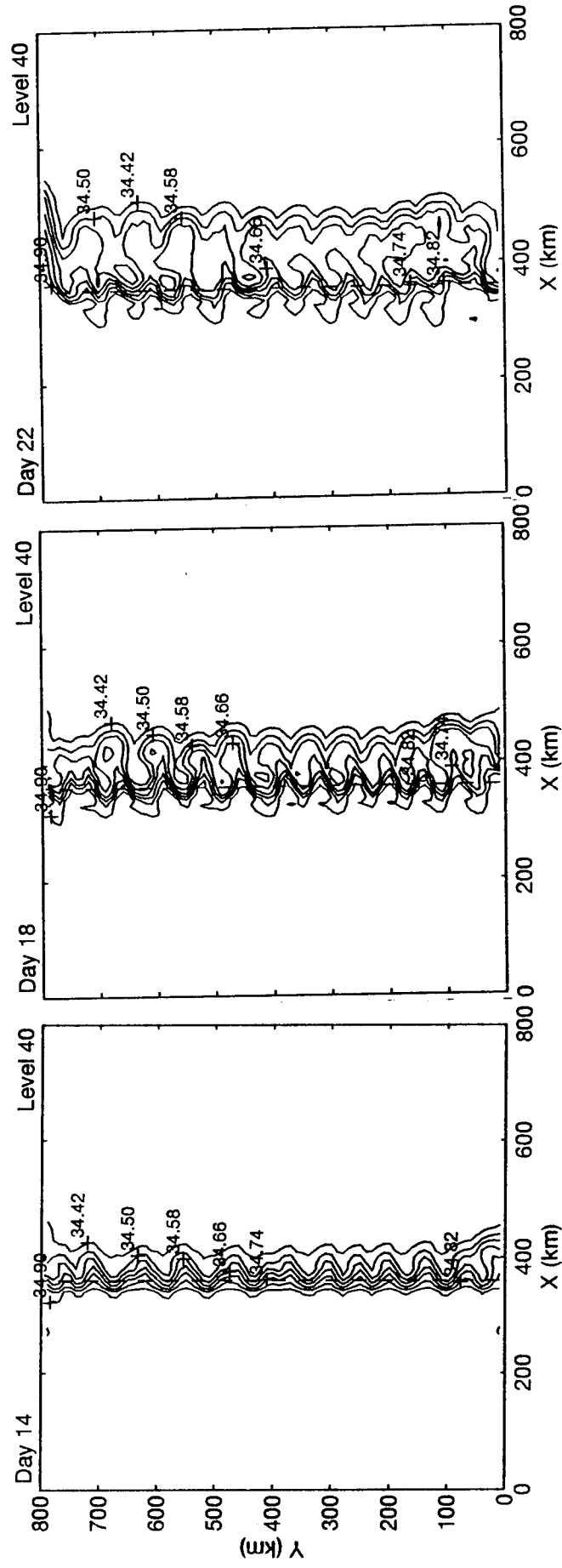


Fig.5

The salinity fields at sigma level 40 at days 14, 18, 22.

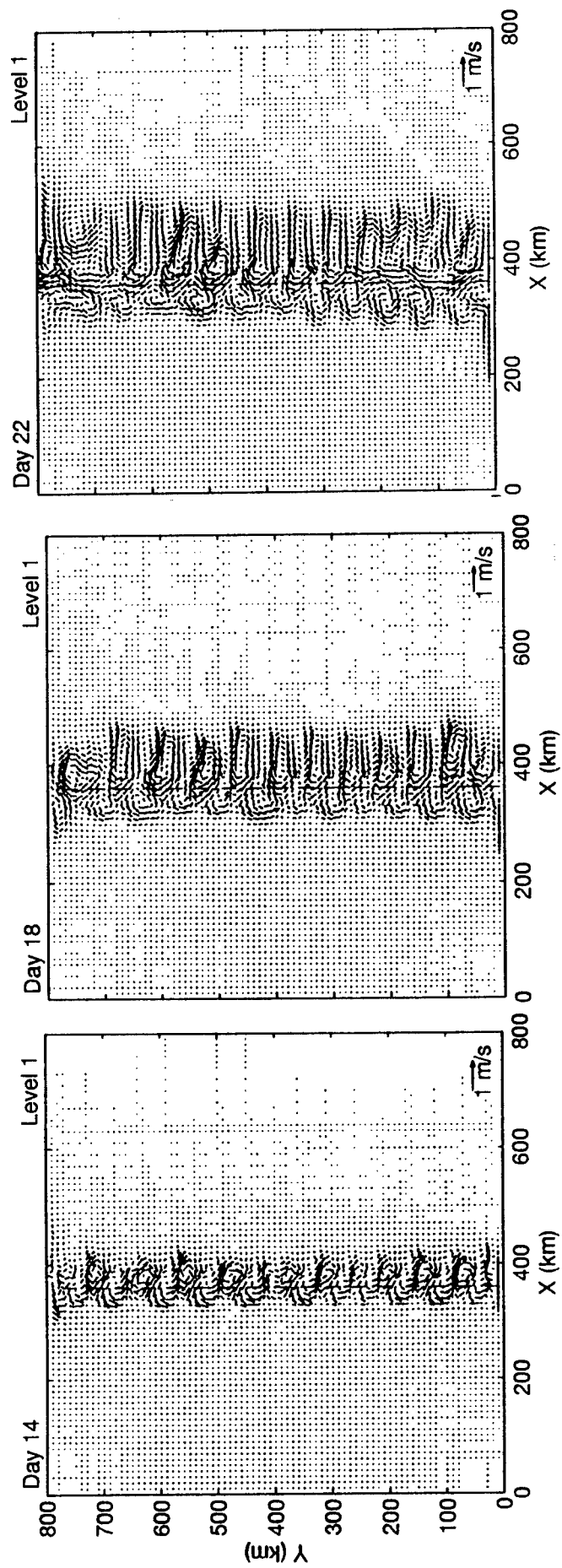
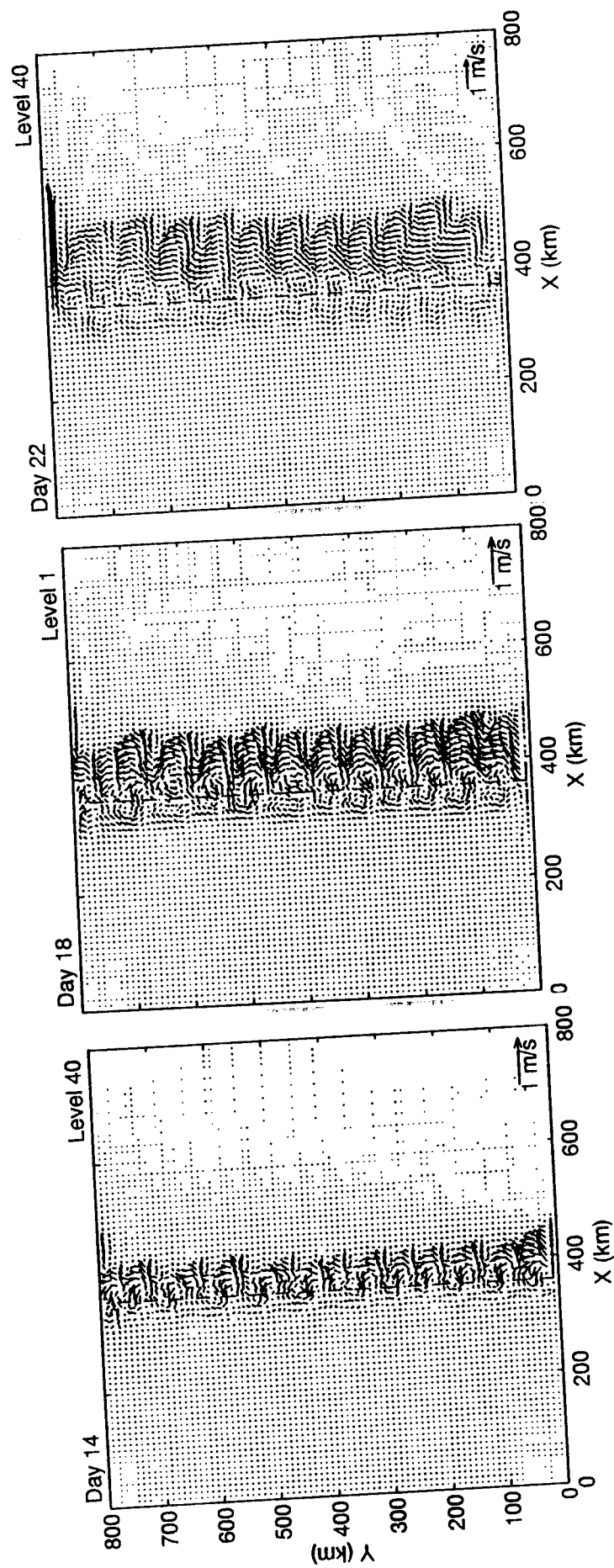


Fig. 6

The velocity fields at sigma level 1 at days 14, 18, 22.



The velocity fields at sigma level 40 at days 14, 18, 22.

Fig. 7

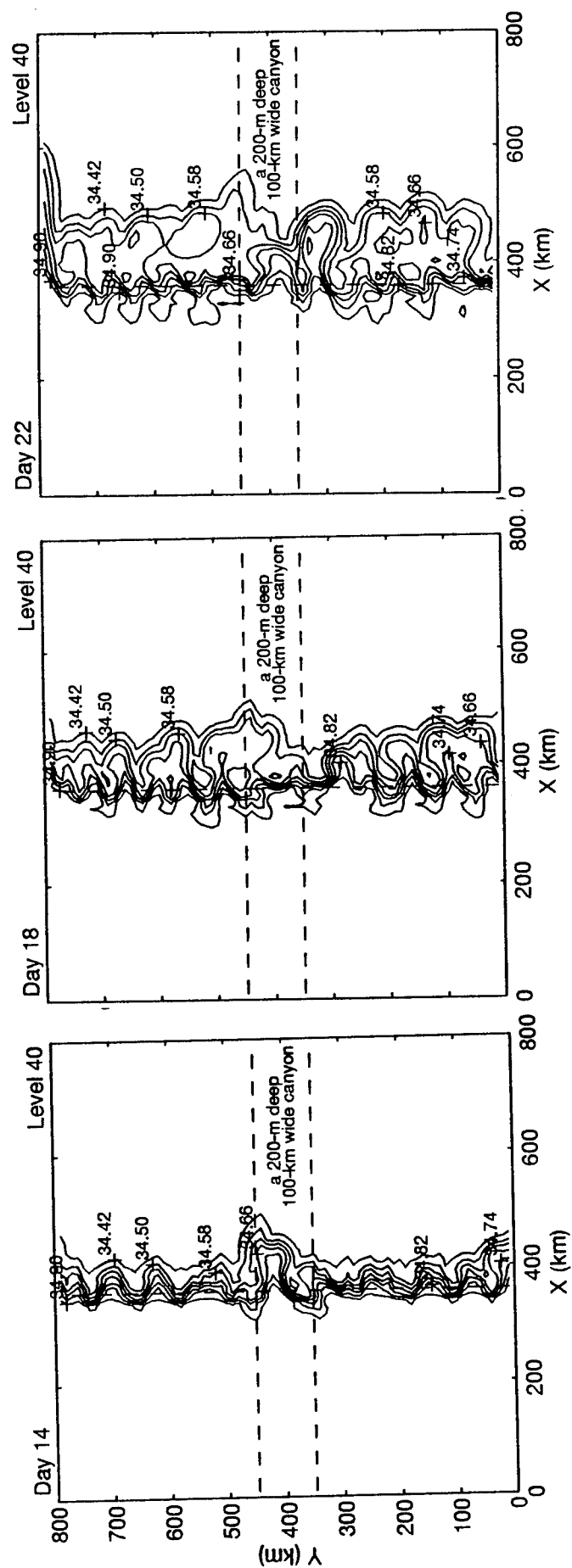


Fig. 8

The salinity fields in the presence of a 100-km wide and 200-m deep canyon at sigma level 40 at days 14, 18, and 22. The horizontal dashed lines show the position of the canyon.

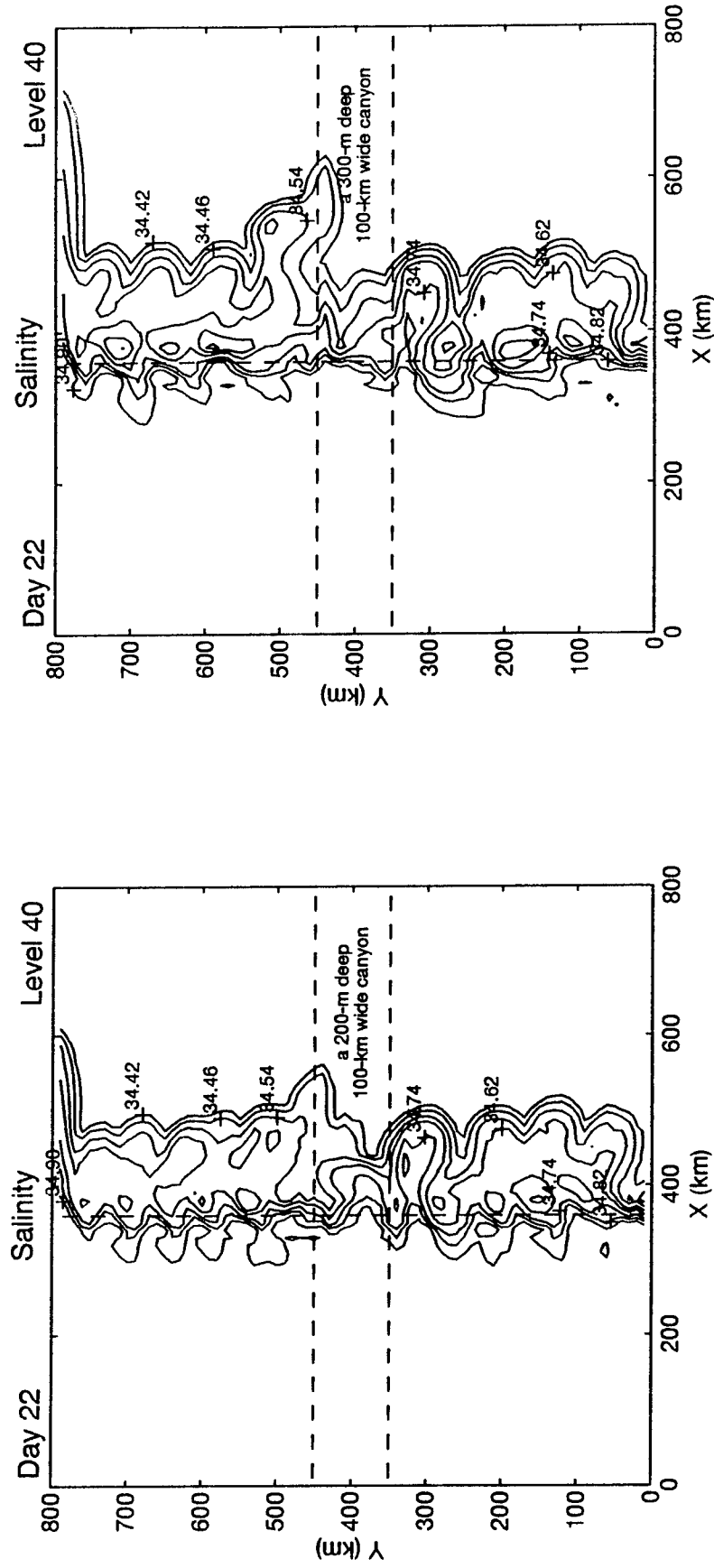


Fig. 9

The salinity fields in the presence of a 200-m deep and 300-m deep canyon at sigma level 40 at day 22.

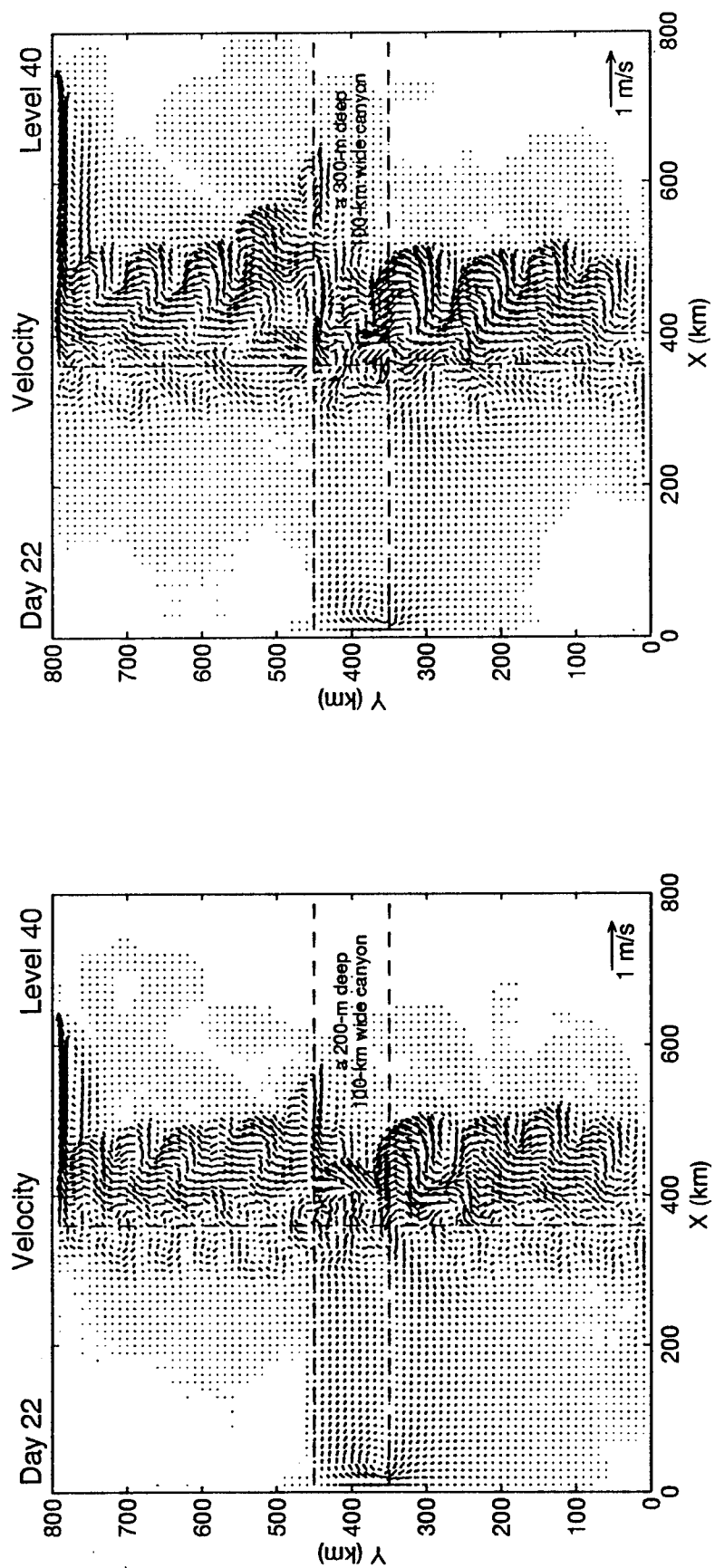


Fig. 10

The velocity fields in the presence of a 200-m deep and 300-m deep canyon at sigma level 40 at day 22.

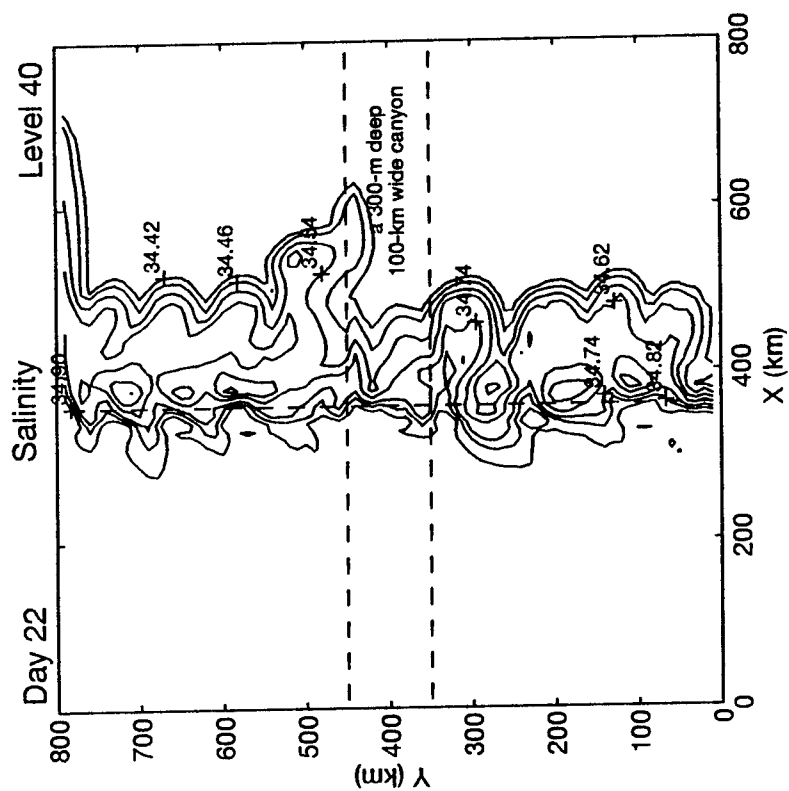
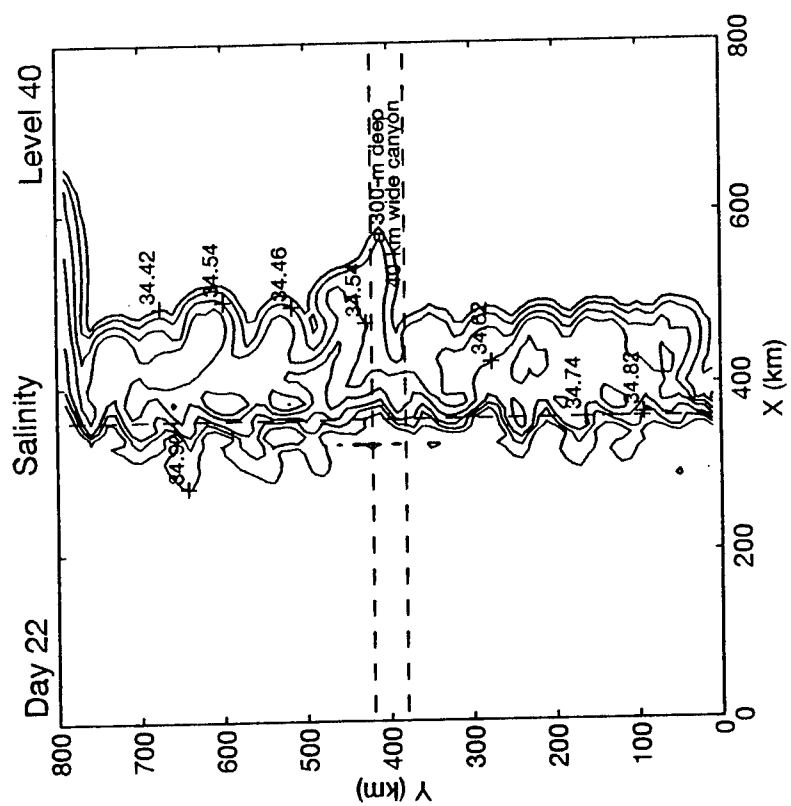


Fig. 14

The salinity fields in the presence of a 300-km wide and 40-km wide canyon at sigma level 40 at day 22.

Summary and Conclusions

Ruth H. Preller and Robert Edson

The purpose of this workshop was to familiarize ANWAP scientists, both modelers and observationalists, with work presently ongoing in the ANWAP. It was intended that such interaction would foster cooperative work and a productive flow of data between the observationalists and the modelers. The workshop initiated that interaction and it is hoped that such interactions continue to flourish in the future.

This workshop made it clear that a large amount of data pertaining to processes important in assessing the Arctic nuclear waste problem already exist. Large amount of data available in the literature as well as new data being collected by ANWAP scientists need to be compiled and made available to ANWAP scientists. This task is presently being addressed via development of a GIS data base and the compilation of an atlas developed from this data to appear in publication in 1995 (Crane).

Real time data, presently being gathered and analyzed, will be needed to understand the magnitude of the existing problem (Brooks). Data on existing source sites and possible future sites need to be validated, compiled and made available to the community.

Past and present field experiments examining sea ice as a mechanism for the uptake and transport of contaminants via sediments raised many important questions. Suspension freezing appears to be a key process in sediment uptake (Reimnitz). Is there any proof that contaminants exist in sea ice? Results of a recent summer field experiment presently being analyzed may shed some light on that question (Tucker). Another important issue was once sediment is incorporated into the ice, what are the mechanisms for the release of those sediments? Does sediment remain in the ice until it reaches the ice edge? Or are there other mechanisms that can cause the release of sediment from sea ice into the water column before it reaches the ice edge? These were raised as key issues for understanding the importance of sea ice as a transport mechanism for nuclear contaminants.

It was also pointed out that there are many available historical data sets dealing with sea ice. Data from Arctic buoys exist and have been analyzed to reveal prevailing patterns of both wind motion and ice drift for the Arctic (Colony). In addition to Arctic buoy data, a Russian historical data set (1967-1990) of sea ice conditions now exists (Rigor). This data set exists in Sea-ice Data in Digital Form (SIGRID) format and emphasizes conditions in the Kara, Laptev and East Siberian Sea.

Not only is Russian sea ice data becoming readily available, but other types of data of interest to the ANWAP program. Ocean circulation, wind and tidal data is available and has been used in the formation of numerical models (Proshutinsky). In addition, Russian historical data is also becoming available for Russian rivers. Of particular interest to the ANWAP program are data available on the Ob, Yenisei and Pechora rivers which empty into the Kara and Barents Seas (Becker).

Another data set of great interest to the nuclear contamination problem is data taken in the vicinity of the seabed (Sternberg). Understanding the motion near the ocean bottom is important to understanding the processes of suspension and settling of particles. A lengthy time series of measurements of deep currents, temperatures and light transmission have been taken in the Barents/Norwegian seas. Preliminary results were presented and a detailed analysis of these data is presently underway.

A final data presentation looked at the use of AVHRR data in studying river outflow effects and characteristic albedo and temperature changes in ice covered regions near river mouths (Fett). Successful past studies in the Beaufort Sea region suggest that a similar study be conducted in the Kara Sea. Data for the fall freeze up period of 1994 is being collected and analyzed to determine if the river plume of the Ob or Yenisei rivers can be seen and described.

Numerical model studies within the ANWAP, range from large scale to regional/basin scale to small scale studies represented by river models. Large scale models, based on the Cox ocean model, covered the Arctic, its marginal seas and subarctic marginal seas. These models were run using source locations mainly in the Kara Sea with values derived from the Yablokov report. Ten year simulations using various sources showed that levels of radiation along the Alaskan coast, in all cases, were approximately 5 orders of magnitude smaller than those in the Kara Sea itself. Results showed that using Sellafield as the only source does not appear to account for radiation levels observed in the Kara Sea (Preller). Ongoing and future work in the large scale modeling effort is focusing on more detailed model to data comparison, particularly in the Kara Sea (Cheng). Future work will use a large scale coupled ice-ocean model to study ice as a transport mechanism for contaminated sediments. This work will have to be done in close cooperation with those scientists conducting the field work on sea ice as well as laboratory experiments of sediment uptake into sea ice, in order to properly parameterize the uptake of these sediments from and release back into the water column.

A complementary study (Rigor) uses ice charts, ice motion and geostrophic wind to look at the net exchange of ice area from the Laptev Sea into the ice pack. This study attempts to determine the mean and interannual variability of ice production in the Laptev and to associate pollution transport with the exchange of ice from this area into the pack.

A second complementary study involves the development of a new ice model, using an anisotropic constitutive law for sea ice (Coon). The new ice model will be designed to account for the physical processes of sea ice as a pathway for the transport of radionuclides. This new model could be adapted by the large and regional scale models if proven an improvement over existing models.

An ongoing cooperative study also exists between the river modeling group and the large scale modeling group. Numerous sources, including the Yablokov report indicate that rivers may act as a major source of radioactive contamination of the Arctic. The river and

large scale modelers are at using both newly obtained river data (Becker) and river model results (Paluszkiewicz and Hibler) as river source data for the large scale models. Studies already underway (Allard) using Russian river data in the large scale coupled ice-ocean model were presented.

Regional models are also investigating the importance of rivers as a source of nuclear contamination into the Arctic. A regional model of the Kara Sea is presently being developed to look at processes which might contribute to the redistribution of nuclear contaminants from rivers. Initial efforts are testing the responses of such a coastal ocean to fresh coastal ocean buoyancy forcing (Smith). Previous work in the Gulf of Maine has shown that multiple river sources can interact, merge and form a single source for the formation of a coastal current (Brooks). The Ob and Yenisei rivers, both with large summer runoff, are speculated to interact in a similar way. Model studies are planned to look at these interactions. It is important to note that the large scale models presently use grid resolutions too coarse to resolve these coastal currents. Regional models will have to be used to understand these river/multi-river interactions with the regional circulation.

At the smaller scales, an effort to model the entire system from land-based sources through the rivers into the estuaries is presently being performed (Paluszkiewicz). The approach is to use a hierarchy of simple models to quantify the transport of contaminated materials through the system. Two scenarios are being evaluated for both river systems: a steady release and a catastrophic release into the system. A study of a catastrophic release scenario from three sites (Krasnoyarsk, Tomsk and Mayak) was presented (Hibler). Using a dynamic, one-dimensional model, results showed that the interaction of the following key parameters, critical shear stress, erodibility and partitioning and rate constants had a pronounced effect on the contaminant transport.

A somewhat different but very important small scale modeling effort was presented. This effort looked at modeling various release mechanisms into the environment from the radioactive waste source of the dumped reactor compartment of the Icebreaker Lenin (Mount). The results of five scenarios, each depending on the integrity of the levels of contaminant were shown. This model is being applied to other forms of radioactive waste dumped in the Kara and Barents Seas. These type of release rates may be used by the regional and large scale models to determine more realistic results than those obtained using constant release rates.

A presentation on atmospheric modeling, another important factor in the atmospheric-ice-ocean system, was given (Thompson). An atmospheric model for the Kara Sea region has been run for the fall 1994 period. This model uses 20 km grid resolution and is being compared to the model results of a corresponding global circulation model presently run by the U. S. Navy. Comparison of these two models should determine whether important atmospheric effects (wind features) are lost in the coarse resolution of the global model. The inability of the global models to calculate these finer scale features may influence model results of the transport of radioactive contaminants in the source regions (the Kara Sea).

Two additional modeling presentations (not part of ANWAP) were presented for information. The first presentation showed some initial results of a sea ice-ocean model in the Sea of Okhotsk (Yang). The Sea of Okhotsk is also a source location for dumped radioactive waste and is composed of a complex ice-ocean system. The final presentation showed the modeling of deep water formation over continental slopes (Jiang). These processes may be important for the transportation of contaminants within the water column but at depth.

The abstracts included in this proceedings indicate that a large effort presently exists to investigate the possible release, dispersion and consequences of radioactive contaminants in the Arctic. Despite this breadth, several issues stand out as problem areas. Most of these areas have components in each of the following three categories: observational evidence, process understanding, and model treatment. We simply do not have enough observational data to accurately quantify the important processes, do not understand the processes due to this lack of evidence, and are, therefore, ignoring or poorly treating these processes in the modeling efforts.

Principal amongst these problems is sea ice as it relates to contaminant transport. The following areas are of note:

- a) coastal dynamics of ice;
- b) methods of sediment entrainment into the ice;
- c) specific characteristics of the ice in each geographic area of major consequence in the contamination problem;
- d) characteristics and movement of the ice in the zone between pack ice and fast ice;
- e) ice contaminant transportation as a mechanism for contaminant source term repositioning; and
- f) treatment of ice contaminant transport processes in large scale models.

All of these points need to be quantified, understood and, where necessary, integrated into the modeling efforts to accurately quantify contaminant transport in the Arctic.

Of equal importance to ice dynamics are the characteristics of the sediment in the Arctic region, and the Kara Sea in particular. Many radionuclides strongly adhere to sediments, making radionuclide transport and sediment dynamics strongly related. The items listed below were highlighted as areas requiring additional information:

- a) sediment transport in the bottom boundary layer;
- b) mid-column sediment transport;
- c) dynamics of the river-sediment plume;
- d) interactions between sediments and ice;
- e) sediment as a transport matrix for contaminants; and
- f) treatment of sediment contaminant transport processes in large and small scale models.

While many of these issues are being addressed in the Arctic, in many cases, they must be investigated in the specific areas of high contamination. The status of sediment research in the Kara Sea must be better understood.

Several additional data/process/model deficiencies, while not specifically noted or discussed in detail during the workshop, should be briefly listed:

- 1) data from periods of maximum river flow;
- 2) data during winter conditions;
- 3) complete annual records for the sediment, ice and hydrographic characteristics of the regions of interest;
- 4) migration patterns of animals that frequent the zones of elevated radionuclide activity on the Russian land-mass and in the localized zones close to Novaya Zemlya with relatively high radionuclide concentrations in the marine sediments;
- 5) modeling pollutant trajectories, from release to the atmosphere to deposition on sea-ice or into ocean waters; and
- 6) understanding of geochemical processes in Siberian Rivers that may inhibit radionuclide transport towards the ocean.

Resolution of these deficiencies is actively being pursued through the ANWAP investigations.

Relative to the modeling efforts as a whole, several points are important and should be highlighted. The relevant time and space scales of the contaminant transport problem need to be investigated. Currently, a comprehensive approach addressing all scales has been adopted, but this approach may not be necessary. To efficiently answer the question of contaminant transport through the Kara Sea and the Arctic basin as a whole, larger regional and basin scale modeling may be all that is needed. Additional concerns lay in model validation. Several of the ANWAP modeling efforts have reached the level of maturity where validation is an important and necessary next step. Those modeling efforts still just beginning should have a thorough model validation effort as an integral part of the research plan. Finally, all model efforts should be initiated with a thorough review of the observational evidence covering the modeled area. The Kara Sea is not a data rich area. However, recent studies, coupled with an increasing amount of newly released Russian data, are allowing for a clearer picture of Kara Sea circulation to be developed. This picture should not be ignored. In the context of ANWAP goals, Russian data will continue to be sought to fill holes in our observational knowledge.

Several generic concerns are also worth noting. First, it is important that the GIS database efforts ongoing at NRL be supported in a timely and meaningful manner. This database serves as an archive of data specific to this program, a tool to assist in the risk assessment evaluations, and as a means of communication results to the international community. Data and cruise information should be forwarded as quickly as feasible, even if it is caveated to prevent dissemination outside ANWAP. Secondly, to assist in communication of the results and inter-comparison of analysis within the program, all principal investigators must transition to SI units. All future papers, reports and figures should be in SI units.

A great deal of information and understanding about the environmental effects of the release of nuclear material in the Arctic can be obtained from the combined efforts of modelers and observationalists. This workshop is a starting point for these types of efforts. It would be beneficial for a second modeling workshop to take place in early 1996 to determine the progress of these efforts.

WORKSHOP ATTENDEES

Richard Allard
Naval Research Laboratory
Code 7322
Stennis Space Center, MS 39529

Robert August
Naval Research Laboratory
Code 6616
Washington, DC 20375-5000

Peter Becker
CCPO/Old Dominion University
768 52nd Street
Norfolk, VA 23529

Robert H. Bourke
Department of Oceanography
Naval Postgraduate School
833 Dyer Road, Rm. 331
Monterey, CA 93943

David A. Brooks
Department of Oceanography
Texas A&M University
College Station, TX 77845

James M. Brooks
Geochemical & Environmental Research Group
Texas A & M University
College Station, TX 77845

Abe Cheng
Sverdrup Tech., Inc.
Bldg. 9110, MSAAP
Stennis Space Center, MS 39529

Roger Colony
Polar Science Center
University of Washington
1013 NE 40th Street
Seattle, WA 98105

Max D. Coon
Northwest Research Associates, Inc.
300 - 120th Avenue. NE
Bellevue, WA 98007

Kathleen Crane
Naval Research Laboratory
Code 7420 Marine Physics
Washington, DC 20375

Robert Edson
Office of Naval Research
Code 322
Rm. 704
800 N. Quincy Street
Arlington, VA 22217

Peter Guest
Department of Meteorology
Naval Postgraduate School
Monterey, CA 93943-5114

Lyle Hibler
Pacific Northwest Laboratory
Marine Science Laboratories
1529 Sequim Bay Rd.
Sequim, WA 98382

Lin Jiang
Department of Oceanography
Naval Postgraduate School
Monterey, CA 93943

Tom Kozo
Naval Research Laboratory
Code 7541
7 Grace Hopper Avenue
Monterey, CA 93943

David W. Layton
Health and Ecological Assessment Division
Lawrence Livermore National Laboratory
7000 East Avenue (L-453)
Livermore, CA 94550

Wieslaw Maslowski
Oceanography Department
Code OC//MA
Naval Postgraduate School
Monterey, CA 93943-5122

Mark Mount
Lawrence Livermore National Laboratory
20201 Century Bldg., 2nd Floor
Germantown, MD

Terri Paluszkiewicz
Pacific Northwest Laboratory
Marine Science Laboratory
1529 West Sequim Bay Rd.
Sequim, WA 98382

A. Rost Parsons
c/o Naval Postgraduate School
Department of Oceanography
833 Dyer Road, Rm. 331
Monterey, CA 93943

Tom Thang Pham
FNMOC, Ocean Models Division
Monterey, CA 93943

Ruth H. Preller
Naval Research Laboratory
Code 7322
Stennis Space Center, MS 39529

Andrey Proshutinsky
Institute of Marine Science
University of Alaska, Fairbanks
P. O. Box 1080
Fairbanks, AK 99775-1080

Erk Rienmitz
U. S. Geological Survey
345 Middlefield Road
Marlo Park, VA 94025-3591

Ignatius Rigor
PSC/APL/UW
1013 NE 40th
Seattle, WA 98103

Michael Rugar
Naval Research Laboratory
Code 5554
4555 Overlook Ave., SW
Washington, DC 20375-5337

Martha Scott
Department of Oceanography
Texas A&M University
College Station, TX 77843-3146

David C. Smith, IV
Institute of Marine Sciences
University of California, Santa Cruz
Santa Cruz, CA 95073

Richard Sternberg
School of Oceanography WB-10
University of Washington
Seattle, WA 98195

William T. Thompson
Naval Research Laboratory
Marine Meteorology Division
7 Grace Hopper Avenue
Monterey, CA 93943-5502

Emeritus Traganza
Naval Postgraduate School
Monterey, CA 93943

Walter (Terry) Tucker
CRREL
72 Lyme Road
Hanover, NH 03755

Carolyn Viscosi-Shirley
College of Oceanic and Atmospheric Sciences
Oregon State University
Corvallis, OR 97330

Michael Van Woert
Office of Naval Research
Code 322
800 N. Quincy Street
Arlington, VA 22217

Jiayan Yang
Department of Physical Oceanography
Woods Hole Oceanographic Institution
Woods Hole, MA 02543